Higher-Order Corrections in the 2HDM, N2HDM and NMSSM

Zur Erlangung des akademischen Grades eines

DOKTORS DER NATURWISSENSCHAFTEN

von der KIT-Fakultät für Physik
des Karlsruher Instituts für Technologie (KIT)

genehmigte

DISSERTATION

von

M.Sc. Marcel Krause

aus Ludwigsburg

Referentin: Prof. Dr. M. M. Mühlleitner (KIT, Karlsruhe)

Korreferent: Prof. Dr. R. Santos (ISEL & ULISBOA, Lissabon)

Tag der mündlichen Prüfung: 19. Juli 2019

Eidesstattliche Versicherung gemäß § 13 Absatz 2 Ziffer 3 der Promotionsordnung des Karlsruher Instituts für Technologie (KIT) für die KIT-Fakultät für Physik:

1. Bei der eingereichten Dissertation zu dem Thema

   Higher-Order Corrections in the 2HDM, N2HDM and NMSSM

   handelt es sich um meine eigenständig erbrachte Leistung.

2. Ich habe nur die angegebenen Quellen und Hilfsmittel benutzt und mich keiner unzulässigen Hilfe Dritter bedient. Insbesondere habe ich wörtlich oder sinngemäß aus anderen Werken übernommene Inhalte als solche kenntlich gemacht.

3. Die Arbeit oder Teile davon habe ich bislang nicht an einer Hochschule des In- oder Auslands als Bestandteil einer Prüfungs- oder Qualifikationsleistung vorgelegt.

4. Die Richtigkeit der vorstehenden Erklärungen bestätige ich.

5. Die Bedeutung der eidesstattlichen Versicherung und die strafrechtlichen Folgen einer unrichtigen oder unvollständigen eidesstattlichen Versicherung sind mir bekannt.

Ich versichere an Eides statt, dass ich nach bestem Wissen die reine Wahrheit erklärt und nichts verschwiegen habe.

Karlsruhe, den 03. Juli 2019

....
(Marcel Krause)

Für meine Eltern.

"Das ist der Weisheit letzter Schluss:
Nur der verdient sich Freiheit wie das Leben,
Der täglich sie erobern muss."

Johann Wolfgang von Goethe
(Faust. Der Tragödie zweiter Teil)

Abstract

Up to this day, the Standard Model of particle physics is widely accepted as the most fundamental quantum field theory which is fully compatible with the precise measurements being carried out at particle collider experiments. Despite this enormous success, the model does not provide answers to all remaining open questions of fundamental physics. In order to overcome this shortcoming, theories beyond the Standard Model are investigated. In this thesis, we compute higher-order corrections to observables in extended Higgs sectors of three different theories beyond the Standard Model.

We investigate the Two-Higgs-Doublet Model and the Next-to-Two-Higgs-Doublet Model as two extensions of the Standard Model with regard to the Higgs potentials of the theories. In both models, we perform the complete electroweak renormalization of all independent parameters of the theories and present several different renormalization schemes for the scalar mixing angles of the extended Higgs sectors. We compute the full electroweak one-loop corrections to the partial decay widths of the decays of all Higgs bosons in the two theories. Furthermore, we provide the two newly developed computer programs 2HDECAY and ewN2HDECAY which allow for the numerical evaluation of the partial decay widths and branching ratios of all Higgs boson decays in the two models. In order to demonstrate the relevance of the newly computed corrections we use the two programs for numerical analyses and estimate the remaining theoretical uncertainties of the calculations.

The third theory investigated in this thesis is the charge-parity-violating Next-to-Minimal Supersymmetric Standard Model. In our work, we provide the $\mathcal{O}(\alpha_t^2)$ two-loop corrections to the masses of the Higgs bosons of this model. To that end, we perform the one- and two-loop renormalization of the theory, restricting ourselves to the contributions relevant for the $\mathcal{O}(\alpha_t^2)$ corrections. The results of our computations are implemented in a new version of NMSSMCALC. As a demonstration of the relevance of the newly computed corrections, we perform a numerical analyses on the size of the $\mathcal{O}(\alpha_t^2)$ two-loop contributions.

Zusammenfassung

Bis zum heutigen Tag ist das Standardmodell der Teilchenphysik weithin als die grundlegendste Quantenfeldtheorie anerkannt welche mit den präzisen Messungen von Teilchenbeschleuniger-Experimenten vollständig kompatibel ist. Trotz dieses enormen Erfolgs vermag das Modell nicht alle verbleibenden offenen Fragen der Grundlagenphysik zu beantworten. Um dieses Manko zu überwinden werden Theorien jenseits des Standardmodells untersucht. In dieser Arbeit berechnen wir Korrekturen höherer Ordnung zu Observablen in den erweiterten Higgs-Sektoren dreier verschiedener Theorien jenseits des Standardmodells.

Wir untersuchen das Zwei-Higgs-Dublett-Modell und das Nichtminiale Zwei-Higgs-Dublett-Modell als zwei Erweiterungen des Standardmodells hinsichtlich der Higgs-Potentiale der Theorien. In beiden Modellen führen wir die vollständige elektroschwache Renormierung aller unabhängigen Parameter der Theorien durch und präsentieren verschiedene Renormierungsschemata für die skalaren Mischungswinkel der erweiterten Higgs-Sektoren. Wir berechnen die vollständigen elektroschwachen ein-Schleifen-Korrekturen zu den partiellen Zerfallsbreiten der Zerfälle aller Higgs-Bosonen in beiden Theorien. Weiterhin stellen wir die zwei neu entwickelte Computerprogramme 2HDECAY und ewN2HDECAY vor, welche die numerische Auswertung der partiellen Zerfallsbreiten und Verzweigungsverhältnisse in beiden Modellen ermöglichen. Um die Relevanz der berechneten Korrekturen zu quantifizieren, nutzen wir die neu entwickelten

Programme für numerische Analysen und schätzen die verbleibende theoretische Unsicherheit unserer Berechnungen ab.

Die dritte in dieser Arbeit untersuchte Theorie ist das ladungs- und paritätsverletzende Nicht-minimale Supersymmetrische Standardmodell. In unserer Arbeit berechnen wir die $\mathcal{O}(\alpha_t^2)$-zwei-Schleifen-Korrekturen zu den Massen der Higgs-Bosonen dieses Modells. Zu diesem Zweck führen wir die ein- und zwei-Schleifen-Renormierung der Theorie durch, wobei wir uns auf Beiträge zu den $\mathcal{O}(\alpha_t^2)$-Korrekturen beschränken. Die Ergebnisse unserer Rechnungen sind in einer neuen Version des Computerprogramms `NMSSMCALC` eingepflegt. Zur Demonstration der Relevanz der neu berechneten Korrekturen analysieren wir die Größe der $\mathcal{O}(\alpha_t^2)$-zwei-Schleifen-Beiträge numerisch.

Contents

Introduction

The Standard Model (SM) of particle physics describes the properties and interactions of the most fundamental particles known to this date in a mathematically consistent way [1–8]. The theoretical predictions made within the SM were confirmed by measurements at particle collider experiments with remarkable precision [9–14] and with the discovery of a SM-like Higgs boson at the Large Hadron Collider (LHC) in 2012 [15, 16], the last missing particle predicted by the SM was discovered.

Despite its enormous success, the SM suffers both from theoretical shortcomings, *e.g.* the *hierarchy problem*, as well as from the fact that it does not postulate a large enough breaking of the charge-parity (CP) symmetry or a suitable candidate for dark matter (DM). Consequently, throughout the last decades tremendous effort was invested into studies of theories beyond the SM (BSM).

Among the simplest candidates for BSM theories are singlet and doublet extensions of the SM Higgs sector. Examples of these BSM theories are the *Two-Higgs-Doublet Model* (2HDM) [17, 18] and the *Next-to-Two-Higgs-Doublet Model* (N2HDM) [19] which are interesting extensions of the SM since they provide candidates for DM, a rich phenomenology and they can describe a successful baryogenesis. For the solution of other shortcomings of the SM, *e.g.* the hierarchy problem, BSM theories based on supersymmetry (SUSY) are considered. The simplest realization of a SUSY theory is given by the *Minimal Supersymmetric Standard Model* (MSSM) [20–36]. Due to the presence of the additional symmetry between the fermionic and bosonic degrees of freedom in the MSSM, the hierarchy problem of the SM Higgs boson sector is naturally solved. Despite this, another form of fine-tuning problem, the μ *problem*, remains in the theory. The *Next-to-Minimal Supersymmetric Standard Model* (NMSSM) [37–46] provides a natural solution to this μ problem. Moreover, the NMSSM features an interesting phenomenology through its extended Higgs sector and the CP-violating realization of the model provides additional sources of CP violation.

The Higgs sector provides a promising portal to BSM physics. The detailed investigation of the discovered Higgs boson and its couplings might indicate signs of new physics due to loop contributions stemming from additional BSM particles or through the mixing with additional Higgs bosons. From the theoretical side, the detailed investigation requires the calculation of the observables of the Higgs sector to the highest possible precision.

Concerning the higher-order corrections to 2HDM Higgs boson decays, several computer programs are available. For example, the `FORTRAN` code `HDECAY 6.52` [47] enables the calculation of the branching ratios (BRs) of the 2HDM Higgs bosons including off-shell and loop-induced decay modes and the state-of-the-art quantum chromodynamics (QCD) corrections, where applicable. Other examples of computer tools include `Prophecy4f` [48–51], enabling the computation of the loop-corrected decay widths corresponding to the decay of the light CP-even Higgs boson to four fermions via pairs of off-shell gauge bosons, `2HDMC` [52] that allows for the computation of all two-body and some three-body decay widths including higher-order QCD corrections, `SPheno` [53,54] which enables the generic calculation of the full one-loop-corrected two-body decays and partially tree-level three-body decays which can be applied to the case of the 2HDM, and `H-COUP` [55] which allows for the computation of loop-corrected partial decay widths of the decays of Higgs bosons of extended Higgs sectors into final-state pairs of fermions and gauge bosons. In order to perform thorough and precise phenomenological analyses, the partial decay widths and BRs of *all* decay channels of the Higgs bosons of the 2HDM need to be considered at the highest possible level of precision. One key goal of this thesis is to provide the electroweak one-loop corrections to the partial decay widths of all on-shell (OS) Higgs boson decays of the 2HDM that are not loop-induced. These decay widths are combined with the state-of-the-art QCD corrections implemented in `HDECAY 6.52` to form the new computer program `2HDECAY` [56]. Since we consider several different renormalization schemes for the scalar mixing angles of the 2HDM in `2HDECAY`, the program additionally allows for an estimate of the remaining theoretical uncertainty of the loop-corrected decay widths.

For the N2HDM on the other hand, only a few computer codes for the computation of higher-order corrections to the Higgs boson decays are available. The `FORTRAN` program `N2HDECAY` [57,58] enables the calculation of the BRs of the N2HDM Higgs bosons, including off-shell and loop-induced decay modes and the state-of-the-art QCD corrections, where applicable. As another example, the generic results for the full one-loop decays of the Higgs bosons provided by the program `SPheno` can be applied to the N2HDM as well. In this thesis, we provide the electroweak one-loop corrections to the partial decay widths of all OS Higgs boson decays of the N2HDM that are not loop-induced. For the calculation of the electroweak one-loop corrections, we consider several different renormalization schemes of the scalar mixing angles of the N2HDM. We present the new computer program `ewN2HDECAY` which combines the electroweak loop-corrected decay widths with the state-of-the-art QCD corrections provided by `N2HDECAY`.

Apart from partial decay widths and BRs, the masses of the Higgs bosons in BSM theories provide another interesting observable for which predictions to the highest level of precision are required. This is particularly the case in SUSY models where the Higgs boson masses are not free parameters but instead, they are calculated from the independent input parameters of the theory. For the MSSM and NMSSM, the higher-order corrections to the Higgs boson masses, dominated by contributions stemming from top quarks and stop squarks, are sizeable. Hence, their calculation to the highest level of precision is of importance in order to provide reliable predictions. While the status of the higher-order corrections to the Higgs boson masses in the NMSSM is not as advanced as in the MSSM, there was still a tremendous progress concerning their calculation throughout the last decades. For the CP-conserving realization of the model, the leading one-loop contributions [59–64] as well as the full one-loop corrections to the Higgs boson masses in several renormalization schemes [65–70] are available. Moreover, the two-loop $\mathcal{O}(\alpha_t\alpha_s + \alpha_b\alpha_s)$ contributions[1] were computed in the approximation of vanishing external momentum [65] and more recently, additional corrections stemming from the genuine NMSSM-specific parameters were computed as well [71]. Analogously, for

---

[1] We refer to Sec. 14.5 for an explanation of the meaning of the $\mathcal{O}(\alpha_i\alpha_j\cdots)$ notations used in this thesis.

the CP-violating NMSSM the dominant one-loop corrections [72–77] as well as the full one-loop corrections together with dominant two-loop corrections in the renormalization group approach [78] were made available. In an independent thorough calculation, the full one-loop corrections as well as the two-loop $\mathcal{O}(\alpha_t \alpha_s)$ contributions to the Higgs boson masses of the complex NMSSM were provided in a mixed $\overline{\text{DR}}$-OS scheme and implemented in the `FORTRAN` program `NMSSMCALC` [67, 79–81]. In order to further increase the precision, it is a key objective of this thesis to calculate the two-loop $\mathcal{O}(\alpha_t^2)$ corrections to the Higgs boson masses in the complex NMSSM and to implement these additional contributions into the updated program version `NMSSMCALC 3.00` [82].

This thesis is structurally and thematically divided into four different parts.

In Part I of the thesis, we lay the theoretical foundations for our work. Starting with Chapter 2, we provide a brief introduction to the SM and its shortcomings and briefly discuss extensions of the SM in general. In the subsequent Chapter 3, we discuss the regularization and OS renormalization of the *ultraviolet* (UV) divergences of loop integrals in general. We provide generic formulae for the calculation of partial decay widths up to one-loop order and discuss the computation of radiative corrections to the masses of particles in a generic way. We conclude Part I with a general discussion about input parameter conversions as well as with a general analysis on gauge dependences in higher-order corrections.

Part II of this thesis deals with the calculation of the electroweak one-loop corrections to the partial decay widths of the Higgs bosons of the real 2HDM. Beginning with Chapter 4, we introduce the electroweak Lagrangian and the Higgs potential of the CP-conserving 2HDM. In the subsequent Chapter 5, we present the renormalization of all independent parameters of the electroweak sector of the 2HDM, focusing in particular on the renormalization of the scalar mixing angles. Following in Chapter 6, we describe the semi-automated calculation of the electroweak partial decay widths and present the computer package `2HDECAY` for the calculation of the BRs and partial decay widths of the 2HDM Higgs bosons. Subsequently, we present in Chapter 7 a numerical analysis on the size of the electroweak one-loop corrections for selected decay channels. Finally, in Chapter 8 we provide a conclusion of Part II of this thesis.

In Part III of this thesis, we focus on the calculation of the electroweak one-loop corrections to the partial decay widths of the Higgs bosons of the real N2HDM. In Chapter 9, we introduce the electroweak Lagrangian and the scalar potential of the CP-conserving N2HDM and present the renormalization of all independent parameters of the N2HDM in the subsequent Chapter 10. We present several different renormalization schemes for the four scalar mixing angles of the N2HDM. In the subsequent Chapter 11, we present the semi-automated computation of the electroweak partial decay widths of all OS decay channels of the N2HDM Higgs bosons that are not loop-induced and present the computer package `ewN2HDECAY`. Following in Chapter 12, we present a numerical analysis on the size of the electroweak corrections to the partial decay widths and BRs. Subsequently, we provide in Chapter 13 a conclusion of Part III of this thesis.

Part IV of this thesis deals with the calculation of the $\mathcal{O}(\alpha_t^2)$ two-loop corrections to the masses of the neutral Higgs bosons in the CP-violating NMSSM. We begin in Chapter 14 with the presentation of the Lagrangian and the scalar potential of the complex NMSSM and present in the subsequent Chapter 15 the renormalization of all independent parameters relevant for the two-loop $\mathcal{O}(\alpha_t^2)$ corrections. In the following Chapter 16, the calculation of the two-loop $\mathcal{O}(\alpha_t^2)$ contributions to the loop-corrected masses of the neutral Higgs bosons of the complex NMSSM and their implementation in `NMSSMCALC 3.00` is described. Subsequently, we present in Chapter 17 a numerical analysis on the size of the two-loop $\mathcal{O}(\alpha_t \alpha_s + \alpha_t^2)$

corrections to the Higgs boson masses. Finally in Chapter 18, we provide a conclusion of Part IV of this thesis.

In Chapter 19, we present a final conclusion as well as an outlook on possible future work. The thesis is completed by an extensive appendix. In App. A, we present the $\mathcal{O}(\varepsilon)$ and $\mathcal{O}(1)$ expansions of the scalar one- and two-loop integrals required for the calculations performed in this work. In the subsequent Appendices B and C, we present the definition of the CTs of the 2HDM and N2HDM as they are implemented in 2HDECAY and ewN2HDECAY, respectively. Following in App. D, we present the analytic formulae for the neutral and charged Higgs boson mass matrix elements as well as their CTs. Subsequently, we present in App. E the Feynman diagrams corresponding to the two-loop contributions to the unrenormalized self-energies of the neutral and charged Higgs bosons. In the final App. F, we provide exemplary input and output files for 2HDECAY.

The calculation of the electroweak corrections to the partial decay widths of the Higgs bosons of the 2HDM and N2HDM as well as the programs 2HDECAY and ewN2HDECAY themselves were presented in [56] and [83], respectively. Moreover, the $\mathcal{O}(\alpha_t^2)$ two-loop corrections to the masses of the Higgs bosons in the complex NMSSM as well as their implementation into the updated version NMSSMCALC 3.00 was presented in [82]. Similarities between the structure and content of these works and Parts II to IV of this thesis are intentional and reflect the contribution of the author.

Part I.

Theoretical Foundations

The Standard Model of Particle Physics and Its Extensions

This thesis covers higher-order corrections to partial decay widths and Higgs boson masses in three different quantum field theories (QFTs): the 2HDM, the N2HDM and the complex NMSSM. The common feature of all three of these models is that they extend the SM of particle physics by introducing additional fields and symmetries. In Sec. 2.1, we present a brief history of particle physics that led to the development of the SM and introduce the particle content of the SM. Moreover, we discuss the remarkable agreement of experimental data with theoretical predictions made within the SM and on the other hand its shortcomings and experimental evidences that indicate that the SM is not sufficient to explain all phenomena observed in the universe. In Sec. 2.2, we introduce first extensions of the SM that are based on the addition of Higgs singlets and doublets to the SM Lagrangian. Both the 2HDM and the N2HDM fall into this category of SM extensions, and we discuss how these models provide solutions to some of the shortcomings of the SM. Finally, in Sec. 2.3 we briefly introduce the concept of SUSY, which doubles the particle content of the SM and provides solutions for most of its open problems. As specific examples of SUSY extensions, we briefly discuss the MSSM and the complex NMSSM, since the calculations of the higher-order corrections to the Higgs masses presented in this thesis are performed in the latter model.

2.1. The Standard Model of Particle Physics

The idea that the physical world consists of fundamental indivisible building blocks is the concept of atomism (from the ancient Greek word *átomos*, meaning "indivisible" [84]) which dates back at least 2500 years from the present day. The original concept of atomism was based on philosophical arguments rather than on experimental observation and the fundamental building blocks were considered to be in the form of geometrical shapes [85, 86]. Through the centuries, scientists discovered the chemical elements and replaced the idea of these shapes as fundamental building blocks in favor of the chemical elements. It was not until the discovery of the *electron* e^- in 1897 [87] that the concept of the atoms as indivisible structures was abandoned, and with the later discovery of the protons and neutrons as sub-atomic particles [88], the apparent fundamental building blocks of nature were found and the Rutherford model of the atom was established [89, 90].

Since then, our understanding of particle physics at the fundamental level progressed in a fast pace throughout the last century. The development of quantum mechanics, especially
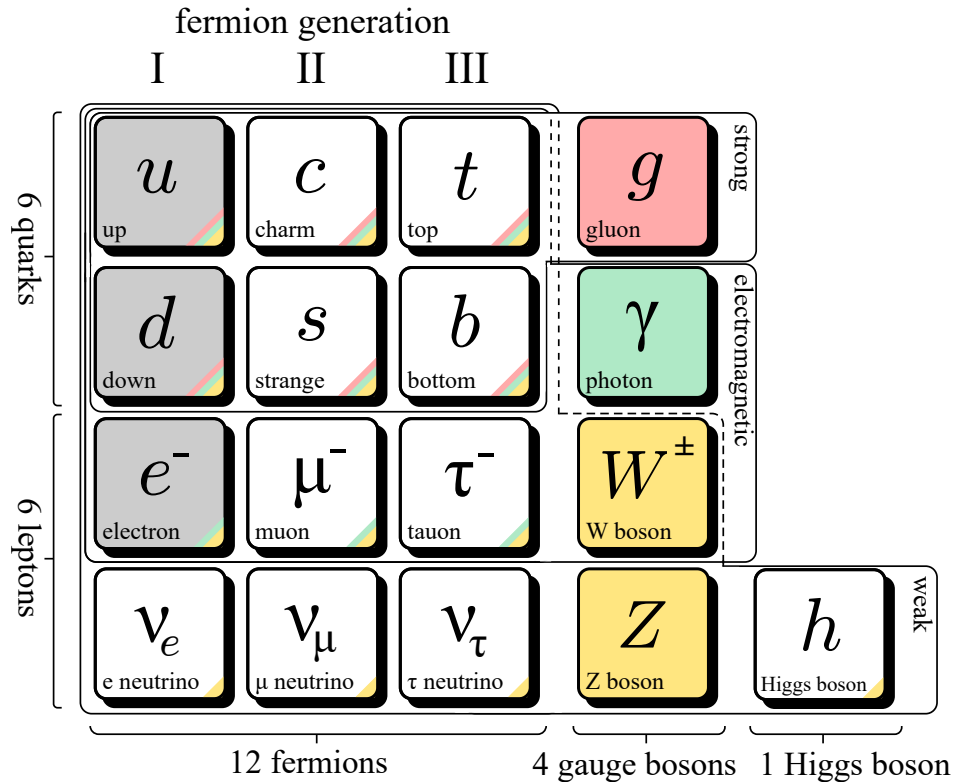
Figure 2.1.: Particle content of the SM of particle physics. The fermions of the SM, namely the quarks and leptons, are grouped into three generations. The gauge bosons mediate the strong, electromagnetic and weak forces, while through the Higgs field, the SM particles acquire their masses. The different boxes around the particles as well as the color codes indicate which particle is affected by each of the fundamental forces, represented by the corresponding colored gauge boson. In the constituent quark model, the u and d quarks form the protons and neutrons and together with the electrons e^- (all three depicted with a gray background), they make up most of the ordinary matter.

of the *spin-statistics theorem* [91, 92], revealed that each fundamental particle belongs to one of two classes of particles: bosons, with an integer spin obeying the Bose-Einstein statistics and fermions, with half-integer spin obeying Fermi-Dirac statistics. While the electrons belong to the latter category, the *photons* γ, the quanta of the electromagnetic field, belong to the bosons. The theoretical concepts of QFTs allowed for the development of quantum electrodynamics (QED), which served as a fundamental theory for describing the *electromagnetic force*, which, together with *gravity*, formed one of the two known forces at the time. Moreover, the formulation of QED allowed for a deeper understanding of electromagnetism, since it enabled a theoretical explanation of many of its phenomena. On the other hand, the observation of radioactive decays led to the development of the concept of the *weak force* [93] as a third fundamental force of nature, with the $W^\pm$ and Z *gauge bosons* as the mediators of the force and the *electron neutrino* ν_e as another fundamental particle which is produced in weak decays. Moreover, experiments carried out at high-energy particle accelerators in the second half of the last century revealed that the protons and neutrons consist of even more fundamental building blocks, namely the up and down *quarks* u and d, respectively, as well as of the *gluons* g. The *strong force* was established as the fourth fundamental force of the universe, mediated between the quarks by these gluons, and mathematically it was described in the framework of QCD [89, 94].

Three of the four known forces, namely the electromagnetic, weak and strong force, where combined into a common mathematical framework of gauge theories, which is nowadays known as the SM of particle physics. The electromagnetic and weak forces were unified as a single *electroweak force*, while the strong force remains as the other individual fundamental force [1, 7, 8]. Furthermore, experiments at high-energy accelerators throughout the second half of the last century revealed that there are several generations of fundamental fermions, where the only formal difference between fermions of different generations is given by their different masses. With the discovery of the top quark t in 1995 [95, 96] and the τ^- lepton in the year 2000 [97], the last fermions of the third generation were discovered. Finally, the *Higgs boson h* of the SM, proposed as a theoretical concept as early as 1968 [2–6], was discovered only recently in the year 2012 [15, 16]. Its discovery completed the whole framework of the SM of particle physics as it is known to date. All fundamental particles of the SM and the forces mediating between them are illustrated in Fig. 2.1.

From a mathematical point of view, the SM of particle physics is established as a gauge QFT based on the direct group product $SU(3)_C \times SU(2)_L \times U(1)_Y$, where the indices refer to color, left-handedness and weak hypercharge, respectively. In the following, we only briefly describe the structure of the SM. For a more detailed overview, we refer to *e.g.* [94]. The first subgroup $SU(3)_C$ describes the strong interaction in the mathematical framework of QCD, with color as the fundamental charge of the gauge group. The gauge bosons mediating the strong force are 8 gluons g in the adjoint representation of the $SU(3)_C$ which each carry a color-less combination of the three color states $\{r, g, b\}$ (red, green and blue) and the three anti-color states $\{\bar{r}, \bar{g}, \bar{b}\}$ (anti-red, anti-green and anti-blue). The only other particles that interact strongly are the quarks which are embedded both in QCD and in the SM as *up-type* and *down-type* quarks, *i.e.* the upper and lower row of quarks presented in Fig. 2.1. Each quark carries any one of the three colors as a color charge.

The other two gauge groups of the SM, given as the direct product $SU(2)_L \times U(1)_Y$, describe the unified electroweak force. The corresponding group charges are the weak isospin I_W as well as the weak hypercharge Y and the gauge boson fields mediating the electroweak force are given by the $SU(2)_L$ triplet (W_1, W_2, W_3) and the gauge singlet B. This force acts on all leptons and quarks of the SM, all of which are represented in the electroweak theory via a chiral representation, *i.e.* the fermions are described via left- and right-chiral fields, indicated with subscripts L and R, respectively. The leptons are represented by the left-chiral $SU(2)_L$ doublet $((\nu_e, \nu_\mu, \nu_\tau), (e, \mu, \tau))_L$ and the right-handed singlet $(e, \mu, \tau)_R$ while the up- and down-type quarks are represented by the left-chiral $SU(2)_L$ doublet $((u, c, t), (d, s, b))_L$ and the two right-handed singlets $(u, c, t)_R$ and $(d, s, b)_R$. Since the subgroups $SU(3)_C$ and $SU(2)_L \times U(1)_Y$ transform independently of each other, the color charge is not affected by this $SU(2)_L \times U(1)_Y$ representation of the quarks [94].

The gauge symmetries of the SM forbid the explicit appearance of mass terms for any fundamental particle of the theory in the Lagrangian. On the other hand, it is experimentally well-established that almost all particles of the SM have a non-vanishing mass [98]. The mechanism of electroweak symmetry breaking (EWSB) provides a solution to this theoretical shortcoming. In addition to the fields described above, the SM contains an $SU(2)_L$ Higgs doublet (ϕ^+, ϕ^0), where ϕ^+ and ϕ^0 represent the charged and neutral components, with a non-vanishing *vacuum expectation value* (VEV) $v \approx 246\,\text{GeV}$ [98] which represents the vacuum state of the scalar potential. Through the *Englert-Brout-Higgs-Guralnik-Hagen-Kibble mechanism* [2, 4, 99], the electroweak symmetry, *i.e.* the internal symmetry of the gauge group product $SU(2)_L \times U(1)_Y$, is spontaneously broken down to the electromagnetic symmetry described by the internal symmetry of the gauge group $U(1)_{\text{em}}$. This group, whose symmetry remains unbroken in the SM after EWSB, corresponds to the electromagnetic force and the corresponding charge Q of the group is the electromagnetic charge. The relationship between

the charges of the original group product and Q is given by an electroweak analogue of the *Gell-Mann–Nishijima formula* [100, 101],

$$Q = I_W^z + \frac{Y}{2} \ , \tag{2.1}$$

where the superscript "z" indicates the third component of the weak isospin. The four gauge boson fields (W_1, W_2, W_3) and B of the unbroken group $SU(2)_L \times U(1)_Y$ are mixed into the massive particle eigenstates $W^\pm$ and Z which mediate the weak force as well as into the massless photon γ which mediates the electromagnetic force. In the broken phase, the matter particles of the SM are still grouped into three generations[2] of up-type and down-type quarks, now with electromagnetic charges $Q = 2/3$ and $Q = -1/3$, respectively, as well as into three generations of charged leptons with $Q = -1$ and neutrinos with $Q = 0$. Moreover, EWSB generates effective mass terms for most of the particles of the SM[3] via the interaction of the particles with the Higgs field. This allows for describing massive particles in the SM while still preserving the underlying gauge symmetries of the QFT.

The theoretical predictions made in the framework of the SM are under ongoing investigation. Especially, the mass of the Higgs boson as well as its production and decay rates have been analyzed in detail and so far, no significant deviations from the SM predictions are observed (cf. [13, 14] and *e.g.* [98, 102] for more recent presentations of results). On the other hand, there are several observations, *e.g.* stemming from cosmology, for which the SM does not offer any theoretical explanation. Moreover, the SM also has some theoretical shortcomings. We briefly review some of both the experimental and theoretical shortcomings in the following, since they serve as a motivation for investigations of BSM physics.

From an experimental point of view, the following observations indicate that the SM is not a sufficient theory to describe nature as a whole:

- **Dark matter:** Cosmological observations indicate that ordinary baryonic matter only accounts for a minority of the matter content of the universe, with the majority of approximately 84% being so-called DM [103]. The SM does not provide a candidate for DM[4].

- **Baryon asymmetry:** A clear dominance of matter over antimatter is observed in the universe [105]. Sakharov formulated three necessary conditions that are required for baryogenesis, *i.e.* for establishing an asymmetry of matter over antimatter in the early universe. Among these conditions is the requirement that a QFT describing the universe must provide sufficient sources of CP violation [106]. While the SM provides a possible source of CP violation through a complex phase of the *Cabibbo-Kobayashi-Maskawa matrix* [107, 108] which mixes the quark flavors, this source is not strong enough to account for the observed baryon asymmetry [109].

- **Gravity:** The SM does not provide any explanation of gravity. While there are several recent attempts to explain gravity not as another fundamental force, but rather as an emergent phenomenon, *e.g.* through entropic gravity [110, 111], some predictions made by these theories seem to be at odds with experimental observations [112]. Hence, at the present date it is far from clear whether gravity should be considered truly as an independent fundamental force or rather an emergent phenomenon, but in both cases, the SM has to be extended in order to accurately describe its effects.

---

[2]In the following, we also use the commonly used word flavor for denoting the different fermions.

[3]The neutrinos, gluons and the photon remain massless in the SM.

[4]While there exist attempts to provide a DM candidate within the SM, *e.g.* through a hexaquark state *uuddss*, none of these attempts seem to explain the observed DM density without being at odds with other experimental results [104].

- **Dark energy:** Apart from ordinary baryonic and dark matter, the majority of approximately 68% of the energy density in the universe stems from *dark energy* [103], hypothesized in order to explain the accelerating expansion of the universe. One attempt to explain the origin of dark energy is through the *cosmological constant*. Within the SM, this constant is connected to the vacuum energy and its contribution can be calculated as zero-point fluctuations in a field-theoretical approach. However, the cosmological constant calculated within the SM and the observed value differ by remarkable 120 orders of magnitude [113, 114] and hence, the SM does not provide a sufficient explanation of dark energy. For a recent review of theoretical approaches to solve the problem of dark energy, we refer to [115].

- **Neutrino masses:** The observation of oscillations between neutrinos of different flavors indicates that neutrinos must have a non-vanishing mass [116], and current experiments like the Karlsruhe Tritium Neutrino Experiment (KATRIN) aim to deliver new upper bounds on the electron neutrino mass or to even measure it with a precision of approximately $0.2\,\mathrm{GeV}$ [117]. In the SM, neutrino masses are not generated through the Higgs mechanism and consequently, the SM has to be extended to account for non-vanishing neutrino masses.

Moreover, the following observations, still requiring more data, are in tension with the SM:

- **$g-2$ of the muon:** The observed value of the anomalous magnetic moment of the muon μ^- differs from the theoretical prediction calculated within the SM at three to four standard deviations [118], which indicates that the SM does not completely explain the anomalous magnetic moment.

- **B meson decays:** Several experiments observed SM deviations in some decays *e.g.* in the B meson decay channel $\overline{B}^0 \to D^{*+}\tau^-\overline{\nu}_\tau$ in which the measured decay rates differ from the theoretical predictions calculated in the SM (cf. [119] for a recent overview). Whether these deviations are large enough to significantly indicate an invalidity of the SM or not is subject to current experimental and theoretical research.

Furthermore, the SM also has theoretical shortcomings, some of which we list in the following:

- **Strong CP problem:** In its most general form, the QCD Lagrangian of the SM can contain a phase θ with arbitrary value which explicitly breaks CP symmetry. However, measurements of the electric dipole moment of the neutron restrict this phase to values $\theta \ll 10^{-9}$ [120]. In the SM, there is no mechanism that explains why θ should be either precisely zero or so exceedingly small. Hence, the strong CP problem embeds a fine-tuning problem into the SM.

- **Hierarchy problem:** As discussed in this section, the Higgs doublet is a necessary ingredient for the SM in order to generate the masses of the SM particles through EWSB. However, higher-order corrections to the Higgs mass that emerge through quantum fluctuations are a function of the squared cut-off energy scale Λ^2 at which the theory breaks down. This is in strong contrast to the higher-order corrections to all other masses in the SM, since these are protected by gauge or chiral symmetries and hence do not depend polynomially on Λ [121]. The hierarchy problem is in essence the question why the observed value of the Higgs mass at approximately $125\,\mathrm{GeV}$ [13] is so much smaller than the expected cut-off scale $\Lambda \approx 10^{19}\,\mathrm{GeV}$, *i.e.* the Planck scale at which the SM is supposed to break down due to effects of gravity. In order to explain the observed value of the Higgs boson in the SM, it is necessary to assume that the higher-order corrections to the Higgs mass cancel with CT[5] in such a way that precisely the

---

[5]The concept of counterterms and renormalization is introduced in detail in Sec. 3.1.

comparatively low Higgs mass of 125 GeV is produced. This requires a cancellation to a precision of approximately 1 part in 10^{30}. Hence, the hierarchy problem is another fine-tuning problem of the SM.

It is debatable whether the theoretical problems of the SM described above should be considered as indications or even motivations for BSM physics. The problem of fine-tuning is in essence more of philosophical than of physical origin, especially if it is mentioned in the context of naturalness, and it is always possible to use *e.g.* the *anthropic principle* as a counterargument for fine-tuning. While in some cases in the past, the removal of fine-tuning problems present in some theories was successfully used as a guiding principle which led to the discovery of more fundamental theories [121, 122], we leave it to the reader whether they consider this reductionistic approach as a valid motivation for BSM physics or not. On the other hand, the experimental observations presented above indicate more clearly that the SM is not a sufficient theory to fully describe nature. While none of the three QFTs considered in this thesis provide solutions to all of the aforementioned problems simultaneously, all of them solve at least some of the experimental and theoretical shortcomings of the SM.

2.2. Singlet and Doublet Extensions of the Standard Model

Among the simplest possibilities to extend the SM of particle physics is the introduction of additional $SU(2)_L$ Higgs singlets and doublets to the Lagrangian. This extends only the scalar sector of the SM in the form of additional Higgs bosons. Since the scalar sector is experimentally the least well-studied sector of the SM so far, BSM theories of this kind become increasingly more interesting since their parameter space is usually less restricted in comparison to other SM extensions where the scalar sector is more restricted *e.g.* due to addtional symmetry relations. One of the most stringent contraints of any BSM model comes from the ρ parameter [33]

$$\rho \equiv \frac{\sum_i v_i^2 \left[4 I_{W,i}(I_{W,i} + 1) - Y_i^2 \right]}{\sum_i 2 Y_{W,i}^2 v_i^2} \,, \tag{2.2}$$

where we sum over any scalar Higgs doublet or singlet with corresponding VEVs v_i, weak isospin $I_{W,i}$ and weak hypercharge Y_i. The currently measured value of this parameter is given by [98]

$$\rho_{\mathrm{exp}} = 1.00039 \pm 0.00019 \,. \tag{2.3}$$

In the SM, the ρ parameter is automatically unity per construction at tree level, since only one Higgs doublet with isospin $I_W = 1/2$ and weak hypercharge $Y = +1$ is contained in the Lagrangian. Likewise, it is possible to add an arbitrary number of additional $SU(2)_L$ doublets or $SU(2)_L$ singlets (with quantum numbers $I_W = 1/2$, $Y = +1$ or $I_W = Y = 0$, respectively) to the Lagrangian, since Eq. (2.2) in all cases evaluates precisely to unity at tree level. While in principle it is possible to add other more complicated $SU(2)_L$ structures to the Lagrangian, the constraint on ρ given by Eq. (2.3) typically leads to a fine-tuning of the parameters in such models [33]. Hence, in Part II of this thesis we consider only the simpler case where we add an additional doublet to the Lagrangian, thus defining the 2HDM, and in Part III, we additionally add a gauge singlet to the 2HDM which gives rise to the N2HDM.

The *unitarity constraints* are another important restriction that models beyond the SM have to fulfill. The mechanism of EWSB does not only introduce effective mass terms to the theory. Moreover, it is a mechanism to unitarize the scattering of *e.g.* longitudinal gauge bosons at high energies. Without the Higgs boson, the scattering amplitude is divergent with respect to an increasing center of mass energy such that unitarity is violated for high energies. However, through EWSB, the Higgs couples to the gauge bosons proportionally

to their squared masses and cancels the divergent contributions in the scattering amplitude, hence preserving unitarity. In theories with extended Higgs sectors, the additional Higgs bosons also couple to the gauge bosons. The unitarity constraints are thus in essence a constraint on the combination of the coupling constants describing the interaction of the Higgs and the gauge bosons. Extensions of the SM which contain $SU(2)_L$ doublets and singlets fulfill the constraints stemming from the couplings to the gauge bosons automatically at tree level per construction [123].

Another set of important constraints are *flavor-changing neutral currents* (FCNCs), *i.e.* decay processes that change the flavor of a quark without a simultaneous change of its electric charge. Experimental data put very stringent constraints on the branching ratios of FCNC processes [124, 125], which implies that models which allow for FCNC couplings at tree level typically need to be fine-tuned in order to be consistent with these data. In the SM, FCNC processes are not present at tree level and are highly suppressed at one-loop order through the *Glashow-Iliopolus-Maiani* (GIM) mechanism [126]. In the 2HDM and N2HDM, however, the most general form of these models introduces FCNCs already at tree level through the Yukawa sector. In Secs. 4.3 and 9.3, we discuss the appearance and removal of FCNCs in the 2HDM and N2HDM, respectively.

While adding another $SU(2)_L$ doublet (and a gauge singlet) to the SM is *ad hoc*, *i.e.* not motivated by a more complex underlying theory or symmetry, the 2HDM and N2HDM are nevertheless interesting models since they provide solutions to some of the aforementioned shortcomings of the SM. A special realization of the 2HDM, the *Inert Doublet Model*, provides a DM candidate [127–130], and so does an inert doublet in the N2HDM. The latter model moreover features the possibility of a dark singlet as another source of DM (cf. [58, 131, 132] for recent analyses). Moreover, the additional Higgs potential parameters of the 2HDM and N2HDM allow for additional sources of CP violation if complex versions of the models are considered[6]. In Parts II and III of this thesis, we provide electroweak one-loop corrections within the CP-conserving realizations of the 2HDM and N2HDM, respectively. These models contain extended Higgs sectors with an interesting phenomenology while at the same time they allow for more freedom with respect to the parameters of the scalar potential since they are not constrained by additional symmetries as it is the case *e.g.* for SUSY models.

2.3. Supersymmetric Extensions of the Standard Model

Among the most popular extensions of the SM are BSM models in the framework of SUSY. In the following, we only briefly introduce the basic concepts and ideas of SUSY. For a general introduction to and a review on the topic, we refer to *e.g.* [36]. In SUSY, additional fermionic operators $\mathcal{Q}$ exist which transform bosonic into fermionic states *et vice versa*:

$$\mathcal{Q} \left| \text{boson} \right\rangle = \left| \text{fermion} \right\rangle , \tag{2.4}$$

$$\mathcal{Q} \left| \text{fermion} \right\rangle = \left| \text{boson} \right\rangle . \tag{2.5}$$

Due to these additional transformations, the bosonic and fermionic fields are directly connected to each other. One motivation for the consideration of SUSY was the fact that in the development of the SM, fundamental symmetries turned out to be fruitful guiding principles (*e.g.* , the formulation of the SM in terms of gauge symmetries allowed for a unification of the electromagnetic and the weak force and their combination with the strong force, and the excellent agreement of many SM predictions with experimental data validated symmetries as a guiding principle). From a theoretical point of view, the Coleman–Mandula theorem [133] provides a stringent no-go theorem which states that in a consistent QFT containing a mass

---

[6]In our work, we restrict ourselves to the real 2HDM and N2HDM.
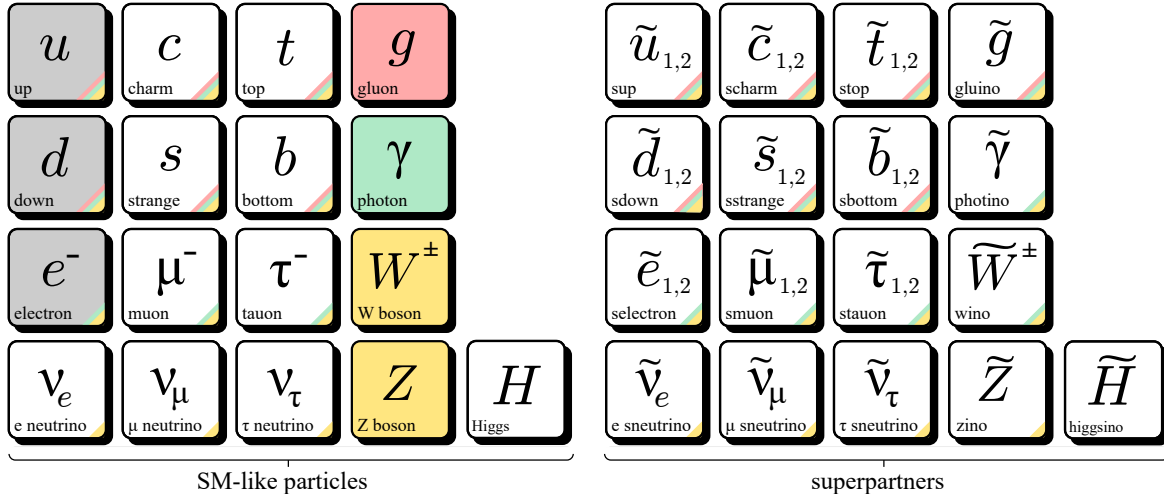
Figure 2.2.: Particle content of the MSSM. Each SM particle (left-hand side of the figure) acquires a superpartner, indicated with a tilde (right-hand side of the figure). Note that in this representation, H and $\tilde{H}$ denote Higgs and higgsino field doublets instead of particles.

gap, only trivial combinations of internal and space-time symmetries can exist, which in essence reduces the possibilities of extending the SM based on additional symmetries. However, the Haag–Łopuszański–Sohnius theorem [134] states a loophole of this no-go theorem. By considering a Lie superalgebra instead of a Lie algebra, *i.e.* by formulating an algebra containing both commuting and anticommuting symmetry generators, the theorem states that there exists a non-trivial combination of both space-time and internal symmetries, providing the basis for a SUSY QFT with a mass gap. Moreover, the theorem states that SUSY is the *only* mechanism through which such a consistent QFT with maximally realized symmetries can be established. Consequently, using symmetries as guiding principles for formulating more fundamental theories naturally leads to the development of SUSY. Moreover, from a theoretical point of view, the unification of gravity with the three other fundamental forces *e.g.* in the framework of superstring theory necessarily requires the superalgebra and hence automatically induces SUSY [135].

SUSY extensions have been studied in great detail up until this day. The MSSM [20–36] is an example of a SUSY theory which provides a supersymmetric extension of the SM via an introduction of a minimal amount of additional particles and which was at the same time compatible with experimental data. Due to the internal symmetries between fermions and bosons in the superalgebra, the MSSM predicts twice as many particles as the SM. Each fundamental fermion and boson of the SM acquires a *superpartner*, also called *sparticles*, whose quantum numbers differ from the respective fundamental particle of the SM only by a half-integer value of the spin, while all other quantum numbers are the same. Per convention, the superpartners of the SM fermions are denoted with the prefix "s" while the superpartners of the bosons are denoted with the suffix "ino". Moreover, due to the holomorphy of the superpotential of the MSSM, the model requires two Higgs doublets instead of one as in the SM and hence, it contains a specific realization of a 2HDM [36]. An overview over the particle content of the MSSM is depicted in Fig. 2.2.

Due to the fact that the superpartners have the same quantum numbers as their SM counterparts (apart from the spin), SUSY extensions like the MSSM predict that each SM particle has a SUSY partner with the same mass. However, this is at odds with experimental results, since we did not observe any superpartners at the mass scale of the SM particles. Due to this, if SUSY is realized in nature, it needs to be broken my some yet unknown mechanism which can be parametrized by adding *soft-SUSY-breaking terms* to the SUSY Lagrangian [24, 136, 137].

These terms are introduced in the form of dimension-two terms, *i.e.* they have a positive dimension of mass, which explains the "softness" of their inclusion: they dominantly affect the physics at the low (*i.e.* soft) energy scale but they do not alter the cancellation of divergent structures (*i.e.* at the high or *hard* scale) in the higher-order scalar masses of the theory. The method of soft SUSY breaking allows for the parametrization of the unknown mechanism of SUSY breaking through the introduction of these additional soft-breaking parameters. Hence, details about the exact origin of the SUSY breaking, still unknown as of today, are not required for the softly-broken theory to yield theoretical predictions for observables. As a potential drawback, the parametrization of the SUSY-breaking mechanism introduces a plethora of new free parameters to the theory. Even the most simple phenomenologically relevant realization of a SUSY model, namely the MSSM, features as much as 105 additional parameters in the soft-SUSY-breaking Lagrangian in its most general form.

Supersymmetric theories provide interesting solutions to many of the shortcomings of the SM mentioned in Sec. 2.1. The MSSM, for example, was originally constructed as a new theory to solve the hierarchy problem inherent to the SM [24]. This solution is based on the SUSY relations between the fermionic and bosonic fields and their coupling constants. As mentioned in Sec. 2.1, the higher-order corrections to the Higgs mass are a function of the cut-off scale Λ^2 up to which the SM is considered to be a valid theory. The dominant contributions to this quadratic term stem from the heaviest particle of the theory, *i.e.* in the SM, the contributions originate from quantum fluctuations involving virtual top quarks. Higher-order corrections to the fermionic particles on the other hand do not feature this quadratic dependence on the cut-off scale, since they are protected by a chiral symmetry. When calculating higher-order corrections to the Higgs boson mass in SUSY extensions, contributions from additional quantum fluctuations involving the superpartners of the top quark need to be taken into account. Due to SUSY, these superpartners couple in the same way to the Higgs boson as the top quark, but since their contribution is bosonic instead of fermionic, they contribute with a different sign. As a consequence, the terms quadratic in the cut-off scale are canceled and the Higgs mass is protected from large corrections due to the symmetry between the fermionic and bosonic sector. Since SUSY is not expected to be an exact symmetry, but rather a softly-broken one, the higher-order corrections to the Higgs mass still receive contributions which depend logarithmically on the cut-off scale, however. As long as the soft SUSY breaking scale is not too large or equivalently the SUSY particles do not become too heavy, *i.e.* at the scale of approximately $\mathcal{O}(1\,\mathrm{TeV})$, no new hierarchy problem is introduced and the Higgs mass is protected against large corrections in the presence of large energy scales[7].

Another open problem of the SM, the observed baryon asymmetry of the universe, can potentially be resolved in SUSY extensions when considering models with complex parameters which yield additional sources of CP violation [138]. Moreover, many SUSY theories provide a candidate for DM. The most general MSSM Lagrangian can contain couplings which allow for processes which violate the conservation of lepton and baryon number L and B, respectively. One theoretical consequence of the existence of these couplings would be *proton decay*, but since experimental observations indicate that the proton is stable at least on a time scale of approximately 10^{34} years [139], additional symmetries are imposed on the MSSM to remove these couplings from the Lagrangian. An example of such an additional symmetry is called *R parity*, which is imposed on the MSSM in the form of a discrete $\mathbb{Z}_2$ symmetry [36] and which yields a conserved quantum number for each particle, the R-parity number

$$P_R = (-1)^{3B+L+2S} \; , \tag{2.6}$$

where S denotes the spin of the corresponding particle. For SM particles, this quantum number is given by $P_R = 1$, while for SUSY particles, it yields $P_R = -1$. Since R parity

---

[7]In the particular case of the MSSM, however, the problem cannot be fully solved since the so-called little hierarchy problem remains in the theory. We discuss this in more detail in Sec. 14.1.

is a conserved quantity, it consequently allows only for the production of SUSY particles in pairs, while the decay of a SUSY particle necessarily involves an odd number of lighter SUSY particles. Hence, *R*-parity-conserving SUSY models predict a stable *lightest supersymmetric particle* (LSP) which serves as a prime candidate for DM if it interacts only weakly and is electrically neutral [36].

In this thesis, we consider the singlet extension of the complex MSSM, *i.e.* the complex Next-to-Minimal Supersymmetric Standard Model (complex NMSSM) [37–46, 140], as a specific realization of a SUSY extension. Due to additional contributions stemming from the gauge singlet, the radiative corrections to the Higgs boson mass are not required to be as large as in the MSSM in order to provide a SM-like Higgs boson with a mass of approximately 125 GeV. We discuss this in more detail in Chapter 14 where we also introduce the model. With its complex parameters, the complex NMSSM provides additional sources of CP violation already at tree level which are less constrained by electric dipole moments (EDMs) in comparison to the MSSM [141]. Moreover, the complex NMSSM is interesting from a phenomenological perspective due to exotic signatures provided by its extended Higgs sector [142]. Furthermore, the theory contains a DM candidate and provides a solution to the hierarchy problem, as outlined above.

Higher-Order Corrections to Higgs Boson Decay Widths and Masses

In this chapter, we give a brief overview over the field-theoretical concepts that are relevant for the calculation of partial decay widths at one-loop level in the 2HDM and N2HDM in Part II and Part III, respectively, as well as for the corrections to Higgs boson masses at two-loop level in the complex NMSSM in Part IV. We assume that the reader is familiar with the concepts of quantum mechanics, special relativity, quantum field theory and the calculation of higher-order corrections in QFTs with the Feynman diagrammatic approach. This thesis is not intended to give a thorough introduction into these topics. For this, we refer the reader to introductory QFT textbooks, *e.g.* [94, 143, 144].

In Sec. 3.1, we briefly review the concepts of regularization and renormalization which are necessary in order to obtain finite partial decay widths and Higgs boson masses in higher-order calculations. One of the main focuses of this thesis is the renormalization of different extensions of the SM. Due to this, we review the renormalization of generic field multiplets in Sec. 3.2 in order to introduce the required notation for the renormalization of the SM extensions and for the concepts of OS renormalization as well as *modified minimal subtraction* ($\overline{\text{MS}}$) and *modified dimensional reduction* ($\overline{\text{DR}}$) renormalization. In the subsequent Secs. 3.3 and 3.4, we discuss the calculation of one-loop partial decay widths and one- and two-loop Higgs boson masses in general. In the subsequent Sec. 3.5, we describe the input parameter conversion which is necessary for the consistent comparison of partial decay widths calculated within different renormalization schemes. This chapter concludes with a brief general discussion of the gauge independence of fixed-order calculations of partial decay widths and Higgs boson masses in Sec. 3.6.

3.1. Regularization and Renormalization of Loop Integrals

As a simple example of a one-loop diagram, we consider a *tadpole diagram* with a virtual scalar particle with mass $m > 0$ in the loop, as depicted in Fig. 3.1. Up to some additional constants, this diagram represents an integral of the form

$$\int \frac{d^4l}{(2\pi)^4} \frac{1}{l^2 - m^2} \, , \tag{3.1}$$

where the four-momentum l is the integration variable. This integral has a divergence in the regime of large momenta (or small spatial distances, respectively), a *UV divergence*. The

Figure 3.1.: Exemplary UV-divergent one-loop *tadpole diagram* with a virtual scalar particle of mass $m > 0$.

appearance of these divergences is inevitable in any fixed-order calculation, *i.e.* they are an artifact of the incompleteness of a quantum-field theoretical description of very small space-time separations [94]. Despite the appearance of these divergences, higher-order calculations of observables, *e.g.* partial decay widths and Higgs boson masses, still yield finite, physical results through the methods of *regularization* and *renormalization*.

Through regularization, the UV divergences of the loop integrals are isolated from their finite contributions in a self-consistent way. There are many different regularization methods, all with their own advantages and shortcomings. In this work, we use *dimensional regularization* (DREG) [145–149] for non-SUSY models and *dimensional reduction* (DRED) [150, 151] for SUSY models in order to isolate the divergences. The key idea common in both regularization methods is that the loop momenta and space-time coordinates are considered in $D = 4 - 2\varepsilon$ dimensions, with $\varepsilon > 0$ being small, instead of the ordinary 4 space-time dimensions. In DREG, this shift to D dimensions is additionally applied to all other tensor and spinor structures of the QFT. While this procedure is applicable to non-SUSY models, in SUSY extensions this would lead to a mismatch between the degrees of freedom of the bosonic and fermionic fields in D dimensions[8]. As a consequence, DREG explicitly violates SUSY [150] which hence needs to be restored *e.g.* through the introduction of SUSY-restoring counterterms [158–161]. In DRED on the other hand, the shift from 4 to D space-time dimensions is restricted to the loop momenta, while the tensor and spinor structure is still considered to be four-dimensional. While it has been analyzed that DRED preserves SUSY at the one-loop level and for the dominant contributions at two- and three-loop level [162–166], a general all-order proof of the preservation of SUSY through DRED is not known to date.

In both regularization schemes, the UV divergence of the loop integral is regularized by the finite shift ε and the loop integral evaluates to a finite part on the one hand and a universal contribution

$$\Delta \equiv \frac{1}{\varepsilon} - \gamma_E + \ln(4\pi) + \ln\left(\frac{\mu^2}{\mu_R^2}\right) \tag{3.2}$$

on the other hand. Here, γ_E denotes the Euler-Mascheroni constant, μ_R is the mass-dimensional renormalization scale which needs to be introduced in order to preserve the dimensionality of the loop integral and μ denotes the mass-dimensional 't Hooft scale which cancels in the calculation of any observable.

While DREG and DRED serve to regulate the UV divergence for any $\varepsilon > 0$, the loop integral, and hence the calculation of any observable, still yields a UV-divergent result. This becomes apparent in the physical limit when considering four space-time dimensions, *i.e.* for $\varepsilon \to 0$ in Eq. (3.2). In order to remove these UV divergences consistently, we use the method of

---

[8]For both SUSY and non-SUSY extensions, care has to be taken when extending the Dirac matrix γ_5 to D dimensions since its definition is given unambigiously only in 4 space-time dimensions. An inconsistent treatment of γ_5 *e.g.* in the framework of DREG leads to the appearance of axial anomalies, the *Adler-Bell-Jackiw* anomalies [152–155]. For an overview over the possible extension of γ_5 to D dimensions, we refer to [156, 157]. In our work, we do not encounter axial anomalies at any stage of our calculations.

renormalization. Each *bare* parameter $\rho_{i,0}$ ($i = 1, 2, ...$) and bare field $\phi_{j,0}$ ($j = 1, 2, ...$) of the QFT is split into a physical *renormalized* parameter ρ_i and field ϕ_j and their corresponding CT $\delta\rho_i$ and *wave-function renormalization constant* (WFRC) $\sqrt{Z_\phi}$ (or its expansion δZ_ϕ) according to

$$\rho_{i,0} = \rho_i + \delta\rho_i \, , \tag{3.3}$$

$$\phi_{j,0} = \sqrt{Z_{\phi_j}}\phi_j \approx \left(1 + \frac{\delta Z_{\phi_j}}{2}\right)\phi_j \, . \tag{3.4}$$

The CTs and WFRCs contain UV divergences which precisely cancel against the UV divergences stemming from loop integrals in a fixed-order calculation. By imposing renormalization conditions, furthermore additional finite contributions are allocated to the CTs and WFRCs that depend on the explicit renormalization conditions that are chosen. The renormalized parameters ρ_i on the other hand are UV-finite and represent the physical values of these parameters. Due to the cancellation of the UV divergences of the loop integrals and the CTs and WFRCs, all divergences are consistently removed from the QFT and the observables become manifestly UV-finite. This procedure works order-by-order for all renormalizable field theories [94]. All models considered in this work, *i.e.* the 2HDM, N2HDM and the complex NMSSM, belong to this class of renormalizable field theories in four space-time dimensions, cf. *e.g.* [36, 167, 168] where the renormalizability of the 2HDM and MSSM is discussed. The singlet extensions of these two models are renormalizable as well, since the additional singlet terms introduced in the Lagrangian are renormalizable.

3.2. On-Shell Renormalization of Field Multiplets

The multiplicative renormalization of scalar fields indicated in Eq. (3.4) is directly applicable for theories with a single scalar field, *e.g.* for the Higgs boson field renormalization in the SM. On the other hand, theories with extended Higgs sectors often contain several scalar fields with the same quantum numbers which consequently can be combined into scalar multiplets. Examples of this are the Higgs sectors of all three models considered in this work, namely the 2HDM, the N2HDM and the complex NMSSM, with several scalar multiplets in each of the models. In the following, we briefly review the renormalization of a scalar multiplet in general. Applications of this general renormalization mechanism to the specific models are discussed in the respective Parts II, III and IV of this thesis.

In the following, we perform the renormalization of the fields in the mass basis. This is a typical approach when the fields are renormalized in an OS scheme and in our work, we apply such a scheme for the Higgs sectors of the 2HDM and N2HDM. Alternatively, the scalar fields can be renormalized in a minimal scheme in the gauge basis where only a minimal amount of WFRCs is introduced. We apply this approach for the renormalization of the Higgs fields in the complex NMSSM and discuss the differences with respect to the renormalization in the mass basis in more detail in Sec. 15.3.1.

We consider a scalar multiplet with n bare scalar fields $\phi_{i,0}$ ($i = 1, ..., n$). In the mass basis, the terms bilinear in the fields define the diagonal mass matrix D_ϕ^2 of the scalar multiplet, with the ith diagonal entry representing the squared mass of the ith scalar. Through multiplicative renormalization by means of an $n \times n$ matrix $\sqrt{Z_\phi}$ (or its expansion δZ_ϕ), the multiplet is rescaled to yield the renormalized multiplet via the n-dimensional generalization of Eq. (3.4),

$$\begin{pmatrix} \phi_1 \\ \vdots \\ \phi_n \end{pmatrix}_0 = \sqrt{Z_\phi} \begin{pmatrix} \phi_1 \\ \vdots \\ \phi_n \end{pmatrix} \approx \left(\mathbb{1}_{n \times n} + \frac{\delta Z_\phi}{2}\right) \begin{pmatrix} \phi_1 \\ \vdots \\ \phi_n \end{pmatrix} \, . \tag{3.5}$$

Figure 3.2.: The 1PI self-energies $i\Sigma_{\phi_i\phi_j}(p^2)$ $(i,j = 1,...,n)$ are defined as the sum of all self-energy diagrams at a given loop order that cannot be split into two different diagrams by cutting a single line in the diagram. They denote the transition of the scalar particle ϕ_i to ϕ_j.

The $n \times n$ matrix δZ_ϕ contains n^2 different WFRCs which are of the considered loop order,

$$
\delta Z_\phi = \begin{pmatrix} \delta Z_{\phi_1\phi_1} & \delta Z_{\phi_1\phi_2} & \cdots & \delta Z_{\phi_1\phi_n} \\ \delta Z_{\phi_2\phi_1} & \delta Z_{\phi_2\phi_2} & & \\ \vdots & & \ddots & \\ \delta Z_{\phi_n\phi_1} & & & \delta Z_{\phi_n\phi_n} \end{pmatrix} .
\tag{3.6}
$$

The probability amplitude of the scalar fields to propagate from one space-time point to another is described by means of the two-point correlation function Γ_ϕ [94]. Since higher-order corrections introduce UV divergences into the two-point correlation function, Γ_ϕ needs to be renormalized. In a renormalizable field theory, it suffices to renormalize all independent parameters and fields of the theory to render the two-point correlation function finite, as well. Accordingly, the renormalized two-point correlation function is defined as:

$$
\widehat{\Gamma}_\phi(p^2) \equiv \begin{pmatrix} \widehat{\Gamma}_{\phi_1\phi_1}(p^2) & \widehat{\Gamma}_{\phi_1\phi_2}(p^2) & \cdots & \widehat{\Gamma}_{\phi_1\phi_n}(p^2) \\ \widehat{\Gamma}_{\phi_2\phi_1}(p^2) & \widehat{\Gamma}_{\phi_2\phi_2}(p^2) & & \\ \vdots & & \ddots & \\ \widehat{\Gamma}_{\phi_n\phi_1}(p^2) & & & \widehat{\Gamma}_{\phi_n\phi_n}(p^2) \end{pmatrix}
$$
$$
\equiv i\sqrt{Z_\phi}^\dagger \left[p^2 \mathbb{1}_{n\times n} - D_\phi^2 + \Sigma_\phi(p^2) - \delta D_\phi^2 \right] \sqrt{Z_\phi} .
\tag{3.7}
$$

Here, we introduced the $n \times n$ matrix CT of D_ϕ^2, that, in contrast to D_ϕ^2 itself, is in general non-diagonal. Its explicit form depends on the renormalization of the minimum of the scalar potential and is presented below. The self-energy matrix $\Sigma_\phi(p^2)$ is a symmetric $n \times n$ matrix given by

$$
\Sigma_\phi(p^2) = \begin{pmatrix} \Sigma_{\phi_1\phi_1}(p^2) & \Sigma_{\phi_1\phi_2}(p^2) & \cdots & \Sigma_{\phi_1\phi_n}(p^2) \\ \Sigma_{\phi_1\phi_2}(p^2) & \Sigma_{\phi_2\phi_2}(p^2) & & \\ \vdots & & \ddots & \\ \Sigma_{\phi_1\phi_n}(p^2) & & & \Sigma_{\phi_n\phi_n}(p^2) \end{pmatrix} .
\tag{3.8}
$$

Each entry of this matrix represents the one-particle irreducible (1PI) self-energy of the transition from the scalar particle ϕ_i to ϕ_j, as shown in Fig. 3.2. By expanding $\sqrt{Z_\phi}$ about the unit matrix, analogously to Eq. (3.5), Eq. (3.7) can be rewritten as

$$
\widehat{\Gamma}_\phi(p^2) \approx i \left[p^2 \mathbb{1}_{n\times n} - D_\phi^2 + \widehat{\Sigma}_\phi(p^2) \right] ,
\tag{3.9}
$$

where we introduced the renormalized self-energy matrix

$$
\widehat{\Sigma}_\phi(p^2) \equiv \Sigma_\phi(p^2) - \delta D_\phi^2 + \frac{\delta Z_\phi^\dagger}{2} \left(p^2 \mathbb{1}_{n\times n} - D_\phi^2 \right) + \left(p^2 \mathbb{1}_{n\times n} - D_\phi^2 \right) \frac{\delta Z_\phi}{2} .
\tag{3.10}
$$

The renormalized propagator of the scalar multiplet is given by the negative inverse of the two-point correlation matrix,

$$\widehat{G}_\phi(p^2) \equiv -\widehat{\Gamma}_\phi^{-1}(p^2) = \frac{i}{(-i)\det\left(\widehat{\Gamma}_\phi(p^2)\right)} \, \mathrm{adj}\left(\widehat{\Gamma}_\phi^{-1}(p^2)\right) \, , \qquad (3.11)$$

where det stands for the determinant and adj for the adjugate of the matrix $\widehat{\Gamma}_\phi(p^2)$. The poles of the renormalized propagator are determined by the zeros of the determinant of the two-point correlation function. According to the *Källéen-Lehmann spectral representation*, these poles correspond to the physical masses m_{ϕ_i} of the scalar particles in the mass basis [94, 169, 170]. By finding the zeros of the determinant, the position of these poles, and consequently the masses of the particles, can be explicitly calculated. Since the calculation of the higher-order corrections to the Higgs masses in the complex NMSSM is part of this work, this concept is discussed in more detail in Sec. 3.4 and Chapter 16.

The matrix CT δD_ϕ^2 and the WFRCs δZ_ϕ contain UV divergences which cancel against the divergences stemming from the unrenormalized self-energies, hence yielding a UV-finite renormalized two-point correlation function in Eq. (3.9). The finite parts of the CTs and WFRCs on the other hand still need to be fixed by imposing suitable renormalization conditions. Among the simplest choices of renormalizing a non-SUSY QFT is to choose an $\overline{\mathrm{MS}}$ scheme in the framework of DREG. In such a scheme, the parameter CTs and WFRCs of the theory are defined to contain only the UV-divergent terms proportional to the universal constant Δ, cf. Eq. (3.2). For SUSY extensions, an equivalent definition in the framework of DRED, namely the $\overline{\mathrm{DR}}$ scheme[9,10], can be defined. In this scheme, the CTs and WFRCs contain only the UV-divergent terms and moreover some additional finite contributions which arise due to the difference between DREG and DRED as discussed in Sec. 3.1. In both cases, the CTs defined in this scheme depend explicitly on the renormalization scale μ_R at which they are defined. The $\overline{\mathrm{MS}}/\overline{\mathrm{DR}}$ scheme has the advantage that the definitions of the CTs and WFRCs become particularly simple.

Another renormalization scheme which is commonly used in literature is the OS scheme by imposing the following three renormalization conditions [94]:

- The mixing of fields with same quantum numbers vanishes on the mass shells $p^2 = m_{\phi_i}^2$ ($i = 1, ..., n$).

- The physical masses m_{ϕ_i} ($i = 1, ..., n$) are defined as the real parts of the poles of the renormalized propagator $\widehat{G}_\phi(p^2)$.

- The normalization of the fields ϕ_i ($i = 1, ..., n$) is such that the residues of the propagator at its poles is equivalent to i.

---

[9] For completeness, we want to mention that in the framework of DRED, there is also an alternative approach for the minimal renormalization called the $\overline{\mathrm{DR}}'$ scheme. This approach differs from the usual $\overline{\mathrm{DR}}$ scheme by a different treatment of the ε-scalar masses which arise in the SUSY Lagrangian through the shift from 4 to D dimensions. For more details about the differences between these approaches, we refer to [171, 172]. In our work, we use the $\overline{\mathrm{DR}}$ scheme for the calculation of the corrections to the Higgs masses in the complex NMSSM and we want to emphasize that to $\mathcal{O}(\alpha_t^2)$, both schemes yield the same results [173].

[10] In principle, we could also apply the $\overline{\mathrm{DR}}$ scheme to non-SUSY models. However, this approach necessitates the consistent treatment of additional contributions stemming from the ε terms, *i.e.* the *evanescent couplings* [165, 174, 175]. Hence, for practical reasons we use the $\overline{\mathrm{MS}}$ scheme for all calculations in non-SUSY models (*i.e.* the 2HDM and N2HDM) and the $\overline{\mathrm{DR}}$ scheme for the complex NMSSM in this work.

The application of these renormalization conditions to the two-point correlation function, cf. Eq. (3.9), and its expansion around its poles determines the diagonal terms of the matrix CT δD_ϕ^2 and the explicit form of the WFRCs in the OS scheme:

$$\delta D^2_{\phi_i\phi_i} = \mathrm{Re}\left[\Sigma_{\phi_i\phi_i}(m^2_{\phi_i})\right] , \tag{3.12}$$

$$\delta Z_{\phi_i\phi_i} = -\mathrm{Re}\left[\frac{\partial\Sigma_{\phi_i\phi_i}(p^2)}{\partial p^2}\right]_{p^2=m^2_{\phi_i}} , \tag{3.13}$$

$$\delta Z_{\phi_i\phi_j} = \frac{2}{m^2_{\phi_i} - m^2_{\phi_j}}\mathrm{Re}\left[\Sigma_{\phi_i\phi_j}(m^2_{\phi_j}) - \delta D^2_{\phi_i\phi_j}\right] \quad (i \neq j) . \tag{3.14}$$

In the OS scheme, the positions of the poles of the propagator are *defined* as the physical masses m_{ϕ_i} ($i = 1, ..., n$), and these mass values are required as an independent input through which the mass parameters and their CTs are fixed. In contrast to the $\overline{\mathrm{MS}}/\overline{\mathrm{DR}}$ scheme, where higher-order corrections to the masses of the particles can be *calculated* by computing the zeros of the determinant of the two-point correlation function, in the OS scheme the physical masses m_{ϕ_i} are per definition given as an input. An advantage of the OS scheme in comparison to the $\overline{\mathrm{MS}}/\overline{\mathrm{DR}}$ scheme is that WFRCs defined in an OS scheme are automatically properly normalized at higher orders and consequently, for a calculation of *e.g.* decay widths of physical particles the *Lehmann-Symanzik-Zimmermann (LSZ) reduction formula* [176] is directly applicable without additional finite rotations [143].

3.3. Decay Widths at Tree Level and Next-to-Leading Order

One way of making theoretical predictions for observables at colliders like the LHC is to use the field-theoretical framework of the LSZ reduction formula together with the Feynman diagrammatic approach in order to calculate decay amplitudes for particles of a specific QFT. In the following, we describe how the decay amplitudes are connected to the partial decay widths of the specific decay channel and how all partial decay widths can be combined to make predictions of the decay probability of a particle that is produced at *e.g.* the LHC. The calculation of the higher-order corrections to the partial decay widths allows for more precise predictions of these decay probabilities.

In Parts II and III of this thesis, we consider the decays of all Higgs bosons of the 2HDM and N2HDM, respectively, and calculate the electroweak corrections to these decays to one-loop order. The relevant formulae for the decay amplitudes are presented in this section in a generic way such that they can be applied to each of the two models in the respective parts of the thesis.

We consider decays of any CP-even, CP-odd or charged Higgs boson ϕ with four-momentum p_1 into a pair of two other particles X_1 and X_2 with four-momenta p_2 and p_3, respectively, *i.e.* we consider the decay process

$$\phi \longrightarrow X_1 X_2 . \tag{3.15}$$

For the calculation of the electroweak corrections, we consider OS decays only, *i.e.* we require

$$m_1^2 \geq (m_2 + m_3)^2 \tag{3.16}$$

with the OS conditions $p_i^2 = m_i^2$ ($i = 1, 2, 3$) for the masses m_i of the three particles. The leading order (LO) decay amplitude

$$i\mathcal{A}^{\mathrm{LO}}_{\phi X_1 X_2} \equiv i\mathcal{A}^{\mathrm{LO}}(\phi \longrightarrow X_1 X_2) \tag{3.17}$$
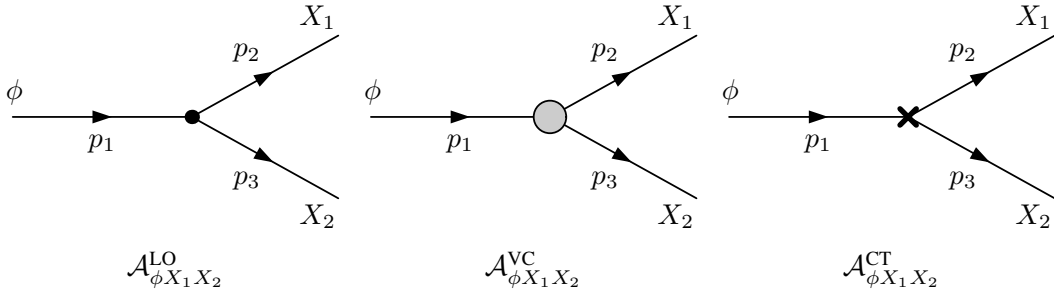
Figure 3.3.: Generic decay amplitudes of the process $\phi \longrightarrow X_1 X_2$. At LO, the decay amplitude is denoted by $\mathcal{A}^{\text{LO}}_{\phi X_1 X_2}$ while at next-to-leading order (NLO), the amplitude consists of the genuine one-loop vertex corrections $\mathcal{A}^{\text{VC}}_{\phi X_1 X_2}$ (center), shown topologically in Fig. 3.4, as well as the sum of all CT and WFRC contributions $\mathcal{A}^{\text{CT}}_{\phi X_1 X_2}$, depicted by a cross.

can be calculated by means of the Feynman diagrammatic approach by calculating the decay generically shown in the left-hand figure in Fig. 3.3. For all decays considered in this thesis, the partial decay width of the decay of ϕ into X_1 and X_2 at LO is subsequently given by

$$\Gamma^{\text{LO}}_{\phi X_1 X_2} = \frac{1}{2m_1} \int d\Pi_2\, S \sum_{\text{d.o.f.}} \left|\mathcal{A}^{\text{LO}}_{\phi X_1 X_2}\right|^2 = S\, \frac{\lambda(m_1^2, m_2^2, m_3^2)}{16\pi m_1^3} \sum_{\text{d.o.f.}} \left|\mathcal{A}^{\text{LO}}_{\phi X_1 X_2}\right|^2 , \qquad (3.18)$$

where $\lambda(x, y, z)$ denotes the *Källén phase space function*

$$\lambda(x, y, z) \equiv \sqrt{x^2 + y^2 + z^2 - 2xy - 2xz - 2yz} \qquad (3.19)$$

and S is a symmetry factor for which we set $S = \text{}^1\!/\!_2$ in case that the two particles X_1 and X_2 are indistinguishable, *e.g.* two Z bosons or neutral CP-even Higgs bosons of the same type, or $S = 1$ otherwise.

At NLO, the decay process receives genuine one-loop corrections to the three-particle vertex, as shown generically in the central figure of Fig. 3.3, as well as CT contributions stemming both from the vertex and from the external field renormalization, depicted generically as a cross in the right-hand figure of Fig. 3.3. We denote these NLO contributions with $\mathcal{A}^{\text{VC}}_{\phi X_1 X_2}$ for the genuine vertex corrections, additionally depicted topologically in Fig. 3.4, and with $\mathcal{A}^{\text{CT}}_{\phi X_1 X_2}$ for the sum of all CT and WFRC contributions, respectively. At one-loop level, in general we also need to consider corrections to the external legs which are not depicted in Fig. 3.3. Due to the OS renormalization of the fields that we use for the calculation of the decays in the 2HDM and N2HDM, most of these external leg corrections are already accounted for. The OS definition of the WFRCs ensures the proper normalization of the fields such that the LSZ reduction formula can still be applied to calculate the decay amplitudes at one-loop level and the external leg corrections are shifted into the WFRCs accordingly. The remaining external leg corrections vanish for all decays that we consider in this work due to *Slavnov-Taylor identities* [177–179]. Hence, the relevant contributions for the NLO decay amplitudes are given by

$$\mathcal{A}^{\text{NLO}}_{\phi X_1 X_2} \equiv \mathcal{A}^{\text{VC}}_{\phi X_1 X_2} + \mathcal{A}^{\text{CT}}_{\phi X_1 X_2} . \qquad (3.20)$$

In order to calculate the partial decay width, we again take the unpolarized absolute square of the decay amplitude, however, at NLO we only expand it up to terms that are relevant at one-loop order,

$$\left|\mathcal{A}^{\text{NLO}}_{\phi X_1 X_2}\right|^2 \approx \left|\mathcal{A}^{\text{LO}}_{\phi X_1 X_2}\right|^2 + 2\,\text{Re}\left[\left(\mathcal{A}^{\text{LO}}_{\phi X_1 X_2}\right)^* \mathcal{A}^{\text{VC}}_{\phi X_1 X_2} + \left(\mathcal{A}^{\text{LO}}_{\phi X_1 X_2}\right)^* \mathcal{A}^{\text{CT}}_{\phi X_1 X_2}\right] . \qquad (3.21)$$

Since Eq. (3.20) is independent of the four-momenta p_i for all decays considered in this work, the phase space integration factorizes out again and the LO formula for the partial decay width, cf. Eq. (3.18), can directly be generalized to the NLO case.
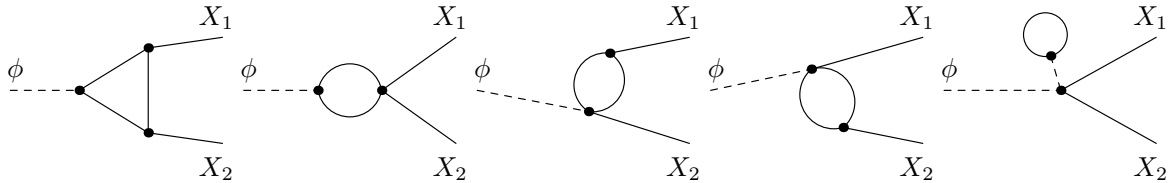
Figure 3.4.: Topological contributions to the vertex corrections $\mathcal{A}^{\mathrm{VC}}_{\phi X_1 X_2}$ to the decay process $\phi \longrightarrow X_1 X_2$ at one-loop level. For the Feynman diagrammatic calculation of a decay in a realistic QFT, the full particle content of the theory has to be mapped into these topologies. The tadpole contributions to the vertex corrections are only relevant in an alternative treatment of the minimum conditions of the potential of a spontaneously broken gauge symmetry.

At one-loop order however, there is one additional complication that needs to be taken into account. Decay processes that contain charged particles in the initial or final state acquire one-loop corrections with virtual photons γ in the loop. Since the photon is a massless particle, these loop integrals develop another type of divergence in the region of small space-time momenta, the so-called *infrared* (IR) regime. The appearance of this divergence in a QFT can be understood via a semi-classical interpretation. The integration of the loop momentum is performed over the whole physical space, *i.e.* over all space-time configurations. Since the photon is a massless particle whose energy is directly proportional to its frequency, its energy can become arbitrarily small. In the asymptotic state of the IR regime, *i.e.* for very small frequencies, an ever-increasing number of photons can occupy the phase-space. Hence, the appearance of an IR divergence is merely an artifact of an insufficient description of the photonic field in this asymptotic space-time configuration. From a field-theoretical point of view, this divergence can be canceled order by order by taking *bremsstrahlung* effects in the NLO decays into account, which is ensured by the Kinoshita-Lee-Nauenberg (KLN) theorem [180, 181]. More specifically, for the NLO decays involving charged particles in the initial or final state, additional Feynman diagrams are computed which correspond to the decays

$$\phi \longrightarrow X_1 X_2 \gamma \,, \tag{3.22}$$

called *real corrections* to the decays. Since these real photons can have arbitrarily small energies as well, in principle an infinite amount could be emitted, since photons with vanishing energies are not detectable. This leads to another divergence that appears in the calculation of the real corrections when the integration over the full phase-space is performed, and this additional IR divergence precisely cancels the IR divergence stemming from the one-loop integrals involving virtual photons. For the calculation of all real corrections $\Gamma^{\mathrm{real}}_{\phi X_1 X_2+\gamma}$ to the decay processes considered in this work, we applied the generic formulae of the real corrections presented in [182] to our models. Additionally, the analytic forms of the phase space integrals required for calculating the real corrections were taken from [183]. Finally, the full partial decay width at NLO is given by

$$\Gamma^{\mathrm{NLO}}_{\phi X_1 X_2} = \Gamma^{\mathrm{LO}}_{\phi X_1 X_2} + S \frac{\lambda(m_1^2, m_2^2, m_3^2)}{16\pi m_1^3} \sum_{\mathrm{d.o.f.}} \left| \mathcal{A}^{\mathrm{NLO}}_{\phi X_1 X_2} \right|^2 + \Gamma^{\mathrm{real}}_{\phi X_1 X_2+\gamma} \,. \tag{3.23}$$

From a field-theoretical point of view, the IR divergences stemming from the virtual photons first need to be regularized before they can be removed by taking real corrections into account. While DREG is a suitable method for the regularization of IR divergences [184] which is often applied in QCD calculations, we use a mass regularization scheme with an infinitesimal photon mass to regulate the IR divergences. This photon mass appears both in the one-loop diagrams containing virtual photons and in the real corrections and cancels in the sum of both contributions. More details about the photon regularization are presented in Secs. 6.1 and 11.1 for the 2HDM and N2HDM decays, respectively.
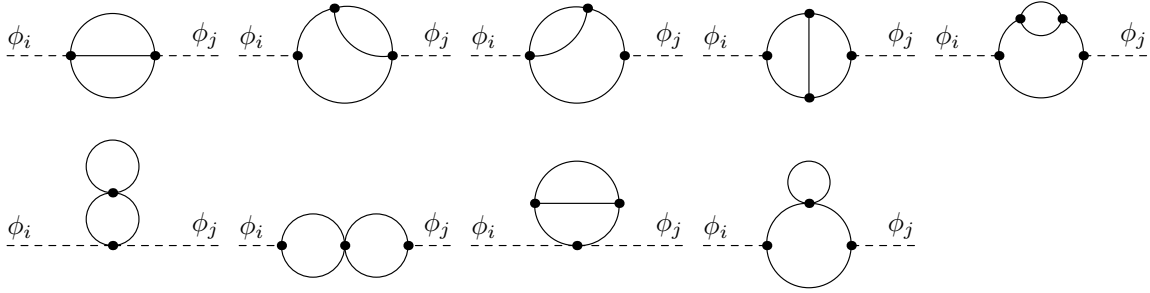
Figure 3.5.: Generic two-loop contributions to the 1PI self-energies $i\Sigma_{\phi_i\phi_j}(p^2)$ $(i, j = 1, ..., n)$ which represent the transition of the scalar particle ϕ_i to ϕ_j.

By summing up all partial decay widths of a specific Higgs boson ϕ, we can calculate the *total decay width* of ϕ at a given loop level:

$$\Gamma_\phi^{\text{tot,(N)LO}} \equiv \sum_{\{X_1,X_2\}} \Gamma_{\phi X_1 X_2}^{(N)LO} . \tag{3.24}$$

With the total decay width at hand, we can define the BR of a specific decay as follows:

$$\text{BR}^{(N)LO} (\phi \longrightarrow X_1 \, X_2) \equiv \frac{\Gamma_{\phi X_1 X_2}^{(N)LO}}{\Gamma_\phi^{\text{tot,(N)LO}}} . \tag{3.25}$$

The BR is a measure of the probability that the Higgs boson ϕ decays specifically into X_1 and X_2. The precise calculation of the BRs, together with precise calculations of the production cross sections, allows for the prediction of the measurable decay rates of the Higgs boson at the LHC.

3.4. Higher-Order Mass Corrections

Important observables at particle colliders are the masses of particles. For example, the 2012 discovery of the Higgs particle [15,16] with SM-like properties and especially the measurement of its mass of approximately 125 GeV [13] is of great importance for our basic understanding of elementary particle physics. The Higgs mass is a particularly interesting observable, since its value is connected to the stability of the electroweak vacuum, and the measured value favors a metastable vacuum over an absolutely stable one [185, 186]. As briefly discussed in Sec. 3.2, from the theoretical approach the mass of elementary particles is a computable quantity as well if not all particle masses are independent parameters of the considered theory. This is typically the case in SUSY models, where due to the SUSY relations connecting the fermionic and bosonic fields, some Higgs boson masses are dependent parameters. Due to this, their CTs are given in terms of CTs of the other independent parameters of the theory. Consequently, the higher-order corrections to the Higgs self-energies lead to a *shift* of the position of the complex pole of the Higgs propagator, cf. Eqs. (3.9) and (3.11).

To one-loop order, the 1PI self-energies are depicted topologically in Fig. 3.2 while at two-loop level, the topological contributions to the self-energies are shown in Fig. 3.5. The loop-corrected masses are then given as the complex poles of the propagator generically defined in Eq. (3.11), *i.e.* the masses of the particles are given as the roots of

$$\det\left(\widehat{\Gamma}(p^2)\right) = 0 \tag{3.26}$$

with respect to p^2. Note that the particle masses that appear in the diagonal matrix D_ϕ^2 in $\widehat{\Gamma}(p^2)$, cf. Eq. (3.9), are the *tree-level* masses while the roots of Eq. (3.26) determine the

loop-corrected masses. Evidently, if $\widehat{\Gamma}(p^2)$ is evaluated only at tree level, then both of these masses are equivalent. Already to one-loop order however, the renormalized self-energies that form the building blocks of $\widehat{\Gamma}(p^2)$ are intricate functions of p^2 which in the most general case do not allow for an analytic solution of Eq. (3.26) for p^2 in closed form. Due to this, the roots often have to be determined numerically. One approach for this numerical determination is given by the iterative solution of Eq. (3.26), *i.e.* by first equating p^2 to the tree-level mass *in the renormalized self-energy only.* This allows to solve Eq. (3.26) for p^2 and this solution is then used as the new value for p^2 in the renormalized self-energies with which Eq. (3.26) can again be solved for p^2, *etc.* Such an iterative approach for calculating the loop-corrected masses is simple to implement, *e.g.* in the form of a *Runge-Kutta method* [187, 188], but it has the disadvantage of automatically mixing different loop orders, which consequently violates the gauge independence of the computed particle masses. We further discuss the gauge dependence of higher-order calculations of particle masses in more detail in Sec. 3.6 and the application of the iterative procedure in the calculation of the complex NMSSM Higgs boson masses in our work in Chapter 16.

3.5. Input Parameter Conversion at Next-to-Leading Order

The calculation of higher-order corrections to partial decay widths and particle masses through the Feynman diagrammatic approach necessarily involves the evaluation of UV-divergent loop integrals, as discussed in detail in Sec. 3.1. In DREG, the evaluation of these loop integrals directly depends on the mass-dimensional renormalization scale, cf. Eq. (3.2). In the following, we denote with μ_{out} this renormalization scale at which the loop integrals (and consequently, *e.g.* the partial decay widths) are evaluated. On the other hand, if some parameters of the QFT are renormalized through $\overline{\text{MS}}/\overline{\text{DR}}$ conditions, their input values and CTs explicitly depend on the renormalization scale μ_R at which these parameters are defined. In the most general case, each $\overline{\text{MS}}/\overline{\text{DR}}$ parameter can be defined at an individual renormalization scale. In the calculation of the electroweak one-loop corrections to the Higgs decays in the 2HDM and N2HDM considered in Parts II and III of this thesis however, we consider all $\overline{\text{MS}}$ parameters to be defined at the same universal scale μ_R. In the following discussion, we restrict ourselves to the case of $\overline{\text{MS}}$ parameters. The case of $\overline{\text{DR}}$ parameters is exactly analogous.

We want to emphasize that both the renormalization scale μ_{out} at which the partial decay widths are evaluated and the renormalization scale μ_R at which the $\overline{\text{MS}}$ parameters are defined can be chosen arbitrarily and in particular, they are not necessarily required to be the same. In case that the two scales are different, the $\overline{\text{MS}}$ parameters that enter the calculation of the decay widths need to be converted from the scale μ_R to the scale μ_{out}. We denote with p a generic parameter of a QFT which is renormalized in the $\overline{\text{MS}}$ scheme by splitting the bare parameter p_0, which is independent of the renormalization scale, into the renormalized parameter $p(\mu_R)$ and its CT[11] $\delta p(\mu_R, p(\mu_R))$, which both are explicitly dependent on the renormalization scale μ_R. Due to the independence of the bare parameter p_0 of the renormalization scale, we can introduce the renormalized parameter and its CT at two different scales, *e.g.* μ_R and μ_{out}, but the sum of both yields the same bare parameter p_0 in both cases:

$$
\begin{aligned}
p_0 &= p(\mu_R) + \delta p\big(\mu_R, p(\mu_R)\big) \\
&= p(\mu_{\text{out}}) + \delta p\big(\mu_{\text{out}}, p(\mu_{\text{out}})\big) \ .
\end{aligned}
\tag{3.27}
$$

---

[11]In the general case, the CT δp depends not only on the parameter p itself, but on several other independent parameters of the theory. In order to keep the notation simple, we express the dependence only in terms of p, but the notation $\delta p\big(\mu_R, p(\mu_R)\big)$ implicitly is to be understood as to represent the dependence on *all* relevant parameters.

This equation can be solved for $p(\mu_{\text{out}})$ which yields an expression for the parameter p at the renormalization scale μ_{out}:

$$
\begin{aligned}
p(\mu_{\text{out}}) &= p(\mu_R) + \delta p\big(\mu_R, p(\mu_R)\big) - \delta p\big(\mu_{\text{out}}, p(\mu_{\text{out}})\big) \\
&\approx p(\mu_R) + \delta p\big(\mu_R, p(\mu_R)\big) - \delta p\big(\mu_{\text{out}}, p(\mu_R)\big) \ .
\end{aligned}
\tag{3.28}
$$

Since the CT δp on the right-hand side of the first line of this equation depends on the parameter $p(\mu_{\text{out}})$ which we want to determine, this equation can only be solved iteratively. In the second line, we therefore applied the linearized approach described in [189] by evaluating the parameter p in every term on the right-hand side of Eq. (3.28) at the scale μ_R where it is known. This allows for a direct determination of $p(\mu_{\text{out}})$ without the need of an iterative procedure. Since the CT δp is defined in the $\overline{\text{MS}}$ scheme, its form at one-loop level is given in terms of the part δp^Δ proportional to the UV-divergent Δ as defined in Eq. (3.2),

$$
\begin{aligned}
\delta p\big(\mu_R, p(\mu_R)\big) &= \delta p^\Delta\big(p(\mu_R)\big) \, \Delta \\
&= \delta p^\Delta\big(p(\mu_R)\big) \left[\frac{1}{\varepsilon} - \gamma_E + \ln(4\pi) + \ln\left(\frac{\mu^2}{\mu_R^2}\right) \right] \ .
\end{aligned}
\tag{3.29}
$$

Inserting this form of the CT into Eq. (3.28) reveals that all terms that are not directly dependent on μ_R or μ_{out} drop out and the formula for the parameter p at the scale μ_{out} simplifies to

$$
p(\mu_{\text{out}}) = p(\mu_R) + \delta p^\Delta\big(p(\mu_R)\big) \ln\left(\frac{\mu_{\text{out}}^2}{\mu_R^2}\right) \ .
\tag{3.30}
$$

This relation allows us to convert the $\overline{\text{MS}}$ renormalized parameter p, defined at a renormalization scale μ_R, to its value at another renormalization scale μ_{out}. However, due to the linearized approach applied in Eq. (3.28), this relation is only approximately valid up to higher-order terms.

Apart from the scale conversion of $\overline{\text{MS}}$ parameters, care has to be taken when higher-order corrections to *e.g.* partial decay widths are calculated within different renormalization schemes for the CTs of the independent parameters. For a consistent comparison of the results calculated within these different schemes, the independent parameters have to be converted from one scheme to another.

In the following, we denote with φ an arbitrary independent parameter of the theory defined in an arbitrary renormalization scheme, *e.g.* the scalar mixing angles of the (N)2HDM considered in this thesis. At one-loop order, we decide to renormalize φ in a *reference scheme* by splitting the bare parameter φ_0 into the physical parameter φ_{ref} and its CT[12] $\delta\varphi_{\text{ref}}\big(\mu_R, \varphi_{\text{ref}}(\mu_R)\big)$ in the reference renormalization scheme, defined at the scale μ_R. Alternatively, we can define both the parameter and its CT in an arbitrary other renormalization scheme at another scale μ_{out}, denoted by φ_i and $\delta\varphi_i\big(\mu_{\text{out}}, \varphi_i(\mu_{\text{out}})\big)$, respectively. Since the bare parameter φ_0 is in both cases the same, we can calculate the parameter φ_i in the other renormalization scheme by a generalization of Eq. (3.28):

$$
\varphi_i(\mu_{\text{out}}) \approx \varphi_{\text{ref}}(\mu_R) + \delta\varphi_{\text{ref}}\big(\mu_R, \varphi_{\text{ref}}(\mu_R)\big) - \delta\varphi_i\big(\mu_{\text{out}}, \varphi_{\text{ref}}(\mu_R)\big) \ .
\tag{3.31}
$$

As for the scale conversion of the $\overline{\text{MS}}$ parameters, this relation is only valid up to higher-order terms since we used the linearized approximation in the last term by evaluating it with the parameter φ_{ref} instead of φ_i in order to avoid the necessity of an iterative procedure.

The finite differences in the definition of any CT are expected to vanish if the CT were to be evaluated precisely to all orders. Hence, it is also expected that the partial decay widths

---

[12]As for the $\overline{\text{MS}}$ CT, the simplified notation $\delta\varphi_{\text{ref}}\big(\mu_R, \varphi_{\text{ref}}(\mu_R)\big)$ implicitly assumes that the CT of the parameter φ may depend on several independent parameters of the theory.

calculated within different renormalization schemes should converge to the same result if they were to be computed in an all-order calculation. At any finite order in perturbation theory, however, the different choices of renormalization schemes lead to different partial decay widths [190]. Due to this, the calculation and comparison of partial decay widths within different renormalization schemes, together with the consistent parameter conversion by means of Eq. (3.31), allows for an estimate of the remaining theoretical uncertainty of the NLO corrections due to missing higher-order contributions.

3.6. Gauge Independence of Fixed-Order Calculations

Since a considerable part of our work deals with the gauge-independent renormalization of mixing angles and questions about gauge dependence of partial decay widths and higher-order corrections to the Higgs masses, the final section of Part I of this thesis is dedicated to a brief discussion about the gauge independence of fixed-order calculations in general.

Gauge theories are characterized by the invariance of the Lagrangian of the gauge theory under specific local gauge transformations. It is a common feature of a quantized gauge theory comprising vector fields to contain redundant degrees of freedom which need to be removed in order to calculate physically sensible predictions. These redundant degrees of freedom appear even in comparatively simple Abelian gauge theories, *e.g.* in QED, where the quantized photon field contains four degrees of freedom from which only two, namely the two transverse modes of the photon polarization, are realized in nature. The other two degrees of freedom of the photon field are redundant and lead to ill-defined expressions in the computation of physical observables. The most straightforward quantity where the problematic redundant degrees of freedom become apparent is the generating functional $\mathcal{Z}[\boldsymbol{J}]$ of the gauge theory within the framework of the path integral formalism [94]. We denote with $\boldsymbol{A}$ a generic vector field with its associated source $\boldsymbol{J}$ and the action of the field theory with $S[\boldsymbol{A}]$. The generating functional of the theory is generically given by

$$\mathcal{Z}[\boldsymbol{J}] \equiv \int \mathcal{D}[\boldsymbol{A}] \exp\left(iS[\boldsymbol{A}] + i \int \mathrm{d}^4 x \boldsymbol{J}(x) \cdot \boldsymbol{A}(x)\right) \ . \tag{3.32}$$

From this quantity, the Feynman rules of the theory as the building blocks of the calculation of S matrix elements can be derived. However, the integration measure $\mathcal{D}[\boldsymbol{A}]$ in Eq. (3.32) implies an integration over *all* possible configuration states of the vector field $\boldsymbol{A}$. Since $\boldsymbol{A}$ contains redundant (*i.e.* unphysical) degrees of freedom which are connected through continuous gauge transformations, Eq. (3.32) implies an integration over arbitrarily many unphysical configuration states[13]. Consequently, Eq. (3.32) is a divergent quantity which *a priori* can not be used to derive physical observables. In order to circumvent this problem, one can *e.g.* apply the *Faddeev-Popov procedure* [191] which consistently cancels the redundant degrees of freedom[14] and allows for the usage of the generating functional for a calculation of physical observables.

In all QFTs we consider in this thesis, we use the class of R_ξ gauges to fix the gauge. Through the *gauge-fixing Lagrangian* of the R_ξ gauges, the generating functional and hence the Feynman rules of *e.g.* the vector boson propagators become functions of GFPs ξ, where

---

[13]Descriptively spoken, the independence of the gauge theory under gauge transformations corresponds to a continuous shear in configuration space. In this sense, the gauge theory forms an equivalence class, and the integration over the infinitely many realizations of the equivalence class leads to the divergence of the generating functional.

[14]Technically, the Faddeev-Popov procedure leads to a factorization of the integration over the redundant degrees of freedom in Eq. (3.32). Through a proper normalization of the generating functional, this global divergent factor stemming from the redundant degrees of freedom is precisely canceled.
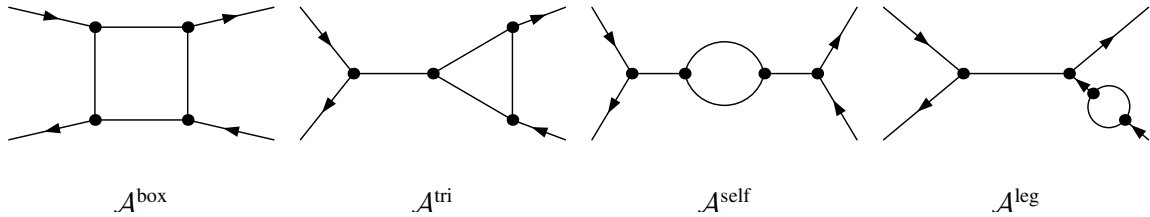
Figure 3.6.: All topological contributions for a two-body toy scattering process of OS fermions at one-loop level, consisting of the box diagrams $\mathcal{A}^{\text{box}}$, triangle diagrams $\mathcal{A}^{\text{tri}}$, self-energy diagrams $\mathcal{A}^{\text{self}}$ and external leg corrections $\mathcal{A}^{\text{leg}}$.

in general, any gauge boson of the theory acquires a distinctive GFP. While the introduction of the gauge-fixing Lagrangian explicitly breaks the invariance of the original Lagrangian of the gauge theory under local gauge transformations, S matrix elements calculated in the gauge-fixed theory are still both gauge-invariant and GFP-independent [192–197]. We want to emphasize that this statement is ensured by the *Becchi-Rouet-Stora-Tyutin* (BRST) symmetry and it is valid order by order in perturbation theory [94, 198, 199]. The only possibility to break the GFP independence of the calculation of observables at a fixed loop order is via imposing improper renormalization conditions on some of the independent parameters of the theory [196, 200]. We discuss this further in Secs. 5.3 and 10.3 for the 2HDM and N2HDM, respectively, where we demonstrate that an improper renormalization of the scalar mixing angles leads to a residual GFP dependence of the partial decay widths at one-loop order.

Apart from an improperly chosen renormalization scheme, there is another possibility to explicitly violate the GFP independence in the calculation of an observable, *e.g.* the higher-order corrections to the Higgs masses, as described in Sec. 3.4. In this case, however, the violation of GFP independence is not introduced via improper renormalization conditions, but via the iterative procedure through which the Higgs masses can be determined, since this procedure mixes different orders of perturbation theory. While the building blocks of the calculation of the Higgs masses, *i.e.* the renormalized diagonal Higgs self-energies (or to be more precise, the complex poles of the corresponding propagator, cf. Eq. (3.26)), are manifestly GFP-independent quantities when considered at a specific fixed loop level and evaluated with the tree-level Higgs masses [196], the iterative procedure leads to the evaluation of these self-energies with loop-corrected masses. This explicitly breaks Slavnov-Taylor identities and hence introduces a GFP dependence into the calculated values of the higher-order Higgs masses, which however is formally of *higher* orders of perturbation theory than the one considered in the calculation. This is in contrast to the violation of gauge-parameter independence introduced through an improper renormalization scheme, where the GFP dependence is formally of the *same* order of perturbation theory as the calculation that is considered [196].

In order to systematically analyze and quantify the GFP dependences arising in perturbative calculations performed in any gauge-fixed gauge theory, there are several theoretical tools available. The *Nielsen identities* [193] allow for a very generic analysis of possible sources of gauge dependences for fixed-order calculations. They can be used to formulate model-independent rigorous proofs *e.g.* about the gauge independence of S matrix elements or the CTs that are required for the fixed-order calculation. While these identities can in principle also be used for analyzing the origin of gauge dependences in different parts of a fixed-order calculation and for tracing their mutual cancellations, there are two other theoretical approaches that are better suited for this purpose in practice.

The first method for the explicit extraction and analysis of the cancellation of GFP-dependent contributions is the so-called *pinch technique* (PT) [201–208]. We briefly illustrate the key ideas of the PT by considering a toy process at one-loop level, *i.e.* the two-body scattering

of OS fermions with momenta p_i and masses m_i as illustrated in Fig. 3.6. The one-loop amplitude is a manifestly GFP-independent quantity, as can be formally proven by application of the Nielsen identities. As mentioned above, this statement is independent of the one-loop renormalization of the process, provided that we do not choose improper renormalization conditions which breaks the manifest GFP independence. More precisely, the diagrammatic origin of all gauge dependences lies in the individual genuine box, triangle and self-energy diagrams as well as in the external leg corrections, which, as discussed above, define the WFRCs. In other words, the cancellation of all gauge dependences occurs between the WFRCs and the genuine one-loop corrections and is independent of the renormalization of the process[15] [196, 200]. In order to illustrate the mechanism of the PT, we consider the full one-loop scattering amplitude, cf. Fig. 3.6. While this is a manifestly GFP-independent quantity, the individual diagrammatic contributions are GFP-dependent,

$$\mathcal{A}^{\mathrm{NLO}}(s,t,m_i) \equiv \mathcal{A}^{\mathrm{box}}(s,t,m,\xi) + \mathcal{A}^{\mathrm{tri}}(s,m,\xi) + \mathcal{A}^{\mathrm{self}}(s,\xi) + \mathcal{A}^{\mathrm{leg}}(s,\xi) , \qquad (3.33)$$

where s and t are the usual s- and t-channel Mandelstam variables and m represents the masses of the virtual particles in the loop. The key idea of the PT is to impose the elementary Ward identity

$$\slashed{l} = \slashed{l} + \slashed{p}_i - m_i - (\slashed{p}_i - m_i) \equiv S^{-1}(l+p_i) - S^{-1}(p_i) , \qquad (3.34)$$

where l denotes the loop momentum of any of the loop diagrams appearing in Fig. 3.6 and S^{-1} denotes the inverse fermion propagator. The term $S^{-1}(p_i)$ on the right-hand side of Eq. (3.34) vanishes in combination with an OS spinor by means of the Dirac equation. The term $S^{-1}(l+p_i)$ on the right-hand side of Eq. (3.34) combines with a fermion propagator $S(l+p_i)$ stemming from an internal fermion, thereby effectively canceling it. Due to this, the internal fermion is *pinched out* of the diagram. By imposing this elementary Ward identity in all loop diagrams, their individual GFP-dependent contributions can be extracted analytically in an unambiguous way. The crucial statement of the PT procedure is that the GFP-dependent contributions stemming from the box and triangle diagrams as well as from the external leg contributions are self-energy-like, *i.e.* they have the same functional dependence as the self-energy contributions. This allows for a reallocation of all GFP-dependent contributions into modified amplitudes for the box, triangle, self-energy and external leg contributions as follows,

$$\mathcal{A}^{\mathrm{NLO}}(s,t,m) \equiv \widehat{\mathcal{A}}^{\mathrm{box}}(s,t,m) + \widehat{\mathcal{A}}^{\mathrm{tri}}(s,m) + \widehat{\mathcal{A}}^{\mathrm{self}}(s) + \widehat{\mathcal{A}}^{\mathrm{leg}}(s) , \qquad (3.35)$$

where the hats over the amplitudes denote that the GFP-dependent contributions have canceled in these quantities. The *pinched self-energy* $\widehat{\mathcal{A}}^{\mathrm{self}}(s)$, as all other topological contributions in Eq. (3.35), are now *individually* GFP-independent. In that sense, the PT is a useful tool for the bookkeeping of the gauge dependences arising in a fixed-order calculation. Moreover, the GFP-independent amplitudes in Eq. (3.35) can be used as building blocks for the definition of GFP-independent renormalization schemes. As a practical example of this, we will use the pinched self-energies for a manifestly GFP-independent definition of the CTs of the scalar mixing matrices in the 2HDM and N2HDM in Secs. 5.1 and 10.1, respectively. For an in-depth introduction to the PT and its numerous interesting applications, we refer to [208].

The second useful tool for analyzing the cancellation of gauge dependences is the *background field method* (BFM) [209–215]. Since we do not apply the BFM in any part of our work and only adopt results from the literature that are calculated within the BFM framework, we only briefly discuss it in the following and refer the reader to the aforementioned literature for an

---

[15]For this statement to be true, it is necessary that the genuine loop corrections to the two-body scattering process as well as the corresponding external leg corrections contain contributions from tadpole diagrams, as well [208]. This corresponds to an alternative treatment of the tadpole renormalization, as discussed further in Secs. 5.1 and 10.1 for the 2HDM and N2HDM, respectively.

in-depth introduction. Essentially, the BFM is an alternative gauge-fixing procedure which allows to fix the gauge of the theory while simultaneously preserving its manifest local gauge invariance. The key idea of the BFM is based on a modification of the building blocks of the generating functional in Eq. (3.32). Each field considered in the generating functional is split into a classical *background field* which is considered to be static, *i.e.* it represents a fixed field configuration, and an additional fluctuating field. Due to the background field being static, a local gauge symmetry of the Lagrangian is preserved, while the fluctuating field allows for a fixation of the gauge. Since both fields appear explicitly in the generating functional, the Feynman rules are modified in comparison to the original theory. In essence, the background fields give rise to additional diagrammatic contributions, and also the renormalization of the fields and parameters of the theory need to be modified accordingly. On the other hand, the separation of the fields into the fluctuating and the background part allows for a separation of the GFP-dependent contributions in a diagrammatic fixed-order calculation and due to this, the cancellation of the GFP dependences is simpler to analyze. As it is the case for the PT, the BFM formalism allows for the definition of *e.g.* self-energies which are manifestly GFP-independent and which can subsequently be used for the definition of GFP-independent CTs. As an example, one of the renormalization schemes used in this work for renormalizing the scalar mixing angles of the 2HDM is based on the BFM [216], as further discussed in Sec. 5.1.

Part II.

Electroweak One-Loop Corrections to Higgs Boson Decays in the 2HDM

A Brief Introduction to the 2HDM

In Part II of this thesis, we consider the electroweak one-loop corrections to the partial decay widths of all Higgs bosons in the real 2HDM with a discrete $\mathbb{Z}_2$ symmetry that is only softly broken. These corrections are implemented in the newly developed computer program 2HDE-CAY, which combines the electroweak corrections with the state-of-the-art QCD corrections to 2HDM Higgs decays already implemented in the tool HDECAY 6.52 [47, 217]. As our work focuses on the electroweak corrections to the partial widths, we do not consider the QCD Lagrangian and its corresponding parameters in the following.

Starting with Sec. 4.1, we first introduce the full electroweak Lagrangian of the 2HDM and briefly discuss the origin of each term contributing to it. In the subsequent Sec. 4.2, we focus on the scalar Lagrangian of the 2HDM together with its accompanying scalar potential and discuss the transformation from the gauge basis to the mass basis of the Higgs boson sector. In Sec. 4.3, we consider the different possibilities of connecting the fermionic and scalar fields in the 2HDM through corresponding Yukawa couplings, leading to four different types of 2HDMs considered in this work. Finally, in Sec. 4.4 we present an overview over two possible full sets of independent parameters which can be used as inputs for the numerical evaluation of the partial decay widths and BRs with the newly developed computer program 2HDECAY presented in this thesis.

4.1. The Electroweak Lagrangian of the 2HDM

We consider a general CP-conserving 2HDM [17, 18] with a discrete global $\mathbb{Z}_2$ symmetry which is softly broken. In contrast to the SM, the 2HDM is comprised of two $SU(2)_L$ Higgs doublets Φ_i ($i = 1, 2$) with weak hypercharge $Y = +1$. The full electroweak Lagrangian of the model is split up into its several different contributions as follows,

$$\mathcal{L}_{\mathrm{2HDM}}^{\mathrm{EW}} = \mathcal{L}_{\mathrm{YM}} + \mathcal{L}_{\mathrm{F}} + \mathcal{L}_{\mathrm{S}}^{\mathrm{2HDM}} + \mathcal{L}_{\mathrm{Yuk}} + \mathcal{L}_{\mathrm{GF}} + \mathcal{L}_{\mathrm{FP}} \ . \tag{4.1}$$

The *Yang-Mills Lagrangian* $\mathcal{L}_{\mathrm{YM}}$ and the *fermion Lagrangian* $\mathcal{L}_{\mathrm{F}}$ contain the kinetic terms of the gauge bosons and fermions as well as the interactions between the gauge bosons with both the fermions and themselves. In the 2HDM, these two Lagrangians are the same as the ones present in the SM and their explicit forms are not needed for the subsequent parts of

this work. Hence, we do not present these two Lagrangians explicitly here but instead refer to *e.g.* [94, 183] where they are presented in detail.

The third term in Eq. (4.1) is the *scalar Lagrangian* $\mathcal{L}_S^{2\mathrm{HDM}}$ of the 2HDM. It contains the kinetic terms of the scalar fields as well as the scalar potential and consequently also the interactions of the scalar particles with the gauge bosons and with themselves. Additionally, the scalar potential defines the vacuum structure of the 2HDM whose explicit treatment is crucial for a GFP-independent renormalization as further discussed in Sec. 5.1. Since the main difference between the SM and the 2HDM lies in the extended scalar sector, we discuss the scalar Lagrangian and the corresponding potential separately in detail in Sec. 4.2.

The fourth term in Eq. (4.1) is the *Yukawa Lagrangian* $\mathcal{L}_{\mathrm{Yuk}}$ which describes the interactions between the fermions and the extended scalar sector. In the SM, the only existing $SU(2)_L$ Higgs doublet couples to the fermions in an unambiguous way. In contrast to that, the two Higgs doublets of the 2HDM can couple in four different combinations to the fermions. Since these combinations can differ significantly with respect to their phenomenology, we discuss the Yukawa Lagrangian in more detail in Sec. 4.3 where we also introduce a short-hand notation for the Yukawa coupling parameters that are used in this work.

The last two terms in Eq. (4.1) are the *gauge-fixing Lagrangian* $\mathcal{L}_{\mathrm{GF}}$ and the *Faddeev-Popov Lagrangian* $\mathcal{L}_{\mathrm{FP}}$. We do not list their explicit forms as they are not needed, but refer instead to [168] for their full form. As briefly discussed in general in Sec. 3.6, these two Lagrangians are required in order to remove the redundant degrees of freedom which arise due to the unphysical polarization states of the gauge bosons. In our work, we use the class of *renormalizable gauges*, the R_ξ gauge [218, 219], to specify the gauge-fixing Lagrangian. As mentioned in Sec. 3.6, the consequence of this gauge-fixing procedure is an explicit dependence of the partial decay widths on the GFPs ξ_V ($V = \{W, Z, \gamma\}$) of each gauge boson. The Faddeev-Popov procedure allows for the removal of the unphysical degrees of freedom by introducing unphysical *Faddeev-Popov ghost fields* $u_{W^\pm}$, u_Z and u_γ for each gauge boson [191]. In our work, we apply the approach of [168] and introduce the Lagrangians $\mathcal{L}_{\mathrm{GF}}$ and $\mathcal{L}_{\mathrm{FP}}$ only after the renormalization of the 2HDM is completed. Hence, all fields contained in these two Lagrangians are already renormalized fields and both the gauge-fixing and the Faddeev-Popov Lagrangian do not receive additional CTs.

4.2. The Scalar Lagrangian and the Scalar Potential

The scalar Lagrangian of the general CP-conserving 2HDM contains the kinetic terms of the scalar fields as well as their interactions with the gauge bosons and the scalar self-interactions. By introducing the *covariant derivative*[16]

$$D_\mu \equiv \partial_\mu + \frac{i}{2}\, g \sum_{a=1}^{3} \sigma_a W_\mu^a + \frac{i}{2}\, g' B_\mu \,, \tag{4.2}$$

with the Pauli matrices σ_a ($a = 1, 2, 3$), the gauge boson fields W_μ^a and B_μ of the gauge groups $SU(2)_L$ and $U(1)_Y$ and their corresponding gauge couplings g and g', respectively, the scalar Lagrangian is given by

$$\mathcal{L}_S^{2\mathrm{HDM}} = \sum_{i=1}^{2} (D_\mu \Phi_i)^\dagger (D^\mu \Phi_i) - V_{2\mathrm{HDM}} \,, \tag{4.3}$$

where Φ_i ($i = 1, 2$) denotes the two complex $SU(2)_L$ Higgs doublets. In comparison to the SM, the scalar potential $V_{2\mathrm{HDM}}$ of the 2HDM contains more interaction terms due to the

---

[16]We want to emphasize that we use the sign convention for the $SU(2)_L$ term that is typically used in MSSM and 2HDM calculations, while in the SM, this term is usually introduced with an opposite sign [183].

existence of two Higgs doublets instead of just one. The CP-conserving scalar potential can be expressed as[17] [18]

$$V_{2\text{HDM}} = m_{11}^2 \left(\Phi_1^\dagger \Phi_1 \right) + m_{22}^2 \left(\Phi_2^\dagger \Phi_2 \right) - m_{12}^2 \left(\Phi_1^\dagger \Phi_2 + \Phi_2^\dagger \Phi_1 \right) + \frac{\lambda_1}{2} \left(\Phi_1^\dagger \Phi_1 \right)^2 + \frac{\lambda_2}{2} \left(\Phi_2^\dagger \Phi_2 \right)^2$$
$$+ \lambda_3 \left(\Phi_1^\dagger \Phi_1 \right) \left(\Phi_2^\dagger \Phi_2 \right) + \lambda_4 \left(\Phi_1^\dagger \Phi_2 \right) \left(\Phi_2^\dagger \Phi_1 \right) + \frac{\lambda_5}{2} \left[\left(\Phi_1^\dagger \Phi_2 \right)^2 + \left(\Phi_2^\dagger \Phi_1 \right)^2 \right] \,, \quad (4.4)$$

with three real mass parameters m_{11}, m_{22} and m_{12} as well as five real dimensionless coupling constants λ_i $(i = 1, ..., 5)$. For later convenience, three of these constants are combined as

$$\lambda_{345} \equiv \lambda_3 + \lambda_4 + \lambda_5 \,. \quad (4.5)$$

The scalar potential of the 2HDM exhibits an approximate discrete $\mathbb{Z}_2$ symmetry under the simultaneous Higgs doublet transformations

$$\Phi_1 \to -\Phi_1 \,, \quad \Phi_2 \to \Phi_2 \,. \quad (4.6)$$

If m_{12} were zero, this symmetry would be exact and Eq. (4.4) would be invariant under these field transformations. The $\mathbb{Z}_2$ symmetry is extended to the Yukawa sector of the 2HDM in order to avoid the appearance of FCNCs on tree level, as further discussed in Sec. 4.3.

The two Higgs doublets Φ_i are expanded around their real VEVs v_i $(i = 1, 2)$,

$$\Phi_1 = \begin{pmatrix} \omega_1^+ \\ \dfrac{v_1 + \rho_1 + i\eta_1}{\sqrt{2}} \end{pmatrix} \,, \quad \Phi_2 = \begin{pmatrix} \omega_2^+ \\ \dfrac{v_2 + \rho_2 + i\eta_2}{\sqrt{2}} \end{pmatrix} \,, \quad (4.7)$$

where we introduced the charged complex fields ω_i^+ as well as the real neutral CP-even and CP-odd fields ρ_i and η_i, respectively. The VEVs of the two doublets, *i.e.* their vacuum states

$$\langle \Phi_1 \rangle = \begin{pmatrix} 0 \\ \dfrac{v_1}{\sqrt{2}} \end{pmatrix} \,, \quad \langle \Phi_2 \rangle = \begin{pmatrix} 0 \\ \dfrac{v_2}{\sqrt{2}} \end{pmatrix} \,, \quad (4.8)$$

represent the minima of the potential. They are connected to the SM VEV v through the relation

$$v^2 = v_1^2 + v_2^2 \approx (246\,\text{GeV})^2 \,, \quad (4.9)$$

with

$$v = \frac{1}{\sqrt{\sqrt{2}G_F}} \,, \quad (4.10)$$

where G_F denotes the Fermi constant. A characteristic parameter of the scalar sector of the 2HDM is given by the ratio of the two VEVs[18],

$$t_\beta \equiv \frac{v_2}{v_1} \,, \quad (4.11)$$

which allows to replace the two VEVs in favor of the new parameter β and the SM-like VEV v as follows,

$$v_1 = c_\beta v \,, \quad (4.12)$$
$$v_2 = s_\beta v \,. \quad (4.13)$$

---

[17]For alternative parametrizations of the 2HDM potential, we refer to [18, 33, 220, 221].
[18]For convenience, we use the short-hand notations $s_x \equiv \sin(x)$, $c_x \equiv \cos(x)$ and $t_x \equiv \tan(x)$ for the trigonometric functions throughout this thesis.

The gauge boson fields in the gauge basis can be rotated to the mass basis by a field redefinition and by means of the Weinberg angle Θ_W,

$$W_\mu^\pm = \frac{1}{\sqrt{2}} \left(W_\mu^1 \mp i W_\mu^2 \right) \; , \tag{4.14}$$

$$\begin{pmatrix} Z_\mu \\ \gamma_\mu \end{pmatrix} = \begin{pmatrix} c_W & -s_W \\ s_W & c_W \end{pmatrix} \begin{pmatrix} W_\mu^3 \\ B_\mu \end{pmatrix} \; , \tag{4.15}$$

where we additionally introduced the short-hand notations $s_W \equiv \sin(\Theta_W)$ and $c_W \equiv \cos(\Theta_W)$. The physical fields $W_\mu^\pm$, Z_μ and γ_μ correspond to the physical gauge bosons $W^\pm$, Z and the photon γ in the mass basis, and their squared masses m_V^2 ($V = \{W, Z, \gamma\}$) are given by

$$m_W^2 = g^2 \frac{v^2}{4} \; , \tag{4.16}$$

$$m_Z^2 = \left(g^2 + g'^2 \right) \frac{v^2}{4} \; , \tag{4.17}$$

$$m_\gamma^2 = 0 \; . \tag{4.18}$$

Furthermore, the diagonalization of the gauge boson sector connects several parameters of the electroweak Lagrangian with each other,

$$c_W = \frac{m_W}{m_Z} \; , \tag{4.19}$$

$$e = \sqrt{4\pi\alpha_{\rm em}} = \frac{gg'}{\sqrt{g^2 + g'^2}} = s_W g \; , \tag{4.20}$$

$$G_F = \frac{\sqrt{2} g^2}{8 m_W^2} = \frac{\alpha_{\rm em}\pi}{\sqrt{2} m_W^2 s_W^2} \; , \tag{4.21}$$

where we additionally introduced the electromagnetic coupling constant e and the corresponding fine-structure constant $\alpha_{\rm em}$.

Since we consider the CP-conserving 2HDM, there are only two terms which are linear in the CP-even fields ρ_i, namely the *tadpole terms*

$$T_1 \equiv m_{11}^2 v_1 - m_{12}^2 v_2 + \frac{1}{2}\lambda_1 v_1^3 + \frac{1}{2}\lambda_{345} v_1 v_2^2 \; , \tag{4.22}$$

$$T_2 \equiv m_{22}^2 v_2 - m_{12}^2 v_1 + \frac{1}{2}\lambda_1 v_3^3 + \frac{1}{2}\lambda_{345} v_1^2 v_2 \; . \tag{4.23}$$

These terms are tightly connected to the vacuum states of the potential. In these states, the scalar potential fulfills the two minimum conditions

$$\left.\frac{\partial V_{\rm 2HDM}}{\partial \Phi_1^\dagger}\right|_{\langle\Phi_1\rangle, \langle\Phi_2\rangle} = \left.\frac{\partial V_{\rm 2HDM}}{\partial \Phi_2^\dagger}\right|_{\langle\Phi_1\rangle, \langle\Phi_2\rangle} = 0 \; , \tag{4.24}$$

which at tree level is equivalent to vanishing tadpole terms,

$$T_1|^{\rm tree} = T_2|^{\rm tree} = 0 \; . \tag{4.25}$$

The two tadpole terms in Eqs. (4.22) and (4.23) can be solved for the two potential parameters m_{11}^2 and m_{22}^2 which consequently can be eliminated in favor of the other parameters of the 2HDM potential,

$$m_{11}^2 = m_{12}^2 \frac{v_2}{v_1} - \frac{1}{2}\lambda_1 v_1^2 - \frac{1}{2}\lambda_{345} v_2^2 + \frac{T_1}{v_1} \; , \tag{4.26}$$

$$m_{22}^2 = m_{12}^2 \frac{v_1}{v_2} - \frac{1}{2}\lambda_2 v_2^2 - \frac{1}{2}\lambda_{345} v_1^2 + \frac{T_2}{v_2} \; . \tag{4.27}$$

The terms in the 2HDM potential which are bilinear in the scalar fields define the three non-diagonal 2×2 mass matrices $\mathcal{M}_\rho^2$, $\mathcal{M}_\eta^2$ and $\mathcal{M}_\omega^2$ of the scalar sector of the 2HDM whose analytic forms are explicitly given by

$$
\mathcal{M}_\rho^2 = \begin{pmatrix} m_{12}^2 \frac{v_2}{v_1} + \lambda_1 v_1^2 & -m_{12}^2 + \lambda_{345} v_1 v_2 \\ -m_{12}^2 + \lambda_{345} v_1 v_2 & m_{12}^2 \frac{v_1}{v_2} + \lambda_2 v_2^2 \end{pmatrix} + \begin{pmatrix} \frac{T_1}{v_1} & 0 \\ 0 & \frac{T_2}{v_2} \end{pmatrix} , \tag{4.28}
$$

$$
\mathcal{M}_\eta^2 = \left(\frac{m_{12}^2}{v_1 v_2} - \lambda_5 \right) \begin{pmatrix} v_2^2 & -v_1 v_2 \\ -v_1 v_2 & v_1^2 \end{pmatrix} + \begin{pmatrix} \frac{T_1}{v_1} & 0 \\ 0 & \frac{T_2}{v_2} \end{pmatrix} , \tag{4.29}
$$

$$
\mathcal{M}_\omega^2 = \left(\frac{m_{12}^2}{v_1 v_2} - \frac{\lambda_4 + \lambda_5}{2} \right) \begin{pmatrix} v_2^2 & -v_1 v_2 \\ -v_1 v_2 & v_1^2 \end{pmatrix} + \begin{pmatrix} \frac{T_1}{v_1} & 0 \\ 0 & \frac{T_2}{v_2} \end{pmatrix} , \tag{4.30}
$$

where we already replaced m_{11}^2 and m_{22}^2 by means of Eqs. (4.26) and (4.27). While the tadpole terms vanish at tree level according to Eq. (4.25), we keep them explicitly in the mass matrices since in the framework of the usual treatment of the tadpoles, they yield higher-order corrections to the mass matrices and consequently also to the CTs of the elements of the mass matrices.

Since the scalar fields ρ_i, η_i and ω_i, representing the *gauge basis* of the scalar potential of the 2HDM, appear pairwise with the same quantum numbers, they mix with each other. In order to interpret these fields as physical particles, the terms bilinear in the scalar fields in the potential are diagonalized, analogously to the gauge boson fields as described above. Since all three mass matrices of the 2HDM are real 2×2 matrices, they are diagonalized by orthogonal matrices of the form

$$
R_\theta \equiv \begin{pmatrix} c_\theta & -s_\theta \\ s_\theta & c_\theta \end{pmatrix} , \tag{4.31}
$$

where $\theta = \{\alpha, \beta_n, \beta_c\}$ are the three scalar mixing angles of the 2HDM[19] that quantify the mixing of the scalar fields. The diagonalized matrices are then given by

$$
D_\rho^2 \equiv R_\alpha^T \mathcal{M}_\rho^2 R_\alpha = \begin{pmatrix} m_H^2 & 0 \\ 0 & m_h^2 \end{pmatrix} + \begin{pmatrix} T_{HH} & T_{Hh} \\ T_{Hh} & T_{hh} \end{pmatrix} , \tag{4.32}
$$

$$
D_\eta^2 \equiv R_{\beta_n}^T \mathcal{M}_\eta^2 R_{\beta_n} = \begin{pmatrix} m_{G^0}^2 & 0 \\ 0 & m_A^2 \end{pmatrix} + \begin{pmatrix} T_{G^0 G^0} & T_{G^0 A} \\ T_{G^0 A} & T_{AA} \end{pmatrix} , \tag{4.33}
$$

$$
D_\omega^2 \equiv R_{\beta_c}^T \mathcal{M}_\omega^2 R_{\beta_c} = \begin{pmatrix} m_{G^\pm}^2 & 0 \\ 0 & m_{H^\pm}^2 \end{pmatrix} + \begin{pmatrix} T_{G^\pm G^\pm} & T_{G^\pm H^\pm} \\ T_{G^\pm H^\pm} & T_{H^\pm H^\pm} \end{pmatrix} , \tag{4.34}
$$

---

[19]As described below, the two mixing angles β_n and β_c are actually equivalent to each other at tree level and consequently, one typically refers to α and β as the only *two* scalar mixing angles of the 2HDM at tree level.

where the squared mass parameters on the right-hand side of these equations are given below
and where we additionally introduced the rotated tadpole parameters

$$
\begin{pmatrix} T_{HH} & T_{Hh} \\ T_{Hh} & T_{hh} \end{pmatrix} \equiv R_\alpha^T \begin{pmatrix} \dfrac{T_1}{v_1} & 0 \\ 0 & \dfrac{T_2}{v_2} \end{pmatrix} R_\alpha \ ,
\tag{4.35}
$$

$$
\begin{pmatrix} T_{G^0 G^0} & T_{G^0 A} \\ T_{G^0 A} & T_{AA} \end{pmatrix} \equiv , R_{\beta_n}^T \begin{pmatrix} \dfrac{T_1}{v_1} & 0 \\ 0 & \dfrac{T_2}{v_2} \end{pmatrix} R_{\beta_n}
\tag{4.36}
$$

$$
\begin{pmatrix} T_{G^\pm G^\pm} & T_{G^\pm H^\pm} \\ T_{G^\pm H^\pm} & T_{H^\pm H^\pm} \end{pmatrix} \equiv R_{\beta_c}^T \begin{pmatrix} \dfrac{T_1}{v_1} & 0 \\ 0 & \dfrac{T_2}{v_2} \end{pmatrix} R_{\beta_c} \ .
\tag{4.37}
$$

At tree level, these tadpole parameters all vanish according to Eq. (4.25) and hence, the
diagonal structure of Eqs. (4.32) to (4.34) is revealed. Through the diagonalization, the
scalar field doublets are transformed to the mass basis by the same orthogonal matrices,

$$
\begin{pmatrix} H \\ h \end{pmatrix} = R_\alpha^T \begin{pmatrix} \rho_1 \\ \rho_2 \end{pmatrix} = \begin{pmatrix} c_\alpha & s_\alpha \\ -s_\alpha & c_\alpha \end{pmatrix} \begin{pmatrix} \rho_1 \\ \rho_2 \end{pmatrix} \ ,
\tag{4.38}
$$

$$
\begin{pmatrix} G^0 \\ A \end{pmatrix} = R_{\beta_b}^T \begin{pmatrix} \eta_1 \\ \eta_2 \end{pmatrix} = \begin{pmatrix} c_{\beta_b} & s_{\beta_b} \\ -s_{\beta_b} & c_{\beta_b} \end{pmatrix} \begin{pmatrix} \eta_1 \\ \eta_2 \end{pmatrix} \ ,
\tag{4.39}
$$

$$
\begin{pmatrix} G^\pm \\ H^\pm \end{pmatrix} = R_\beta^T \begin{pmatrix} \omega_1^\pm \\ \omega_2^\pm \end{pmatrix} = \begin{pmatrix} c_{\beta_c} & s_{\beta_c} \\ -s_{\beta_c} & c_{\beta_c} \end{pmatrix} \begin{pmatrix} \omega_1^\pm \\ \omega_2^\pm \end{pmatrix} \ .
\tag{4.40}
$$

In this basis, h and H represent the light and heavy CP-even Higgs bosons, A represents the
CP-odd Higgs boson and $H^\pm$ represents the charged Higgs boson pair, while G^0 and $G^\pm$ are
the CP-odd and charged Goldstone bosons. The squared masses of the physical Higgs bosons
in the mass basis are given by

$$
m_H^2 = c_{\alpha-\beta}^2 \mathcal{M}_{11}^2 + s_{2(\alpha-\beta)} \mathcal{M}_{12}^2 + s_{\alpha-\beta}^2 \mathcal{M}_{22}^2 \ ,
\tag{4.41}
$$

$$
m_h^2 = s_{\alpha-\beta}^2 \mathcal{M}_{11}^2 - s_{2(\alpha-\beta)} \mathcal{M}_{12}^2 + c_{\alpha-\beta}^2 \mathcal{M}_{22}^2 \ ,
\tag{4.42}
$$

$$
m_A^2 = v^2 \left(\frac{m_{12}^2}{v_1 v_2} - \lambda_5 \right) \ ,
\tag{4.43}
$$

$$
m_{H^\pm}^2 = v^2 \left(\frac{m_{12}^2}{v_1 v_2} - \frac{\lambda_4 + \lambda_5}{2} \right) \ ,
\tag{4.44}
$$

where we additionally introduced

$$
\mathcal{M}_{11}^2 \equiv v^2 \left[c_\beta^4 \lambda_1 + s_\beta^4 \lambda_2 + 2 s_\beta^2 c_\beta^2 \lambda_{345} \right] \ ,
\tag{4.45}
$$

$$
\mathcal{M}_{12}^2 \equiv s_\beta c_\beta v^2 \left[-c_\beta^2 \lambda_1 + s_\beta^2 \lambda_2 + c_{2\beta} \lambda_{345} \right] \ ,
\tag{4.46}
$$

$$
\mathcal{M}_{22}^2 \equiv \frac{m_{12}^2}{s_\beta c_\beta} + \frac{v^2}{8} \left(1 - c_{4\beta} \right) \left[\lambda_1 + \lambda_2 - 2 \lambda_{345} \right] \ .
\tag{4.47}
$$

The unphysical Goldstone bosons are massless,

$$
m_{G^0}^2 = 0 \ ,
\tag{4.48}
$$

$$
m_{G^\pm}^2 = 0 \ .
\tag{4.49}
$$

The scalar mixing angle α of the CP-even Higgs bosons can be expressed by the other parameters of the 2HDM potential as

$$t_{2(\alpha-\beta)} = \frac{2\mathcal{M}_{12}^2}{\mathcal{M}_{11}^2 - \mathcal{M}_{22}^2} \ . \tag{4.50}$$

The inversion of this relation, together with Eqs. (4.41) to (4.44), yields expressions for the 2HDM potential parameters λ_i $(i = 1, ..., 5)$ in terms of the physical parameters, *i.e.* in terms of the masses of the physical Higgs bosons and the scalar mixing angle α [222],

$$\lambda_1 = \frac{1}{v^2 c_\beta^2} \left(c_\alpha^2 m_H^2 + s_\alpha^2 m_h^2 - \frac{s_\beta}{c_\beta} m_{12}^2 \right) \ , \tag{4.51}$$

$$\lambda_2 = \frac{1}{v^2 s_\beta^2} \left(s_\alpha^2 m_H^2 + c_\alpha^2 m_h^2 - \frac{c_\beta}{s_\beta} m_{12}^2 \right) \ , \tag{4.52}$$

$$\lambda_3 = \frac{2m_{H^\pm}^2}{v^2} + \frac{s_{2\alpha}}{s_{2\beta} v^2} \left(m_H^2 - m_h^2 \right) - \frac{m_{12}^2}{s_\beta c_\beta v^2} \ , \tag{4.53}$$

$$\lambda_4 = \frac{1}{v^2} \left(m_A^2 - 2m_{H^\pm}^2 + \frac{m_{12}^2}{s_\beta c_\beta} \right) \ , \tag{4.54}$$

$$\lambda_5 = \frac{1}{v^2} \left(\frac{m_{12}^2}{s_\beta c_\beta} - m_A^2 \right) \ . \tag{4.55}$$

The two mixing angles β_n and β_c are in general different from each other as well as from the parameter β which is defined through the ratio of the VEVs, cf. Eq. (4.11). At tree level however, all three of these parameters are equal,

$$\beta_n|^{\text{tree}} = \beta_c|^{\text{tree}} = \beta|^{\text{tree}} \ . \tag{4.56}$$

Consequently, the scalar mixing angle β and the mixing angle α of the CP-even Higgs bosons are at tree level considered as the two independent scalar mixing angles of the 2HDM in this work.

The Goldstone bosons, remaining massless in the unitary gauge, acquire the squared masses

$$m_{G^0}^2 = \xi_Z m_Z^2 \ , \tag{4.57}$$

$$m_{G^\pm}^2 = \xi_W m_W^2 \ . \tag{4.58}$$

in R_ξ gauge and the squared masses of the ghost fields are given by

$$m_{u_Z}^2 = \xi_Z m_Z^2 \ , \tag{4.59}$$

$$m_{u_{W^\pm}}^2 = \xi_W m_W^2 \ , \tag{4.60}$$

$$m_{u_\gamma}^2 = 0 \ . \tag{4.61}$$

For the renormalization of the 2HDM described in Chapter 5, all Goldstone and ghost particles are still considered to be massless since we employ the gauge-fixing and Faddeev-Popov Lagrangians only *after* the renormalization of the theory is completed [223].

4.3. The Yukawa Couplings and the Four Types of 2HDMs

The Yukawa Lagrangian $\mathcal{L}_{\text{Yuk}}$ contains the interactions between the fermionic and scalar fields. In order to avoid FCNCs at tree level that occur in the 2HDM [18], the $\mathbb{Z}_2$ symmetry of the scalar sector is extended to the Yukawa sector in such a form that each Higgs doublet couples only to one specific type of fermion multiplet which is a sufficient condition to ensure

	u-type	d-type	leptons
I	Φ_2	Φ_2	Φ_2
II	Φ_2	Φ_1	Φ_1
lepton-specific	Φ_2	Φ_2	Φ_1
flipped	Φ_2	Φ_1	Φ_2

Table 4.1.: The four possible assignments of the Higgs doublets Φ_i ($i = 1, 2$) to the up-type (u) and down-type (d) quarks and the charged leptons in the $\mathbb{Z}_2$-symmetric 2HDM.

that no FCNCs appear at tree level in the theory [224]. Per convention, the second Higgs doublet Φ_2 always couples to the up-type fermions. This leaves four different possibilities for the coupling of the first Higgs doublet Φ_1 to the up-type and down-type fermions and the charged leptons, corresponding to the four types of 2HDM as presented in Table 4.1. Due to the resulting different coupling structures between the physical Higgs bosons with the fermions, each 2HDM type is phenomenologically different from the other and hence, the contraints on the 2HDM parameters gained by experimental data differ for each type. The different assignments of the Higgs doublets to each of the field multiplets of the fermions gives rise to different Yukawa couplings between the Higgs bosons and the down-type quarks d and charged leptons l. In our work, we parametrize these couplings by means of six different Yukawa coupling parameters Y_i ($i = 1, ..., 6$) as defined by the corresponding terms in the Yukawa Lagrangian,

$$\mathcal{L}_{\text{Yuk}} \supset -\frac{m_d}{v} \left(Y_1 \overline{\psi}_d \psi_d h + Y_2 \overline{\psi}_d \psi_d H\right) - \frac{m_l}{v} \left(Y_4 \overline{\psi}_l \psi_l h + Y_5 \overline{\psi}_l \psi_l H\right) \tag{4.62}$$
$$+ \frac{2im_d}{v} I_W^{z,d} Y_3 \overline{\psi}_d \gamma_5 \psi_d A + \frac{2im_l}{v} I_W^{z,l} Y_6 \overline{\psi}_l \gamma_5 \psi_l A \ ,$$

where $I_W^{z,f}$ denotes the third component of the weak isospin of the corresponding fermion field ψ_f. In Table 4.2, we present the explicit values of the Yukawa coupling parameters for each type of 2HDM.

4.4. Set of Independent Parameters

In the final section of this chapter, we conclude with the full set of independent parameters used by us to parametrize the electroweak Lagrangian of the 2HDM. These independent parameters are used as input for the calculation of the electroweak corrections to the partial decay widths of the Higgs bosons of the 2HDM with the newly developed computer program `2HDECAY`, as further described in Chapter 6. Since `2HDECAY` does not only calculate the electroweak corrections, but moreover combines them with the state-of-the-art QCD corrections already available in the computer program `HDECAY`, the following additional independent input parameters are required for the computations performed by `2HDECAY`:

- The electromagnetic coupling constant α_{em} in the Thomson limit is required for the calculation of loop-induced decays into $Z\gamma$ and $\gamma\gamma$ final states.

- The strong coupling constant α_s is used for the calculation of the loop-induced decays into pairs of gluons as well as for the computation of the state-of-the-art QCD corrections.

- The total decay widths Γ_W and Γ_Z of the W and Z bosons, respectively, are required for the computation of the off-shell decays into final states containing these massive gauge bosons.

2HDM type	Y_1	Y_2	Y_3	Y_4	Y_5	Y_6
I	c_α/s_β	s_α/s_β	$-1/t_\beta$	c_α/s_β	s_α/s_β	$-1/t_\beta$
II	$-s_\alpha/c_\beta$	c_α/c_β	t_β	$-s_\alpha/c_\beta$	c_α/c_β	t_β
lepton-specific	c_α/s_β	s_α/s_β	$-1/t_\beta$	$-s_\alpha/c_\beta$	c_α/c_β	t_β
flipped	$-s_\alpha/c_\beta$	c_α/c_β	t_β	c_α/s_β	s_α/s_β	$-1/t_\beta$

Table 4.2.: Yukawa coupling parameters Y_i ($i = 1, ..., 6$) in the $\mathbb{Z}_2$-symmetric 2HDM, parametrizing the Yukawa couplings for each 2HDM type.

These additional parameters are combined with the other independent parameters from the gauge, fermion and scalar sectors of the electroweak Lagrangian as presented in the preceding sections into the full set of independent parameters in the mass basis of the 2HDM potential,

$$\{G_F, \alpha_s, \Gamma_W, \Gamma_Z, \alpha_{\rm em}, m_W, m_Z, m_f, V_{ij}, t_\beta, m_{12}^2, \alpha, m_h, m_H, m_A, m_{H^\pm}\} \ . \tag{4.63}$$

In this set, m_f represents the masses of all fermions $f = \{s, c, b, t, \mu, \tau\}$ and V_{ij} ($i, j = 1, 2, 3$) denotes the *Cabibbo-Kobayashi-Maskawa matrix* (CKM) [107, 108] matrix elements. The fermions of the first generation, as well as the neutrinos, are assumed to be massless in the computation of the partial decay widths. As an alternative to Eq. (4.63), we can consider the scalar sector in the gauge basis and instead of the physical Higgs boson masses and the mixing angle α, we use the 2HDM potential parameters λ_i ($i = 1, ..., 5$) as independent input. In this case, the set of independent parameters is given by

$$\{G_F, \alpha_s, \Gamma_W, \Gamma_Z, \alpha_{\rm em}, m_W, m_Z, m_f, V_{ij}, t_\beta, m_{12}^2, \lambda_1, \lambda_2, \lambda_3, \lambda_4, \lambda_5\} \ , \tag{4.64}$$

and the relation between the two sets is given by the formulae of the 2HDM potential parameters λ_i in terms of the physical parameters in Eqs. (4.51) to (4.55). We want to emphasize that for the calculation of the electroweak corrections to the partial decay widths, we use the OS masses m_W and m_Z of the $W^\pm$ and Z bosons, respectively, as well as the electromagnetic coupling constant $\alpha_{\rm em}(m_Z^2)$ at the scale of the Z boson mass, which is directly related to the Fermi constant G_F via Eq. (4.21). On the other hand, the state-of-the-art QCD corrections implemented in HDECAY require G_F as fundamental input and the fine-structure constant is only used in the Thomson limit, *i.e.* $\alpha_{\rm em}(0)$, for the calculation of the loop-induced decays into $Z\gamma$ and $\gamma\gamma$ as described above. We come back to this in Sec. 6.2.

For completeness, we want to mention that the tadpole parameters T_1 and T_2 formally belong to these two sets of independent parameters, as well. However, as discussed in detail in Sec. 5.1, these parameters either vanish at each order in perturbation theory in the framework of the standard renormalization of the tadpoles or they do not appear in the first place as independent input in the framework of an alternative tadpole renormalization. Since in both cases the parameters T_1 and T_2 do not contribute to the calculation of the electroweak partial decay widths, we do not include them in the two sets in Eqs. (4.63) and (4.64).

The Renormalization of the 2HDM in a Nutshell

The calculation of partial decay widths of the Higgs bosons of the 2HDM at higher orders in perturbation theory necessarily involves the evaluation of UV-divergent loop integrals. In this chapter, we specify the renormalization conditions applied to all independent input parameters for the calculation of the electroweak corrections in order to cancel all UV divergences that appear at the electroweak one-loop level.

The one-loop renormalization of the 2HDM was considered in several publications before [168, 222, 225]. One subtlety in the renormalization concerns the two scalar mixing angles α and β of the 2HDM, since in the schemes proposed in *e.g.* [222], intricate GFP dependences are introduced into the calculation of observables. In [226–228], several GFP-independent renormalization schemes were proposed for the first time for the 2HDM. Subsequently, several other GFP-independent renormalization schemes for the scalar mixing angles were introduced in [189, 216, 229]. In this thesis, we adopt the renormalization schemes presented in [226] and extend them to all sectors of the 2HDM and moreover additionally adopt the renormalization schemes for the scalar mixing angles presented in [216]. We describe how these renormalization schemes are implemented in the newly developed computer program `2HDECAY`. Since in Part II of this thesis we focus on the calculation of the electroweak one-loop corrections to the partial decay widths and since the renormalization schemes for the 2HDM that we employ in our work were presented in great detail before, we only briefly recapitulate these schemes here while for a detailed description, we refer to the aforementioned literature.

Since the proper renormalization of the minimum conditions of the 2HDM potential is crucial in order to obtain GFP-independent observables at one-loop level, we recapitulate the tadpole renormalization in Sec. 5.1. In the subsequent Sec. 5.2, we briefly present the renormalization of the gauge, fermion and scalar sectors, mostly based on the OS scheme. Since the renormalization of the scalar mixing angles potentially violates the GFP independence of the electroweak one-loop partial decay widths, we review several renormalization schemes and their GFP dependence and independence in a detailed overview in Sec. 5.3. Finally, in Sec. 5.4 we present the renormalization scheme for the soft-$\mathbb{Z}_2$-breaking parameter m_{12}^2 applied in our work.

5.1. Renormalization of the Tadpoles

In the literature, there are two different approaches for determining the VEVs at loop level, and the exact definitions of all CTs of the 2HDM depend on the chosen renormalization of the VEVs. The difference between the two schemes was analyzed in detail in [226] for the 2HDM. In the following, we therefore only briefly recapitulate the key ideas of the two schemes.

In the *standard (tadpole) scheme*, commonly used in electroweak calculations of the SM [183] and the 2HDM [222, 230], the VEVs are determined through the loop-corrected scalar potential. Since the VEVs represent the minimum states of the potential, the renormalization of the tadpole terms in Eqs. (4.22) and (4.23) is tightly connected to the NLO treatment of the VEVs. In the standard scheme, the tadpole parameters are promoted to one-loop order by splitting them into their renormalized values and their CTs as follows,

$$T_i \to T_i + \delta T_i \quad (i = 1, 2) . \tag{5.1}$$

Demanding the minimum conditions of Eq. (4.24) to hold at one-loop order for the loop-corrected potential implies that the renormalized tadpole parameters vanish again:

$$T_i = 0 \quad (i = 1, 2) . \tag{5.2}$$

As a consequence of this condition, the tadpole CTs in the standard scheme are given by[20] Eq. (B.1). By promoting the tadpole terms to one-loop order in Eq. (5.1), the rotated tadpole terms in Eqs. (4.35) to (4.37) receive CT contributions as well, all of which are functions of the CTs δT_i already fixed through Eq. (B.1). The resulting CTs of the rotated tadpole parameters in the standard tadpole scheme are presented in App. B.1 for convenience.

The loop-corrected scalar potential of the 2HDM is manifestly GFP-dependent. Hence, fixing the minima of this potential through Eq. (4.24) necessarily leads to loop-corrected VEVs which are manifestly GFP-dependent quantities. As a consequence, all renormalized parameters and their CTs defined through these loop-corrected VEVs become GFP-dependent quantities as well. As discussed in Sec. 3.6, such a GFP dependence of the CTs is acceptable as long as in the calculation of a physical observable, all GFP dependences arising from different parts of the calculation cancel with each other. In the 2HDM, however, the standard tadpole scheme requires a specific form of GFP dependence which needs to be included in the CTs of the scalar mixing angles in order to cancel the GFP dependences of the full partial decay widths for decay processes involving these mixing angle CTs. Renormalizing the mixing angles in schemes as suggested *e.g.* in [222] leads to the inclusion of GFP dependences in the definitions of their CTs which do not match the GFP dependences arising in other parts of the calculation of the partial decay widths. Instead, these schemes introduce additional intricate GFP-dependent terms and hence they break the GFP independence of the full one-loop partial decay width. From a technical point of view, the application of the standard tadpole scheme complicates tracing the various cancellations of all GFP dependences in the one-loop calculation, since in general all CTs defined through the GFP-dependent VEVs contribute GFP-dependent terms to the decay amplitudes.

In order to more systematically remove the GFP-dependent terms from the one-loop partial decay widths, an alternative treatment of the minimum conditions can be applied. Such an approach was first established in the SM in [231] and extended to the 2HDM for the first time in [226, 227]. We refer to this scheme as *alternative (FJ tadpole) scheme* in the following. The key idea of this alternative scheme is to consider the VEVs as the fundamental quantities which are promoted to higher orders and whose values are fixed through the tree-level scalar

---

[20]Note that the tadpole terms and diagrams in Eq. (B.1) are defined in the mass basis, related to the corresponding terms in the gauge basis by means of the rotation matrix R_α, cf. Eq. (4.31).

Figure 5.1.: Topological contributions to the one-loop self-energy. In the standard tadpole scheme, we consider the usual 1PI self-energy $\Sigma(p^2)$ while in the alternative FJ tadpole scheme, the self-energy $\Sigma^{\text{tad}}(p^2)$ additionally contains contributions from the tadpole topology. For the actual calculations of the 2HDM self-energies, the full particle content of the 2HDM has to be inserted into these topologies.

potential. This is in contrast to the standard scheme, where the fundamental quantities are the tadpole terms which are promoted to higher orders and where the VEVs are fixed through the loop-corrected potential. Since the VEVs are connected to the tree-level potential in the alternative scheme, they *a priori* do not represent the proper minimum at one-loop level, however. In order to maintain the proper minimum conditions at one-loop order, it is therefore necessary to split the VEVs into renormalized VEVs and their CTs as

$$v_i \to v_i + \delta v_i \quad (i = 1, 2) . \tag{5.3}$$

By imposing the condition that the tree-level VEVs represent the proper minimum of the scalar potential even at one-loop order, all effects of the shift of the minima are allocated to the CTs of the VEVs δv_i, which directly connects them to the genuine tadpole diagrams as depicted in Eq. (B.11). As a consequence of the VEV shifts, explicit tadpole topologies have to be considered in the calculation of all vertex corrections to the Higgs decay widths as well as in all self-energies. The latter case is depicted in Fig. 5.1 where apart from the generic 1PI one-loop self-energy $\Sigma(p^2)$ we moreover show the generic self-energy $\Sigma^{\text{tad}}(p^2)$ which additionally contains one-loop contributions from the tadpole diagrams. All implications of the alternative FJ scheme on the renormalization of the tadpoles were presented in [226] for the 2HDM for the first time and are summarized in App. B.1 for convenience.

The application of the alternative FJ tadpole scheme has several important consequences for the calculation of the Higgs decay widths at one-loop order. In this scheme, the VEVs are defined through the proper minimum of the scalar potential, *i.e.* the renormalized VEVs represent the tree-level minima to one-loop order as well. Due to this, the VEVs are manifestly GFP-independent and consequently, all quantities defined through these VEVs, *e.g.* the masses of all particles of the 2HDM as well as their CTs, become manifestly GFP-independent, as well. Moreover, applying the alternative FJ tadpole scheme allows for a GFP-independent definition of the mixing angle CTs, since the one-loop decay amplitude calculated within this tadpole scheme, but with the mixing angle CTs set to zero, is already a manifestly GFP-independent quantity. Consequently, by defining the mixing angle CTs in a GFP-independent scheme, the full partial decay width maintains the GFP independence as well. We come back to this point in Sec. 5.3 where we present all renormalization schemes of the mixing angle CTs that are considered in this work.

5.2. Renormalization of the Gauge, Scalar and Fermion Sectors

The renormalization of the gauge, scalar and fermion sectors is mostly performed in the OS scheme. Since the gauge and fermion sectors of the 2HDM are essentially the same as

those of the SM, we adopt the OS schemes presented in [183] for these sectors. For the renormalization of the scalar doublets of the 2HDM, we impose OS conditions as generically described in Sec. 3.2. In the following, we only briefly summarize the renormalization of the gauge, scalar and fermion sectors and refer to [226, 227] for a detailed description of the renormalization of the 2HDM.

Renormalization of the gauge sector
For the renormalization of the gauge sector, we split each parameter belonging to the weak sector into its renormalized value and its CT and introduce one-loop WFRCs for the gauge boson fields as follows,

$$m_W^2 \rightarrow m_W^2 + \delta m_W^2 \ , \tag{5.4}$$

$$m_Z^2 \rightarrow m_Z^2 + \delta m_Z^2 \ , \tag{5.5}$$

$$e \rightarrow e\left(1 + \delta Z_e\right) \ , \tag{5.6}$$

$$g \rightarrow g + \delta g \ , \tag{5.7}$$

$$\alpha_{\rm em} \rightarrow \alpha_{\rm em} + \delta\alpha_{\rm em} \equiv \alpha_{\rm em} + 2\alpha_{\rm em}\delta Z_e \ , \tag{5.8}$$

$$W_\mu^\pm \rightarrow \left(1 + \frac{\delta Z_{WW}}{2}\right) W_\mu^\pm \ , \tag{5.9}$$

$$\begin{pmatrix} Z \\ \gamma \end{pmatrix} \rightarrow \begin{pmatrix} 1 + \dfrac{\delta Z_{ZZ}}{2} & \dfrac{\delta Z_{Z\gamma}}{2} \\ \dfrac{\delta Z_{\gamma Z}}{2} & 1 + \dfrac{\delta Z_{\gamma\gamma}}{2} \end{pmatrix} \begin{pmatrix} Z \\ \gamma \end{pmatrix} \ . \tag{5.10}$$

As can be inferred from Eq. (4.63), from the five constants presented in Eqs. (5.4) to (5.8), we only use m_W^2, m_Z^2 and $\alpha_{\rm em}$ as independent parameters. Nevertheless, we additionally introduce CTs for the coupling constants e and g for later convenience. We impose OS conditions for the renormalization of all CTs and WFRCs of the gauge sector. The corresponding generic formulae from Eqs. (3.12) to (3.14) can be straightforwardly adapted to the gauge bosons by replacing the self-energies in these formulae with the transverse parts of the gauge boson self-energies. In the framework of the alternative tadpole scheme, all self-energies additionally contain tadpole contributions, cf. Fig. 5.1. For the renormalization of the electromagnetic coupling constant e, we impose the same condition as presented in [183], *i.e.* we define δZ_e via the vertex corrections to the OS $e^+e^-\gamma$ coupling. In our case, however, we do not impose this condition in the Thomson limit but instead, we consider e to be renormalized at the scale of the Z boson mass. All CTs and WFRCs of the gauge sector defined in this OS scheme are presented explicitly in App. B.2.

Renormalization of the scalar sector
The masses and fields of all scalar particles of the 2HDM are promoted to one-loop order by the introduction of mass CTs and WFRCs. For the unphysical Goldstone bosons, no mass CTs are introduced since they remain massless to higher orders and only receive effective mass terms through the gauge-fixing Lagrangian after the renormalization is completed, cf. Eqs. (4.57) and (4.58). In order to cancel all UV divergences for the calculation of the decay amplitudes, the Goldstone boson fields acquire non-vanishing WFRCs, however. The corresponding renormalized squared masses, mass CTs and WFRCs are introduced as follows,

$$m_H^2 \rightarrow m_H^2 + \delta m_H^2 \ , \tag{5.11}$$

$$m_h^2 \rightarrow m_h^2 + \delta m_h^2 \ , \tag{5.12}$$

$$m_A^2 \rightarrow m_A^2 + \delta m_A^2 \ , \tag{5.13}$$

$$m_{H^\pm}^2 \rightarrow m_{H^\pm}^2 + \delta m_{H^\pm}^2 \ , \tag{5.14}$$

$$\begin{pmatrix} H \\ h \end{pmatrix} \rightarrow \begin{pmatrix} 1 + \dfrac{\delta Z_{HH}}{2} & \dfrac{\delta Z_{Hh}}{2} \\ \dfrac{\delta Z_{hH}}{2} & 1 + \dfrac{\delta Z_{hh}}{2} \end{pmatrix} \begin{pmatrix} H \\ h \end{pmatrix} , \tag{5.15}$$

$$\begin{pmatrix} G^0 \\ A \end{pmatrix} \rightarrow \begin{pmatrix} 1 + \dfrac{\delta Z_{G^0 G^0}}{2} & \dfrac{\delta Z_{G^0 A}}{2} \\ \dfrac{\delta Z_{A G^0}}{2} & 1 + \dfrac{\delta Z_{AA}}{2} \end{pmatrix} \begin{pmatrix} G^0 \\ A \end{pmatrix} , \tag{5.16}$$

$$\begin{pmatrix} G^\pm \\ H^\pm \end{pmatrix} \rightarrow \begin{pmatrix} 1 + \dfrac{\delta Z_{G^\pm G^\pm}}{2} & \dfrac{\delta Z_{G^\pm H^\pm}}{2} \\ \dfrac{\delta Z_{H^\pm G^\pm}}{2} & 1 + \dfrac{\delta Z_{H^\pm H^\pm}}{2} \end{pmatrix} \begin{pmatrix} G^\pm \\ H^\pm \end{pmatrix} . \tag{5.17}$$

The generic formulae for the renormalization of scalar multiplets presented in Eqs. (3.12) to (3.14) can be directly applied to the scalar particles of the 2HDM. The resulting explicit forms of the CTs and WFRCs are presented in App. B.3.

Renormalization of the fermion sector

We introduce CTs for all fermion masses, the CKM matrix elements as well as for the Yukawa coupling parameters defined in Table 4.2 and additionally introduce WFRCs for all fermionic fields f_i of the 2HDM as follows,

$$m_f \rightarrow m_f + \delta m_f , \tag{5.18}$$

$$V_{ij} \rightarrow V_{ij} + \delta V_{ij} , \tag{5.19}$$

$$Y_i \rightarrow Y_i + \delta Y_i , \tag{5.20}$$

$$f_i^L \rightarrow \sum_j \left(\delta_{ij} + \frac{\delta Z_{ij}^{f,L}}{2} \right) f_j^L , \tag{5.21}$$

$$f_i^R \rightarrow \sum_j \left(\delta_{ij} + \frac{\delta Z_{ij}^{f,R}}{2} \right) f_j^R . \tag{5.22}$$

The generic formulae for the OS definition of the mass CTs and WFRCs from Eqs. (3.12) to (3.14) can again be straightforwardly adapted to the case of the fermion self-energies. In this case, the self-energy contributions are split up according to their chiral structures as outlined in [183]. The CTs δY_i of the Yukawa coupling parameters are not independent CTs but instead, they are functions of the CTs of the scalar mixing angles whose renormalization is discussed in the subsequent Sec. 5.3. For the renormalization of the CKM matrix elements, several schemes were proposed in the literature [183, 232–237]. Using the scheme proposed in [183] leads to an inclusion of intricate GFP-dependent terms originating from the off-diagonal fermion WFRCs into the calculation of one-loop partial decay widths which involve the CTs of the CKM matrix elements. Since the CKM matrix is approximately a unit matrix [98], the numerical effects of these GFP-dependent terms are typically small, but nevertheless, the complete one-loop partial decay widths involving these CTs become manifestly GFP-dependent. For our work, we employ the CKM matrix renormalization scheme presented in [236] which allows for a manifestly GFP-independent definition of the CTs of the CKM matrix elements. The explicit definitions of all CTs and WFRCs of the fermion sector are presented in App. B.4.

5.3. Renormalization of the Scalar Mixing Angles α and β

The scalar mixing angles α and β are promoted to one-loop order by splitting them into their renormalized values and their CTs as follows,

$$\alpha \to \alpha + \delta\alpha \, , \tag{5.23}$$

$$\beta \to \beta + \delta\beta \, . \tag{5.24}$$

The renormalization of the scalar mixing angles is a non-trivial task. While for physical fields and masses physically motivated renormalization schemes, *e.g.* the OS scheme, can be applied, there is no analogon of an obvious physical renormalization scheme for the scalar mixing angles. This situation is similar in the MSSM, where the scalar mixing angle β needs to be renormalized. In [238], three desirable criteria for the renormalization of this mixing angle were suggested:

- **GFP independence:** The definition of the mixing angle CT shall not introduce intricate uncanceled GFP dependences into the calculation of the one-loop partial decay widths.

- **Numerical stability:** The renormalization scheme imposed on the scalar mixing angle shall not introduce unnaturally large contributions to the finite terms of the mixing angle CT and consequently also to the full partial decay width. More specifically, the finite term of the mixing angle CT shall not introduce large uncanceled contributions to the one-loop partial decay widths such that they become orders of magnitude larger than the decay widths at tree level.

- **Process independence:** The mixing angle CT shall not be defined via a physical decay process.

In [238], a no-go theorem was formulated which states that for the MSSM, no renormalization scheme for the scalar mixing angle β exists that fulfills all of the three aforementioned criteria simultaneously. In [56, 216, 226, 227], these criteria were adopted to the case of the two mixing angles in the 2HDM and several different renormalization schemes were analyzed with respect to the fulfillment of these criteria. In the following, we present an overview over these schemes, all of which are implemented in the program package 2HDECAY developed in this thesis.

$\overline{\text{MS}}$ scheme
The application of the $\overline{\text{MS}}$ scheme is among the simplest renormalization schemes for the mixing angle CTs. It was analyzed in [226, 239] that the renormalization of $\delta\alpha$ and $\delta\beta$ in the $\overline{\text{MS}}$ scheme can lead to one-loop-corrected partial decay widths that are orders of magnitude larger than the tree level widths[21]. Moreover, in the framework of the standard tadpole scheme, an $\overline{\text{MS}}$ condition for the mixing angle CTs breaks the GFP independence of the one-loop decay amplitude since per definition, the finite parts of the mixing angle CTs vanish and hence do not contribute GFP-dependent terms which could cancel the GFP dependences appearing in the residual decay amplitude in the standard scheme. Nevertheless, we consider this scheme in this work as a reference. Imposing the $\overline{\text{MS}}$ condition on the mixing angle CTs means that only the UV-divergent parts proportional to Δ, cf. Eq. (3.2), are allocated to the CTs $\delta\alpha$ and $\delta\beta$, while no finite parts are assigned to these CTs. The resulting CTs are presented in App. B.5.1.

KOSY scheme
The KOSY scheme, named after the authors' initials, was first proposed in [222] in the

---

[21]On the other hand, a detailed analysis performed in [229] showed that the $\overline{\text{MS}}$ renormalization of the mixing angle CTs can be useful for certain decay processes when they involve a partial cancellation of large contributions stemming from the tadpoles. This is not the case for any of the Higgs boson decay processes considered in our work, however.

framework of the standard tadpole scheme. The key idea in this approach is to consider an alternative real symmetric matrix $\sqrt{Z_{\tilde{\phi}}}$ containing the WFRCs for each scalar doublet in the gauge basis, denoted by $\tilde{\phi}$, which is connected to the mass basis through an expansion of the rotation matrix at one-loop order. This yields an alternative WFRC matrix in the mass basis,

$$\sqrt{Z_{\phi}^{\text{KOSY}}} \approx R_{\delta\theta}^{T} R_{\theta}^{T} \sqrt{Z_{\tilde{\phi}}} R_{\theta} \approx \begin{pmatrix} 1 + \dfrac{\delta Z_{\phi_1\phi_1}}{2} & \delta C_{\phi} + \delta\theta \\ \delta C_{\phi} - \delta\theta & 1 + \dfrac{\delta Z_{\phi_2\phi_2}}{2} \end{pmatrix} , \tag{5.25}$$

where the rotation matrix R_{θ} is defined in Eq. (4.31) and the constants $\delta Z_{\phi_1\phi_1}$, $\delta Z_{\phi_2\phi_2}$ and δC_{ϕ} denote the three independent parameters of the matrix $\sqrt{Z_{\tilde{\phi}}}$. Comparing Eq. (5.25) with Eqs. (5.15) to (5.17) reveals a connection between the scalar mixing angle CTs $\delta\theta \in \{\delta\alpha, \delta\beta\}$ and the WFRCs of the scalar sector. Since the latter are defined in the OS scheme in our case, the KOSY approach hence yields an OS-motivated[22] scheme for the scalar mixing angles. The renormalization of the mixing angles is applied *after* the rotation from the gauge to the mass basis is performed, when the tree-level relation in Eq. (4.56) is satisfied. Hence, the mixing angle β diagonalizes the CP-odd and charged sectors simultaneously, but since we do not have enough free constants in Eq. (5.25) for both the CP-odd and the charged sectors, we are not able to apply the OS conditions for the definition of the mixing angle CT $\delta\beta$ through the CP-odd and charged sectors simultaneously. Instead, we have to choose through which of the two sectors the CT $\delta\beta$ shall be defined. In our work, we define $\delta\beta$ either solely through the CP-odd or solely through the charged sector, which we refer to as $\delta\beta^o$ and $\delta\beta^c$ respectively. While the KOSY scheme is process-independent and typically leads to moderate one-loop corrections, hence featuring numerical stability in the aforementioned sense, it introduces an explicit GFP dependence into the calculation of the partial decay widths at one-loop order. The situation is unchanged in the framework of the alternative FJ tadpole scheme, where again uncanceled GFP dependences are introduced. We nevertheless consider the KOSY scheme in both tadpole schemes and implement them into `2HDECAY` since the partial decay widths calculated in these schemes serve as a reference for a comparison with the ones computed in other schemes. The resulting explicit formulae for the mixing angle CTs in the KOSY scheme are presented in App. B.5.2.

p_*-pinched scheme

One approach of avoiding the GFP dependence of the KOSY scheme but keeping its OS-motivated definition is the p_*-*pinched scheme* [226, 227] which is based on the PT [201–208]. The main drawback of the KOSY scheme is the fact that it does not allow for an unambiguous extraction of the gauge-dependent parts of the full partial decay widths. As a first step to solve this problem, the one-loop partial decay widths are evaluated within the alternative FJ tadpole scheme instead of the standard one. As briefly mentioned at the end of Sec. 5.1, this tadpole scheme requires the CTs $\delta\alpha$ and $\delta\beta$ to be manifestly GFP-independent quantities. By defining the mixing angle CTs in the same OS-motivated approach as in the KOSY scheme, but by using the manifestly GFP-independent pinched scalar self-energies instead of the usual self-energies $\Sigma^{\text{tad}}(p^2)$ with tadpole contributions included, this scheme leads to manifestly GFP-independent partial decay widths at one-loop level. The definition of the mixing angle CTs via the pinched self-energies in this scheme leaves the additional freedom at which scale p^2 the CTs shall be defined. In the p_*-pinched scheme, we follow the approach of [240] in the MSSM and evaluate the CTs at the p_* scale given by

$$p_*^2 \equiv \frac{m_i^2 + m_j^2}{2} , \tag{5.26}$$

---

[22]Following the argument presented in [216], we do not denote the KOSY scheme as a true OS scheme for the scalar mixing angles, since $\delta\alpha$ and $\delta\beta$ are defined through off-diagonal WFRCs in the KOSY scheme, which have no interpretation in the sense of physical OS quantities.

where m_i and m_j denote the masses of the scalar particles h_i and h_j whose self-energy transition $\Sigma_{h_i h_j}(p^2)$ is considered. As shown in [226] for the 2HDM for the first time, the pinched self-energies are equivalent to the usual self-energies $\Sigma^{\mathrm{tad}}(p^2)$ with tadpole contributions evaluted in the Feynman-'t Hooft gauge, *i.e.* $\xi_V = 1$ ($V \in \{W^\pm, Z, \gamma\}$), up to additional UV-finite contributions $\Sigma^{\mathrm{add}}(p^2)$. These additional contributions identically vanish for $p^2 = p_*^2$, however. Hence, the mixing angle CTs are solely defined through $\Sigma^{\mathrm{tad}}(p_*^2)$ at $\xi_V = 1$. The resulting mixing angle CTs in the p_*-pinched scheme are presented in App. B.5.3. Since they are manifestly GFP-independent, process-independent and yield moderate NLO corrections to the partial decay widths as analyzed in [227, 228], the p_*-pinched scheme is a prime candidate for a renormalization scheme of the scalar mixing angles fulfilling all three of the aforementioned desirable criteria simultaneously.

OS-pinched scheme
The *OS-pinched scheme* [226, 227] is another OS-motivated definition of the mixing angle CTs, closely related to the p_*-pinched scheme from which it differs solely by the scale p^2 at which the mixing angle CTs are defined. In the OS-pinched scheme, this scale is chosen analogously to the original scale definition of the KOSY scheme, *i.e.* the scale p^2 in the pinched self-energies, introduced through the connection to the off-diagonal WFRCs, is set to the corresponding squared scalar masses as in the KOSY scheme. In this case, the additional UV-finite self-energy contributions $\Sigma^{\mathrm{add}}(p^2)$, derived in [226] for the 2HDM, are non-zero and need to be included in the definition of $\delta\alpha$ and $\delta\beta$. The resulting mixing angle CTs are explicitly presented in App. B.5.4. Analogous to the p_*-pinched scheme, the mixing angle CTs defined in the OS-pinched scheme are manifestly GFP-independent, process-independent and their application typically leads to moderate NLO corrections [227, 228], hence fulfilling the three aforementioned desirable criteria simultaneously as well.

Process-dependent schemes
The connection of the definition of a mixing angle CT with an observable, *e.g.* a partial decay width, was proposed for the mixing angle β in the MSSM in [238, 241] and for α and β in the 2HDM in [242]. Such a scheme is per definition process-dependent, *i.e.* the mixing angle CTs become functions of genuine vertex corrections and other CT contributions to loop-corrected decay processes. Due to this, the definition of the mixing angle CTs is technically more involved and moreover, the CTs themselves can become numerically large due to uncanceled contributions stemming from the vertex corrections. Hence, these schemes can often lead to numerical instabilities. On the other hand, since the mixing angle CTs are defined via observables, using the process-dependent scheme automatically leads to manifestly GFP-independent one-loop partial decay widths. For the definition of the mixing angle CTs in the 2HDM, many possible processes could be considered through which the CTs could be defined. Independent of the chosen decay $\phi \longrightarrow X_1 X_2$ of a Higgs boson ϕ to two other particles X_1 and X_2, the common idea of a process-dependent scheme is to equate the partial decay widths of the chosen process at LO and NLO,

$$\Gamma^{\mathrm{LO}}_{\phi X_1 X_2} \equiv \Gamma^{\mathrm{NLO}}_{\phi X_1 X_2} \equiv \Gamma^{\mathrm{LO}}_{\phi X_1 X_2} \left(1 + 2 \, \mathrm{Re} \left[\mathcal{F}^{\mathrm{VC}}_{\phi X_1 X_2} + \mathcal{F}^{\mathrm{CT}}_{\phi X_1 X_2} \right] \right), \tag{5.27}$$

where we introduce form factors $\mathcal{F}^{\mathrm{VC}}_{\phi X_1 X_2}$ and $\mathcal{F}^{\mathrm{CT}}_{\phi X_1 X_2}$ for the genuine vertex corrections and the CT contributions including the WFRCs, respectively and where we exclude real corrections to the decay width as further described below. This condition can be reformulated as follows,

$$\mathrm{Re} \left[\mathcal{F}^{\mathrm{CT}}_{\phi X_1 X_2} \right] = -\mathrm{Re} \left[\mathcal{F}^{\mathrm{VC}}_{\phi X_1 X_2} \right]. \tag{5.28}$$

The form factor $\mathcal{F}^{\mathrm{CT}}_{\phi X_1 X_2}$ contains, amongst other CTs and WFRCs, either one or both mixing angle CTs $\delta\alpha$ and $\delta\beta$. Hence, the reformulated renormalization condition in Eq. (5.28) can

be solved for the mixing angle CTs which consequently become functions of a combination of CTs and WFRCs of the 2HDM as well as of the genuine vertex corrections $\mathcal{F}^{\text{VC}}_{\phi X_1 X_2}$. Care has to be taken when the chosen process involves charged particles in the initial or final states due to the appearance of IR divergences in the vertex corrections and hence, also in the definition of the mixing angle CTs, which is disfavored [238]. In order to circumvent this problem, a process can be chosen which either does not contain charged particles in the initial or final states or whose genuine IR-divergent QED-like contributions in the vertex corrections form a UV-finite subset which is excluded from the renormalization condition, hence justifying the approach of not including real corrections in the renormalization condition in Eq. (5.27). The former case is unfavorable in the 2HDM due to the intricate structure of the mixing angle CTs which would arise by solely using neutral-current decay channels[23]. In the latter case, Eq. (5.28) contains only genuine weak contributions everywhere, *i.e.* the IR-divergent QED-like contributions are neglected in both of the two form factors $\mathcal{F}^{\text{VC}}_{\phi X_1 X_2}$ and $\mathcal{F}^{\text{CT}}_{\phi X_1 X_2}$. In our work, we have chosen three different combinations of decay processes of the CP-even and CP-odd Higgs bosons into pairs of tauons, all of which are implemented in `2HDECAY`:

1. define $\delta\beta$ via $A \to \tau^+ \tau^-$ and subsequently $\delta\alpha$ via $H \to \tau^+ \tau^-$,

2. define $\delta\beta$ via $A \to \tau^+ \tau^-$ and subsequently $\delta\alpha$ via $h \to \tau^+ \tau^-$

3. and define $\delta\alpha$ and $\delta\beta$ simultaneously via $h \to \tau^+ \tau^-$ and $H \to \tau^+ \tau^-$.

The resulting explicit forms of the mixing angle CTs for these three combinations are presented in App. B.5.5. While their forms are the same for both the standard and alternative FJ tadpole scheme, the actual values of the mixing angle CTs differ between these two schemes. On the other hand, the full one-loop partial decay width is independent of the chosen tadpole renormalization when the mixing angle CTs are defined in a process-dependent scheme.

Physical OS scheme
In a process-dependent scheme, the mixing angle CTs are functions of not only S matrix elements, but moreover of other CTs and WFRCs of the theory as well. In order to exploit the advantageous feature of these schemes, namely their manifest GFP independence, while simultaneously avoiding their shortcomings, *i.e.* potentially large NLO corrections stemming from uncanceled contributions between the vertex corrections and the WFRCs and CTs, the mixing angle CTs can be defined purely through S matrix elements, only. Such a *physical OS scheme* was proposed for the renormalization of the quark mixing matrix in the SM in [243] and for $\delta\alpha$ and $\delta\beta$ in the 2HDM in [216]. In the following, we only briefly review the physical OS scheme while for a detailed derivation in the 2HDM, we refer to the latter reference. Solely for the purpose of renormalizing the mixing angles, the 2HDM is temporarily extended by adding two right-handed fermion singlets $\nu_{i\text{R}}$ ($i = 1, 2$) to the 2HDM Lagrangian, together with imposing an additional discrete $\mathbb{Z}_2$ symmetry under which the singlets transform as

$$\nu_{1\text{R}} \to -\nu_{1\text{R}} \ , \tag{5.29}$$

$$\nu_{2\text{R}} \to \nu_{2\text{R}} \ , \tag{5.30}$$

and which prevents the mixture of different lepton generations for simplicity[24]. Due to the additional two right-handed neutrino singlets, the mechanism of EWSB now generates mass

---

[23]Suitable decays for the neutral-current process-dependent renormalization of the mixing angles involve two-body decays with neutral initial and final states for which the mixing angles appear at tree level in the corresponding coupling constants. This is the case for all Higgs decays to fermions, but since these always involve charged particles in the final state, they can not be used. Other candidates are $h/H \to Z A$ or $h/H \to Z Z$, but these decays only allow for a definition of the CT combination $\delta\alpha - \delta\beta$ but not for a definition of the CTs separately. The only remaining candidates are the neutral-current Higgs-to-Higgs decays $h/H \to A A$ or $H \to h h$, but due to the structures of the corresponding coupling constants, their application leads to intricate definitions of the mixing angle CTs.

[24]The mixing of neutrino generations is observed in nature in form of neutrino oscillations [116] and theoretically described by the *Pontecorvo–Maki–Nakagawa–Sakata* (PMNS) neutrino mixing matrix [244, 245]. The addi-

terms for two arbitrarily chosen neutrinos ν_j ($j = 1, 2$) in the mass basis[25], together with tree-level couplings between the massive neutrinos and the Higgs bosons, all of which are proportional to new Yukawa coupling constants y_{ν_j}. The limit $y_{\nu_j} \to 0$ is then the 2HDM limit in which the neutrinos become massless again and the contributions from the right-handed neutrino singlets decouple. The CT of the mixing angle α is fixed by demanding a modified process-dependent renormalization condition. Instead of imposing a condition equivalent to Eq. (5.28), it is proposed in [216] to impose the condition that the *ratios* of the amplitudes of two Higgs decays into massive neutrinos are the same at tree level and one-loop order. Consequently, choosing the decay into a pair of *e.g.* massive ν_1 neutrinos leads to the condition

$$\frac{\mathcal{A}^{\text{NLO}}_{H\bar{\nu}_1\nu_1}}{\mathcal{A}^{\text{NLO}}_{h\bar{\nu}_1\nu_1}} \equiv \frac{\mathcal{A}^{\text{LO}}_{H\bar{\nu}_1\nu_1}}{\mathcal{A}^{\text{LO}}_{h\bar{\nu}_1\nu_1}} \ , \tag{5.31}$$

while choosing the decay into the second pair of massive neutrinos leads to the condition

$$\frac{\mathcal{A}^{\text{NLO}}_{H\bar{\nu}_2\nu_2}}{\mathcal{A}^{\text{NLO}}_{h\bar{\nu}_2\nu_2}} \equiv \frac{\mathcal{A}^{\text{LO}}_{H\bar{\nu}_2\nu_2}}{\mathcal{A}^{\text{LO}}_{h\bar{\nu}_2\nu_2}} \ . \tag{5.32}$$

Either of these two conditions can be solved for $\delta\alpha$. Imposing this process-dependent definition on the ratios has the advantage that contributions appearing universally in both decays in the nominator and denominator cancel against each other. As a consequence, the mixing angle CT $\delta\alpha$ is defined solely through the CP-even Higgs WFRCs as well as through genuine vertex corrections to the tree-level vertices of the CP-even Higgs bosons h/H and the massive neutrinos ν_j. For the definition of the CT for the mixing angle β, analogous conditions can be imposed. In [216], it is suggested that one of the following conditions can be chosen,

$$\frac{\mathcal{A}^{\text{NLO}}_{A\bar{\nu}_1\nu_1}}{\mathcal{A}^{\text{NLO}}_{H\bar{\nu}_1\nu_1}} \equiv \frac{\mathcal{A}^{\text{LO}}_{A\bar{\nu}_1\nu_1}}{\mathcal{A}^{\text{LO}}_{H\bar{\nu}_1\nu_1}} \ , \tag{5.33}$$

$$\frac{\mathcal{A}^{\text{NLO}}_{A\bar{\nu}_2\nu_2}}{\mathcal{A}^{\text{NLO}}_{H\bar{\nu}_2\nu_2}} \equiv \frac{\mathcal{A}^{\text{LO}}_{A\bar{\nu}_2\nu_2}}{\mathcal{A}^{\text{LO}}_{H\bar{\nu}_2\nu_2}} \ . \tag{5.34}$$

However, the drawback of these conditions is that Eq. (5.33) leads to a definition of $\delta\beta$ which becomes singular for $c_\beta \to 0$ while Eq. (5.34) leads to a singular behavior for $s_\beta \to 0$. While these singularities might not be relevant for any phenomenological analysis of the 2HDM, this singular behavior still can lead to numerical instabilities in certain corners of the parameter space. In order to circumvent this problem, a third condition is suggested in [216]. By introducing form factors as follows,

$$\mathcal{A}^{\text{(N)LO}}_{H/h\bar{\nu}_j\nu_j} \equiv \left[\bar{u}_{\nu_j} v_{\nu_j}\right] \widetilde{\mathcal{F}}^{\text{(N)LO}}_{H/h\bar{\nu}_j\nu_j} \ , \tag{5.35}$$

$$\mathcal{A}^{\text{(N)LO}}_{A\bar{\nu}_j\nu_j} \equiv \left[\bar{u}_{\nu_j} i\gamma_5 v_{\nu_j}\right] \widetilde{\mathcal{F}}^{\text{(N)LO}}_{A\bar{\nu}_j\nu_j} \ , \tag{5.36}$$

where the terms in brackets denote the full decay kinematics of the spinor chains of the massive neutrinos, the following renormalization condition is imposed,

$$0 = \frac{\widetilde{\mathcal{F}}^{\text{LO}}_{A\bar{\nu}_1\nu_1}}{c_\alpha \widetilde{\mathcal{F}}^{\text{LO}}_{H\bar{\nu}_1\nu_1} - s_\alpha \widetilde{\mathcal{F}}^{\text{LO}}_{h\bar{\nu}_1\nu_1}} c_\beta + \frac{\widetilde{\mathcal{F}}^{\text{LO}}_{A\bar{\nu}_2\nu_2}}{s_\alpha \widetilde{\mathcal{F}}^{\text{LO}}_{H\bar{\nu}_2\nu_2} + c_\alpha \widetilde{\mathcal{F}}^{\text{LO}}_{h\bar{\nu}_2\nu_2}} s_\beta \tag{5.37}$$

$$\equiv \frac{\widetilde{\mathcal{F}}^{\text{NLO}}_{A\bar{\nu}_1\nu_1}}{c_\alpha \widetilde{\mathcal{F}}^{\text{NLO}}_{H\bar{\nu}_1\nu_1} - s_\alpha \widetilde{\mathcal{F}}^{\text{NLO}}_{h\bar{\nu}_1\nu_1}} c_\beta + \frac{\widetilde{\mathcal{F}}^{\text{NLO}}_{A\bar{\nu}_2\nu_2}}{s_\alpha \widetilde{\mathcal{F}}^{\text{NLO}}_{H\bar{\nu}_2\nu_2} + c_\alpha \widetilde{\mathcal{F}}^{\text{NLO}}_{h\bar{\nu}_2\nu_2}} s_\beta \ ,$$

---

tional $\mathbb{Z}_2$ symmetry imposed on the neutrino singlets in the physical OS scheme prevents this mixing. We want to emphasize, however, that imposing this additional $\mathbb{Z}_2$ symmetry does not further restrict the considered model since in the original 2HDM without neutrino singlets, as considered in this work, neutrinos are assumed to be massless and hence, no neutrino mixing is present in the first place.

[25]We adopt the nomenclature of [216] and refer to the massive neutrinos as ν_1 and ν_2 instead of using flavor indices $\{e, \mu, \tau\}$, since ν_e, ν_μ and ν_τ are reserved for the three generations of *massless* neutrinos in our work.

i.e. it is demanded that the tree-level relation in the first line of Eq. (5.37) remains valid at one-loop level as well. The hereby defined CT $\delta\beta$ is free from numerical instabilities arising from specific regions of the parameter space. Out of all presented renormalization conditions, the three different combinations named and chosen in [216] are as follows:

- *OS1*: define $\delta\alpha$ via Eq. (5.31) and $\delta\beta$ via Eq. (5.33) ,

- *OS2*: define $\delta\alpha$ via Eq. (5.32) and $\delta\beta$ via Eq. (5.34) and

- *OS12*: define $\delta\alpha$ via Eq. (5.32) and $\delta\beta$ via Eq. (5.37) .

The resulting explicit forms of the mixing angle CTs are presented in App. B.5.6 and all three combinations are implemented as different renormalization schemes in `2HDECAY`. All genuine vertex corrections for the tree-level couplings of the Higgs bosons with the massive neutrinos, required for the definition of the mixing angle CTs, yield non-vanishing contributions even in the limit $y_{\nu_j} \to 0$. After the renormalization is imposed on the mixing angles in these schemes, this 2HDM limit is applied and the neutrino singlets are effectively removed from the model again. Analogous to the process-dependent definition, defining the mixing angle CTs in the physical OS schemes leads to an invariance of the one-loop partial decay width with respect to the chosen tadpole scheme. In our work, we therefore apply the physical OS scheme only in the framework of the alternative FJ tadpole scheme for simplicity.

Apart from the fact that the mixing angle CTs are defined solely through WFRCs and genuine vertex corrections, another crucial difference between the physical OS scheme and the other process-dependent schemes considered before lies in the definition of the renormalized values of the mixing angles themselves. In the process-dependent schemes, both the mixing angle CTs as well as their renormalized values are determined via Eq. (5.27), *i.e.* the measured values of α and β in the process-dependent scheme are determined by the measured values of the partial decay widths of the decays through which the mixing angle CTs are defined. In the physical OS scheme on the other hand, the mixing angle CTs are defined via Higgs decays to massive neutrinos. Since after the renormalization the 2HDM limit is applied and the neutrinos become massless again, the renormalization conditions in Eqs. (5.31) to (5.34) and (5.37) can not be directly applied to determine the measured values of the mixing angles in the physical OS scheme since the corresponding decays into massive neutrinos do not exist anymore in the 2HDM. Instead, their values are determined through the measured partial decay widths of other measurable decay channels.

Rigid symmetry scheme (BFMS scheme)
In the KOSY scheme, the mixing angle CTs are defined by temporarily switching between the mass and gauge bases which allows for a connection of the CTs with the scalar WFRCs in the mass basis. In an alternative approach, the rigid symmetry of the Lagrangian in the unbroken, *i.e.* symmetric, phase can be used to define the mixing angle CTs through alternative WFRCs. In this *rigid symmetry scheme*, a minimal set of WFRCs is introduced in the gauge basis of the 2HDM to ensure the UV finiteness of the calculated observables. Through a rotation and an introduction of the mixing angle CTs in the rotation matrices, the CTs $\delta\alpha$ and $\delta\beta$ can be connected to the rotated WFRCs which in general differ from the OS-defined WFRCs. Such a scheme is applied for renormalizing the SM in [246] and in [216] for defining the mixing angle CTs in the 2HDM. Since we only briefly present the key idea of the scheme here, we refer to the latter reference for details. In order to ensure GFP independence of the hereby defined CTs and the full one-loop partial decay widths, the WFRCs $\delta Z_{\hat{h}\hat{H}}$ and $\delta Z_{\hat{H}\hat{h}}$ used in the definition of the CTs are defined through the BFM [209–215] with $\hat{h}$ and $\hat{H}$ denoting the CP-even Higgs fields defined in the BFM framework. The CP-even self-energies required for the definition of these background-field WFRCs differ from the usual self-energies Σ^{tad} with tadpole contributions by the additional terms stated in App. B of [216]. Due to the close

connection between the PT and the BFM, these additional terms coincide with the additional terms derived in the PT framework, cf. Eq. (B.75). Consequently, the definition of the CT $\delta\alpha$ defined in the rigid symmetry scheme coincides with the definition of $\delta\alpha$ in the OS-pinched scheme. The CT $\delta\beta$ on the other hand is connected to the CP-even WFRCs as well due to the rigid symmetry and hence, the definition of the CT differs in comparison to the schemes based on the PT. Explicit forms of both mixing angle CTs in the rigid symmetry scheme are presented in App. B.5.7.

5.4. Renormalization of the Soft-$\mathbb{Z}_2$-Breaking Parameter m_{12}^2

The only remaining independent parameter which requires renormalization is the soft-$\mathbb{Z}_2$-breaking parameter m_{12}^2 which is split into a renormalized value and its CT as usual,

$$m_{12}^2 \to m_{12}^2 + \delta m_{12}^2 \ . \tag{5.38}$$

In contrast to *e.g.* the masses of the particles of the 2HDM, the parameter m_{12}^2 has no direct physical interpretation and hence, there is no straightforward OS definition which could be imposed in order to fix its CT. Since m_{12}^2 appears in the trilinear and quartic Higgs couplings, it is in principle possible to fix the CT δm_{12}^2 at one-loop order through a Higgs-to-Higgs decay. The renormalized value of m_{12}^2 would then depend on the measured value of the partial decay width of the chosen decay channel. Apart from the fact that Higgs-to-Higgs decay channels are rather difficult to measure directly in current collider experiments, it was found in [228] that such a process-dependent renormalization condition for δm_{12}^2 is additionally unfavorable from a theoretical perspective since it introduces genuine one-loop vertex corrections of the Higgs-to-Higgs decays into the finite parts of the CT. Due to this, δm_{12}^2 itself as well as partial decay widths containing this CT typically become orders of magnitude larger than the tree-level partial decay widths, thereby leading to a numerical instability of the one-loop calculation. Hence, for practical reasons, a process-dependent renormalization scheme for the soft-$\mathbb{Z}_2$-breaking parameter m_{12}^2 is not used in this work. Instead, we fix the CT in the $\overline{\text{MS}}$ scheme and the explicit form of the CT is given in App. B.6. Since Δ explicitly depends on the renormalization scale μ_R, the $\overline{\text{MS}}$-renormalized CT δm_{12}^2 depends on this scale at which the CT is defined as well and its value must be specified for the calculation of partial decay widths involving the renormalization of m_{12}^2.

Calculation of Higher-Order Higgs Boson Decays with 2HDECAY

The main objective of Part II of this thesis is the calculation of the electroweak one-loop corrections to the partial decay widths and branching ratios of all Higgs bosons of the 2HDM. To this end, the corresponding decay amplitudes need to be calculated and all parameters relevant for the electroweak corrections need to be renormalized. Due to the large amount of Feynman diagrams contributing to the different decay channels of all Higgs bosons of the 2HDM already at one-loop level, it is sensible that the calculation of the decay amplitudes is automated as far as possible.

In Sec. 6.1, we describe in detail which decay channels are considered in the calculation of the electroweak one-loop corrections and all approximations that are applied in the course of the computation. We introduce the computer routine 2HDMCalc which allows for a semi-automated calculation of all one-loop corrections to the decay amplitudes of the Higgs bosons of the 2HDM. In the subsequent Sec. 6.2, we explain the integration of all analytic results into the newly developed computer program 2HDECAY and introduce its main features. Moreover, we describe how the state-of-the-art QCD corrections implemented in HDECAY are combined with the electroweak one-loop corrections to the partial decay widths of the Higgs bosons of the 2HDM.

6.1. Calculation of the Electroweak Decay Widths with 2HDM-Calc

For the calculation of the electroweak corrections to the partial decay widths of the Higgs bosons of the 2HDM, we consider all OS decays that are not loop-induced and that acquire electroweak corrections at the one-loop level. For the 2HDM, this amounts to the following list of decays:

- $h/H/A \longrightarrow f \bar{f} \quad (f \bar{f} = s \bar{s}, c \bar{c}, b \bar{b}, t \bar{t}, \mu^- \mu^+, \tau^- \tau^+)$,

- $h/H \longrightarrow V V \quad (V V = Z Z, W^\pm W^\mp)$,

- $h/H \longrightarrow V S \quad (V S = Z A, W^\pm H^\mp)$,

- $h/H \longrightarrow S S \quad (S S = A A, H^\pm H^\mp)$,

- $H \longrightarrow h\,h$,

- $H^{\pm} \longrightarrow V\,S$ $(V\,S = W^{\pm}\,h,\, W^{\pm}\,H,\, W^{\pm}\,A)$,

- $H^{+} \longrightarrow f\,\bar{f}$ $(f\,\bar{f} = u\,\bar{s},\, u\,\bar{b},\, c\,\bar{d},\, c\,\bar{s},\, c\,\bar{b},\, t\,\bar{d},\, t\,\bar{s},\, t\,\bar{b},\, \nu_{\mu}\,\mu^{+},\, \nu_{\tau}\,\tau^{+})$,

- $A \longrightarrow V\,S$ $(V\,S = Z\,h,\, Z\,H,\, W^{\pm}\,H^{\mp})$.

While we calculate also the one-loop corrections to the decays of the Higgs bosons into pairs of fermions of the first generation,

- $h/H/A \longrightarrow f\,\bar{f}$ $(f\,\bar{f} = u\,\bar{u},\, d\,\bar{d},\, e^{-}\,e^{+})$,

- $H^{+} \longrightarrow f\,\bar{f}$ $(f\,\bar{f} = u\,\bar{d},\, \nu_{e}\,e^{+})$,

- $H^{-} \longrightarrow f\,\bar{f}$ $(f\,\bar{f} = d\,\bar{u},\, e^{-}\,\bar{\nu}_{e})$,

these decay channels are neglected in the implementation of the one-loop corrections in *2HDE-CAY* since they are overwhelmed by Dalitz decays $S \to f\,\bar{f}^{(')}\,\gamma$ $(S = h, H, A, H^{\pm})$ which are induced *e.g.* by the off-shell $\gamma^{*} \to f\,\bar{f}$ splitting.

For the calculation of the decay amplitudes and partial widths at tree level and NLO, we follow the approach described in Sec. 3.3. For each decay of a Higgs boson ϕ to any pair of other particles X_1 and X_2 presented in the aforementioned list, we calculate the tree-level amplitude $\mathcal{A}^{\mathrm{LO}}_{\phi X_1 X_2}$ as well as all genuine vertex corrections $\mathcal{A}^{\mathrm{VC}}_{\phi X_1 X_2}$ to the amplitude, shown generically in Figs. 3.3 and 3.4, respectively, by generating the Feynman diagrams and the corresponding decay amplitudes with the *Mathematica* [247] package *FeynArts 3.9* [248]. The 2HDM model file required for this is a slightly modified version of the model file contained in *FeynArts* in order to account for the lepton-specific and flipped 2HDM types as well.

The computation of the traces of the spinor structures and the reduction of the tensor integrals to scalar loop integrals [249] is performed with the *Mathematica* package *FeynCalc 8.2.0* [250, 251]. The CT amplitudes $\mathcal{A}^{\mathrm{CT}}_{\phi X_1 X_2}$ for all decays are generated by expanding the tree-level vertex $\mathcal{A}^{\mathrm{LO}}_{\phi X_1 X_2}$ to one-loop order. This includes the one-loop expansion of all required CTs and WFRCs that are defined through diagrammatic contributions in form of tadpole diagrams, self-energies and vertex corrections, that are calculated with the help of the tools *FeynArts* and *FeynCalc*.

All analytic results are combined according to Eqs. (3.18) and (3.23) to form the electroweak partial decay widths at tree level and NLO, respectively. For the latter quantity for all decays involving charged particles in the initial or final states, we additionally take into account the real corrections $\Gamma^{\mathrm{real}}_{\phi X_1 X_2 + \gamma}$. As described in Sec. 3.3, these real corrections are implemented fully analytically by adapting the generic formulae given in [182,183] to the case of the 2HDM decays. In our work, we regulate the corresponding IR-divergent integrals contained in both the real corrections and the vertex corrections containing virtual photons by introducing a photon mass as a regulator. For the real corrections, this photon mass is introduced as an additional parameter while in the calculation of the virtual corrections, *FeynArts* automatically introduces an infinitesimal photon mass to regularize the IR divergences. Due to the large number of considered decay channels and diagrammatic contributions at one-loop level, all the aforementioned steps are performed in a semi-automated way. To that end, the computer program *2HDMCalc* was developed which allows for the calculation of the two-body decays of the 2HDM Higgs bosons and which automatically converts the analytic results of the computations to *Fortran* 90 code. *2HDMCalc* can be obtained from

https://github.com/marcel-krause/2HDMCalc .
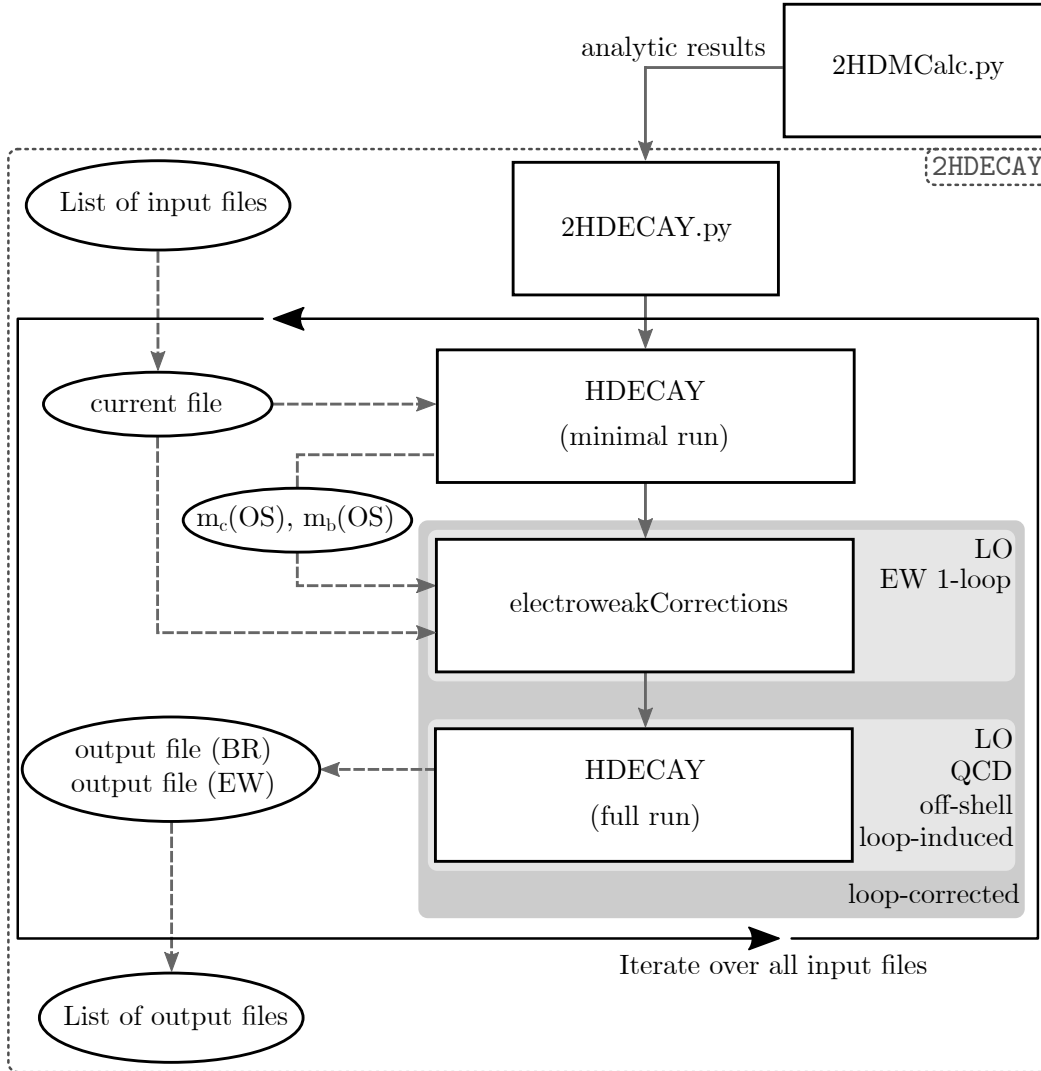
Figure 6.1.: Flowchart of 2HDECAY. The program consists of a main wrapper file 2HDECAY.py which iterates over all input files provided by the user. For each input file, the wrapper calls the subprograms HDECAY and electroweakCorrections. The program generates two output files for each input file, one containing the electroweak partial decay widths (EW) and one containing the branching ratios with and without the electroweak corrections (BR).

In this repository, we additionally provide the full analytic results of all contributions to the partial decay widths at tree level and one-loop order, including the analytic formulae of all tadpole diagrams, self-energies and vertex corrections required for the definition of all CTs and WFRCs of the 2HDM.

6.2. Description of 2HDECAY

All analytic results for all electroweak partial decay widths at tree level and one-loop order generated with the help of 2HDMCalc are implemented into the newly developed computer program 2HDECAY [56] which can be obtained from

<div align="center">https://github.com/marcel-krause/2HDECAY .</div>

The program combines the electroweak corrections to the non-loop-induced OS decays of all Higgs bosons of the 2HDM with the state-of-the-art QCD corrections already implemented in the program HDECAY 6.52 which can be obtained from

`http://tiger.web.psi.ch/hdecay` .

These corrections provided by HDECAY comprise

- the state-of-the-art QCD corrections to the partial decay widths, where applicable,

- the calculation of the loop-induced decays into the final states $g\,g$, $\gamma\,\gamma$ and $Z\,\gamma$, where apart from the final state $Z\,\gamma$, higher-order QCD corrections are taken into account and

- the calculation of partial decay widths for the following off-shell decays into final states containing an off-shell particle, denoted by an asterisk,

  ○ $h/H/A \;\longrightarrow\; t^*\bar{t}$,

  ○ $h/H \;\longrightarrow\; Z^*A$,

  ○ $h/H/A \;\longrightarrow\; W^{\pm*}H^{\mp}$,

  ○ $h/H \;\longrightarrow\; W^{\pm*}W^{\mp*}$,

  ○ $h/H \;\longrightarrow\; Z^*Z^*$,

  ○ $H^{\pm} \;\longrightarrow\; W^{\pm*}S \quad (S = h,\,H,\,A)$,

  ○ $H^+ \;\longrightarrow\; t^*\bar{f} \quad (\bar{f} = \bar{d},\,\bar{s},\,\bar{b})$,

  ○ $A \;\longrightarrow\; Z^*S \quad (S = h,\,H)$,

  ○ $h/H \;\longrightarrow\; A^*A$,

  ○ $H \;\longrightarrow\; h^*h$,

where for the last two decay modes presented in the list, *i.e.* the decays into neutral Higgs boson pairs with one off-shell Higgs boson, it is assumed that the off-shell Higgs boson predominantly decays into the $b\bar{b}$ final state. The total width of the top quark in the 2HDM, required for the calculation of the decay modes containing off-shell top quarks in the final state, is calculated internally in HDECAY.

Structure of 2HDECAY
Depicted in Fig. 6.1 is the flowchart of 2HDECAY. The main component of the program is the wrapper file 2HDECAY.py, written in Python. The user provides arbitrarily many input files that contain the numerical values for the input parameters based on either of the two sets of independent parameters presented in Eqs. (4.63) and (4.64), where the choice on the used input set is left to the user by setting the corresponding flag PARAM in the input file, cf. the presentation of the input file format below. The wrapper file iterates over all provided input files. For each file, HDECAY is called in a minimal run in which the charm and bottom quark masses, provided in the input file as $\overline{\text{MS}}$ parameters, are converted to OS parameters. Subsequently, the wrapper file calls the subroutine electroweakCorrections which reads the input files, together with the calculated OS masses of the two quarks, and calculates the electroweak partial decay widths to all OS decays of the Higgs bosons at tree level and one-loop order. The numerical evaluation of the scalar one-loop integrals contained in the analytic formulae of the electroweak partial decay widths is performed by linking the Fortran library Loop-Tools 2.15 [252]. Finally, HDECAY is called in a second run in which the program computes the tree-level partial decay widths together with the aforementioned state-of-the-art QCD corrections and combines these consistently with the electroweak corrections. Subsequently, the BRs are computed. They are calculated by 2HDECAY once without the inclusion of the newly computed electroweak partial decay widths and once with them being included. We want to emphasize that in 2HDECAY, the combination of the electroweak and QCD corrections

ID	Scheme	Abbreviation	Tadpole scheme	$\delta\alpha$	$\delta\beta$
1/2	KOSY	KOSY$^{o/c}$	standard	(B.66)	(B.67)/(B.68)
3/4	KOSY	KOSY$^{o/c}$	alternative FJ	(B.69)	(B.70)/(B.71)
5/6	p_*-pinched	p$_*^{o/c}$	alternative FJ	(B.72)	(B.73)/(B.74)
7/8	OS-pinched	pOS$^{o/c}$	alternative FJ	(B.78)	(B.79)/(B.80)
9	Process-dependent 1	proc1	alternative FJ	(B.81)	(B.82)
10	Process-dependent 2	proc2	alternative FJ	(B.83)	(B.84)
11	Process-dependent 3	proc3	alternative FJ	(B.85)	(B.86)
12	Physical on-shell 1	OS1	alternative FJ	(B.87)	(B.88)
13	Physical on-shell 2	OS2	alternative FJ	(B.89)	(B.90)
14	Physical on-shell 12	OS12	alternative FJ	(B.91)	(B.92)
15	Rigid symmetry (BFMS)	BFMS	alternative FJ	(B.93)	(B.94)
16	$\overline{\text{MS}}$	$\overline{\text{MS}}$(stand)	standard	(B.64)	(B.65)
17	$\overline{\text{MS}}$	$\overline{\text{MS}}$(FJ)	alternative FJ	(B.64)	(B.65)

Table 6.1.: Renormalization schemes of the two scalar mixing angles α and β of the real 2HDM used for the numerical analyses in Sec. 7.2, together their abbreviations and the equations through which the mixing angle CTs are defined in each scheme.

is performed in such a way that the electroweak corrections are only computed for OS decays in the subroutine `electroweakCorrections`, while `HDECAY` computes the widths of off-shell decays as well.

The subprogram `HDECAY` generates two output files for each input file, one containing the BRs with and without the electroweak corrections included, denoted as "BR" in Fig. 6.1, and a second file containing the LO and NLO electroweak partial decay widths of all decays denoted as "EW". The latter output is particularly interesting for dedicated studies on the renormalization scheme dependence of the electroweak one-loop corrections. To that end, `2HDECAY` provides the parameter conversion necessary for comparing one-loop partial decay widths calculated within different renormalization schemes, cf. Sec. 3.5. In `2HDECAY 1.1.3`, the 17 different renormalization schemes for the scalar mixing angles α and β as shown in Table 6.1 are implemented. In the table, we moreover provide the required ID of each renormalization scheme as used in the input file, cf. the presentation of the input file format below, as well as a short-hand notation which is used for the identification of the schemes in the numerical analysis in Chapter 7 and the formulae via which the mixing angle CTs are defined for each scheme. The user chooses in the input file one of these renormalization schemes as a reference scheme while the calculation of the electroweak partial decay widths can be performed either in one selected scheme or in all 17 schemes simultaneously. Moreover, the input parameter for the soft-$\mathbb{Z}_2$-breaking scale m_{12}^2 can be specified at an arbitrary renormalization scale μ_R, while the scale μ_{out} at which the one-loop decay widths are computed can be any other arbitrarily chosen scale. `2HDECAY` converts the input parameters of the mixing angles and m_{12}^2 for the case that the one-loop decay widths are evaluated within another renormalization scheme than the chosen reference scheme or in case that $\mu_R \neq \mu_{\text{out}}$ is chosen, as described in Sec. 3.5.

Combination of the electroweak corrections with `HDECAY`
As mentioned in Sec. 4.4, `HDECAY` uses the Fermi constant G_F as a fundamental parameter while for the calculation of the electroweak corrections, the fine-structure constant $\alpha_{\text{em}}(m_Z)$ at the scale of the Z boson mass is used as independent input. For the consistent combina-

	QCD-corrected	QCD&EW-corrected
on-shell and non-loop-induced	$\dfrac{G_F^{\mathrm{calc}}}{G_F}\Gamma_{\phi X_1 X_2}^{\mathrm{HD,QCD}}$	$\dfrac{G_F^{\mathrm{calc}}}{G_F}\left[1+\delta^{\mathrm{EW}}\right]\Gamma_{\phi X_1 X_2}^{\mathrm{HD,QCD}}$
off-shell or loop-induced	$\dfrac{G_F^{\mathrm{calc}}}{G_F}\Gamma_{\phi X_1 X_2}^{\mathrm{HD,QCD}}$	$\dfrac{G_F^{\mathrm{calc}}}{G_F}\Gamma_{\phi X_1 X_2}^{\mathrm{HD,QCD}}$

Table 6.2.: The QCD-corrected and QCD&EW-corrected partial decay widths as computed by `2HDECAY`, where the superscript "QCD" indicates that QCD corrections are included where applicable.

tion of the partial decay widths calculated within the subprograms `electroweakCorrections` and `HDECAY`, a conversion between the two input parameter schemes is required which necessitates the inclusion of the 2HDM-specific higher-order corrections in the conversion formulae. Since these conversion formulae are not implemented yet, we choose instead a pragmatic approximate solution. In the default configuration of `2HDECAY`, *i.e.* when the electroweak contributions to the partial decay widths in the 2HDM are taken into account, the fine-structure constant $\alpha_{\mathrm{em}}(m_Z)$ is read from the input file and is used as the fundamental input for the calculation of the electroweak partial decay widths at tree level and NLO. For the computation of the state-of-the-art QCD corrections in `HDECAY`, `2HDECAY` calculates the Fermi constant G_F^{calc} as a function of $\alpha_{\mathrm{em}}(m_Z)$, m_W and m_Z by means of Eq. (4.21). We expect the differences between the observables calculated within these two schemes to be small. The partial widths calculated in `HDECAY` are rescaled by the factor G_F^{calc}/G_F to account for the change of the input parameter scheme. Moreover, we assume that all higher-order corrections to the decay widths factorize. The combined partial decay widths of the decay of a Higgs boson ϕ into two particles X_1 and X_2, excluding and including the electroweak corrections to the decays respectively, are then given by

$$\Gamma_{\phi X_1 X_2}^{\mathrm{QCD}} \equiv \frac{G_F^{\mathrm{calc}}}{G_F}\Gamma_{\phi X_1 X_2}^{\mathrm{HD,LO}}\left[1+\delta^{\mathrm{QCD}}\right] \equiv \frac{G_F^{\mathrm{calc}}}{G_F}\Gamma_{\phi X_1 X_2}^{\mathrm{HD,QCD}} \;, \tag{6.1}$$

$$\Gamma_{\phi X_1 X_2}^{\mathrm{QCD\&EW}} \equiv \frac{G_F^{\mathrm{calc}}}{G_F}\Gamma_{\phi X_1 X_2}^{\mathrm{HD,LO}}\left[1+\delta^{\mathrm{QCD}}\right]\left[1+\delta^{\mathrm{EW}}\right] \equiv \Gamma_{\phi X_1 X_2}^{\mathrm{QCD}}\left[1+\delta^{\mathrm{EW}}\right] \;, \tag{6.2}$$

where δ^{QCD} and δ^{EW} denote the factorized higher-order contributions to the partial decay widths calculated by the subroutines `HDECAY` and `electroweakCorrections`, respectively, while $\Gamma_{\phi X_1 X_2}^{\mathrm{HD,LO}}$ and $\Gamma_{\phi X_1 X_2}^{\mathrm{HD,QCD}}$ denote the partial decay widths at tree level and at higher orders including all state-of-the-art QCD corrections from `HDECAY`, respectively. The factorized higher-order QCD contributions δ^{QCD} are normalized to the LO width $\Gamma_{\phi X_1 X_2}^{\mathrm{HD,LO}}$, calculated internally by `HDECAY`. This means that for example in the case of final states consisting of quark pairs, the LO width includes the running quark mass in order to improve the perturbative behavior. The factorized higher-order electroweak corrections δ^{EW} on the other hand are obtained by a normalization to the LO width with OS particle masses. Since the electroweak one-loop corrections implemented in the subroutine `electroweakCorrections` are only calculated for OS decays that are not loop-induced, while in `HDECAY` also off-shell and loop-induced decays are computed, the electroweak corrections are only included for OS and non-loop-induced decays. In all other cases, there are no contributions from δ^{EW} and the partial decay width is given by Eq. (6.1). This is shown in Table 6.2 where we present an overview of the partial decay widths as they are calculated by `2HDECAY` for all aforementioned cases. In the table, "QCD-corrected" refers to the widths as defined in Eq. (6.1), including the widths of loop-induced and off-shell decay modes as well as QCD corrections where applicable. The "QCD&EW-corrected" widths additionally contain the electroweak one-loop corrections to the partial decay widths for all non-loop-induced OS decay modes.

Line	Input name	Allowed values and meaning
6	OMIT ELW2	0: electroweak corrections (2HDM) are calculated 1: electroweak corrections (2HDM) are neglected
9	2HDM	0: considered model is not the 2HDM 1: considered model is the 2HDM
56	PARAM	1: 2HDM Higgs masses and α (lines 66-70) are given as input 2: 2HDM potential parameters (lines 72-76) are given as input
57	TYPE	1,2,3,4: 2HDM type I, II, lepton-specific, flipped
58	RENSCHEM	0: all renormalization schemes are calculated 1-17: only the chosen scheme (*cf.* Table 6.1) is calculated
59	REFSCHEM	1-17: the input values of α, β and m_{12}^2 (*cf.* Table 6.4) are given in the chosen reference scheme and at the scale μ_R as given by INSCALE in case of $\overline{\mathrm{MS}}$ parameters

Table 6.3.: Basic control input parameters for 2HDECAY. The table is adopted from [56].

The BRs of the Higgs decays are calculated separately without and with the electroweak contributions in the HDECAY subroutine by means of the loop-corrected partial decay widths in Eqs. (6.1) and (6.2), respectively. The BRs without and with the EW correctons are hence given by

$$\mathrm{BR}^{\mathrm{QCD}}\left(\phi \longrightarrow X_1\,X_2\right) \equiv \frac{\Gamma^{\mathrm{QCD}}_{\phi X_1 X_2}}{\Gamma^{\mathrm{tot,QCD}}_{\phi}}\ , \tag{6.3}$$

$$\mathrm{BR}^{\mathrm{QCD\&EW}}\left(\phi \longrightarrow X_1\,X_2\right) \equiv \frac{\Gamma^{\mathrm{QCD\&EW}}_{\phi X_1 X_2}}{\Gamma^{\mathrm{tot,QCD\&EW}}_{\phi}}\ , \tag{6.4}$$

where $\Gamma^{\mathrm{tot,QCD}}_{\phi}$ and $\Gamma^{\mathrm{tot,QCD\&EW}}_{\phi}$ denote the total decay width of the scalar particle ϕ excluding and including the electroweak corrections, respectively.

Input file format

In App. F.1, we present an exemplary input file 2hdecay.in, where we restrict the presentation only to the input parameters that are relevant for the calculations performed with 2HDECAY. The input file contains two classes of inputs. The first class contains the input parameters that are relevant for the main flow of the program. In Table 6.3, we present the input parameters of this class together with their line numbers in the input file, their allowed values and the meaning of the parameters. In order to calculate the BRs and partial decay widths in the 2HDM, the value 2HDM = 1 has to be set by the user. For the input value OMIT ELW2 = 0, the QCD&EW-corrected partial decay widths and the corresponding BRs are calculated as described in the preceding paragraph. For this choice, 2HDECAY automatically sets 2HDM = 1 internally. If the user on the other hand sets OMIT ELW2 = 1, then the electroweak corrections are not calculated and 2HDECAY provides the same corrections as the original version of HDECAY 6.52. In this case, the QCD-corrected decay widths are not rescaled by G_F^{calc} but instead calculated by using the value of G_F as provided in the input file. The parametrization of the input values of the scalar sector is specified by the input parameter PARAM. For PARAM = 1, the parameter set shown in Eq. (4.63) is used, *i.e.* the masses of the Higgs bosons and the CP-even scalar mixing angle α are considered as independent input, while for PARAM = 2, the 2HDM potential parameters λ_i $(i = 1, ..., 5)$ are used as independent input as denoted by the parameter set in Eq. (4.64). We want to emphasize however

Line	Input name	Name in Chapter 4	Allowed values and meaning
18	ALS(MZ)	$\alpha_s(m_Z)$	strong coupling constant (at m_Z)
19	MSBAR(2)	$m_s(2\,\text{GeV})$	s-quark $\overline{\text{MS}}$ mass at 2 GeV in GeV
20	MCBAR(3)	$m_c(3\,\text{GeV})$	c-quark $\overline{\text{MS}}$ mass at 3 GeV in GeV
21	MBBAR(MB)	$m_b(m_b)$	b-quark $\overline{\text{MS}}$ mass at m_b in GeV
22	MT	m_t	t-quark pole mass in GeV
23	MTAU	m_τ	τ-lepton pole mass in GeV
24	MMUON	m_μ	μ-lepton pole mass in GeV
25	1/ALPHA	$\alpha_{\text{em}}^{-1}(0)$	inverse fine-structure constant (Thomson limit)
26	ALPHAMZ	$\alpha_{\text{em}}(m_Z)$	fine-structure constant (at m_Z)
29	GAMW	Γ_W	partial decay width of the W boson
30	GAMZ	Γ_Z	partial decay width of the Z boson
31	MZ	m_Z	Z boson on-shell mass in GeV
32	MW	m_W	W boson on-shell mass in GeV
33-41	Vij	V_{ij}	CKM matrix elements ($i \in \{u,c,t\}$, $j \in \{d,s,b\}$)
61	TGBET2HDM	t_β	ratio of the VEVs in the 2HDM
62	M_12^2	m_{12}^2	squared soft-$\mathbb{Z}_2$-breaking scale in GeV^2
63	INSCALE	μ_R	renormalization scale for $\overline{\text{MS}}$ inputs in GeV
64	OUTSCALE	μ_{out}	renormalization scale for the evaluation of the partial decay widths in GeV or in terms of MIN
66	ALPHA_H	α	CP-even Higgs mixing angle in radians
67	MHL	m_h	light CP-even Higgs boson mass in GeV
68	MHH	m_H	heavy CP-even Higgs boson mass in GeV
69	MHA	m_A	CP-odd Higgs boson mass in GeV
70	MH+-	$m_{H^\pm}$	charged Higgs boson mass in GeV
72-76	LAMBDAi	λ_i	Higgs potential parameters, cf. Eq. (4.4)

Table 6.4.: Relevant physical input parameters for the calculations performed in 2HDECAY. The table is adopted from [56].

that the analytic results for the electroweak partial decay widths are implemented in terms of the former input parameter set and hence, if PARAM = 2 is chosen, the masses of the Higgs bosons and the mixing angle α are calculated internally by 2HDECAY by means of Eqs. (4.41) to (4.44) and Eq. (4.50) for the calculation of the electroweak partial decay widths. The input value TYPE specifies the type of 2HDM that is considered as described in Sec. 4.3. The value of RENSCHEM determines the renormalization scheme for the scalar mixing angles which is used for the calculation of the electroweak partial decay widths. For RENSCHEM = 0, the electroweak-corrected widths and BRs are calculated for all 17 implemented renormalization schemes shown in Table 6.1 simultaneously. If RENSCHEM is set to any integer between 1 and 17, the partial decay widths are calculated for the scheme corresponding to the ID shown in Table 6.1. The input parameter REFSCHEM with integer values between 1 and 17 denotes the reference renormalization scheme at which the input values of the scalar mixing angles α and β are defined. The input value for the $\overline{\text{MS}}$ parameter m_{12}^2 is always defined at the input scale μ_R and the same applies for the scalar mixing angles in case that the $\overline{\text{MS}}$ scheme is chosen as a reference scheme, while the evaluation of the electroweak partial decay widths is performed at the renormalization scale μ_{out}. The values of α, β and m_{12}^2 at the scale μ_{out} and in the chosen input renormalization scheme RENSCHEM are calculated from their values at μ_R and in the reference scheme by means of Eqs. (3.30) and (3.31), respectively.

The second class of input parameters for `2HDECAY` are the relevant physical input parameters presented in Table 6.4, together with their line numbers in the exemplary input file shown in App. F.1, the corresponding parameters introduced in Chapter 4 as well as their allowed values and meanings. The `OUTSCALE` renormalization scale μ_{out} is given either in GeV or in terms of the mass `MIN` of the decaying Higgs boson for each decay channel that is calculated, *i.e.* the input value `OUTSCALE = MIN` sets the renormalization scale at which the partial decay widths are evaluated to $\mu_{\text{out}} = m_1$ for each decay channel, where m_1 denotes the mass of the decaying Higgs boson. Apart from `OUTSCALE`, all other input parameters shown in Table 6.4 are entered in `FORTRAN` double-precision format into the input file. In case that `PARAM = 1` is set, `2HDECAY` reads the masses of the Higgs bosons and α as independent input and ignores the values of the 2HDM potential parameters λ_i in the input file, while for `PARAM = 2`, the λ_i are read in and the Higgs boson masses and α are instead calculated by means of Eqs. (4.41) to (4.44) and Eq. (4.50).

Output file format
For each input file, `2HDECAY` generates one output file containing the BRs of all decay channels and, in case that `OMIT ELW2 = 0` is set, additionally one output file containing the electroweak partial decay widths of the OS non-loop-induced decay modes. In App. F.2, we present exemplary output files for the BRs and electroweak decay widths which are shortened to two decay channels of the lighter CP-even Higgs boson h since we focus on the description of the general structure of the output files here. The output file format follows the SUSY Les Houch Accord (SLHA) [253, 254] which however is modified in order to account for the electroweak corrections to the partial decay widths calculated in the 2HDM. In the first four blocks given out for both output files and not shown explicitly in App. F.2, basic information about `2HDECAY` as well as the input values used for the calculations are provided. The value of G_F which is printed in this block corresponds to the value of G_F^{calc} in case that `OMIT ELW2 = 0` is set and is consequently not necessarily the same as the value of G_F provided in the input file, as discussed above.

Subsequently, in the output file that contains the BRs, for each Higgs boson h, H, A and $H^{\pm}$ two blocks `DECAY QCD` and `DECAY QCD&EW` are printed. Both blocks start with the total decay width of the corresponding Higgs boson, followed by the ID of the renormalization scheme for which the widths and BRs are calculated and the values of α, β and m_{12}^2 in the considered scheme and at the scale μ_{out} which, due to the conversion routine implemented in `2HDECAY`, can differ from the corresponding values provided in the input file defined in the reference renormalization scheme and at the scale μ_R. The first block `DECAY QCD` for each Higgs boson contains the BRs of the respective Higgs boson as they are implemented in `HDECAY`, comprising the tree-level decays, the off-shell decay modes presented at the beginning of this section as well as loop-induced decays into $g\,g$, $\gamma\,\gamma$ and $Z\,\gamma$ final states, together with the state-of-the-art QCD corrections, where applicable. In case that `OMIT ELW2 = 1` is set, these BRs correspond to the ones which are printed out in the original `HDECAY 6.52` version. For `OMIT ELW2 = 0` on the other hand, the printed BRs differ from the ones given out by the original `HDECAY` version due to the rescaling with the calculated Fermi constant G_F^{calc}, as explained before. In the second block `DECAY QCD&EW` printed out for each Higgs boson, the BRs of all decay modes of the corresponding Higgs boson, containing both the corrections to the tree-level widths as implemented in `HDECAY` as well as the electroweak corrections provided by the subroutine `electroweakCorrections`, are given. We want to note that since the electroweak corrections are calculated only for OS decays that are not loop-induced, the BRs of off-shell or loop-induced decay modes given out in the block `DECAY QCD&EW` are still only QCD-corrected BRs and not QCD&EW-corrected ones. In the last block of the file, which is not explicitly shown in App. F.2, the QCD-corrected BR of the top quark in the 2HDM is given out since it is required for the calculation of the Higgs boson decays into final states containing an off-shell top quark as mentioned at the beginning of this section.

In the output file that contains the electroweak partial decay widths, after the first four blocks containing the basic information about `2HDECAY` and the input parameters used for the calculation, two subsequent blocks `LO DECAY WIDTH` and `NLO DECAY WIDTH` are printed out for each Higgs boson h, H, A and $H^{\pm}$. Each block starts with the ID of the renormalization scheme, followed by the parameters α, β and m_{12}^2 in the considered renormalization scheme and at the renormalization scale μ_{out} which are used for the calculation of the decay widths. Subsequently, the electroweak partial decay widths of all OS and non-loop-induced decays of the corresponding Higgs boson are given out. The decay widths printed in the block `LO DECAY WIDTH` correspond to the tree-level partial decay widths while the ones printed in the block `NLO DECAY WIDTH` are the one-loop decay widths. The widths provided by this second output file are particularly useful for studies on the renormalization scheme dependence of the electroweak one-loop corrections. We want to emphasize that since the electroweak corrections are calculated for OS and non-loop-induced decays only, it can happen that the output file for the electroweak partial decay widths does not contain all decay channels that are provided by the output file containing the BRs, since for the latter, `HDECAY` also calculates the BRs of off-shell and loop-induced decays.

Caveats

We want to note that it can happen that the electroweak-corrected partial decay widths calculated by `2HDECAY` can become very large or negative due to large contributions from the one-loop partial decay widths with respect to the tree-level widths, for which there are several different reasons:

- The electroweak corrections can be enhanced due to unsuitable schemes used for the renormalization of the independent parameters of the 2HDM. In our work, this is referred to as the numerical instability of a chosen renormalization scheme, cf. the discussion in Sec. 5.3.

- The electroweak corrections can be parametrically enhanced in case that some coupling constants involved in the calculation of the widths become very large or small for the considered parameter point or due to virtual particles with very small masses in the one-loop integrals, cf. [227, 228, 255]. In these cases, resummation methods could be applied to improve the perturbative behavior of the partial decay widths, which in turn requires the inclusion of electroweak corrections beyond the fixed one-loop level however.

- The tree-level partial decay widths can be suppressed due to small coupling constants of the tree-level decay amplitude. As an example, the tree-level coupling constant between the non-SM-like Higgs boson and two massive gauge bosons can be suppressed due to the sum rules of the gauge boson couplings of the 2HDM. In case that the electroweak one-loop corrections are not suppressed by the same powers of the coupling constant, the loop-corrected decay width can become comparatively large with respect to the tree-level width.

We want to note that since negative partial decay widths or too large loop-corrected widths with respect to the tree-level results are unphysical, the electroweak-corrected widths and BRs in these cases are not suitable for phenomenological analyses and should be discarded.

Numerical Analysis with 2HDECAY

In this chapter, we perform numerical analyses on the BRs and partial decay widths of the Higgs bosons of the real 2HDM by using 2HDECAY 1.1.3, focusing on the size of the electroweak corrections to the decays implemented in this work.

In Sec. 7.1, we describe the scans over the parameter space of the real 2HDM and present all constraints applied to the scans in order to obtain valid input parameter sets. In the subsequent Sec. 7.2, we perform the numerical calculation of the branching ratios and partial decay widths of selected Higgs decay channels for our chosen input parameter sets. We compare the size of the electroweak corrections computed within different renormalization schemes and present exemplary analyses of selected decay channels with respect to the remaining theoretical uncertainty and the numerical stability of the renormalization schemes of the scalar mixing angles.

7.1. Input Parameters

For the calculation of the numerical results presented in this chapter, we set the input values of the SM parameters in 2HDECAY to the following values [98, 256],

$$
\begin{aligned}
m_\mu &\equiv 105.658\,371\,\text{MeV} , & m_\tau &= 1.776\,82\,\text{GeV} , & (7.1)\\
m_s^{\overline{\text{MS}}}(2\,\text{GeV}) &= 95.0\,\text{MeV} , & m_c^{\overline{\text{MS}}}(3\,\text{GeV}) &\equiv 0.986\,\text{GeV} , \\
m_b^{\overline{\text{MS}}}(m_b^{\overline{\text{MS}}}) &\equiv 4.18\,\text{GeV} , & m_t &= 173.2\,\text{GeV} , \\
\alpha_s^{\overline{\text{MS}}}(m_Z) &= 0.1181 , & G_F &= 1.166\,3787 \cdot 10^{-5}\,\text{GeV}^{-2} , \\
m_W &= 80.385\,\text{GeV} , & m_Z &= 91.1876\,\text{GeV} , \\
\Gamma_W &= 2.085\,\text{GeV} , & \Gamma_Z &= 2.4952\,\text{GeV} , \\
\alpha_{\text{em}}^{-1}(m_Z) &= 128.962 , & \alpha_{\text{em}}^{-1}(0) &= 137.036 ,
\end{aligned}
$$

while the electron and the up and down quarks are massless in our approximation. The masses of the gauge bosons are given as OS masses and all other masses without a superscript are

	$m_{h/H/A}$	$m_{H^\pm}$ (II/flipped)	$m_{H^\pm}$ (I/lepton-specific)	m_{12}^2	α	t_β
min	30 GeV	580 GeV	80 GeV	0 GeV^2	$-\pi/2$	0.25
max	1500 GeV	1500 GeV	1500 GeV	100 000 GeV^2	$\pi/2$	35

Table 7.1.: Allowed ranges of the input values of the real 2HDM for the parameter scan. Each parameter is separately varied between its corresponding minimum and maximum values.

given as pole masses of the respective particles. For the CKM matrix, we consider a general non-diagonal representation and set the nine different entries of the matrix to the values [98]

$$
V = \begin{pmatrix}
0.974\,460 & 0.224\,520 & 0.003\,650 \\
-0.224\,380 & 0.973\,590 & 0.042\,140 \\
0.008\,960 & -0.041\,330 & 0.999\,105
\end{pmatrix} . \tag{7.2}
$$

For the generation of the input parameter sets that are compatible with most recent theoretical and experimental constraints, we scan over the parameter space of the real 2HDM. In the following, we only briefly present the parameters of the scan and the constraints applied to generate valid input parameter sets. For a detailed description about the scan procedure, we refer to [257, 258].

For all scans that are performed, we require that either the lighter CP-even Higgs boson h or the heavier CP-even Higgs boson H corresponds to the SM-like Higgs boson, with its mass given by [13]

$$
m_{h_{\mathrm{SM}}} = 125.09 \,\mathrm{GeV} . \tag{7.3}
$$

In order to avoid parameter sets that lead to Higgs signals being built up by two close resonances, we demand that no other Higgs boson with a mass in the range of $\pm 5\,\mathrm{GeV}$ around the value given in Eq. (7.3) is produced in the scan. Apart from the SM parameters and one of the Higgs masses being fixed by Eq. (7.3), all other parameters of the 2HDM are free input parameters. In the scan, we allow these parameters to lie within the minimal and maximal values presented in Table 7.1. For the mass of the charged Higgs boson, the lower limit of $m_{H^\pm} \geq 580\,\mathrm{GeV}$ [259] for the 2HDM types II and flipped are applied.

The parameter scan is performed with the help of the tool `ScannerS` [57, 260, 261]. The various generated parameter scenarios are checked against the following constraints:

- The Higgs exclusion limits stemming from experiments at the Large Electron Positron collider (LEP), Tevatron and LHC are checked with `HiggsBounds 5.3.2` [262–264].

- The Higgs rates are checked with `HiggsSignals 2.2.3` [265].

Each parameter set passing these constraints is considered as a valid input parameter set. Out of all valid sets, we choose a few exemplary ones for the sets used in our numerical analysis. In the following, we present the values of the 2HDM-specific parameters for each of the sets.

Parameter set "P1".
For the SM parameters, the input values presented in Eqs. (7.1) and (7.2) are used, while the 2HDM-specific parameters are set to

$$
\begin{aligned}
m_h &= 125.09\,\text{GeV}\,, & m_H &= 381.767\,\text{GeV}\,, & (7.4) \\
m_A &= 350.665\,\text{GeV}\,, & m_{H^\pm} &= 414.114\,\text{GeV}\,, \\
m_{12}^2(m_{h_{\text{SM}}}) &= 28\,505.5\,\text{GeV}^2\,, & \alpha|_{p_*^o} &= -0.189\,345\,, \\
t_\beta|_{p_*^o} &= 4.236\,35\,, & \text{2HDM type} &= \text{I}\,,
\end{aligned}
$$

where for m_{12}^2, the argument in brackets indicates that the input value is defined at the scale $\mu_R = m_{h_{\text{SM}}}$. Moreover, the subscripts denote that the two mixing angles are defined in the p_*-pinched (odd) scheme, defined through Eqs. (B.72) and (B.73), as the reference scheme considered for our numerical analysis. The renormalization scale μ_{out} at which the electroweak partial decay widths are evaluated is set to the mass of the decaying particle for each decay channel, separately.

Parameter set "P2".
Analogous to the former set, the input values of the SM parameters are set as presented in Eqs. (7.1) and (7.2), while the 2HDM-specific parameters are chosen as follows,

$$
\begin{aligned}
m_h &= 125.09\,\text{GeV}\,, & m_H &= 302.324\,\text{GeV}\,, & (7.5) \\
m_A &= 494.618\,\text{GeV}\,, & m_{H^\pm} &= 300.077\,\text{GeV}\,, \\
m_{12}^2(m_{h_{\text{SM}}}) &= 28\,328.8\,\text{GeV}^2\,, & \alpha|_{p_*^o} &= -0.200\,175\,, \\
t_\beta|_{p_*^o} &= 2.660\,82\,, & \text{2HDM type} &= \text{I}\,,
\end{aligned}
$$

For an analysis of the size of the electroweak corrections to selected decay channels, we moreover perform a variation of some of the input parameters of this set:

- Variation of $m_H \in [130\,\text{GeV}, 550\,\text{GeV}]$, while all other parameters are given by the fixed values in Eq. (7.5).

- Variation of $m_A \in [130\,\text{GeV}, 550\,\text{GeV}]$, while all other parameters are given by the fixed values in Eq. (7.5).

These variations of the input parameters can lead to points in the parameter space of the real 2HDM that do not fulfill the aforementioned experimental constraints anymore. Since we do not perform a dedicated phenomenological analysis in this work, however, we nevertheless use the parameter sets generated by the variations in order to demonstrate the size of the electroweak corrections implemented in `2HDECAY` and to provide examples for analyses which can be extended in future work. The renormalization scale μ_{out} at which the electroweak partial decay widths are evaluated is again set to the mass of the decaying particle for each decay channel, separately.

Parameter sets "P3".
For another analysis of the size of the electroweak corrections of a selected Higgs decay channel computed within different renormalization schemes, we use several additional parameter sets which we collectively define as the "P3" set. The set includes 15 000 different parameter points for a 2HDM type I with large varieties with respect to the values of the masses, mixing angles and m_{12}^2, while the SM values are again set according to Eqs. (7.1) and (7.2). We evaluate the electroweak partial decay widths again at the renormalization scale μ_{out} which is set to the mass of the decaying particle of the respective decay channel. In contrast to the other two aforementioned parameter sets, the values of the mixing angles in set "P3" are defined within each considered renormalization scheme separately such that no conversion between

their input values is required. All points fulfill the aforementioned experimental constraints. Since the amount of points considered in the set "P3" is too large, we do not present the explicit values of the 2HDM-specific parameters for each point here.

7.2. Numerical Results and Analysis

In this section, we perform several analyses on the BRs and partial decay widths computed for different renormalization schemes with `2HDECAY`. In order to quantify the size of the electroweak contributions newly computed in this thesis, we define

$$\Delta \mathrm{BR} \equiv \frac{\mathrm{BR}^{\mathrm{QCD\&EW}}(\phi \to X_1\, X_2) - \mathrm{BR}^{\mathrm{QCD}}(\phi \to X_1\, X_2)}{\mathrm{BR}^{\mathrm{QCD}}(\phi \to X_1\, X_2)} \tag{7.6}$$

as a measure for the relative contributions of the electroweak corrections to the BRs with respect to the BRs already contained in `HDECAY`. Analogously, we define the deviation

$$\Delta \Gamma^{\mathrm{EW}} \equiv \frac{\Gamma_{\phi X_1 X_2}^{\mathrm{NLO,EW}} - \Gamma_{\phi X_1 X_2}^{\mathrm{LO,EW}}}{\Gamma_{\phi X_1 X_2}^{\mathrm{LO,EW}}} \tag{7.7}$$

as a measure of the size of the genuine one-loop contributions to the electroweak partial decay widths with respect to the tree-level widths. Furthermore, we define the quantity

$$\Delta \Gamma^{\mathrm{EW,x}} \equiv \frac{\left.\Gamma_{\phi X_1 X_2}^{\mathrm{NLO,EW}}\right|_{\mathrm{x}} - \left.\Gamma_{\phi X_1 X_2}^{\mathrm{NLO,EW}}\right|_{\mathrm{p}_*^o}}{\left.\Gamma_{\phi X_1 X_2}^{\mathrm{NLO,EW}}\right|_{\mathrm{p}_*^o}} \tag{7.8}$$

as a measure of the difference of the one-loop electroweak partial decay width computed in a renormalization scheme of the scalar mixing angles, denoted by the index "x", with respect to the one-loop width computed in the p_*-pinched scheme "p_*^o". In order to consistently compare the electroweak partial decay widths computed within the different renormalization schemes, `2HDECAY` converts the scalar mixing angles from the scheme "p_*^o" to scheme "x", as described in Sec. 6.2. Since we restrict the computation of the electroweak corrections to OS decays which are not loop-induced, the deviation of the electroweak decay widths in Eqs. (7.7) and (7.8) are only calculated for electroweak decay amplitudes that are in general non-vanishing at tree-level, while the deviation of the BRs defined in Eq. (7.6) is computed for all decay channels implemented in `2HDECAY`.

We begin our numerical analysis by computing the BRs and electroweak partial decay widths of all decay channels for the parameter set "P1". For the computation, we fix the renormalization scheme of the scalar mixing angles to the OS-pinched scheme "pOS^o" defined via the CP-odd sector, cf. Table 6.1. Since the input values of the two mixing angles in the set "P1" are defined in the p_*-pinched scheme "p_*^o", they are converted to the "pOS^o" scheme before being used for the calculation of the decays, cf. Sec. 3.5. Moreover, the $\overline{\mathrm{MS}}$ parameter m_{12}^2 is defined at the scale $\mu_R = m_{h_{\mathrm{SM}}}$ while the scale μ_{out} at which the electroweak decay widths are evaluated is set equal to the mass of the decaying particle. Consequently, the parameter m_{12}^2 is converted from the scale μ_R to the scale μ_{out} wherever these two scales are not equal.

In Table 7.2, the BRs excluding and including the electroweak contributions as well as the electroweak partial decay widths at tree level and one-loop order for all decay channels are presented as they are given as output by `2HDECAY`. Moreover, we present the calculated deviations defined in Eqs. (7.6) and (7.7) for all decay channels, where applicable. For the SM-like Higgs boson h, the relative electroweak contributions to the BRs are comparatively small, ranging from $-3.5\,\%$ to $3.0\,\%$ compared to the BRs computed without the electroweak corrections. Analogously, the electroweak one-loop contributions shift the partial decay widths

Decay channel	$\mathrm{BR}^{\mathrm{QCD}}_{(\phi \to X_1 X_2)}$	$\mathrm{BR}^{\mathrm{QCD\&EW}}_{(\phi \to X_1 X_2)}$	$\Delta\mathrm{BR}$	$\Gamma^{\mathrm{LO,EW}}_{\phi X_1 X_2}$ in GeV	$\Gamma^{\mathrm{NLO,EW}}_{\phi X_1 X_2}$ in GeV	$\Delta\Gamma^{\mathrm{EW}}$
$h \to b\,\bar{b}$	$5.934 \cdot 10^{-1}$	$5.850 \cdot 10^{-1}$	-1.4 %	$5.968 \cdot 10^{-3}$	$5.715 \cdot 10^{-3}$	-4.3 %
$h \to \tau^+\,\tau^-$	$6.388 \cdot 10^{-2}$	$6.304 \cdot 10^{-2}$	-1.3 %	$2.699 \cdot 10^{-4}$	$2.587 \cdot 10^{-4}$	-4.2 %
$h \to \mu^+\,\mu^-$	$2.262 \cdot 10^{-4}$	$2.183 \cdot 10^{-4}$	-3.5 %	$9.555 \cdot 10^{-7}$	$8.958 \cdot 10^{-7}$	-6.3 %
$h \to s\,\bar{s}$	$2.239 \cdot 10^{-4}$	$2.254 \cdot 10^{-4}$	0.7 %	$2.317 \cdot 10^{-6}$	$2.266 \cdot 10^{-6}$	-2.2 %
$h \to c\,\bar{c}$	$2.904 \cdot 10^{-2}$	$2.906 \cdot 10^{-2}$	0.1 %	$5.268 \cdot 10^{-4}$	$5.119 \cdot 10^{-4}$	-2.8 %
$h \to g\,g$	$7.785 \cdot 10^{-2}$	$8.015 \cdot 10^{-2}$	3.0 %	–	–	–
$h \to \gamma\,\gamma$	$2.199 \cdot 10^{-3}$	$2.265 \cdot 10^{-3}$	3.0 %	–	–	–
$h \to Z\,\gamma$	$1.541 \cdot 10^{-3}$	$1.587 \cdot 10^{-3}$	3.0 %	–	–	–
$h \to W^+\,W^-$	$2.059 \cdot 10^{-1}$	$2.120 \cdot 10^{-1}$	3.0 %	–	–	–
$h \to Z\,Z$	$2.570 \cdot 10^{-2}$	$2.646 \cdot 10^{-2}$	3.0 %	–	–	–
$H \to b\,\bar{b}$	$1.236 \cdot 10^{-3}$	$1.057 \cdot 10^{-3}$	-14.5 %	$6.653 \cdot 10^{-4}$	$6.342 \cdot 10^{-4}$	-4.7 %
$H \to \tau^+\,\tau^-$	$1.641 \cdot 10^{-4}$	$1.335 \cdot 10^{-4}$	-18.7 %	$2.988 \cdot 10^{-5}$	$2.707 \cdot 10^{-5}$	-9.4 %
$H \to \mu^+\,\mu^-$	$5.805 \cdot 10^{-7}$	$4.611 \cdot 10^{-7}$	-20.6 %	$1.057 \cdot 10^{-7}$	$9.352 \cdot 10^{-8}$	-11.5 %
$H \to s\,\bar{s}$	$4.655 \cdot 10^{-7}$	$3.897 \cdot 10^{-7}$	-16.3 %	$2.563 \cdot 10^{-7}$	$2.391 \cdot 10^{-7}$	-6.7 %
$H \to c\,\bar{c}$	$6.044 \cdot 10^{-5}$	$5.012 \cdot 10^{-5}$	-17.1 %	$5.829 \cdot 10^{-5}$	$5.386 \cdot 10^{-5}$	-7.6 %
$H \to t\,\bar{t}$	$5.399 \cdot 10^{-1}$	$4.755 \cdot 10^{-1}$	-11.9 %	$6.327 \cdot 10^{-2}$	$6.208 \cdot 10^{-2}$	-1.9 %
$H \to g\,g$	$4.236 \cdot 10^{-3}$	$3.802 \cdot 10^{-3}$	-10.3 %	–	–	–
$H \to \gamma\,\gamma$	$1.816 \cdot 10^{-5}$	$1.629 \cdot 10^{-5}$	-10.3 %	–	–	–
$H \to Z\,\gamma$	$1.068 \cdot 10^{-5}$	$9.580 \cdot 10^{-6}$	-10.3 %	–	–	–
$H \to W^+\,W^-$	$1.272 \cdot 10^{-1}$	$1.191 \cdot 10^{-1}$	-6.3 %	$2.314 \cdot 10^{-2}$	$2.416 \cdot 10^{-2}$	4.4 %
$H \to Z\,Z$	$5.900 \cdot 10^{-2}$	$6.650 \cdot 10^{-2}$	12.7 %	$1.074 \cdot 10^{-2}$	$1.349 \cdot 10^{-2}$	25.6 %
$H \to A\,A$	$1.190 \cdot 10^{-10}$	$1.068 \cdot 10^{-10}$	-10.3 %	–	–	–
$H \to h\,h$	$2.680 \cdot 10^{-1}$	$3.337 \cdot 10^{-1}$	24.5 %	$4.879 \cdot 10^{-2}$	$6.769 \cdot 10^{-2}$	38.7 %
$H \to Z\,A$	$1.709 \cdot 10^{-4}$	$1.533 \cdot 10^{-4}$	-10.3 %	–	–	–
$A \to b\,\bar{b}$	$7.263 \cdot 10^{-4}$	$6.831 \cdot 10^{-4}$	-6.0 %	$8.953 \cdot 10^{-4}$	$8.366 \cdot 10^{-4}$	-6.6 %
$A \to \tau^+\,\tau^-$	$9.737 \cdot 10^{-5}$	$8.639 \cdot 10^{-5}$	-11.3 %	$4.019 \cdot 10^{-5}$	$3.542 \cdot 10^{-5}$	-11.9 %
$A \to \mu^+\,\mu^-$	$3.443 \cdot 10^{-7}$	$2.983 \cdot 10^{-7}$	-13.4 %	$1.421 \cdot 10^{-7}$	$1.223 \cdot 10^{-7}$	-13.9 %
$A \to s\,\bar{s}$	$2.603 \cdot 10^{-7}$	$2.379 \cdot 10^{-7}$	-8.6 %	$3.447 \cdot 10^{-7}$	$3.129 \cdot 10^{-7}$	-9.2 %
$A \to c\,\bar{c}$	$3.671 \cdot 10^{-5}$	$3.322 \cdot 10^{-5}$	-9.5 %	$7.841 \cdot 10^{-5}$	$7.050 \cdot 10^{-5}$	-10.1 %
$A \to t\,\bar{t}$	$9.622 \cdot 10^{-1}$	$9.710 \cdot 10^{-1}$	0.9 %	$1.782 \cdot 10^{-1}$	$1.786 \cdot 10^{-1}$	0.3 %
$A \to g\,g$	$9.650 \cdot 10^{-3}$	$9.714 \cdot 10^{-3}$	0.7 %	–	–	–
$A \to \gamma\,\gamma$	$3.973 \cdot 10^{-5}$	$4.000 \cdot 10^{-5}$	0.7 %	–	–	–
$A \to Z\,\gamma$	$6.741 \cdot 10^{-6}$	$6.785 \cdot 10^{-6}$	0.7 %	–	–	–
$A \to Z\,h$	$2.723 \cdot 10^{-2}$	$1.846 \cdot 10^{-2}$	-32.2 %	$1.124 \cdot 10^{-2}$	$7.570 \cdot 10^{-3}$	-32.7 %
$H^+ \to c\,\bar{b}$	$6.671 \cdot 10^{-7}$	$6.537 \cdot 10^{-7}$	-2.0 %	$2.042 \cdot 10^{-6}$	$1.925 \cdot 10^{-6}$	-5.7 %
$H^+ \to \tau^+\,\nu_\tau$	$4.986 \cdot 10^{-5}$	$4.720 \cdot 10^{-5}$	-5.3 %	$4.746 \cdot 10^{-5}$	$4.322 \cdot 10^{-5}$	-8.9 %
$H^+ \to \mu^+\,\nu_\mu$	$1.763 \cdot 10^{-7}$	$1.631 \cdot 10^{-7}$	-7.5 %	$1.678 \cdot 10^{-7}$	$1.493 \cdot 10^{-7}$	-11.0 %
$H^+ \to u\,\bar{b}$	$4.772 \cdot 10^{-9}$	$4.579 \cdot 10^{-9}$	-4.0 %	$1.409 \cdot 10^{-8}$	$1.300 \cdot 10^{-8}$	-7.7 %
$H^+ \to u\,\bar{s}$	$6.672 \cdot 10^{-9}$	$6.498 \cdot 10^{-9}$	-2.6 %	$2.052 \cdot 10^{-8}$	$1.922 \cdot 10^{-8}$	-6.3 %
$H^+ \to c\,\bar{d}$	$8.766 \cdot 10^{-7}$	$8.493 \cdot 10^{-7}$	-3.1 %	$4.662 \cdot 10^{-6}$	$4.345 \cdot 10^{-6}$	-6.8 %
$H^+ \to c\,\bar{s}$	$1.663 \cdot 10^{-5}$	$1.608 \cdot 10^{-5}$	-3.3 %	$8.815 \cdot 10^{-5}$	$8.200 \cdot 10^{-5}$	-7.0 %
$H^+ \to t\,\bar{b}$	$9.702 \cdot 10^{-1}$	$9.660 \cdot 10^{-1}$	-0.4 %	$9.203 \cdot 10^{-1}$	$8.815 \cdot 10^{-1}$	-4.2 %
$H^+ \to t\,\bar{s}$	$1.659 \cdot 10^{-3}$	$1.651 \cdot 10^{-3}$	-0.4 %	$1.573 \cdot 10^{-3}$	$1.507 \cdot 10^{-3}$	-4.2 %
$H^+ \to t\,\bar{d}$	$7.795 \cdot 10^{-5}$	$7.786 \cdot 10^{-5}$	-0.1 %	$7.394 \cdot 10^{-5}$	$7.105 \cdot 10^{-5}$	-3.9 %
$H^+ \to W^+\,h$	$2.600 \cdot 10^{-2}$	$3.012 \cdot 10^{-2}$	15.8 %	$2.475 \cdot 10^{-2}$	$2.758 \cdot 10^{-2}$	11.4 %
$H^+ \to W^+\,H$	$5.028 \cdot 10^{-5}$	$5.227 \cdot 10^{-5}$	4.0 %	–	–	–
$H^+ \to W^+\,A$	$1.918 \cdot 10^{-3}$	$1.994 \cdot 10^{-3}$	4.0 %	–	–	–

Table 7.2.: Higher-order BRs excluding and including electroweak contributions as well as electroweak parial decay widths at tree level and one-loop order for all decay channels implemented in `2HDECAY` as calculated for the parameter set "P1" defined in Eq. (7.4). The relative sizes $\Delta\mathrm{BR}$ and $\Delta\Gamma^{\mathrm{EW}}$ of the BRs and electroweak partial decay widths are defined in Eqs. (7.6) and (7.7), respectively. For the computation of all BRs including the electroweak corrections as well as for the one-loop partial decay widths, the scalar mixing angles are renormalized in the OS-pinched scheme "pOS^o", cf. Table 6.1.
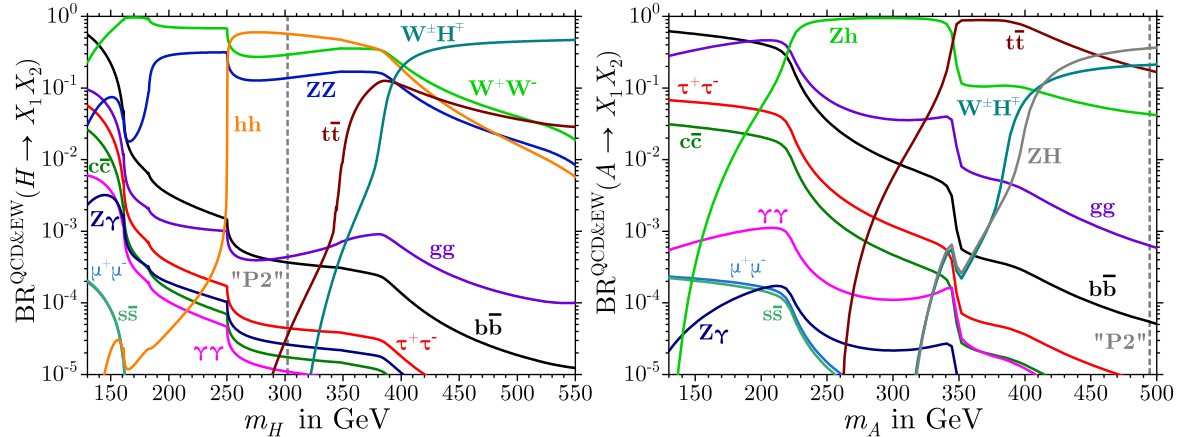
Figure 7.1.: Scenario "P2": BRs of the heavy CP-even Higgs boson H as a function of m_H (left) and the CP-odd Higgs boson A as a function of m_A (right) into various OS final states including both the electroweak and the QCD corrections. For the computation of all BRs, the scalar mixing angles are renormalized in the OS-pinched scheme "pOS^o", cf. Table 6.1.

moderately by $-6.3\,\%$ to $-2.2\,\%$ compared to the tree-level widths. The computed BRs, both including and excluding the newly computed electroweak contributions, are compatible with the BRs of the Higgs boson of the SM, cf. Table 11.3 of [98].

For the other Higgs bosons of the 2HDM, the electroweak contributions to the partial decay widths and BRs are considerably larger for some decay channels. In the following, we restrict the discussion to the relative change of the BRs since the discussion about the change of the electroweak partial decay widths is analogous. In the considered scenario, the decay of the heavy Higgs boson H is dominated by OS decays into a top quark pair, followed by OS decays into a pair of SM-like Higgs bosons h as well as into pairs of $W^\pm$ bosons, with BRs at the level of tens of percents for all three decay channels. Due to the mass values of the H and A Higgs bosons, the former does not decay OS into AA and hence, this decay mode is realized only off-shell with a very small BR of $\mathcal{O}(10^{-10})$. The electroweak corrections change the BRs relatively by $-20.6\,\%$ to $24.5\,\%$ and are hence sizeable. For the CP-odd Higgs boson A, the dominant decay mode by far is the decay into a top quark pair. Moreover, the scenario provides an OS decay of A into a Z boson and the SM-like Higgs boson h with a BR in the percent level. Like the heavy CP-even Higgs boson, the electroweak corrections to the BRs of the CP-odd Higgs boson range from $-32.2\,\%$ to $0.9\,\%$ and are sizeable in particular for the decay into Zh. The charged Higgs boson $H^\pm$ decays dominantly into a top-bottom quark pair with a BR of $97\,\%$, while the scenario additionally allows for an OS decay of $H^\pm$ into $W^\pm h$, with a BR at the percent level. In the parameter set "P1", the decays of $H^\pm$ into $W^\pm$ and either H or A are realized only off-shell with BRs of $\mathcal{O}(10^{-5})$ and $\mathcal{O}(10^{-3})$, respectively. The electroweak contributions shift the BRs by $-7.5\,\%$ to $15.8\,\%$. The analysis shows that the electroweak corrections to the partial decay widths and to the BRs are not negligible. In contrast, especially for the additional Higgs bosons of the 2HDM with respect to the SM, they can be of relevant size. Consequently, the inclusion of the electroweak corrections is mandatory of a more precise calculation of the Higgs boson observables.

In order to analyze the sensitivity of the BRs on the 2HDM-specific input parameters and to compare the electroweak one-loop partial decay widths computed within different renormalization schemes for the scalar mixing angles, we consider the second parameter set "P2" as defined in Eq. (7.5). The scenario features a heavy Higgs boson H and a pair of charged Higgs bosons $H^\pm$ both with masses of $\mathcal{O}(300\,\text{GeV})$ as well as a comparatively heavy CP-odd Higgs boson A with a mass of $\mathcal{O}(500\,\text{GeV})$. Due to the distribution of the masses, the scenario
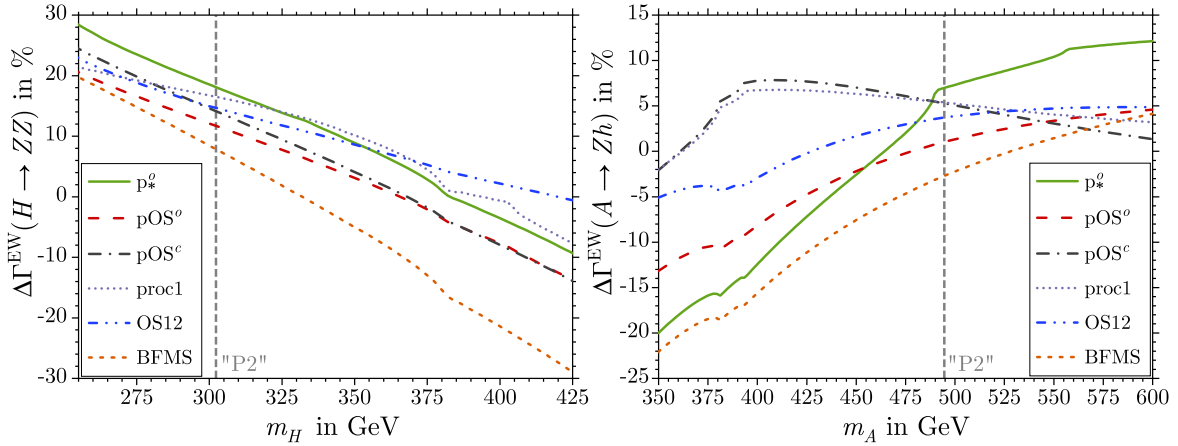
Figure 7.2.: Scenario "P2": Relative correction $\Delta\Gamma^{\mathrm{EW}}$ as defined in Eq. (7.7) between the one-loop and tree-level electroweak partial decay width of the decay channel $H \to ZZ$ as a function of m_H (left) and of the decay channel $A \to Zh$ as a function of m_A (right) for several renormalization schemes (for a definition of the abbreviations used, cf. Table 6.1).

allows, among other decay modes, for an OS decay of the heavy CP-even Higgs into a pair of SM-like Higgs bosons h as well as for an OS decay of the CP-odd Higgs boson into $t\bar{t}$, $Z\,h$ and $W^{\pm}H^{\mp}$ final states. In order to analyze the dependence of the BRs on the 2HDM-specific input parameters, we perform a variation of the masses of the heavy CP-even and the CP-odd Higgs boson separately, in the ranges specified in the preceding Sec. 7.1[26].

Figure 7.1 shows the electroweak-corrected BRs of all decay modes of the heavy CP-even Higgs boson H and of the CP-odd Higgs boson A as a function of either m_H or m_A on the left-hand and right-hand sides of the figure, respectively, where the color code denotes the various final states. The dashed vertical lines indicate the value of the respective Higgs mass corresponding to its initial value defined in the parameter set "P2", cf. Eq. (7.5). As can be inferred from the plots, the BRs strongly depend on the chosen values of m_H and m_A. For increasing masses, additional decay channels are realized OS and their corresponding BRs potentially suppress those of other decay modes. This is the case *e.g.* for the decay of the CP-odd Higgs boson A into the $Z\,h$ final state, with the corresponding BRs exceeding the BRs of all other decay modes for intermediate values of m_A between $220\,\mathrm{GeV}$ and $330\,\mathrm{GeV}$, and for the decay of the A boson into the final state $Z\,H$ for values $m_A > 450\,\mathrm{GeV}$. The heavy CP-even Higgs boson H dominantly decays into pairs of $W^{\pm}$ or Z bosons for values of m_H below $250\,\mathrm{GeV}$. For $m_H \gtrsim 2m_h$, the OS decay of the heavy CP-even Higgs into two SM-like Higgs bosons becomes kinematically allowed and hence, the BR for this decay channel becomes relevant for masses m_H up to approximately $400\,\mathrm{GeV}$. In particular, for scenario "P2", this decay channel is the dominant one with a BR of $57\,\%$. For values of m_H larger than $400\,\mathrm{GeV}$, the BR for the decay into $W^{\pm}H^{\mp}$ final states exceeds the BRs of all other decay channels.

In order to analyze the dependence of the size of the electroweak one-loop corrections to the partial decay widths on the renormalization scheme of the scalar mixing angles, we again perform a numerical analysis with the input parameter set "P2" with the same variations of the masses m_H and m_A as before. For the analysis performed in this work, we compute the relative correction $\Delta\Gamma^{\mathrm{EW}}$ defined in Eq. (7.7) as a function of m_H and m_A for two specific decay channels, namely for the decay channels $H \to Z\,Z$ and $A \to Z\,h$, and for five different

---

[26]For some of the figures presented in the following, however, we reduce the range for both parameters for a better legibility of the plots.
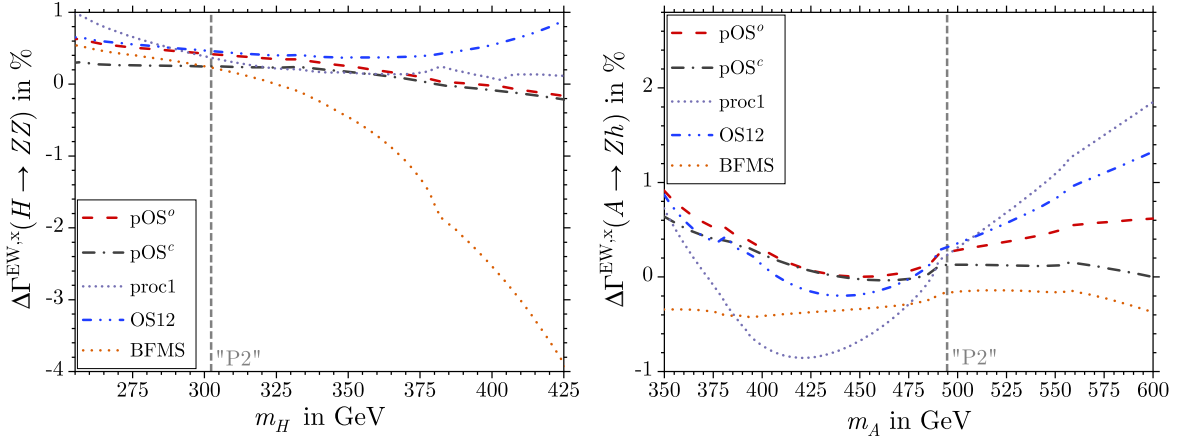
Figure 7.3.: The difference $\Delta\Gamma^{\text{EW,x}}$ as defined in Eq. (7.8) between the one-loop electroweak partial decay width of the decay channel $H \rightarrow ZZ$ computed in several renormalization schemes "x" (cf. Table 6.1 for a definition of the abbreviations used) with respect to the one-loop width as computed in the p_*-pinched scheme "p_*^o". The difference is presented for the decay channel $H \rightarrow ZZ$ as a function of m_H (left-hand side) and for the decay channel $A \rightarrow Zh$ as a function of m_A (right-hand side). For the calculation of all values in the plots, the input parameters were set according to the set "P2".

renormalization schemes. For each of the five schemes considered in this analysis, the tree-level and one-loop decay widths entering the calculation of $\Delta\Gamma^{\text{EW}}$ are always defined in the same input renormalization scheme. For a direct comparison of the decay widths calculated within the different schemes, we convert the input parameters as described in Sec. 6.2. In Fig. 7.2, we present the relative deviations $\Delta\Gamma^{\text{EW}}$ between the one-loop and tree-level decay widths of the two decay channels as a function of m_H and m_A on the left-hand and right-hand sides of the figure, respectively. The vertical dashed line indicates the values of m_H and m_A corresponding to the respective initial values defined as the parameter set "P2" in Eq. (7.5). As can be inferred from the plots, the sizes of the electroweak one-loop corrections are sensitive on the choice of the renormalization scheme for a large range of the Higgs boson masses. For the mass values corresponding to the set "P2" for instance, the relative size of the one-loop corrections $\Delta\Gamma^{\text{EW}}$ to the process $H \rightarrow ZZ$ varies between 9% and 20% and for the process $A \rightarrow Zh$ between -3% and 7% for the different renormalization schemes considered here.

In order to get a rough estimate of the remaining theoretical uncertainty of the partial decay widths due to missing higher-order corrections, we compare the decays widths computed in different renormalization schemes "x" with the reference scheme that we choose here to be "p_*^o". We hence compute the relative difference $\Delta\Gamma^{\text{EW,x}}$, defined in Eq. (7.8), where we again compute the tree-level and one-loop partial decay widths in the same renormalization scheme "x" for each of the considered schemes. In Fig. 7.3 we show the relative difference $\Delta\Gamma^{\text{EW,x}}$ for the same two decay channels analyzed before, *i.e.* for $H \rightarrow ZZ$ as a function of m_H on the left-hand side and for $A \rightarrow Zh$ as a function of m_A on the right-hand side of the figure. As can be inferred from the plots, the relative difference between the widths computed in the different schemes varies between approximately -4% and 1% for the former decay channel and between approximately -1% and 2% for the latter decay channel over the whole range of varied masses presented in the plots. We want to emphasize again that for the computation of the widths within different renormalization schemes, a parameter conversion as described in Sec. 3.5 is performed in `2HDECAY` which allows for a consistent comparison of the widths computed within these different schemes. From the plots, it can be inferred that the relative
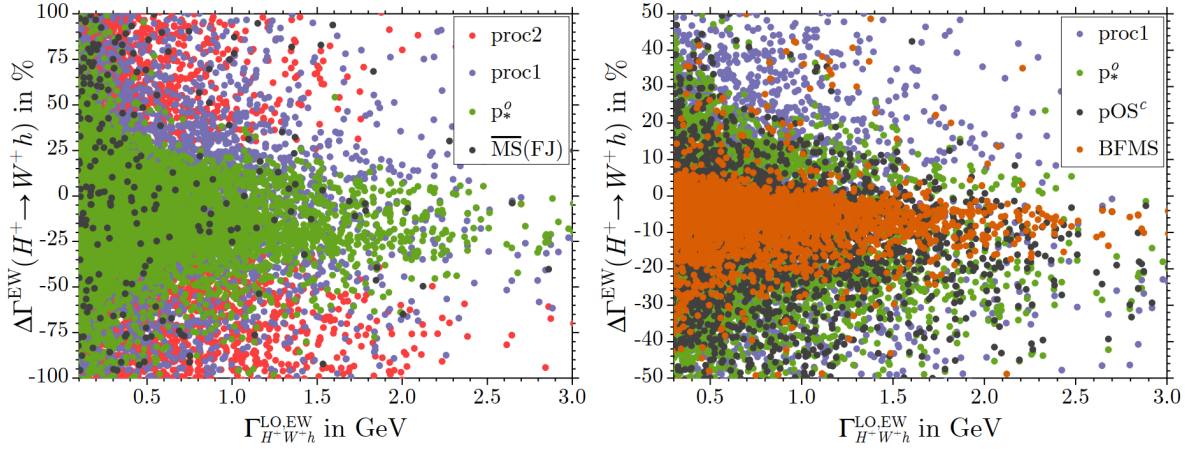
Figure 7.4.: Parameter Set "P3": The relative size of the electroweak corrections $\Delta\Gamma^{\mathrm{EW}}$ as defined in Eq. (7.7) between the one-loop and tree-level electroweak partial decay width of the decay channel $H^+ \to W^+ h$ as a function of the tree-level electroweak decay width $\Gamma^{\mathrm{LO,EW}}_{H^+W^+h}$ for two different scales on the $\Delta\Gamma^{\mathrm{EW}}$ axis and for different renormalization schemes used for the computation of the one-loop widths (left and right).

uncertainty on the one-loop electroweak partial decay widths, estimated from a change of the renormalization schemes, is of the order of a few percent for the decay channels and points in parameter space considered.

As briefly mentioned in Sec. 5.3, some renormalization schemes for the scalar mixing angles considered in this thesis can lead to numerical instabilities, *i.e.* their application can lead to large one-loop contributions to the electroweak partial decay widths. On the one hand, this numerical instability of the one-loop results can appear in certain regions of parameter space of the real 2HDM if *e.g.* the mixing angles α and β are set to such values that certain combinations of these two mixing angles become very small. Since these combinations typically appear in the denominators of either the genuine one-loop vertex corrections or of certain CTs of the partial decay widths, such a choice of α and β leads to an enhancement of uncanceled one-loop contributions. On the other hand, an unsuitable choice of mixing angle CTs can lead to an artificial increase of the one-loop partial decay widths if the mixing angle CTs *themselves* become very small or large, leading to uncanceled contributions to the partial decay width. While the former effect of numerical instability is restricted to certain corners of parameter space, the latter appears more generally for a large variety of different parameter sets.

In order to disentangle these two effects for a categorization of a renormalization scheme with respect to its numerical stability, we perform a numerical analysis on the relative size of the electroweak one-loop corrections, again quantified through $\Delta\Gamma^{\mathrm{EW}}$ as defined in Eq. (7.7), for 15 000 different input parameter sets randomly distributed in the parameter space of the real 2HDM denoted by the set "P3", cf. Sec. 7.1. The electroweak tree-level and one-loop partial decay widths are again calculated within the same input renormalization scheme. In contrast to the analyses performed before, we consider the reference scheme of the mixing angles to be equal to the input renormalization scheme for each parameter point in the set "P3" and for each considered renormalization scheme, separately. Consequently, no conversion of the mixing angles between the different schemes is required since we do not compare the results computed within the different renormalization schemes directly with each other but instead analyze each renormalization scheme with respect to its numerical stability separately. In Fig. 7.4, we show the relative size $\Delta\Gamma^{\mathrm{EW}}$ of the electroweak one-loop corrections as a function of the tree-level partial decay width $\Gamma^{\mathrm{LO,EW}}_{H^+W^+h}$ for the decay of a charged Higgs boson H^+ into

a pair of W^+ and h bosons for several different renormalization schemes of the scalar mixing angles. For both plots in the figure, we exclude the region where the tree-level partial decay width is vanishing since in this case, the measure $\Delta\Gamma^{\mathrm{EW}}$ becomes very sensitive to the one-loop corrections and is consequently not a suitable quantity for the estimate of the numerical stability of the renormalization schemes.

On the left-hand side of Fig. 7.4, the difference $\Delta\Gamma^{\mathrm{EW}}$ is plotted up to values of $\pm\,100\,\%$ as a function of the tree-level width $\Gamma^{\mathrm{LO,EW}}_{H^+W^+h}$. The results for the $\overline{\mathrm{MS}}$ scheme, defined in the framework of the alternative FJ tadpole scheme, mostly lie outside the plotted region with relative differences up to $\pm\,10\,000\,\%$. Hence, the $\overline{\mathrm{MS}}$ scheme leads to one-loop corrections to the partial decay widths that are orders of magnitude larger than the tree-level widths over a large range of input parameter sets and the loop-corrected decay widths become unphysical. This reconfirms the analysis performed in [227] for the same decay channel and indicates that the $\overline{\mathrm{MS}}$ scheme of the scalar mixing angles is an unsuitable scheme for the computation of partial decay widths and BRs for the decays of the Higgs bosons in the 2HDM[27]. Analogously, the process-dependent scheme "proc2" defined via the loop-corrected decay widths of the decay channels $A \to \tau^+\tau^-$ and $h \to \tau^+\tau^-$ also leads to huge one-loop corrections. While in this case the relative differences $\Delta\Gamma^{\mathrm{EW}}$ are typically smaller than the ones computed in the $\overline{\mathrm{MS}}$ scheme, they nevertheless are as large as $\pm 1000\,\%$ over a large region of the parameter space. Such huge corrections indicate that the decay widths need to be corrected by *e.g.* including two-loop contributions or applying resummation methods, since corrections up to $\pm\,10\,000\,\%$ are unphysical at fixed one-loop order, as discussed in Sec. 6.2. Moreover, relative corrections below $-100\,\%$ correspond to negative one-loop partial decay widths, which is unphysical as well. In these cases, the loop-corrected partial decay widths should be discarded and not used for any phenomenological studies.

For the process-dependent scheme "proc1" and the p_*-pinched scheme "p$^o_*$" on the other hand, the relative corrections are typically orders of magnitude smaller. In order to analyze their size further, we present on the right-hand side of Fig. 7.4 again the relative electroweak corrections $\Delta\Gamma^{\mathrm{EW}}$ as a function of the tree-level decay widths, but with a smaller range of the $\Delta\Gamma^{\mathrm{EW}}$ axis. Apart from the "proc1" and "p$^o_*$" schemes also presented on the left-hand side of the figure, we moreover present the numerical results for the OS-pinched scheme "pOS^c" and the rigid symmetry scheme "BFMS". As can be inferred from the plot, the results for the process-dependent scheme are relatively widespread and can become larger than $25\,\%$ over a wide range of input parameter sets, while most of the results computed in the two pinched schemes and the rigid symmetry scheme lie in a band within $\pm 25\,\%$, with the majority of the deviations $\Delta\Gamma^{\mathrm{EW}}$ being between $-12\,\%$ and $10\,\%$. Consequently, these three renormalization schemes lead to numerically stable results for the considered decay channel and for the parameter sets used for the analysis. While we do not show the numerical results for the other renormalization schemes introduced in Sec. 5.3 explicitly here, we have verified that the relative corrections $\Delta\Gamma^{\mathrm{EW}}$ computed within the other PT-based schemes and the physical OS schemes are of a similar size as the ones computed in the two pinched schemes and the rigid symmetry scheme shown on the right-hand side of Fig. 7.4.

---

[27]Although we only present results for the $\overline{\mathrm{MS}}$ scheme in the alternative FJ tadpole scheme here, we confirmed that analogous conclusions can be drawn for the $\overline{\mathrm{MS}}$ scheme defined in the standard tadpole scheme. However, since the latter not only leads to numerically unstable results but moreover also to GFP-dependent partial decay widths, we do not present the numerical results for this scheme here explicitly.

Conclusion of Part II

The key objective of Part II of this thesis was the calculation of the electroweak one-loop corrections to the partial decay widths of all Higgs bosons of the 2HDM and the development of the new computer program `2HDECAY`, thereby increasing the precision of the partial decay widths and BRs of all Higgs boson decays.

To that end, we presented the electroweak Lagrangian and the scalar potential of the 2HDM. In the mass basis, the model features two CP-even Higgs bosons h and H, one CP-odd Higgs boson A and the charged Higgs bosons $H^\pm$ together with the corresponding scalar mixing angles α and β of the CP-even and CP-odd/charged sectors, respectively.

We presented the electroweak one-loop renormalization of the independent parameters of the 2HDM. For the renormalization of the scalar mixing angles, we presented several different renormalization schemes based on $\overline{\text{MS}}$ conditions, (physical) OS-motivated approaches, rigid symmetries, process-dependent definitions and on the application of the PT. We characterized the different schemes with respect to the three desirable criteria of process independence, GFP independence and numerical stability.

The electroweak partial decay widths of all Higgs bosons of the 2HDM at tree level and one-loop order were calculated with the newly developed tool `2HDMCalc` and the resulting decay widths were consistently combined with the tree-level and loop-corrected widths provided by `HDECAY 6.52`, including state-of-the-art QCD corrections, where applicable, to form the newly developed `Python` program `2HDECAY`. The program allows for the computation of the BRs and partial decay widths of all Higgs bosons of the real 2HDM both excluding and including the newly computed electroweak corrections to the Higgs decays. Being fast, `2HDECAY` moreover enables efficient phenomenological studies on the decays of the Higgs bosons of the real 2HDM.

We demonstrated a compact numerical analysis on the size of the electroweak corrections implemented in `2HDECAY`. To that end, we defined input parameter sets for the real 2HDM which are compatible with most recent theoretical and experimental constraints. We showed that the electroweak corrections to the partial decay widths and BRs, in particular for those of the additional non-SM-like Higgs bosons of the 2HDM, can become sizeable and hence, they are of importance for the calculation of the BRs and partial decay widths to highest precision. We presented a comparison of the size of selected one-loop decay widths computed within different renormalization schemes of the scalar mixing angles, thereby providing an estimate

of the remaining theoretical uncertainties of the numerical results due to missing higher-order corrections. For the considered decay channels, we found that the remaining uncertainty is of the order of a few percent over a large range of chosen input parameter values. Moreover, we compared the size of the one-loop corrections computed within different renormalization schemes for $15\,000$ different input parameter sets in order to categorize the schemes with respect to their numerical stability. For the decay channel considered in this analysis, we found that the $\overline{\text{MS}}$ and the process-dependent schemes led to numerically unstable results for a majority of the considered input parameters. On the other hand, the analysis showed that the PT-based schemes, the physical OS scheme as well as the rigid symmetry scheme lead to numerically stable results for a majority of all input parameter sets considered.

Part III.

Electroweak One-Loop Corrections to Higgs Boson Decays in the N2HDM

A Brief Introduction to the N2HDM

Part III of this thesis is dedicated to the calculation of the partial decay widths of all Higgs bosons of the N2HDM at tree level and one-loop order in the electroweak corrections, with the latter being calculated for OS and non-loop induced decays, and their combination with the state-of-the-art QCD corrections implemented in `N2HDECAY` in form of a newly developed program `ewN2HDECAY`, thereby enabling a more precise calculation of the BRs and partial decay widths of the Higgs bosons of the N2HDM. In our work, we consider a CP-conserving N2HDM with an additional discrete $\mathbb{Z}_2$ symmetry which is softly broken.

We start in Sec. 9.1 with the introduction of the electroweak Lagrangian of the N2HDM and all its contributing terms. Since we consider the calculation of the electroweak corrections in our work, we restrict the introduction of the N2HDM to its electroweak sector. In Sec. 9.2, we discuss the scalar potential of the N2HDM in greater detail, focusing on the differences between the N2HDM and the 2HDM with respect to the extended scalar sector of the former model. In the subsequent Sec. 9.3, we briefly discuss the different realizations of the N2HDM concerning the Yukawa couplings of the Higgs doublets to the fermion sector. This chapter concludes in Sec. 9.4 with an overview over the set of independent parameters which are used for the calculation of the partial decay widths and branching ratios of the Higgs boson decays in `ewN2HDECAY`.

9.1. The Electroweak Lagrangian of the N2HDM

We consider a general CP-conserving N2HDM [19] with two additional discrete global $\mathbb{Z}_2$ symmetries, one of which is softly broken while the other one is retained as an exact symmetry of the Lagrangian in the unbroken phase. In contrast to the CP-conserving 2HDM considered in Part II, the N2HDM contains an additional real $SU(2)_L$ singlet Φ_s with weak hypercharge $Y = 0$. The electroweak Lagrangian of the N2HDM is given by

$$\mathcal{L}_{\mathrm{N2HDM}}^{\mathrm{EW}} = \mathcal{L}_{\mathrm{YM}} + \mathcal{L}_{\mathrm{F}} + \mathcal{L}_{\mathrm{S}}^{\mathrm{N2HDM}} + \mathcal{L}_{\mathrm{Yuk}} + \mathcal{L}_{\mathrm{GF}} + \mathcal{L}_{\mathrm{FP}} \ . \tag{9.1}$$

Most of these terms are formally equivalent to the ones present in the electroweak Lagrangian of the 2HDM as defined in Sec. 4.1 and their explicit forms are presented for the 2HDM *e.g.* in [168] from which their forms for the N2HDM can be directly inferred. As for the 2HDM, we use the class of R_ξ gauges [218, 219] as a gauge-fixing procedure.

The scalar Lagrangian $\mathcal{L}_S^{N2HDM}$ of the N2HDM contains the kinetic terms of the scalar fields as well as the scalar potential. It comprises of all additional contributions stemming from the gauge singlet which give rise to the additional scalar sector of the N2HDM in comparison to the 2HDM. We describe these additional contributions to the scalar Lagrangian in detail in the subsequent Sec. 9.2. Due to the extended scalar sector and the resulting modified rotation of the scalar fields from the gauge to the mass basis, the Yukawa Lagrangian $\mathcal{L}_{Yuk}$ containing the couplings between the fermionic and scalar fields is slightly modified in comparison to the 2HDM as well. We discuss these modifications and present the Yukawa coupling parameters of the N2HDM in Sec. 9.3.

9.2. The Scalar Potential

The scalar Lagrangian of the general CP-conserving N2HDM is an extension of the scalar Lagrangian of the 2HDM presented in Eq. (4.3) which accounts for the additional $SU(2)_L$ singlet Φ_s contained in the model. The explicit form of the Lagrangian is given by

$$\mathcal{L}_S^{N2HDM} = \sum_{i=1}^{2}(D_\mu\Phi_i)^\dagger(D^\mu\Phi_i) + (\partial_\mu\Phi_s)(\partial^\mu\Phi_s) - V_{N2HDM} \ , \qquad (9.2)$$

where the covariant derivative D_μ is defined in Eq. (4.2). The explicit form of the scalar potential is given by [19]

$$V_{N2HDM} = \frac{1}{2}m_s^2\Phi_s^2 + \frac{1}{8}\lambda_6\Phi_s^4 + \frac{1}{2}\lambda_7\left(\Phi_1^\dagger\Phi_1\right)\Phi_s^2 + \frac{1}{2}\lambda_8\left(\Phi_2^\dagger\Phi_2\right)\Phi_s^2 + V_{2HDM} \ . \qquad (9.3)$$

The potential contains the real mass parameter m_s and the three dimensionless coupling constants λ_i ($i = 6, 7, 8$) which, together with the parameters m_{11}, m_{22}, m_{12} and λ_i ($i = 1, ..., 5$) stemming from the 2HDM potential V_{2HDM}, are all independent parameters of the tree-level scalar potential of the N2HDM in the gauge basis.

We impose two discrete symmetries $\mathbb{Z}_2$ on the Lagrangian of the N2HDM. The first discrete $\mathbb{Z}_2$ symmetry is analogous to the 2HDM and corresponds to the invariance of the Lagrangian under the simultaneous field transformations

$$\Phi_1 \to \Phi_1 \ , \quad \Phi_2 \to -\Phi_2 \ , \quad \Phi_s \to \Phi_s \ . \qquad (9.4)$$

We break this symmetry softly by allowing the parameter m_{12}^2 to be non-vanishing. The second discrete $\mathbb{Z}_2$ symmetry corresponds to the invariance of the Lagrangian under the simultaneous transformations

$$\Phi_1 \to \Phi_1 \ , \quad \Phi_2 \to \Phi_2 \ , \quad \Phi_s \to -\Phi_s \ . \qquad (9.5)$$

In the realization of the N2HDM studied in our work, this symmetry is retained in the unbroken phase of the potential.

Analogous to the 2HDM, we introduce two VEVs v_i ($i = 1, 2$) for the two $SU(2)_L$ doublets Φ_i and additionally a VEV v_s for the $SU(2)_L$ singlet Φ_s. After EWSB the doublet and singlet fields can be expanded as follows,

$$\Phi_1 = \begin{pmatrix} \omega_1^+ \\ \dfrac{v_1 + \rho_1 + i\eta_1}{\sqrt{2}} \end{pmatrix} \ , \quad \Phi_2 = \begin{pmatrix} \omega_2^+ \\ \dfrac{v_2 + \rho_2 + i\eta_2}{\sqrt{2}} \end{pmatrix} \ , \quad \Phi_s = v_s + \rho_s \ , \qquad (9.6)$$

where in comparison to the 2HDM we introduced the additional real scalar field ρ_s which leads to the presence of an additional CP-even Higgs boson in the N2HDM. The CP-odd and

charged sectors on the other hand do not change with respect to the 2HDM. Likewise, the characteristic parameter describing the ratios of the VEVs is given by

$$t_\beta \equiv \frac{v_2}{v_1} \ . \tag{9.7}$$

By inserting the doublet and singlet expansions of Eq. (9.6) into the scalar potential in Eq. (9.3), we obtain[28]

$$V_{\text{N2HDM}} = \frac{1}{2} \begin{pmatrix} \rho_1 & \rho_2 & \rho_s \end{pmatrix} \mathcal{M}_\rho^2 \begin{pmatrix} \rho_1 \\ \rho_2 \\ \rho_s \end{pmatrix} + T_1 \rho_1 + T_2 \rho_2 + T_s \rho_s + \ \cdots \ . \tag{9.8}$$

The application of the minimum conditions leads to the tree-level conditions

$$T_1|^{\text{tree}} = T_2|^{\text{tree}} = T_s|^{\text{tree}} = 0 \tag{9.9}$$

for the three tadpole terms

$$T_1 \equiv m_{11}^2 v_1 - m_{12}^2 v_2 + \frac{1}{2}\lambda_1 v_1^3 + \frac{1}{2}\lambda_{345} v_1 v_2^2 + \frac{1}{2}\lambda_7 v_1 v_s^2 \ , \tag{9.10}$$

$$T_2 \equiv m_{22}^2 v_2 - m_{12}^2 v_1 + \frac{1}{2}\lambda_1 v_3^3 + \frac{1}{2}\lambda_{345} v_1^2 v_2 + \frac{1}{2}\lambda_8 v_2 v_s^2 \ , \tag{9.11}$$

$$T_s \equiv m_s^2 v_s + \frac{1}{2}\lambda_6 v_s^3 + \frac{1}{2}\lambda_7 v_1^2 v_s + \frac{1}{2}\lambda_8 v_2^2 v_s \ , \tag{9.12}$$

where λ_{345} is defined in Eq. (4.5). The minimum conditions can be used to eliminate m_{11}^2, m_{22}^2 and m_s^2 in favor of the tadpole terms and the other parameters of the scalar potential. The 3×3 mass matrix $\mathcal{M}_\rho^2$ introduced in Eq. (9.8) is given by

$$\mathcal{M}_\rho^2 \equiv \begin{pmatrix} m_{12}^2 \dfrac{v_2}{v_1} + \lambda_1 v_1^2 & -m_{12}^2 + \lambda_{345} v_1 v_2 & \lambda_7 v_1 v_s \\ -m_{12}^2 + \lambda_{345} v_1 v_2 & m_{12}^2 \dfrac{v_1}{v_2} + \lambda_2 v_2^2 & \lambda_8 v_2 v_s \\ \lambda_7 v_1 v_s & \lambda_8 v_2 v_s & \lambda_6 v_s^2 \end{pmatrix} + \begin{pmatrix} \dfrac{T_1}{v_1} & 0 & 0 \\ 0 & \dfrac{T_2}{v_2} & 0 \\ 0 & 0 & \dfrac{T_s}{v_s} \end{pmatrix} , \tag{9.13}$$

while the mass matrices $\mathcal{M}_\eta^2$ and $\mathcal{M}_\omega^2$ of the CP-odd and charged scalar fields are the same as the ones presented for the 2HDM in Eqs. (4.29) and (4.30), respectively. We transform the scalar potential from the gauge basis to the mass basis by means of the CP-even 3×3 rotation matrix

$$R \equiv \begin{pmatrix} c_{\alpha_1} c_{\alpha_2} & s_{\alpha_1} c_{\alpha_2} & s_{\alpha_2} \\ -(c_{\alpha_1} s_{\alpha_2} s_{\alpha_3} + s_{\alpha_1} c_{\alpha_3}) & c_{\alpha_1} c_{\alpha_3} - s_{\alpha_1} s_{\alpha_2} s_{\alpha_3} & c_{\alpha_2} s_{\alpha_3} \\ -c_{\alpha_1} s_{\alpha_2} c_{\alpha_3} + s_{\alpha_1} s_{\alpha_3} & -(c_{\alpha_1} s_{\alpha_3} + s_{\alpha_1} s_{\alpha_2} c_{\alpha_3}) & c_{\alpha_2} c_{\alpha_3} \end{pmatrix} , \tag{9.14}$$

where we introduced the three CP-even scalar mixing angles α_i $(i = 1, 2, 3)$, as well as by means of the CP-odd and charged 2×2 rotation matrices R_{β_n} and R_{β_c}, respectively, generically

---

[28]Here and in the following, we do not explicitly introduce a superscript "N2HDM" for indicating that the parameters, tadpole terms, etc. differ with respect to the corresponding quantities presented for the 2HDM in Sec. 4.2. Instead, the difference of the parameters between the two models is implicitly understood.

defined in Eq. (4.31). Analogously to the CP-odd and charged sectors, the rotation matrix R transforms the CP-even mass matrix into the diagonal form

$$D_\rho^2 \equiv R_\alpha^{\mathrm{T}} \mathcal{M}_\rho^2 R_\alpha = \begin{pmatrix} m_{H_1}^2 & 0 & 0 \\ 0 & m_{H_2}^2 & 0 \\ 0 & 0 & m_{H_3}^2 \end{pmatrix} + \begin{pmatrix} T_{H_1 H_1} & T_{H_1 H_2} & T_{H_1 H_3} \\ T_{H_1 H_2} & T_{H_2 H_2} & T_{H_2 H_3} \\ T_{H_1 H_3} & T_{H_2 H_3} & T_{H_3 H_3} \end{pmatrix} , \tag{9.15}$$

where we introduced the squared masses $m_{H_i}^2$ $(i = 1, 2, 3)$ and rotated tadpole parameters as

$$T_{H_i H_j} \equiv R_{i1} R_{j1} \frac{T_1}{v_1} + R_{i2} R_{j2} \frac{T_2}{v_2} + R_{i3} R_{j3} \frac{T_s}{v_s} \quad (i, j = 1, 2, 3) . \tag{9.16}$$

Per convention, we impose an ordering of the CP-even Higgs bosons with ascending mass,

$$m_{H_1} \leq m_{H_2} \leq m_{H_3} . \tag{9.17}$$

The CP-even rotation matrix R transforms the fields in the gauge basis into the physical Higgs boson fields H_i via the transformation

$$\begin{pmatrix} H_1 \\ H_2 \\ H_3 \end{pmatrix} = R \begin{pmatrix} \rho_1 \\ \rho_2 \\ \rho_s \end{pmatrix} . \tag{9.18}$$

Together with the CP-odd Higgs boson A and the charged Higgs bosons $H^\pm$, these form the mass basis of the scalar potential. The dimensionless coupling constants λ_i $(i = 1, ..., 8)$ of the unbroken scalar potential are connected to the parameters in the mass basis via the relations [57]

$$\lambda_1 = \frac{1}{v^2 c_\beta^2} \left[\sum_{i=1}^3 m_{H_i}^2 R_{i1}^2 - \frac{s_\beta}{c_\beta} m_{12}^2 \right] , \tag{9.19}$$

$$\lambda_2 = \frac{1}{v^2 s_\beta^2} \left[\sum_{i=1}^3 m_{H_i}^2 R_{i2}^2 - \frac{c_\beta}{s_\beta} m_{12}^2 \right] , \tag{9.20}$$

$$\lambda_3 = \frac{1}{v^2} \left[\frac{1}{s_\beta c_\beta} \sum_{i=1}^3 m_{H_i}^2 R_{i1} R_{i2} + 2 m_{H^\pm}^2 - \frac{1}{s_\beta c_\beta} m_{12}^2 \right] , \tag{9.21}$$

$$\lambda_4 = \frac{1}{v^2} \left[\frac{m_{12}^2}{s_\beta c_\beta} + m_A^2 - 2 m_{H^\pm}^2 \right] , \tag{9.22}$$

$$\lambda_5 = \frac{1}{v^2} \left[\frac{m_{12}^2}{s_\beta c_\beta} - m_A^2 \right] , \tag{9.23}$$

$$\lambda_6 = \frac{1}{v_s^2} \sum_{i=1}^3 m_{H_i}^2 R_{i3}^2 , \tag{9.24}$$

$$\lambda_7 = \frac{1}{v v_s c_\beta} \sum_{i=1}^3 m_{H_i}^2 R_{i1} R_{i3} , \tag{9.25}$$

$$\lambda_8 = \frac{1}{v v_s s_\beta} \sum_{i=1}^3 m_{H_i}^2 R_{i2} R_{i3} . \tag{9.26}$$

	$\kappa_{H_i VV}$	$\tilde{\kappa}_{H_i VH}$
H_1	$c_{\alpha_2} c_{\beta-\alpha_1}$	$-c_{\alpha_2} s_{\beta-\alpha_1}$
H_2	$-s_{\alpha_2} s_{\alpha_3} c_{\beta-\alpha_1} + c_{\alpha_3} s_{\beta-\alpha_1}$	$s_{\alpha_2} s_{\alpha_3} s_{\beta-\alpha_1} + c_{\alpha_3} c_{\beta-\alpha_1}$
H_3	$-s_{\alpha_2} c_{\alpha_3} c_{\beta-\alpha_1} - s_{\alpha_3} s_{\beta-\alpha_1}$	$s_{\alpha_2} c_{\alpha_3} s_{\beta-\alpha_1} - s_{\alpha_3} c_{\beta-\alpha_1}$

Table 9.1.: Definition of the coupling factors $\kappa_{H_i VV}$ and $\tilde{\kappa}_{H_i VH}$ which characterize the interaction between a CP-even Higgs and two gauge bosons as well as pairs of $W^{\mp} H^{\pm}$ and $Z A$, respectively.

All other relations concerning the CP-odd and charged sectors are the same as in the 2HDM and presented in Sec. 4.2. Especially, the masses of the Goldstone bosons G^0 and $G^{\pm}$, before and after the introduction of the gauge-fixing Lagrangian, as well as the masses of the corresponding Faddeev-Popov ghosts and gauge bosons are unchanged.

Due to the extended CP-even sector in the N2HDM, the coupling constants between the Higgs bosons and the gauge bosons are modified in comparison to the SM. The Feynman rules corresponding to the tree-level interaction of a CP-even Higgs boson H_i with two massive gauge bosons V ($V = W^{\pm}, Z$) is given by

$$i g_{\mu\nu} \kappa_{H_i VV} g_{h_{\mathrm{SM}} VV} \ , \tag{9.27}$$

where $g_{h_{\mathrm{SM}} VV}$ denotes the SM coupling factor, while for the interaction of a CP-even Higgs boson H_i with either $Z A$ or $W^{\mp} H^{\pm}$, the Feynman rules are given by

$$\frac{m_Z}{v} (p_{H_i} - p_A)_\mu \tilde{\kappa}_{H_i VH} \ , \tag{9.28}$$

$$\frac{\pm i m_W}{v} (p_{H_i} - p_{H^{\pm}})_\mu \tilde{\kappa}_{H_i VH} \ , \tag{9.29}$$

where p_x ($x = H_i, A, H^{\pm}$) denotes the four-momentum of the corresponding particle. In Table 9.1, we present the coupling factors $\kappa_{H_i VV}$ and $\tilde{\kappa}_{H_i VH}$. For later convenience, we moreover introduce the short-hand notations $\mathcal{O}^{(x)}_{H_i H_j}$ ($x = 1, 2, 3$) for combinations of the coupling constants between the Higgs bosons and the gauge bosons,

$$\mathcal{O}^{(1)}_{H_i H_j} = \tilde{\kappa}_{H_i VH} \, \tilde{\kappa}_{H_j VH} \ , \tag{9.30}$$

$$\mathcal{O}^{(2)}_{H_i H_j} = \kappa_{H_i VV} \, \kappa_{H_j VV} \ , \tag{9.31}$$

$$\mathcal{O}^{(3)}_{H_i H_j} = \kappa_{H_i VV} \, \tilde{\kappa}_{H_j VH} \ . \tag{9.32}$$

The 2HDM limit of the N2HDM is obtained by simultaneously applying the limits

$$\alpha_1 \longrightarrow \alpha + \frac{\pi}{2} \ , \tag{9.33}$$

$$\alpha_2 \longrightarrow 0 \ , \tag{9.34}$$

$$\alpha_3 \longrightarrow 0 \ , \tag{9.35}$$

$$v_s \longrightarrow \infty \ . \tag{9.36}$$

With this phase convention, the mixing angle α_1 of the N2HDM is related to the mixing angle α of the 2HDM and the Higgs bosons are assigned as $H_1 \to h$ and $H_2 \to H$. In the 2HDM limit, all contributions stemming from the $SU(2)_L$ singlet Φ_s and the corresponding physical Higgs boson H_3 decouple and the particle spectrum of the 2HDM is obtained.

N2HDM type	Y_1^l	Y_2^l	Y_3^l	Y_4^l	Y_1^d	Y_2^d	Y_3^d	Y_4^d
I	R_{12}/s_β	R_{22}/s_β	R_{32}/s_β	$1/t_\beta$	R_{12}/s_β	R_{22}/s_β	R_{32}/s_β	$1/t_\beta$
II	R_{11}/c_β	R_{21}/c_β	R_{31}/c_β	$-t_\beta$	R_{11}/c_β	R_{21}/c_β	R_{31}/c_β	$-t_\beta$
lepton-specific	R_{11}/c_β	R_{21}/c_β	R_{31}/c_β	$-t_\beta$	R_{12}/s_β	R_{22}/s_β	R_{32}/s_β	$1/t_\beta$
flipped	R_{12}/s_β	R_{22}/s_β	R_{32}/s_β	$1/t_\beta$	R_{11}/c_β	R_{21}/c_β	R_{31}/c_β	$-t_\beta$

Table 9.2.: Introduction of the Yukawa coupling parameters for each type of the N2HDM considered in this work.

9.3. The Yukawa Couplings and the Four Types of N2HDMs

The Yukawa Lagrangian $\mathcal{L}_{\text{Yuk}}$ connects the scalar sector of the N2HDM with the fermion sector. Since the singlet field Φ_s does not directly couple to the fermion doublets and singlets, the description of the Yukawa Lagrangian is analogous to the corresponding Lagrangian in the 2HDM as presented in Sec. 4.3. Due to imposing the discrete $\mathbb{Z}_2$ symmetry on the two Higgs doublets, which is only softly broking in the case of a non-vanishing term m_{12}^2, there are four different possibilities of coupling the two Higgs doublets to the fermions as presented in Table 4.1. Analogous to the 2HDM, the softly broken $\mathbb{Z}_2$ symmetry leads to the assignment of exactly one Higgs doublet per fermion field type and consequently, the N2HDM considered in our work is free of FCNCs at tree level.

While the Yukawa Lagrangians of the 2HDM and N2HDM are formally the same, the coupling constants of the physical Higgs bosons H_i to the fermions f nevertheless differ between the two models due to the extended CP-even sector, parametrized by the CP-even rotation matrix in Eq. (9.14). In our work, we parametrize the Yukawa coupling constants through Yukawa coupling parameters Y_i^f $(i = 1, ..., 4)$ as defined by the corresponding terms in the Yukawa Lagrangian,

$$\mathcal{L}_{\text{Yuk}} \supset -\sum_{i=1}^{3} \frac{m_f}{v} Y_i^f \overline{\psi}_f \psi_f H_i + \frac{2im_f}{v} I_W^{z,f} Y_4^f \overline{\psi}_f \gamma_5 \psi_f A \ , \tag{9.37}$$

where $I_W^{z,f}$ denotes the third component of the weak isospin of the corresponding fermion field ψ_f. In Table 9.2, we present the explicit values of Y_i^f for each type of N2HDM.

9.4. Set of Independent Parameters

We conclude this chapter with a presentation of all independent parameters necessary for the calculation of the electroweak one-loop corrections to the decay widths of the Higgs bosons in the N2HDM with the newly developed computer program ewN2HDECAY, further described in Chapter 11. To that end, we combine the electroweak one-loop corrections with the state-of-the-art QCD corrections implemented in the computer program N2HDECAY. As described in Sec. 4.4 for the 2HDM, N2HDECAY analogously requires the electromagnetic coupling constant $\alpha_{\text{em}}(0)$ in the Thomson limit, the strong coupling constant α_s as well as the total decay widths Γ_W and Γ_Z of the $W^\pm$ and Z bosons. These, together with the parameters required for the evaluation of the electroweak one-loop corrections, are combined into the set of independent parameters in the mass basis of the N2HDM as used in our work,

$$\{G_F, \alpha_s, \Gamma_W, \Gamma_Z, \alpha_{\text{em}}, m_W, m_Z, m_f, V_{ij}, t_\beta, m_{12}^2, v_s, \alpha_1, \alpha_2, \alpha_3, m_{H_1}, m_{H_2}, m_{H_3}, \tag{9.38}$$
$$m_A, m_{H^\pm}\} \ .$$

For the calculation of the electroweak corrections, most of these input parameters require renormalization. In the subsequent Chapter 10, we present the electroweak renormalization of these parameters.

The Renormalization of the N2HDM in a Nutshell

The calculation of the electroweak one-loop corrections to the partial decay widths of the Higgs bosons of the N2HDM entails the computation of UV-divergent loop integrals. As discussed in Sec. 3.1 in general, we regulate these UV divergences by means of DREG. For the renormalization of these UV divergences, we adopt the schemes applied to the independent parameters of the 2HDM in Chapter 5 and extend them to account for the additional CP-even Higgs boson in the N2HDM. Since these two models mainly differ with respect to their CP-even sectors, we restrict the discussion of the renormalization of the N2HDM to the differences arising through its extended scalar sector in the following.

Starting with Sec. 10.1, we recapitulate the importance of the proper renormalization of the minimum conditions of the scalar potential with respect to GFP-independent one-loop partial decay widths. In the subsequent Sec. 10.2, we present the renormalization of the gauge, scalar and fermion sectors while the renormalization of the four scalar mixing angles of the N2HDM is presented in Sec. 5.3. Finally, in Sec. 10.4 and Sec. 10.5, we present the $\overline{\text{MS}}$ renormalization of the soft-$\mathbb{Z}_2$-breaking scale m_{12}^2 and the singlet VEV v_s, respectively.

10.1. Renormalization of the Tadpoles

As discussed in detail in Sec. 5.1 for the 2HDM, the proper application of the minimum conditions of the scalar potential beyond tree level is crucial for the formulation of GFP-independent renormalization schemes for the scalar mixing angles as well as for obtaining GFP-independent partial decay widths at the one-loop level. The corresponding treatment of the vacuum structure of the scalar potential, or equivalently of the tadpole terms, can be directly transferred to the case of the N2HDM. Since we discussed both the standard and the alternative FJ tadpole scheme in detail in Sec. 5.1 for the 2HDM, we only recapitulate the key ideas behind the two approaches in the following.

In the commonly applied standard tadpole scheme, we introduce CTs for the tadpole terms defined in Eqs. (9.10) to (9.12) by splitting the bare tadpole terms into renormalized tadpole terms and their corresponding CTs,

$$T_i \rightarrow T_i + \delta T_i \quad (i = 1, 2, s) \ . \tag{10.1}$$

The renormalization conditions imposed on the tadpoles in the standard tadpole scheme are given by

$$T_i = 0 \ (i = 1, 2, s) \quad , \tag{10.2}$$

thereby minimizing the loop-corrected potential. As a consequence of this condition, no explicit tadpole topologies have to be considered in a one-loop calculation with the exception of the appearance of the rotated tadpole CTs $\delta T_{H_i H_j}$ $(i, j = 1, 2, 3)$ in the CTs of the scalar mass matrices. We present their explicit forms in Eqs. (C.5) to (C.11).

In the alternative FJ tadpole scheme, extended to the N2HDM for the first time in the course of this thesis and published in [255], the proper minima of the scalar potential are defined through the GFP-independent tree-level scalar potential. In order to account for the proper minimization of the NLO potential, the VEVs receive the shifts

$$v_i \rightarrow v_i + \delta v_i \quad (i = 1, 2, s) \ , \tag{10.3}$$

with the VEV CTs δv_i. In the alternative FJ scheme, we impose the renormalization condition that the VEVs v_i on the right-hand side of Eq. (10.3) correspond to the tree-level VEVs which represent the proper minima of the potential. Thereby, the CTs δv_i of the VEVs are connected to tadpole diagrams as shown in Eq. (C.12) and as a consequence, tadpole diagrams have to be considered in the calculation of all self-energies and vertex corrections. We summarize the effects of this alternative treatment of the minimum conditions in App. C.1.

Since the VEVs defined in the alternative FJ tadpole scheme are manifestly GFP-independent quantities, the mass CTs defined through these VEVs become GFP-independent as well. In the alternative treatment of the tadpoles, a GFP-independent definition of the scalar mixing angle CTs is required. Providing such GFP-independent renormalization schemes, cf. Sec. 10.3, allows for the calculation of partial decay widths at electroweak one-loop level which become manifestly GFP-independent quantities as well.

10.2. Renormalization of the Gauge, Scalar and Fermion Sectors

We perform the renormalization of the gauge, scalar and fermion sectors mostly in the OS scheme. Due to the similarities of the gauge and the fermion sectors of the N2HDM and the 2HDM, we restrict the presentation of the renormalization to the differences between the two models.

Renormalization of the gauge sector
The gauge sectors of the N2HDM and 2HDM are identical. As a consequence, we can directly adopt the renormalization of the gauge sector in the latter model, presented in Sec. 5.2, to the N2HDM. The explicit forms of the corresponding CTs are given in App. C.2.

Renormalization of the scalar sector
The masses and the fields corresponding to the CP-even Higgs bosons of the N2HDM are promoted to one-loop order by introducing CTs and WFRCs as follows,

$$m_{H_i}^2 \ \rightarrow \ m_{H_i}^2 + \delta m_{H_i}^2 \ , \tag{10.4}$$

$$\begin{pmatrix} H_1 \\ H_2 \\ H_3 \end{pmatrix} \rightarrow \begin{pmatrix} 1 + \dfrac{\delta Z_{H_1 H_1}}{2} & \dfrac{\delta Z_{H_1 H_2}}{2} & \dfrac{\delta Z_{H_1 H_3}}{2} \\ \dfrac{\delta Z_{H_2 H_1}}{2} & 1 + \dfrac{\delta Z_{H_2 H_2}}{2} & \dfrac{\delta Z_{H_2 H_3}}{2} \\ \dfrac{\delta Z_{H_3 H_1}}{2} & \dfrac{\delta Z_{H_3 H_2}}{2} & 1 + \dfrac{\delta Z_{H_3 H_3}}{2} \end{pmatrix} \begin{pmatrix} H_1 \\ H_2 \\ H_3 \end{pmatrix} \ . \tag{10.5}$$

These CTs and WFRCs of the CP-even sector are directly given by applying the generic formulae for the OS renormalization of scalar multiplets presented in Eqs. (3.12) to (3.14). Since the CP-odd and charged sectors of the N2HDM do not change with respect to the 2HDM, they are promoted to one-loop order as described in Sec. 5.2. The explicit forms of the CTs and WFRCs of all scalar fields of the N2HDM are presented in App. C.3.

Renormalization of the fermion sector
The introduction of WFRCs for all fermionic fields and the promotion of the fermion masses and the CKM matrix elements to one-loop order is exactly analogous to the 2HDM. For the Yukawa coupling parameters defined in Table 9.2, we introduce renormalized parameters and their CTs as follows,

$$Y_i^f \;\to\; Y_i^f + \delta Y_i^f \quad (f = l, d) \; . \tag{10.6}$$

The fermion WFRCs and mass CTs are renormalized in the OS scheme, while for the CKM matrix elements, we adopt the manifestly GFP-independent scheme presented in [236]. The explicit forms of all WFRCs and CTs of the fermion sector, together with explicit expressions for the CTs of the Yukawa coupling parameters δY_i^f $(f = l, d)$, are given in App. C.4.

10.3. Renormalization of the Scalar Mixing Angles α_i and β

We promote the scalar mixing angles α_i $(i = 1, 2, 3)$ and β to one-loop order by splitting them up into renormalized mixing angles and CTs as follows,

$$\alpha_i \to \alpha_i + \delta\alpha_i \quad (i = 1, 2, 3) \; , \tag{10.7}$$

$$\beta \to \beta + \delta\beta \; . \tag{10.8}$$

As for the scalar mixing angles in the 2HDM, renormalizing α_i and β in the N2HDM is non-trivial since there is no obvious renormalization scheme that connects the CTs to *e.g.* observables as it is the case for OS-renormalized masses. In our work, we adopt the three desirable criteria for a renormalization scheme of the mixing angle β as presented in [238], namely GFP independence, process independence and numerical stability, and use them as a guideline for the renormalization of all four scalar mixing angles in the N2HDM. Some of the renormalization schemes for the mixing angle CTs considered in this chapter resemble the ones presented in Sec. 5.3 for the 2HDM. Hence, we only briefly present these adopted schemes in the following. All renormalization schemes presented in this section are implemented in the newly developed computer program `ewN2HDECAY`.

$\overline{\text{MS}}$ scheme
The simplest choice of renormalizing the angles α_i and β in the N2HDM is the renormalization via $\overline{\text{MS}}$ conditions. As analyzed in [226, 239] for the 2HDM, such a scheme can lead to one-loop partial decay widths which commonly become orders of magnitude larger than the corresponding widths at tree level. Consequently, we expect similarly large NLO corrections to appear in the N2HDM when the $\overline{\text{MS}}$ scheme is imposed on the renormalization of the mixing angles. Moreover, we want to emphasize that the $\overline{\text{MS}}$ scheme in the framework of the standard tadpole scheme leads to manifestly GFP-dependent one-loop decay widths. Nevertheless, we implement this scheme in `ewN2HDECAY` as a reference for a numerical comparison with results computed in other renormalization schemes. Technically, imposing $\overline{\text{MS}}$ conditions on the mixing angle CTs $\delta\alpha_i$ and $\delta\beta$ is equivalent with allocating solely the UV-divergent parts proportional to Δ as defined inEq. (3.2) to them while setting their finite parts to zero. As a consequence of these $\overline{\text{MS}}$ conditions, the mixing angle CTs become dependent on the renormalization scale μ_R at which they are defined. The resulting CTs in the $\overline{\text{MS}}$ scheme are presented in App. C.5.1.

Adapted KOSY scheme

The KOSY scheme, proposed for the CTs of the scalar mixing angles of the 2HDM in [222], can be adapted to the extended scalar sector of the N2HDM in a straightforward way. The key idea of the scheme is the connection of the scalar mixing angle CTs to off-diagonal scalar WFRCs by temporarily switching between the gauge and mass bases of the scalar sector. As a consequence, the CTs α_i and β are connected to the off-diagonal WFRCs of the CP-even and CP-odd or charged sectors, respectively. In the framework of both the standard and the alternative FJ tadpole scheme, these WFRCs contain intricate GFP dependences which remain uncanceled in the calculation of a decay amplitude containing either of the mixing angle CTs. As a consequence, the adapted KOSY scheme leads to manifestly GFP-dependent partial decay widths at one-loop order. Nevertheless, we consider this scheme in our work and implement it in `ewN2HDECAY` as a reference, since the one-loop corrections to the decay widths calculated in this scheme are typically of moderate size and hence, the scheme is considered to be numerically stable. The explicit expressions for the CTs $\delta\alpha_i$ and β in the adapted KOSY scheme, defined both within the standard and the alternative FJ tadpole schemes, are presented in App. C.5.2.

p_*-pinched scheme

In order to retain the OS-motivated definition provided by the adapted KOSY scheme without introducing intricate GFP dependences into the calculation of the one-loop partial decay widths, the p_*-pinched scheme, based on the pinch technique, can be extended from the 2HDM to the N2HDM as worked out for the first time in this thesis and as published in [255]. The scheme relies on the application of the alternative FJ tadpole scheme which requires a manifestly GFP-independent definition of the scalar mixing angle CTs. By replacing the self-energies appearing in the definitions of the CTs $\delta\alpha_i$ and $\delta\beta$ in the adapted KOSY scheme with the pinched scalar self-energies of the N2HDM, the mixing angle CTs become manifestly GFP-independent quantities themselves and as a consequence, the one-loop partial decay widths calculated in this scheme become GFP-independent as well. The pinched scalar self-energies differ from the self-energies $\Sigma^{\mathrm{tad}}(p^2)$ in the alternative FJ scheme by additional terms $\Sigma^{\mathrm{add}}(p^2)$. However, at the p_* scale defined in Eq. (5.26), these additional terms identically vanish and as a consequence, the mixing angle CTs are solely defined through the self-energies $\Sigma^{\mathrm{tad}}(p_*^2)$. In App. C.5.3, we present the explicit forms of the CTs $\delta\alpha_i$ and $\delta\beta$ in the p_*-pinched scheme.

OS-pinched scheme

The OS-pinched scheme differs from the p_*-pinched scheme solely by the scale p^2 at which the pinched self-energies are evaluated. In this scheme, the scales used in the off-diagonal WFRCs resemble the scales used in the adapted KOSY scheme. Due to this, the aforementioned additional self-energy contributions $\Sigma^{\mathrm{add}}(p^2)$ contained in the pinched self-energies, derived for the N2HDM for the first time in the course of this thesis and as published in [255], need to be taken into account. In contrast to the 2HDM, these additional contributions are UV-divergent by themselves. However, in the definition of the mixing angle CTs they appear solely in UV-finite combinations and hence they retain the UV finiteness of the one-loop partial decay widths. The analytic forms of $\delta\alpha_i$ and $\delta\beta$ in the OS-pinched scheme together with the additional self-energy contributions $\Sigma^{\mathrm{add}}(p^2)$ are presented in App. C.5.4.

10.4. Renormalization of the Soft-$\mathbb{Z}_2$-Breaking Parameter m_{12}^2

The soft-$\mathbb{Z}_2$-breaking parameter m_{12}^2 is promoted to one-loop order by splitting it into its renormalized parameter and its CT,

$$m_{12}^2 \rightarrow m_{12}^2 + \delta m_{12}^2 \ . \tag{10.9}$$

In our work, we choose to renormalize m_{12}^2 in the $\overline{\text{MS}}$ scheme, *i.e.* δm_{12}^2 contains only UV-divergent parts proportional to Δ, cf. Eq. (3.2). Since m_{12}^2 is a genuine parameter of the N2HDM potential in the unbroken phase, its CT is independent of the tadpole renormalization and consequently, the UV-divergent terms allocated to δm_{12}^2 do not differ in both tadpole schemes. We present their explicit forms in App. C.6. Due to the $\overline{\text{MS}}$ renormalization of m_{12}^2, both the CT of the parameter as well as the parameter itself depend on the renormalization scale μ_R at which the parameter is defined.

10.5. Renormalization of the Singlet Vacuum Expectation Value v_s

The last remaining parameter of the N2HDM that requires renormalization is the singlet VEV v_s. We split the parameter into its renormalized value and its CT according to

$$v_s \rightarrow v_s + \Delta v_s \ , \tag{10.10}$$

where we used the notation Δv_s to distinguish the additional CT Δv_s of the tree-level VEV v_s from the shift of the tadpoles introduced in Eq. (10.3) which accounts for the proper minimum of the potential. This distinction is also applied for the doublet VEVs v_1 and v_2. Once these two VEVs are shifted via δv_1 and δv_2 through Eq. (10.3), they are connected to the renormalized VEV v via Eq. (4.9). In the alternative tadpole scheme, the renormalized VEV v^{ren} corresponds to the tree-level VEV v^{tree} which, by means of Eq. (4.16), can be expressed in terms of the independent parameters m_W and g as follows,

$$v^{\text{ren}}\big|_{\text{FJ}} = v^{\text{tree}} = \frac{2m_W}{g}\bigg|^{\text{tree}} \ . \tag{10.11}$$

After the shift of the VEVs is performed, the tree-level parameters m_W and g still need to be renormalized by replacing them with their renormalized values and their corresponding CTs,

$$\frac{2m_W}{g}\bigg|^{\text{tree}} \rightarrow \frac{2m_W}{g}\bigg|^{\text{ren}}_{\text{FJ}} + \underbrace{\frac{2m_W}{g}\left(\frac{\delta m_W^2}{2m_W^2} - \frac{\delta g}{g}\right)\bigg|_{\text{FJ}}}_{\equiv \Delta v} \ . \tag{10.12}$$

We want to emphasize that Δv is unrelated to δv_1 and δv_2, which can also be inferred from their different divergent structures.

For the singlet VEV v_s, we similarly distinguish between δv_s and Δv_s. In the alternative tadpole scheme, δv_s corresponds to the shift of the singlet VEV as shown in Eq. (10.3) and the renormalized VEV v_s^{ren} equals the tree-level VEV v_s^{tree}. Subsequently, the tree-level VEV is renormalized by the CT Δv_s which we renormalize in the $\overline{\text{MS}}$ scheme. In the standard tadpole scheme on the other hand, no VEV shift δv_s is introduced and only the additional VEV CT Δv_s needs to be specified. Within the standard tadpole scheme, it was shown in [266] that such an additional CT of the VEV can contain at most UV-finite contributions if the Lagrangian contains a rigid symmetry with respect to the field which corresponds to the VEV. In the N2HDM, this is precisely the case for the $SU(2)_L$ gauge singlet Φ_s. Consequently, in the standard tadpole scheme Δv_s is UV-finite and in this case, we choose to set the finite part of the CT to zero. In App. C.7, we present an overview of the definition of Δv_s in both tadpole schemes.

Calculation of Higher-Order Higgs Boson Decays with `ewN2HDECAY`

In this chapter, we present the calculation of the electroweak one-loop corrections to the partial decay widths and BRs of all Higgs bosons of the N2HDM and present the computer program `ewN2HDECAY` which allows for a subsequent numerical analysis on the size of the electroweak corrections. Due to the numerous decay channels that are considered and the large amount of Feynman diagrams contributing to the decay amplitudes at one-loop level, their calculation is automated as much as possible.

In Sec. 11.1, we present all Higgs boson decay channels considered in our work for the calculation of the electroweak one-loop corrections. We briefly introduce the computer program `N2HDMCalc` which allows for the automated calculation of the electroweak partial decay widths. In the subsequent Sec. 11.2, we describe the computer program `ewN2HDECAY` which combines the electroweak corrections computed with `N2HDMCalc` with the state-of-the-art QCD corrections from `N2HDECAY`. Since `ewN2HDECAY` is structurally very similar to `2HDECAY` and the aspects of combining the electroweak corrections with the corrections implemented in `N2HDECAY` is analogous to the connection with `HDECAY` for the 2HDM, we only briefly recapitulate the key ideas of the combination here.

11.1. Calculation of the Electroweak Decay Widths with `N2HDM-Calc`

We consider the OS decays of all Higgs bosons of the N2HDM that are not loop-induced, *i.e.* for the calculation of the electroweak corrections, we consider the following decays at tree level and one-loop order:

- $H_1/H_2/H_3/A \longrightarrow f\,\bar{f} \quad (f\,\bar{f} = s\,\bar{s},\, c\,\bar{c},\, b\,\bar{b},\, t\,\bar{t},\, \mu^-\,\mu^+,\, \tau^-\,\tau^+)$,

- $H_1/H_2/H_3 \longrightarrow V\,V \quad (V\,V = Z\,Z,\, W^\pm\,W^\mp)$,

- $H_1/H_2/H_3 \longrightarrow V\,S \quad (V\,S = Z\,A,\, W^\pm\,H^\mp)$,

- $H_1/H_2/H_3 \longrightarrow S\,S \quad (S\,S = A\,A,\, H^\pm\,H^\mp)$,

- $H_2 \longrightarrow H_1\,H_1$,

- $H_3 \longrightarrow H_1\,H_1$,

- $H_3 \longrightarrow H_2\, H_2$,

- $H_3 \longrightarrow H_1\, H_2$,

- $H^{\pm} \longrightarrow V\, S \quad (V\, S = W^{\pm}\, H_1, W^{\pm}\, H_2, W^{\pm}\, H_3, W^{\pm}\, A)$,

- $H^{+} \longrightarrow f\, \bar{f} \quad (f\, \bar{f} = u\, \bar{s}, u\, \bar{b}, c\, \bar{d}, c\, \bar{s}, c\, \bar{b}, t\, \bar{d}, t\, \bar{s}, t\, \bar{b}, \nu_{\mu}\, \mu^{+}, \nu_{\tau}\, \tau^{+})$,

- $A \longrightarrow V\, S \quad (V\, S = Z\, H_1, Z\, H_2, Z\, H_3, W^{\pm}\, H^{\mp})$.

In `N2HDMCalc`, we moreover compute the decays of the Higgs bosons into pairs of first-generation fermions:

- $H_1/H_2/H_3/A \longrightarrow f\, \bar{f} \quad (f\, \bar{f} = u\, \bar{u}, d\, \bar{d}, e^{-}\, e^{+})$,

- $H^{+} \longrightarrow f\, \bar{f} \quad (f\, \bar{f} = u\, \bar{d}, \nu_e\, e^{+})$.

Since these decays are overwhelmed by Dalitz decays $S \to f\, \bar{f}^{(')}\, \gamma$ $(S = H_1, H_2, H_3, A, H^{\pm})$, induced *e.g.* by the off-shell $\gamma^{*} \to f\, \bar{f}$ splitting, they are not considered for any computations performed in `ewN2HDECAY`, however.

The calculation of the partial decay widths at tree level and one-loop order is analogous to the corresponding calculations in the 2HDM, described in Sec. 6.1. Therefore, we only briefly recapitulate the key points of the calculation. All Feynman diagrams and corresponding decay amplitudes of the Higgs decays are generated with the help of the `Mathematica` [247] package `FeynArts 3.9` [248]. The `FeynArts` model file of the real N2HDM required for generating the amplitudes is obtained from `SARAH 4.14.0` [267–270] with slight modifications added by hand to account for the four different types of the N2HDM, cf. Sec. 9.3. The traces over the spinor structures and the reduction of all tensor integrals to the basic set of 't Hooft-Veltman scalar integrals [249] is performed with the help of `FeynCalc 8.2.0` [250,251]. Moreover, all tadpole and self-energy diagrams required for the definition of the CTs and WFRCs are generated with `FeynArts` and simplified with `FeynCalc`, as well. All analytic results are combined to form the electroweak partial decay widths at tree level and one-loop order according to Eqs. (3.18) and (3.23). For the numerical evaluation of the latter, we link `LoopTools 2.15` [252]. For all decays involving charged particles in the initial or final state, we moreover include the generic formulae for the real corrections to the decay widths presented in [182, 183], applied to the case of the N2HDM decays. The IR divergences stemming from the virtual massless photons as well as from the radiated real photons are regulated by introducing a infinitesimal photon mass as a regulator. The newly developed computer program `N2HDMCalc` allows for a semi-automated computation of all aforementioned steps and automatically produces `Fortran 90` code for all analytic results. `N2HDMCalc` can be downloaded from

https://github.com/marcel-krause/N2HDMCalc .

In the repository, we provide analytic results of all partial decay widths at LO and NLO, including analytic formulae for the tadpole diagrams, self-energies and vertex corrections through which the CTs and WFRCs are defined.

11.2. Description of `ewN2HDECAY`

The analytic results of the OS electroweak partial decay widths provided by `N2HDMCalc` are integrated into the newly developed tool `ewN2HDECAY` [83] which can be downloaded from

https://github.com/marcel-krause/ewN2HDECAY .

It combines the electroweak corrections in a consistent fashion with all corrections already implemented in `N2HDECAY`[29] [57, 58], consisting of

- state-of-the-art QCD corrections to the partial decay widths, where applicable,

- the calculation of the loop-induced decays into the final states $g\,g$, $\gamma\,\gamma$ and $Z\,\gamma$, where apart from the final state $Z\,\gamma$, higher-order QCD corrections are taken into account and

- the calculation of the following off-shell partial decay widths consisting of one particle in the final state which is considered off-shell[30], denoted by an asterisk,

  - $H_1/H_2/H_3/A \longrightarrow t^*\,\bar{t}$,

  - $H_1/H_2/H_3 \longrightarrow Z^*\,A$,

  - $H_1/H_2/H_3/A \longrightarrow W^{\pm*}\,H^{\mp}$,

  - $H_1/H_2/H_3 \longrightarrow W^{\pm*}\,W^{\mp*}$,

  - $H_1/H_2/H_3 \longrightarrow Z^*\,Z^*$,

  - $H^{\pm} \longrightarrow W^{\pm*}\,S \quad (S = H_1,\,H_2,\,H_3,\,A)$,

  - $H^{+} \longrightarrow t^*\,\bar{f} \quad (\bar{f} = \bar{d},\,\bar{s},\,\bar{b})$,

  - $A \longrightarrow Z^*\,S \quad (S = H_1,\,H_2,\,H_3)$,

For the calculation of the decay modes containing off-shell top quarks in the final state, the required total width of the top quark is calculated internally in `N2HDECAY`.

Structure of `ewN2HDECAY`

In Fig. 11.1, we depict the flowchart of the program `ewN2HDECAY`, consisting of the main wrapper file `ewN2HDECAY.py` written in `Python`. The wrapper iterates over all provided input files. For each selected file, `N2HDECAY` is called first in a minimal run in order to convert the provided $\overline{\text{MS}}$ charm and bottom quark masses to their OS values. These, together with all additional input parameters provided in the selected input file, are then used for the calculation of the electroweak partial decay widths at tree level and at one-loop order in the EW corrections in the subprogram `electroweakCorrections`. Subsequently, the wraper calls `N2HDECAY` in a second run in which all aforementioned state-of-the-art QCD corrections are computed and consistently combined with the electroweak corrections. Finally, the wrapper produces two output files for each selected input file. One file containing the BRs with and without electroweak contributions and one file containing the OS and non-loop-induced partial decay widths at tree level and one-loop order in the electroweak corrections, denoted by "BR" and "EW" in Fig. 11.1 respectively. The latter file is particularly useful for studying the renormalization scheme dependence of the electroweak one-loop corrected partial decay widths. As described generically in Sec. 3.5, the consistent comparison of the electroweak one-loop corrected partial decay widths evaluated within different renormalization schemes requires the conversion of the input parameters between the compared renormalization schemes. In `ewN2HDECAY`, 10 different renormalization schemes for the scalar mixing angle CTs are implemented. Moreover, the $\overline{\text{MS}}$ input parameters m_{12}^2 and v_s (and and also the mixing angles α_i ($i = 1, 2, 3$) and β in case that an $\overline{\text{MS}}$ scheme is chosen for their renormalization) are defined at an arbitrarily chosen renormalization scale μ_R, while the computation of the partial decay widths is performed at the arbitrarily chosen scale μ_{out}. In case that the two scales are chosen to be different, an additional scale evolution of the $\overline{\text{MS}}$ parameters from μ_R to μ_{out} is required.

---

[29]The program package `N2HDECAY` can be downloaded from `https://www.itp.kit.edu/~maggie/N2HDECAY/`.

[30]Note that in `N2HDECAY`, the calculation of Higgs decays including off-shell Higgs bosons is disabled. These decays are included in `HDECAY` for the approximation that the off-shell Higgs bosons dominantly decay into $b\bar{b}$ final states, which is not justified for the additional Higgs bosons of the N2HDM in all ranges of parameter space.
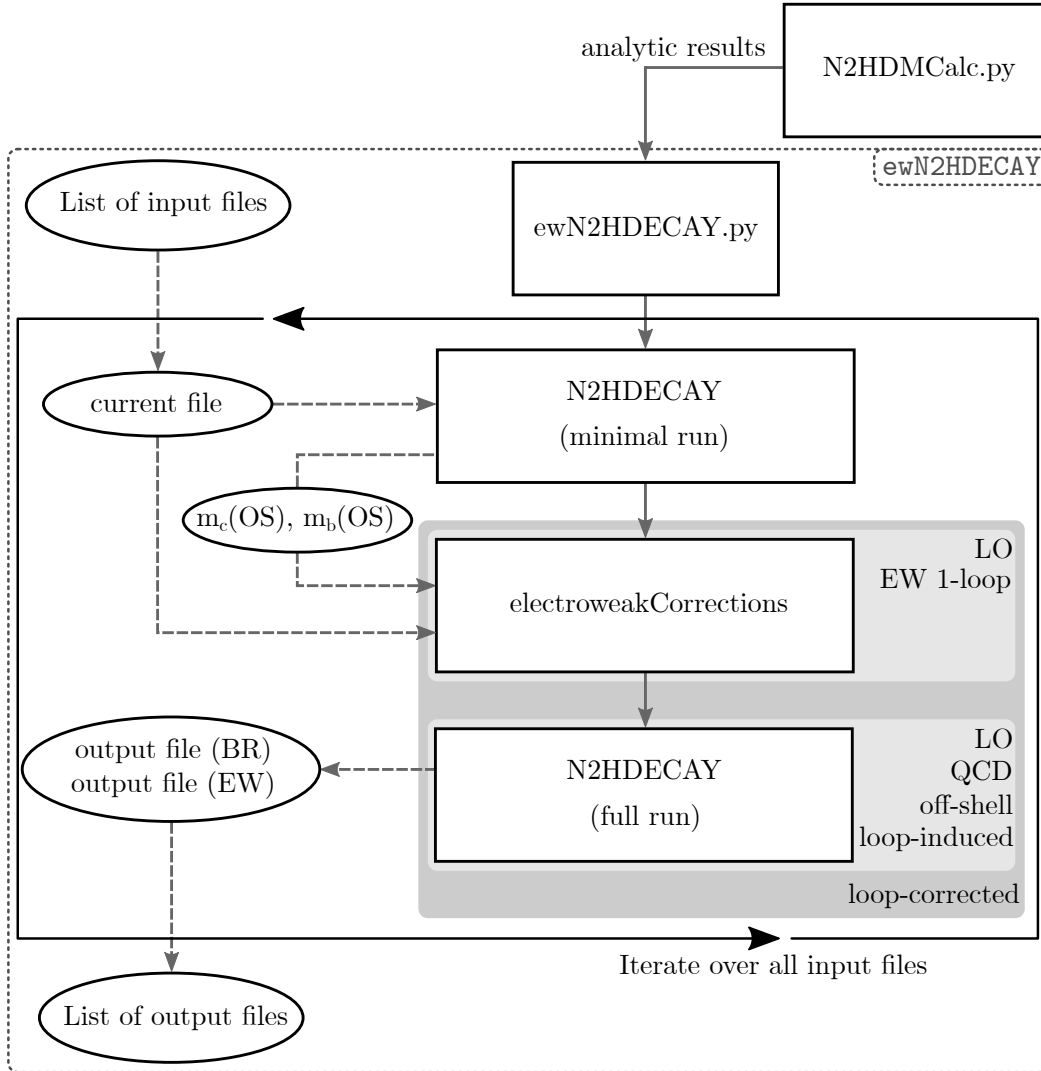
Figure 11.1.: Flowchart of `ewN2HDECAY`. The program consists of a main wrapper file `ewN2HDECAY.py` which iterates over all input files provided by the user. For each input file, the wrapper calls the subprograms `N2HDECAY` and `electroweakCorrections`. The program creates two output files for each input file, one containing the electroweak partial decay widths (EW) and one containing the BRs with and without the electroweak corrections (BR).

Combination of the electroweak corrections with `N2HDECAY`

Comparing the flowchart with the one of `2HDECAY` in Fig. 6.1 reveals the narrow relationship between the two programs. In fact, large parts of the program code of `ewN2HDECAY` are directly inherited from `2HDECAY`. Moreover, due to the similarities of the codes `N2HDECAY` and `HDECAY`, the combination of the electroweak corrections with `N2HDECAY` can be analogously described as in Sec. 11.2 for `2HDECAY`. Consequently, we only briefly recapitulate the important aspects of the combination in the following.

While the electroweak corrections use the fine-structure constant $\alpha_{\mathrm{em}}(m_Z)$ at the Z boson mass as independent input, `N2HDECAY` requires the Fermi constant G_F for the calculation of the state-of-the-art QCD corrections. For the conversion between the two schemes, higher-order corrections in the conversion formulae would need to be included. Since these conversion formulae are not implemented yet, we chose instead a pragmatic approximate solution in `ewN2HDECAY` where we do not implement a full conversion between the two input schemes but instead calculate the Fermi constant G_F^{calc} as a function of the gauge boson masses m_W

ID	Scheme	Abbreviation	Tadpole scheme	$\delta\alpha_i$	$\delta\beta$
1/2	Adapted KOSY	KOSY$^{o/c}$	standard	(C.26)-(C.28)	(C.29)/(C.30)
3/4	Adapted KOSY	KOSY$^{o/c}$	alternative FJ	(C.31)-(C.33)	(C.34)/(C.35)
5/6	p_*-pinched	p$_*^{o/c}$	alternative FJ	(C.36)-(C.38)	(C.39)/(C.40)
7/8	OS-pinched	pOS$^{o/c}$	alternative FJ	(C.42)-(C.44)	(C.45)/(C.46)
9	$\overline{\text{MS}}$	$\overline{\text{MS}}$(stand)	standard	(C.24)	(C.25)
10	$\overline{\text{MS}}$	$\overline{\text{MS}}$(FJ)	alternative FJ	(C.24)	(C.25)

Table 11.1.: Renormalization schemes of the four scalar mixing angles α_i ($i = 1, 2, 3$) and β of the real N2HDM used for the numerical analyses in Sec. 12.2, together their abbreviations and the equations through which the mixing angle CTs are defined in each scheme.

and m_Z and $\alpha_{\text{em}}(m_Z)$ by means of Eq. (4.21). We expect the numerical differences for the decay widths calculated within the two schemes to be small. For consistently matching the electroweak decay widths with the ones computed in `N2HDECAY`, we consequently rescale the latter by powers of G_F^{calc}/G_F, where applicable. As for `2HDECAY`, the fully combined partial decay width is then given by Eq. (6.2), where we again assume that both the electroweak and the state-of-the-art QCD corrections factorize. Since we calculate the electroweak corrections only for non-loop-induced OS decays while the state-of-the-art QCD corrections implemented in `N2HDECAY` moreover contain decay widths for off-shell and loop-induced decays, we want to emphasize that the factorized electroweak contributions δ^{EW} given in Eq. (6.2) are only taken into account if the considered decay channel is OS and not loop-induced. In all other cases, only the state-of-the-art QCD contributions δ^{QCD} are taken into account and the partial decay widths are calculated as given by Eq. (6.1). The calculation of the partial decay widths for all of the aforementioned cases is presented as an overview in Table 6.2 for `2HDECAY` which analogously applies to `ewN2HDECAY` as well. The BRs of all decay channels are subsequently calculated separately without and with the electroweak corrections by `N2HDECAY` via analogous relations as the ones shown in Eqs. (6.3) and (6.4) for `2HDECAY`, respectively.

Input file format
Since the input file format of `ewN2HDECAY` is similar to the one of `2HDECAY` presented in App. F.1, we restrict the presentation of the former to the differences with respect to `2HDECAY` in the following. The key difference between the input files of the two programs lies in the extended scalar sector of the N2HDM with respect to the 2HDM. In the following listing, the relevant differences in the input file are shown, together with the corresponding line numbers in the input file:

```
   ...
10 N2HDM     = 1
   ...
80 MH1       = 125.09D0
81 MH2       = 286.094D0
82 MH3       = 648.564D0
83 alpha1    = 0.909079D0
84 alpha2    = -0.155397D0
85 alpha3    = -1.54459D0
86 V_SING    = 2440.84D0
   ...
```

The input parameter `N2HDM` is analogous to the parameter `2HDM` for `2HDECAY` and in order to calculate the BRs and partial decay widths for the N2HDM in `ewN2HDECAY`, the value `N2HDM = 1` has to be set. In contrast to `2HDECAY`, the input value `PARAM = 1` is always set

Line	Input name	Name in Chapter 9	Allowed values and meaning
80	MH1	m_{H_1}	mass of the CP-even Higgs boson H_1 in GeV
81	MH2	m_{H_2}	mass of the CP-even Higgs boson H_2 in GeV
82	MH3	m_{H_3}	mass of the CP-even Higgs boson H_3 in GeV
83	alpha1	α_1	CP-even Higgs mixing angle α_1 in radians
84	alpha2	α_2	CP-even Higgs mixing angle α_2 in radians
85	alpha3	α_3	CP-even Higgs mixing angle α_3 in radians
86	V_SING	v_s	singlet VEV in GeV

Table 11.2.: Relevant physical input parameters for the calculations performed in `ewN2HDECAY` which differ from the ones used in the input file of `2HDECAY`, cf. Table 6.4. The table is adopted from [83].

in `ewN2HDECAY` since the BRs and partial decay widths are always calculated as functions of the masses of the physical Higgs bosons and the CP-even scalar mixing angles α_i ($i = 1, 2, 3$) and not in terms of the N2HDM potential parameters, cf. Eq. (9.38). The reference renormalization scheme `REFSCHEM` and the renormalization scheme `REFSCHEM` in which the electroweak partial decay widths are evaluated are specified by the IDs as shown in Table 11.2. The N2HDM-specific physical input parameters are shown in Table 11.2 together with their line numbers in the input file as shown in the listing above, the corresponding parameters as introduced in Chapter 9 and their allowed values and meanings. These parameters are entered into the input file in `FORTRAN` double-precision format. All other input parameters required for running `ewN2HDECAY` are analogous to the ones presented in Sec. 6.2 for `2HDECAY`.

Output file format

For each input file, `ewN2HDECAY` provides one output file for the BRs of all implemented decay channels as well as one output file containing the electroweak partial decay widths of the OS non-loop-induced decay modes in case that `OMIT ELW2 = 0` is set. The format of the output files is analogous to the format of the output files of `2HDECAY` as shown in App. F.2, with the only difference between the output format of `ewN2HDECAY` being that in each block containing the BRs or partial decay widths, the values of the three scalar mixing angles α_i (instead of α in the 2HDM) and additionally the value of the singlet VEV v_s in the renormalization scheme `RENSCHEM` and at the scale μ_{out} are printed out. Apart from this difference, the output files provided by `ewN2HDECAY` follow the format as described in Sec. 6.2 for `2HDECAY`.

Caveats

We want to point out that the electroweak partial decay widths calculated by `ewN2HDECAY` can become very large or negative for certain points in the parameter space of the N2HDM. The origin of these large contributions is analogously explained as in Sec. 6.2 for `2HDECAY`, *i.e.* unsuitable renormalization schemes can lead to numerical instabilities in the partial decay widths, the electroweak one-loop corrections can be parametrically enhanced in case that some coupling constants of the N2HDM become very large or small or the one-loop decay widths become larger than the tree-level widths if the latter are more suppressed than the former by small tree-level couplings. In these cases, the very large or negative partial decay widths become unphysical and should hence be discarded and not used for phenomenological analyses.

Numerical Analysis with `ewN2HDECAY`

In this chapter, we present numerical analyses on the electroweak corrections to the BRs and partial decay widths of the Higgs bosons of the real N2HDM by using `ewN2HDECAY 1.0.1`.

Beginning with Sec. 12.1, we briefly describe the scan procedure over the parameter space of the real NMSSM for determining the input parameter sets that are used for the calculation of the results presented in this chapter. In the subsequent Sec. 12.2, analyses on the BRs and partial decay widths for selected Higgs decay channels are presented. Moreover, a comparison of the size of the electroweak corrections computed within different renormalization schemes of the scalar mixing angles is performed and the different schemes are analyzed with respect to their numerical stability for selected decay channels.

12.1. Input Parameters

For the computation of all BRs and partial decay widths of the Higgs bosons of the N2HDM with `ewN2HDECAY`, we set the values of the SM-like parameters to the ones presented in Sec. 7.1 for the performed numerical analyses with `2HDECAY`. The generation of the input parameter sets compatible with up-to-date theoretical and experimental constraints is achieved by scanning through the parameter space of the real N2HDM. To that end, initial parameter sets are generated by randomly choosing values of the N2HDM-specific parameters in the ranges presented in Table 12.1 while demanding that one of the three CP-even Higgs bosons H_i ($i = 1, 2, 3$) corresponds to the SM-like Higgs boson with its mass given by Eq. (7.3). Subsequently, the thereby created initial parameter sets are checked against several theoretical and experimental constraints with help of the tool `ScannerS` [57, 260, 261]. Since all constraints and additional conditions applied for the scan of the real N2HDM are analogous to the ones applied for the real 2HDM, we do not state them here again explicitly and refer to Sec. 7.1 and moreover to [258] for a detailed description about the scan procedure. Out of all valid parameter sets generated by the scan, we choose the following sets for the numerical analyses performed in this thesis.

	$m_{H_i/A}$	$m_{H^\pm}$ (II/flip.)	$m_{H^\pm}$ (I/lep.-sp.)	m_{12}^2	v_s	α_i	t_β
min	30 GeV	580 GeV	80 GeV	0 GeV^2	1 GeV	$-\pi/2$	0.25
max	1500 GeV	1500 GeV	1500 GeV	100 000 GeV^2	1500 GeV	$\pi/2$	35

Table 12.1.: Allowed ranges of the input values of the real N2HDM for the parameter scan, where $i = 1, 2, 3$. Each parameter is separately varied between its corresponding minimum and maximum value.

Parameter set "P1".
For the SM-like parameters, we use the input values presented in Eqs. (7.1) and (7.2), while the N2HDM-specific parameters are set to

$$
\begin{aligned}
m_{H_1} &= 76.524 \text{ GeV} , & m_{H_2} &= 125.09 \text{ GeV} , & (12.1) \\
m_{H_3} &= 185.782 \text{ GeV} , & m_A &= 304.936 \text{ GeV} , \\
m_{H^\pm} &= 298.729 \text{ GeV} , & m_{12}^2(m_{h_{\text{SM}}}) &= 1712.82 \text{ GeV}^2 , \\
v_s(m_{h_{\text{SM}}}) &= 1454.24 \text{ GeV} , & \alpha_1|_{p_*^o} &= 0.334\,442 , \\
\alpha_2|_{p_*^o} &= 1.352\,66 \text{ GeV} , & \alpha_3|_{p_*^o} &= -0.726\,926 , \\
t_\beta|_{p_*^o} &= 2.385\,25 , & \text{N2HDM type} &= \text{I} ,
\end{aligned}
$$

where for m_{12}^2 and v_s, the arguments in brackets indicate that these input values are defined at the scale $\mu_R = m_{h_{\text{SM}}}$. The subscripts denote that the four scalar mixing angles and their CTs are given in the p_*-pinched (odd) scheme, defined through Eqs. (C.36) to (C.39), which is used as the reference renormalization scheme for this set. The renormalization scale μ_{out} at which all electroweak partial decay widths are evaluated is set to the mass of the decaying particle for each decay mode, separately.

Parameter set "P2".
The SM-like parameters are again set to the values presented in Eqs. (7.1) and (7.2) while the N2HDM-specific parameters are set to the values

$$
\begin{aligned}
m_{H_1} &= 91.123 \text{ GeV} , & m_{H_2} &= 125.09 \text{ GeV} , & (12.2) \\
m_{H_3} &= 696.389 \text{ GeV} , & m_A &= 766.781 \text{ GeV} , \\
m_{H^\pm} &= 672.106 \text{ GeV} , & m_{12}^2(m_{h_{\text{SM}}}) &= 208\,360.0 \text{ GeV}^2 , \\
v_s(m_{h_{\text{SM}}}) &= 2196.48 \text{ GeV} , & \alpha_1|_{p_*^o} &= 0.697\,912 , \\
\alpha_2|_{p_*^o} &= -1.459\,21 \text{ GeV} , & \alpha_3|_{p_*^o} &= 1.516\,15 , \\
t_\beta|_{p_*^o} &= 0.950\,614 , & \text{N2HDM type} &= \text{II} ,
\end{aligned}
$$

where the $\overline{\text{MS}}$ parameters are again defined at the scale $\mu_R = m_{h_{\text{SM}}}$ and the four scalar mixing angles are given in the p_*-pinched (odd) scheme. Moreover, we perform a variation of some of the N2HDM-specific input parameters in order to analyze the sensitivity of the BRs and partial decay widths on these parameters:

- Variation of $m_{H_3} \in [500 \text{ GeV}, 800 \text{ GeV}]$, while all other parameters are given by the fixed values in Eq. (12.2).

- Variation of $m_{H^\pm} \in [580 \text{ GeV}, 1200 \text{ GeV}]$, while all other parameters are given by the fixed values in Eq. (12.2).

- Variation of $m_A \in [300 \text{ GeV}, 1100 \text{ GeV}]$, while all other parameters are given by the fixed values in Eq. (12.2).

For all input parameter points defined in set "P2", the renormalization scale μ_{out} at which the partial decay widths are evaluated is set to the mass of the decaying Higgs boson for each decay channel, separately. The variation of the input parameters as presented above potentially leads to the generation of parameter sets that do not fulfill all the experimental constraints anymore. We nevertheless use them for the purpose of the numerical analysis on the size of the electroweak corrections computed within different renormalization schemes in this work.

Parameter sets "P3".
In order to systematically analyze the size of the electroweak corrections to the partial decay widths computed within different renormalization schemes for a larger sample of input parameters, we use 15 000 input parameter sets, collectively denoted by "P3", that fulfill all of the aforementioned theoretical and experimental constraints. All parameter points in the set correspond to an N2HDM type II and feature a large variety of different values of the N2HDM-specific masses, mixing angles, m_{12}^2 and v_s. In contrast to the other two input parameter sets, the mixing angles in set "P3" are defined for each renormalization scheme separately as a reference scheme for the numerical analysis and hence, their values do not require a parameter conversion from one scheme to the other. As for the sets defined above, the renormalization scale μ_{out} at which the partial decay widths are evaluated is set to the mass of the decaying particle for each decay channel separately. For the majority of all input parameter sets generated, the lightest CP-even Higgs boson H_1 corresponds to the SM-like Higgs boson with its mass given in Eq. (7.3). However, the set "P3" also features a few scenarios in which H_1 is lighter than the SM-like Higgs boson which in all these scenarios corresponds to H_2. Due to the large amount of different points considered for this set, we do not present the values of the N2HDM-specific input parameters for all points here explicitly.

12.2. Numerical Results and Analysis

For the quantification of the numerical results, we use the same measures as introduced in Sec. 7.2, *i.e.* we adopt the definitions of the relative size ΔBR of the electroweak contributions to the BRs from Eq. (7.6) and of the relative size $\Delta\Gamma^{\text{EW}}$ of the electroweak corrections to the partial decay widths for OS and non-loop induced decays from Eq. (7.7). Moreover, we adopt the definition of the relative difference $\Delta\Gamma^{\text{EW,x}}$ of the electroweak one-loop partial decay widths computed within different renormalization schemes with respect to a defined reference renormalization scheme from Eq. (7.8).

We first analyze the BRs and electroweak partial decay widths of all decay channels implemented in `ewN2HDECAY` for the parameter set "P1". For the calculation of all electroweak corrections to the OS and non-loop-induced decays, we renormalize the four mixing angle CTs in the p_*-pinched scheme "p_*^o", cf. Table 11.1. Since the input values of the mixing angles in the set "P1" are defined in the same scheme, no input parameter conversion needs to be applied for them[31]. Shown in Table 12.2 are all BRs excluding and including the electroweak corrections as well as, where applicable, the tree-level and one-loop electroweak partial decay widths for all decay channels implemented in `ewN2HDECAY` for the parameter set "P1". In the table, we additionally present the quantities ΔBR and $\Delta\Gamma^{\text{EW}}$ as measures for the relative size of the electroweak contributions to the BRs and partial widths, all for the OS and non-loop induced decays.

For the lightest CP-even Higgs boson H_1, the relative one-loop contributions $\Delta\Gamma^{\text{EW}}$ to the electroweak decay widths are rather small, ranging from $-5.4\,\%$ to $-0.7\,\%$ and hence, their

---

[31]Of course, the $\overline{\text{MS}}$ parameters m_{12}^2 and v_s are nevertheless automatically converted from μ_R to μ_{out} for each decay channel, separately.

Decay channel	$\mathrm{BR}^{\mathrm{QCD}}_{(\phi \to X_1 X_2)}$	$\mathrm{BR}^{\mathrm{QCD\&EW}}_{(\phi \to X_1 X_2)}$	$\Delta\mathrm{BR}$	$\Gamma^{\mathrm{LO,EW}}_{\phi X_1 X_2}$ in GeV	$\Gamma^{\mathrm{NLO,EW}}_{\phi X_1 X_2}$ in GeV	$\Delta\Gamma^{\mathrm{EW}}$
$H_1 \to b\,\bar{b}$	$8.319 \cdot 10^{-1}$	$8.260 \cdot 10^{-1}$	-0.7 %	$2.098 \cdot 10^{-5}$	$1.985 \cdot 10^{-5}$	-5.4 %
$H_1 \to \tau^+\tau^-$	$8.091 \cdot 10^{-2}$	$8.300 \cdot 10^{-2}$	2.6 %	$9.611 \cdot 10^{-7}$	$9.398 \cdot 10^{-7}$	-2.2 %
$H_1 \to \mu^+\mu^-$	$2.870 \cdot 10^{-4}$	$2.881 \cdot 10^{-4}$	0.4 %	$3.410 \cdot 10^{-9}$	$3.263 \cdot 10^{-9}$	-4.3 %
$H_1 \to s\,\bar{s}$	$3.144 \cdot 10^{-4}$	$3.275 \cdot 10^{-4}$	4.2 %	$8.269 \cdot 10^{-9}$	$8.210 \cdot 10^{-9}$	-0.7 %
$H_1 \to c\,\bar{c}$	$4.078 \cdot 10^{-2}$	$4.230 \cdot 10^{-2}$	3.7 %	$1.877 \cdot 10^{-6}$	$1.856 \cdot 10^{-6}$	-1.1 %
$H_1 \to g\,g$	$4.055 \cdot 10^{-2}$	$4.254 \cdot 10^{-2}$	4.9 %	–	–	–
$H_1 \to \gamma\,\gamma$	$3.415 \cdot 10^{-3}$	$3.582 \cdot 10^{-3}$	4.9 %	–	–	–
$H_1 \to W^+W^-$	$1.471 \cdot 10^{-3}$	$1.543 \cdot 10^{-3}$	4.9 %	–	–	–
$H_1 \to Z\,Z$	$4.095 \cdot 10^{-4}$	$4.296 \cdot 10^{-4}$	4.9 %	–	–	–
$H_2 \to b\,\bar{b}$	$5.923 \cdot 10^{-1}$	$5.828 \cdot 10^{-1}$	-1.7 %	$5.824 \cdot 10^{-3}$	$5.532 \cdot 10^{-3}$	-5.0 %
$H_2 \to \tau^+\tau^-$	$6.382 \cdot 10^{-2}$	$6.300 \cdot 10^{-2}$	-1.3 %	$2.634 \cdot 10^{-4}$	$2.512 \cdot 10^{-4}$	-4.6 %
$H_2 \to \mu^+\mu^-$	$2.260 \cdot 10^{-4}$	$2.181 \cdot 10^{-4}$	-3.5 %	$9.324 \cdot 10^{-7}$	$8.699 \cdot 10^{-7}$	-6.7 %
$H_2 \to s\,\bar{s}$	$2.237 \cdot 10^{-4}$	$2.253 \cdot 10^{-4}$	0.7 %	$2.261 \cdot 10^{-6}$	$2.201 \cdot 10^{-6}$	-2.7 %
$H_2 \to c\,\bar{c}$	$2.902 \cdot 10^{-2}$	$2.904 \cdot 10^{-2}$	0.1 %	$5.141 \cdot 10^{-4}$	$4.972 \cdot 10^{-4}$	-3.3 %
$H_2 \to g\,g$	$7.778 \cdot 10^{-2}$	$8.048 \cdot 10^{-2}$	3.5 %	–	–	–
$H_2 \to \gamma\,\gamma$	$2.053 \cdot 10^{-3}$	$2.125 \cdot 10^{-3}$	3.5 %	–	–	–
$H_2 \to Z\,\gamma$	$1.506 \cdot 10^{-3}$	$1.558 \cdot 10^{-3}$	3.5 %	–	–	–
$H_2 \to W^+W^-$	$2.067 \cdot 10^{-1}$	$2.139 \cdot 10^{-1}$	3.5 %	–	–	–
$H_2 \to Z\,Z$	$2.580 \cdot 10^{-2}$	$2.670 \cdot 10^{-2}$	3.5 %	–	–	–
$H_3 \to b\,\bar{b}$	$1.880 \cdot 10^{-1}$	$1.833 \cdot 10^{-1}$	-2.5 %	$1.553 \cdot 10^{-3}$	$1.499 \cdot 10^{-3}$	-3.5 %
$H_3 \to \tau^+\tau^-$	$2.184 \cdot 10^{-2}$	$2.065 \cdot 10^{-2}$	-5.4 %	$6.991 \cdot 10^{-5}$	$6.545 \cdot 10^{-5}$	-6.4 %
$H_3 \to \mu^+\mu^-$	$7.725 \cdot 10^{-5}$	$7.143 \cdot 10^{-5}$	-7.5 %	$2.473 \cdot 10^{-7}$	$2.264 \cdot 10^{-7}$	-8.5 %
$H_3 \to s\,\bar{s}$	$7.087 \cdot 10^{-5}$	$6.869 \cdot 10^{-5}$	-3.1 %	$5.999 \cdot 10^{-7}$	$5.756 \cdot 10^{-7}$	-4.1 %
$H_3 \to c\,\bar{c}$	$9.197 \cdot 10^{-3}$	$8.839 \cdot 10^{-3}$	-3.9 %	$1.364 \cdot 10^{-4}$	$1.298 \cdot 10^{-4}$	-4.8 %
$H_3 \to g\,g$	$5.876 \cdot 10^{-2}$	$5.935 \cdot 10^{-2}$	1.0 %	–	–	–
$H_3 \to \gamma\,\gamma$	$7.840 \cdot 10^{-5}$	$7.919 \cdot 10^{-5}$	1.0 %	–	–	–
$H_3 \to Z\,\gamma$	$3.478 \cdot 10^{-6}$	$3.513 \cdot 10^{-6}$	1.0 %	–	–	–
$H_3 \to W^+W^-$	$1.218 \cdot 10^{-2}$	$2.911 \cdot 10^{-2}$	139.0 %	$3.898 \cdot 10^{-5}$	$9.226 \cdot 10^{-5}$	136.7 %
$H_3 \to Z\,Z$	$2.526 \cdot 10^{-3}$	$3.269 \cdot 10^{-3}$	29.4 %	$8.087 \cdot 10^{-6}$	$1.036 \cdot 10^{-5}$	28.1 %
$H_3 \to H_1 H_1$	$7.073 \cdot 10^{-1}$	$6.953 \cdot 10^{-1}$	-1.7 %	$2.265 \cdot 10^{-3}$	$2.204 \cdot 10^{-3}$	-2.7 %
$A \to b\,\bar{b}$	$1.187 \cdot 10^{-3}$	$1.104 \cdot 10^{-3}$	-6.9 %	$2.536 \cdot 10^{-3}$	$2.272 \cdot 10^{-3}$	-10.4 %
$A \to \tau^+\tau^-$	$1.551 \cdot 10^{-4}$	$1.391 \cdot 10^{-4}$	-10.3 %	$1.138 \cdot 10^{-4}$	$9.830 \cdot 10^{-5}$	-13.6 %
$A \to \mu^+\mu^-$	$5.484 \cdot 10^{-7}$	$4.800 \cdot 10^{-7}$	-12.5 %	$4.025 \cdot 10^{-7}$	$3.392 \cdot 10^{-7}$	-15.7 %
$A \to s\,\bar{s}$	$4.251 \cdot 10^{-7}$	$3.927 \cdot 10^{-7}$	-7.6 %	$9.762 \cdot 10^{-7}$	$8.683 \cdot 10^{-7}$	-11.1 %
$A \to c\,\bar{c}$	$5.996 \cdot 10^{-5}$	$5.485 \cdot 10^{-5}$	-8.5 %	$2.221 \cdot 10^{-4}$	$1.956 \cdot 10^{-4}$	-11.9 %
$A \to t\,\bar{t}$	$1.083 \cdot 10^{-3}$	$1.125 \cdot 10^{-3}$	3.9 %	–	–	–
$A \to g\,g$	$4.638 \cdot 10^{-3}$	$4.817 \cdot 10^{-3}$	3.9 %	–	–	–
$A \to \gamma\,\gamma$	$1.434 \cdot 10^{-5}$	$1.490 \cdot 10^{-5}$	3.9 %	–	–	–
$A \to Z\,\gamma$	$2.811 \cdot 10^{-6}$	$2.920 \cdot 10^{-6}$	3.9 %	–	–	–
$A \to Z\,H_1$	$1.957 \cdot 10^{-1}$	$1.958 \cdot 10^{-1}$	0.1 %	$1.436 \cdot 10^{-1}$	$1.384 \cdot 10^{-1}$	-3.6 %
$A \to Z\,H_2$	$1.176 \cdot 10^{-3}$	$5.442 \cdot 10^{-4}$	-53.7 %	$8.629 \cdot 10^{-4}$	$3.846 \cdot 10^{-4}$	-55.4 %
$A \to Z\,H_3$	$7.960 \cdot 10^{-1}$	$7.964 \cdot 10^{-1}$	0.1 %	$5.842 \cdot 10^{-1}$	$5.628 \cdot 10^{-1}$	-3.7 %
$A \to W^+ H^-$	$8.446 \cdot 10^{-9}$	$8.771 \cdot 10^{-9}$	3.9 %	–	–	–
$A \to W^- H^+$	$8.446 \cdot 10^{-9}$	$8.771 \cdot 10^{-9}$	3.9 %	–	–	–
$H^+ \to c\,\bar{b}$	$6.543 \cdot 10^{-7}$	$6.251 \cdot 10^{-7}$	-4.5 %	$4.797 \cdot 10^{-6}$	$4.216 \cdot 10^{-6}$	-12.1 %
$H^+ \to \tau^+ \nu_\tau$	$4.624 \cdot 10^{-5}$	$4.266 \cdot 10^{-5}$	-7.8 %	$1.115 \cdot 10^{-4}$	$9.471 \cdot 10^{-5}$	-15.1 %
$H^+ \to \mu^+ \nu_\mu$	$1.635 \cdot 10^{-7}$	$1.471 \cdot 10^{-7}$	-10.0 %	$3.943 \cdot 10^{-7}$	$3.267 \cdot 10^{-7}$	-17.2 %
$H^+ \to u\,\bar{b}$	$4.683 \cdot 10^{-9}$	$4.379 \cdot 10^{-9}$	-6.5 %	$3.309 \cdot 10^{-8}$	$2.849 \cdot 10^{-8}$	-13.9 %
$H^+ \to u\,\bar{s}$	$6.547 \cdot 10^{-9}$	$6.211 \cdot 10^{-9}$	-5.1 %	$4.821 \cdot 10^{-8}$	$4.211 \cdot 10^{-8}$	-12.7 %
$H^+ \to c\,\bar{d}$	$8.601 \cdot 10^{-7}$	$8.101 \cdot 10^{-7}$	-5.8 %	$1.095 \cdot 10^{-5}$	$9.499 \cdot 10^{-6}$	-13.3 %
$H^+ \to c\,\bar{s}$	$1.632 \cdot 10^{-5}$	$1.537 \cdot 10^{-5}$	-5.8 %	$2.071 \cdot 10^{-4}$	$1.796 \cdot 10^{-4}$	-13.3 %
$H^+ \to t\,\bar{b}$	$6.613 \cdot 10^{-1}$	$6.472 \cdot 10^{-1}$	-2.1 %	1.400	1.262	-9.9 %
$H^+ \to t\,\bar{s}$	$1.131 \cdot 10^{-3}$	$1.107 \cdot 10^{-3}$	-2.1 %	$2.393 \cdot 10^{-3}$	$2.156 \cdot 10^{-3}$	-9.9 %
$H^+ \to t\,\bar{d}$	$5.314 \cdot 10^{-5}$	$5.203 \cdot 10^{-5}$	-2.1 %	$1.125 \cdot 10^{-4}$	$1.014 \cdot 10^{-4}$	-9.9 %
$H^+ \to W^+ H_1$	$5.942 \cdot 10^{-2}$	$6.162 \cdot 10^{-2}$	3.7 %	$1.433 \cdot 10^{-1}$	$1.368 \cdot 10^{-1}$	-4.5 %
$H^+ \to W^+ H_2$	$3.617 \cdot 10^{-4}$	$3.534 \cdot 10^{-4}$	-2.3 %	$8.723 \cdot 10^{-4}$	$7.845 \cdot 10^{-4}$	-10.1 %
$H^+ \to W^+ H_3$	$2.777 \cdot 10^{-1}$	$2.896 \cdot 10^{-1}$	4.3 %	$6.696 \cdot 10^{-1}$	$6.429 \cdot 10^{-1}$	-4.0 %

Table 12.2.: Parameter set "P1": Higher-order BRs without and with electroweak corrections as well as tree-level and one-loop electroweak partial decay widths for OS and non-loop-induced decays as computed by `ewN2HDECAY`. For the computation, the scalar mixing angles are renormalized in the p_*-pinched scheme "p^{o}_*". $\Delta\mathrm{BR}$ and $\Delta\Gamma^{\mathrm{EW}}$ are defined in Eqs. (7.6) and (7.7) respectively.
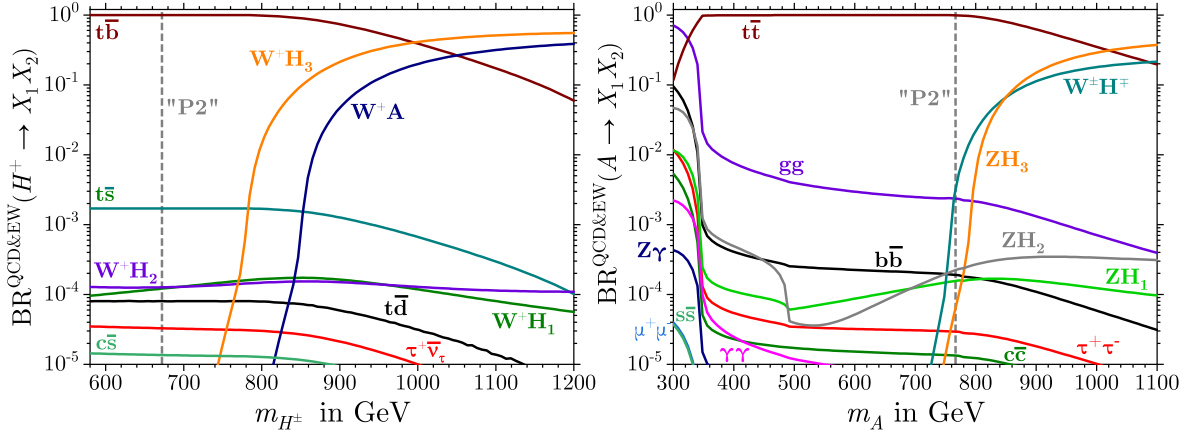
Figure 12.1.: Parameter set "P2": Shown are the BRs of the charged Higgs boson H^+ as a function of $m_{H^\pm}$ (left) and the BRs of the CP-odd Higgs boson A as a function of m_A (right). The BRs contain the newly computed electroweak one-loop corrections to all OS decay that are not loop-induced. For the calculation of all BRs, the four scalar mixing angles are renormalized in the p_*-pinched scheme "p_*^o", cf. Table 6.1.

inclusion changes the BRs of the decay channels of the H_1 boson between $-0.7\,\%$ to $4.9\,\%$. The H_1 boson dominantly decays into $b\,\bar{b}$ with a BR of $83\,\%$ and subdominantly into $\tau^+\,\tau^-$, $c\,\bar{c}$ and $g\,g$, with BRs of the order of a few percent. The BRs for the off-shell decays into $W^+\,W^-$ and $Z\,Z$ are very small since the corresponding coupling between the H_1 boson and the two gauge bosons is suppressed due to the sum rules of the gauge boson couplings in the N2HDM. For the Higgs boson H_2, which in the input parameter set "P1" corresponds to the SM-like Higgs boson with mass $125.09\,\text{GeV}$, the relative corrections to the electroweak decay widths are rather small as well and range between $-6.7\,\%$ and $-2.7\,\%$ and consequently, the change of the BRs is rather small as well, ranging between $-3.5\,\%$ and $3.5\,\%$. As can be inferred from a comparison with Table 11.3 of [98], the BRs of H_2, both excluding and including the electroweak contributions, are compatible with the BRs of the Higgs boson of the SM.

For the heaviest CP-even Higgs boson H_3, the inclusion of the electroweak corrections to the partial decay widths leads to mostly moderate relative corrections to the electroweak decay widths between $-8.5\,\%$ and $-2.7\,\%$ and to the BRs between $-7.5\,\%$ and $1.0\,\%$, with exception of the decays into $Z\,Z$ and $W^\pm\,W^\mp$ where the relative corrections to the electroweak decay widths become as large as $28.1\,\%$ and $136.7\,\%$. For these two decay channels, the large one-loop corrections stem from the mixing angle CTs and the off-diagonal WFRCs of the CP-even Higgs bosons which appear together with a specific combination of tree-level scalar mixing angles in the one-loop decay width of the two decay channels. In the parameter set "P1", these contributions are parametrically enhanced and hence lead to large one-loop corrections to the rather small tree-level decay width. Due to the mass values in the parameter set "P1", the scenario allows for the OS decay of H_3 into a pair of H_1 Higgs bosons, which with a BR of approximately $70\,\%$ is the dominant decay channel for the heaviest CP-even Higgs boson, followed by the decay into $b\,\bar{b}$.

For the decays of the CP-odd Higgs boson A, the relative electroweak corrections are sizeable, ranging from $-55.4\,\%$ to $-3.6\,\%$ and hence, the relative corrections to the BRs between $-53.7\,\%$ to $3.9\,\%$ are sizeable as well. The large electroweak one-loop corrections to the decay $A \to Z\,H_2$ stem from parametrically enhanced contributions from the mixing angle CTs and WFRCs in the parameter set "P1", as it was the case for the decays of the H_3 boson into the gauge bosons. As can be inferred from the table, the A boson dominantly decays into
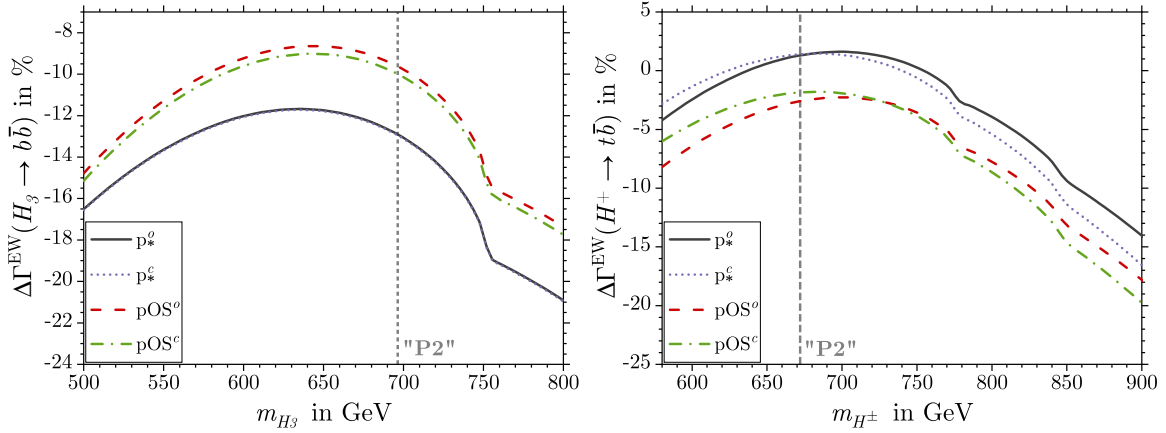
Figure 12.2.: Parameter set "P2": The relative one-loop corrections $\Delta\Gamma^{\mathrm{EW}}$ as defined in Eq. (7.7) for the decay channel $H_3 \to b\bar{b}$ as a function of m_{H_3} (left) and for the decay channel $H^+ \to t\bar{b}$ as a function of $m_{H^\pm}$ (right) for four different renormalization schemes as specified in the figure. For a definition of the abbreviations used to identify the schemes, cf. Table 6.1.

$Z\,H_3$ and $Z\,H_1$. Since the masses of the CP-odd and charged Higgs boson are close to each other, the decays of A into $W^\pm H^\mp$ and are not possible OS and hence, the BRs for these off-shell decays are very small. For the charged Higgs boson $H^\pm$, the relative corrections to the electroweak decay widths range from $-17.2\,\%$ to $-4.0\,\%$ and the corrections to the BRs between $-10.0\,\%$ and $4.3\,\%$ and are hence sizeable. The charged Higgs dominantly decays into a top-bottom pair and $W^\pm H_3$. The numerical analysis for the parameter set "P1" shows that the electroweak corrections to the electroweak partial decay widths and BRs of the Higgs bosons of the N2HDM, in particular for the non-SM-like bosons, can become sizeable. Consequently, the electroweak contributions provided in this thesis are relevant for a more precise evaluation of the BRs and partial decay widths of the N2HDM Higgs bosons.

For an analysis of the sensitivity of the BRs on the N2HDM-specific parameters, we consider the input parameter set "P2", featuring a CP-even Higgs boson H_1 which again is lighter than the SM-like Higgs boson H_2. The masses of the heaviest CP-even, CP-odd and charged Higgs bosons are rather large. In order to analyze the behavior of the BRs with respect to a change of the masses of the Higgs bosons, we perform a variation of $m_{H^\pm}$, m_A and m_{H_3} separately[32]. We show in Fig. 12.1 the BRs of the charged Higgs boson H^+ as a function of $m_{H^\pm}$ as well as the BRs of the CP-odd Higgs boson A as a function of m_A on the left-hand and right-hand sides of the figure, respectively. All BRs presented in the plots contain the newly computed electroweak corrections to all OS decays that are not loop-induced, computed within the p_*-pinched scheme "p_*^o". The dashed vertical lines indicate the masses of the two Higgs bosons corresponding to the original definition of the parameter set "P2" where no variation is applied. As can be inferred from the plots, the BRs show a strong behavior on the two varied masses. The charged Higgs boson dominantly decays into $t\bar{b}$ over a large range of the mass $m_{H^\pm}$ and only for larger values above about $1\,\mathrm{TeV}$ the BRs of the decays into $W^+ H_3$ and $W^+ A$ exceed the ones of all other decay channels. The BRs of the decays into $W^+ H_1$ and $W^+ H_2$ are similarly small over the whole range of chosen values of $m_{H^\pm}$. For the BRs of the CP-odd Higgs boson A shown in the right-hand side of the figure, the threshold of OS $t\bar{t}$ production is clearly visible for $m_A \gtrsim 2m_t$. Above the threshold, this decay mode is the dominant one for the A boson over a large range of its mass until values of m_A about

---

[32]We want to emphasize again that while the variation of the masses potentially leads to the definition of input parameter sets that do not fulfill the theoretical and experimental constraints anymore, we only perform the analysis of the BRs implemented in `ewN2HDECAY` to investigate the size of the electroweak corrections provided in this thesis.
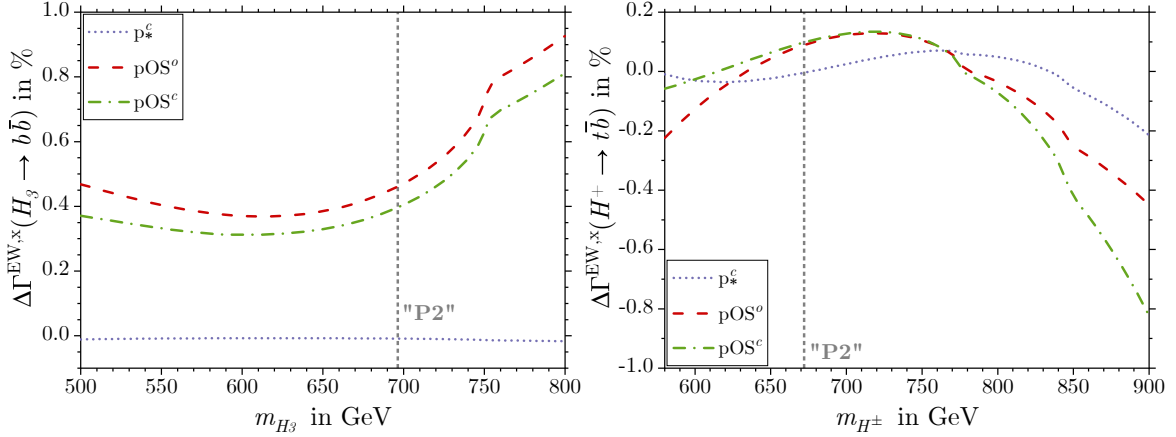
Figure 12.3.: Parameter set "P2": The relative difference $\Delta\Gamma^{\mathrm{EW,x}}$ of the one-loop partial decay widths evaluated in the renormalization scheme "x" in comparison to the ones computed in the "p_*^o" scheme, cf. Eq. (7.8), for the decay channel $H_3 \to b\bar{b}$ as a function of m_{H_3} (left) and for the decay channel $H^+ \to t\bar{b}$ as a function of $m_{H^\pm}$ (right).

1 TeV are reached, where the BRs of the decays into $Z\,H_3$ and $W^\pm\,H^\mp$ exceed the BRs of all other decay modes.

For the analysis of the size of the electroweak-corrected one-loop partial decay widths with respect to the choice of the renormalization scheme for the scalar mixing angles, we again consider the parameter set "P2" together with a variation of the masses of the H_3 and $H^\pm$ Higgs bosons. To that end, we compute the relative one-loop corrections $\Delta\Gamma^{\mathrm{EW}}$ for the decay of the heaviest CP-even Higgs boson H_3 into $b\bar{b}$ and for the decay of the charged Higgs boson H^+ into $t\bar{b}$ for the four different renormalization schemes "$\mathrm{p}_*^{o/c}$" and "$\mathrm{pOS}^{o/c}$" of the scalar mixing angles. For each of the four renormalization schemes, both the tree-level and the one-loop partial decay widths that enter Δ^{EW} are calculated for the same renormalization scheme. In case that this scheme differs from the reference scheme "p_*^o" in which the mixing angles are defined in the parameter set "P2", their values are converted from the reference scheme to the input renormalization scheme in `ewN2HDECAY`. In Fig. 12.2, we show the corresponding relative corrections $\Delta\Gamma^{\mathrm{EW}}$ for $H_3 \to b\bar{b}$ as a function of m_{H_3} on the left-hand side and for $H^+ \to t\bar{b}$ as a function of $m_{H^\pm}$ on the right-hand side of the figure, respectively. The relative one-loop corrections are sensitive to the change of the masses of the two Higgs bosons. Depending on the renormalization scheme, they range from approximately $-21\,\%$ to $-8\,\%$ for the decay $H_3 \to b\bar{b}$ and from $-20\,\%$ to $3\,\%$ for the decay $H^+ \to t\bar{b}$ and hence, they are sizeable for the two decay modes and the parameter set "P2" used for this analysis.

For a rough estimate of the remaining theoretical uncertainty of the partial decay widths due to missing higher-order corrections, we define the "p_*^o" as a reference scheme and compute the difference $\Delta\Gamma^{\mathrm{EW,x}}$, cf. Eq. (7.8), between the one-loop partial decay widths computed within any other scheme "x" with respect to the one computed in the reference scheme. As before, the tree-level and one-loop electroweak decay widths are evaluated in the same renormalization scheme for each considered scheme "x" and the mixing angles are converted from the reference scheme to scheme "x" via the parameter conversion routine that is implemented in `ewN2HDECAY`. Figure 12.3 shows the difference $\Delta\Gamma^{\mathrm{EW,x}}$, again for the decay channel $H_3 \to b\bar{b}$ as a function of m_{H_3} and for $H^+ \to t\bar{b}$ as a function of $m_{H^\pm}$ on the left-hand and right-hand sides of the figure, respectively. As can be seen in the plots, the difference between the one-loop corrections computed within the different variations of the pinched schemes is only below the percent level over the range of m_{H_3} and $m_{H^\pm}$ that is considered. This serves as a rough indicator that the estimated remaining theoretical uncertainty for the two consid-
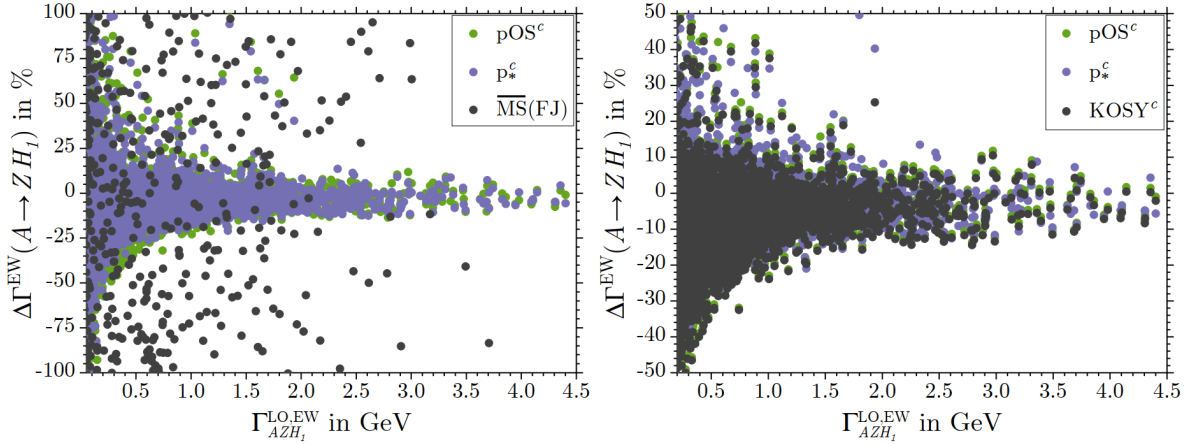
Figure 12.4.: Parameter set "P3": The relative one-loop corrections $\Delta\Gamma^{\mathrm{EW}}$ as defined in Eq. (7.7) for the decay channel $A \to ZH_1$ as a function of the electroweak decay width $\Gamma^{\mathrm{LO,EW}}_{AZH_1}$ at tree level. The results are presented for two different scales of the $\Delta\Gamma^{\mathrm{EW}}$ axis and for different choices of the renormalization schemes used for the computation of the one-loop widths (left and right).

ered decay channels and for the input parameters as defined in set "P2" is small. In order to formulate more general statements about the remaining theoretical uncertainties due to missing higher-order corrections, it is required to analyze all decay channels implemented in ewN2HDECAY for a large amount of different input parameter sets, however.

As analyzed *e.g.* in [255] for selected decay channels of the Higgs bosons of the N2HDM, some renormalization schemes of the scalar mixing angles presented in Sec. 10.3 potentially introduce large uncanceled one-loop contributions to the partial decay widths and hence lead to numerical instabilities in the sense that the one-loop partial decay widths become orders of magnitude larger than the tree-level widths. In order to systematically categorize the different renormalization schemes implemented into ewN2HDECAY with respect to their numerical stability, we perform a numerical analysis on the electroweak one-loop corrections to the partial decay widths of the sample decay channel $A \to Z H_1$. To that end, we use the 15 000 different parameter sets collectively denoted by "P3", for all of which the decay channel is OS. For each parameter set, we compute the relative one-loop corrections $\Delta\Gamma^{\mathrm{EW}}$ for several different renormalization schemes of the scalar mixing angles, where again the tree-level and the one-loop partial decay widths are calculated in the same input renormalization scheme. In contrast to the analyses before however, the reference scheme of the scalar mixing angles for each of the 15 000 points is always set to the considered input renormalization scheme. Hence, the mixing angle CTs are not converted from one scheme to the other which is not required since we focus on the size of the relative electroweak corrections $\Delta\Gamma^{\mathrm{EW}}$ computed for a large amount of input parameters for each renormalization scheme separately and we do not directly compare the results computed within the different schemes with each other. The results of the analysis are presented in Fig. 12.4 as a function of the electroweak partial decay width of the process at tree level for two different scale choices of the $\Delta\Gamma^{\mathrm{EW}}$ axis and for different choices of renormalization schemes presented on the left- and right-hand sides of the figure, respectively.

On the left-hand side of Fig. 12.4, we present the relative difference $\Delta\Gamma^{\mathrm{EW}}$ in the range of $\pm 100\,\%$ as a function of the tree-level width $\Gamma^{\mathrm{LO,EW}}_{AZH_1}$. For the $\overline{\mathrm{MS}}$ scheme, defined in the framework of the alternative FJ tadpole scheme, the relative differences become as large as $\pm 10\,000\,\%$ and lie outside of the plotted region for most of the input parameter points. Consequently, the $\overline{\mathrm{MS}}$ scheme yields huge relative one-loop corrections that are not sensible at the

fixed one-loop order. Moreover, we analyzed that the corrections in this scheme are typically negative and below -100% for a large amount of input parameter sets which corresponds to negative and unphysical one-loop partial decay widths. Hence, the loop-corrected widths can not be used anymore for phenomenological studies and should be discarded in these cases. As discussed in [255], the origin of these large corrections stems from both the genuine one-loop vertex corrections to the decay process as well as from the WFRCs, both introducing introducing here huge corrections that cannot canceled by finite contributions from the mixing angle CTs. This reconfirms that the $\overline{\text{MS}}$ scheme for the scalar mixing angles is in general not a well-suited renormalization scheme for the computation of electroweak corrections to the partial decay widths of the N2HDM Higgs bosons. On the other hand, as can be observed on the right-hand side of Fig. 12.4 the KOSY scheme, p_*-pinched scheme and the OS-pinched scheme, all three defined over the charged sector for t_β, all yield relative one-loop corrections that are mostly between $\pm 10\%$ and consequently, the schemes are considered to fulfill the criterion of numerical stability.

Conclusion of Part III

In Part III of this thesis, we dealt with the calculation of the electroweak one-loop corrections to the partial decay widths of all Higgs bosons of the CP-conserving (*i.e.* real) N2HDM and presented the new computed program `ewN2HDECAY` which allows for a more precise calculation of the BRs and partial decay widths.

We introduced the electroweak Lagrangian and the scalar potential of the N2HDM. The scalar sector of the model contains the three CP-even Higgs bosons H_i ($i = 1, 2, 3$) together with the three CP-even tree-level mixing angles α_i as well as the CP-odd Higgs boson A and the charged Higgs bosons $H^\pm$ with the tree-level mixing angle β of the CP-odd/charged sectors.

We presented the electroweak one-loop renormalization of the N2HDM and introduced several different renormalization schemes of the four scalar mixing angles that are based the $\overline{\text{MS}}$ scheme, OS-motivated approaches as well as on the PT. As for the 2HDM in Part II, we categorized these different renormalization schemes with respect to the three desirable criteria of GFP independence, process independence and numerical stability.

For the automated calculation of all electroweak partial decay widths at tree level and one-loop order, we presented the program `N2HDMCalc`. The resulting analytic formulae for the partial decay widths were implemented in the newly developed program `ewN2HDECAY` which combines the electroweak corrections with the tree-level and loop-corrected decay widths already implemented in `N2HDECAY`, including off-shell decays and state-of-the-art QCD corrections, where applicable. The program `ewN2HDECAY` allows for the fast calculation of the BRs, excluding and including the electroweak corrections, as well as for the calculation of the electroweak tree-level and one-loop partial decay widths of all Higgs bosons of the real N2HDM.

In order to demonstrate the relevance of the newly computed electroweak corrections, we presented a numerical analysis on the BRs and electroweak partial decay widths with `ewN2HDECAY`. To that end, we defined input parameter sets compatible with most recent theoretical and experimental constraints. The size of the electroweak contributions to the BRs were analyzed and particularly for the additional non-SM-like Higgs bosons of the N2HDM, they were found to be sizeable. A comparison of the electroweak partial decay widths computed within different renormalization schemes of the scalar mixing angles allowed for a rough estimate of the remaining theoretical uncertainties. For the two decay channels and the parameter sets

considered, the remaining uncertainty was roughly estimated to be small. For a systematic analysis on numerical stability, we analyzed the electroweak one-loop corrections for 15 000 input parameter sets computed within different renormalization schemes of the scalar mixing angles. For the decay channel considered in our analysis, it was found that the $\overline{\text{MS}}$ scheme is numerically unstable, leading to one-loop partial decay widths that are orders of magnitude larger than the corresponding tree-level widths. On the other hand, the four pinched schemes implemented in `ewN2HDECAY` typically lead to moderate radiative corrections for the analyzed decay channel and the input parameter sets used. The numerical analysis has shown that the electroweak corrections to the partial decay widths of the Higgs bosons of the N2HDM, provided in `ewN2HDECAY` for the first time, are of relevant size and that they should be included in order to make more precise predictions for the BRs and partial widths.

Part IV.

The $\mathcal{O}(\alpha_t^2)$ Corrections to Higgs Boson Masses in the Complex NMSSM

A Brief Introduction to the Complex NMSSM

The main objective of Part IV of this thesis is the calculation of the $\mathcal{O}(\alpha_t^2)$ two-loop corrections to the masses of the Higgs bosons of the complex NMSSM, thereby allowing for a more precise prediction. Since for the $\mathcal{O}(\alpha_t^2)$ corrections only a subset of the particle content of the complex NMSSM contributes, we restrict the introduction to the parameters and particles relevant for the calculations performed in this work.

Starting with Sec. 14.1, we provide the Lagrangian relevant for our calculations and introduce our notation. In Sec. 14.2, we discuss the Higgs potential and describe the tree-level Higgs spectrum of the complex NMSSM. Since the $\mathcal{O}(\alpha_t^2)$ contributions to the Higgs masses dominantly stem from the top and stop sectors, we introduce their particle spectrum in Sec. 14.3. Moreover, we introduce the chargino and neutralino sectors in the subsequent Sec. 14.4, since they also contribute to the two-loop corrections in our work. In Sec. 14.5, we present an overview over all approximations applied for the calculation of the two-loop corrections to $\mathcal{O}(\alpha_t^2)$. We conclude this chapter in Sec. 14.6 with an overview over the full set of independent parameters through which we parametrize the higher-order corrections to the Higgs masses in our work.

14.1. The Lagrangian of the Complex NMSSM

The complex NMSSM is an extension of the simplest and well-studied SUSY theory, the MSSM. Due to this, we first briefly introduce the MSSM and motivate its extension to the NMSSM in the following. As depicted graphically in Fig. 2.2, in the MSSM each field of the SM acquires a superpartner whose spin differs by $1/2$ with respect to the spin of the corresponding SM field. Consequently, the fermions of the SM, *i.e.* the quarks and leptons, acquire the spin 0 *sfermions* as superpartners, consisting of the *squarks* and *sleptons*. In contrast to the SM with only one Higgs doublet, the MSSM contains two Higgs doublets, as further described below. The superpartners of the Higgs fields contained in the doublets are spin $1/2$ Weyl fermions called the *higgsinos*, while the gauge bosons of the SM acquire the *gauginos* (consisting of the *gluinos*, *winos* and the *bino*) also with spin $1/2$ as their superpartners. The fermion and Higgs fields[33] as well as their superpartners are combined into the chiral super-

---

[33] We want to emphasize that in comparison to Parts II and III of this thesis, we slightly alter the notation of the Higgs fields in Part IV of this thesis to follow the convention that the subscripts u and d denote the quark type to which the Higgs fields couple, cf. *e.g.* [36].

names		spin 0	spin $\frac{1}{2}$	$(SU(3)_C \times SU(2)_L \times U(1)_Y)$
squarks and quarks (3 generations)	$\widehat{Q}$	$\widetilde{Q}_L = (\widetilde{u}_L, \widetilde{d}_L)^T$	$Q_L = (u_L, d_L)^T$	$(\mathbf{3}, \mathbf{2}, \frac{1}{6})$
	$\widehat{U}$	$\widetilde{u}_R^*$	$u_R^\dagger$	$(\overline{\mathbf{3}}, \mathbf{1}, -\frac{2}{3})$
	$\widehat{D}$	$\widetilde{d}_R^*$	$d_R^\dagger$	$(\overline{\mathbf{3}}, \mathbf{1}, \frac{1}{3})$
sleptons and leptons (3 generations)	$\widehat{L}$	$\widetilde{L}_L = (\widetilde{\nu}_L, \widetilde{e}_L)^T$	$L_L = (\nu_L, e_L)^T$	$(\mathbf{1}, \mathbf{2}, -\frac{1}{2})$
	$\widehat{E}$	$\widetilde{e}_R^*$	$e_R^\dagger$	$(\mathbf{1}, \mathbf{1}, 1)$
Higgs and higgsinos	$\widehat{H}_u$	$H_u = (H_u^+, H_u^0)^T$	$\widetilde{H}_u = (\widetilde{H}_u^+, \widetilde{H}_u^0)^T$	$(\mathbf{1}, \mathbf{2}, \frac{1}{2})$
	$\widehat{H}_d$	$H_d = (H_d^0, H_d^-)^T$	$\widetilde{H}_d = (\widetilde{H}_d^0, \widetilde{H}_d^-)^T$	$(\mathbf{1}, \mathbf{2}, -\frac{1}{2})$
singlet	$\widehat{S}$	S	$\widetilde{S}$	$(\mathbf{1}, \mathbf{1}, 0)$

Table 14.1.: Chiral supermultiplets of the MSSM (excluding the singlet multiplet $\widehat{S}$ in the last row) and the NMSSM (including $\widehat{S}$) and the corresponding spin 0 and spin 1/2 fields which form the superfields, adopted from [36]. The last column denotes the gauge transformation properties of the supermultiplets with respect to the three gauge subgroups.

multiplets presented in Table 14.1 (where for the case of the MSSM, the singlet multiplet $\widehat{S}$ shown in the last row of the table is excluded), while the gauge boson fields and their super-partners are combined into gauge supermultiplets as presented in Table 14.2. In the former table, the chiral superfields are indicated with a hat while all superpartners of the particles of the SM are denoted with a tilde in both tables.

One fundamental building block of each SUSY model is the holomorphic superpotential W which determines the most general forms of non-gauge interactions of the chiral supermulti-plets of any SUSY extension [36]. The superpotential of the MSSM contains two Higgs su-perfields in comparison to the SM with one Higgs doublet. In fact, trying to build a minimal SUSY model analogous to the MSSM but with just one Higgs superfield leads to inconsisten-cies due to the appearance of gauge anomalies and due to the fact that the requirement of the holomorphy of the superpotential cannot be fulfilled in this case.

Both problems are avoided by adding a second Higgs superfield to the model. Per construc-tion, one of the Higgs superfields only couples to the up-type superfields $\widehat{U}$ while the other one only couples to the down-type superfields $\widehat{D}$ as well as to the leptonic superfields $\widehat{L}$. In-specting Table 4.1 reveals that this configuration resembles a type II 2HDM. Following from these considerations, the superpotential of the MSSM is given by[34] [36]

$$W_{\mathrm{MSSM}} = \widehat{U} Y^U \left(\widehat{Q}^T \epsilon \widehat{H}_u \right) - \widehat{D} Y^D \left(\widehat{Q}^T \epsilon \widehat{H}_d \right) - \widehat{E} Y^E \left(\widehat{L}^T \epsilon \widehat{H}_d \right) + \mu \left(\widehat{H}_u^T \epsilon \widehat{H}_d \right) , \quad (14.1)$$

where ϵ denotes the two-dimensional totally anti-symmetric tensor, the matrices Y^f ($f = U, D, E$) denote the 3×3 Yukawa coupling matrices in flavor space and μ is an additional mass-dimensional parameter.

---

[34]For simplicity, we suppress all gauge and generation indices since they are not required for the following discussions.

names	spin 1	spin $\frac{1}{2}$	$(SU(3)_C \times SU(2)_L \times U(1)_Y)$
gluons and gluinos	g	$\widetilde{g}$	$(\mathbf{8}, \mathbf{1}, 0)$
W bosons and winos	$W^{\pm}, W^0$	$\widetilde{W}^{\pm}, \widetilde{W}^0$	$(\mathbf{1}, \mathbf{3}, 0)$
B boson and bino	B	$\widetilde{B}$	$(\mathbf{1}, \mathbf{1}, 0)$

Table 14.2.: Gauge supermultiplets of the NMSSM and the corresponding spin 1 and spin $1/2$ fields which form the superfields, adopted from [36]. For the charged W bosons, the corresponding fields are already presented in the mass basis $W^{\pm}$, cf Eq. (4.14). The last column denotes the gauge transformation properties of the supermultiplets with respect to the three gauge subgroups.

By deriving the tree-level spectrum of the MSSM it is revealed that the tree-level mass of the lightest CP-even Higgs boson h is bounded from above by the mass of the Z boson due to the SUSY relations between the Higgs and the gauge sectors,

$$\left(m_h^{\mathrm{MSSM}}\right)^2 < m_Z^2 c_{2\beta}^2 \ , \tag{14.2}$$

where the parameter β, connected to the ratios of the VEVs of the two Higgs doublets, is introduced in the subsequent Sec. 14.2. Since the value of the Z boson mass is given by 91.1876 GeV [98], it is clear that the tree-level mass relation of Eq. (14.2) cannot be fulfilled if the lightest CP-even Higgs boson h is considered to be the SM-like Higgs boson with a measured mass of 125.09 GeV [13]. Instead, large higher-order corrections to the Higgs mass m_h^{MSSM} are required in order to allow for an interpretation of h as the SM-like Higgs observed at the LHC. The dominant contributions of these higher-order corrections stem from virtual top and stop particles and rather large stop masses are required to match the calculated mass m_h^{MSSM} with the measured SM Higgs boson mass. However, a too large discrepancy between the top and stop masses leads to a reintroduction of the hierarchy problem into the MSSM, cf. Sec. 2.3. From a theoretical point of view, this is unfavorable since the proposed solution of the hierarchy problem is considered as a main theoretical motivation for the formulation of the MSSM. But even if the stop masses turn out to be not too large, a closer look at the superpotential of the MSSM reveals that the model is not capable of solving all fine-tuning problems completely. The mass-dimensional parameter μ contributes to the mass terms of the Higgs superfields and for phenomenological reasons, it is expected to be of the order of the electroweak scale or the SUSY scale. However, since μ is in principle a free parameter of the superpotential of the MSSM, there is no mechanism that would necessarily enforce the parameter to be at these scales. This fine-tuning problem of the parameter μ is referred to as the μ *problem* of the MSSM [271].

One possible solution to the μ problem is to consider the μ parameter to be generated dynamically instead of adding it explicitly to the superpotential. This is the key idea realized in the NMSSM. Extending the superfield content of the MSSM by an additional superfield $\widehat{S}$, consisting of the singlet field S and the singlino $\widetilde{S}$ as component fields, allows for a replacement of the μ term in the superpotential with the new term

$$\lambda \widehat{S} \left(\widehat{H}_u^T \epsilon \widehat{H}_d \right) \ , \tag{14.3}$$

where λ is a dimensionless complex coupling constant. By assigning a non-vanishing VEV $\langle S \rangle$ to the singlet field S, an effective μ term

$$\mu_{\mathrm{eff}} \equiv \lambda \langle S \rangle \tag{14.4}$$

is generated in the vacuum state of the potential. Since the VEV is connected to the mechanism of EWSB, its scale and consequently also the scale of μ_{eff} are automatically of the desired order. Hence, the NMSSM provides a solution to the μ problem without relying on a fine-tuning of the parameter.

The most general form of the superpotential of the NMSSM contains all combinations of the superfields that maintain the holomorphy of the superpotential. In principle, this allows for the appearance of terms which are linear or quadratic in the singlet superfield $\widehat{S}$, and a dimensional analysis reveals that the corresponding parameters proportional to these terms would have positive mass-dimension. This in turn would reintroduce the μ problem to the NMSSM. In order to avoid these additional terms in the superpotential, the invariance under an additional discrete $\mathbb{Z}_3$ symmetry is imposed on the model, which forbids the appearance of terms proportional to $\widehat{S}$ and $\widehat{S}^2$ in the superpotential. For simplicity, throughout this thesis we refer to this realization of the NMSSM as *the* NMSSM. Consequently, the $\mathbb{Z}_3$-conserving superpotential of the NMSSM considered in this work is given by

$$W_{\text{NMSSM}} = \widehat{U} Y^U \left(\widehat{Q}^T \epsilon \widehat{H}_u \right) - \widehat{D} Y^D \left(\widehat{Q}^T \epsilon \widehat{H}_d \right) - \widehat{E} Y^E \left(\widehat{L}^T \epsilon \widehat{H}_d \right) + \lambda \widehat{S} \left(\widehat{H}_u^T \epsilon \widehat{H}_d \right) \quad (14.5)$$
$$+ \frac{1}{3} \kappa \widehat{S}^3 \ .$$

The additional term cubic in the singlet superfield is in accordance with the discrete $\mathbb{Z}_3$ symmetry. A vanishing value of κ would lead to an invariance of the superpotential under an additional global $U(1)$ gauge transformation, the so-called *Peccei–Quinn symmetry* [272,273]. As soon as the singlet field acquires its VEV through EWSB, this additional symmetry would be spontaneously broken, giving rise to the *Peccei-Quinn axion* as the massless Goldstone boson of the global symmetry breaking. The appearance of such an axion leads to strict constraints on the parameters of the NMSSM through experimental data [274]. Hence, in the realization of the NMSSM considered in this thesis, a non-vanishing value of κ is assumed which prevents the appearance of the Peccei-Quinn axion.

In the NMSSM, the upper bound on the tree-level mass of the lightest CP-even Higgs boson is elevated in comparison to the MSSM due to additional contributions stemming from the term proportional to λ,

$$\left(m_{h_1}^{\text{NMSSM}} \right)^2 < m_Z^2 c_{2\beta}^2 + \frac{1}{2} |\lambda|^2 v^2 s_{2\beta}^2 \ . \quad (14.6)$$

Consequently, the NMSSM allows for more moderate higher-order corrections to the Higgs boson mass in order to assign h_1 to the observed SM-like Higgs boson with a mass of $125.09\,\text{GeV}$. Moreover, while the spectrum of the complex MSSM at tree level does not allow for CP violation in the Higgs sector since all CP-violating phases can be rotated away or vanish due to the minimum conditions of the potential [275], the complex NMSSM studied in this work contains additional phases which introduce CP-violating terms in the spectrum even at tree level. Hence, the complex NMSSM also provides a possible solution to the shortcoming of the SM with respect to its insufficient amount of CP violation [141].

Apart from the favorabale theoretical features, the NMSSM spectrum is moreover interesting from an experimental point of view. Due to its extended Higgs sector in comparison to the MSSM, the NMSSM allows for additional Higgs bosons which can be substantially lighter than the Higgs boson with a mass of $125.09\,\text{GeV}$ observed at the LHC and whose existences are not yet excluded by experimental constraints stemming from data taken at LEP, Tevatron and the LHC. Moreover, the NMSSM, containing more than two Higgs bosons in its spectrum, allows for cascade decays of the Higgs bosons which in turn can lead to interesting and exotic signatures, cf. *e.g.* [142].

The Lagrangian of the complex NMSSM consists of SUSY-conserving and symmetry-breaking contributions. The Lagrangian can be expressed as

$$\mathcal{L}_{\text{NMSSM}} = \mathcal{L}_{\text{SUSY}} + \mathcal{L}_{\text{GF}} + \mathcal{L}_{\text{FP}} + \mathcal{L}_{\text{soft}} \ . \tag{14.7}$$

The SUSY Lagrangian $\mathcal{L}_{\text{SUSY}}$ contains the kinetic terms of the particles of the NMSSM as well as parts of the scalar potential and the Yukawa interactions. Its form follows from the superpotential of the NMSSM, presented in Eq. (14.5), and from the transformation properties of the superfields under gauge transformations. Analogous to the SM and its doublet and singlet extensions, the Lagrangian is extended with the gauge-fixing and Faddeev-Popov Lagrangians $\mathcal{L}_{\text{GF}}$ and $\mathcal{L}_{\text{FP}}$ respectively in order to remove the redundant unphysical degrees of freedom from the model. Finally, the soft-SUSY-breaking Lagrangian $\mathcal{L}_{\text{soft}}$ contains terms that break SUSY softly, *i.e.* the coupling constants of the SUSY-violating operators have positive mass-dimension. Due to this, these additional terms do not introduce additional quadratically divergent contributions *e.g.* to the calculation of the higher-order corrections to the Higgs mass, which in turn would reintroduce the hierarchy problem to the model. The inclusion of the soft-SUSY-breaking terms is required due to the fact that we have not observed superpartners with the same mass as their SM counterparts. The so far unknown mechanism of SUSY breaking is parametrized by the introduction of the soft-SUSY-breaking Lagrangian, given by

$$
\begin{aligned}
\mathcal{L}_{\text{soft}} = &-\frac{1}{2} \left[M_1 \widetilde{B}\widetilde{B} + M_2 \sum_i \widetilde{W}^i \widetilde{W}^i + M_3 \sum_{\widetilde{g}} \widetilde{g}\widetilde{g} + \text{h.c.} \right] \\
&- \left[A_U Y^U \widetilde{U}_R^* (\widetilde{Q}^T \epsilon H_u) - A_D Y^D \widetilde{D}_R^* (\widetilde{Q}^T \epsilon H_d) - A_E Y^E \widetilde{E}_R^* (\widetilde{L}^T \epsilon H_d) + \text{h.c.} \right] \\
&- \left[A_\lambda \lambda \left(H_u^T \epsilon H_d \right) S + \tfrac{1}{3} A_\kappa \kappa S^3 + \text{h.c.} \right] \\
&- m_{\widetilde{Q}}^2 \widetilde{Q}^\dagger \widetilde{Q} - m_{\widetilde{U}_R}^2 |\widetilde{U}_R|^2 - m_{\widetilde{D}_R}^2 |\widetilde{D}_R|^2 - m_{\widetilde{L}}^2 \widetilde{L}^\dagger \widetilde{L} - m_{\widetilde{E}_R}^2 |\widetilde{E}_R|^2 \\
&- m_{H_u}^2 H_u^\dagger H_u - m_{H_d}^2 H_d^\dagger H_d - m_s^2 |S|^2 \ .
\end{aligned}
\tag{14.8}
$$

In principle, any term that breaks SUSY only softly can be added to the Lagrangian. In Eq. (14.8), the soft-SUSY-breaking terms included are

- the complex mass parameters M_i ($i = 1, 2, 3$) for the gauginos presented in the first line of Eq. (14.8),

- the soft-SUSY-breaking trilinear terms A_i ($i = U, D, E, \lambda, \kappa$) for the MSSM in the second and for the singlet contributions in the third line of Eq. (14.8) which, together with the Yukawa coupling matrices, are complex 3×3 matrices in flavor space,

- the complex hermitian 3×3 matrices m_i^2 ($i = \widetilde{Q}, \widetilde{U}_R, \widetilde{D}_R, \widetilde{L}, \widetilde{E}_R$) presented in the fourth line of Eq. (14.8) which provide additional mass terms *e.g.* for the sfermions and

- the real soft-SUSY-breaking terms m_i^2 ($i = H_u, H_d, s$) of the Higgs potential presented in the fifth line of Eq. (14.8).

For the calculation of the genuine $\mathcal{O}(\alpha_t^2)$ two-loop corrections to the Higgs boson masses in the NMSSM performed in this work, we apply the approximation that the masses of all SM fermions apart from the top quark vanish and we do not consider any flavor violation in the quark sector. As a consequence, the Yukawa coupling matrices Y^f ($f = U, D, E$) simplify considerably and only a subset of the free parameters of the complex NMSSM yield contributions to our calculations.

14.2. The Scalar Sector and the Higgs Potential

The Higgs potential V_{NMSSM} of the complex NMSSM consists of contributions from the SUSY Lagrangian $\mathcal{L}_{\mathrm{SUSY}}$ as well as from the soft-SUSY-breaking Lagrangian $\mathcal{L}_{\mathrm{soft}}$. In component field notation, the potential reads

$$
\begin{aligned}
V_{\mathrm{NMSSM}} = {} & \left(|\lambda|^2|S|^2 + m_{H_u}^2\right)H_u^\dagger H_u + \left(|\lambda|^2|S|^2 + m_{H_d}^2\right)H_d^\dagger H_d + m_s^2|S|^2 \\
& + \frac{1}{8}(g'^{\,2} + g^2)\left(H_u^\dagger H_u - H_d^\dagger H_d\right)^2 + \frac{1}{2}g_2^2\left|H_u^\dagger H_d\right|^2 \\
& + \left|\lambda(H_u^T \epsilon H_d) + \kappa S^2\right|^2 + \left(A_\lambda \lambda(H_u^T \epsilon H_d)S + \frac{1}{3}A_\kappa \kappa S^3 + \mathrm{h.c.}\right) ,
\end{aligned}
\tag{14.9}
$$

where g' and g are the coupling constants associated to the gauge groups $U(1)_Y$ and $SU(2)_L$, respectively. Through the mechanism of EWSB, the two Higgs doublets H_u and H_d as well as the Higgs singlet S acquire non-vanishing VEVs[35] v_u, v_d and v_s, respectively. The VEVs of the two doublets are connected to the measured VEV v via [98]

$$
v^2 = v_u^2 + v_d^2 \approx (246\,\mathrm{GeV})^2 ,
\tag{14.10}
$$

and their ratio defines the characteristic parameter β of the NMSSM,

$$
t_\beta \equiv \frac{v_u}{v_d} .
\tag{14.11}
$$

The corresponding multiplets are expanded around their VEVs as follows,

$$
H_d = \begin{pmatrix} \dfrac{v_d + h_d + ia_d}{\sqrt{2}} \\ h_d^- \end{pmatrix} , \quad
H_u = e^{i\varphi_u}\begin{pmatrix} h_u^+ \\ \dfrac{v_u + h_u + ia_u}{\sqrt{2}} \end{pmatrix} , \quad
S = e^{i\varphi_s}\frac{v_s + h_s + ia_s}{\sqrt{2}} , \tag{14.12}
$$

where we introduced the neutral fields h_i, a_i $(i = d, u, s)$ and the charged fields $h_i^\pm$ $(i = d, u)$ as well as two additional phases φ_i $(i = u, s)$ which account for the possible phase differences between the multiplets[36]. Since the doublet H_u couples to the up-type quarks, cf. Eq. (14.5), the phase φ_u is shifted to the Yukawa sector and hence it appears in the mass eigenvalues and Yukawa couplings of the up-type quarks. In order to simplify the analytic calculations, we redefine the up-type quark fields according to

$$
u_L \longrightarrow e^{-i\varphi_u/2}u_L , \quad u_R \longrightarrow e^{i\varphi_u/2}u_R .
\tag{14.13}
$$

Through this redefinition, the phase φ_u is absorbed in the up-type quark fields and disappears from the mass eigenvalues and Yukawa couplings of two up-type quarks, while for couplings involving only one up-type quark, the phase now explicitly appears in the corresponding coupling constants. Apart from the aforementioned phases, we could in principle express all complex parameters of the NMSSM through their absolute values and their complex phases. However, in order to comply with the SLHA, we express the soft-SUSY-breaking parameters A_λ and A_κ through their real and imaginary parts,

$$
A_\lambda \equiv \mathrm{Re}(A_\lambda) + \mathrm{Im}(A_\lambda) , \quad A_\kappa \equiv \mathrm{Re}(A_\kappa) + \mathrm{Im}(A_\kappa) ,
\tag{14.14}
$$

while the parameters λ and κ are expressed through their absolute values and complex phases,

$$
\lambda \equiv e^{i\varphi_\lambda}|\lambda| , \quad \kappa \equiv e^{i\varphi_\kappa}|\kappa| .
\tag{14.15}
$$

---

[35]The VEVs of the Higgs doublets of the complex NMSSM and of the 2HDM are related as $v_d \leftrightarrow v_1$ and $v_u \leftrightarrow v_2$.
[36]To describe the phase differences between the three multiplets, two complex phases are sufficient. One phase, *e.g.* the one of the doublet H_d, can always be absorbed through a redefinition of the fields and hence, only the two phases φ_i $(i = u, s)$ describing the *relative* phases between the multiplets are relevant.

Together with φ_u and φ_s, the phases enter the spectrum of the complex NMSSM in the combinations

$$\varphi_y \equiv \varphi_\kappa - \varphi_\lambda + 2\varphi_s - \varphi_u \;, \tag{14.16}$$

$$\varphi_\omega \equiv \varphi_\kappa + 3\varphi_s \;. \tag{14.17}$$

The insertion of the multiplet expansion of Eq. (14.12) into the Higgs potential in Eq. (14.9) yields terms that are linear and bilinear in the fields h_i and a_i $(i = d, u, s)$,

$$V_{\mathrm{NMSSM}} = \left(T_{h_d}, T_{h_u}, T_{h_s}, T_{a_d}, T_{a_u}, T_{a_s}\right)\phi^n + \frac{1}{2}\,\phi^{n,T}\mathcal{M}^2_{\phi\phi}\phi^n + \phi^{c,\dagger}\mathcal{M}^2_{h^+h^-}\phi^c + \cdots \;, \tag{14.18}$$

where we present only the terms T_{ϕ_i} $(\phi_i = h_d, h_u, h_s, a_d, a_u, a_s)$ as well as $\mathcal{M}^2_{\phi\phi}$ and $\mathcal{M}^2_{h^+h^-}$ linear and bilinear in the fields, respectively, since all other constant, cubic and quartic terms are not relevant for the following discussion. In Eq. (14.18), we moreover introduce the neutral and charged scalar field multiplets in the gauge basis of the complex NMSSM,

$$\phi^{n,T} \equiv \left(h_d, h_u, h_s, a_d, a_u, a_s\right)^T \;, \tag{14.19}$$

$$\phi^{c,T} \equiv \left((h_d^-)^*, h_u^+\right)^T \;. \tag{14.20}$$

The terms linear in the neutral scalar fields are the tadpole terms whose explicit forms are given by

$$\frac{T_{h_d}}{vc_\beta} \equiv m^2_{H_d} + \frac{1}{2}m^2_Z c_{2\beta} - \frac{1}{2}|\lambda|t_\beta v_s\left(|\kappa|v_s c_{\varphi_y} - \sqrt{2}s_{\varphi_\omega - \varphi_y}\mathrm{Im}(A_\lambda) + \sqrt{2}c_{\varphi_\omega - \varphi_y}\mathrm{Re}(A_\lambda)\right)$$

$$+ \frac{1}{2}|\lambda|^2\left(s_\beta^2 v^2 + v_s^2\right) \;, \tag{14.21}$$

$$\frac{T_{h_u}}{vs_\beta} \equiv m^2_{H_u} - \frac{1}{2}m^2_Z c_{2\beta} - \frac{|\lambda|v_s}{2t_\beta}\left(|\kappa|c_{\varphi_y}v_s - \sqrt{2}s_{\varphi_\omega - \varphi_y}\mathrm{Im}(A_\lambda) + \sqrt{2}c_{\varphi_\omega - \varphi_y}\mathrm{Re}(A_\lambda)\right)$$

$$+ \frac{1}{2}|\lambda|^2\left(c_\beta^2 v^2 + v_s^2\right) \;, \tag{14.22}$$

$$\frac{T_{h_s}}{v_s} \equiv m^2_s + |\kappa|^2 v_s^2 + \frac{1}{2}|\lambda|^2 v^2 + \frac{|\lambda|s_\beta c_\beta v^2}{\sqrt{2}v_s}\left(s_{\varphi_\omega - \varphi_y}\mathrm{Im}(A_\lambda) - c_{\varphi_\omega - \varphi_y}\mathrm{Re}(A_\lambda) - \sqrt{2}v_s|\kappa|c_{\varphi_y}\right)$$

$$+ \frac{1}{\sqrt{2}}|\kappa|v_s\left(c_{\varphi_\omega}\mathrm{Re}(A_\kappa) - s_{\varphi_\omega}\mathrm{Im}(A_\kappa)\right) \;, \tag{14.23}$$

$$\frac{T_{a_d}}{vs_\beta} \equiv \frac{1}{2}|\lambda|v_s\left(-|\kappa|v_s s_{\varphi_y} + \sqrt{2}c_{\varphi_\omega - \varphi_y}\mathrm{Im}(A_\lambda) + \sqrt{2}s_{\varphi_\omega - \varphi_y}\mathrm{Re}(A_\lambda)\right) \;, \tag{14.24}$$

$$T_{a_u} \equiv \frac{1}{t_\beta}T_{a_d} \;, \tag{14.25}$$

$$T_{a_s} \equiv \frac{1}{2}|\lambda|c_\beta s_\beta v^2\left(2|\kappa|v_s s_{\varphi_y} + \sqrt{2}c_{\varphi_\omega - \varphi_y}\mathrm{Im}(A_\lambda) + \sqrt{2}s_{\varphi_\omega - \varphi_y}\mathrm{Re}(A_\lambda)\right)$$

$$- \frac{1}{\sqrt{2}}|\kappa|v_s^2\left(c_{\varphi_\omega}\mathrm{Im}(A_\kappa) + s_{\varphi_\omega}\mathrm{Re}(A_\kappa)\right) \;, \tag{14.26}$$

where Eq. (14.25) reveals that the tadpole parameters T_{a_u} and T_{a_d} are linearly dependent and hence, the total amount of independent tadpole parameters is five. The minimum conditions

$$\left.\frac{\partial V_{\mathrm{NMSSM}}}{\partial H_d}\right|_{\langle H_d\rangle,\langle H_u\rangle,\langle S\rangle} = \left.\frac{\partial V_{\mathrm{NMSSM}}}{\partial H_u}\right|_{\langle H_d\rangle,\langle H_u\rangle,\langle S\rangle} = \left.\frac{\partial V_{\mathrm{NMSSM}}}{\partial S}\right|_{\langle H_d\rangle,\langle H_u\rangle,\langle S\rangle} = 0 \;, \tag{14.27}$$

imply that the tadpole parameters vanish at tree level,

$$T_{h_d}|^{\mathrm{tree}} = T_{h_u}|^{\mathrm{tree}} = T_{h_s}|^{\mathrm{tree}} = T_{a_d}|^{\mathrm{tree}} = T_{a_u}|^{\mathrm{tree}} = T_{a_s}|^{\mathrm{tree}} = 0 \;. \tag{14.28}$$

Nevertheless, we explicitly keep the tadpole parameters in the following expressions since they require renormalization and hence receive higher-order corrections. The tadpole parameters in Eqs. (14.21) to (14.23) can be solved for $m_{H_d}^2$, $m_{H_u}^2$ and m_s^2 which allows for eliminating these three parameters in favor of the other Higgs potential parameters, while Eqs. (14.24) and (14.26) allow for eliminating $\text{Im}(A_\lambda)$ and $\text{Im}(A_\kappa)$. To summarize, we replace the five Higgs potential parameters as follows,

$$m_{H_d}^2 = \frac{T_{h_d}}{vc_\beta} - \frac{1}{2}c_{2\beta}m_Z^2 + \frac{1}{2}|\lambda|t_\beta v_s \left(|\kappa|c_{\varphi_y}v_s - \sqrt{2}\text{Im}(A_\lambda)s_{\varphi_\omega-\varphi_y} + \sqrt{2}\text{Re}(A_\lambda)c_{\varphi_\omega-\varphi_y}\right)$$
$$- \frac{1}{2}|\lambda|^2\left(s_\beta^2v^2 + v_s^2\right) , \tag{14.29}$$

$$m_{H_u}^2 = \frac{T_{h_u}}{vs_\beta} + \frac{1}{2}c_{2\beta}m_Z^2 + \frac{1}{2}\frac{|\lambda|v_s}{t_\beta}\left(|\kappa|c_{\varphi_y}v_s - \sqrt{2}\text{Im}(A_\lambda)s_{\varphi_\omega-\varphi_y} + \sqrt{2}\text{Re}(A_\lambda)c_{\varphi_\omega-\varphi_y}\right)$$
$$- \frac{1}{2}|\lambda|^2\left(c_\beta^2v^2 + v_s^2\right) , \tag{14.30}$$

$$m_s^2 = \frac{T_{h_s}}{v_s} - |\kappa|^2v_s^2 - \frac{1}{2}|\lambda|^2v^2 - |\lambda|c_\beta s_\beta v^2 \left(\frac{\text{Im}(A_\lambda)s_{\varphi_\omega-\varphi_y} - \text{Re}(A_\lambda)c_{\varphi_\omega-\varphi_y}}{\sqrt{2}v_s} - |\kappa|c_{\varphi_y}\right)$$
$$- \frac{1}{\sqrt{2}}|\kappa|v_s\left(\text{Re}(A_\kappa)c_{\varphi_\omega} - \text{Im}(A_\kappa)s_{\varphi_\omega}\right) , \tag{14.31}$$

$$\text{Im}(A_\lambda) = \frac{1}{\sqrt{2}c_{\varphi_\omega-\varphi_y}}\left(\frac{2}{vv_s|\lambda|s_\beta}T_{a_d} + |\kappa|v_ss_{\varphi_y} - \sqrt{2}s_{\varphi_\omega-\varphi_y}\text{Re}(A_\lambda)\right) , \tag{14.32}$$

$$\text{Im}(A_\kappa) = \frac{\sqrt{2}}{|\kappa|v_s^2c_{\varphi_\omega}}\left(\frac{3}{2}|\lambda||\kappa|s_\beta c_\beta v^2v_ss_{\varphi_y} + \frac{c_\beta v}{v_s}T_{a_d} - T_{a_s}\right) - t_{\varphi_\omega}\text{Re}(A_\kappa) . \tag{14.33}$$

The bilinear terms in Eq. (14.18) form the mass matrices $\mathcal{M}_{\phi\phi}^2$ and $\mathcal{M}_{h^+h^-}^2$ of the neutral and charged fields. The analytic form of the former is further discussed below, while the one of the latter is presented in App. D.3. The 2×2 mass matrix $\mathcal{M}_{h^+h^-}^2$ is diagonalized by means of the 2×2 rotation matrix

$$R^c \equiv \begin{pmatrix} -c_{\beta_c} & s_{\beta_c} \\ s_{\beta_c} & c_{\beta_c} \end{pmatrix} \tag{14.34}$$

where β_c denotes the scalar mixing angle of the charged sector of the NMSSM. The rotation matrix R^c transforms the charged doublet from the gauge basis to the mass basis,

$$\begin{pmatrix} G^\pm \\ H^\pm \end{pmatrix} \equiv R^c \begin{pmatrix} h_d^{\mp,*} \\ h_u^\pm \end{pmatrix} , \tag{14.35}$$

and the mass matrix $\mathcal{M}_{h^+h^-}^2$ is transformed as follows,

$$D_{h^+h^-}^2 \equiv R^c\mathcal{M}_{h^+h^-}^2R^{c,T} \equiv \begin{pmatrix} m_{G^\pm}^2 & m_{G^\pm H^\pm}^2 \\ m_{H^\pm G^\pm}^2 & m_{H^\pm}^2 \end{pmatrix} . \tag{14.36}$$

The four elements of this transformed matrix are explicitly given by

$$m_{H^\pm}^2 = \frac{|\lambda|c_{\beta-\beta_c}^2v_s}{s_{2\beta}c_{\varphi_\omega-\varphi_y}}\left(|\kappa|v_sc_{\varphi_\omega} + \sqrt{2}\text{Re}(A_\lambda)\right) - \frac{1}{2}|\lambda|^2c_{\beta-\beta_c}^2v^2 + c_{\beta-\beta_c}^2m_W^2 \tag{14.37}$$
$$+ \frac{c_{\beta_c}^2}{vs_\beta}T_{h_u} + \frac{s_{\beta_c}^2}{vc_\beta}T_{h_d} + \frac{c_{\beta-\beta_c}^2t_{\varphi_y-\varphi_\omega}}{s_\beta^2c_\beta v}T_{a_d} ,$$

$$m^2_{G^\pm} = t^2_{\beta-\beta_c} m^2_{H^\pm} - \frac{s_{\beta-2\beta_c}}{vc^2_{\beta-\beta_c}} T_{h_u} + \frac{c_{\beta-2\beta_c}}{vc^2_{\beta-\beta_c}} T_{h_d} \ , \tag{14.38}$$

$$m^2_{G^\pm H^\pm} = -t_{\beta-\beta_c} m^2_{H^\pm} + \frac{c_{\beta_c}}{vc_{\beta-\beta_c}} T_{h_u} - \frac{s_{\beta_c}}{vc_{\beta-\beta_c}} T_{h_d} + \frac{i}{vs_\beta} T_{a_d} \ , \tag{14.39}$$

$$m^2_{H^\pm G^\pm} = \left(m^2_{G^+ H^+}\right)^* \ . \tag{14.40}$$

At tree level, the mixing angle β_c coincides with β defined in Eq. (14.11) and all tadpole parameters vanish, cf. Eq. (14.28). Consequently, the three matrix elements $m^2_{G^\pm}$, $m^2_{G^\pm H^\pm}$ and $m^2_{H^\pm G^\pm}$ vanish, the transformed mass matrix $D^2_{h^+ h^-}$ becomes diagonal and the charged Higgs bosons acquire the squared mass $m^2_{H^\pm}$. The analytic expression in Eq. (14.37) allows to eliminate one further parameter of the Higgs potential in favor of another. In our work, we consider the choice whether to take $m^2_{H^\pm}$ or $\mathrm{Re}(A_\lambda)$ as independent input. In case of the latter choice, $m^2_{H^\pm}$ can be calculated by means of Eq. (14.37) as a function of the other potential parameters, while choosing the former option implies that Eq. (14.37) has to be solved for $\mathrm{Re}(A_\lambda)$, yielding

$$\mathrm{Re}(A_\lambda) = \frac{s_{2\beta} c_{\varphi_\omega - \varphi_y}}{\sqrt{2}|\lambda|c^2_{\beta-\beta_c} v_s} \left(m^2_{H^\pm} + \frac{1}{2}|\lambda|^2 c^2_{\beta-\beta_c} v^2 - c^2_{\beta-\beta_c} m^2_W - \frac{c^2_{\beta_c}}{vs_\beta} T_{h_u} - \frac{s^2_{\beta_c}}{vc_\beta} T_{h_d} \right. \tag{14.41}$$

$$\left. - \frac{c^2_{\beta-\beta_c} t_{\varphi_y - \varphi_\omega}}{s^2_\beta c_\beta v} T_{a_d} \right) - \frac{|\kappa| v_s c_{\varphi_\omega}}{\sqrt{2}} \ ,$$

which is then calculated as a function of the other parameters. For the neutral multiplet, we split the rotation from the gauge to the mass basis into two consecutive rotations,

$$(h_d, h_u, h_s, a, a_s, G^0)^T \equiv R^G (h_d, h_u, h_s, a_d, a_u, a_s)^T \ , \tag{14.42}$$

$$(h_1, h_2, h_3, h_3, h_4, h_5, G^0)^T \equiv R (h_d, h_u, h_s, a, a_s, G^0)^T \ . \tag{14.43}$$

The basis on the left-hand side of Eq. (14.42) is gained from the gauge basis by extracting the Goldstone boson G^0 by means of the rotation matrix

$$R^G \equiv \begin{pmatrix} \mathbb{1}_{3\times3} & \emptyset_{3\times3} \\ \emptyset_{3\times3} & \widetilde{R}^G \end{pmatrix} \quad \text{with} \quad \widetilde{R}^G \equiv \begin{pmatrix} s_{\beta_n} & c_{\beta_n} & 0 \\ 0 & 0 & 1 \\ c_{\beta_n} & -s_{\beta_n} & 0 \end{pmatrix} \ , \tag{14.44}$$

where the mixing angle β_n is introduced. The rotation matrix R^G rotates the mass matrix into the matrix $\mathcal{M}^2_{hh}$,

$$\mathcal{M}^2_{hh} \equiv R^G \mathcal{M}^2_{\phi\phi} R^{G,T} \ , \tag{14.45}$$

and the analytic forms of all elements of this matrix are presented explicitly in App. D.1. We want to mention already at this stage that while $\mathcal{M}^2_{hh}$ is a 6×6 matrix, we restrict the presentation of its elements in App. D.1 to the 5×5-dimensional sub-matrix in which the admixture with the Goldstones is neglected. Hence, the corresponding modified 5×5-dimensional mass matrix $\mathcal{M}^2_{hh}$ used for calculating the loop-corrected neutral Higgs boson masses accounts for the mixing of the neutral Higgs boson fields only, neglecting the Goldstone boson contributions. Likewise, while the rotation matrix R introduced in Eq. (14.43) is a 6×6 matrix, we consider only a 5×5-dimensional modified rotation matrix R where the Goldstone boson admixture is neglected for the calculation of the loop-corrected masses in Sec. 16.2.

The complete mass basis of the neutral sector given on the left-hand side of Eq. (14.43) is gained by a second rotation with the rotation matrix[37] R,

$$D^2_{hh} \equiv R\mathcal{M}^2_{hh}R^T \equiv \mathrm{diag}\left(m^2_{h_1}, m^2_{h_2}, m^2_{h_3}, m^2_{h_4}, m^2_{h_5}, 0\right) , \qquad (14.46)$$

where in this equation, the tree-level tadpole conditions from Eq. (14.28) are applied together with the fact that at tree level, the mixing angle β_n coincides with β defined in Eq. (14.11) and moreover with β_c from Eq. (14.34),

$$\beta_n|_{\mathrm{tree}} = \beta_c|_{\mathrm{tree}} = \beta|_{\mathrm{tree}} . \qquad (14.47)$$

The physical neutral CP-mixed Higgs bosons h_i ($i = 1, ..., 5$) are per convention sorted by ascending mass,

$$m^2_{h_1} \leq m^2_{h_2} \leq m^2_{h_3} \leq m^2_{h_4} \leq m^2_{h_5} . \qquad (14.48)$$

The effective μ parameter μ_{eff} of the complex NMSSM, dynamically generated through the VEV of the singlet field is given by

$$\mu_{\mathrm{eff}} = \frac{1}{\sqrt{2}}\lambda v_s e^{i\varphi_s} \equiv |\mu_{\mathrm{eff}}|e^{i\varphi_{\mu_{\mathrm{eff}}}} , \qquad (14.49)$$

where we defined the absolute value and the phase of μ_{eff} as

$$|\mu_{\mathrm{eff}}| \equiv \frac{1}{\sqrt{2}}|\lambda|v_s , \qquad (14.50)$$

$$\varphi_{\mu_{\mathrm{eff}}} \equiv \varphi_s + \varphi_\lambda . \qquad (14.51)$$

The MSSM limit of the complex NMSSM is gained by letting the NMSSM-specific parameters λ and κ vanish, *i.e.* by simultaneously taking the limits $\lambda \to 0$ and $\kappa \to 0$, while λ/κ and the effective Higgs mass parameter μ_{eff} in Eq. (14.4) are kept at a constant non-vanishing value.

14.3. The Quark, Lepton, Sfermion and Gauge Boson Sectors

The next sectors of the complex NMSSM we consider are the SM-like fermions, *i.e.* the quark and lepton sector, the sfermions as well as the gauge bosons. In the following, we restrict the presentation of each sector to the parts that yield contributions to the two-loop $\mathcal{O}(\alpha^2_t)$ corrections to the Higgs boson masses.

Quark and lepton sectors
In the approximations used in our two-loop calculations, cf. Sec. 14.5 for further discussions, we consider all quarks and leptons to be massless apart from the top quark with a non-zero mass m_t. Moreover, we neglect all generation mixing in the quark sector as well, *i.e.* we replace the CKM matrix V with a unit matrix. Due to these approximations, only the massive top quark and the approximately massless bottom quark are relevant for our calculations, while all other quarks and leptons do not contribute at the $\mathcal{O}(\alpha^2_t)$ two-loop level.

Up-squark sector
Due to the aforementioned approximation in the quark and lepton sector, *i.e.* neglecting all generation mixing and considering all quarks and leptons apart from the top quark to be massless, the up-squark mixing matrix reduces considerably. Moreover, the since we apply the *gaugeless limit* $g' = g = 0$ in our $\mathcal{O}(\alpha^2_t)$ two-loop calculations, the diagonal elements of

---

[37]We do not introduce subscripts for the neutral mixing matrix in order to distinguish it from the one presented in the N2HDM in Eq. (9.14). Throughout Part IV of this thesis, the matrix R denotes the one defined via Eq. (14.43).

the squark mass matrix simplify even further. With these approximations, the only non-zero contributions stem from the superpartners of the top quark and the corresponding reduces 2×2 mass matrix reads

$$
\mathcal{M}_{\tilde{t}}^2 = \begin{pmatrix} m_{\tilde{Q}_3}^2 + m_t^2 & m_t \left(A_t^* e^{-i\varphi_u} - \dfrac{\mu_{\text{eff}}}{t_\beta} \right) \\ m_t \left(A_t e^{i\varphi_u} - \dfrac{\mu_{\text{eff}}^*}{t_\beta} \right) & m_{\tilde{t}_R}^2 + m_t^2 \end{pmatrix} \ , \tag{14.52}
$$

where $m_{\tilde{Q}_3}^2$ and $m_{\tilde{t}_R}^2$ denote the only entries of the soft-SUSY-breaking mass matrices $m_{\tilde{Q}}^2$ and $m_{\tilde{U}_R}^2$ which are relevant in this approximation and A_t is the soft-SUSY-breaking trilinear coupling of the stop sector. The 2×2 matrix is diagonalized by the unitary matrix $\mathcal{U}_{\tilde{t}}$. The corresponding eigenstates are the two physical stop squarks in the mass basis

$$
\left(\tilde{t}_1, \tilde{t}_2 \right)^T = \mathcal{U}_{\tilde{t}} \left(\tilde{t}_L, \tilde{t}_R \right)^T \ , \tag{14.53}
$$

and the diagonalized matrix contains the squared masses of the stop squarks,

$$
\mathcal{D}_{\tilde{t}}^2 = \mathcal{U}_{\tilde{t}} \mathcal{M}_{\tilde{t}}^2 \mathcal{U}_{\tilde{t}}^\dagger = \text{diag}\left(m_{\tilde{t}_1}^2, m_{\tilde{t}_2}^2 \right) \ . \tag{14.54}
$$

For later convenience, we additionally define the off-diagonal matrix element of the diagonalized stop matrix,

$$
Y_{\tilde{t}} \equiv \left(\mathcal{U}_{\tilde{t}} \mathcal{M}_{\tilde{t}}^2 \mathcal{U}_{\tilde{t}}^\dagger \right)_{12} \ , \tag{14.55}
$$

which vanishes at tree level according to Eq. (14.54) but receives higher-order corrections through renormalization.

Down-squark sector
By applying the aforementioned approximations of vanishing quark and lepton masses (apart from m_t) and the gaugeless limit, the down-squark mass matrix simplifies considerably and moreover, it is revealed that only the left-handed sbottom squark contributes to our calculations. The mass eigenstate of the first sbottom squark corresponds to the left-handed sbottom squark,

$$
\tilde{b}_1 \longleftrightarrow \tilde{b}_L \ , \tag{14.56}
$$

and the squared mass of the particle is given by

$$
m_{\tilde{b}_1}^2 = m_{\tilde{Q}_3}^2 \ . \tag{14.57}
$$

The second sbottom squark $\tilde{b}_2$, corresponding to the right-handed sbottom state, decouples and does not contribute to our two-loop calculations at $\mathcal{O}(\alpha_t^2)$.

Gauge boson sector
The squared masses of the gauge bosons $W^\pm$ and Z, generated through the mechanism of EWSB, are defined as in Eqs. (4.16) and (4.17). While the masses m_W and m_Z of the gauge bosons vanish in the gaugeless limit, they nevertheless yield non-vanishing contributions through their renormalization as further described in Sec. 15.4.

14.4. The Chargino and Neutralino Sectors

Chargino sector
The mass matrix of the charged winos $\widetilde{W}^\pm$ and the charged higgsinos $\widetilde{H}_{u,d}^\pm$ in the gauge basis $(\widetilde{W}^-, \widetilde{H}_d^-)$ and $(\widetilde{W}^+, \widetilde{H}_u^+)$ is given by

$$
\mathcal{M}_{\tilde{\chi}^\pm} = \begin{pmatrix} M_2 & \sqrt{2} e^{-i\varphi_u} s_\beta m_W \\ \sqrt{2} c_\beta m_W & \mu_{\text{eff}} \ . \end{pmatrix} \tag{14.58}
$$

The physical eigenstates in the mass basis are given by the *charginos* $\widetilde{\chi}_i^\pm$ ($i = 1, 2$). In the gaugeless limit, cf. Sec. 14.5, the mass matrix simplifies to the diagonal form

$$\mathcal{M}_{\widetilde{\chi}^\pm} = \mathrm{diag}\big(M_2, \mu_{\mathrm{eff}}\big) \ . \tag{14.59}$$

The charged winos decouple and the charginos $\widetilde{\chi}_2^\pm$ are directly connected to the charged higgsinos. The diagonalization of the fermion mass matrix yields the masses of the charginos,

$$\mathcal{D}_{\widetilde{\chi}^\pm} = \mathrm{diag}\big(m_{\widetilde{\chi}_1}, m_{\widetilde{\chi}_2}\big) = \mathrm{diag}\big(M_2, |\mu_{\mathrm{eff}}|\big) \ , \tag{14.60}$$

where we absorbed the phase $\varphi_{\mu_{\mathrm{eff}}}$ into the mixing matrix elements which, as a consequence, leads to the reappearance of this phase in the chargino couplings. In the approximations that we consider for the calculation of the two-loop corrections to the Higgs boson masses, the charginos $\widetilde{\chi}_1^\pm$ decouple and only the charginos $\widetilde{\chi}_2^\pm$ contribute to our calculations.

Neutralino sector

In the gauge basis $(\widetilde{B}, \widetilde{W}^0, \widetilde{H}_d^0, \widetilde{H}_u^0, \widetilde{S})$, the 5×5-dimensional mass matrix of the neutralinos is given by

$$\mathcal{M}_{\widetilde{\chi}^0} = \begin{pmatrix} M_1 & 0 & -c_\beta m_Z s_W & s_\beta e^{-i\varphi_u} m_Z s_W & 0 \\ 0 & M_2 & c_\beta m_W & -s_\beta e^{-i\varphi_u} m_W & 0 \\ -c_\beta m_Z s_W & c_\beta m_W & 0 & -\mu_{\mathrm{eff}} & -\dfrac{v s_\beta e^{i\varphi_u} \lambda}{\sqrt{2}} \\ s_\beta e^{-i\varphi_u} m_Z s_W & -s_\beta e^{-i\varphi_u} m_W & -\mu_{\mathrm{eff}} & 0 & -\dfrac{v s_\beta e^{i\varphi_u} \lambda}{\sqrt{2}} \\ 0 & 0 & -\dfrac{v s_\beta e^{i\varphi_u} \lambda}{\sqrt{2}} & -\dfrac{v s_\beta e^{i\varphi_u} \lambda}{\sqrt{2}} & \sqrt{2} v_s e^{i\varphi_s} \kappa \end{pmatrix} \ , \tag{14.61}$$

where we use the short-hand notation $s_W \equiv \sin(\Theta_W)$ for the Weinberg angle Θ_W. The diagonalization of the mass matrix yields the five *neutralinos* $\widetilde{\chi}_i^0$ ($i = 1, ..., 5$). In the gaugeless limit, the mass matrix reduces to a block-diagonal form consisting of two block matrices

$$\mathcal{M}_{\widetilde{\chi}^0} = \mathrm{diag}\big(\mathcal{M}_{\widetilde{\chi}^0}^G, \mathcal{M}_{\widetilde{\chi}^0}^N\big) \ , \tag{14.62}$$

with the diagonal 2×2 gaugino mass matrix

$$\mathcal{M}_{\widetilde{\chi}^0}^G = \mathrm{diag}\big(M_1, M_2\big) \ , \tag{14.63}$$

and the 3×3 higgsino-singlino mass matrix

$$\mathcal{M}_{\widetilde{\chi}^0}^N = \begin{pmatrix} 0 & -\mu_{\mathrm{eff}} & -\dfrac{v s_\beta e^{i\varphi_u} \lambda}{\sqrt{2}} \\ -\mu_{\mathrm{eff}} & 0 & -\dfrac{v s_\beta e^{i\varphi_u} \lambda}{\sqrt{2}} \\ -\dfrac{v s_\beta e^{i\varphi_u} \lambda}{\sqrt{2}} & -\dfrac{v s_\beta e^{i\varphi_u} \lambda}{\sqrt{2}} & \sqrt{2} v_s e^{i\varphi_s} \kappa \end{pmatrix} \ . \tag{14.64}$$

The already diagonalized form of $\mathcal{M}_{\widetilde{\chi}^0}^G$,

$$\mathcal{D}_{\widetilde{\chi}^0}^G = \mathcal{M}_{\widetilde{\chi}^0}^G = \mathrm{diag}\big(m_{\widetilde{\chi}_1^0}, m_{\widetilde{\chi}_2^0}\big) = \mathrm{diag}\big(M_1, M_2\big) \ , \tag{14.65}$$

corresponds to the two neutralino eigenstates $\widetilde{\chi}_i^0$ ($i = 1, 2$). In our approximations, these eigenstates decouple and do not contribute to our two-loop results at $\mathcal{O}(\alpha_t^2)$. On the other hand, the diagonalization of the other fermion block matrix $\mathcal{M}_{\widetilde{\chi}^0}^N$ yields the three neutralinos $\widetilde{\chi}_i^0$ ($i = 3, 4, 5$) which contribute to our two-loop results. The diagonalized mass matrix is gained by applying the mixing matrix $\mathcal{N}$ to the mass matrix,

$$\mathcal{D}_{\widetilde{\chi}^0}^N = \mathcal{N}^* \mathcal{M}_{\widetilde{\chi}^0}^N N^\dagger = \mathrm{diag}\big(m_{\widetilde{\chi}_3^0}, m_{\widetilde{\chi}_4^0}, m_{\widetilde{\chi}_5^0}\big) \ . \tag{14.66}$$

14.5. Approximations for the Two-Loop Calculations

For convenience, we provide an overview over all aforementioned approximations applied in the calculation of the $\mathcal{O}(\alpha_t^2)$ two-loop corrections to the Higgs boson masses in the complex NMSSM in this section and moreover present another approximation which we apply for the calculation of the genuine two-loop Feynman diagrams. To that end, we first define the exact meaning of denoting the two-loop corrections by $\mathcal{O}(\alpha_t^2)$. We define the coupling constant α_t as

$$\alpha_t \equiv \frac{y_t^2}{4\pi} \equiv \frac{1}{4\pi} \frac{2m_t^2}{v^2 s_\beta^2} \,, \tag{14.67}$$

where we defined the top Yukawa coupling constant y_t for convenience. In general, the notation $\mathcal{O}(\alpha_i \alpha_j \cdots)$ used in this thesis implies that only certain powers of the coupling constants $\alpha_i, \alpha_j, \ldots$ defined via relations analogous to Eq. (14.67), are taken into account. Consequently, the notation $\mathcal{O}(\alpha_t^2)$ implies that only diagrammatic contributions proportional to α_t^2 are taken into account. Strictly speaking however, we actually calculate contributions proportional to $m_t^2 \alpha_t^2$ in this work and hence, our two-loop results are of $\mathcal{O}(m_t^2 \alpha_t^2)$. In order to comply with the conventional notation however, we nevertheless refer to our two-loop calculations as being of $\mathcal{O}(\alpha_t^2)$ throughout this thesis.

Concerning the independent input parameters, we apply the approximations that

- in the *gaugeless limit*, the gauge couplings g' and g of the gauge subgroups $U(1)_Y$ and $SU(2)_L$, respectively and consequently also the gauge boson masses vanish[38],

$$g' \to 0 \,, \quad g \to 0 \,, \quad m_W \to 0 \,, \quad m_Z \to 0 \,, \tag{14.68}$$

- all quarks and leptons, apart from the top quark, have vanishing mass,

$$m_t \neq 0 \,, \quad m_f \to 0 \quad \text{(all other quarks and leptons)} \,, \tag{14.69}$$

- no mixing of generations in the quark and lepton sectors are present and especially, the CKM matrix V equals a unit matrix,

$$V_{ij} \to \delta_{ij} \,. \tag{14.70}$$

As a consequence of these approximations, only a reduced amount of particles compared to the full particle content of the complex NMSSM as shown in Fig. 14.1 are relevant for the $\mathcal{O}(\alpha_t^2)$ two-loop corrections to the Higgs masses. These particles are given by

- the top quark t and the bottom quark b,

- the stop squarks $\widetilde{t}_i$ ($i = 1, 2$) and the sbottom squark $\widetilde{b}_1$,

- the neutral CP-mixed Higgs bosons h_i ($i = 1, ..., 5$) and the charged Higgs bosons $H^\pm$,

- the neutral Goldstone boson G^0 and the charged Goldstone bosons $G^\pm$,

- the chargino $\widetilde{\chi}_2^\pm$ and the three neutralinos $\widetilde{\chi}_i^0$ ($i = 3, 4, 5$) and

- the $W^\pm$ and Z gauge bosons.

Apart from these approximations, we moreover simplify the calculation of the genuine two-loop Feynman diagrams by taking the limit of *vanishing external momentum*, i.e. we evaluate
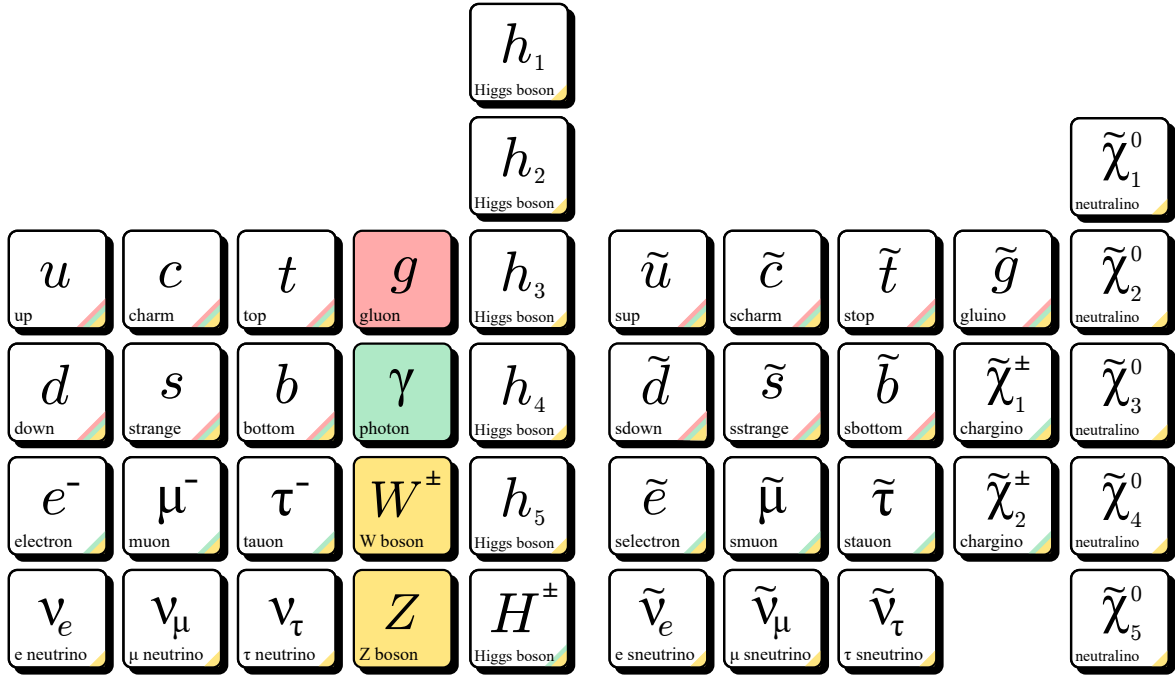
Figure 14.1.: Particle content of the complex NMSSM in the mass basis. In the complex realization of the NMSSM, the five Higgs bosons h_i $(i = 1, ..., 5)$ represent CP-mixed states.

the genuine two-loop diagrams in the limit $p^2 \to 0$. In this limit, the calculated Feynman amplitudes correspond to their counterparts derived in the effective potential approach.

We want to emphasize that we apply all aforementioned approximations only for the calculation of the $\mathcal{O}(\alpha_t^2)$ two-loop corrections to the Higgs boson masses. For the numerical evaluation presented in Chapter 17 on the other hand, we also evaluate the Higgs boson masses at full one-loop order, without any approximations applied, and at $\mathcal{O}(\alpha_t \alpha_s)$ two-loop order, with the same approximations applied as for the calculation of the $\mathcal{O}(\alpha_t^2)$ corrections.

14.6. Set of Independent Parameters and Particle Content

In the following, we present the independent input parameters relevant for the $\mathcal{O}(\alpha_t^2)$ corrections. For practical reasons, we include in this set only the parameters which are relevant for the $\mathcal{O}(\alpha_t^2)$ two-loop corrections to the Higgs masses when all approximations in the preceding Sec. 14.5 are applied. When choosing $m_{H^\pm}$ as an independent parameter, $\text{Re}(A_\lambda)$ is calculated as a function of the other parameters of the scalar potential through Eq. (14.41) and the set of independent parameters is given by

$$\left\{ T_{\phi_i}, v, s_W, e, t_\beta, |\lambda|, |\kappa|, v_s, m_{H^\pm}, \text{Re}(A_\kappa), \varphi_j, m_t, m_{\widetilde{Q}_3}, m_{\widetilde{t}_R}, A_t \right\} , \tag{14.71}$$

where $\phi_i = h_d, h_u, h_s, a_d, a_u, a_s$ and $j = \lambda, \kappa, u, s$. If we instead choose $\text{Re}(A_\lambda)$ to be an independent parameter, $m_{H^\pm}^2$ is calculated as a function of the other Higgs potential parameters by means of Eq. (14.37) and the set of independent parameters is given by

$$\left\{ T_{\phi_i}, v, s_W, e, t_\beta, |\lambda|, |\kappa|, v_s, \text{Re}(A_\lambda), \text{Re}(A_\kappa), \varphi_j, m_t, m_{\widetilde{Q}_3}, m_{\widetilde{t}_R}, A_t \right\} . \tag{14.72}$$

---

[38] We want to emphasize here already that while g', g, m_W and m_Z all vanish in the gaugeless limit, constants defined over the ratio of these quantities, *e.g.* the VEV v or the sine and cosine of the Weinberg angle Θ_W, are unaffected by these limit and remain at their constant non-zero values.

The Renormalization of the Complex NMSSM for the $\mathcal{O}(\alpha_t^2)$ Corrections

The computation of the higher-order corrections to the Higgs boson masses necessitates the evaluation of one- and two-loop integrals which in general contain UV divergences. Consequently, the independent parameters presented at the end of the preceding Chapter 14 require renormalization. In contrast to Parts II and III of this thesis, where we considered corrections at the one-loop level, the two-loop corrections require the renormalization of the relevant parameters not only at one-loop level but additionally also at two-loop order. Throughout this chapter, the definition of the one- and two-loop CTs of the independent parameters is restricted to contain only contributions which are relevant for the genuine $\mathcal{O}(\alpha_t^2)$ two-loop corrections and for all approximations which are used in the course of the calculations, cf. Sec. 14.5. The resulting CTs are implemented in a new version of the computer program `NMSSMCALC` which is used for the numerical computation of the higher-order corrections to the Higgs boson masses in the complex NMSSM. The discussion of the renormalization which is required for the computation of the $\mathcal{O}(\alpha_t^2)$ two-loop corrections presented in this chapter closely follows the recent publication [82].

Starting with Sec. 15.1, we introduce CTs for all independent parameters of the complex NMSSM that are relevant for the calculations performed in our work. In Sec. 15.2, we present the renormalization of the top and stop sector which is of particular relevance for the $\mathcal{O}(\alpha_t^2)$ corrections. In the subsequent Sec. 15.3, we present the renormalization of the scalar sector including the definition of the CTs for the neutral Higgs mass matrix, the WFRCs of the scalar fields as well as the renormalization of the charged Higgs boson mass and t_β. Moreover, we discuss the renormalization of the minimum conditions of the scalar potential and define the tadpole CTs required for the higher-order corrections to the Higgs masses. Subsequently, we present in Sec. 15.4 the renormalization of the gauge sector of the complex NMSSM. Finally, we discuss the renormalization of all remaining independent parameters of the complex NMSSM in Sec. 15.5.

15.1. The Counterterms for the $\mathcal{O}(\alpha_t^2)$ Corrections

In the first section of this chapter, we first formally introduce the CTs of all independent parameters given by either of the two sets in Eqs. (14.71) and (14.72). For each indepen-

dent parameter, we split the bare parameter into a renormalized value and its corresponding genuine one- and two-loop CTs as follows[39],

$$T_{\phi_i} \rightarrow T_{\phi_i} + \delta^{(1)}T_{\phi_i} + \delta^{(2)}T_{\phi_i} \; , \tag{15.1}$$

$$v \rightarrow v + \delta^{(1)}v + \delta^{(2)}v \; , \tag{15.2}$$

$$e \rightarrow e\left(1 + \delta^{(1)}Z_e + \delta^{(2)}Z_e\right) \; , \tag{15.3}$$

$$s_W \rightarrow s_W + \delta^{(1)}s_W + \delta^{(2)}s_W \; , \tag{15.4}$$

$$m_W^2 \rightarrow m_W^2 + \delta^{(1)}m_W^2 + \delta^{(2)}m_W^2 \; , \tag{15.5}$$

$$m_Z^2 \rightarrow m_Z^2 + \delta^{(1)}m_Z^2 + \delta^{(2)}m_Z^2 \; , \tag{15.6}$$

$$m_{H^\pm}^2 \rightarrow m_{H^\pm}^2 + \delta^{(1)}m_{H^\pm}^2 + \delta^{(2)}m_{H^\pm}^2 \; , \tag{15.7}$$

$$m_{G^\pm H^\pm}^2 \rightarrow m_{G^\pm H^\pm}^2 + \delta^{(1)}m_{G^\pm H^\pm}^2 + \delta^{(2)}m_{G^\pm H^\pm}^2 \; , \tag{15.8}$$

$$(\mathcal{M}_{hh}^2)_{\phi_i\phi_j} \rightarrow (\mathcal{M}_{hh}^2)_{\phi_i\phi_j} + (\delta^{(1)}\mathcal{M}_{hh}^2)_{\phi_i\phi_j} + (\delta^{(2)}\mathcal{M}_{hh}^2)_{\phi_i\phi_j} \; , \tag{15.9}$$

$$t_\beta \rightarrow t_\beta + \delta^{(1)}t_\beta + \delta^{(2)}t_\beta \; , \tag{15.10}$$

$$\mathrm{Re}(A_\lambda) \rightarrow \mathrm{Re}(A_\lambda) + \delta^{(1)}\mathrm{Re}(A_\lambda) + \delta^{(2)}\mathrm{Re}(A_\lambda) \; , \tag{15.11}$$

$$|\lambda| \rightarrow |\lambda| + \delta^{(1)}|\lambda| + \delta^{(2)}|\lambda| \; , \tag{15.12}$$

$$|\kappa| \rightarrow |\kappa| + \delta^{(1)}|\kappa| + \delta^{(2)}|\kappa| \; , \tag{15.13}$$

$$v_s \rightarrow v_s + \delta^{(1)}v_s + \delta^{(2)}v_s \; , \tag{15.14}$$

$$\mathrm{Re}(A_\kappa) \rightarrow \mathrm{Re}(A_\kappa) + \delta^{(1)}\mathrm{Re}(A_\kappa) + \delta^{(2)}\mathrm{Re}(A_\kappa) \; , \tag{15.15}$$

$$\varphi_i \rightarrow \varphi_i + \delta^{(1)}\varphi_i + \delta^{(2)}\varphi_i \quad (i = u, s, \lambda, \kappa) \; , \tag{15.16}$$

$$\mu_{\mathrm{eff}} \rightarrow \mu_{\mathrm{eff}} + \delta^{(1)}\mu_{\mathrm{eff}} + \delta^{(2)}\mu_{\mathrm{eff}} \; , \tag{15.17}$$

$$m_t \rightarrow m_t + \delta^{(1)}m_t \; , \tag{15.18}$$

$$m_{\widetilde{Q}_3}^2 \rightarrow m_{\widetilde{Q}_3}^2 + \delta^{(1)}m_{\widetilde{Q}_3}^2 \; , \tag{15.19}$$

$$m_{\widetilde{t}_R}^2 \rightarrow m_{\widetilde{t}_R}^2 + \delta^{(1)}m_{\widetilde{t}_R}^2 \; , \tag{15.20}$$

$$A_t \rightarrow A_t + \delta^{(1)}A_t \; , \tag{15.21}$$

$$m_{\widetilde{t}_i}^2 \rightarrow m_{\widetilde{t}_i}^2 + \delta^{(1)}m_{\widetilde{t}_i}^2 \quad (i = 1, 2) \; , \tag{15.22}$$

$$m_{\widetilde{b}_1}^2 \rightarrow m_{\widetilde{b}_1}^2 + \delta^{(1)}m_{\widetilde{b}_1}^2 \; , \tag{15.23}$$

$$Y_{\widetilde{t}} \rightarrow Y_{\widetilde{t}} + \delta^{(1)}Y_{\widetilde{t}} \; , \tag{15.24}$$

with $\phi_i = h_d, h_u, h_s, a_d, a_u, a_s$ for Eq. (15.1) and $\phi_i, \phi_j = h_d, h_u, h_s, a, a_s$ for Eq. (15.9). For later convenience we additionally introduced CTs of the squared gauge boson masses m_W^2 and m_Z^2, for the effective parameter μ_{eff} defined in Eq. (14.49), for the off-diagonal entry $m_{G^\pm H^\pm}^2$ of the diagonalized charged Higgs mass matrix defined in Eq. (14.39), for the neutral mass matrix elements $(\mathcal{M}_{hh}^2)_{\phi_i\phi_j}$ as given in App. D.1 as well as for the additional parameters $m_{\widetilde{t}_i}^2$ $(i = 1, 2)$, $m_{\widetilde{b}_1}^2$ and $Y_{\widetilde{t}}$ of the top and stop sectors which are promoted only up to one-loop order, since the two-loop CTs are not required in our calculations.

In order to incorporate the newly calculated $\mathcal{O}(\alpha_t^2)$ contributions consistently with the full one-loop and $\mathcal{O}(\alpha_t\alpha_s)$ two-loop corrections for the complex NMSSM already implemented in NMSSMCALC [79, 81], we adopt the mixed $\overline{\mathrm{DR}}$-OS scheme used in these computations, *i.e.* in case that $m_{H^\pm}^2$ is chosen as independent input the independent parameters of the complex NMSSM are renormalized as follows,

$$\underbrace{T_{\phi_i}, m_{H^\pm}^2, v, e, s_W}_{\text{OS scheme}}, \underbrace{t_\beta, |\lambda|, v_s, |\kappa|, \mathrm{Re}(A_\kappa), \varphi_i}_{\overline{\mathrm{DR}} \text{ scheme}}, \underbrace{m_t, m_{\widetilde{Q}_3}, m_{\widetilde{t}_R}, A_t}_{\text{OS}/\overline{\mathrm{DR}} \text{ scheme}} \; . \tag{15.25}$$

---

[39]In Part IV, we introduce the CT $\delta^{(n)}p$ of the parameter p required for the two-loop calculations with a superscript (n) denoting the nth loop level at which the CT is defined.

where OS/$\overline{\text{DR}}$ denotes that the parameters of the top and stop sectors are renormalized either in the OS or in the $\overline{\text{DR}}$ scheme as described in the subsequent Sec. 15.2. If instead $\text{Re}(A_\lambda)$ is considered as input, then the CTs in the mixed $\overline{\text{DR}}$-OS scheme are fixed according to

$$\underbrace{T_{\phi_i}, v, e, s_W}_{\text{OS scheme}}, \underbrace{t_\beta, |\lambda|, v_s, |\kappa|, \text{Re}(A_\lambda), \text{Re}(A_\kappa), \varphi_i}_{\overline{\text{DR}} \text{ scheme}}, \underbrace{m_t, m_{\widetilde{Q}_3}, m_{\widetilde{t}_R}, A_t}_{\text{OS/}\overline{\text{DR}} \text{ scheme}}, \tag{15.26}$$

In the subsequent sections, we present the renormalization conditions imposed on the different sectors of the complex NMSSM in more detail and present the resulting CTs explicitly. However, we want to emphasize again that we restrict the presentation and definition of all CTs solely to the terms which contribute to the newly calculated two-loop corrections to the Higgs masses at $\mathcal{O}(\alpha_t^2)$. For the one-loop corrections to the Higgs masses implemented in NMSSMCALC on the other hand, the full CTs including contributions from all independent parameters are considered. We do not show these full one-loop CTs in this work and instead refer to [79] for their presentation.

15.2. Renormalization of the Top and Stop Sectors

The first sector considered for renormalization in the complex NMSSM is the top and stop sector of the theory. The relevant parameters of the top/stop sectors are split into renormalized parameters and one-loop CTs as presented in Eqs. (15.18) to (15.21). In our work, we proceed along the lines of [81] and consider the two possibilities of renormalizing the top/stop sector either in the OS or in the $\overline{\text{DR}}$ scheme. In case the former is chosen, it is more practical to directly define the CTs for the masses of the two stops $\widetilde{t}_i$ ($i = 1, 2$), for the sbottom $\widetilde{b}_1$ as well as for the off-diagonal mixing element $Y_{\widetilde{t}}$ of the stop sector as defined in Eq. (14.55). These additional CTs are introduced analogously by splitting the bare parameters into the sum of the renormalized parameters and their CTs as presented in Eqs. (15.22) to (15.24).

We first consider the case that the parameters of the top/stop sectors are renormalized OS. For the OS conditions of the top/stop sector, we adopt the scheme definitions of the CTs presented in [276, 277]. The four CTs are given by

$$\delta^{(1)} m_t = \frac{m_t}{2} \text{Re} \left[\Sigma_{tt}^{(1),L}(m_t^2) + \Sigma_{tt}^{(1),R}(m_t^2) + 2\Sigma_{tt}^{(1),S}(m_t^2) \right] , \tag{15.27}$$

$$\delta^{(1)} m_{\widetilde{t}_1}^2 = \widetilde{\text{Re}} \left[\Sigma_{\widetilde{t}_1 \widetilde{t}_1}^{(1)}(m_{\widetilde{t}_1}^2) \right] , \tag{15.28}$$

$$\delta^{(1)} m_{\widetilde{t}_2}^2 = \widetilde{\text{Re}} \left[\Sigma_{\widetilde{t}_2 \widetilde{t}_2}^{(1)}(m_{\widetilde{t}_2}^2) \right] , \tag{15.29}$$

$$\delta^{(1)} Y_{\widetilde{t}} = \frac{1}{2} \widetilde{\text{Re}} \left[\Sigma_{\widetilde{t}_1^* \widetilde{t}_2^*}^{(1)}(m_{\widetilde{t}_2}^2) + \Sigma_{\widetilde{t}_1^* \widetilde{t}_2^*}^{(1)}(m_{\widetilde{t}_2}^2) \right] , \tag{15.30}$$

where the superscripts denote the left-chiral (L), right-chiral (R) and scalar (S) projections of the unrenormalized one-loop top quark self-energies in terms of the chirality projectors $\omega_{\mp}$ (cf. *e.g.* [183] for more details). The terms $\Sigma_{\widetilde{t}_i^{(*)} \widetilde{t}_j^{(*)}}^{(1)}(p^2)$ ($i, j = 1, 2$) denote the unrenormalized one-loop self-energies of the stop transitions $\widetilde{t}_i^{(*)} \to \widetilde{t}_j^{(*)}$ and $\widetilde{\text{Re}}$ implies that the real part is applied only to the loop integrals but not to the coupling constants of the complex NMSSM appearing in the stop self-energies. For the calculation of the $\mathcal{O}(\alpha_t^2)$ two-loop corrections, only the subsets of self-energy diagrams shown in Fig. 15.1 and Fig. 15.2 for the top and stop self-energies, respectively, are required. The CTs of the soft-SUSY-breaking masses, trilinear coupling constants and of the squared sbottom mass are derived as functions of other CTs as follows,

$$\delta^{(1)} A_t = \frac{e^{-i\varphi_u}}{m_t} \left[(\mathcal{U}_{\widetilde{t}})_{11}(\mathcal{U}_{\widetilde{t}})_{12}^* \left(\delta^{(1)} m_{\widetilde{t}_1}^2 - \delta^{(1)} m_{\widetilde{t}_2}^2 \right) + (\mathcal{U}_{\widetilde{t}})_{11}(\mathcal{U}_{\widetilde{t}})_{22}^* (\delta^{(1)} Y_{\widetilde{t}})^* \right. \tag{15.31}$$
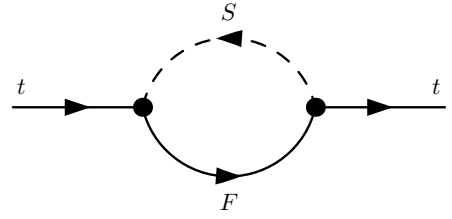
$$S, F = \{h_a, G^0, H^+, G^+, \tilde{t}_b, \tilde{b}_1\}, \{t, b, \chi_c^0, \chi_2^+\}$$

Figure 15.1.: Generic one-loop self-energies of the top quark relevant for the $\mathcal{O}(\alpha_t)$ renormalization of m_t. We implicitly sum over the indices $a = 1, ..., 5$, $b = 1, 2$ and $c = 3, 4, 5$ of all internal particles.

$$+ (\mathcal{U}_{\tilde{t}})_{21}(\mathcal{U}_{\tilde{t}})_{12}^* \delta^{(1)} Y_{\tilde{t}} - \left(A_t e^{i\varphi_u} - \frac{\mu_{\text{eff}}^*}{t_\beta} \right) \delta^{(1)} m_t \right] - \frac{e^{-i\varphi_u} \mu_{\text{eff}}^* \delta^{(1)} t_\beta}{t_\beta^2} + \frac{e^{-i\varphi_u} (\delta^{(1)} \mu_{\text{eff}})^*}{t_\beta}$$

$$\delta^{(1)} m_{\tilde{Q}_3}^2 = |(\mathcal{U}_{\tilde{t}})_{11}|^2 \delta^{(1)} m_{\tilde{t}_1}^2 + |(\mathcal{U}_{\tilde{t}})_{12}|^2 \delta^{(1)} m_{\tilde{t}_2}^2 + (\mathcal{U}_{\tilde{t}})_{21}(\mathcal{U}_{\tilde{t}})_{11}^* \delta^{(1)} Y_{\tilde{t}} + (\mathcal{U}_{\tilde{t}})_{11}(\mathcal{U}_{\tilde{t}})_{21}^* (\delta^{(1)} Y_{\tilde{t}})^* \quad (15.32)$$

$$\qquad - 2 m_t \delta^{(1)} m_t \ ,$$

$$\delta^{(1)} m_{\tilde{t}_R}^2 = |(\mathcal{U}_{\tilde{t}})_{12}|^2 \delta^{(1)} m_{\tilde{t}_1}^2 + |(\mathcal{U}_{\tilde{t}})_{22}|^2 \delta^{(1)} m_{\tilde{t}_2}^2 + (\mathcal{U}_{\tilde{t}})_{22}(\mathcal{U}_{\tilde{t}})_{12}^* \delta^{(1)} Y_{\tilde{t}} + (\mathcal{U}_{\tilde{t}})_{12}(\mathcal{U}_{\tilde{t}})_{22}^* (\delta^{(1)} Y_{\tilde{t}})^* \quad (15.33)$$

$$\qquad - 2 m_t \delta^{(1)} m_t \ ,$$

$$\delta^{(1)} m_{\tilde{b}_1}^2 = \delta^{(1)} m_{\tilde{Q}_3}^2 \ , \quad (15.34)$$

where $\delta^{(1)} t_\beta$ and $\delta^{(1)} \mu_{\text{eff}}$ are defined in the upcoming Subsec. 15.3.4 and Sec. 15.5, respectively.

For the two-loop calculations, we need to expand the one-loop CT $\delta^{(1)} p$ for any parameter p *a priori* up to $\mathcal{O}(\varepsilon)$ terms[40] as follows,

$$\delta^{(1)} p^{\text{OS}} = \frac{1}{\varepsilon} \delta^{(1)} p_{\text{div}} + \delta^{(1)} p_{\text{fin}} + \varepsilon \delta^{(1)} p_\varepsilon \ , \quad (15.35)$$

where the subscripts denote the divergent (div) and finite (fin) parts of the CT as well as the part which is proportional to ε. While the latter terms can in principle be included in the calculation, cf. [278, 279], it turns out that all $\varepsilon \delta^{(1)} p_\varepsilon$ terms of each OS-defined CT do not contribute to the $\mathcal{O}(\alpha_t^2)$ two-loop corrections of the Higgs masses, which was checked explicitly by us. As a consequence, we set the parts proportional to ε of all OS-defined CTs to zero and consider only the expansion up to the finite part in the following,

$$\delta^{(1)} p^{\text{OS}} \rightarrow \frac{1}{\varepsilon} \delta^{(1)} p^{\text{div}} + \delta^{(1)} p^{\text{fin}} \ . \quad (15.36)$$

The $\overline{\text{DR}}$ CT on the other hand is given by

$$\delta^{(1)} p^{\overline{\text{DR}}} = \frac{1}{\varepsilon} \delta^{(1)} p^{\text{div}} \ . \quad (15.37)$$

According to the SLHA, the top quark mass used in the higher-order computations of the Higgs boson masses is understood as the pole mass while the soft-SUSY-breaking mass terms $m_{\tilde{Q}_3}^2$ and $m_{\tilde{t}_R}^2$ as well as the soft-SUSY-breaking trilinear coupling A_t are parameters defined in the $\overline{\text{DR}}$ scheme at the renormalization scale $\mu_R = M_{\text{SUSY}}$, where M_{SUSY} denotes the SUSY mass scale. In our work, we consider both possibilities that the top/stop sector is renormalized either through OS or $\overline{\text{DR}}$ conditions. Since we apply the SLHA, this, however, requires that in both cases, some of the parameters need to be converted from one scheme to the other:

---

[40]The $\mathcal{O}(\varepsilon)$ terms of the CTs are relevant when calculating one-loop Feynman diagrams with CT insertions at *e.g.* one of the vertices of the diagram. The $\mathcal{O}(\varepsilon)$ terms of the CT can combine with the UV-divergent $\mathcal{O}(\varepsilon^{-1})$ terms of the one-loop integral and hence contribute at two-loop order to the finite part of the diagram.

$$F_1, F_2 = \{t, b\}, \{\chi_c^0, \chi_2^+\} \qquad S_1, S_2 = \{h_a, G^0, H^+, G^+\}, \{\tilde{t}_b, \tilde{b}_1\} \qquad S = \{h_a, G^0, H^+, G^+, \tilde{t}_b, \tilde{b}_1\}$$
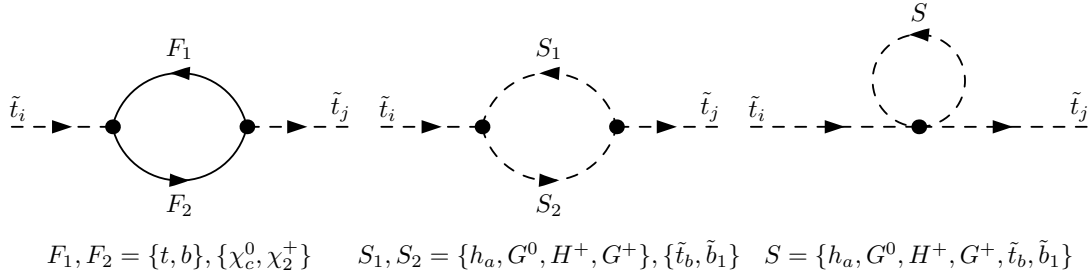
Figure 15.2.: Generic one-loop self-energies of the stops relevant for the $\mathcal{O}(\alpha_t)$ renormalization of the stop sector. We implicitly sum over the indices $a = 1, ..., 5$, $b = 1, 2$ and $c = 3, 4, 5$ of all internal particles.

- In case the $\overline{\text{DR}}$ scheme is chosen for renormalizing the top/stop sector, the $\overline{\text{DR}}$-defined parameters $m_{\widetilde{Q}_3}^2$, $m_{\tilde{t}_R}^2$ and A_t are taken as they are, but the pole mass m_t needs to be converted to the $\overline{\text{DR}}$ top quark mass $m_t^{\overline{\text{DR}}}$. For this, we follow the approach as described in detail in App. C of [82].

- In case the OS scheme is chosen for renormalizing the top/stop sector, the top quark pole mass m_t is taken as input while the $\overline{\text{DR}}$ parameters $m_{\widetilde{Q}_3}$, $m_{\tilde{t}_R}$ and A_t are converted to their corresponding values in the OS scheme by applying the generic formula presented in Eq. (3.31) to the case of the three $\overline{\text{DR}}$ parameters,

$$A_t^{\text{OS}} = A_t^{\overline{\text{DR}}} - \delta^{(1)} A_t^{\text{fin}} , \tag{15.38}$$

$$(m_{\widetilde{Q}_3}^2)^{\text{OS}} = (m_{\widetilde{Q}_3}^2)^{\overline{\text{DR}}} - (\delta^{(1)} m_{\widetilde{Q}_3}^2)^{\text{fin}} , \tag{15.39}$$

$$(m_{\tilde{t}_R}^2)^{\text{OS}} = (m_{\tilde{t}_R}^2)^{\overline{\text{DR}}} - (\delta^{(1)} m_{\tilde{t}_R}^2)^{\text{fin}} . \tag{15.40}$$

In contrast to Eq. (3.31) however, we evaluate the finite parts of the CTs on the right-hand sides of Eqs. (15.38) to (15.40) with the OS parameters A_t^{OS}, $(m_{\widetilde{Q}_3}^2)^{\text{OS}}$ and $(m_{\tilde{t}_R}^2)^{\text{OS}}$ instead of the $\overline{\text{DR}}$ parameters. But since these are defined through these equations, this requires an iterative procedure for solving Eqs. (15.38) to (15.40) for the OS parameters, as discussed in Sec. 3.5. In NMSSMCALC, such an iterative procedure is implemented for the conversion of the $\overline{\text{DR}}$ parameters $m_{\widetilde{Q}_3}$, $m_{\tilde{t}_R}$ and A_t.

Both the OS and the $\overline{\text{DR}}$ scheme of the top/stop sectors are implemented in NMSSMCALC and the user can decide in the input file which renormalization scheme is chosen. Since both schemes differ by finite terms in the CTs of the top/stop sector, the resulting computed higher-order corrections to the Higgs masses differ between the two schemes, as well. We discuss this in more detail in Chapter 17.

15.3. Renormalization of the Scalar Sector

The next sector considered for renormalization is the scalar sector of the theory. This comprises of the renormalization of the scalar field multiplets, the treatment of the tadpoles at one- and two-loop order and the renormalization of the charged Higgs boson mass $m_{H^\pm}$ and t_β. We discuss each of these sectors separately in the following subsections.

15.3.1. The Scalar Wave Function Renormalization Constants

As discussed for scalar field multiplets in general in Sec. 3.2, the scalar fields of the complex NMSSM receive higher-order corrections due to which the bare fields are rescaled to form the

renormalized fields. We introduce one WFRC for each Higgs doublet and singlet[41], expanded up to two-loop order as follows,

$$
H_d \; \to \; \left(1 + \frac{\delta^{(1)} Z_{H_d}}{2} + \frac{\delta^{(2)} Z_{H_d}}{2} - \frac{1}{2} \left(\frac{\delta^{(1)} Z_{H_d}}{2} \right)^2 \right) H_d \tag{15.41}
$$

$$
\equiv \left(1 + \frac{\Delta^{(1)} Z_{H_d}}{2} + \frac{\Delta^{(2)} Z_{H_d}}{2} \right) H_d \; ,
$$

$$
H_u \; \to \; \left(1 + \frac{\delta^{(1)} Z_{H_u}}{2} + \frac{\delta^{(2)} Z_{H_u}}{2} - \frac{1}{2} \left(\frac{\delta^{(1)} Z_{H_u}}{2} \right)^2 \right) H_u \tag{15.42}
$$

$$
\equiv \left(1 + \frac{\Delta^{(1)} Z_{H_u}}{2} + \frac{\Delta^{(2)} Z_{H_u}}{2} \right) H_u \; ,
$$

$$
S \; \to \; \left(1 + \frac{\delta^{(1)} Z_S}{2} + \frac{\delta^{(2)} Z_S}{2} - \frac{1}{2} \left(\frac{\delta^{(1)} Z_S}{2} \right)^2 \right) S \tag{15.43}
$$

$$
\equiv \left(1 + \frac{\Delta^{(1)} Z_S}{2} + \frac{\Delta^{(2)} Z_S}{2} \right) S \; ,
$$

where for later convenience we define the short-hand notations

$$
\Delta^{(1)} Z_{\Phi_i} \equiv \delta^{(1)} Z_{\Phi_i} \; , \tag{15.44}
$$

$$
\Delta^{(2)} Z_{\Phi_i} \equiv \delta^{(2)} Z_{\Phi_i} - \left(\frac{\delta^{(1)} Z_{\Phi_i}}{2} \right)^2 \; , \tag{15.45}
$$

for the genuine one-loop WFRCs as well as for the combination of the genuine two-loop WFRC with the squared one-loop contributions, where $(\Phi_i = H_d, H_u, S)$. For the renormalization of the three WFRCs, we follow the approach used in the calculation of the full one-loop and $\mathcal{O}(\alpha_t \alpha_s)$ two-loop corrections in NMSSMCALC [67, 79, 81] and fix the WFRCs at n-loop level by applying the $\overline{\text{DR}}$ conditions

$$
\left. \frac{\partial \widehat{\Sigma}^{(n)}_{\phi_i \phi_i}}{\partial p^2} \right|_{\text{div}} = 0 \tag{15.46}
$$

to any scalar component field $(\phi_i = h_d, h_u, h_s, a_d, a_u, a_s)$ in the gauge basis, where the subscript denotes that only the UV-divergent contributions proportional to ε^{-1}, cf. Eq. (3.2), in the framework of DRED are taken into account. Since for Eq. (15.46) we have six component fields at our disposal but only three WFRCs that need to be determined, we could in principle choose any combination of three scalar fields[42] to fix the WFRCs through these renormalization conditions. In our case, we choose the three fields $\phi_i = h_d, h_u, h_s$ to define the three WFRCs,

$$
\delta^{(n)} Z_{H_d} = - \left. \frac{\partial \Sigma^{(n)}_{h_d h_d}(p^2)}{\partial p^2} \right|_{\text{div}} \; , \tag{15.47}
$$

$$
\delta^{(n)} Z_{H_u} = - \left. \frac{\partial \Sigma^{(n)}_{h_u h_u}(p^2)}{\partial p^2} \right|_{\text{div}} \; , \tag{15.48}
$$

$$
\delta^{(n)} Z_S = - \left. \frac{\partial \Sigma^{(n)}_{h_s h_s}(p^2)}{\partial p^2} \right|_{\text{div}} \; . \tag{15.49}
$$

---

[41] As discussed in [280] for the MSSM, the introduction of one WFRC for each fundamental $SU(2)_L$ doublet or singlet is sufficient for the UV finiteness of observables calculated as a function of these WFRCs.

[42] In fact, we could also apply Eq. (15.46) to all six fields $(\phi_i = h_d, h_u, h_s, a_d, a_u, a_s)$ and solve the six equations for the three WFRCs. Three of these six equations are linearly dependent, so that the system of equations is always well-determined.
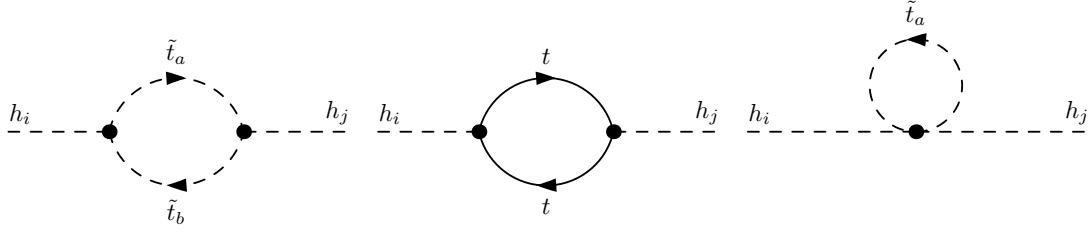
Figure 15.3.: Generic Feynman-diagrammatic contributions to the self-energies of the neutral Higgs bosons $h_{i,j}$ $(i,j = 1, ..., 5)$ relevant at $\mathcal{O}(\alpha_t)$. We implicitly sum over the indices $a, b = 1, 2$ of all internal particles.

In these definitions, the corresponding one- and two-loop self-energies $\Sigma_{\phi_i \phi_i}^{(n)}(p^2)$ are given in the gauge basis. In practical calculations, however, we perform all calculations of the self-energies $\Sigma_{h_i h_j}^{(n)}(p^2)$ $(i, j = 1, ..., 5)$ in the mass basis consisting of the physical particles of the complex NMSSM as depicted in Fig. 14.1. A straightforward translation of the two quantities can be achieved by calculating the diagonal self-energies $\Sigma_{h_i h_i}^{(n)}(p^2)$ in the mass basis in the limit of a diagonal mixing matrix of the neutral Higgs sector, which directly relates the diagonal components of the self-energies in the mass basis to the ones in the gauge basis.

For our computations at $\mathcal{O}(\alpha_t^2)$ and with all approximations as discussed in Sec. 14.5 applied, the one-loop self-energies required for the definition of the WFRCs are depicted in Fig. 15.3, while the two-loop self-energies are presented in App. E.1. For the one-loop WFRCs, we find for the $\mathcal{O}(\alpha_t)$ contributions relevant for our two-loop calculations the analytic results

$$\delta^{(1)} Z_{H_d} = 0 \; , \tag{15.50}$$

$$\delta^{(1)} Z_{H_u} = \frac{-3m_t^2}{8\pi^2 v^2 s_\beta^2} \frac{1}{\varepsilon} \; , \tag{15.51}$$

$$\delta^{(1)} Z_S = 0 \; . \tag{15.52}$$

Since the $\mathcal{O}(\alpha_t^2)$ two-loop WFRCs are among others derived from Feynman-diagrammatic contributions containing CTs from the top/stop sector as depicted by the CT insertions in Fig. E.1, the analytic form of the scalar WFRCs at two-loop level depend on the renormalization scheme of the top/stop sector that is chosen, cf. the discussion at the end of the preceding Sec. 15.2. In case that the sector is renormalized in the $\overline{\text{DR}}$ scheme, the WFRCs are given by

$$\delta^{(2)} Z_{H_d}^{\overline{\text{DR}}} = 0 \; , \tag{15.53}$$

$$\delta^{(2)} Z_{H_u}^{\overline{\text{DR}}} = \frac{9(m_t^{\overline{\text{DR}}})^4}{128\pi^4 v^4 s_\beta^4} \left(\frac{1}{\varepsilon} - \frac{1}{\varepsilon}^2 \right) \; , \tag{15.54}$$

$$\delta^{(2)} Z_S^{\overline{\text{DR}}} = 0 \; . \tag{15.55}$$

If the top/stop sector is renormalized in the OS scheme, then the WFRCs gain additional contributions stemming from the finite parts of the OS CTs, cf. Eq. (15.36), and the WFRCs are explicitly given by

$$\delta^{(2)} Z_{H_d}^{\text{OS}} = 0 \; , \tag{15.56}$$

$$\delta^{(2)} Z_{H_u}^{\text{OS}} = \frac{9(m_t^{\text{OS}})^4}{128\pi^4 v^4 s_\beta^4} \left(\frac{1}{\varepsilon} - \frac{1}{\varepsilon}^2 \right) - \frac{3(m_t^{\text{OS}})^2}{4\pi^2 v^2 s_\beta^2} \left(\frac{\delta m_t^{\alpha_t,\text{fin}}}{m_t^{\text{OS}}} - \frac{\delta v^{\alpha_t,\text{fin}}}{v} \right) \frac{1}{\varepsilon} \; , \tag{15.57}$$

$$\delta^{(2)} Z_S^{\text{OS}} = 0 \; , \tag{15.58}$$

where the finite shifts are given in terms of OS parameters by

$$\delta m_t^{\alpha_t,\text{fin}} = -\frac{m_t^3}{16\pi^2 v^2 s_\beta^2}\text{Re}\left[c_\beta^2 B_1^{\text{fin}}(m_t^2;0,m_{H^\pm}^2) + B_1^{\text{fin}}(m_t^2;|\mu_{\text{eff}}|^2,m_{\tilde{Q}_3}^2)\right. \tag{15.59}$$

$$\left. + 2c_\beta^2 B_1^{\text{fin}}(m_t^2;m_t^2,m_{H^\pm}^2) + B_1^{\text{fin}}(m_t^2;|\mu_{\text{eff}}|^2,m_{\tilde{t}_1}^2) + B_1^{\text{fin}}(m_t^2;|\mu_{\text{eff}}|^2,m_{\tilde{t}_2}^2)\right] ,$$

$$\delta v^{\alpha_t,\text{fin}} = \frac{3}{32\pi^2 s_W^2 v}\left[(c_W^2 - s_W^2)\left(|(\mathcal{U}^{\tilde{t}})_{11}|^2 F_0(m_{\tilde{t}_1}^2,m_{\tilde{Q}_3}^2) + |(\mathcal{U}^{\tilde{t}})_{21}|^2 F_0(m_{\tilde{t}_2}^2,m_{\tilde{Q}_3}^2)\right)\right. \tag{15.60}$$

$$\left. - c_W^2|(\mathcal{U}^{\tilde{t}})_{11}|^2|(\mathcal{U}^{\tilde{t}})_{12}|^2 F_0(m_{\tilde{t}_1}^2,m_{\tilde{t}_2}^2)\right],$$

as a function of

$$F_0(m_1^2,m_2^2) \equiv m_1^2 + m_2^2 - \frac{2m_1^2 m_2^2}{m_1^2 - m_2^2}\ln\left(\frac{m_1^2}{m_2^2}\right) , \tag{15.61}$$

as well as of the finite part of the loop integral

$$B_1^{\text{fin}}(p^2;m_1^2,m_2^2) = \frac{1}{2p^2}\left[A_0^{\text{fin}}(m_1^2) - A_0^{\text{fin}}(m_2^2) - (p^2 + m_1^2 - m_2^2)B_0^{\text{fin}}(p^2;m_1^2,m_2^2)\right] , \tag{15.62}$$

evaluated at $\mu_R = M_{\text{SUSY}}$, where the finite parts of the scalar A_0^{fin} and B_0^{fin} integrals are presented in App. A. In the formulae for the finite shifts, the top quark mass m_t is given as the NMSSM running mass at the SUSY scale $\mu_R = M_{\text{SUSY}}$. The analytic formulae of the one- and two-loop WFRCs in the $\overline{\text{DR}}$ scheme presented in Eqs. (15.50) to (15.55) and derived in the Feynman-diagrammatic approach are in agreement with the formulae presented in [266, 281] which are derived on the basis of the renormalization group.

So far, we considered the WFRCs defined in the minimal scheme solely in the gauge basis $(h_d, h_u, h_s, a_d, a_u, a_s)^T$, where the two WFRC matrices for the neutral and charged sectors are given by

$$\Delta^{(\text{n})}Z_{\phi^0} \equiv \text{diag}\left(\Delta^{(\text{n})}Z_{H_d}, \Delta^{(\text{n})}Z_{H_u}, \Delta^{(\text{n})}Z_S, \Delta^{(\text{n})}Z_{H_d}, \Delta^{(\text{n})}Z_{H_u}, \Delta^{(\text{n})}Z_S\right) , \tag{15.63}$$

$$\Delta^{(\text{n})}Z_{\phi^\pm} \equiv \text{diag}\left(\Delta^{(\text{n})}Z_{H_d}, \Delta^{(\text{n})}Z_{H_u}\right) . \tag{15.64}$$

For practical calculations, however, it is additionally useful to present the explicit formulae for all WFRCs in the corresponding mass bases of the scalar fields. By introducing symmetric WFRCs $\delta^{(\text{n})}Z_{h_i h_j}$ (where $h_i, h_j = h_1, ..., h_5$ and additionally $h_6 \equiv G^0$ for the symmetry between the two bases) for the neutral and $\delta^{(\text{n})}Z_{H_i^\pm H_j^\pm}$ (with $H_{i,j}^\pm = H^\pm, G^\pm$) for the charged sectors, the WFRCs in the gauge basis are related to the ones in the mass basis by the field transformations shown in Eqs. (14.35), (14.42) and (14.43),

$$\delta^{(\text{n})}Z_{h_i h_j} = \left(R R^G \Delta^{(\text{n})}Z_{\phi^0} R^{G,\dagger} R^\dagger\right)_{ij} , \tag{15.65}$$

$$\delta^{(\text{n})}Z_{H_i^\pm H_j^\pm} = \left(R^c \Delta^{(\text{n})}Z_{\phi^\pm} R^{c,\dagger}\right)_{ij} . \tag{15.66}$$

Since the elements of the rotation matrix R can in general not be given analytically in closed form, we are not able to express the matrix elements $\delta^{(\text{n})}Z_{h_i h_j}$ analytically in general, either. For the charged sector, however, we insert the rotation matrix R^c given in Eq. (14.34) and find the following analytic expressions of the matrix elements $\delta^{(\text{n})}Z_{H_i^\pm,H_j^\pm}$,

$$\delta^{(\text{n})}Z_{H^\pm H^\pm} = s_{\beta_c}^2 \Delta^{(\text{n})}Z_{H_d} + c_{\beta_c}^2 \Delta^{(\text{n})}Z_{H_u} , \tag{15.67}$$

$$\delta^{(\text{n})}Z_{G^\pm G^\pm} = c_{\beta_c}^2 \Delta^{(\text{n})}Z_{H_d} + s_{\beta_c}^2 \Delta^{(\text{n})}Z_{H_u} , \tag{15.68}$$

$$\delta^{(\text{n})}Z_{G^\pm H^\pm} = s_{\beta_c} c_{\beta_c}\left(\Delta^{(\text{n})}Z_{H_u} - \Delta^{(\text{n})}Z_{H_d}\right) , \tag{15.69}$$

$$\delta^{(\text{n})}Z_{H^\pm G^\pm} = \delta^{(\text{n})}Z_{G^\pm H^\pm} . \tag{15.70}$$
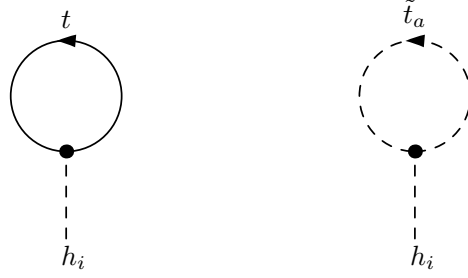
Figure 15.4.: One-loop tadpole diagrams of all neutral Higgs bosons h_i ($i = 1, ..., 5$). Tadpole diagrams stemming from the Goldstone boson $h_6 \equiv G^0$ do not contribute to our calculations. We implicitly sum over the index $a = 1, 2$ of the internal stops.

For later convenience, it is additionally useful to define the WFRC matrix $\delta^{(n)} Z_{\widetilde{\phi}^0}$ after the rotation with the neutral Goldstone matrix R^G is performed:

$$(\delta^{(n)} Z_{\widetilde{\phi}^0})_{ij} = \left(R^G \Delta^{(n)} Z_{\phi^0} R^{G,\dagger} \right)_{ij} . \tag{15.71}$$

This WFRC matrix is a 6×6-dimensional matrix with the elements of the sixth row and column describing the admixture of the neutral Goldstone boson with all other neutral Higgs bosons in the basis of (14.42). However, for the actual calculation of the higher-order corrections to the neutral Higgs boson masses in Sec. 16.2, we neglect the admixture with the Goldstone bosons. Consequently, it is useful to define the 5×5-dimensional sub-matrix of the WFRCs by restricting the indices of Eq. (15.71) to $i, j \leq 5$. In this case, the reduced WFRC matrix is given by

$$\delta^{(n)} Z_{\widetilde{\phi}^0} \equiv \mathrm{diag}\Big(\Delta^{(n)} Z_{H_d}, \Delta^{(n)} Z_{H_u}, \Delta^{(n)} Z_S, s_{\beta_n}^2 \Delta^{(n)} Z_{H_d} + c_{\beta_n}^2 \Delta^{(n)} Z_{H_u}, \Delta^{(n)} Z_S \Big) . \tag{15.72}$$

15.3.2. Renormalization of the Tadpoles

In order for the VEVs to represent the vacua states at higher orders in perturbation theory, it is necessary to renormalize them properly such that at two-loop order, the minimum conditions of the scalar potential apply again. As outlined in detail in Secs. 5.1 and 10.1 for the 2HDM and N2HDM respectively, the proper renormalization of the minimum conditions of the scalar potential through the alternative FJ tadpole scheme is crucial for defining *e.g.* renormalized masses and their CTs in a GFP-independent way. In Part IV of this thesis on the other hand, we solely renormalize the minima of the potential in the standard tadpole scheme as used *e.g.* in [183] in the SM. We want to emphasize that at the level of the newly calculated $\mathcal{O}(\alpha_t^2)$ contributions to the Higgs boson masses in the gaugeless limit and in the limit of vanishing external momentum, the framework of the standard tadpole scheme does not introduce additional one- or two-loop GFP dependences into the calculation of the Higgs boson masses. All GFP-dependent contributions are proportional to g and g' (or m_W and m_Z, equivalently) and hence, these contributions vanish in the gaugeless limit. Consequently, we are able to perform all calculations in the standard tadpole scheme without introducing additional GFP-dependent terms into the two-loop Higgs masses.

In the framework of the standard tadpole scheme, we introduce CTs for the tadpoles as shown in Eq. (15.1) which account for the shift of the scalar potential such that the VEVs represent the vacuum states at higher orders again. At one- and two-loop level, the one-point functions in the scalar potential not only acquire contributions from the tadpole CTs $\delta^{(n)} T_{\phi_i}$ for all fields ($\phi_i = h_d, h_u, h_s, a_d, a_u, a_s$) but moreover additional contributions stemming from the genuine tadpole diagrams $T_{\phi_i}^{(n)}$ ($n = 1, 2$). The tadpole CTs are fixed by imposing the renormalization

$S = \{h_c, G^0, H^+, G^+, \tilde{t}_d, \tilde{b}_1\}$ $S_1, S_2 = \{h_b, G^0, H^+, G^+\}, \{\tilde{t}_c, \tilde{b}_1\}$ $F_1, F_2 = \{\chi_c^0, \chi_2^+\}, \{t, b\}$ $S_1, S_2 = \{h_c, G^0, H^+, G^+\}, \{\tilde{t}_d, \tilde{b}_1\}$ $S, F = \{\tilde{t}_a, \tilde{b}_1\}, \{\chi_b^0, \chi_2^+\}$

$S, F = \{h_a, G^0, H^+, G^+\}, \{t, b\}$
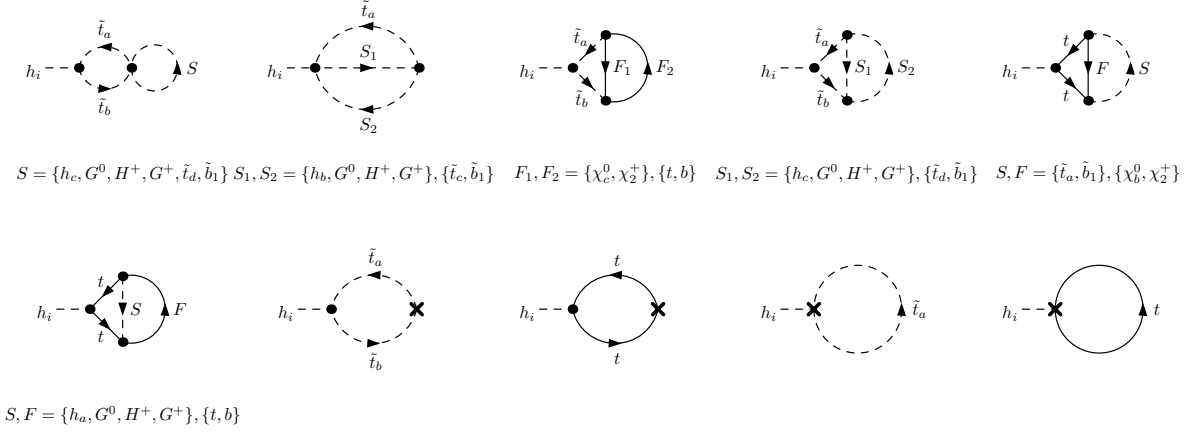
Figure 15.5.: Two-loop tadpole diagrams of all neutral Higgs bosons h_i $(i = 1, ..., 5)$. Tadpole diagrams stemming from the Goldstone boson $h_6 \equiv G^0$ do not contribute to our calculations. All placeholders $S_{(i)}$ and $F_{(i)}$ $(i = 1, 2)$ represent the particle content, specified below each individual Feynman diagram. We implicitly sum over the indices $a, b = 1, 2$ of the internal stops.

condition that the renormalized tadpoles T_{ϕ_i} vanish again at higher orders, leading to the relations

$$T_{\phi_i}^{(\text{n})} - \Delta^{(\text{n})} T_{\phi_i} \equiv 0 \ . \tag{15.73}$$

As a consequence, the tadpole CTs absorb the contributions stemming from the genuine one- and two-loop tadpole diagrams and their explicit forms are given by

$$\delta^{(1)} T_{\phi_i} = \Delta^{(1)} T_{\phi_i} \tag{15.74}$$
$$= T_{\phi_i}^{(1)} \ ,$$
$$\delta^{(2)} T_{\phi_i} = \Delta^{(2)} T_{\phi_i} + T_{\phi_i}^{(1)} \delta^{(1)} Z_{\phi_i} \tag{15.75}$$
$$= T_{\phi_i}^{(2)} + \delta^{(1)} T_{\phi_i} \delta^{(1)} Z_{\phi_i} \ .$$

Since we perform the calculations in the mass basis, we can transform these CT definitions given in the gauge basis to the mass basis by means of the rotation matrices R and R^G. Consequently, the tadpole CTs in the mass basis are given by

$$\delta^{(1)} T_{h_i} = T_{h_i}^{(1)} \ , \tag{15.76}$$
$$\delta^{(2)} T_{h_i} = T_{h_i}^{(2)} + \sum_j \delta^{(1)} T_{h_j} \delta^{(1)} Z_{h_j h_i} \ , \tag{15.77}$$

with $h_i, h_j = h_1, ..., h_5$ and additionally $h_6 \equiv G^0$. However, we want to emphasize that the tadpole diagrams and CTs stemming from the Goldstone boson G^0 do not contribute to our calculations. In the mass basis, the genuine tadpole diagrams $T_{h_i}^{(\text{n})}$ are presented at one-loop level in Fig. 15.4 and to two-loop order in Fig. 15.5.

15.3.3. Renormalization of the Charged Higgs Boson Mass and $\text{Re}(A_\lambda)$

The squared charged Higgs boson mass $m_{H^\pm}^2$ and the real part $\text{Re}(A_\lambda)$ of the soft-SUSY-breaking trilinear coupling A_λ are promoted to higher orders as given in Eqs. (15.7) and (15.11). Depending on the choice whether $m_{H^\pm}^2$ or $\text{Re}(A_\lambda)$ are considered as an independent parameter for our calculations, only the chosen parameter needs to be renormalized and

$$S = \{\tilde{t}_a, \tilde{b}_1\}$$
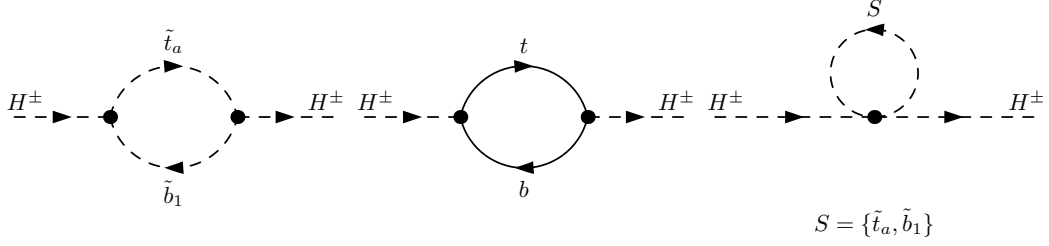
Figure 15.6.: Generic one-loop self-energies of the charged Higgs boson transition $H^\pm \to H^\pm$ that contribute at $\mathcal{O}(\alpha_t)$, required for the renormalization of the squared charged Higgs mass $m_{H^\pm}^2$. We implicitly sum over the indices $a = 1, 2$ of the internal stops.

receives an independent CT, while the CT of the other parameter becomes a function of other independent CTs.

We first consider the case that $m_{H^\pm}^2$ is chosen as an independent parameter. In this case, we renormalize $m_{H^\pm}^2$ in the OS scheme. However, since the $\mathcal{O}(\alpha_t^2)$ two-loop corrections to the Higgs boson masses are calculated in the limit of vanishing external momentum, we apply the OS scheme in the same limit. To that end, we adapt the generic presentation of the OS renormalization outlined in Sec. 3.2 to account for the fact that now, we employ the OS conditions at vanishing external momentum, i.e. for $p^2 = 0$. A look at Eq. (3.10) reveals that in this limit, the OS-defined scalar mass CTs additionally are dependent on the WFRCs already at one-loop level. Moreover, the charged Higgs mass CT receives contributions from the off-diagonal element $m_{G^\pm H^\pm}^2$ defined in Eq. (14.39) which at tree level vanishes. The one-loop CT of $m_{G^\pm H^\pm}^2$ is given by

$$\delta^{(1)} m_{G^\pm H^\pm}^2 = \frac{c_\beta}{v} \delta^{(1)} T_{h_u} - \frac{s_\beta}{v} \delta^{(1)} T_{h_d} - c_\beta^2 m_{H^\pm}^2 \delta^{(1)} t_\beta + \frac{i}{v s_\beta} \delta^{(1)} T_{a_d} \; . \tag{15.78}$$

The resulting charged Higgs mass CTs at one- and two-loop level in the limit of vanishing external momentum read

$$\delta^{(1)} m_{H^\pm}^2 = \text{Re}\left[\Sigma_{H^\pm H^\pm}^{(1)}(0) - m_{H^\pm}^2 \delta^{(1)} Z_{H^\pm H^\pm} \right] , \tag{15.79}$$

$$\delta^{(2)} m_{H^\pm}^2 = \text{Re}\left[\Sigma_{H^\pm H^\pm}^{(2)}(0) - m_{H^\pm}^2 \left(\frac{\delta^{(1)} Z_{H^\pm H^\pm}}{2} \right)^2 - \delta^{(1)} Z_{H^\pm H^\pm} \delta^{(1)} m_{H^\pm}^2 - \delta^{(1)} Z_{G^\pm H^\pm} \delta^{(1)} m_{H^\pm G^\pm}^2 \right.$$

$$\left. - m_{H^\pm}^2 \delta^{(2)} Z_{H^\pm H^\pm} \right] , \tag{15.80}$$

where $\Sigma_{H^\pm H^\pm}^{(n)}(0)$ denotes the unrenormalized n-loop self-energy of the charge Higgs transition $H^\pm \to H^\pm$ in the limit of vanishing external momentum. At one-loop order, the corresponding Feynman diagrams are depicted in Fig. 15.6 and the analytic formula for the self-energy relevant for the $\mathcal{O}(\alpha_t^2)$ corrections is given by

$$\Sigma_{H^\pm H^\pm}^{(1)}(0) = \frac{3m_t^2}{8\pi^2 t_\beta^2 v^2} \left(A_0^{\text{fin}}(m_{\tilde{Q}_3}^2) - 2A_0^{\text{fin}}(m_t^2) + \left| (\mathcal{U}_{\tilde{t}})_{12} \right|^2 A_0^{\text{fin}}(m_{\tilde{t}_1}^2) + \left| (\mathcal{U}_{\tilde{t}})_{22} \right|^2 A_0^{\text{fin}}(m_{\tilde{t}_2}^2) \right.$$

$$+ \left| m_t \left| (\mathcal{U}_{\tilde{t}})_{11} \right| + \left| A_t \right| e^{i(\varphi_\omega - \varphi_y + \varphi_{A_\lambda})} \left| (\mathcal{U}_{\tilde{t}})_{12} \right| + \frac{\left| \lambda \left| t_\beta v_s \right| (\mathcal{U}_{\tilde{t}})_{12} \right|}{\sqrt{2}} \right|^2 B_0^{\text{fin}}(0; m_{\tilde{Q}_3}^2, m_{\tilde{t}_1}^2) \tag{15.81}$$

$$+ \left| m_t \left| (\mathcal{U}_{\tilde{t}})_{21} \right| + \left| A_t \right| e^{i(\varphi_\omega - \varphi_y + \varphi_{A_\lambda})} \left| (\mathcal{U}_{\tilde{t}})_{22} \right| + \frac{\left| \lambda \left| t_\beta v_s \right| (\mathcal{U}_{\tilde{t}})_{22} \right|}{\sqrt{2}} \right|^2 B_0^{\text{fin}}(0; m_{\tilde{Q}_3}^2, m_{\tilde{t}_2}^2) \right) ,$$

where the finite parts of the scalar integrals A_0^{fin} and B_0^{fin} are presented in App. A. At two-loop order, all Feynman-diagrammatic contributions to the charged Higgs self-energy are depicted in App. E.2. Since the resulting analytic form of the two-loop self-energy is rather intricate, we do not present it explicitly. The CTs $\delta^{(n)}\text{Re}(A_\lambda)$ are given as functions of the CTs of the other parameters by inserting their renormalized values and CTs, cf. Eqs. (15.1) to (15.21), into Eq. (14.41). The resulting formulae are presented analytically in App. D.5.

In the second case that the parameter $\text{Re}(A_\lambda)$ is considered as the independent parameter, we renormalize its CTs $\delta^{(n)}\text{Re}(A_\lambda)$ in a $\overline{\text{DR}}$ scheme at the SUSY scale $\mu_R = M_{\text{SUSY}}$. In this case, the one- and two-loop CTs $\delta^{(n)}m_{H^\pm}^2$ of the charged Higgs mass are given as functions of the other CTs of the NMSSM by inserting the corresponding higher-order expansions, cf. Eqs. (15.1) to (15.21), into Eq. (14.37). The resulting analytic formulae for the CTs $\delta^{(n)}m_{H^\pm}^2$ are presented in App. D.4. Moreover, the charged Higgs mass receives higher-order corrections since it is not renormalized in the OS scheme in case that $\text{Re}(A_\lambda)$ is chosen as the independent parameter. We define the renormalized self-energy of the charged Higgs boson at one-loop level by adapting the generic formula of Eq. (3.10) to the case of the charged Higgs,

$$\widehat{\Sigma}_{H^\pm H^\pm}^{(1)}(p^2) = \Sigma_{H^\pm H^\pm}^{(1)}(p^2) + (p^2 - m_{H^\pm}^2)\delta^{(1)}Z_{H^\pm H^\pm} - \delta^{(1)}m_{H^\pm}^2 \ , \tag{15.82}$$

where the one-loop contributions of the unrenormalized self-energy $\Sigma_{H^\pm H^\pm}^{(1)}(p^2)$ are given in [79]. Analogously, the renormalized self-energy at two-loop order in the approximation of vanishing external momentum is given by

$$\widehat{\Sigma}_{H^\pm H^\pm}^{(2),\mathcal{O}}(0) = \Sigma_{H^\pm H^\pm}^{(2),\mathcal{O}}(0) - m_{H^\pm}^2 \left(\frac{\delta^{(1)}Z_{H^\pm H^\pm}}{2}\right)^2 - \delta^{(1)}Z_{H^\pm H^\pm}\delta^{(1)}m_{H^\pm}^2 \tag{15.83}$$

$$- \delta^{(1)}Z_{H^\pm G^\pm}\delta^{(1)}m_{G^\pm H^\pm}^2 - m_{H^\pm}^2\delta^{(2)}Z_{H^\pm H^\pm} - \delta^{(2)}m_{H^\pm}^2 \ , \tag{15.84}$$

where $\mathcal{O} \in \{\alpha_t\alpha_s, \alpha_t^2\}$. The $\mathcal{O}(\alpha_t\alpha_s)$ two-loop unrenormalized self-energy $\Sigma_{H^\pm H^\pm}^{(2),\mathcal{O}}(0)$ is given in [81], while at $\mathcal{O}(\alpha_t^2)$, the corresponding Feynman diagrams contributing to the self-energy are again depicted in App. E.2. The loop-corrected value of the charged Higgs boson mass at two-loop order is then given as the solution of the equation

$$p^2 - m_{H^\pm}^2 + \widehat{\Sigma}_{H^\pm H^\pm}^{(1)}(p^2) + \widehat{\Sigma}_{H^\pm H^\pm}^{(2),\alpha_t\alpha_s}(0) + \widehat{\Sigma}_{H^\pm H^\pm}^{(2),\alpha_t^2}(0) = 0 \tag{15.85}$$

with respect to p^2 which corresponds to the two-loop expansion of the generic formula presented in Eq. (3.26). In NMSSMCALC, Eq. (15.85) is solved iteratively.

15.3.4. Renormalization of t_β

The parameter t_β, defined as the ratio of the VEVs in Eq. (14.11), is promoted to higher orders by means of Eq. (15.10). In our work, we renormalize t_β through $\overline{\text{DR}}$ conditions. In this case, the CTs at one- and two-loop level are given by [238, 282–286]

$$\delta^{(n)}t_\beta = \frac{1}{2}t_\beta \left(\delta^{(n)}Z_{H_u} - \delta^{(n)}Z_{H_d}\right)\Big|_{\text{div}} = \frac{1}{2}t_\beta \, \delta^{(n)}Z_{H_u}\big|_{\text{div}} \ , \tag{15.86}$$

where the subscript denotes that only the UV-divergent part of the WFRCs presented in Subsec. 15.3.1 are taken into account. We want to emphasize that the last identity in Eq. (15.86) only holds at one-loop $\mathcal{O}(\alpha_t)$ and two-loop $\mathcal{O}(\alpha_t^2)$ level, but not in general. As shown in [238] and discussed in Secs. 5.3 and 10.3, imposing the $\overline{\text{DR}}$ scheme for fixing the CTs of t_β in the framework of the standard tadpole scheme has the drawback that such a scheme is manifestly GFP-dependent. At the level of the $\mathcal{O}(\alpha_t^2)$ two-loop corrections to the Higgs masses however, no additional GFP dependences are introduced since all GFP-dependent contributions vanish in the gaugeless limit in which the two-loop corrections are calculated.
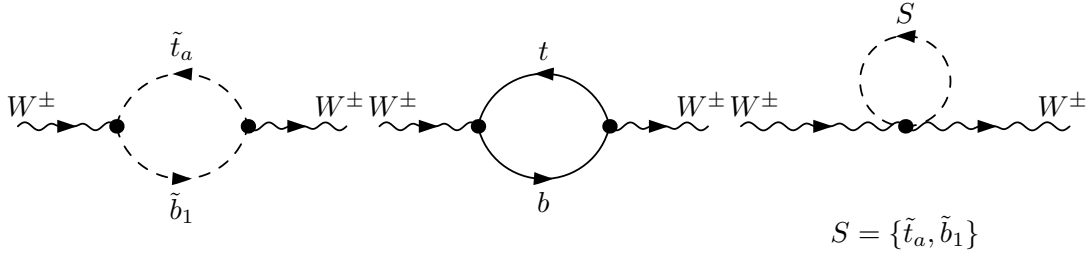
Figure 15.7.: Generic one-loop self-energies of the $W^\pm$ boson transition $W^\pm \to W^\pm$ contributing at $\mathcal{O}(\alpha_t)$ to the renormalization of m_W^2 and v. We implicitly sum over the index $a = 1, 2$ of the internal stops.

15.3.5. Renormalization of the Neutral Higgs Boson Mass Matrix

The elements of the neutral Higgs mass matrix $(\mathcal{M}_{hh}^2)_{\phi_i \phi_j}$, defined in the basis $(\phi_i, \phi_j = h_d, h_u, h_s, a, a_s)$, are not independent parameters but instead given analytically as functions of the other independent parameters of the complex NMSSM in App. D.1. Nevertheless, we formally promote them to higher orders in Eq. (15.9) for convenience, since the CTs of the neutral Higgs mass matrix elements, $(\delta^{(n)} \mathcal{M}_{hh}^2)_{\phi_i \phi_j}$, explicitly appear in the calculation of the higher-order corrections to the Higgs boson masses, as further discussed in Sec. 16.2. By inserting the CT expansions of all independent parameters, cf. Eqs. (15.1) to (15.24), into the formulae for the matrix elements $(\mathcal{M}_{hh}^2)_{\phi_i \phi_j}$, the corresponding dependent CTs $(\delta^{(n)} \mathcal{M}_{hh}^2)_{\phi_i \phi_j}$ at one- and two-loop order are gained. Their analytic forms are presented in App. D.2.

15.4. Renormalization of the Gauge Sector

We turn to the renormalization of the gauge sector of the complex NMSSM. From the five parameters promoted to higher orders in Eqs. (15.2) to (15.6), only three are independent parameters whose CTs are fixed by independent renormalization conditions, while the other two are presented as a function of the independent parameters and CTs in the following. The CT $\delta^{(n)} Z_e$ of the electromagnetic coupling constant e is fixed by adopting the approach presented in [183], *i.e.* via the vertex corrections to the OS coupling $e^+ e^- \gamma$. At $\mathcal{O}(\alpha_t^2)$ both e and $\delta^{(n)} Z_e$ vanish in the gaugeless limit and hence, the CTs $\delta^{(n)} Z_e$ do not contribute to our computations. Consequently, for $n = 1, 2$ we set

$$\delta^{(n)} Z_e = 0 . \tag{15.87}$$

For the renormalization of the squared gauge boson masses m_W^2 and m_W^2, we impose OS conditions. However, since we perform our calculations in the gaugeless approximation where the gauge boson masses vanish, the OS conditions are applied in the gaugeless approximation as well, leading to the following definitions of the CTs of the squared gauge boson masses at one-loop level,

$$\delta^{(1)} m_W^2 = \text{Re} \left[\Sigma_{WW}^{(1),T}(0) \right] , \tag{15.88}$$

$$\delta^{(1)} m_Z^2 = \text{Re} \left[\Sigma_{ZZ}^{(1),T}(0) \right] , \tag{15.89}$$

where $\Sigma_{VV}^{(1),T}(0)$ $(V = W, Z)$ denotes the transverse part of the unrenormalized self-energies of the W and Z bosons presented diagrammatically at $\mathcal{O}(\alpha_t)$ in Figs. 15.7 and 15.8 respectively, evaluated in the limit of vanishing external momentum. While the unrenormalized gauge boson self-energies vanish in the gaugeless limit analogously to the gauge boson masses themselves, we want to emphasize that for the $\mathcal{O}(\alpha_t^2)$ corrections to the Higgs boson masses, the
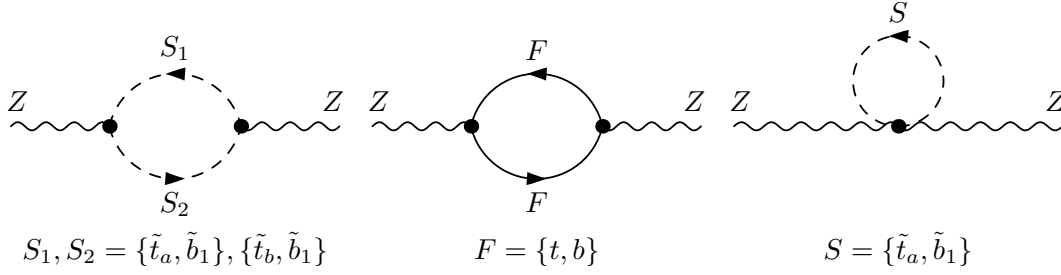
Figure 15.8.: Generic one-loop self-energies of the Z boson transition $Z \to Z$ contributing at $\mathcal{O}(\alpha_t)$ to the renormalization of m_Z^2 and v. We implicitly sum over the indices $a, b = 1, 2$ of the internal stops.

CTs of the squared gauge boson masses often appear in the combination $\delta^{(1)} m_V^2 / m_V^2$ which is in general non-vanishing in the gaugeless limit.

In our work, the one-loop CT of the sine of the Weinberg angle is not an independent quantity but instead given as a function of the CTs of the squared gauge boson masses,

$$\delta^{(1)} s_W^2 = c_W^2 \left(\frac{\delta^{(1)} m_Z^2}{m_Z^2} - \frac{\delta^{(1)} m_W^2}{m_W^2} \right) \ . \tag{15.90}$$

Analogously, we do not consider the VEV v to be an independent quantity but instead a function of m_W^2, m_Z^2 and e, cf. Eq. (4.16). Hence, we renormalize the one-loop CT of v in the OS scheme by expressing $\delta^{(1)} v$ as a function of the OS-defined CTs $\delta^{(1)} m_V^2$ as well as $\delta^{(1)} Z_e$,

$$
\begin{aligned}
\delta^{(1)} v &= v \left[\frac{c_W^2}{2 s_W^2} \left(\frac{\delta^{(1)} m_Z^2}{m_Z^2} - \frac{\delta^{(1)} m_W^2}{m_W^2} \right) + \frac{\delta^{(1)} m_W^2}{2 m_W^2} + \delta^{(1)} Z_e \right] \\
&= v \left[\frac{c_W^2}{2 s_W^2} \left(\frac{\delta^{(1)} m_Z^2}{m_Z^2} - \frac{\delta^{(1)} m_W^2}{m_W^2} \right) + \frac{\delta^{(1)} m_W^2}{2 m_W^2} \right] ,
\end{aligned}
\tag{15.91}
$$

where in the second line, we used the fact that $\delta^{(1)} Z_e$ vanishes in the gaugeless approximation, cf. Eq. (15.87).

In principle, the OS conditions can be extended to provide definitions of all CTs of the gauge boson sector to two-loop order as well. While *e.g.* the two-loop CT $\delta^{(2)} v$ explicitly appears in the analytic formulae of the CTs of the neutral Higgs boson mass matrix elements, cf. App. D.2, it turns out that at $\mathcal{O}(\alpha_t^2)$ in the gaugeless limit, the two-loop CTs of the gauge boson sector do not contribute to the calculation of the Higgs boson masses. Consequently, for our work we effectively set

$$\delta^{(2)} m_W^2 = 0 \ , \tag{15.92}$$

$$\delta^{(2)} m_Z^2 = 0 \ , \tag{15.93}$$

$$\delta^{(2)} s_W = 0 \ , \tag{15.94}$$

$$\delta^{(2)} v = 0 \ . \tag{15.95}$$

15.5. Renormalization of the Remaining Parameters

The remaining independent parameters of the complex NMSSM, namely $|\lambda|$, $|\kappa|$, v_s, $\text{Re}(A_\kappa)$ and φ_i ($i = u, s, \lambda, \kappa$), are all renormalized by $\overline{\text{DR}}$ conditions. For the one-loop CT of $|\lambda|$ introduced in Eq. (15.12), we find at one-loop $\mathcal{O}(\alpha_t)$ the analytic expression

$$\delta^{(1)}|\lambda| = -\frac{|\lambda|}{2}\left(c_\beta^2 \delta^{(1)}Z_{H_u} + \frac{2}{v}\delta^{(1)}v\Big|_{\text{div}}\right) = -\frac{|\lambda|}{2}\delta^{(1)}Z_{H_u} \tag{15.96}$$

$$\overset{(15.51)}{=} \frac{-3m_t^2|\lambda|}{16\pi^2 v^2 s_\beta^2}\frac{1}{\varepsilon} \ .$$

The two-loop CT $\delta^{(2)}|\lambda|$ as well as the one- and two-loop CTs of all other remaining parameters, introduced in Eqs. (15.13) to (15.16), vanish in our approximations and hence yield no contributions to the $\mathcal{O}(\alpha_t^2)$ two-loop Higgs mass corrections:

$$\delta^{(2)}|\lambda| = 0 \ , \tag{15.97}$$

$$\delta^{(n)}|\kappa| = 0 \ , \tag{15.98}$$

$$\delta^{(n)}v_s = 0 \ , \tag{15.99}$$

$$\delta^{(n)}\text{Re}(A_\kappa) = 0 \ , \tag{15.100}$$

$$\delta^{(n)}\varphi_i = 0 \ . \tag{15.101}$$

For convenience, we additionally provide the dependent CT of the effective parameter μ_{eff}, introduced in Eq. (14.49) and promoted to higher orders in Eq. (15.17). For the dependent CT, we find at one-and two-loop order

$$\delta^{(1)}\mu_{\text{eff}} = \mu_{\text{eff}}\left[\frac{\delta^{(1)}|\lambda|}{|\lambda|} + \frac{\delta^{(1)}v_s}{v_s} + i\left(\delta^{(1)}\varphi_s + \delta^{(1)}\varphi_\lambda\right)\right] \ , \tag{15.102}$$

$$\delta^{(2)}\mu_{\text{eff}} = \mu_{\text{eff}}\left[\frac{\delta^{(2)}|\lambda|}{|\lambda|} + \frac{\delta^{(2)}v_s}{v_s} + i\left(\delta^{(2)}\varphi_s + \delta^{(2)}\varphi_\lambda\right) + \frac{\delta^{(1)}|\lambda|}{|\lambda|}\frac{\delta^{(1)}v_s}{v_s}\right. \tag{15.103}$$

$$\left. + i\left(\delta^{(1)}\varphi_s + \delta^{(1)}\varphi_\lambda\right)\left(\frac{\delta^{(1)}|\lambda|}{|\lambda|} + \frac{\delta^{(1)}v_s}{v_s} + i\left(\delta^{(1)}\varphi_s + \delta^{(1)}\varphi_\lambda\right)\right)\right] \ . \tag{15.104}$$

However, as most of the CTs in these formulae vanish in our approximations, the CTs of μ_{eff} relevant for the $\mathcal{O}(\alpha_t^2)$ corrections for the Higgs boson masses reduce to the simple forms

$$\delta^{(1)}\mu_{\text{eff}} = \frac{\mu_{\text{eff}}}{|\lambda|}\delta^{(1)}|\lambda| = -\frac{1}{2}\delta^{(1)}Z_{H_u} \tag{15.105}$$

$$\overset{(15.51)}{=} \frac{-3m_t^2}{16\pi^2 v^2 s_\beta^2}\frac{1}{\varepsilon} \ ,$$

$$\delta^{(2)}\mu_{\text{eff}} = 0 \ . \tag{15.106}$$

Calculation of the Higgs Boson Masses at $\mathcal{O}(\alpha_t^2)$

In order to calculate the loop corrections to the Higgs boson masses, the only missing ingredients are the unrenormalized self-energies of the neutral Higgs bosons which are consistently combined with the CTs introduced in the preceding Chapter 15 to form the renormalized self-energies.

Starting with Sec. 16.1, we present the calculation of the genuine one- and two-loop corrections to the unrenormalized self-energies of the neutral Higgs bosons as key ingredients for the calculation of the higher-order corrections to the Higgs masses. Moreover, we present an overview over all computer tools used in the course of the calculations and provide technical details about the calculations themselves. In the subsequent Sec. 16.2, we describe how the unrenormalized self-energies are combined with the CTs defined in the preceding Chapter 15 in order to form the renormalized self-energies of the neutral Higgs bosons of the complex NMSSM. Subsequently, we describe the implementation of all analytic results into a new version of `NMSSMCALC` and discuss how the loop-corrected masses are calculated from the renormalized self-energies through an iterative procedure.

16.1. The Unrenormalized Self-Energies of the Neutral Higgs Bosons at $\mathcal{O}(\alpha_t^2)$

The first contributions considered for the calculation of the loop corrections to the Higgs boson masses in the complex NMSSM are the genuine one- and two-loop corrections to the self-energies of the Higgs bosons. We adopt the notation from Subsec. 15.3.1 and denote by $\Sigma_{h_i h_j}^{(\mathrm{n})}(p^2)$ the corrections to the physical Higgs self-energy transitions $h_i \to h_j$ $(i, j = 1, ..., 5)$ at the n-loop order as a function of the squared external momentum p^2. For some parts of the calculation of the loop-corrected Higgs boson masses, products of one-loop terms stemming from *e.g.* the unrenormalized one-loop neutral Higgs boson self-energy arise. These products yield contributions to the two-loop $\mathcal{O}(\alpha_t^2)$ corrections of the Higgs boson masses. Since in our work we focus on these $\mathcal{O}(\alpha_t^2)$ corrections, we restrict the calculation of the self-energy to one-loop $\mathcal{O}(\alpha_t)$ and to two-loop $\mathcal{O}(\alpha_t^2)$ contributions in order to be consistent with the rest of the calculation. We moreover restrict ourselves to the gaugeless limit and apply the approximation of vanishing external momentum, *i.e.* we set $p^2 = 0$. We want to emphasize that the restriction to the $\mathcal{O}(\alpha_t)$ contributions to the unrenormalized one-loop self-energy

$\Sigma_{h_i h_j}^{(1)}(p^2)$, with all aforementioned approximations applied, is considered in `NMSSMCALC` only when computing the genuine two-loop $\mathcal{O}(\alpha_t^2)$ contributions to the neutral Higgs boson masses. For the calculation of the genuine one-loop corrections to the masses in `NMSSMCALC` on the other hand, the full one-loop self-energy without any approximations as published in [79], *i.e.* without the gaugeless limit and the approximation of vanishing external momentum, is considered.

As a consequence of the application of these approximations, we effectively consider the MSSM limit of the complex NMSSM[43]. The diagrams that contribute at one-loop $\mathcal{O}(\alpha_t)$ are depicted in Fig. 15.3. At two-loop order, the number of diagrams increases significantly, with all relevant diagrammatic contributions being presented in App. E.1. In this case, $\Sigma_{h_i h_j}^{(2)}$ consists not only of contributions stemming from genuine two-loop diagrams but moreover from one-loop diagrams with CT insertions, depicted as a cross in the corresponding diagrams in the next-to-last and last rows of Fig. E.1, that are formally of two-loop order as well. All independent CTs required for the calculation of the Feynman diagrams containing CT insertions have been presented in the preceding Chapter 15.

The calculation of all contributions to the unrenormalized self-energies is performed in the framework of DRED which, as discussed in Sec. 3.1, preserves SUSY. The calculation of all one- and two-loop diagrams required for the unrenormalized self-energies of the neutral Higgs bosons are performed fully analytically by generating all Feynman diagrams and the corresponding amplitudes with the help of the `Mathematica` [247] package `FeynArts 3.9` [248]. To that end, the model file of the complex NMSSM required by `FeynArts` is obtained from `SARAH 4.14.0` [267–270], where we slightly modified the built-in model file of the complex NMSSM to account for the phase shifts introduced in Eq. (14.13). For the diagrams that contribute to the unrenormalized two-loop self-energies, we apply the approximation of vanishing external momentum as well as the gaugeless limit at this stage[44], since this considerably simplifies the subsequent parts of the calculations.

The computations of all traces of spinor structures in the Feynman amplitudes are performed with `FeynCalc 8.2.0` [250, 251]. As an independent cross-check, we additionally performed the calculation of the spinor traces with the `Mathematica` package `FormTracer 2.3.6` [287] which evaluates the fifth Dirac matrix γ_5 appearing in the spinor traces in the *Larin scheme* [288]. In contrast, `FeynCalc 8.2.0` evaluates γ_5 in the default configuration in the *"naive" scheme* [157]. Consequently, the independent cross-check between the trace calculations performed with the help of the tools `FeynCalc` and `FormTracer` allows for a comparison of the results gained within the two different approaches for treating γ_5. For all spinor traces required for the computation of the $\mathcal{O}(\alpha_t^2)$ contributions, we find that both tools and hence both the naive and Larin scheme yield the same analytic results for the traces.

After the calculation of the traces is performed, the Feynman amplitudes are further simplified by reducing the tensor structures of all one- and two-loop integrals to a set of basis integrals. For the one-loop integrals, the reduction is performed with the package `FeynCalc 8.2.0` while for the two-loop integrals, moreover the `FeynCalc` package `TARCER` [289] is used for the tensor decomposition. The resulting simplified Feynman amplitudes are functions of the basic scalar loop integrals. In the one-loop case, the corresponding analytic results of the 't Hooft-Veltman scalar loop integrals are presented in [249, 290] while for the two-loop case, the analytic results for the corresponding integrals required for the $\mathcal{O}(\alpha_t^2)$ corrections to the

---

[43] Note, however, that the MSSM limit is taken only for the computation of the two-loop $\mathcal{O}(\alpha_t^2)$ corrections performed in the gaugeless limit to ensure the cancellation of all UV divergences. All other parts of the calculations performed in `NMSSMCALC` are not restricted to the MSSM limit.

[44] Note, however, that the unrenormalized two-loop self-energies of the neutral Higgs bosons are also required for the WFRCs as defined in Eqs. (15.47) to (15.49). For the calculation of these, we only apply the approximation of vanishing external momentum *after* the derivatives of the self-energies with respect to p^2 are taken.

Higgs boson masses in the limit of vanishing external momentum are presented in [291]. For convenience, we moreover present the analytic results for all these integrals in App. A.

The resulting analytic formulae for all Feynman diagrams are converted to `FORTRAN` code and implemented in the newly developed version `3.00` of `NMSSMCALC`[45] [82]. Since the analytic formulae of the unrenormalized self-energies of the neutral Higgs bosons at $\mathcal{O}(\alpha_t^2)$ are intricate, we do not present the results explicitly in this thesis and refer to the source code of `NMSSMCALC` where the formulae for the self-energies are implemented.

Since at $\mathcal{O}(m_t^2 \alpha_t^2)$ the self-energies of the NMSSM are equivalent to the ones in the MSSM when μ_{eff} is used as the input value for the μ parameter and when further $\mathcal{O}(\alpha_t^2)$ contributions are neglected, we can compare our results for the Higgs boson self-energies in the NMSSM with the ones implemented in `FeynHiggs` [292–300] for the MSSM. To that end, we adapted the CTs of the VEV v and the weak mixing angle to the renormalization scheme used in `FeynHiggs`, cf. *e.g.* [301], and ensured that the same input values for `NMSSMCALC` and `FeynHiggs` were used. In the comparison, we found agreement between the results computed by us and the ones implemented in `FeynHiggs`. As a further check, we compared our results, computed for real input parameters and with m_A as an independent input, in the OS and $\overline{\text{DR}}$ scheme with the results and the corresponding computer program presented in [302] and found an agreement between the results as well.

16.2. The Renormalized Self-Energies and Loop-Corrected Masses of the Neutral Higgs Bosons at $\mathcal{O}(\alpha_t^2)$

We define the renormalized self-energies of the transition $h_i \rightarrow h_j$ ($i, j = 1, ..., 5$) of the physical neutral Higgs bosons as a function of the squared external momentum p^2 by

$$\widehat{\Sigma}_{h_i h_j}^{(\text{n})}(p^2) \equiv \widehat{\Sigma}_{h_i h_j}^{(1)}(p^2) + \widehat{\Sigma}_{h_i h_j}^{(2)}(0) \;, \tag{16.1}$$

composed of the renormalized self-energy $\widehat{\Sigma}_{h_i h_j}^{(1)}(p^2)$ at the one-loop level as published in [79] and $\widehat{\Sigma}_{h_i h_j}^{(2)}(0)$ at the two-loop level, where the latter is evaluated in the approximation of vanishing external momentum and in the gaugeless limit. In the two-loop case, we moreover split the renormalized self-energy as

$$\widehat{\Sigma}_{h_i h_j}^{(2)}(0) \equiv \widehat{\Sigma}_{ij}^{(2),\alpha_t \alpha_s}(0) + \widehat{\Sigma}_{ij}^{(2),\alpha_t^2}(0) \;, \tag{16.2}$$

where $\widehat{\Sigma}_{ij}^{(2),\alpha_t \alpha_s}(0)$ denotes the renormalized two-loop self-energy containing the $\mathcal{O}(\alpha_t \alpha_s)$ contributions as computed and implemented into `NMSSMCALC` in [81], while $\widehat{\Sigma}_{ij}^{(2),\alpha_t^2}(0)$ represents the new $\mathcal{O}(\alpha_t^2)$ corrections to the renormalized two-loop self-energies as computed and implemented in `NMSSMCALC` in this thesis and published in [82]. In this work, we restrict all discussions to the genuine $\mathcal{O}(\alpha_t^2)$ two-loop contributions to the neutral Higgs bosons masses and drop the corresponding superscript indicating the considered subgroup of diagrams in the following.

For the parts of the calculation where products of one-loop terms stemming from the unrenormalized neutral Higgs boson self-energies appear, we limit the calculation of the renormalized self-energy $\widehat{\Sigma}_{h_i h_j}^{(1)}$ to one-loop $\mathcal{O}(\alpha_t)$ contributions as well and apply the approximations of vanishing external momentum and the gaugeless limit. We want to emphasize again that we limit the renormalized one-loop self-energy to these approximations only in the case where products of one-loop terms relevant to the newly computed $\mathcal{O}(\alpha_t^2)$ corrections appear, while for the computation of the loop-corrected masses to one-loop order in `NMSSMCALC`, the full renormalized one-loop self-energy is taken into account.

---

[45] The computer program `NMSSMCALC` can be obtained from `https://www.itp.kit.edu/~maggie/NMSSMCALC/`.

The renormalized one-loop self-energy of the neutral Higgs boson transition $h_i \to h_j$ at $\mathcal{O}(\alpha_t)$ is decomposed analogously to the generic formula presented in Eq. (3.10) as[46]

$$\widehat{\Sigma}_{h_i h_j}^{(1)}(p^2) \equiv \Sigma_{h_i h_j}^{(1)}(p^2) - (R\delta^{(1)}\mathcal{M}_{hh}^2 R^T)_{ij} \tag{16.3}$$
$$+ \left[R \left\{ (p^2 \mathbb{1}_{5\times 5} - \mathcal{M}_{hh}^2) \frac{\delta^{(1)}Z_{\widetilde{\phi}^0}}{2} + \frac{(\delta^{(1)}Z_{\widetilde{\phi}^0})^\dagger}{2} (p^2 \mathbb{1}_{5\times 5} - \mathcal{M}_{hh}^2) \right\} R^T \right]_{ij} ,$$

where the 5×5 WFRC matrix $\delta^{(1)}Z_{\widetilde{\phi}^0}$ is defined in Eq. (15.72), the elements of the neutral Higgs mass matrix $\mathcal{M}_{hh}^2$ and their one-loop CTs $\delta^{(1)}\mathcal{M}_{hh}^2$ are given in Appendices D.1 and D.2, respectively, and the matrix R describes the rotation to the physical Higgs boson basis. As mentioned in Sec. 14.2, while the matrices R, $\mathcal{M}_{hh}^2$ and $\delta^{(1)}\mathcal{M}_{hh}^2$ are originally defined as 6×6 matrices to account for the full spectrum of the neutral scalar fields of the complex NMSSM, we perform the approximation of neglecting the Goldstone boson admixture with the physical Higgs boson fields. Consequently, the matrices R, $\mathcal{M}_{hh}^2$ and $\delta^{(1)}\mathcal{M}_{hh}^2$ used for the calculation of the renormalized self-energy in Eq. (16.3) represent the corresponding 5×5-dimensional sub-matrices without the Goldstone boson admixture. We explicitly checked that this admixture is numerically small for the parameter sets used in the numerical analysis presented in Chapter 17.

Analogously to the one-loop case, we define the two-loop renormalized self-energy contributing up to $\mathcal{O}(\alpha_t^2)$ as

$$\widehat{\Sigma}_{h_i h_j}^{(2)}(p^2) \equiv \Sigma_{h_i h_j}^{(2)}(p^2) - (R\delta^{(2)}\mathcal{M}_{hh}^2 R^T)_{ij} \tag{16.4}$$
$$+ \left[R \left\{ (p^2 \mathbb{1}_{5\times 5} - \mathcal{M}_{hh}^2) \frac{\delta^{(2)}Z_{\widetilde{\phi}^0}}{2} + \frac{(\delta^{(2)}Z_{\widetilde{\phi}^0})^\dagger}{2} (p^2 \mathbb{1}_{5\times 5} - \mathcal{M}_{hh}^2) \right. \right.$$
$$\left. \left. + \frac{(\delta^{(1)}Z_{\widetilde{\phi}^0})^\dagger}{2} (p^2 \mathbb{1}_{5\times 5} - \mathcal{M}_{hh}^2) \frac{\delta^{(1)}Z_{\widetilde{\phi}^0}}{2} - \frac{(\delta^{(1)}Z_{\widetilde{\phi}^0})^\dagger}{2} \delta^{(1)}\mathcal{M}_{hh}^2 - \delta^{(1)}\mathcal{M}_{hh}^2 \frac{\delta^{(1)}Z_{\widetilde{\phi}^0}}{2} \right\} R^T \right]_{ij} ,$$

where the 5×5 matrix $\delta^{(2)}\mathcal{M}_{hh}^2$ contains the two-loop contributions to the CTs of the neutral Higgs mixing matrix elements given in App. D.2 and the two-loop WFRC matrix $\delta^{(2)}Z_{\widetilde{\phi}^0}$ is defined in Eq. (15.72). As before, the matrices R, $\mathcal{M}_{hh}^2$ and $\delta^{(1)}\mathcal{M}_{hh}^2$ in Eq. (16.4) denote the 5×5 sub-matrices without the Goldstone boson admixture. Note that in contrast to the one-loop case, the renormalized two-loop self-energy contains additional products of one-loop terms which provide contributions at $\mathcal{O}(\alpha_t^2)$ as well.

Both $\widehat{\Sigma}_{h_i h_j}^{(1)}(p^2)$ and $\widehat{\Sigma}_{h_i h_j}^{(2)}(p^2)$ are renormalized, *i.e.* they contain no UV divergences. As described in the preceding Sec. 16.1, we perform all calculations in the framework of DRED which regulates the UV divergences as poles in the dimensional regulator ε. We calculate all UV-divergent terms proportional to ε^{-2} and ε^{-1} analytically and we explicitly verify numerically that all UV-divergent contributions within the renormalized one- and two-loop self-energies cancel with each other. All UV-finite contributions to the renormalized self-energies are evaluated numerically in NMSSMCALC. To that end, the required finite parts of the one- and two-loop integrals, cf. App. A, are implemented as FORTRAN functions in NMSSMCALC. Consequently, no additional library is required for performing the numerical evaluation of the loop integrals.

In order to calculate the loop-corrected masses of the neutral Higgs bosons, we apply the generic procedure described in Sec. 3.4 to the case of the complex NMSSM. The quantity

---

[46] Here and in the following, even when considering the corresponding self-energies in the approximation of vanishing external momentum, we present the renormalized self-energies in the most general way for completeness, *i.e.* we include the terms proportional to p^2 as well.

required for the calculation of the masses at n-loop order is the renormalized two-point correlation function of the neutral Higgs bosons, given by

$$\widehat{\Gamma}(p^2) = i \left(p^2 \mathbb{1}_{5\times 5} - \mathcal{M}^{(\mathrm{n})} \right) \ . \tag{16.5}$$

The mass matrix part of the two-point correlation function is given by

$$\left(\mathcal{M}^{(\mathrm{n})} \right)_{ij} \equiv m_{h_i}^2 \mathbb{1}_{5\times 5} - \widehat{\Sigma}_{h_i h_j}^{(\mathrm{n})}(p^2) \qquad (i,j = 1, ..., 5) \ , \tag{16.6}$$

where $m_{h_i}^2$ denotes the square of the neutral Higgs boson masses at tree level as introduced in Eq. (14.46). As discussed in Sec. 3.4, the loop-corrected neutral Higgs boson masses up to n-loop order are given by the real parts of the poles of the propagator matrix of the neutral Higgs bosons. Consequently, they are calculated as the zeros of the determinant of the two-point correlation function $\widehat{\Gamma}(p^2)$. The n-loop-corrected masses $m_{h_i}^{(\mathrm{n})}$ are hence obtained from

$$\widehat{\Gamma}\left((m_{h_i}^{(\mathrm{n})})^2 \right) = 0 \qquad (i = 1, ..., 5) \ . \tag{16.7}$$

These equations are solved numerically in `NMSSMCALC` by an iterative procedure. For the calculation of the loop-corrected mass $m_{h_i}^{(\mathrm{n})}$ of the ith neutral Higgs boson, this iterative procedure follows the subsequently described steps:

1. As the first iteration step, the square of the external momentum is set to the tree-level value of the ith neutral Higgs boson mass, *i.e.* $p^2 = m_{h_i}^2$.

2. With the chosen value of p^2, the matrix part of the two-point correlation function, *i.e.* Eq. (16.6), is diagonalized.

3. The ith eigenvalue gained by the diagonalization is an approximate value of the loop-corrected mass $m_{h_i}^{(\mathrm{n})}$ of the ith Higgs boson.

4. The squared external momentum is set to the ith eigenvalue calculated in the previous step.

5. Steps 2 to 4 are repeated until the difference of the ith eigenvalue between two consecutive steps falls below 10^{-9}, at which point the procedure terminates.

This iterative procedure is applied for the calculation of the loop-corrected masses of all five neutral Higgs bosons in `NMSSMCALC`. As briefly discussed in general in Sec. 3.4, computing the masses via such an iterative procedure has the advantage of a straightforward implementation through *e.g.* the fourth-order Runge-Kutta algorithm [187,188] which is implemented in `NMSSMCALC`. Moreover, in general the procedure leads to a fast convergence.

On the other hand, the iterative procedure mixes orders of perturbation theory since the loop-corrected squared masses are inserted as values of p^2 into higher-order renormalized self-energies which again are used for the calculation of the next approximation of the masses. Nevertheless, as it was argued at least for the one-loop case in [280], using this iterative procedure is considered to yield a better approximate result of the loop-corrected masses than gained through a fixed-order calculation. One drawback of the iterative procedure is the introduction of GFP dependences into the loop-corrected masses. As argued in general in Sec. 3.6, these GFP dependences arise since the usage of a loop-corrected instead of a tree-level mass in the renormalized self-energies leads to a violation of Slavnov-Taylor identities. For the genuine $\mathcal{O}(\alpha_t^2)$ contributions computed in this work, however, no additional GFP dependences are introduced since all new contributions are calculated in the gaugeless limit in which the GFP-dependent terms vanish.

Numerical Analysis with `NMSSMCALC`

In the following chapter, we perform a numerical analysis of the loop-corrected masses of the neutral Higgs bosons of the complex NMSSM with the up-to-date version `NMSSMCALC 3.00`, including the $\mathcal{O}(\alpha_t^2)$ corrections derived in this work.

Beginning with Sec. 17.1, we describe the scanning procedure over the parameter space of the complex NMSSM which is applied for generating the valid input parameter sets for the computation of the higher-order corrections to the Higgs masses with `NMSSMCALC`. We discuss all constraints applied and present all input parameters of each of the two sets used in this thesis. In the subsequent Sec. 17.2, for each of the two input parameter sets we present the numerical results for the higher-order Higgs masses calculated with `NMSSMCALC 3.00`. We analyze the higher-order corrections to the neutral Higgs masses for these two sets and describe the relative size and importance of the newly calculated $\mathcal{O}(\alpha_t^2)$ corrections.

17.1. Input Parameters

For the computation of all numerical results presented in this chapter, we use the following fixed values for the input parameters of the SM [98, 303],

$$
\begin{aligned}
m_e &= 510.9989\,\text{keV} , & m_\mu &= 105.6584\,\text{MeV} , & (17.1) \\
m_\tau &= 1.77682\,\text{GeV} , & m_u &= 2.2\,\text{MeV} , \\
m_d &= 4.7\,\text{MeV} , & m_s &= 95.0\,\text{MeV} , \\
m_c &= 1.274\,\text{GeV} , & m_b^{\overline{\text{MS}}}(m_b^{\overline{\text{MS}}}) &= 4.18\,\text{GeV} , \\
m_t &= 172.74\,\text{GeV} , & G_F &= 1.166\,37 \cdot 10^{-5}\,\text{GeV}^{-2} , \\
m_Z &= 91.1876\,\text{GeV} , & m_W &= 80.379\,\text{GeV} , \\
\alpha_{\text{em}}^{-1}(m_Z) &= 127.955 , & \alpha_s^{\overline{\text{MS}}}(m_Z) &= 0.1181 .
\end{aligned}
$$

In order to obtain input parameter sets compatible with current theoretical and experimental constraints that are subsequently used for the numerical analysis of the higher-order Higgs boson masses, we apply a scan procedure over the parameter space of the complex NMSSM[47], cf. also [82]. For the scan, we fix the gluino mass parameter to the value

$$
M_3 = 1.85\,\text{TeV} , \tag{17.2}
$$

---

[47]For a detailed description about the scan procedure, we refer to [142, 304, 305].

while the mass parameters of the sfermions of the first and second generations are all set to the value

$$m_i = 3\,\text{TeV} \quad \left(i \in \{\widetilde{u}_R, \widetilde{d}_R, \widetilde{s}_R, \widetilde{c}_R, \widetilde{e}_R, \widetilde{\mu}_R, \widetilde{Q}_1, \widetilde{Q}_2, \widetilde{L}_1, \widetilde{L}_2\}\right) . \tag{17.3}$$

Since the newly computed $\mathcal{O}(\alpha_t^2)$ contributions are obtained in the MSSM limit of the complex NMSSM, we do not allow for too large contributions stemming from the singlet in the NMSSM in our numerical analysis. We therefore make sure not to choose to large values of λ and κ in the following. We furthermore apply the rough constraint

$$|\lambda|^2 + |\kappa|^2 \leq 0.7 , \tag{17.4}$$

to ensure unitarity. Since the one-loop corrections to the Higgs masses implemented in `NMSSM-CALC` are not restricted to the MSSM limit and hence include contributions from λ and κ, however, the numerical results for the loop-corrected Higgs boson masses should not be significantly affected by these missing contributions at two-loop order as long as λ and κ do not become too large[48]. We demand λ and κ to lie in the ranges

$$10^{-4} \ \leq \ \lambda \ \leq \ 0.4 , \tag{17.5}$$
$$0 \ \leq \ \kappa \ \leq \ 0.6 , \tag{17.6}$$

which also satisfies the constraint from Eq. (17.4). We additionally restrict λ and κ to real values for the scan. For the other parameters of the complex NMSSM, we allow a variation of their input values in the ranges presented in Table 17.1. As can be inferred from the table, we use $m_{H^\pm}$ as independent input parameter instead of $\text{Re}(A_\lambda)$ for our scan. Furthermore, we want to emphasize that since we follow the SLHA format [253, 254], we use μ_{eff} as an independent input and obtain the values of v_s and φ_s by means of Eq. (14.49). Not shown in Table 17.1 are the soft-SUSY-breaking trilinear terms of the first and second generation. Their values are set equal to the values of the trilinear terms of the corresponding third generation,

$$A_e = A_\mu = A_\tau , \tag{17.7}$$
$$A_d = A_s = A_b , \tag{17.8}$$
$$A_u = A_c = A_t . \tag{17.9}$$

In accordance with the SLHA, all soft-SUSY-breaking trilinear and mass terms as well as the parameters λ, κ, A_κ, μ_{eff} and t_β are considered to be $\overline{\text{DR}}$ parameters given at the SUSY scale[49] M_{SUSY} given by

$$\mu_R = M_{\text{SUSY}} = \sqrt{m_{\widetilde{Q}_3} m_{\widetilde{t}_R}} . \tag{17.10}$$

One of the neutral CP-even Higgs bosons is identified with the SM-like Higgs boson, called h_{SM} in the following, and its mass, calculated at $\mathcal{O}(\alpha_t \alpha_s + \alpha_t^2)$, is required to lie in the range

$$122\,\text{GeV} \leq m_{h_i}^{(2)} \leq 128\,\text{GeV} \quad (\text{for one } h_i \equiv h_{\text{SM}}) . \tag{17.11}$$

For the parameter scan, initial parameter values are created by randomly fixing the NMSSM parameters within the aforementioned ranges. We restrict the scan to the real NMSSM while for the numerical analysis, some of the complex phases are turned on as described below. The generated parameter sets are checked against the following experimental constraints:

- The Higgs exclusion limits stemming from experiments at LEP, Tevatron and LHC are checked with `HiggsBounds 5.3.2` [262–264].

---

[48]We also refer to [306] for a discussion about the size of these contributions.

[49]According to the SLHA format, this is only the case for t_β if its value is read in from the block `EXTPAR`, which is the case in `NMSSMCALC`. Otherwise, t_β is considered as a $\overline{\text{DR}}$ parameter defined at the scale m_Z.

	M_1	M_2	A_τ	A_b	A_t	A_κ	$m_{H^\pm}$	$m_{\widetilde{\tau}_R}$	$m_{\widetilde{L}_3}$	$m_{\widetilde{b}_R}$	$m_{\widetilde{t}_R}$	$m_{\widetilde{Q}_3}$	μ_{eff}	t_β
							all values apart from t_β in TeV							
min	0.4	0.4	-2.0	-2.0	-2.0	-2.0	0.2	0.4	0.4	2.0	0.4	0.4	0.2	1.5
max	1.0	1.0	2.0	2.0	2.0	2.0	1.0	3.0	3.0	3.0	3.0	3.0	0.3	10.0

Table 17.1.: Scan ranges of the input values of the complex NMSSM. Each parameter is separately varied between its corresponding minimum and maximum value. The soft-SUSY-breaking trilinear terms of the first two generations are set equal to the trilinear terms of their corresponding third generation.

- The Higgs rates are checked with `HiggsSignals 2.2.3` [265]. To that end, the effective coupling factors computed by `NMSSMCALC` are used as an input in `HiggsSignals` and we demand that the total χ^2 value calculated by `HiggsSignals` using these coupling factors is compatible with the χ^2 value of the SM within $1\,\sigma$.

- Current LHC exclusion bounds on the masses of the SUSY particles are applied, including

  - the slepton masses to be larger than $400\,\text{GeV}$ [307],

  - the stop and sbottom masses to be larger than $800\,\text{GeV}$ [307, 308],

  - the gluino masses as well as the masses of the lightest squarks of the second generation to be larger than $1.8\,\text{TeV}$ [307].

- While we perform the scan in the real NMSSM, checks against constraints stemming from the EDMs become relevant as soon as non-vanishing complex phases are considered [141, 309]. In this case, the input parameter set is checked in `NMSSMCALC` against the experimental limits given by the ACME collaboration [310].

For our numerical analysis we use parameter sets that pass all these constraints. From all valid sets generated in the scan, we choose the two parameter sets which are presented and used in [82] for our numerical analysis of the loop-corrected Higgs boson masses in this thesis. The two parameter points differ with respect to the treatment of the top and stop sectors applied in `NMSSMCALC` during the scan, cf. Sec. 15.2. For the first parameter set, denoted by "P1OS", the top and stop sectors are renormalized in the OS scheme while for the second parameter set, denoted by "P2DR", the $\overline{\text{DR}}$ scheme is applied. In the following, we present all input values of the two corresponding sets.

Parameter set "P1OS".
The input values of the SM parameters are as stated in Eq. (17.1), while the mass parameter of the gluino and the soft-SUSY-breaking mass parameters are fixed to the values given in Eqs. (17.2) and (17.3), respectively. The input values of the remaining parameters are set as follows[50],

$$
\begin{aligned}
m_{\widetilde{\tau}_R} &= 2967\,\text{GeV} , & m_{\widetilde{L}_3} &= 1369\,\text{GeV} , & (17.12)\\
m_{\widetilde{b}_R} &= 2765\,\text{GeV} , & m_{\widetilde{t}_R} &= 881\,\text{GeV} , \\
m_{\widetilde{Q}_3} &= 1226\,\text{GeV} , & A_e = A_\mu = A_\tau &= 1170\,\text{GeV} , \\
A_d = A_s = A_b &= -1885\,\text{GeV} , & A_u = A_c = A_t &= -1922\,\text{GeV} ,
\end{aligned}
$$

---

[50]The imaginary part of A_κ is not an independent input parameter but instead determined via the other parameters of the Higgs sector as shown in Eq. (14.33).

$$
\begin{aligned}
M_1 &= 644\,\text{GeV}\,, & M_2 &= 585\,\text{GeV}\,, \\
\lambda &= 0.301\,, & \kappa &= 0.299\,, \\
\text{Re}(A_\kappa) &= -791\,\text{GeV}\,, & \mu_{\text{eff}} &= 209\,\text{GeV}\,, \\
t_\beta &= 4.44\,, & m_{H^\pm} &= 898\,\text{GeV}\,,
\end{aligned}
$$

which fixes the complex phases of the parameters to the values

$$
\varphi_{A_u} = \varphi_{A_d} = \varphi_{A_s} = \varphi_{A_c} = \varphi_{A_b} = \varphi_{A_t} = \pi\,, \tag{17.13}
$$
$$
\varphi_{A_e} = \varphi_{A_\mu} = \varphi_{A_\tau} = \varphi_{M_1} = \varphi_{M_2} = \varphi_{M_3} = \varphi_\lambda = \varphi_\kappa = \varphi_{\mu_{\text{eff}}} = \varphi_u = 0\,.
$$

All parameters in this set are generated by using the OS scheme in the top and stop sectors, cf. Sec. 15.2. For the numerical evaluation, we moreover perform a variation of some of the input parameters of this set:

- Variation of $A_t \in [-3000\,\text{GeV}, 3000\,\text{GeV}]$, while all other parameters are kept fixed as described above.

- Variation of $\varphi_{A_t} \in [-\pi, \pi]$, while all other parameters are kept fixed as described above[51].

- Variation of $\varphi_{\mu_{\text{eff}}} \in [-\pi, \pi]$ with a simultaneous variation of the phases of λ and A_κ according to $\varphi_\lambda = 2/3\varphi_{\mu_{\text{eff}}}$ and $\varphi_{A_\kappa} = -\varphi_{\mu_{\text{eff}}}$, while all other parameters are kept fixed as described above[52]. As a consequence of these phase variations, the CP-violating phase φ_y, defined in Eq. (14.16), which appears already at tree level in the Higgs sector, is ensured to vanish for all chosen values of the phases. Consequently, the main effects of the phase variations only appear at one-loop level and beyond.

We want to point out that the variation of some of the input parameters as described above might lead to points in the parameter space of the complex NMSSM which do not fulfill the aforementioned experimental constraints anymore[53]. We nevertheless perform this variation of the input parameters in order to demonstrate the effects of the input parameters on the newly computed $\mathcal{O}(\alpha_t^2)$ corrections to the Higgs boson masses in `NMSSMCALC 3.00`.

Parameter set "P2DR".
As for the former set, the input values of the SM parameters are set according to Eq. (17.1), while the mass parameter of the gluino and the soft-SUSY-breaking mass parameters are given as in Eqs. (17.2) and (17.3), respectively. The input values of all remaining parameters are set as follows,

$$
\begin{aligned}
m_{\widetilde{\tau}_R} &= 3000\,\text{GeV}\,, & m_{\widetilde{L}_3} &= 3000\,\text{GeV}\,, \quad (17.14) \\
m_{\widetilde{b}_R} &= 3000\,\text{GeV}\,, & m_{\widetilde{t}_R} &= 1247\,\text{GeV}\,, \\
m_{\widetilde{Q}_3} &= 1353\,\text{GeV}\,, & A_e = A_\mu = A_\tau &= 173\,\text{GeV}\,, \\
A_d = A_s = A_b &= 753\,\text{GeV}\,, & A_u = A_c = A_t &= 2987\,\text{GeV}\,, \\
M_1 &= 614\,\text{GeV}\,, & M_2 &= 528\,\text{GeV}\,, \\
\lambda &= 0.096\,, & \kappa &= 0.372\,,
\end{aligned}
$$

---

[51]Since `NMSSMCALC` follows the SLHA format and hence uses $\text{Re}(A_t)$ and $\text{Im}(A_t)$ as input instead of $|A_t|$ and φ_{A_t}, the variation of φ_{A_t} is converted to a variation of the real and imaginary parts of A_t for the numerical analysis. The same applies for the variation of $\varphi_{\mu_{\text{eff}}}$ as well.

[52]The phase of v_s is additionally automatically varied in `NMSSMCALC` according to $\varphi_s = 1/3\varphi_{\mu_{\text{eff}}}$ by means of Eq. (14.49).

[53]For the input parameter set "P1OS", choosing complex phases $|\varphi_{A_t}| \gtrsim 0.08\pi$ or $|\varphi_{\mu_{\text{eff}}}| \gtrsim 9.5 \cdot 10^{-10}\,\pi$ (with all other phases being fixed as described before) leads to points in the parameter space of the complex NMSSM which are excluded by the EDM constraints.

	$h_1\ (h_s)$	$h_2\ (h_u)$	$h_3\ (a_s)$	$h_4\ (a)$	$h_5\ (h_d)$
			in GeV		
m_{h_i}	74.29	91.43	704.12	895.91	897.83
$m_{h_i}^{(1),\mathrm{OS}}$	86.58	135.00	700.03	895.83	897.83
$m_{h_i}^{(2,\mathcal{O}(\alpha_t\alpha_s)),\mathrm{OS}}$	86.16	118.11	700.04	895.83	897.76
$m_{h_i}^{(2,\mathcal{O}(\alpha_t\alpha_s+\alpha_t^2)),\mathrm{OS}}$	86.35	125.05	700.04	895.83	897.79
$m_{h_i}^{(1),\overline{\mathrm{DR}}}$	85.93	112.77	700.05	895.79	897.71
$m_{h_i}^{(2,\mathcal{O}(\alpha_t\alpha_s)),\overline{\mathrm{DR}}}$	86.21	118.62	700.04	895.78	897.73
$m_{h_i}^{(2,\mathcal{O}(\alpha_t\alpha_s+\alpha_t^2)),\overline{\mathrm{DR}}}$	86.22	119.10	700.04	895.78	897.73

Table 17.2.: Parameter set "P1OS": Mass values of the five neutral Higgs bosons of the complex NMSSM at tree level, one-loop level and two-loop $\mathcal{O}(\alpha_t\alpha_s)$ and $\mathcal{O}(\alpha_t\alpha_s + \alpha_t^2)$ levels. The superscripts OS and $\overline{\mathrm{DR}}$ denote the two renormalization schemes of the top and stop sectors used at two-loop order. In brackets, we give the dominant components of the Higgs fields in the gauge basis.

$$\mathrm{Re}(A_\kappa) \quad = \quad -61.8\,\mathrm{GeV}\ , \qquad\qquad \mu_{\mathrm{eff}} \quad = \quad 237\,\mathrm{GeV}\ ,$$
$$t_\beta \quad = \quad 9.97\ , \qquad\qquad m_{H^\pm} \quad = \quad 793\,\mathrm{GeV}\ ,$$

which fixes the complex phases of the parameters to the values

$$\varphi_{A_u} = \varphi_{A_d} = \varphi_{A_s} = \varphi_{A_c} = \varphi_{A_b} = \varphi_{A_t} = 0\ , \qquad (17.15)$$
$$\varphi_{A_e} = \varphi_{A_\mu} = \varphi_{A_\tau} = \varphi_{M_1} = \varphi_{M_2} = \varphi_{M_3} = \varphi_\lambda = \varphi_\kappa = \varphi_{\mu_{\mathrm{eff}}} = \varphi_u = 0\ .$$

All parameters in this set are generated by using the $\overline{\mathrm{DR}}$ scheme in the top and stop sectors, cf. Sec. 15.2. As for the other set, we perform a variation of the input parameters to analyze the numerical effects of the parameter changes on the computed Higgs boson masses. For the set "P2DR", we restrict the variation only to one parameter:

- Variation of $A_t \in [-4000\,\mathrm{GeV}, 4000\,\mathrm{GeV}]$, while all other parameters are kept fixed as described above.

As for the other input parameter set, the variation of the parameters might lead to points in the parameter space of the complex NMSSM which do not fulfill the experimental constraints anymore. Nevertheless, we use these points in order to demonstrate the effect of these parameters on the $\mathcal{O}(\alpha_t^2)$ corrections.

17.2. Numerical Results and Analysis

Numerical results for the parameter set "P1OS".
We start with the analysis of the results for "P1OS". For this parameter set, the tree-level masses of the two stops, computed in the OS and $\overline{\mathrm{DR}}$ schemes respectively, are given by

$$m_{\tilde{t}_i}^{\mathrm{OS}} = \begin{cases} 811\,\mathrm{GeV}\ , & i = 1 \\ 1276\,\mathrm{GeV}\ , & i = 2 \end{cases} , \qquad m_{\tilde{t}_i}^{\overline{\mathrm{DR}}} = \begin{cases} 837\,\mathrm{GeV}\ , & i = 1 \\ 1271\,\mathrm{GeV}\ , & i = 2 \end{cases} . \qquad (17.16)$$

In case the $\overline{\mathrm{DR}}$ scheme is chosen for the renormalization of the top and stop sectors, the OS top mass, which is an input value, is converted to the $\overline{\mathrm{DR}}$ scheme as described in detail in App. C of [82], resulting in the value

$$m_t^{\overline{\mathrm{DR}}} = 141.80\,\mathrm{GeV}\ . \qquad (17.17)$$

Table 17.2 displays the masses of the five physical Higgs bosons h_i $(i = 1, ..., 5)$ at tree level, one-loop level as well as at two-loop $\mathcal{O}(\alpha_t \alpha_s)$ and $\mathcal{O}(\alpha_t \alpha_s + \alpha_t^2)$ levels. For the loop-corrected masses, we additionally use the superscripts OS and $\overline{\text{DR}}$ to indicate which of the two renormalization schemes of the top and stop sectors where applied, cf. Sec. 15.2. Additionally, we denote in brackets the main gauge field component which contributes to the respective Higgs eigenstates in the mass basis. In general, the main components of each physical Higgs field may differ at different loop levels. For all values computed with the parameter set "P1OS", however, the main component for each field h_i remains the same at each loop order. The scenario "P1OS" features a SM-like Higgs boson given by h_2, with its mass computed at two-loop $\mathcal{O}(\alpha_t \alpha_s + \alpha_t^2)$ to $125.05\,\text{GeV}$ when the top and stop sectors are renormalized in the OS scheme. The SM-like Higgs boson is dominantly produced at the LHC through gluon fusion in a loop-induced process with major contributions stemming from virtual top quarks. Due to this, the Higgs boson h_2 is dominated by contributions stemming from the field h_u in the gauge basis in order to be compatible with the Higgs rates measurements of the LHC. The lighter Higgs boson h_1 has a mass of $86.35\,\text{GeV}$ in the OS scheme and the three heavier neutral Higgs bosons h_i $(i = 3, 4, 5)$ have masses between $700\,\text{GeV}$ and $900\,\text{GeV}$.

In order to compare the relative size of the higher-order corrections to the Higgs masses, we define the relative change of the mass values computed by `NMSSMCALC` as

$$\frac{\left| m_{h_i}^b - m_{h_i}^a \right|}{m_{h_i}^a} \;, \tag{17.18}$$

where a and b denote two subsequent loop orders including the corresponding levels of the corrections. For the h_s-dominated lightest Higgs boson h_1 the relative change between the tree-level and one-loop mass value, both in the OS and the $\overline{\text{DR}}$ scheme, amounts $\mathcal{O}(16\,\%)$. On the other hand, the two-loop corrections at $\mathcal{O}(\alpha_t \alpha_s)$ and at $\mathcal{O}(\alpha_t \alpha_s + \alpha_t^2)$ change the mass of h_1 only below the percent level for both renormalization schemes of the top and stop sectors. For the h_u-dominated Higgs boson h_2, the one-loop corrections increase the tree-level mass by sizeable $\mathcal{O}(48\,\%)$ in the OS scheme and by $\mathcal{O}(23\,\%)$ in the $\overline{\text{DR}}$ scheme. The $\mathcal{O}(\alpha_t \alpha_s)$ two-loop corrections reduce the mass of the Higgs boson h_2 by $\mathcal{O}(12\,\%)$ in the OS scheme, while in the $\overline{\text{DR}}$ the mass is again increased by $\mathcal{O}(5\,\%)$. As can be inferred from Table 17.2, at the level of the two-loop $\mathcal{O}(\alpha_t \alpha_s)$ corrections, the computed masses $m_{h_i}^{(2, \mathcal{O}(\alpha_t \alpha_s))}$ are very close to each other for both renormalization schemes of the top and stop sectors. The newly computed $\mathcal{O}(\alpha_t \alpha_s + \alpha_t^2)$ corrections add another $\mathcal{O}(6\,\%)$ to the mass of h_2 in the OS scheme while in the $\overline{\text{DR}}$ scheme, the relative change of the mass induced by these additional corrections is only below the percent level. Consequently, the difference between the SM-like Higgs boson mass computed in the OS scheme and in the $\overline{\text{DR}}$ scheme becomes larger again at $\mathcal{O}(\alpha_t \alpha_s + \alpha_t^2)$. For the three heavier Higgs bosons, the relative change of the mass values remains below the percent level for each pair of loop orders and hence they receive only very small radiative corrections.

For the comparison of the Higgs boson masses computed within the two renormalization schemes of the top and stop sectors, we define their relative difference by

$$\Delta_1 \equiv \frac{\left| m_{h_i}^{(\text{x}), \overline{\text{DR}}} - m_{h_i}^{(\text{x}), \text{OS}} \right|}{m_{h_i}^{(\text{x}), \overline{\text{DR}}}} \tag{17.19}$$

for each loop order denoted by the superscript (x) separately. We vary the input parameters A_t and φ_{A_t} as described in the previous Sec. 17.1 in order to investigate the sensitivity of the Higgs masses to a change of these two parameters. Among the neutral Higgs bosons, the h_u-dominated Higgs boson receives the largest higher-order corrections and consequently, we restrict the subsequent numerical analysis to this Higgs boson. The two upper plots of
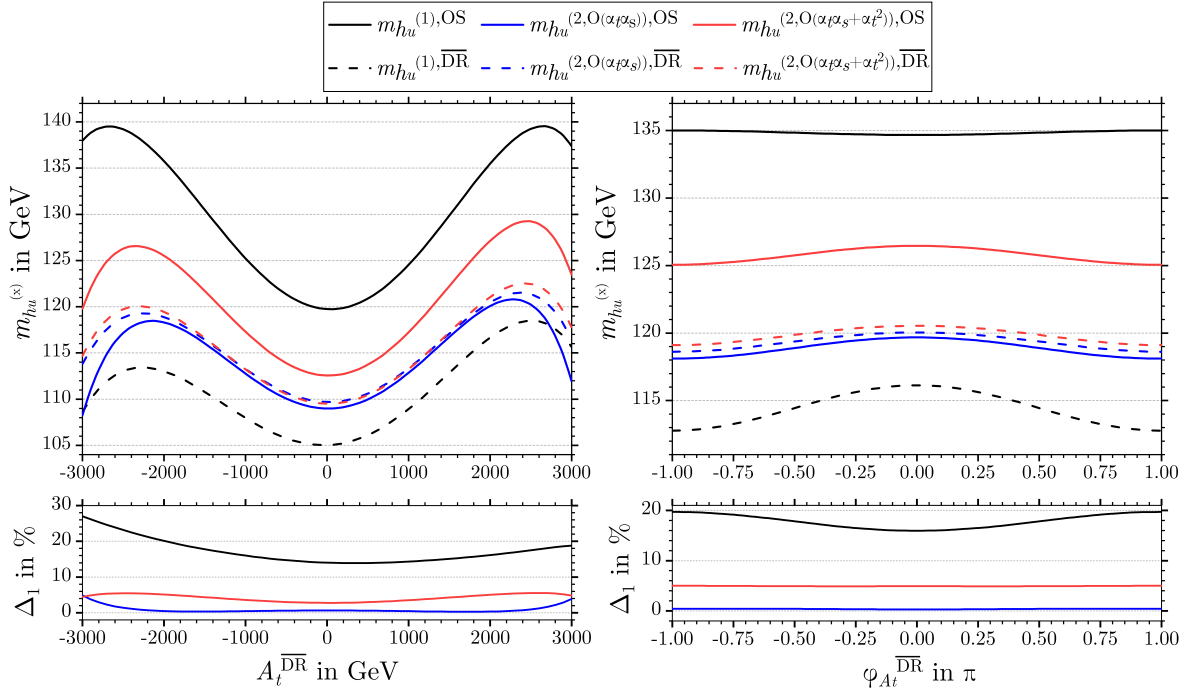
Figure 17.1.: Top: The mass $m_{h_u}^{(x)}$ of the h_u-dominated Higgs boson at one-loop order (black lines), two-loop $\mathcal{O}(\alpha_t\alpha_s)$ (blue lines) and at two-loop $\mathcal{O}(\alpha_t\alpha_s + \alpha_t^2)$ (red lines) as a function of A_t (left) and of φ_{A_t} (right). The masses are calculated for both the OS (straight lines) and $\overline{\text{DR}}$ (dashed lines) renormalization schemes of the top and stop sectors. **Bottom:** Absolute value of the relative difference between $m_{h_u}^{(x)}$ in the OS and $\overline{\text{DR}}$, cf. Eq. (17.19), as a function of A_t (left) and of φ_{A_t} (right). The difference is computed at one-loop order (black line), two-loop $\mathcal{O}(\alpha_t\alpha_s)$ (blue line) and two-loop $\mathcal{O}(\alpha_t\alpha_s + \alpha_t^2)$ (red line).

Fig. 17.1 shows the mass $m_{h_u}^{(x)}$ of the h_u-dominated Higgs boson as a function of A_t on the left and as a function of φ_{A_t} on the right. As can be inferred from the plots, the mass of the h_u-dominated Higgs boson shows a rather strong dependence on A_t, while the dependence on φ_{A_t} is relatively small. Furthermore, the one-loop corrections computed in the OS scheme are almost symmetric with respect to a sign change of A_t while they are asymmetric for the one-loop corrections calculated in the $\overline{\text{DR}}$ scheme. For the computation of the Higgs boson masses in the OS scheme, the $\overline{\text{DR}}$ input parameters of the top and stop sectors are converted to the OS scheme. The dependence on the sign of A_t almost exactly cancels out in this conversion, hence leading for the one-loop corrections to a weak dependence on the sign. For the computation of the Higgs boson masses in the $\overline{\text{DR}}$ scheme on the other hand, the OS top quark mass is converted to the $\overline{\text{DR}}$ top quark mass. Due to threshold effects, the conversion depends more strongly on the sign of A_t and hence, the one-loop Higgs boson masses in the $\overline{\text{DR}}$ scheme show a stronger asymmetry around $A_t = 0$.

The two lower plots of Fig. 17.1 show the relative difference Δ_1 between the h_u-dominated Higgs boson masses computed in the OS scheme and $\overline{\text{DR}}$ scheme, cf. Eq. (17.19), as a function of A_t (left) and φ_{A_t} (right). As can be inferred from the plots, while the difference Δ_1 between the Higgs boson masses computed within the two renormalization schemes is relatively large at one-loop level, the values lie closer to each other at $\mathcal{O}(\alpha_t\alpha_s)$. On the other hand, the inclusion of the $\mathcal{O}(\alpha_t^2)$ contributions only leads to a minor change of the Higgs boson mass in the $\overline{\text{DR}}$ scheme while for the OS scheme the $\mathcal{O}(\alpha_t^2)$ contributions are larger. Consequently, in the plot on the left-hand side of the bottom row of Fig. 17.1 the relative difference Δ_1 at $\mathcal{O}(\alpha_t\alpha_s + \alpha_t^2)$ lies above the corresponding difference at $\mathcal{O}(\alpha_t\alpha_s)$. From the plots on the

right-hand side of Fig. 17.1, we infer that the SM-like Higgs boson mass is less dependent on φ_{A_t} than on A_t for all loop levels. The dependence of the relative difference Δ_1 between the masses computed in the OS and $\overline{\text{DR}}$ on the phase φ_{A_t} is analogously described as the dependence on A_t. The difference between the masses computed in the two schemes is largest at one-loop order, lowest at the order of the $\mathcal{O}(\alpha_t\alpha_s)$ two-loop corrections and becomes larger again when including the $\mathcal{O}(\alpha_t^2)$ corrections.

The larger difference Δ_1 between the masses computed in the two renormalization schemes at $\mathcal{O}(\alpha_t\alpha_s + \alpha_t^2)$ in comparison to $\mathcal{O}(\alpha_t\alpha_s)$ can be understood by considering the conversion of the top mass m_t between the OS and $\overline{\text{DR}}$ scheme at the SUSY scale $\mu_R = M_{\text{SUSY}}$, described in detail in App. C of [82]. For the conversion, the OS top quark mass is first converted within the SM to the $\overline{\text{MS}}$ mass at the Z boson scale $\mu_R = m_Z$, including corrections up to $\mathcal{O}(\alpha_s + \alpha_t + \alpha_s^2)$. Subsequently, the converted top quark mass is evolved to the SUSY scale $\mu_R = M_{\text{SUSY}}$ via renormalization group equation (RGE) running, including corrections of $\mathcal{O}(\alpha_s + \alpha_t)$ as well as $\mathcal{O}(\alpha_t\alpha_s + \alpha_s^2 + \alpha_t^2)$. Hence, already at one-loop level, the Higgs boson masses contain higher-order corrections beyond the fixed one-loop order when the top and stop sectors are renormalized in the $\overline{\text{DR}}$ scheme. As a consequence, the Higgs mass $m_{h_u}^{(\text{x})}$ calculated at one-loop order differs less from the one calculated at two-loop order for the $\overline{\text{DR}}$ scheme in comparison to the same difference in the OS scheme and moreover, the inclusion of the $\mathcal{O}(\alpha_t^2)$ corrections does not change the computed Higgs masses significantly in the $\overline{\text{DR}}$ while for the OS scheme, the mass of the h_u-dominated Higgs is shifted again by a few GeV.

The difference Δ_1 plotted in the lower row of Fig. 17.1 is related to the remaining theoretical uncertainty of the Higgs mass calculations due to missing higher-order corrections. While in an all-order calculation both the OS and the $\overline{\text{DR}}$ schemes would lead to the same numerical results, the computation of the contributions to the Higgs masses up to a fixed order leads to differences of these values between the two schemes. These differences, as large as a few tens of percent in the given scenario at one-loop order, decrease significantly at the $\mathcal{O}(\alpha_t\alpha_s)$ two-loop level, while the inclusion of the $\mathcal{O}(\alpha_t^2)$ increases the difference again. Consequently, the estimated remaining theoretical uncertainty of the calculated Higgs masses is higher at $\mathcal{O}(\alpha_t\alpha_s + \alpha_t^2)$ compared to $\mathcal{O}(\alpha_t\alpha_s)$. This fact, at first seeming counter-intuitive, can be explained by realizing that both the $\mathcal{O}(\alpha_t\alpha_s)$ and the $\mathcal{O}(\alpha_t\alpha_s + \alpha_t^2)$ are of two-loop order and consequently, it is not necessarily expected that the remaining theoretical uncertainty decreases when further contributions of the same loop level are included. While the former corrections, combined with the higher orders introduced in the conversion of the top quark mass, allow for an estimate of the missing three-loop $\mathcal{O}(\alpha_t^2\alpha_s + \alpha_t\alpha_s^2)$ and four-loop $\mathcal{O}(\alpha_t^3\alpha_s + \alpha_t^2\alpha_s^2 + \alpha_s^3\alpha_t)$ corrections, the inclusion of the two-loop $\mathcal{O}(\alpha_t^2)$ corrections allows for an estimate of the missing three-loop $\mathcal{O}(\alpha_t^3)$ and four-loop $\mathcal{O}(\alpha_t^4)$ corrections, respectively, in addition to the estimate of the missing contributions as before. Hence, the newly computed $\mathcal{O}(\alpha_t\alpha_s + \alpha_t^2)$ corrections show that care has to be taken when estimating the uncertainty due to missing higher-order corrections at a given loop level when only parts of the loop contributions at this given order are taken into account.

In order to further analyze the phase dependence of the higher-order Higgs boson masses, we perform an additional variation of the phase μ_{eff} with a simultaneous variation of the phases of λ, v_s and A_κ as described in the preceding Sec. 17.1, while all other phases are kept fixed at their initial values according to the parameter set "P1OS". Separately for the OS and $\overline{\text{DR}}$ renormalization schemes of the top and stop sectors, we define the absolute value of the relative difference between the two- and one-loop corrections as

$$\Delta_2^{\text{OS}/\overline{\text{DR}}} \equiv \frac{\left| m_{h_i}^{(2,\text{x}),\text{OS}/\overline{\text{DR}}} - m_{h_i}^{(1),\text{OS}/\overline{\text{DR}}} \right|}{m_{h_i}^{(1),\text{OS}/\overline{\text{DR}}}} \tag{17.20}$$
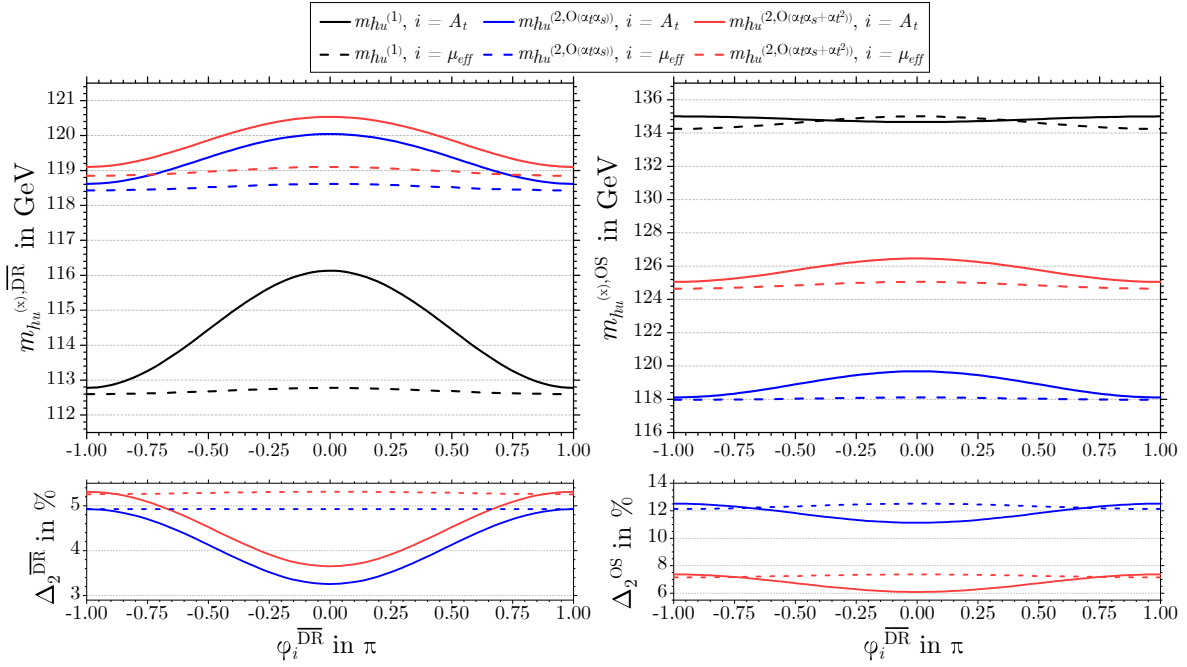
Figure 17.2.: Top: The mass $m_{h_u}^{(\times)}$ of the h_u-dominated Higgs boson at one-loop order (black lines), two-loop $\mathcal{O}(\alpha_t\alpha_s)$ (blue lines) and two-loop $\mathcal{O}(\alpha_t\alpha_s + \alpha_t^2)$ (red lines) as a function of φ_i (with $i = \{A_t, \mu_{\text{eff}}\}$) for the $\overline{\text{DR}}$ scheme (left) and the OS scheme (right). **Bottom:** Absolute value of the relative difference Δ_2, cf. Eq. (17.20), of either the $\mathcal{O}(\alpha_t\alpha_s)$ (blue line) or $\mathcal{O}(\alpha_t\alpha_s + \alpha_t^2)$ (red line) two-loop masses of h_u with respect to the one-loop mass as a function of the phases φ_i, again for the $\overline{\text{DR}}$/OS schemes (left/right).

where the superscript (x) denotes either the $\mathcal{O}(\alpha_t\alpha_s)$ or the $\mathcal{O}(\alpha_t\alpha_s+\alpha_t^2)$ two-loop corrections to the Higgs boson masses. The two upper plots of Fig. 17.2 show the mass of the h_u-dominated Higgs boson as a function of the phases φ_{A_t} and $\varphi_{\mu_{\text{eff}}}$. The plot on the left-hand side is computed for the $\overline{\text{DR}}$ scheme in the top and stop sectors, while for the plot on the right-hand side the OS scheme was used. As can be inferred from the plots, the dependence of the mass of the h_u-dominated Higgs boson on φ_{A_t} is in general stronger than on $\varphi_{\mu_{\text{eff}}}$ where for the latter, the computed masses vary only mildly as a function of $\varphi_{\mu_{\text{eff}}}$. However, the overall dependence of the computed values of the SM-like Higgs boson mass on both phases is rather small since we consider only radiatively induced CP violation in our analysis.

The two lower plots of Fig. 17.2 show the relative difference Δ_2 between the $\mathcal{O}(\alpha_t\alpha_s)$ or $\mathcal{O}(\alpha_t\alpha_s+\alpha_t^2)$ two-loop masses with respect to the one-loop mass, cf. Eq. (17.20), as a function of the phases φ_{A_t} and $\varphi_{\mu_{\text{eff}}}$ for the $\overline{\text{DR}}$ scheme (left) and for the OS scheme (right) of the top and stop sectors. The comparison of the differences Δ_2 between the two renormalization schemes reveals that the absolute difference is larger in the OS scheme than in the $\overline{\text{DR}}$ scheme. While in the latter scheme, both the two-loop corrections at $\mathcal{O}(\alpha_t\alpha_s)$ and at $\mathcal{O}(\alpha_t\alpha_s + \alpha_t^2)$ change the one-loop result by up to $\mathcal{O}(5\%)$, in the OS scheme the change from one-loop order to $\mathcal{O}(\alpha_t\alpha_s)$ introduces relatively large corrections up to $\mathcal{O}(12\%)$. This can again be explained by the resummation of the higher-order corrections into the fixed-order calculation when the top quark mass is converted from the OS to the $\overline{\text{DR}}$ scheme, hence leading to a lower difference Δ_2 in the $\overline{\text{DR}}$ scheme at $\mathcal{O}(\alpha_t\alpha_s)$. At the level of the two-loop $\mathcal{O}(\alpha_t\alpha_s + \alpha_t^2)$ contributions, the difference Δ_2 is slightly increased in the $\overline{\text{DR}}$ scheme and decreased in the OS scheme and the convergence of the Higgs boson mass in the former scheme is worsened.

Since the main focus in Part IV of this thesis lies on the calculation of the genuine $\mathcal{O}(\alpha_t^2)$ contributions to the Higgs boson masses, as described in detail in Chapter 16, we restrict

	h_1 (h_u)	h_2 (a_s)	h_3 (h_d)	h_4 (a)	h_5 (h_s)
			in GeV		
m_{h_i}	89.38	409.50	788.76	790.98	1828.56
$m_{h_i}^{(1),\text{OS}}$	142.91	407.74	788.62	790.90	1827.81
$m_{h_i}^{(2,\mathcal{O}(\alpha_t\alpha_s)),\text{OS}}$	123.92	407.71	788.57	790.91	1827.81
$m_{h_i}^{(2,\mathcal{O}(\alpha_t\alpha_s+\alpha_t^2)),\text{OS}}$	133.56	407.71	788.59	790.91	1827.81
$m_{h_i}^{(1),\overline{\text{DR}}}$	120.86	407.68	788.64	791.01	1827.81
$m_{h_i}^{(2,\mathcal{O}(\alpha_t\alpha_s)),\overline{\text{DR}}}$	124.58	407.69	788.65	791.00	1827.81
$m_{h_i}^{(2,\mathcal{O}(\alpha_t\alpha_s+\alpha_t^2)),\overline{\text{DR}}}$	125.67	407.69	788.65	791.00	1827.81

Table 17.3.: Parameter set "P2DR": Mass values of the five neutral Higgs bosons of the complex NMSSM at tree level, one-loop level and two-loop $\mathcal{O}(\alpha_t\alpha_s)$ and $\mathcal{O}(\alpha_t\alpha_s + \alpha_t^2)$ levels. The superscripts OS and $\overline{\text{DR}}$ denote the two renormalization schemes of the top and stop sectors used at two-loop order. In brackets, we give the dominant components of the Higgs fields in the gauge basis.

the numerical analysis on the effects stemming from these newly computed contributions, as presented above. For a more detailed numerical analysis with respect to the scale dependence as well as for an analysis of the numerical effects of gauge contributions on the higher-order Higgs boson masses, we refer to [82].

Numerical results for the parameter set "P2DR".
For the input values of the parameter set "P2DR", the tree-level masses of the stops, computed in the OS and $\overline{\text{DR}}$ schemes respectively, evaluate to

$$m_{\tilde{t}_i}^{\text{OS}} = \begin{cases} 1100\,\text{GeV}\,, & i=1 \\ 1469\,\text{GeV}\,, & i=2 \end{cases} \quad , \quad m_{\tilde{t}_i}^{\overline{\text{DR}}} = \begin{cases} 1121\,\text{GeV}\,, & i=1 \\ 1473\,\text{GeV}\,, & i=2 \end{cases} \quad , \quad (17.21)$$

while the converted top quark mass in the $\overline{\text{DR}}$ scheme is given by

$$m_t^{\overline{\text{DR}}} = 146.64\,\text{GeV}\,. \quad (17.22)$$

In Table 17.3, we again present the numerical results of the masses of the five physical Higgs bosons h_i ($i = 1, ..., 5$) at tree level, one-loop level as well as at two-loop $\mathcal{O}(\alpha_t\alpha_s)$ and two-loop $\mathcal{O}(\alpha_t\alpha_s + \alpha_t^2)$ both in the OS and $\overline{\text{DR}}$ scheme of the top and stop sectors. Analogous to the parameter set "P1OS", the main gauge field components for each of the five physical Higgs bosons does not change between the different loop levels. Hence, we present the main component of each Higgs boson in brackets in the header of Table 17.3. The "P2DR" scenario features the SM-like Higgs boson h_1 as the lightest of the five Higgs bosons with a mass of 125.67 GeV computed at two-loop $\mathcal{O}(\alpha_t\alpha_s + \alpha_t^2)$ in the $\overline{\text{DR}}$ scheme. The four other Higgs bosons are considerably heavier than the SM-like Higgs, namely we have a CP-odd singlet-like Higgs h_2 with a mass of around 407 GeV, two CP-even and CP-odd MSSM-like Higgs bosons h_3 and h_4 with masses around 790 GeV and finally a CP-even singlet-like Higgs h_5 with a mass of approximately 1828 GeV. As can be inferred from Table 17.3, the higher-order corrections lead to sizable contributions to the mass of the SM-like Higgs h_1 only, while the masses of the other four Higgs bosons are barely modified by the radiative corrections. Consequently, we restrict the numerical analysis on h_1 in the following.

For the comparison of the relative size of the higher-order corrections between two subsequent loop levels, we again compute the quantity defined in Eq. (17.18) for each pair of loop levels
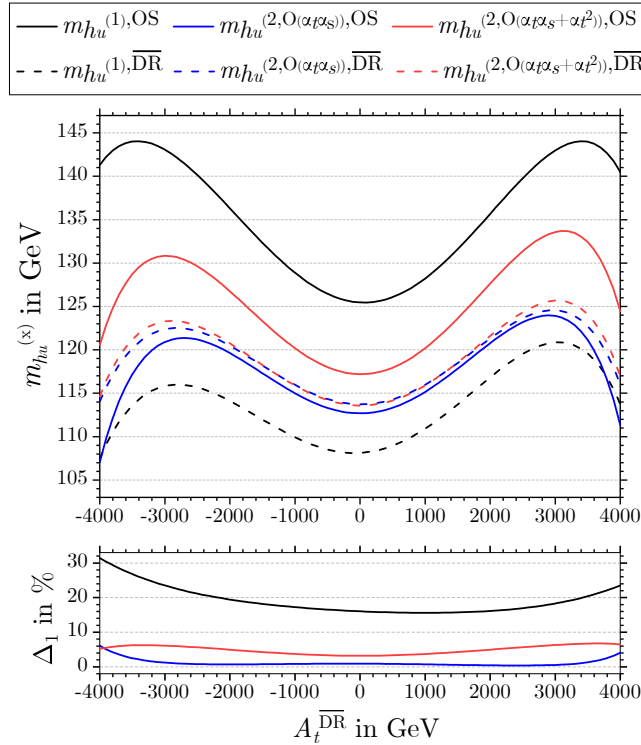
Figure 17.3.: Top: The mass $m_{h_u}^{(\times)}$ of the h_u-dominated Higgs boson at one-loop order (black lines), two-loop $\mathcal{O}(\alpha_t\alpha_s)$ (blue lines) and two-loop $\mathcal{O}(\alpha_t\alpha_s + \alpha_t^2)$ (red lines) as a function of A_t. The masses are calculated for both the OS (straight lines) and $\overline{\text{DR}}$ (dashed lines) renormalization schemes of the top and stop sectors. **Bottom:** Absolute value of the relative difference between $m_{h_u}^{(\times)}$ in the OS and $\overline{\text{DR}}$ schemes, cf. Eq. (17.19), as a function of A_t. The difference is computed at one-loop order (black line), two-loop $\mathcal{O}(\alpha_t\alpha_s)$ (blue line) and two-loop $\mathcal{O}(\alpha_t\alpha_s + \alpha_t^2)$ (red line).

for both renormalization schemes of the top and stop sectors. The comparison between the masses of h_1 at tree level and one-loop order reveals an increase of $\mathcal{O}(60\,\%)$ in the OS scheme and of $\mathcal{O}(35\,\%)$ in the $\overline{\text{DR}}$ scheme, indicating the importance of the one-loop corrections to the Higgs boson masses. The $\mathcal{O}(\alpha_t\alpha_s)$ two-loop corrections decrease the mass of the SM-like Higgs by $\mathcal{O}(13\,\%)$ in the OS scheme while they add another $\mathcal{O}(3\,\%)$ to the mass calculated in the $\overline{\text{DR}}$ scheme. As for the parameter set "P1OS", the values of the mass of the SM-like Higgs lie close to each other for both renormalization schemes at this loop level. The additional inclusion of the $\mathcal{O}(\alpha_t^2)$ two-loop corrections increases the mass computed in the OS scheme again by $\mathcal{O}(8\,\%)$ while in the $\overline{\text{DR}}$ scheme, the mass only mildly increases by $\mathcal{O}(1\,\%)$, consequently pushing the masses computed within the two different schemes further apart again. While the overall radiative corrections to the mass of h_1 in the "P2DR" scenario are larger than in the "P1OS" scenario, the numerical behavior of the masses at the different loop orders is very similar to the latter scenario considered above.

Analogous to the parameter set "P1OS", we perform a variation of the input parameter A_t in the set "P2DR" as described in the preceding Sec. 17.1 in order to investigate the sensitivity of the SM-like Higgs boson mass on this parameter. The upper plot of Fig. 17.3 shows the mass of the h_u-dominated Higgs boson as a function of A_t for both renormalization schemes of the top and stop sectors. A comparison with the plot shown on the left-hand side of Fig. 17.1 reveals that the behavior of $m_{h_u}^{(\times)}$ with varying A_t is very similar for both parameter sets considered in this thesis. Since the previously explained approximate symmetry of the one-loop Higgs mass in the OS scheme and the asymmetry in the $\overline{\text{DR}}$ scheme with respect

to a sign change of A_t are generic features of the conversion of the parameters of the top and stop sectors from one renormalization scheme to the other, they are not specific to a particular parameter set and hence, they are observable in Fig. 17.3 as well.

In the bottom row of Fig. 17.3, the difference Δ_1 between the h_u-dominated Higgs mass computed in the OS and $\overline{\text{DR}}$ schemes at a specific loop level, cf. Eq. (17.19), is presented as a function of A_t. As for the previously considered parameter set, it can be inferred from the plot that the $\mathcal{O}(\alpha_t\alpha_s)$ two-loop corrections considerably reduce the difference between the Higgs masses computed within these two renormalization schemes, while the addition of the $\mathcal{O}(\alpha_t^2)$ corrections increase the difference again. As explained above, the origin of the larger discrepancies at $\mathcal{O}(\alpha_t\alpha_s + \alpha_t^2)$ is the inclusion of additional three-loop $\mathcal{O}(\alpha_t^3)$ and four-loop $\mathcal{O}(\alpha_t^4)$ terms in the conversion of the top quark mass from the OS to the $\overline{\text{DR}}$ scheme. Consequently, at two-loop $\mathcal{O}(\alpha_t\alpha_s + \alpha_t^2)$, we find a slightly worse convergence of the results calculated in the two renormalization schemes, which leads to a more conservative estimate of the remaining theoretical uncertainty of the computed Higgs boson masses in comparison to the estimate derived at two-loop $\mathcal{O}(\alpha_t\alpha_s)$.

A futher analysis of the behavior of the Higgs boson masses with respect to variations of other parameters of the set "P2DR", *e.g.* for a variation of φ_{A_t} or $\varphi_{\mu_{\text{eff}}}$, reveals qualitatively similar results as for the previously analyzed parameter set "P1OS". We therefore do not present the results and plots for the variation of these parameters within the set "P2DR" explicitly here, since no additional conclusions can be drawn from their analyses.

Conclusion of Part IV

The main objective of Part IV of this thesis was the calculation of the $\mathcal{O}(\alpha_t^2)$ two-loop corrections to the Higgs boson masses of the CP-violating (*i.e.* complex) NMSSM and the implementation of the newly computed contributions to the computer program `NMSSMCALC`.

We introduced the Lagrangian of the complex NMSSM, focusing on a detailed presentation of the Higgs potential of the NMSSM. By rotating from the gauge basis to the mass basis, we presented the physical spectrum of the scalar sector of the complex NMSSM, consisting of five physical CP-mixed Higgs bosons h_i $(i = 1, ..., 5)$.

We presented the one-loop and two-loop renormalization of the independent parameters of the complex NMSSM that are relevant for the calculation of the two-loop $\mathcal{O}(\alpha_t^2)$ corrections to the Higgs boson masses. All CTs were defined in the approximation of vanishing external momentum as well as in the gaugeless limit. For the parameters of the top and stop sectors, we considered the two different approaches of renormalizing them either via $\overline{\mathrm{DR}}$ conditions or in an OS scheme, both of which are implemented in `NMSSMCALC`.

For the calculation of the $\mathcal{O}(\alpha_t^2)$ two-loop corrections to the Higgs boson masses, we applied the Feynman-diagrammatic approach and presented the computations in full detail. As for the definition of the CTs, we applied the approximation of vanishing external momentum and the gaugeless limit for the calculation of the Feynman amplitudes. All analytic results relevant for the two-loop $\mathcal{O}(\alpha_t^2)$ calculations were implemented in `NMSSMCALC 3.00`.

As an analysis of the size of the newly computed $\mathcal{O}(\alpha_t^2)$ two-loop contributions to the Higgs boson masses, we provided numerical results for two input parameter sets that fulfill up-to-date theoretical and experimental constraints. At the level of the newly computed $\mathcal{O}(\alpha_t\alpha_s + \alpha_t^2)$ corrections, the loop-corrected mass of the SM-like Higgs boson is increased by $\mathcal{O}(6-8\,\%)$ in the OS scheme for both sets compared to the loop-corrected mass values at two-loop $\mathcal{O}(\alpha_t\alpha_s)$. From this, we inferred that the $\mathcal{O}(\alpha_t^2)$ corrections are not negligible but instead they are of relevant size.

We further studied the differences of the SM-like Higgs boson mass computed within the OS or $\overline{\mathrm{DR}}$ scheme of the top and stop sectors by performing variations of the soft-SUSY-breaking trilinear term A_t as well as of the phases of A_t and μ_{eff}. We found that the loop-corrected masses at all levels of corrections depend relatively strongly on A_t while the dependence of the

mass values on the phases was rather small for both renormalization schemes. At the level of the two-loop $\mathcal{O}(\alpha_t\alpha_s + \alpha_t^2)$ corrections, the difference of the loop-corrected mass of the SM-like Higgs boson between the OS and the $\overline{\text{DR}}$ scheme turned out to be larger than at two-loop $\mathcal{O}(\alpha_t\alpha_s)$. From this, we drew the conclusion that at the level of the two-loop $\mathcal{O}(\alpha_t\alpha_s + \alpha_t^2)$ corrections to the Higgs boson masses, the estimated remaining theoretical uncertainty is increased in comparison to the estimate based on the two-loop $\mathcal{O}(\alpha_t\alpha_s)$ corrections and that care has to be taken when estimating the remaining uncertainty at a given loop level when only parts of the higher-order corrections at this loop level are taken into account.

Final Conclusion and Outlook

This thesis has dealt with higher-order corrections in several different models beyond the SM of particle physics. Despite the remarkable agreement of experimental data with the predictions made within the SM, the SM alone does not provide sufficient explanations of many other phenomena observed in our universe. It is therefore expected that the SM reflects only the low-energy limit of another more fundamental theory capable of providing explanations of these phenomena.

In this thesis, we considered the CP-conserving realizations of the 2HDM and the N2HDM as two rather simple extensions of the Higgs sector of the SM as well as the CP-violating NMSSM as an example of a more complex SUSY extension. While none of these three models is capable of providing solutions to all of the unanswered questions about our universe simultaneously, each of the models provides at least solutions to a subset of the shortcomings of the SM. Since the discovery of the SM-like Higgs boson at the LHC in 2012, the scalar sector of the SM has been under ongoing investigation from both the experimental as well as the theoretical point of view. By exploring the properties of the Higgs boson and thereby the structure of the scalar potential in more detail in current or future particle collider experiments, the Higgs sector itself serves as a portal to the exploration of BSM theories. However, However, the increasing precision in the Higgs sector requires improvements on the precision of the theoretical predictions, as well. Therefore, this thesis focused on higher-order corrections to observables connected to the Higgs sectors of the 2HDM, N2HDM and the NMSSM, respectively, in order to provide more precise predictions for the observables considered in this work.

In Part I of this thesis, we gave a brief description of the SM and its shortcomings as a motivation for the introduction of BSM theories. As examples, we briefly discussed $SU(2)_L$ singlet and doublet extensions of the SM Higgs sector as well as SUSY theories. For the calculation of the higher-order corrections to the observables of the Higgs sectors of the 2HDM, N2HDM and NMSSM in later parts of the thesis, we provided the theoretical framework and generic formulae for the observables that were applied in the corresponding parts.

Parts II and III of this thesis dealt with the calculation of the electroweak corrections to the OS partial decay widths of all decays of the Higgs bosons of the CP-conserving 2HDM and N2HDM that are not loop-induced. Due to the similar structure of the two models, Parts II

and III were both structurally and conceptionally similar as well. After having introduced the electroweak Lagrangians of the two models and in particular their Higgs sectors in detail, we presented the complete renormalization of the 2HDM and N2HDM. For the scalar mixing angles, introduced through the rotation of the Higgs potential from the gauge to the physical mass eigenstates, we presented several different renormalization schemes and categorized them with respect to the three desirable criteria of GFP independence, process independence and numerical stability. The electroweak one-loop corrections to the partial decay widths of all Higgs bosons of the 2HDM and N2HDM were computed fully analytically with the help of the `Mathematica` packages `SARAH 4.14.0`, `FeynArts 3.9` and `FeynCalc 8.2.0`. The resulting electroweak partial decay widths were consistently combined with the `FORTRAN` codes `HDECAY 6.52` and `N2HDECAY` for the 2HDM and N2HDM, respectively, both of which contain the state-of-the-art QCD corrections to the BRs of the Higgs boson decays for the two models. The combined corrections were provided as the newly developed `Python/FORTRAN` program packages `2HDECAY` and `ewN2HDECAY`, again for the 2HDM and N2HDM, respectively. Being fast, the programs allow for an efficient numerical evaluation of the partial decay widths and BRs of all decay modes of the Higgs bosons of the 2HDM and N2HDM. We concluded Parts II and III with numerical analyses on the size of the electroweak corrections and found that they can be of relevant size in particular for the non-SM-like Higgs bosons of the two models. Based on the change of the renormalization schemes for the scalar mixing angles, where we took care of the consistent conversion of the input parameters as well, we estimated the remaining theoretical uncertainties on the decay widths to be of a few percent for selected decay channels and input parameter sets. Additionally, we reconfirmed that the $\overline{\text{MS}}$ and process-dependent schemes typically lead to very large one-loop corrections for a large amount of different parameter sets, while the renormalization schemes based on the PT are considered to be numerically stable for the decay channels and parameters considered. For the 2HDM, we found that the additionally implemented renormalization schemes based on rigid symmetries and physical OS approaches can be considered as being numerically stable as well.

The final Part IV of this thesis dealt with the calculation of the $\mathcal{O}(\alpha_t^2)$ two-loop corrections to the masses of the Higgs bosons of the CP-violating NMSSM. After having introduced the superpotential and the Lagrangian of the complex NMSSM, we presented in full detail the renormalization of all parameters up to $\mathcal{O}(\alpha_t^2)$ contributions relevant for the cancellation of all UV divergences appearing in the course of the calculation of the mass corrections. As a key ingredient for the computation of the higher-order corrections to the masses, we provided the genuine $\mathcal{O}(\alpha_t^2)$ two-loop corrections to the unrenormalized self-energies of the Higgs bosons and combined them with the CTs to obtain the renormalized self-energies of the complex NMSSM. For the calculation of all loop integrals, we applied the Feynman-diagrammatic approach and generated and evaluated all Feynman amplitudes with the help of the `Mathematica` packages `SARAH 4.14.0`, `FeynArts 3.9`, `FeynCalc 8.2.0`, `FormTracer 2.3.6` and `TARCER`. Throughout the calculations of the self-energies and the CTs, we applied the approximations of vanishing external momentum and the gaugeless limit in order to simplify the evaluation of the two-loop tensor integrals. In the limit of vanishing external momentum, all one- and two-loop integrals could be reduced to a set of scalar integrals for which analytic expressions are well known. We expanded these expressions up to terms linear in the dimensional regulator ε which allowed us to explicitly confirm the UV finiteness of our results. The full analytic results for the $\mathcal{O}(\alpha_t^2)$ two-loop corrections to the Higgs boson masses were implemented in the new `NMSSMCALC 3.00` version. We concluded Part IV with a numerical analysis for two exemplary input parameter sets which fulfill up-to-date theoretical and experimental constraints. Our analysis showed that at the two-loop $\mathcal{O}(\alpha_t \alpha_s + \alpha_t^2)$ level, the mass of the SM-like Higgs boson is shifted by several percent in the OS scheme when compared to the results obtained at $\mathcal{O}(\alpha_t \alpha_s)$. From this, we concluded that the $\mathcal{O}(\alpha_t^2)$ corrections yield relevant contributions for the precise calculation of the masses of the NMSSM Higgs bosons. For

the $\overline{\text{DR}}$ scheme on the other hand, the shift of the masses between the two different orders is only below the percent level. Based on the results when the $\mathcal{O}(\alpha_t^2)$ corrections are included, we arrived at a more conservative estimate on the remaining theoretical uncertainties of the loop-corrected Higgs boson masses due to missing higher-order corrections. Further numerical analyses revealed that the loop corrections to the mass of the SM-like Higgs boson are rather sensitive to the chosen value of A_t while the dependence on the complex phases of A_t and μ_{eff} turned out to be relatively small, showing that radiatively induced CP violation has only a minor effect on the mass of the SM-like Higgs boson.

Only recently, the second run of data-taking at the LHC at a center-of-mass energy of $13\,\text{TeV}$ concluded, providing more data than ever on the particle collisions observed at the experiments at the LHC. In the future, the data acquired by the experiments will be analyzed in detail. The Higgs sector, as one of the lesser precisely studied aspects of the SM, might provide a portal for the search of new physics. Through the calculations performed in this work, we provided relevant contributions for more precise predictions of observables in the Higgs boson sector of the CP-conserving 2HDM and N2HDM as well as of the CP-violating NMSSM. We hope that the computer programs developed in the course of this work, namely `2HDECAY`, `ewN2HDECAY` and `NMSSMCALC 3.00`, will be useful for detailed studies of the 2HDM, N2HDM and the NMSSM, respectively, thereby providing a contribution to the ongoing quest of understanding the fundamental theories that describe nature in more detail.

For future work, it would be interesting to further extend the studies and computations presented in this thesis. The time-efficient calculation of the BRs and electroweak partial decay widths of the Higgs bosons of the 2HDM and N2HDM with `2HDECAY` and `ewN2HDECAY` enables dedicated phenomenological studies on all decay channels for these two BSM theories. It would be additionally of interest to analyze the effects of the electroweak higher-order contributions on certain regions of parameter space of the 2HDM and N2HDM, *e.g.* the alignment or the decoupling limits, and whether the electroweak corrections are sizeable enough to have an effect on these limits. For the renormalization schemes of the scalar mixing angles implemented in the two tools, a dedicated numerical analysis including large amounts of different input parameter sets would be of interest, thereby allowing for a more general categorization of the renormalization schemes with respect to their numerical stability. Regarding `NMSSM-CALC`, future work could include the computation of other higher-order contributions beyond the $\mathcal{O}(\alpha_t\alpha_s + \alpha_t^2)$ two-loop level, focusing *e.g.* on the NMSSM-specific two-loop contributions stemming from terms mediated by λ or κ. Moreover, it might be of interest to recompute the existing contributions without the approximations of the gaugeless limit and vanishing external momentum. Furthermore, the existing version `NMSSMCALC 3.00` can be used in future work for dedicated phenomenological studies on the CP-violating NMSSM.

Scalar One-Loop and Two-Loop Integrals

A.1. Scalar One-Loop Integrals up to $\mathcal{O}(\varepsilon)$

In this section, we present the expansion of the scalar one-loop one-point, two-point and three-point integrals up to $\mathcal{O}(\varepsilon)$, where ε is the dimensional regulator in DREG/DRED, cf. Sec. 3.1. For the one-loop electroweak corrections to the partial decay widths of the Higgs bosons in the 2HDM and N2HDM, presented in Parts II and III of this thesis, we use the expansion of the scalar one-loop integrals up to $\mathcal{O}(1)$, while for the $\mathcal{O}(\alpha_t^2)$ two-loop corrections to the Higgs boson masses in the complex NMSSM as presented in Part IV, their expansion up to $\mathcal{O}(\varepsilon)$ is required.

A.1.1. Used Conventions

For convenience, we define a modified renormalization scale Q_R which is related to the renormalization scale μ_R of DREG/DRED via the relation

$$Q_R^2 \equiv 4\pi \mu_R^2 e^{-\gamma_E} \ . \tag{A.1}$$

Additionally, we define a short-hand notation for the logarithm at the scale Q_R,

$$\overline{\ln}\,(m_i^2) \equiv \ln\left(\frac{m_i^2}{Q_R^2}\right) \ , \tag{A.2}$$

where m_i is an arbitrary mass-dimensional parameter. The $\mathcal{O}(\varepsilon)$ expansion of the one-loop two-point integral can be expressed in terms of this logarithm and additionally the polylogarithm of order 2 (also called *dilogarithm* or *Spence's function*), defined as a function of $z \in \mathbb{C}$ by [311]

$$\mathrm{Li}_2(z) \equiv -\int_0^z \mathrm{d}x \frac{\ln(1-x)}{x} \ . \tag{A.3}$$

Special analytic solutions of the dilogarithm are given by

$$\mathrm{Li}_2(-1) = -\frac{\pi^2}{12} \ , \tag{A.4}$$

$$\mathrm{Li}_2(1) \equiv \zeta(2) = \frac{\pi^2}{6} \ , \tag{A.5}$$

where $\zeta(2)$ denotes the Riemann zeta function $\zeta(s)$ evaluated at the value $s = 2$. The expansion of the scalar one-loop two-point integral can be expressed by means of the two solutions r_1 and r_2 of the equation [312]

$$\frac{m_2^2}{m_1^2}r^2 + \frac{p^2 - m_1^2 - m_2^2 + i\epsilon}{m_1 m_2}\frac{m_2}{m_1}r + 1 = 0 \ . \tag{A.6}$$

In closed form, the solutions are given by

$$r_{1/2} = \frac{-p^2 + m_1^2 + m_2^2 - i\epsilon \pm \sqrt{(p^2 - m_1^2 - m_2^2 + i\epsilon)^2 - 4m_1^2 m_2^2}}{2m_2^2} \ , \tag{A.7}$$

where the infinitesimal shift $\epsilon > 0$ with $\epsilon \ll m_i^2$ and $\epsilon \ll p^2$ is required to evaluate the logarithms containing these complex roots on the correct branch. By defining the two dimensionless quantities

$$x \equiv \frac{p^2}{m_2^2} \ , \tag{A.8}$$

$$y \equiv \frac{m_1^2}{m_2^2} \ , \tag{A.9}$$

the two solutions are related via

$$y = r_1 r_2 \ , \tag{A.10}$$
$$x = (1 - r_1)(1 - r_2) \ . \tag{A.11}$$

A.1.2. The Scalar One-Loop One-Point Integral A_0 to $\mathcal{O}(\varepsilon)$

We define the scalar one-loop one-point integral in $D = 4 - 2\varepsilon$ dimensions as in [149],

$$A_0(m^2) \equiv 16\pi^2 \mu_R^{4-D} \int \frac{d^D l}{i(2\pi)^D} \frac{1}{[l^2 - m^2]} \ . \tag{A.12}$$

Up to $\mathcal{O}(\varepsilon)$, the solution of this integral is given by

$$A_0(m^2) = \frac{m^2}{\varepsilon} + m^2\left\{1 - \overline{\ln}(m^2)\right\} + m^2\left\{\frac{\zeta(2)}{2} + \frac{1}{2}\overline{\ln}^2(m^2) - \overline{\ln}(m^2) + 1\right\}\varepsilon \ . \tag{A.13}$$

In the massless case, *i.e.* for a vanishing argument $m^2 = 0$, the integral vanishes as well,

$$A_0(0) = 0 \ . \tag{A.14}$$

A.1.3. The Scalar One-Loop Two-Point Integral B_0 to $\mathcal{O}(\varepsilon)$

We define the scalar one-loop two-point integral in $D = 4 - 2\varepsilon$ dimensions as in [149],

$$B_0(p^2, m_1^2, m_2^2) \equiv 16\pi^2 \mu_R^{4-D} \int \frac{d^D l}{i(2\pi)^D} \frac{1}{[l^2 - m_1^2][(l + p)^2 - m_2^2]} \ . \tag{A.15}$$

Up to $\mathcal{O}(\varepsilon)$, the most general solution of the B_0 integral can be expressed as [312]

$$B_0(p^2; m_1^2, m_2^2) = \frac{1}{\varepsilon} + \left\{ 2 - \frac{\overline{\ln}(m_1^2) + \overline{\ln}(m_2^2)}{2} - \frac{y-1}{2x}\ln(y) + \frac{r_1 - r_2}{2x}\left(\ln(r_1) - \ln(r_2)\right) \right\}$$

$$+ \left\{ \frac{\zeta(2)}{2} + 4 + \frac{\left(\overline{\ln}(m_1^2) + \overline{\ln}(m_2^2)\right)^2}{8} + \frac{1}{8}\ln^2(y) - \frac{y-1}{x}\ln(y) \right. \tag{A.16}$$

$$+ \left(\overline{\ln}(m_1^2) + \overline{\ln}(m_2^2)\right)\left(-1 + \frac{y-1}{4x}\ln(y) - \frac{r_1 - r_2}{4x}(\ln(r_1) - \ln(r_2))\right)$$

$$+ \frac{r_1 - r_2}{2x}\left[2\ln(r_1) - 2\ln(r_2) + \mathrm{Li}_2\left(\frac{-r_1(1-r_2)}{r_2 - r_1}\right) - \mathrm{Li}_2\left(\frac{-r_2(1-r_1)}{r_1 - r_2}\right) \right.$$

$$+ \ln\left(\frac{1-r_1}{r_2 - r_1}\right)\ln\left(\frac{-r_1(1-r_2)}{r_2 - r_1}\right) - \ln\left(\frac{1-r_2}{r_1 - r_2}\right)\ln\left(\frac{-r_2(1-r_1)}{r_1 - r_2}\right)$$

$$\left. \left. + \mathrm{Li}_2\left(\frac{1-r_1}{r_2 - r_1}\right) - \mathrm{Li}_2\left(\frac{1-r_2}{r_1 - r_2}\right) \right] \right\} \varepsilon \quad .$$

While this general solution is valid for arbitrary values of p^2, m_1^2 and m_2^2, in a practical calculation, its implementation can lead to numerical instabilities due to the appearance of vanishing denominators or large (di)logarithms. Therefore, we present several special cases for the $\mathcal{O}(\varepsilon)$ expansion of the B_0 integral:

$$B_0(p^2; 0, m^2) = \frac{1}{\varepsilon} + \left\{ 2 - \overline{\ln}(m^2) + \frac{m^2 - p^2}{p^2}\ln\left(\frac{-p^2 + m^2 - i\epsilon}{m^2}\right) \right\} \tag{A.17}$$

$$+ \left\{ \frac{\zeta(2)}{2} + 4 + \frac{1}{2}\overline{\ln}^2(m^2) - 2\overline{\ln}(m^2) + \frac{p^2 - m^2}{p^2}\overline{\ln}(m^2)\ln\left(\frac{-p^2 + m^2 - i\epsilon}{m^2}\right) \right.$$

$$+ \frac{p^2 - m^2}{p^2}\left[\frac{1}{2}\ln^2\left(\frac{-p^2 + m^2 - i\epsilon}{m^2}\right) - 2\ln\left(\frac{-p^2 + m^2 - i\epsilon}{m^2}\right) \right.$$

$$\left. \left. - \mathrm{Li}_2\left(\frac{-p^2 - i\epsilon}{-p^2 + m^2 - i\epsilon}\right) \right] \right\} \varepsilon$$

$$B_0(p^2; 0, 0) = \frac{1}{\varepsilon} + \left\{ 2 - \overline{\ln}(-p^2 - i\epsilon) \right\} \tag{A.18}$$

$$+ \left\{ 4 - \frac{\zeta(2)}{2} + \frac{\overline{\ln}^2(-p^2 - i\epsilon)}{2} - 2\overline{\ln}(-p^2 - i\epsilon) \right\} \varepsilon$$

$$B_0(m^2; 0, m^2) = \frac{1}{\varepsilon} + \left\{ 2 - \overline{\ln}(m^2) \right\} + \left\{ \frac{\zeta(2)}{2} + 4 + \frac{\overline{\ln}^2(m^2)}{2} - 2\overline{\ln}(m^2) \right\} \varepsilon \tag{A.19}$$

$$B_0(0; m_1^2, m_2^2) = \frac{1}{\varepsilon} + \left\{ 1 - \frac{m_1^2}{m_1^2 - m_2^2}\overline{\ln}(m_1^2) + \frac{m_2^2}{m_1^2 - m_2^2}\overline{\ln}(m_2^2) \right\} \tag{A.20}$$

$$+ \left\{ \frac{\zeta(2)}{2} + 1 - \frac{y}{2(1-y)}\overline{\ln}^2(m_1^2) + \frac{1}{2(1-y)}\overline{\ln}^2(m_2^2) + \frac{y}{1-y}\overline{\ln}(m_1^2) \right.$$

$$\left. - \frac{1}{1-y}\overline{\ln}(m_2^2) \right\} \varepsilon$$

$$B_0(0; m^2, m^2) = \frac{1}{\epsilon} - \overline{\ln}(m^2) + \left\{ \frac{\zeta(2)}{2} + \frac{1}{2}\overline{\ln}^2(m^2) \right\} \varepsilon \tag{A.21}$$

$$B_0(0; 0, m^2) = \frac{1}{\varepsilon} + \left\{ 1 - \overline{\ln}(m^2) \right\} + \left\{ \frac{\zeta(2)}{2} + 1 + \frac{\overline{\ln}^2(m^2)}{2} - \overline{\ln}(m^2) \right\} \varepsilon \tag{A.22}$$

$$B_0(0; 0, 0) \equiv \frac{1}{\varepsilon} - \frac{1}{\varepsilon_{\mathrm{IR}}} \quad . \tag{A.23}$$

We also refer to [297], where several of these special cases are presented. The last integral in Eq. (A.23) represents the scalar one-loop two-point function with vanishing momentum and vanishing masses. In the framework of DREG/DRED, this integral yields the same UV-divergent structure as the most general solution of the B_0 integral, *i.e.* a simple pole in the regulator ε. However, in the limit that all arguments of the integral are vanishing, the integral moreover contains an IR divergence. In Eq. (A.23), we regulated this divergence also in DREG/DRED with an IR regulator ε_{IR} in order to make it explicit. The appearance of these IR-divergent integrals is typical when the approximations of vanishing external momentum, *i.e.* $p^2 = 0$, and the gaugeless limit, *i.e.* massless Goldstone bosons, are applied. This is known in literature as the *Goldstone boson catastrophe* (GBC) and several possible solutions were proposed for dealing with these divergent contributions [313–316]. For the results derived in our work, the GBC does not appear. In the case of the one-loop corrections to the partial decay widths of the Higgs bosons in the 2HDM and N2HDM, the loop integrals are computed with full momentum dependence, while for the two-loop corrections to the Higgs masses in the complex NMSSM, there are no diagrammatic contributions to $\mathcal{O}(\alpha_t^2)$ that would give rise to B_0 integrals with vanishing arguments[54]. Hence, all results derived in our work are independent of the IR regulator ε_{IR}.

For the derivative of the most general result in Eq. (A.16), we find

$$
\begin{aligned}
\frac{\partial B_0(p^2; m_1^2, m_2^2)}{\partial p^2}\bigg|_{p^2=0} = &\; \frac{m_1^4 - m_2^4 - 2m_1^2 m_2^2 \ln\left(\frac{m_1^2}{m_2^2}\right)}{2\left(m_1^2 - m_2^2\right)^3} \\
&+ \Bigg\{ \frac{m_2^2\left(2m_1^2 + m_2^2\right)\overline{\ln}(m_2^2) - m_1^2\left(m_1^2 + 2m_2^2\right)\overline{\ln}(m_1^2)}{2(m_1^2 - m_2^2)^3} \\
&+ \frac{3\left(m_1^2 + m_2^2\right)}{4\left(m_1^2 - m_2^2\right)^2} + \frac{m_1^2 m_2^2}{2(m_1^2 - m_2^2)^3}\left(\overline{\ln}^2(m_1^2) - \overline{\ln}^2(m_2^2)\right) \Bigg\}\, \varepsilon \; .
\end{aligned}
\tag{A.24}
$$

A.1.4. The Scalar One-Loop Three-Point Integral C_0 to $\mathcal{O}(\varepsilon)$

We define the scalar one-loop three-point integral in $D = 4 - 2\varepsilon$ dimensions as in [149],

$$
C_0(p^2, q^2, (p+q)^2, m_1^2, m_2^2, m_3^2) \equiv 16\pi^2 \mu_R^{4-D}
\tag{A.25}
$$

$$
\cdot \int \frac{d^D l}{i(2\pi)^D} \frac{1}{[l^2 - m_1^2][(l+p)^2 - m_2^2][(l+p+q)^2 - m_3^2]} \; .
$$

The most general result of this integral to $\mathcal{O}(1)$ is presented in [183]. For the calculation of the $\mathcal{O}(\alpha_t^2)$ corrections to the Higgs boson masses in the complex NMSSM, the following special solution of the integral to $\mathcal{O}(\varepsilon)$ is required:

$$
C_0(0, 0, 0; m^2, m^2, m^2) = -\frac{1}{2m^2} + \frac{\overline{\ln}(m^2)}{2m^2}\, \epsilon \; .
\tag{A.26}
$$

A.2. Scalar Two-Loop Integrals to $\mathcal{O}(1)$

In this section, we present the expansion of the two-loop integrals up to $\mathcal{O}(1)$, where ε is the dimensional regulator in DREG/DRED, cf. Sec. 3.1, as they are needed for the calculation of the two-loop corrections to the Higgs boson masses in the complex NMSSM presented in

---

[54]For completeness, we want to mention that as soon as other NMSSM-specific contributions (*e.g.* the $\mathcal{O}(\alpha_t \alpha_\lambda)$ corrections) are taken into account, the GBC explicitly appears at two-loop level when the approximations of vanishing external momentum and the gaugeless limit are applied.

Part IV of this thesis. For the calculation of the two-loop tensor integrals and their decomposition into the basic scalar two-loop integrals, we use the `Mathematica` package `TARCER` [289] which implements the reduction algorithms presented in [317, 318]. In the `TARCER` notation, the most general form of a two-loop integral is given by

$$\texttt{TFI[D,p}^2\texttt{,}\Delta\texttt{p,\{a,b\},\{u,v,r,s,t\},\{\{}\nu_1\texttt{,m}_1\texttt{\},\{}\nu_2\texttt{,m}_2\texttt{\}, \ldots ,\{}\nu_5\texttt{,m}_5\texttt{\}\}]} \tag{A.27}$$
$$\equiv \frac{1}{\pi^D} \iint \frac{\mathrm{d}^D l_1 \mathrm{d}^D l_2 \, (\Delta \cdot l_1)^a \, (\Delta \cdot l_2)^b \, (l_1^2)^u \, (l_2^2)^v \, (p \cdot l_1)^r \, (p \cdot l_2)^s \, (l_1 \cdot l_2)^t}{[l_1^2 - m_1^2]^{\nu_1}[l_2^2 - m_2^2]^{\nu_2}[(l_1-p)^2 - m_3^2]^{\nu_3}[(l_2-p)^2 - m_4^2]^{\nu_4}[(l_1-l_2)^2 - m_5^2]^{\nu_5}} \; ,$$

where a, b, u, v, r, s, t and ν_i ($i = 1, ..., 5$) are non-negative integers and Δ represents a light-like four-vector, *i.e.* it satisfies $\Delta^2 = 0$. The reduction algorithm reduces all integrals to a combination of basic integrals, defined as [289]

$$\texttt{TFI[D,p}^2\texttt{,\{\{}\nu_1\texttt{,m}_1\texttt{\},\{}\nu_2\texttt{,m}_2\texttt{\},\{}\nu_3\texttt{,m}_3\texttt{\},\{}\nu_4\texttt{,m}_4\texttt{\},\{}\nu_5\texttt{,m}_5\texttt{\}\}]} \tag{A.28}$$
$$\equiv \frac{1}{\pi^D} \iint \frac{\mathrm{d}^D l_1 \mathrm{d}^D l_2}{[l_1^2 - m_1^2]^{\nu_1}[l_2^2 - m_2^2]^{\nu_2}[(l_1-p)^2 - m_3^2]^{\nu_3}[(l_2-p)^2 - m_4^2]^{\nu_4}[(l_1-l_2)^2 - m_5^2]^{\nu_5}} \; ,$$
$$\texttt{TVI[D,p}^2\texttt{,\{\{}\nu_1\texttt{,m}_1\texttt{\},\{}\nu_2\texttt{,m}_2\texttt{\},\{}\nu_3\texttt{,m}_3\texttt{\},\{}\nu_4\texttt{,m}_4\texttt{\}\}]} \tag{A.29}$$
$$\equiv \frac{1}{\pi^D} \iint \frac{\mathrm{d}^D l_1 \mathrm{d}^D l_2}{[(l_1-l_2)^2 - m_1^2]^{\nu_1}[l_2^2 - m_2^2]^{\nu_2}[(l_1-p)^2 - m_3^2]^{\nu_3}[(l_2-p)^2 - m_4^2]^{\nu_4}} \; ,$$
$$\texttt{TJI[D,p}^2\texttt{,\{\{}\nu_1\texttt{,m}_1\texttt{\},\{}\nu_2\texttt{,m}_2\texttt{\},\{}\nu_3\texttt{,m}_3\texttt{\}\}]} \tag{A.30}$$
$$\equiv \frac{1}{\pi^D} \iint \frac{\mathrm{d}^D l_1 \mathrm{d}^D l_2}{[l_1^2 - m_1^2]^{\nu_1}[(l_1-l_2)^2 - m_2^2]^{\nu_2}[(l_2-p)^2 - m_3^2]^{\nu_3}} \; ,$$
$$\texttt{TJI[D,0,\{\{}\nu_1\texttt{,m}_1\texttt{\},\{}\nu_2\texttt{,m}_2\texttt{\},\{}\nu_3\texttt{,m}_3\texttt{\}\}]} \tag{A.31}$$
$$\equiv \frac{1}{\pi^D} \iint \frac{\mathrm{d}^D l_1 \mathrm{d}^D l_2}{[l_1^2 - m_1^2]^{\nu_1}[(l_1-l_2)^2 - m_2^2]^{\nu_2}[l_2^2 - m_3^2]^{\nu_3}} \; ,$$
$$\texttt{TBI[D,p}^2\texttt{,\{\{}\nu_1\texttt{,m}_1\texttt{\},\{}\nu_2\texttt{,m}_2\texttt{\}\}]} \tag{A.32}$$
$$\equiv \frac{1}{\pi^{D/2}} \int \frac{\mathrm{d}^D l_1}{[l_1^2 - m_1^2]^{\nu_1}[(l_1-p)^2 - m_2^2]^{\nu_2}} \; ,$$
$$\texttt{TAI[D,0,\{\{}\nu_1\texttt{,m}_1\texttt{\}\}]} \tag{A.33}$$
$$\equiv \frac{1}{\pi^{D/2}} \int \frac{\mathrm{d}^D l_1}{[l_1^2 - m_1^2]^{\nu_1}} \; .$$

For the calculation of the corrections to the Higgs masses in the complex NMSSM to $\mathcal{O}(\alpha_t^2)$, we only need a subset of these integrals. For those, we implemented the analytic results presented in [291, 319] to the order that is required for our calculations. The integrals in the notation used in this reference are connected to the integrals in the `TARCER` notation via the following relations:

$$\texttt{TAI[D,0,\{\{1,m}_1\texttt{\}\}]} = -i\pi^2 \, \mathbf{A}(m_1^2) \; , \tag{A.34}$$
$$\texttt{TBI[D,p}^2\texttt{,\{\{1,m}_1\texttt{\},\{1,m}_2\texttt{\}\}]} = i\pi^2 \, \mathbf{B}(m_1^2, m_2^2) \; , \tag{A.35}$$
$$\texttt{TJI[D,0,\{\{1,m}_1\texttt{\},\{1,m}_2\texttt{\},\{1,m}_3\texttt{\}\}]} = \pi^4 \, \mathbf{I}(m_1^2, m_2^2, m_3^2) \; , \tag{A.36}$$
$$\texttt{TJI[D,p,\{\{1,m}_1\texttt{\},\{1,m}_2\texttt{\},\{1,m}_3\texttt{\}\}]} = \pi^4 \, \mathbf{S}(m_1^2, m_2^2, m_3^2) \; , \tag{A.37}$$
$$\texttt{TJI[D,p,\{\{2,m}_1\texttt{\},\{1,m}_2\texttt{\},\{1,m}_3\texttt{\}\}]} = -\pi^4 \, \mathbf{T}(m_1^2, m_2^2, m_3^2) \; , \tag{A.38}$$
$$\texttt{TVI[D,p}^2\texttt{,\{\{1,m}_4\texttt{\},\{1,m}_1\texttt{\},\{1,m}_3\texttt{\},\{1,m}_2\texttt{\}\}]} = -\pi^4 \, \mathbf{U}(m_1^2, m_2^2, m_3^2, m_4^2) \; . \tag{A.39}$$

The analytic results of these integrals are given by [291,319]

$$\mathbf{A}(m_1^2) = -\frac{m_1^2}{\varepsilon} - A_0^{\text{fin}}(m_1^2) - \varepsilon A_0^\varepsilon(m_1^2) \ , \tag{A.40}$$

$$\mathbf{B}(m_1^2, m_2^2) = \frac{1}{\varepsilon} + B_0^{\text{fin}}(p^2, m_1^2, m_2^2) + \varepsilon B_0^\varepsilon(p^2, m_1^2, m_2^2) \ , \tag{A.41}$$

$$\mathbf{I}(m_1^2, m_2^2, m_3^2) = -\frac{m_1^2 + m_2^2 + m_3^2}{2\varepsilon^2} + \frac{A_0^{\text{fin}}(m_1^2) + A_0^{\text{fin}}(m_2^2) + A_0^{\text{fin}}(m_3^2) - \frac{m_1^2 + m_2^2 + m_3^2}{2}}{\varepsilon}$$
$$+ \text{TJI}^{\text{fin}}(m_1^2, m_2^2, m_3^2) \ , \tag{A.42}$$

$$\mathbf{S}(m_1^2, m_2^2, m_3^2) = -\frac{m_1^2 + m_2^2 + m_3^2}{2\varepsilon^2} \tag{A.43}$$
$$+ \frac{A_0^{\text{fin}}(m_1^2) + A_0^{\text{fin}}(m_2^2) + A_0^{\text{fin}}(m_3^2) - \frac{m_1^2 + m_2^2 + m_3^2}{2} + \frac{p^2}{4}}{\varepsilon} \ ,$$

$$\mathbf{T}(m_1^2, m_2^2, m_3^2) = \frac{1}{2\varepsilon^2} - \frac{\frac{A_0(m_1^2)}{m_1^2} + \frac{1}{2}}{\varepsilon} \ , \tag{A.44}$$

$$\mathbf{U}(m_1^2, m_2^2, m_3^2, m_4^2) = \frac{1}{2\varepsilon^2} + \frac{B_0^{\text{fin}}(p^2, m_1^2, m_2^2) + \frac{1}{2}}{\varepsilon} \ , \tag{A.45}$$

where the superscripts fin and ε denote the $\mathcal{O}(1)$ and $\mathcal{O}(\varepsilon)$ terms of the A_0 and B_0 integrals given in Eqs. (A.13) and (A.16), respectively. Moreover, the finite part of the $\mathbf{I}$ integral is given by [320]

$$\text{TJI}^{\text{fin}}(m_1^2, m_2^2, m_3^2) = \sum_{i=1}^{3} \left\{ A_0^\varepsilon(m_i^2) - \frac{m_i^2}{2} \left(\overline{\ln}(m_i^2) \left[\overline{\ln}(m_i^2) - 4 \right] + 5 \right) \right\} - \frac{m_3^2}{2} \lambda^2(x, y) \Phi(x, y)$$
$$+ \frac{m_1^2 + m_2^2 - m_3^2}{4} \overline{\ln}^2(z) + \frac{m_1^2 - m_2^2 + m_3^2}{4} \overline{\ln}^2(x) + \frac{-m_1^2 + m_2^2 + m_3^2}{4} \overline{\ln}^2(y) \ , \tag{A.46}$$

where

$$x \equiv \frac{m_1^2}{m_3^2} \ , \quad y \equiv \frac{m_2^2}{m_3^2} \ , \quad z \equiv \frac{m_1^2}{m_2^2} \ , \tag{A.47}$$

and

$$\lambda(x, y) \equiv \sqrt{(1 - x - y)^2 - 4xy} \ , \tag{A.48}$$

$$\Phi(x, y) \equiv \frac{1}{\lambda(x, y)} \left[2 \ln \left(\frac{1 + x - y - \lambda(x, y)}{2} \right) \ln \left(\frac{1 - x + y - \lambda(x, y)}{2} \right) - \ln(x) \ln(y) + 2 \zeta(2) \right.$$
$$\left. - 2 \text{Li}_2 \left(\frac{1 + x - y - \lambda(x, y)}{2} \right) - 2 \text{Li}_2 \left(\frac{1 - x + y - \lambda(x, y)}{2} \right) \right] \ . \tag{A.49}$$

The Riemann zeta function $\zeta(s)$ evaluated at $s = 2$ is given in Eq. (A.5). Moreover, we implemented the following special cases of the integral in order to avoid numerical instabilities due to large (di)logarithms,

$$\text{TJI}^{\text{fin}}(0, m_2^2, m_3^2) = -\sum_{i=2}^{3} m_i^2 \left[\overline{\ln}(m_i^2) \left(\overline{\ln}(m_i^2) - 3 \right) + \frac{7 + \zeta(2)}{2} \right] + \frac{m_2^2}{2} \overline{\ln}^2(y) \tag{A.50}$$
$$- (m_2^2 - m_3^2) \left[\text{Li}_2(y) + \ln(1 - y) \ln(y) - \zeta(2) \right] \ ,$$

$$\text{TJI}^{\text{fin}}(0, 0, m_3^2) = -m_3^2 \left[\overline{\ln}(m_3^2) \left(\overline{\ln}(m_3^2) - 3 \right) + \frac{7 + 3\zeta(2)}{2} \right] \ , \tag{A.51}$$

$$\text{TJI}^{\text{fin}}(0, 0, 0) = 0 \ , \tag{A.52}$$

where the first of these relations is also presented in [321].

One-Loop Electroweak Renormalization Constants of the 2HDM

B.1. One-Loop Renormalization Constants of the Tadpoles

In the standard tadpole scheme, the tadpole terms T_i $(i = 1, 2)$ are promoted to one-loop order by means of Eq. (5.1) and fixed by demanding that the loop-corrected VEVs represent the minima of the loop-corrected scalar potential. This connects the tadpole CTs δT_i directly to the one-loop tadpole diagrams,

$$
i\delta T_{H/h} = \begin{pmatrix} \begin{array}{c} \bigcirc \\ \vdots \\ H/h \end{array} \end{pmatrix} ,
\tag{B.1}
$$

where we additionally rotated the tadpole CTs from the gauge basis to the mass basis by means of the rotation matrix R_α as defined in Eq. (4.31). The nine distinct tadpole terms appearing in the diagonalized mass matrices in Eqs. (4.32) to (4.34) receive CTs as well which are given by [226]

Renormalization of the tadpoles (standard scheme)

$$
\delta T_{HH} = \frac{c_\alpha^3 s_\beta + s_\alpha^3 c_\beta}{v s_\beta c_\beta} \delta T_H - \frac{s_{2\alpha} s_{\beta-\alpha}}{v s_{2\beta}} \delta T_h ,
\tag{B.2}
$$

$$
\delta T_{Hh} = -\frac{s_{2\alpha} s_{\beta-\alpha}}{v s_{2\beta}} \delta T_H + \frac{s_{2\alpha} c_{\beta-\alpha}}{v s_{2\beta}} \delta T_h ,
\tag{B.3}
$$

$$
\delta T_{hh} = \frac{s_{2\alpha} c_{\beta-\alpha}}{v s_{2\beta}} \delta T_H - \frac{s_\alpha^3 s_\beta - c_\alpha^3 c_\beta}{v s_\beta c_\beta} \delta T_h ,
\tag{B.4}
$$

$$
\delta T_{G^0 G^0} = \frac{c_{\beta-\alpha}}{v} \delta T_H + \frac{s_{\beta-\alpha}}{v} \delta T_h ,
\tag{B.5}
$$

$$
\delta T_{G^0 A} = -\frac{s_{\beta-\alpha}}{v} \delta T_H + \frac{c_{\beta-\alpha}}{v} \delta T_h ,
\tag{B.6}
$$

$$
\delta T_{AA} = \frac{c_\alpha s_\beta^3 + s_\alpha c_\beta^3}{v s_\beta c_\beta} \delta T_H - \frac{s_\alpha s_\beta^3 - c_\alpha c_\beta^3}{v s_\beta c_\beta} \delta T_h ,
\tag{B.7}
$$

$$
\delta T_{G^\pm G^\pm} = \frac{c_{\beta-\alpha}}{v} \delta T_H + \frac{s_{\beta-\alpha}}{v} \delta T_h ,
\tag{B.8}
$$

$$\delta T_{G^\pm H^\pm} = -\frac{s_{\beta-\alpha}}{v}\delta T_H + \frac{c_{\beta-\alpha}}{v}\delta T_h \ , \tag{B.9}$$

$$\delta T_{H^\pm H^\pm} = \frac{c_\alpha s_\beta^3 + s_\alpha c_\beta^3}{v s_\beta c_\beta}\delta T_H - \frac{s_\alpha s_\beta^3 - c_\alpha c_\beta^3}{v s_\beta c_\beta}\delta T_h \ . \tag{B.10}$$

In the alternative tadpole scheme, the VEVs are the fundamental quantities and hence, the tadpole terms do not receive CTs. Instead, the condition that the tree-level VEVs represent the proper minimum of the potential is imposed at one-loop level, leading to the following definition of the VEV CTs [226]:

$$\delta v_1 = \frac{-ic_\alpha}{m_H^2}\left(\begin{array}{c} \bigcirc \\ \vdots \\ H \end{array}\right) - \frac{-is_\alpha}{m_h^2}\left(\begin{array}{c} \bigcirc \\ \vdots \\ h \end{array}\right) \ , \quad \delta v_2 = \frac{-is_\alpha}{m_H^2}\left(\begin{array}{c} \bigcirc \\ \vdots \\ H \end{array}\right) + \frac{-ic_\alpha}{m_h^2}\left(\begin{array}{c} \bigcirc \\ \vdots \\ h \end{array}\right) \ . \tag{B.11}$$

As a consequence of this renormalization condition of the minimum of the scalar potential, explicit tadpole contributions in all self-energies and vertex corrections need to be included:

Renormalization of the tadpoles (alternative FJ scheme)

$$\delta T_{ij} = 0 \ , \tag{B.12}$$

$$\Sigma(p^2) \ \rightarrow \ \Sigma^{\text{tad}}(p^2) \ , \tag{B.13}$$

Tadpole diagrams have to be considered in the vertex corrections .

B.2. One-Loop Renormalization Constants of the Gauge Sector

The explicit forms of the gauge boson mass CTs depend on the chosen tadpole scheme. By denoting the transverse part of the gauge boson self-energies with the superscript T, the corresponding CTs are given by [226]

Renormalization of the gauge sector (standard scheme)

$$\delta m_W^2 = \text{Re}\left[\Sigma_{WW}^T\left(m_W^2\right)\right] \ , \tag{B.14}$$

$$\delta m_Z^2 = \text{Re}\left[\Sigma_{ZZ}^T\left(m_Z^2\right)\right] \ , \tag{B.15}$$

Renormalization of the gauge sector (alternative FJ scheme)

$$\delta m_W^2 = \text{Re}\left[\Sigma_{WW}^{\text{tad},T}\left(m_W^2\right)\right] \ , \tag{B.16}$$

$$\delta m_Z^2 = \text{Re}\left[\Sigma_{ZZ}^{\text{tad},T}\left(m_Z^2\right)\right] \ . \tag{B.17}$$

The $SU(2)_L$ coupling constant g is not an independent parameter in our work, but for convenience, we nevertheless present its CT as a function of the CTs of the independent parameters as follows:

$$\frac{\delta g}{g} = \delta Z_e + \frac{c_W^2}{2s_W^2}\left(\frac{\delta m_W^2}{m_W^2} - \frac{\delta m_Z^2}{m_Z^2}\right) \ . \tag{B.18}$$

The WFRCs of the gauge bosons as well as the definition of the CT for the electromagnetic charge e are independent of the tadpole scheme and explicitly given by [226]

Renormalization of the gauge sector (both schemes)

$$\delta Z_e(m_Z^2) = \frac{1}{2} \left. \frac{\partial \Sigma_{\gamma\gamma}^T (p^2)}{\partial p^2} \right|_{p^2=0} + \frac{s_W}{c_W} \frac{\Sigma_{\gamma Z}^T (0)}{m_Z^2} - \frac{1}{2} \Delta\alpha(m_Z^2) \,, \tag{B.19}$$

$$\delta Z_{WW} = -\mathrm{Re} \left[\frac{\partial \Sigma_{WW}^T (p^2)}{\partial p^2} \right]_{p^2=m_W^2} \,, \tag{B.20}$$

$$\begin{pmatrix} \delta Z_{ZZ} & \delta Z_{Z\gamma} \\ \delta Z_{\gamma Z} & \delta Z_{\gamma\gamma} \end{pmatrix} = \begin{pmatrix} -\mathrm{Re} \left[\dfrac{\partial \Sigma_{ZZ}^T (p^2)}{\partial p^2} \right]_{p^2=m_Z^2} & \dfrac{2}{m_Z^2} \Sigma_{Z\gamma}^T (0) \\[2ex] -\dfrac{2}{m_Z^2} \mathrm{Re} \left[\Sigma_{Z\gamma}^T (m_Z^2) \right] & -\mathrm{Re} \left[\dfrac{\partial \Sigma_{\gamma\gamma}^T (p^2)}{\partial p^2} \right]_{p^2=0} \end{pmatrix} . \tag{B.21}$$

Since we do not define δZ_e in the Thomson limit but instead at the scale of the Z boson mass, we additionally introduce the term

$$\Delta\alpha(m_Z^2) = \left. \frac{\partial \Sigma_{\gamma\gamma}^{\mathrm{light},T}(p^2)}{\partial p^2} \right|_{p^2=0} - \frac{\Sigma_{\gamma\gamma}^T(m_Z^2)}{m_Z^2} \tag{B.22}$$

which accounts for this scale shift. The transverse photon self-energy $\Sigma_{\gamma\gamma}^{\mathrm{light},T}(p^2)$ contains only contributions from light fermions, *i.e.* from all fermions apart from the top quark. Due to this, the one-loop corrections to the decay widths containing δZ_e are independent of large logarithms stemming from light fermion contributions [183].

B.3. One-Loop Renormalization Constants of the Scalar Sector

The diagonal WFRCs of the Higgs bosons of the 2HDM are independent from tadpole contributions since they are defined over the derivatives of the scalar self-energies. Hence, their explicit forms are the same in both tadpole schemes [226]:

Renormalization of the scalar sector (both schemes)

$$\delta Z_{HH} = -\mathrm{Re} \left[\frac{\partial \Sigma_{HH} (p^2)}{\partial p^2} \right]_{p^2=m_H^2} \,, \tag{B.23}$$

$$\delta Z_{hh} = -\mathrm{Re} \left[\frac{\partial \Sigma_{hh} (p^2)}{\partial p^2} \right]_{p^2=m_h^2} \,, \tag{B.24}$$

$$\delta Z_{G^0 G^0} = -\mathrm{Re} \left[\frac{\partial \Sigma_{G^0 G^0} (p^2)}{\partial p^2} \right]_{p^2=0} \,, \tag{B.25}$$

$$\delta Z_{AA} = -\mathrm{Re} \left[\frac{\partial \Sigma_{AA} (p^2)}{\partial p^2} \right]_{p^2=m_A^2} \,, \tag{B.26}$$

$$\delta Z_{G^\pm G^\pm} = -\mathrm{Re} \left[\frac{\partial \Sigma_{G^\pm G^\pm} (p^2)}{\partial p^2} \right]_{p^2=0} \,, \tag{B.27}$$

$$\delta Z_{H^\pm H^\pm} = -\mathrm{Re} \left[\frac{\partial \Sigma_{H^\pm H^\pm} (p^2)}{\partial p^2} \right]_{p^2=m_{H^\pm}^2} . \tag{B.28}$$

The mass CTs of the scalar Higgs bosons as well as their off-diagonal WFRCs depend on the chosen tadpole scheme and are explicitly given as follows [226],

---

Renormalization of the scalar sector (standard scheme)

$$\delta Z_{Hh} = \frac{2}{m_H^2 - m_h^2} \text{Re}\Big[\Sigma_{Hh}(m_h^2) - \delta T_{Hh} \Big] \,, \tag{B.29}$$

$$\delta Z_{hH} = -\frac{2}{m_H^2 - m_h^2} \text{Re}\Big[\Sigma_{Hh}(m_H^2) - \delta T_{Hh} \Big] \,, \tag{B.30}$$

$$\delta Z_{G^0 A} = -\frac{2}{m_A^2} \text{Re}\Big[\Sigma_{G^0 A}(m_A^2) - \delta T_{G^0 A} \Big] \,, \tag{B.31}$$

$$\delta Z_{A G^0} = \frac{2}{m_A^2} \text{Re}\Big[\Sigma_{G^0 A}(0) - \delta T_{G^0 A} \Big] \,, \tag{B.32}$$

$$\delta Z_{G^\pm H^\pm} = -\frac{2}{m_{H^\pm}^2} \text{Re}\Big[\Sigma_{G^\pm H^\pm}(m_{H^\pm}^2) - \delta T_{G^\pm H^\pm} \Big] \,, \tag{B.33}$$

$$\delta Z_{H^\pm G^\pm} = \frac{2}{m_{H^\pm}^2} \text{Re}\Big[\Sigma_{G^\pm H^\pm}(0) - \delta T_{G^\pm H^\pm} \Big] \,, \tag{B.34}$$

$$\delta m_H^2 = \text{Re}\Big[\Sigma_{HH}(m_H^2) - \delta T_{HH} \Big] \,, \tag{B.35}$$

$$\delta m_h^2 = \text{Re}\Big[\Sigma_{hh}(m_h^2) - \delta T_{hh} \Big] \,, \tag{B.36}$$

$$\delta m_A^2 = \text{Re}\Big[\Sigma_{AA}(m_A^2) - \delta T_{AA} \Big] \,, \tag{B.37}$$

$$\delta m_{H^\pm}^2 = \text{Re}\Big[\Sigma_{H^\pm H^\pm}(m_{H^\pm}^2) - \delta T_{H^\pm H^\pm} \Big] \,, \tag{B.38}$$

Renormalization of the scalar sector (alternative FJ scheme)

$$\delta Z_{Hh} = \frac{2}{m_H^2 - m_h^2} \text{Re}\Big[\Sigma_{Hh}^{\text{tad}}(m_h^2) \Big] \,, \tag{B.39}$$

$$\delta Z_{hH} = -\frac{2}{m_H^2 - m_h^2} \text{Re}\Big[\Sigma_{Hh}^{\text{tad}}(m_H^2) \Big] \,, \tag{B.40}$$

$$\delta Z_{G^0 A} = -\frac{2}{m_A^2} \text{Re}\Big[\Sigma_{G^0 A}^{\text{tad}}(m_A^2) \Big] \,, \tag{B.41}$$

$$\delta Z_{A G^0} = \frac{2}{m_A^2} \text{Re}\Big[\Sigma_{G^0 A}^{\text{tad}}(0) \Big] \,, \tag{B.42}$$

$$\delta Z_{G^\pm H^\pm} = -\frac{2}{m_{H^\pm}^2} \text{Re}\Big[\Sigma_{G^\pm H^\pm}^{\text{tad}}(m_{H^\pm}^2) \Big] \,, \tag{B.43}$$

$$\delta Z_{H^\pm G^\pm} = \frac{2}{m_{H^\pm}^2} \text{Re}\Big[\Sigma_{G^\pm H^\pm}^{\text{tad}}(0) \Big] \,, \tag{B.44}$$

$$\delta m_H^2 = \text{Re}\Big[\Sigma_{HH}^{\text{tad}}(m_H^2) \Big] \,, \tag{B.45}$$

$$\delta m_h^2 = \text{Re}\Big[\Sigma_{hh}^{\text{tad}}(m_h^2) \Big] \,, \tag{B.46}$$

$$\delta m_A^2 = \text{Re}\Big[\Sigma_{AA}^{\text{tad}}(m_A^2) \Big] \,, \tag{B.47}$$

$$\delta m_{H^\pm}^2 = \text{Re}\Big[\Sigma_{H^\pm H^\pm}^{\text{tad}}(m_{H^\pm}^2) \Big] \,. \tag{B.48}$$

B.4. One-Loop Renormalization Constants of the Fermion Sector

The mass CTs of the fermions and their off-diagonal WFRCs dependent on the tadpole scheme,

---

Renormalization of the fermion sector (standard scheme)

$$\delta m_{f,i} = \frac{m_{f,i}}{2}\mathrm{Re}\left(\Sigma_{ii}^{f,L}(m_{f,i}^2) + \Sigma_{ii}^{f,R}(m_{f,i}^2) + 2\Sigma_{ii}^{f,S}(m_{f,i}^2)\right) \ , \tag{B.49}$$

$$\delta Z_{ij}^{f,L} = \frac{2}{m_{f,i}^2 - m_{f,j}^2}\mathrm{Re}\left[m_{f,j}^2\Sigma_{ij}^{f,L}(m_{f,j}^2) + m_{f,i}m_{f,j}\Sigma_{ij}^{f,R}(m_{f,j}^2)\right. \tag{B.50}$$

$$\left. + (m_{f,i}^2 + m_{f,j}^2)\Sigma_{ij}^{f,S}(m_{f,j}^2)\right] \qquad (i \neq j) \ ,$$

$$\delta Z_{ij}^{f,R} = \frac{2}{m_{f,i}^2 - m_{f,j}^2}\mathrm{Re}\left[m_{f,j}^2\Sigma_{ij}^{f,R}(m_{f,j}^2) + m_{f,i}m_{f,j}\Sigma_{ij}^{f,L}(m_{f,j}^2)\right. \tag{B.51}$$

$$\left. + 2m_{f,i}m_{f,j}\Sigma_{ij}^{f,S}(m_{f,j}^2)\right] \qquad (i \neq j) \ ,$$

Renormalization of the fermion sector (alternative FJ scheme)

$$\delta m_{f,i} = \frac{m_{f,i}}{2}\mathrm{Re}\left(\Sigma_{ii}^{f,L}(m_{f,i}^2) + \Sigma_{ii}^{f,R}(m_{f,i}^2) + 2\Sigma_{ii}^{\mathrm{tad},f,S}(m_{f,i}^2)\right) \ , \tag{B.52}$$

$$\delta Z_{ij}^{f,L} = \frac{2}{m_{f,i}^2 - m_{f,j}^2}\mathrm{Re}\left[m_{f,j}^2\Sigma_{ij}^{f,L}(m_{f,j}^2) + m_{f,i}m_{f,j}\Sigma_{ij}^{f,R}(m_{f,j}^2)\right. \tag{B.53}$$

$$\left. + (m_{f,i}^2 + m_{f,j}^2)\Sigma_{ij}^{\mathrm{tad},f,S}(m_{f,j}^2)\right] \qquad (i \neq j) \ ,$$

$$\delta Z_{ij}^{f,R} = \frac{2}{m_{f,i}^2 - m_{f,j}^2}\mathrm{Re}\left[m_{f,j}^2\Sigma_{ij}^{f,R}(m_{f,j}^2) + m_{f,i}m_{f,j}\Sigma_{ij}^{f,L}(m_{f,j}^2)\right. \tag{B.54}$$

$$\left. + 2m_{f,i}m_{f,j}\Sigma_{ij}^{\mathrm{tad},f,S}(m_{f,j}^2)\right] \qquad (i \neq j) \ .$$

The diagonal WFRCs are independent of the tadpole renormalization. For the CTs of the CKM matrix elements, we implement the scheme presented in [236] which defines the CTs over the pinched fermion self-energies which are equivalent to the ordinary fermion self-energies, but evaluated in the Feynman-'t Hooft gauge. The corresponding CTs and WFRCs are given as

---

Renormalization of the fermion sector (both schemes)

$$\delta V_{ij} = \frac{1}{4}\left[\left(\delta Z_{ik}^{u,L} - \delta Z_{ik}^{u,L\dagger}\right)V_{kj} - V_{ik}\left(\delta Z_{kj}^{d,L} - \delta Z_{kj}^{d,L\dagger}\right)\right]_{\xi=1} \ , \tag{B.55}$$

$$\delta Z_{ii}^{f,L} = -\mathrm{Re}\left[\Sigma_{ii}^{f,L}(m_{f,i}^2)\right] - m_{f,i}^2\mathrm{Re}\left[\frac{\partial\Sigma_{ii}^{f,L}(p^2)}{\partial p^2} + \frac{\partial\Sigma_{ii}^{f,R}(p^2)}{\partial p^2} + 2\frac{\partial\Sigma_{ii}^{f,S}(p^2)}{\partial p^2}\right]_{p^2=m_{f,i}^2} \ , \tag{B.56}$$

$$\delta Z_{ii}^{f,R} = -\mathrm{Re}\left[\Sigma_{ii}^{f,R}(m_{f,i}^2)\right] - m_{f,i}^2\mathrm{Re}\left[\frac{\partial\Sigma_{ii}^{f,L}(p^2)}{\partial p^2} + \frac{\partial\Sigma_{ii}^{f,R}(p^2)}{\partial p^2} + 2\frac{\partial\Sigma_{ii}^{f,S}(p^2)}{\partial p^2}\right]_{p^2=m_{f,i}^2} \ . \tag{B.57}$$

As argued in [216], we want to note that the CT definition in Eq. (B.55) can also be used in the framework of the standard tadpole scheme, which effectively resembles the original GFP-dependent definition of the CTs of the CKM matrix elements presented in [183], but evaluated at a specific gauge.

The Yukawa coupling parameters introduced in Table 4.2 are not independent parameters. For convenience, we nevertheless present their CTs as functions of the mixing angle CTs $\delta\alpha$ and $\delta\beta$, presented in the subsequent App. B.5. The explicit forms of the Yukawa coupling parameter CTs, independently of the 2HDM type chosen, are given by

$$\delta Y_1 = Y_1 \left(-\frac{Y_2}{Y_1}\delta\alpha + Y_3\delta\beta \right) \ , \tag{B.58}$$

$$\delta Y_2 = Y_2 \left(\frac{Y_1}{Y_2}\delta\alpha + Y_3\delta\beta \right) \ , \tag{B.59}$$

$$\delta Y_3 = \left(1 + Y_3^2\right)\delta\beta \ , \tag{B.60}$$

$$\delta Y_4 = Y_4 \left(-\frac{Y_5}{Y_4}\delta\alpha + Y_6\delta\beta \right) \ , \tag{B.61}$$

$$\delta Y_5 = Y_5 \left(\frac{Y_4}{Y_5}\delta\alpha + Y_6\delta\beta \right) \ , \tag{B.62}$$

$$\delta Y_6 = \left(1 + Y_6^2\right)\delta\beta \ . \tag{B.63}$$

B.5. One-Loop Renormalization Constants of the Scalar Mixing Angles

B.5.1. $\overline{\text{MS}}$ Scheme

In the $\overline{\text{MS}}$ scheme, the mixing angle CTs do not receive finite contributions $\delta\alpha^{\text{fin}}$ and $\delta\beta^{\text{fin}}$ but instead, they only contain the UV-divergent parts proportional to Δ, defined in Eq. (3.2). The resulting CTs are independent of the tadpole scheme and are hence given by

Renormalization of $\delta\alpha$ and $\delta\beta$: $\overline{\text{MS}}$ scheme (both schemes)
$$\delta\alpha|_{\text{fin}} = 0 \ , \tag{B.64}$$ $$\delta\beta|_{\text{fin}} = 0 \ . \tag{B.65}$$

The analytic forms of the UV-divergent parts of $\delta\alpha$ and $\delta\beta$ are rather intricate. Hence, we do not display them here explicitly but refer to [189] for their presentation.

B.5.2. KOSY Scheme

The KOSY scheme [222] connects the definition of the mixing angle CTs with the WFRCs of the scalar doublets. For the CP-even scalar mixing angle α this connection is unambiguous, while for the CP-odd and charged mixing angle β, different combinations of WFRCs in the definition of $\delta\beta$ are possible. We choose the two combinations where $\delta\beta$ is defined solely through the CP-odd sector, denotes by $\delta\beta^o$, and where it is defined solely through the charged sector, denoted by $\delta\beta^c$. The corresponding CTs in the standard and alternative FJ tadpole scheme are given by [222, 226]

Renormalization of $\delta\alpha$ and $\delta\beta$: KOSY scheme (standard scheme)

$$\delta\alpha = \frac{1}{2(m_H^2 - m_h^2)}\mathrm{Re}\left[\Sigma_{Hh}(m_H^2) + \Sigma_{Hh}(m_h^2) - 2\delta T_{Hh}\right] \ , \tag{B.66}$$

$$\delta\beta^o = -\frac{1}{2m_A^2}\mathrm{Re}\left[\Sigma_{G^0 A}(m_A^2) + \Sigma_{G^0 A}(0) - 2\delta T_{G^0 A}\right] \ , \tag{B.67}$$

$$\delta\beta^c = -\frac{1}{2m_{H^\pm}^2}\mathrm{Re}\left[\Sigma_{G^\pm H^\pm}(m_{H^\pm}^2) + \Sigma_{G^\pm H^\pm}(0) - 2\delta T_{G^\pm H^\pm}\right] \ , \tag{B.68}$$

Renormalization of $\delta\alpha$ and $\delta\beta$: KOSY scheme (alternative FJ scheme)

$$\delta\alpha = \frac{1}{2(m_H^2 - m_h^2)}\mathrm{Re}\left[\Sigma_{Hh}^{\mathrm{tad}}(m_H^2) + \Sigma_{Hh}^{\mathrm{tad}}(m_h^2)\right] \ , \tag{B.69}$$

$$\delta\beta^o = -\frac{1}{2m_A^2}\mathrm{Re}\left[\Sigma_{G^0 A}^{\mathrm{tad}}(m_A^2) + \Sigma_{G^0 A}^{\mathrm{tad}}(0)\right] \ , \tag{B.70}$$

$$\delta\beta^c = -\frac{1}{2m_{H^\pm}^2}\mathrm{Re}\left[\Sigma_{G^\pm H^\pm}^{\mathrm{tad}}(m_{H^\pm}^2) + \Sigma_{G^\pm H^\pm}^{\mathrm{tad}}(0)\right] \ . \tag{B.71}$$

We want to emphasize that the KOSY scheme features mixing angle CTs which are manifestly GFP-dependent and that their usage one-loop order yields GFP-dependent partial decay widths.

B.5.3. p_*-Pinched Scheme

In the p_*-pinched scheme, the OS-motivated approach of the KOSY scheme is connected with an unambiguous definition of the GFP-independent part of the self-energies involved in the definition of the mixing angle CTs, given by the pinched scalar self-energies. For the p_* scale, cf. Eq. (5.26), the pinched scalar self-energies of the 2HDM are equivalent to the usual self-energies $\Sigma^{\mathrm{tad}}(p^2)$ including tadpole contributions, evaluated at the Feynman-'t Hooft gauge $\xi_V = 1$ ($V \in \{W^\pm, Z, \gamma\}$). For consistency, the p_*-pinched scheme requires the framework of the alternative FJ scheme. The mixing angle CTs in this scheme are given by [226]

Renormalization of $\delta\alpha$ and $\delta\beta$: p_*-pinched scheme (alternative FJ scheme)

$$\delta\alpha = \frac{1}{m_H^2 - m_h^2}\mathrm{Re}\left[\Sigma_{Hh}^{\mathrm{tad}}\left(\frac{m_H^2 + m_h^2}{2}\right)\right]_{\xi=1} \ , \tag{B.72}$$

$$\delta\beta^o = -\frac{1}{m_A^2}\mathrm{Re}\left[\Sigma_{G^0 A}^{\mathrm{tad}}\left(\frac{m_A^2}{2}\right)\right]_{\xi=1} \ , \tag{B.73}$$

$$\delta\beta^c = -\frac{1}{m_{H^\pm}^2}\mathrm{Re}\left[\Sigma_{G^\pm H^\pm}^{\mathrm{tad}}\left(\frac{m_{H^\pm}^2}{2}\right)\right]_{\xi=1} \ , \tag{B.74}$$

---

where $\delta\beta^o$ and $\delta\beta^c$ are the two variations of the CT definition of the mixing angle β, adopted from the KOSY scheme.

B.5.4. OS-Pinched Scheme

The OS-pinched scheme is analogous to the p_*-pinched scheme, however, the original scale p^2 of the self-energies from the KOSY scheme is adopted in the definition of the mixing angle

CTs instead of the p_*^2 scale. Due to this, the additional UV-finite self-energy contributions derived for the 2HDM in [226] need to be taken into account,

$$\Sigma_{Hh}^{\text{add}}(p^2) = \frac{\alpha_{\text{em}} m_Z^2 s_{\beta-\alpha} c_{\beta-\alpha}}{8\pi m_W^2 \left(1 - \frac{m_W^2}{m_Z^2}\right)} \left(p^2 - \frac{m_H^2 + m_h^2}{2}\right) \left\{ \left[B_0(p^2; m_Z^2, m_A^2) - B_0(p^2; m_Z^2, m_Z^2)\right] \right.$$
$$\left. + 2\frac{m_W^2}{m_Z^2} \left[B_0(p^2; m_W^2, m_{H^\pm}^2) - B_0(p^2; m_W^2, m_W^2)\right] \right\}, \tag{B.75}$$

$$\Sigma_{G^0 A}^{\text{add}}(p^2) = \frac{\alpha_{\text{em}} m_Z^2 s_{\beta-\alpha} c_{\beta-\alpha}}{8\pi m_W^2 \left(1 - \frac{m_W^2}{m_Z^2}\right)} \left(p^2 - \frac{m_A^2}{2}\right) \left[B_0(p^2; m_Z^2, m_H^2) - B_0(p^2; m_Z^2, m_h^2)\right], \tag{B.76}$$

$$\Sigma_{G^\pm H^\pm}^{\text{add}}(p^2) = \frac{\alpha_{\text{em}} s_{\beta-\alpha} c_{\beta-\alpha}}{4\pi \left(1 - \frac{m_W^2}{m_Z^2}\right)} \left(p^2 - \frac{m_{H^\pm}^2}{2}\right) \left[B_0(p^2; m_W^2, m_H^2) - B_0(p^2; m_W^2, m_h^2)\right]. \tag{B.77}$$

As for the p_*-pinched scheme, the OS-pinched scheme requires the alternative FJ tadpole scheme for consistency. The mixing angle CTs in the OS-pinched scheme are given by [226]

Renormalization of $\delta\alpha$ and $\delta\beta$: OS-pinched scheme (alternative FJ scheme)

$$\delta\alpha = \frac{\text{Re}\left[\left[\Sigma_{Hh}^{\text{tad}}(m_H^2) + \Sigma_{Hh}^{\text{tad}}(m_h^2)\right]_{\xi=1} + \Sigma_{Hh}^{\text{add}}(m_H^2) + \Sigma_{Hh}^{\text{add}}(m_h^2)\right]}{2\left(m_H^2 - m_h^2\right)}, \tag{B.78}$$

$$\delta\beta^o = -\frac{\text{Re}\left[\left[\Sigma_{G^0 A}^{\text{tad}}(m_A^2) + \Sigma_{G^0 A}^{\text{tad}}(0)\right]_{\xi=1} + \Sigma_{G^0 A}^{\text{add}}(m_A^2) + \Sigma_{G^0 A}^{\text{add}}(0)\right]}{2m_A^2}, \tag{B.79}$$

$$\delta\beta^c = -\frac{\text{Re}\left[\left[\Sigma_{G^\pm H^\pm}^{\text{tad}}(m_{H^\pm}^2) + \Sigma_{G^\pm H^\pm}^{\text{tad}}(0)\right]_{\xi=1} + \Sigma_{G^\pm H^\pm}^{\text{add}}(m_{H^\pm}^2) + \Sigma_{G^\pm H^\pm}^{\text{add}}(0)\right]}{2m_{H^\pm}^2}, \tag{B.80}$$

---

where again the two chosen combinations $\delta\beta^o$ and $\delta\beta^c$ where adopted from the KOSY scheme.

B.5.5. Process-Dependent Schemes

The process-dependent scheme imposes the renormalization condition that the partial decay widths at LO and NLO for a set of chosen decay processes $\phi \longrightarrow X_1 X_2$ of Higgs bosons ϕ into two other particles X_1 and X_2 are equivalent, *i.e.* the full one-loop effects are shifted into the definition of the mixing angle CTs. In order to avoid the appearance of IR-divergent contributions, only the genuine weak one-loop corrections are considered, requiring that for the chosen processes the QED-like contributions form a UV-divergent subset. For the three different combinations of decay processes presented in Sec. 5.3, the resulting mixing angle CTs are given as:

Renormalization of $\delta\alpha$ and $\delta\beta$: process-dependent scheme 1 (both schemes)

$$\delta\alpha = \frac{-Y_5}{Y_4} \left[\mathcal{F}_{H\tau\tau}^{\text{VC}} + \frac{\delta g}{g} + \frac{\delta m_\tau}{m_\tau} - \frac{\delta m_W^2}{2m_W^2} + Y_6\delta\beta + \frac{\delta Z_{HH}}{2} + \frac{Y_4}{Y_5}\frac{\delta Z_{hH}}{2} + \frac{\delta Z_{\tau\tau}^{\text{L}}}{2} \right.$$
$$\left. + \frac{\delta Z_{\tau\tau}^{\text{R}}}{2} \right], \tag{B.81}$$

$$\delta\beta = \frac{-Y_6}{1 + Y_6^2} \left[\mathcal{F}_{A\tau\tau}^{\text{VC}} + \frac{\delta g}{g} + \frac{\delta m_\tau}{m_\tau} - \frac{\delta m_W^2}{2m_W^2} + \frac{\delta Z_{AA}}{2} - \frac{1}{Y_6}\frac{\delta Z_{G^0 A}}{2} + \frac{\delta Z_{\tau\tau}^{\text{L}}}{2} + \frac{\delta Z_{\tau\tau}^{\text{R}}}{2} \right], \tag{B.82}$$

Renormalization of $\delta\alpha$ and $\delta\beta$: process-dependent scheme 2 (both schemes)

$$\delta\alpha = \frac{Y_4}{Y_5}\left[\mathcal{F}_{h\tau\tau}^{\mathrm{VC}} + \frac{\delta g}{g} + \frac{\delta m_\tau}{m_\tau} - \frac{\delta m_W^2}{2m_W^2} + Y_6\delta\beta + \frac{\delta Z_{hh}}{2} + \frac{Y_5}{Y_4}\frac{\delta Z_{Hh}}{2} + \frac{\delta Z_{\tau\tau}^{\mathrm{L}}}{2}\right. \tag{B.83}$$

$$\left. + \frac{\delta Z_{\tau\tau}^{\mathrm{R}}}{2}\right],$$

$$\delta\beta = \frac{-Y_6}{1+Y_6^2}\left[\mathcal{F}_{A\tau\tau}^{\mathrm{VC}} + \frac{\delta g}{g} + \frac{\delta m_\tau}{m_\tau} - \frac{\delta m_W^2}{2m_W^2} + \frac{\delta Z_{AA}}{2} - \frac{1}{Y_6}\frac{\delta Z_{G^0 A}}{2} + \frac{\delta Z_{\tau\tau}^{\mathrm{L}}}{2} + \frac{\delta Z_{\tau\tau}^{\mathrm{R}}}{2}\right],$$

$$\tag{B.84}$$

Renormalization of $\delta\alpha$ and $\delta\beta$: process-dependent scheme 3 (both schemes)

$$\delta\alpha = \frac{Y_4 Y_5}{Y_4^2 + Y_5^2}\left[\mathcal{F}_{h\tau\tau}^{\mathrm{VC}} - \mathcal{F}_{H\tau\tau}^{\mathrm{VC}} + \frac{\delta Z_{hh}}{2} - \frac{\delta Z_{HH}}{2} + \frac{Y_5}{Y_4}\frac{\delta Z_{Hh}}{2} - \frac{Y_4}{Y_5}\frac{\delta Z_{hH}}{2}\right], \tag{B.85}$$

$$\delta\beta = \frac{-1}{Y_6(Y_4^2 + Y_5^2)}\left[(Y_4^2 + Y_5^2)\left(\frac{\delta g}{g} + \frac{\delta m_\tau}{m_\tau} - \frac{\delta m_W^2}{2m_W^2} + \frac{\delta Z_{\tau\tau}^{\mathrm{L}}}{2} + \frac{\delta Z_{\tau\tau}^{\mathrm{R}}}{2}\right)\right. \tag{B.86}$$

$$\left. + Y_4 Y_5\left(\frac{\delta Z_{Hh}}{2} + \frac{\delta Z_{hH}}{2}\right) + Y_4^2\left(\frac{\delta Z_{hh}}{2} + \mathcal{F}_{h\tau\tau}^{\mathrm{VC}}\right) + Y_5^2\left(\frac{\delta Z_{HH}}{2} + \mathcal{F}_{H\tau\tau}^{\mathrm{VC}}\right)\right],$$

---

where the first process-dependent scheme was already presented in [226]. Formally, these definitions of the mixing angle CTs are the same for the standard and alternative FJ tadpole scheme. However, since some of the CTs involved in these definitions differ between the two schemes, the actual values of the mixing angle CTs differ between these schemes, as well.

B.5.6. Physical On-Shell Schemes

The formal definition of the mixing angle CTs in the physical OS schemes from [216] are independent of the tadpole scheme and explicitly given by

---

Renormalization of $\delta\alpha$ and $\delta\beta$: physical (on-shell) scheme OS1 (both schemes)

$$\delta\alpha = s_\alpha c_\alpha\left(\delta_{H\nu_1\bar{\nu}_1} - \delta_{h\nu_1\bar{\nu}_1}\right) + s_\alpha c_\alpha\frac{\delta Z_{HH} - \delta Z_{hh}}{2} + \frac{c_\alpha^2\delta Z_{Hh} - s_\alpha^2\delta Z_{hH}}{2}, \tag{B.87}$$

$$\delta\beta = t_\beta\left[c_\alpha^2\delta_{H\nu_1\bar{\nu}_1} + s_\alpha^2\delta_{h\nu_1\bar{\nu}_1} - \delta_{A\nu_1\bar{\nu}_1} + \frac{c_\alpha^2\delta Z_{HH} + s_\alpha^2\delta Z_{hh} - \delta Z_{AA}}{2}\right. \tag{B.88}$$

$$\left. - s_\alpha c_\alpha\frac{\delta Z_{Hh} + \delta Z_{hH}}{2}\right] + \frac{\delta Z_{G^0 A}}{2},$$

Renormalization of $\delta\alpha$ and $\delta\beta$: physical (on-shell) scheme OS2 (both schemes)

$$\delta\alpha = s_\alpha c_\alpha\left(\delta_{h\nu_2\bar{\nu}_2} - \delta_{H\nu_2\bar{\nu}_2}\right) + s_\alpha c_\alpha\frac{\delta Z_{hh} - \delta Z_{HH}}{2} + \frac{s_\alpha^2\delta Z_{Hh} - c_\alpha^2\delta Z_{hH}}{2}, \tag{B.89}$$

$$\delta\beta = \frac{1}{t_\beta}\left[\delta_{A\nu_2\bar{\nu}_2} - s_\alpha^2\delta_{H\nu_2\bar{\nu}_2} - c_\alpha^2\delta_{h\nu_2\bar{\nu}_2} + \frac{\delta Z_{AA} - s_\alpha^2\delta Z_{HH} - c_\alpha^2\delta Z_{hh}}{2}\right. \tag{B.90}$$

$$\left. - s_\alpha c_\alpha\frac{\delta Z_{Hh} + \delta Z_{hH}}{2}\right] + \frac{\delta Z_{G^0 A}}{2},$$

> **Renormalization of $\delta\alpha$ and $\delta\beta$: physical (on-shell) scheme OS12 (both schemes)**
>
> $$\delta\alpha = s_\alpha c_\alpha \left(\delta_{h\nu_2\bar{\nu}_2} - \delta_{H\nu_2\bar{\nu}_2}\right) + s_\alpha c_\alpha \frac{\delta Z_{hh} - \delta Z_{HH}}{2} + \frac{s_\alpha^2 \delta Z_{Hh} - c_\alpha^2 \delta Z_{hH}}{2} \ , \qquad \text{(B.91)}$$
>
> $$\delta\beta = s_\beta c_\beta \left[c_{2\alpha} \frac{\delta Z_{HH} - \delta Z_{hh}}{2} - s_{2\alpha} \frac{\delta Z_{Hh} + \delta Z_{hH}}{2} \right] + \frac{\delta Z_{G^0 A}}{2} \qquad \text{(B.92)}$$
>
> $$+ s_\beta c_\beta \left[\delta_{A\nu_2\bar{\nu}_2} - \delta_{A\nu_1\bar{\nu}_1} + c_\alpha^2 \delta_{H\nu_1\bar{\nu}_1} - s_\alpha^2 \delta_{H\nu_2\bar{\nu}_2} + s_\alpha^2 \delta_{h\nu_1\bar{\nu}_1} - c_\alpha^2 \delta_{h\nu_2\bar{\nu}_2} \right] \ .$$

The genuine factorized vertex corrections $\delta_{H\nu_i\bar{\nu}_i}$, $\delta_{h\nu_i\bar{\nu}_i}$ and $\delta_{A\nu_i\bar{\nu}_i}$ (all for $i = 1, 2$) to the couplings of the Higgs bosons with the massive neutrinos are presented in App. D of [216].

B.5.7. Rigid Symmetry Scheme (BFMS scheme)

The definition of the rigid symmetry scheme (BFMS scheme) from [216] is formally independent of the renormalization scheme. The mixing angle CTs are defined through alternative WFRCs which are introduced in the symmetric phase of the potential in the framework of the BFM. In this scheme, the CTs are given by

> **Renormalization of $\delta\alpha$ and $\delta\beta$: BFMS scheme (alternative FJ scheme)**
>
> $$\delta\alpha = \frac{\mathrm{Re}\left[\left[\Sigma_{Hh}^{\mathrm{tad}}(m_H^2) + \Sigma_{Hh}^{\mathrm{tad}}(m_h^2)\right]_{\xi=1} + \Sigma_{Hh}^{\mathrm{add}}(m_H^2) + \Sigma_{Hh}^{\mathrm{add}}(m_h^2)\right]}{2\left(m_H^2 - m_h^2\right)} \ , \qquad \text{(B.93)}$$
>
> $$\delta\beta = \frac{s_{2\beta}}{s_{2\alpha}} \frac{\mathrm{Re}\left[\left[\Sigma_{Hh}^{\mathrm{tad}}(m_h^2) - \Sigma_{Hh}^{\mathrm{tad}}(m_H^2)\right]_{\xi=1} + \Sigma_{Hh}^{\mathrm{add}}(m_h^2) - \Sigma_{Hh}^{\mathrm{add}}(m_H^2)\right]}{2\left(m_H^2 - m_h^2\right)} \qquad \text{(B.94)}$$
>
> $$+ \frac{e}{2m_W \sqrt{1 - \frac{m_W^2}{m_Z^2}}} \left[s_{\beta-\alpha} \frac{\delta T_H}{m_H^2} - c_{\beta-\alpha} \frac{\delta T_h}{m_h^2} \right] \ .$$

B.6. One-Loop Renormalization Constant of the Soft-Z_2-Breaking Parameter m_{12}^2

As a genuine parameter of the tree-level 2HDM potential, the soft-$\mathbb{Z}_2$-breaking parameter m_{12}^2 and its CT are independent of the tadpole renormalization and the latter reads

> **Renormalization of m_{12}^2 (both schemes)**
>
> $$\delta m_{12}^2 = \frac{\alpha_{\mathrm{em}} m_{12}^2}{16\pi m_W^2 \left(1 - \frac{m_W^2}{m_Z^2}\right)} \left[\frac{8m_{12}^2}{s_{2\beta}} - 2m_{H^\pm}^2 - m_A^2 + \frac{s_{2\alpha}}{s_{2\beta}}(m_H^2 - m_h^2) - 3(2m_W^2 + m_Z^2) \right.$$
>
> $$\left. + \sum_u 3m_u^2 \frac{1}{s_\beta^2} - \sum_d 6m_d^2 Y_3 \left(-Y_3 - \frac{1}{t_{2\beta}}\right) - \sum_l 2m_l^2 Y_6 \left(-Y_6 - \frac{1}{t_{2\beta}}\right) \right] \Delta \ , \quad \text{(B.95)}$$

where we sum over all up-type (u) and down-type (d) quarks and charged leptons (l).

One-Loop Electroweak Renormalization Constants of the N2HDM

C.1. One-Loop Renormalization Constants of the Tadpoles

In the standard tadpole scheme, the tadpole terms T_i $(i = 1, 2, s)$ are promoted to one-loop order by means of Eq. (5.1) and fixed by demanding that the loop-corrected VEVs represent the minimum of the loop-corrected scalar potential. This connects the tadpole CTs δT_i directly to the one-loop tadpole diagrams $T_{H_i}^{\text{loop}}$,

$$i\delta T_{H_i} \equiv iT_{H_i}^{\text{loop}} \equiv \begin{pmatrix} \\ \bigcirc \\ \vdots \\ H_i \end{pmatrix} . \tag{C.1}$$

The relations between the tadpole CTs in the mass and gauge bases are given by

$$\delta T_1 = \sum_{j=1}^{3} R_{j1}\delta T_{H_j} \ , \tag{C.2}$$

$$\delta T_2 = \sum_{j=1}^{3} R_{j2}\delta T_{H_j} \ , \tag{C.3}$$

$$\delta T_s = \sum_{j=1}^{3} R_{j3}\delta T_{H_j} \ , \tag{C.4}$$

where the CP-even rotation matrix R is defined in Eq. (9.14). The twelve distinct tadpole terms appearing in the diagonalized mass matrices in Eq. (9.15) and Eqs. (4.33)-(4.34), the latter two presented for the 2HDM being equivalent to the ones in the N2HDM, receive CTs as well which are given by

---

Renormalization of the tadpoles (standard scheme)

$$\delta T_{H_i H_j} = R_{i1} R_{j1} \frac{\delta T_1}{v_1} + R_{i2} R_{j2} \frac{\delta T_2}{v_2} + R_{i3} R_{j3} \frac{\delta T_s}{v_s} \quad (i,j = 1,2,3) \tag{C.5}$$

$$\delta T_{G^0 G^0} = c_\beta \frac{\delta T_1}{v} + s_\beta \frac{\delta T_2}{v} \tag{C.6}$$

$$\delta T_{G^0 A} = -s_\beta \frac{\delta T_1}{v} + c_\beta \frac{\delta T_2}{v} \tag{C.7}$$

$$\delta T_{AA} = \frac{s_\beta^2}{c_\beta} \frac{\delta T_1}{v} + \frac{c_\beta^2}{s_\beta} \frac{\delta T_2}{v} \tag{C.8}$$

$$\delta T_{G^\pm G^\pm} = c_\beta \frac{\delta T_1}{v} + s_\beta \frac{\delta T_2}{v} \tag{C.9}$$

$$\delta T_{G^\pm H^\pm} = -s_\beta \frac{\delta T_1}{v} + c_\beta \frac{\delta T_2}{v} \tag{C.10}$$

$$\delta T_{H^\pm H^\pm} = \frac{s_\beta^2}{c_\beta} \frac{\delta T_1}{v} + \frac{c_\beta^2}{s_\beta} \frac{\delta T_2}{v} \ . \tag{C.11}$$

In the alternative tadpole scheme, the VEVs are the fundamental quantities and hence, the tadpole terms do not receive CTs. Instead, the condition that the tree-level VEVs represent the proper minimum of the potential is imposed at one-loop level, leading to the following definition of the VEV CTs:

$$\begin{pmatrix} \delta v_1 \\ \delta v_2 \\ \delta v_s \end{pmatrix} = R^T \begin{pmatrix} T_{H_1}^{\text{loop}}/m_{H_1}^2 \\ T_{H_2}^{\text{loop}}/m_{H_2}^2 \\ T_{H_3}^{\text{loop}}/m_{H_3}^2 \end{pmatrix} \ . \tag{C.12}$$

As a consequence of this renormalization condition of the minimum of the scalar potential, explicit tadpole contributions in all self-energies and vertex corrections need to be included:

Renormalization of the tadpoles (alternative FJ scheme)

$$\delta T_{ij} = 0 \ , \tag{C.13}$$

$$\Sigma(p^2) \ \rightarrow \ \Sigma^{\text{tad}}(p^2) \ , \tag{C.14}$$

Tadpole diagrams have to be considered in the vertex corrections.

C.2. One-Loop Renormalization Constants of the Gauge Sector

The definitions of all CTs and WFRCs of the gauge sector of the N2HDM are equivalent to the ones of the gauge sector of the 2HDM. Consequently, we do not present the resulting definitions here explicitly but refer to App. B.2 for their presentation.

C.3. One-Loop Renormalization Constants of the Scalar Sector

The diagonal WFRCs of the CP-even Higgs bosons of the 2HDM are independent from tadpole contributions since they are defined over the derivatives of the scalar self-energies. Hence, their explicit forms are the same in both tadpole schemes:

Renormalization of the scalar sector (both schemes)

$$\delta Z_{H_i H_i} = -\text{Re}\left[\frac{\partial \Sigma_{H_i H_i}\left(p^2\right)}{\partial p^2}\right]_{p^2 = m_{H_i}^2} . \tag{C.15}$$

The mass CTs of the CP-even Higgs bosons as well as their off-diagonal WFRCs depend on the chosen tadpole scheme and are explicitly given as follows,

---

Renormalization of the scalar sector (standard scheme)

$$\delta Z_{H_i H_j} = \frac{2}{m_{H_i}^2 - m_{H_j}^2}\text{Re}\left[\Sigma_{H_i H_j}(m_{H_j}^2) - \delta T_{H_i H_j}\right] \quad (i \neq j) , \tag{C.16}$$

$$\delta m_{H_i}^2 = \text{Re}\left[\Sigma_{H_i H_i}(m_{H_i}^2) - \delta T_{H_i H_i}\right] , \tag{C.17}$$

Renormalization of the scalar sector (alternative FJ scheme)

$$\delta Z_{H_i H_j} = \frac{2}{m_{H_i}^2 - m_{H_j}^2}\text{Re}\left[\Sigma_{H_i H_j}^{\text{tad}}(m_{H_j}^2)\right] \quad (i \neq j) , \tag{C.18}$$

$$\delta m_{H_i}^2 = \text{Re}\left[\Sigma_{H_i H_i}^{\text{tad}}(m_{H_i}^2)\right] . \tag{C.19}$$

The CTs and WFRCs of the CP-odd and charged Higgs bosons of the N2HDM are analogous to the ones defined in the 2HDM. Their explicit forms are presented in App. B.3.

C.4. One-Loop Renormalization Constants of the Fermion Sector

The CTs and WFRCs of the fermion sector of the N2HDM are analogously defined to the ones in the 2HDM. For an explicit presentation of their definitions, we refer to App. B.4.

The only difference between the fermion sectors of the two models lies in the different structure of the Yukawa interactions between the Higgs bosons and the fermions. The Yukawa coupling parameters introduced in Table 9.2 are not independent parameters. For convenience, we nevertheless present their CTs as functions of the mixing angle CTs $\delta\alpha_i$ ($i = 1, 2, 3$) and $\delta\beta$, presented in the subsequent App. C.5. The explicit forms of the Yukawa coupling parameter CTs, independently of the 2HDM type chosen, are given by

$$\delta Y_1^f = c_{\alpha_2}\left(c_{\alpha_3}Y_2^f - s_{\alpha_3}Y_3^f\right)\delta\alpha_1 - t_{\alpha_2}Y_1^f\delta\alpha_2 - Y_1^f Y_4^f\delta\beta \tag{C.20}$$

$$\delta Y_2^f = \left(s_{\alpha_2}Y_3^f - c_{\alpha_2}c_{\alpha_3}Y_1^f\right)\delta\alpha_1 - s_{\alpha_3}Y_1^f\delta\alpha_2 + Y_3^f\delta\alpha_3 - Y_2^f Y_4^f\delta\beta \tag{C.21}$$

$$\delta Y_3^f = \left(c_{\alpha_2}s_{\alpha_3}Y_1^f - s_{\alpha_2}Y_2^f\right)\delta\alpha_1 - c_{\alpha_3}Y_1^f\delta\alpha_2 - Y_2^f\delta\alpha_3 - Y_3^f Y_4^f\delta\beta \tag{C.22}$$

$$\delta Y_4^f = -\left(1 + \left(Y_4^f\right)^2\right)\delta\beta . \tag{C.23}$$

C.5. One-Loop Renormalization Constants of the Scalar Mixing Angles

C.5.1. $\overline{\text{MS}}$ Scheme

In the $\overline{\text{MS}}$ scheme, the mixing angle CTs do not receive finite contributions $\delta\alpha_i^{\text{fin}}$ ($i = 1, 2, 3$) and $\delta\beta^{\text{fin}}$ but instead, they only contain the UV-divergent parts proportional to Δ, defined in Eq. (3.2). The resulting CTs are independent of the tadpole scheme and are hence given by

Renormalization of $\delta\alpha_i$ and $\delta\beta$: $\overline{\text{MS}}$ scheme (both schemes)

$$\delta\alpha_i|_{\text{fin}} = 0 \quad (i = 1, 2, 3) \tag{C.24}$$
$$\delta\beta|_{\text{fin}} = 0 \tag{C.25}$$

The analytic forms of the UV-divergent parts of $\delta\alpha$ and $\delta\beta$ are rather intricate. Hence, we do not display them here explicitly.

C.5.2. Adapted KOSY Scheme

The KOSY scheme [222] which connects the definition of the mixing angle CTs with the WFRCs of the scalar doublets is adapted to the N2HDM. Following the same conventions as in the 2HDM presented in App. B.5.2, the corresponding CTs in the standard and alternative FJ tadpole scheme are given by

Renormalization of $\delta\alpha_i$ and $\delta\beta$: adapted KOSY scheme (standard scheme)

$$\delta\alpha_1 = \frac{c_{\alpha_3}\left(\text{Re}\left[\Sigma_{H_1H_2}(m_{H_1}^2) + \Sigma_{H_1H_2}(m_{H_2}^2)\right] - 2\delta T_{H_1H_2}\right)}{2c_{\alpha_2}(m_{H_1}^2 - m_{H_2}^2)} \tag{C.26}$$
$$- \frac{s_{\alpha_3}\left(\text{Re}\left[\Sigma_{H_1H_3}(m_{H_1}^2) + \Sigma_{H_1H_3}(m_{H_3}^2)\right] - 2\delta T_{H_1H_3}\right)}{2c_{\alpha_2}(m_{H_1}^2 - m_{H_3}^2)} \,,$$

$$\delta\alpha_2 = \frac{s_{\alpha_3}\left(\text{Re}\left[\Sigma_{H_1H_2}(m_{H_1}^2) + \Sigma_{H_1H_2}(m_{H_2}^2)\right] - 2\delta T_{H_1H_2}\right)}{2(m_{H_1}^2 - m_{H_2}^2)} \tag{C.27}$$
$$+ \frac{c_{\alpha_3}\left(\text{Re}\left[\Sigma_{H_1H_3}(m_{H_1}^2) + \Sigma_{H_1H_3}(m_{H_3}^2)\right] - 2\delta T_{H_1H_3}\right)}{2(m_{H_1}^2 - m_{H_3}^2)} \,,$$

$$\delta\alpha_3 = \frac{\text{Re}\left[\Sigma_{H_2H_3}(m_{H_2}^2) + \Sigma_{H_2H_3}(m_{H_3}^2)\right] - 2\delta T_{H_2H_3}}{2(m_{H_2}^2 - m_{H_3}^2)} \tag{C.28}$$
$$- \frac{s_{\alpha_2}c_{\alpha_3}\left(\text{Re}\left[\Sigma_{H_1H_2}(m_{H_1}^2) + \Sigma_{H_1H_2}(m_{H_2}^2)\right] - 2\delta T_{H_1H_2}\right)}{2c_{\alpha_2}(m_{H_1}^2 - m_{H_2}^2)}$$
$$+ \frac{s_{\alpha_2}s_{\alpha_3}\left(\text{Re}\left[\Sigma_{H_1H_3}(m_{H_1}^2) + \Sigma_{H_1H_3}(m_{H_3}^2)\right] - 2\delta T_{H_1H_3}\right)}{2c_{\alpha_2}(m_{H_1}^2 - m_{H_3}^2)} \,,$$

$$\delta\beta^o = -\frac{\text{Re}\left[\Sigma_{G^0A}(m_A^2) + \Sigma_{G^0A}(0)\right] - 2\delta T_{G^0A}}{2m_A^2} \,, \tag{C.29}$$

$$\delta\beta^c = -\frac{\text{Re}\left[\Sigma_{G^\pm H^\pm}(m_{H^\pm}^2) + \Sigma_{G^\pm H^\pm}(0)\right] - 2\delta T_{G^\pm H^\pm}}{2m_{H^\pm}^2} \,. \tag{C.30}$$

Renormalization of $\delta\alpha_i$ and $\delta\beta$: adapted KOSY scheme (alternative FJ scheme)

$$\delta\alpha_1 = \frac{c_{\alpha_3}\left(\text{Re}\left[\Sigma^{\text{tad}}_{H_1 H_2}(m^2_{H_1}) + \Sigma^{\text{tad}}_{H_1 H_2}(m^2_{H_2})\right]\right)}{2c_{\alpha_2}(m^2_{H_1} - m^2_{H_2})} - \frac{s_{\alpha_3}\left(\text{Re}\left[\Sigma^{\text{tad}}_{H_1 H_3}(m^2_{H_1}) + \Sigma^{\text{tad}}_{H_1 H_3}(m^2_{H_3})\right]\right)}{2c_{\alpha_2}(m^2_{H_1} - m^2_{H_3})},$$
(C.31)

$$\delta\alpha_2 = \frac{s_{\alpha_3}\left(\text{Re}\left[\Sigma^{\text{tad}}_{H_1 H_2}(m^2_{H_1}) + \Sigma^{\text{tad}}_{H_1 H_2}(m^2_{H_2})\right]\right)}{2(m^2_{H_1} - m^2_{H_2})} + \frac{c_{\alpha_3}\left(\text{Re}\left[\Sigma^{\text{tad}}_{H_1 H_3}(m^2_{H_1}) + \Sigma^{\text{tad}}_{H_1 H_3}(m^2_{H_3})\right]\right)}{2(m^2_{H_1} - m^2_{H_3})},$$
(C.32)

$$\delta\alpha_3 = \frac{\text{Re}\left[\Sigma^{\text{tad}}_{H_2 H_3}(m^2_{H_2}) + \Sigma^{\text{tad}}_{H_2 H_3}(m^2_{H_3})\right]}{2(m^2_{H_2} - m^2_{H_3})} - \frac{s_{\alpha_2}c_{\alpha_3}\left(\text{Re}\left[\Sigma^{\text{tad}}_{H_1 H_2}(m^2_{H_1}) + \Sigma^{\text{tad}}_{H_1 H_2}(m^2_{H_2})\right]\right)}{2c_{\alpha_2}(m^2_{H_1} - m^2_{H_2})}$$
$$+ \frac{s_{\alpha_2}s_{\alpha_3}\left(\text{Re}\left[\Sigma^{\text{tad}}_{H_1 H_3}(m^2_{H_1}) + \Sigma^{\text{tad}}_{H_1 H_3}(m^2_{H_3})\right]\right)}{2c_{\alpha_2}(m^2_{H_1} - m^2_{H_3})},$$
(C.33)

$$\delta\beta^o = -\frac{\text{Re}\left[\Sigma^{\text{tad}}_{G^0 A}(m^2_A) + \Sigma^{\text{tad}}_{G^0 A}(0)\right]}{2m^2_A},$$
(C.34)

$$\delta\beta^c = -\frac{\text{Re}\left[\Sigma^{\text{tad}}_{G^\pm H^\pm}(m^2_{H^\pm}) + \Sigma^{\text{tad}}_{G^\pm H^\pm}(0)\right]}{2m^2_{H^\pm}},$$
(C.35)

We want to emphasize that the adapted KOSY scheme features mixing angle CTs which are manifestly GFP-dependent and that their usage one-loop order yields GFP-dependent partial decay widths.

C.5.3. p_*-Pinched Scheme

In the p_*-pinched scheme, the OS-motivated approach of the adapted KOSY scheme is connected with an unambiguous definition of the GFP-independent part of the self-energies involved in the definition of the mixing angle CTs, given by the pinched scalar self-energies. The mixing angle CTs in this scheme are given by

Renormalization of $\delta\alpha_i$ and $\delta\beta$: p_*-pinched scheme (alternative FJ scheme)

$$\delta\alpha_1 = \frac{c_{\alpha_3}\text{Re}\left[\Sigma^{\text{tad}}_{H_1 H_2}\left(p^2_{*,12}\right)\right]_{\xi=1}}{c_{\alpha_2}(m^2_{H_1} - m^2_{H_2})} - \frac{s_{\alpha_3}\text{Re}\left[\Sigma^{\text{tad}}_{H_1 H_3}\left(p^2_{*,13}\right)\right]_{\xi=1}}{c_{\alpha_2}(m^2_{H_1} - m^2_{H_3})},$$
(C.36)

$$\delta\alpha_2 = \frac{s_{\alpha_3}\text{Re}\left[\Sigma^{\text{tad}}_{H_1 H_2}\left(p^2_{*,12}\right)\right]_{\xi=1}}{m^2_{H_1} - m^2_{H_2}} + \frac{c_{\alpha_3}\text{Re}\left[\Sigma^{\text{tad}}_{H_1 H_3}\left(p^2_{*,13}\right)\right]_{\xi=1}}{m^2_{H_1} - m^2_{H_3}},$$
(C.37)

$$\delta\alpha_3 = \frac{\text{Re}\left[\Sigma^{\text{tad}}_{H_2 H_3}\left(p^2_{*,23}\right)\right]_{\xi=1}}{m^2_{H_2} - m^2_{H_3}} + \frac{s_{\alpha_2}s_{\alpha_3}\text{Re}\left[\Sigma^{\text{tad}}_{H_1 H_3}\left(p^2_{*,13}\right)\right]_{\xi=1}}{c_{\alpha_2}(m^2_{H_1} - m^2_{H_3})}$$
$$- \frac{s_{\alpha_2}c_{\alpha_3}\text{Re}\left[\Sigma^{\text{tad}}_{H_1 H_2}\left(p^2_{*,12}\right)\right]_{\xi=1}}{c_{\alpha_2}(m^2_{H_1} - m^2_{H_2})},$$
(C.38)

$$\delta\beta^o = -\frac{1}{m^2_A}\text{Re}\left[\Sigma^{\text{tad}}_{G^0 A}\left(\frac{m^2_A}{2}\right)\right]_{\xi=1},$$
(C.39)

$$\delta\beta^c = -\frac{1}{m^2_{H^\pm}}\text{Re}\left[\Sigma^{\text{tad}}_{G^\pm H^\pm}\left(\frac{m^2_{H^\pm}}{2}\right)\right]_{\xi=1},$$
(C.40)

where $\delta\beta^o$ and $\delta\beta^c$ are the two variations of the CT definition of the mixing angle β in correspondence to the adapted KOSY scheme and the $p_{*,ij}^2$ are given by

$$p_{*,ij}^2 \equiv \frac{m_{H_i}^2 + m_{H_j}^2}{2} \; . \tag{C.41}$$

C.5.4. OS-Pinched Scheme

The mixing angle CTs in the OS-pinched scheme are given by

Renormalization of $\delta\alpha_i$ and $\delta\beta$: OS-pinched scheme (alternative FJ scheme)

$$\delta\alpha_1 = \frac{c_{\alpha_3}\left(\mathrm{Re}\left[\Sigma_{H_1 H_2}^{\mathrm{tad}}(m_{H_1}^2) + \Sigma_{H_1 H_2}^{\mathrm{tad}}(m_{H_2}^2)\right]_{\xi=1} + \Sigma_{H_1 H_2}^{\mathrm{add}}(m_{H_1}^2) + \Sigma_{H_1 H_2}^{\mathrm{add}}(m_{H_2}^2)\right)}{2c_{\alpha_2}(m_{H_1}^2 - m_{H_2}^2)}$$

$$\tag{C.42}$$

$$- \frac{s_{\alpha_3}\left(\mathrm{Re}\left[\Sigma_{H_1 H_3}^{\mathrm{tad}}(m_{H_1}^2) + \Sigma_{H_1 H_3}^{\mathrm{tad}}(m_{H_3}^2)\right]_{\xi=1} + \Sigma_{H_1 H_3}^{\mathrm{add}}(m_{H_1}^2) + \Sigma_{H_1 H_3}^{\mathrm{add}}(m_{H_3}^2)\right)}{2c_{\alpha_2}(m_{H_1}^2 - m_{H_3}^2)} \; ,$$

$$\delta\alpha_2 = \frac{s_{\alpha_3}\left(\mathrm{Re}\left[\Sigma_{H_1 H_2}^{\mathrm{tad}}(m_{H_1}^2) + \Sigma_{H_1 H_2}^{\mathrm{tad}}(m_{H_2}^2)\right]_{\xi=1} + \Sigma_{H_1 H_2}^{\mathrm{add}}(m_{H_1}^2) + \Sigma_{H_1 H_2}^{\mathrm{add}}(m_{H_2}^2)\right)}{2(m_{H_1}^2 - m_{H_2}^2)}$$

$$\tag{C.43}$$

$$+ \frac{c_{\alpha_3}\left(\mathrm{Re}\left[\Sigma_{H_1 H_3}^{\mathrm{tad}}(m_{H_1}^2) + \Sigma_{H_1 H_3}^{\mathrm{tad}}(m_{H_3}^2)\right]_{\xi=1} + \Sigma_{H_1 H_3}^{\mathrm{add}}(m_{H_1}^2) + \Sigma_{H_1 H_3}^{\mathrm{add}}(m_{H_3}^2)\right)}{2(m_{H_1}^2 - m_{H_3}^2)} \; ,$$

$$\delta\alpha_3 = \frac{\mathrm{Re}\left[\Sigma_{H_2 H_3}^{\mathrm{tad}}(m_{H_2}^2) + \Sigma_{H_2 H_3}^{\mathrm{tad}}(m_{H_3}^2)\right]_{\xi=1} + \Sigma_{H_2 H_3}^{\mathrm{add}}(m_{H_2}^2) + \Sigma_{H_2 H_3}^{\mathrm{add}}(m_{H_3}^2)}{2(m_{H_2}^2 - m_{H_3}^2)} \tag{C.44}$$

$$- \frac{s_{\alpha_2} c_{\alpha_3}\left(\mathrm{Re}\left[\Sigma_{H_1 H_2}^{\mathrm{tad}}(m_{H_1}^2) + \Sigma_{H_1 H_2}^{\mathrm{tad}}(m_{H_2}^2)\right]_{\xi=1} + \Sigma_{H_1 H_2}^{\mathrm{add}}(m_{H_1}^2) + \Sigma_{H_1 H_2}^{\mathrm{add}}(m_{H_2}^2)\right)}{2c_{\alpha_2}(m_{H_1}^2 - m_{H_2}^2)}$$

$$+ \frac{s_{\alpha_2} s_{\alpha_3}\left(\mathrm{Re}\left[\Sigma_{H_1 H_3}^{\mathrm{tad}}(m_{H_1}^2) + \Sigma_{H_1 H_3}^{\mathrm{tad}}(m_{H_3}^2)\right]_{\xi=1} + \Sigma_{H_1 H_3}^{\mathrm{add}}(m_{H_1}^2) + \Sigma_{H_1 H_3}^{\mathrm{add}}(m_{H_3}^2)\right)}{2c_{\alpha_2}(m_{H_1}^2 - m_{H_3}^2)} \; ,$$

$$\delta\beta^o = -\frac{\mathrm{Re}\left[\Sigma_{G^0 A}^{\mathrm{tad}}(m_A^2) + \Sigma_{G^0 A}^{\mathrm{tad}}(0)\right]_{\xi=1} + \Sigma_{G^0 A}^{\mathrm{add}}(m_A^2) + \Sigma_{G^0 A}^{\mathrm{add}}(0)}{2m_A^2} \; , \tag{C.45}$$

$$\delta\beta^c = -\frac{\mathrm{Re}\left[\Sigma_{G^\pm H^\pm}^{\mathrm{tad}}(m_{H^\pm}^2) + \Sigma_{G^\pm H^\pm}^{\mathrm{tad}}(0)\right]_{\xi=1} + \Sigma_{G^\pm H^\pm}^{\mathrm{add}}(m_{H^\pm}^2) + \Sigma_{G^\pm H^\pm}^{\mathrm{add}}(0)}{2m_{H^\pm}^2} \; , \tag{C.46}$$

---

where again the two chosen combinations $\delta\beta^o$ and $\delta\beta^c$ where adapted from the KOSY scheme.

The OS-pinched scheme is analogous to the p_*-pinched scheme, however, the original scale p^2 of the self-energies from the adapted KOSY scheme is adapted in the definition of the mixing angle CTs instead of the p_*^2 scale. Due to this, the additional self-energy contributions derived in [255] for the N2HDM need to be taken into account,

$$\Sigma_{H_i H_j}^{\mathrm{add}}(p^2) = -\frac{\alpha_{\mathrm{em}} m_Z^2}{8\pi m_W^2\left(1 - \frac{m_W^2}{m_Z^2}\right)}\left(p^2 - \frac{m_{H_i}^2 + m_{H_j}^2}{2}\right) \tag{C.47}$$

$$\cdot \left\{\mathcal{O}_{H_i H_j}^{(1)} B_0(p^2; m_Z^2, m_A^2) + \mathcal{O}_{H_i H_j}^{(2)} B_0(p^2; m_Z^2, m_Z^2)\right.$$

$$+ 2\frac{m_W^2}{m_Z^2}\left[\mathcal{O}_{H_iH_j}^{(1)}B_0(p^2;m_W^2,m_{H^\pm}^2) + \mathcal{O}_{H_iH_j}^{(2)}B_0(p^2;m_W^2,m_W^2)\right]\Bigg\}$$

$$\Sigma_{G^0A}^{\text{add}}(p^2) = -\frac{\alpha_{\text{em}}m_Z^2}{8\pi m_W^2\left(1-\frac{m_W^2}{m_Z^2}\right)}\left(p^2 - \frac{m_A^2}{2}\right)\sum_{k=1}^{3}\mathcal{O}_{H_kH_k}^{(3)}B_0(p^2;m_Z^2,m_{H_k}^2) \tag{C.48}$$

$$\Sigma_{G^\pm H^\pm}^{\text{add}}(p^2) = -\frac{\alpha_{\text{em}}}{4\pi\left(1-\frac{m_W^2}{m_Z^2}\right)}\left(p^2 - \frac{m_{H^\pm}^2}{2}\right)\sum_{k=1}^{3}\mathcal{O}_{H_kH_k}^{(3)}B_0(p^2;m_Z^2,m_{H_k}^2) \tag{C.49}$$

where the short-hand notations $\mathcal{O}_{H_iH_j}^{(x)}$ $(x = 1, 2, 3)$ are introduced in Eqs. (9.30) to (9.32). While some of these additional self-energy contributions are UV-divergent, they only appear in the definition of the mixing angle CTs in combinations which are explicitly UV-finite.

C.6. One-Loop Renormalization Constant of the Soft-Z_2-Breaking Parameter m_{12}^2

As a genuine parameter of the tree-level N2HDM potential, the soft-$\mathbb{Z}_2$-breaking parameter m_{12}^2 and its CT are independent of the tadpole renormalization and in both schemes read

---

Renormalization of m_{12}^2 (both schemes)

$$\delta m_{12}^2 = \frac{\alpha_{\text{em}}m_{12}^2}{16\pi m_W^2\left(1-\frac{m_W^2}{m_Z^2}\right)}\left[\frac{8m_{12}^2}{s_{2\beta}} - 2m_{H^\pm}^2 - m_A^2 + \sum_{i=1}^{3}R_{i1}R_{i2}m_{H_i}^2 - 3(2m_W^2 + m_Z^2)\right.$$

$$\left. + \sum_u 3m_u^2\frac{1}{s_\beta^2} + \sum_d 6m_d^2 Y_4^d\left(Y_4^d - \frac{1}{t_{2\beta}}\right) + \sum_l 2m_l^2 Y_4^l\left(Y_4^l - \frac{1}{t_{2\beta}}\right)\right]\Delta \tag{C.50}$$

---

where we sum over all up-type (u) and down-type (d) quarks and charged leptons (l).

C.7. One-Loop Renormalization Constant of v_s

The CT Δv_s of the singlet VEV is renormalized in an $\overline{\text{MS}}$ scheme. In the standard tadpole scheme, the CT contains at most finite contributions $\Delta v_s|_{\text{fin}}$ due to the rigid symmetry of the potential and hence, we can choose to set the finite contributions to zero. In the alternative FJ tadpole scheme on the other hand, Δv_s contains UV-divergent contributions but since we apply an $\overline{\text{MS}}$ scheme, its finite contributions vanish again. Consequently, the CT in both schemes is given by

---

Renormalization of the tree-level v_s (both schemes)

$$\Delta v_s|_{\text{fin}} = 0 . \tag{C.51}$$

Due to its intricate analytic structure, we do not state the UV-divergent part of the CT in the alternative FJ tadpole scheme explicitly.

NMSSM Higgs Boson Mass Matrices and Their Counterterms

In this appendix, we present the analytic expressions of the mass matrices of the neutral and charged Higgs bosons in the complex NMSSM together with their CTs at one- and two-loop order. Furthermore, we present the CTs of the charged Higgs boson mass and of the parameter $\mathrm{Re}(A_\lambda)$. The tree-level matrices presented in this appendix are given in the most general form, *i.e.* for their presentation we do not apply any of the approximations which are used for the actual calculation of the two-loop corrections of the Higgs boson masses, while for the CTs, we restrict the presentation to the contributions relevant for the $\mathcal{O}(\alpha_t^2)$ two-loop contributions.

D.1. Neutral Higgs Boson Mass Matrix at Tree Level

All elements of the neutral Higgs mass matrix in the complex NMSSM, expressed through the set of independent parameters presented in Eq. (14.71), are given in analytic form in the following. We restrict the presentation of the matrix elements to the 5×5-dimensional sub-matrix without the Goldstone boson admixture. Since the tadpole parameters, actually vanishing at tree level, and moreover the parameter β, defined via the ratio of the VEVs of the two Higgs doublets in Eq. (14.11), receive CT contributions while the mixing angle β_n, introduced in Eq. (14.44), does not, we present these parameters here explicitly as well. At tree level as well as after the promotion of all independent parameters to higher orders through the introduction of their CTs, the tadpole parameters vanish and $\beta_n \to \beta$ holds. The elements of the neutral Higgs mass matrix are given by

$$(\mathcal{M}_{hh}^2)_{h_d h_d} = \frac{1}{2}|\lambda|^2 s_\beta^2 v^2 + c_\beta^2 m_Z^2 - m_W^2 s_\beta^2 + \frac{m_{H^\pm}^2 s_\beta^2}{c_{\beta-\beta_n}^2} + \frac{c_{\beta_n} T_{h_d}(c_\beta c_{\beta_n} + 2 s_\beta s_{\beta_n})}{c_{\beta-\beta_n}^2 v} \qquad (\text{D.1})$$
$$- \frac{c_{\beta_n}^2 s_\beta T_{h_u}}{c_{\beta-\beta_n}^2 v} \; ,$$

$$(\mathcal{M}_{hh}^2)_{h_d h_u} = \frac{1}{2}|\lambda|^2 s_{2\beta} v^2 + \frac{m_W^2 s_{2\beta}}{2} - \frac{m_Z^2 s_{2\beta}}{2} - \frac{m_{H^\pm}^2 s_{2\beta}}{2 c_{\beta-\beta_n}^2} + \frac{c_\beta c_{\beta_n}^2 T_{h_u}}{c_{\beta-\beta_n}^2 v} + \frac{s_\beta s_{\beta_n}^2 T_{h_d}}{c_{\beta-\beta_n}^2 v} \; , \qquad (\text{D.2})$$

$$(\mathcal{M}^2_{hh})_{h_d h_s} = -\frac{1}{2}|\kappa||\lambda|c_{\varphi_y}s_\beta v v_s - \frac{|\lambda|^2 c_\beta v(s_\beta^2 v^2 - 2v_s^2)}{2v_s} - \frac{c_\beta m_{H^\pm}^2 s_\beta^2 v}{c_{\beta-\beta_n}^2 v_s} \tag{D.3}$$

$$+ \frac{c_\beta m_W^2 s_\beta^2 v}{v_s} + \frac{c_{\beta_n}^2 s_{2\beta} T_{h_u}}{2c_{\beta-\beta_n}^2 v_s} + \frac{s_\beta^2 s_{\beta_n}^2 T_{h_d}}{c_{\beta-\beta_n}^2 v_s} \,,$$

$$(\mathcal{M}^2_{hh})_{h_d a} = \frac{c_{\beta_n} T_{a_d}}{s_\beta v} \,, \tag{D.4}$$

$$(\mathcal{M}^2_{hh})_{h_d a_s} = \frac{3}{2}|\kappa||\lambda|s_\beta s_{\varphi_y} v v_s + \frac{T_{a_d}}{v_s} \,, \tag{D.5}$$

$$(\mathcal{M}^2_{hh})_{h_u h_u} = \frac{1}{2}|\lambda|^2 c_\beta^2 v^2 + \frac{c_\beta^2 m_{H^\pm}^2}{c_{\beta-\beta_n}^2} - c_\beta^2 m_W^2 + m_Z^2 s_\beta^2 + \frac{s_{\beta_n} T_{h_u}(2c_\beta c_{\beta_n} + s_\beta s_{\beta_n})}{c_{\beta-\beta_n}^2 v} \tag{D.6}$$

$$- \frac{c_\beta s_{\beta_n}^2 T_{h_d}}{c_{\beta-\beta_n}^2 v} \,,$$

$$(\mathcal{M}^2_{hh})_{h_u h_s} = -\frac{1}{2}|\kappa||\lambda|c_\beta c_{\varphi_y} v v_s - \frac{|\lambda|^2 s_\beta v(c_\beta^2 v^2 - 2v_s^2)}{2v_s} - \frac{c_\beta^2 m_{H^\pm}^2 s_\beta v}{c_{\beta-\beta_n}^2 v_s} \tag{D.7}$$

$$+ \frac{c_\beta^2 m_W^2 s_\beta v}{v_s} + \frac{c_\beta^2 c_{\beta_n}^2 T_{h_u}}{c_{\beta-\beta_n}^2 v_s} + \frac{s_{2\beta} s_{\beta_n}^2 T_{h_d}}{2c_{\beta-\beta_n}^2 v_s} \,,$$

$$(\mathcal{M}^2_{hh})_{h_u a} = \frac{s_{\beta_n} T_{a_d}}{s_\beta v} \,, \tag{D.8}$$

$$(\mathcal{M}^2_{hh})_{h_u a_s} = \frac{3}{2}|\kappa||\lambda|c_\beta s_{\varphi_y} v v_s + \frac{c_\beta T_{a_d}}{s_\beta v_s} \,, \tag{D.9}$$

$$(\mathcal{M}^2_{hh})_{h_s h_s} = 2|\kappa|^2 v_s^2 - \frac{|\kappa||\lambda|s_{2\beta} v^2(c_{\varphi_\omega} c_{\varphi_y} + 3s_{\varphi_\omega} s_{\varphi_y})}{4c_{\varphi_\omega}} + \frac{|\kappa|\mathrm{Re}(A_\kappa)v_s}{\sqrt{2}c_{\varphi_\omega}} + \frac{m_{H^\pm}^2 s_{2\beta}^2 v^2}{4c_{\beta-\beta_n}^2 v_s^2} \tag{D.10}$$

$$+ \frac{|\lambda|^2 s_{2\beta}^2 v^4}{8v_s^2} - \frac{m_W^2 s_{2\beta}^2 v^2}{4v_s^2} - \frac{c_\beta^2 c_{\beta_n}^2 s_\beta T_{h_u} v}{c_{\beta-\beta_n}^2 v_s^2} - \frac{c_\beta s_\beta^2 s_{\beta_n}^2 T_{h_d} v}{c_{\beta-\beta_n}^2 v_s^2} + \frac{T_{h_s}}{v_s}$$

$$+ \frac{s_{\varphi_\omega}(T_{a_s} v_s - c_\beta T_{a_d} v)}{c_{\varphi_\omega} v_s^2} \,,$$

$$(\mathcal{M}^2_{hh})_{h_s a} = -\frac{1}{2}|\kappa||\lambda|c_{\beta-\beta_n} s_{\varphi_y} v v_s + \frac{c_{\beta-\beta_n} T_{a_d}}{s_\beta v_s} \,, \tag{D.11}$$

$$(\mathcal{M}^2_{hh})_{h_s a_s} = -|\kappa||\lambda|s_{2\beta} s_{\varphi_y} v^2 + \frac{2T_{a_s} v_s - 2c_\beta T_{a_d} v}{v_s^2} \,, \tag{D.12}$$

$$(\mathcal{M}^2_{hh})_{aa} = \frac{1}{2}|\lambda|^2 c_{\beta-\beta_n}^2 v^2 - c_{\beta-\beta_n}^2 m_W^2 + m_{H^\pm}^2 \,, \tag{D.13}$$

$$(\mathcal{M}^2_{hh})_{aa_s} = -\frac{3}{2}|\kappa||\lambda|c_{\beta-\beta_n}c_{\varphi_y}vv_s + \frac{|\lambda|^2c_{\beta-\beta_n}s_{2\beta}v^3}{4v_s} + \frac{m^2_{H^\pm}s_{2\beta}v}{2c_{\beta-\beta_n}v_s} - \frac{c_{\beta-\beta_n}m^2_Ws_{2\beta}v}{2v_s} \quad \text{(D.14)}$$

$$- \frac{c_\beta c^2_{\beta_n}T_{h_u}}{c_{\beta-\beta_n}v_s} - \frac{s_\beta s^2_{\beta_n}T_{h_d}}{c_{\beta-\beta_n}v_s} \; ,$$

$$(\mathcal{M}^2_{hh})_{a_s a_s} = \frac{3|\kappa||\lambda|s_{2\beta}v^2(c_{\varphi_\omega}c_{\varphi_y} + 3s_{\varphi_\omega}s_{\varphi_y})}{4c_{\varphi_\omega}} - \frac{3|\kappa|\text{Re}(A_\kappa)v_s}{\sqrt{2}c_{\varphi_\omega}} + \frac{|\lambda|^2s^2_{2\beta}v^4}{8v^2_s} + \frac{T_{h_s}}{v_s} \quad \text{(D.15)}$$

$$- \frac{m^2_Ws^2_{2\beta}v^2}{4v^2_s} - \frac{c^2_\beta c^2_{\beta_n}s_\beta T_{h_u}v}{c^2_{\beta-\beta_n}v^2_s} - \frac{c_\beta s^2_\beta s^2_{\beta_n}T_{h_d}v}{c^2_{\beta-\beta_n}v^2_s} + \frac{m^2_{H^\pm}s^2_{2\beta}v^2}{4c^2_{\beta-\beta_n}v^2_s}$$

$$+ \frac{3s_{\varphi_\omega}(c_\beta T_{a_d}v - T_{a_s}v_s)}{c_{\varphi_\omega}v^2_s} \; .$$

In order to apply the gaugeless limit to the mass matrix elements, the simultaneous limits $m_W, m_Z \to 0$ are applied while the VEV v is kept at a constant non-vanishing value.

D.2. Neutral Higgs Boson Mass Matrix Counterterm at One- and Two-Loop Level

The one-loop CT of the neutral Higgs boson mass matrix consists of genuine one-loop CT contributions $(\Delta^{(1)}\mathcal{M}^2_{hh})_{\phi_i\phi_j}$, while the two-loop CT contains not only genuine two-loop CT contributions $(\Delta^{(2)}\mathcal{M}^2_{hh})_{\phi_i\phi_j}$, but moreover contributions $(\Delta^{(1)(1)}\mathcal{M}^2_{hh})_{\phi_i\phi_j}$ from products of two one-loop CTs (all terms given in the basis $(\phi_i, \phi_j = h_d, h_u, h_s, a, a_s)$ without the Goldstone boson admixture). The genuine CT contributions to n^{th} loop order ($n = 1, 2$) are given by

$$(\Delta^{(n)}\mathcal{M}^2_{hh})_{h_dh_d} = v|\lambda|^2s^2_\beta\delta^{(n)}v + s^2_\beta\delta^{(n)}m^2_{H^\pm} + \frac{\delta^{(n)}T_{h_d}(1-s^4_\beta)}{vc_\beta} - \frac{\delta^{(n)}T_{h_u}s_\beta c^2_\beta}{v} \quad \text{(D.16)}$$

$$+ c^3_\beta s_\beta\left(|\lambda|^2v^2 + 2m^2_{H^\pm}\right)\delta^{(n)}t_\beta + s^2_\beta v^2|\lambda|\delta^{(n)}|\lambda|$$

$$(\Delta^{(n)}\mathcal{M}^2_{hh})_{h_dh_u} = v|\lambda|^2s_\beta c_\beta\delta^{(n)}v - s_\beta c_\beta\delta^{(n)}m^2_{H^\pm} + \frac{s^3_\beta\delta^{(n)}T_{h_d}}{v} + \frac{c^3_\beta\delta^{(n)}T_{h_u}}{v} \quad \text{(D.17)}$$

$$+ s_\beta c_\beta v^2|\lambda|\delta^{(n)}|\lambda| + \frac{1}{2}c^2_\beta c_{2\beta}(|\lambda|^2v^2 - 2m^2_{H^\pm})\delta^{(n)}t_\beta$$

$$(\Delta^{(n)}\mathcal{M}^2_{hh})_{h_dh_s} = \frac{c^3_\beta\delta^{(n)}T_{h_u}s_\beta}{v_s} + \frac{\delta^{(n)}T_{h_d}s^4_\beta}{v_s} - \frac{c_\beta\delta^{(n)}m^2_{H^\pm}s^2_\beta v}{v_s} \quad \text{(D.18)}$$

$$+ \delta^{(n)}v\left[-\frac{c_\beta m^2_{H^\pm}s^2_\beta}{v_s} - \frac{1}{2}|\kappa||\lambda|c_{\varphi_y}s_\beta v_s - \frac{|\lambda|^2c_\beta(3s^2_\beta v^2 - 2v^2_s)}{2v_s}\right]$$

$$- \frac{1}{2}|\lambda|c_{\varphi_y}\delta^{(n)}|\kappa|s_\beta vv_s + \delta^{(n)}|\lambda|\left[-\frac{1}{2}|\kappa|c_{\varphi_y}s_\beta vv_s + |\lambda|c_\beta\left(2vv_s - \frac{s^2_\beta v^3}{v_s}\right)\right]$$

$$+ \delta^{(n)}v_s\left[-\frac{1}{2}|\kappa||\lambda|c_{\varphi_y}s_\beta v + \frac{c_\beta m^2_{H^\pm}s^2_\beta v}{v^2_s} + \frac{|\lambda|^2c_\beta v(s^2_\beta v^2 + 2v^2_s)}{2v^2_s}\right]$$

$$+ \delta^{(n)}t_\beta\left[\frac{c^2_\beta m^2_{H^\pm}s_\beta(-2c^2_\beta + s^2_\beta)v}{v_s} - \frac{1}{2}|\kappa||\lambda|c^3_\beta c_{\varphi_y}vv_s\right]$$

$$\left. - \frac{|\lambda|^2 c_\beta^2 s_\beta v \left(\left(2c_\beta^2 - s_\beta^2\right)v^2 + 2v_s^2 \right)}{2v_s} \right]$$

$$(\Delta^{(n)} \mathcal{M}_{hh}^2)_{h_d a} = \frac{\delta^{(n)} T_{a_d}}{t_\beta v} \tag{D.19}$$

$$(\Delta^{(n)} \mathcal{M}_{hh}^2)_{h_d a_s} = \frac{\delta^{(n)} T_{a_d}}{v_s} + \frac{3}{2}|\kappa||\lambda|\delta^{(n)}v s_\beta s_{\varphi_y} v_s + \frac{3}{2}|\kappa||\lambda|\delta^{(n)}v_s s_\beta s_{\varphi_y} v \tag{D.20}$$

$$+ \frac{3}{2}|\kappa||\lambda|c_\beta^3 \, \delta^{(n)} t_\beta s_{\varphi_y} v v_s + \frac{3}{2}|\lambda|\delta^{(n)}|\kappa| s_\beta s_{\varphi_y} v v_s + \frac{3}{2}|\kappa|\delta^{(n)}|\lambda| s_\beta s_{\varphi_y} v v_s$$

$$(\Delta^{(n)} \mathcal{M}_{hh}^2)_{h_u h_u} = c_\beta^2 \delta^{(n)} m_{H^\pm}^2 - \frac{c_\beta \delta^{(n)} T_{h_d} s_\beta^2}{v} + \frac{\delta^{(n)} T_{h_u} \left(2c_\beta^2 s_\beta + s_\beta^3\right)}{v} \tag{D.21}$$

$$+ |\lambda|c_\beta^2 \delta^{(n)}|\lambda|v^2 + \delta^{(n)} t_\beta \left(-2c_\beta^3 m_{H^\pm}^2 s_\beta - |\lambda|^2 c_\beta^3 s_\beta v^2\right) + |\lambda|^2 v c_\beta^2 \delta^{(n)} v$$

$$(\Delta^{(n)} \mathcal{M}_{hh}^2)_{h_u h_s} = \frac{c_\beta^4 \delta^{(n)} T_{h_u}}{v_s} + \frac{c_\beta \delta^{(n)} T_{h_d} s_\beta^3}{v_s} - \frac{c_\beta^2 \delta^{(n)} m_{H^\pm}^2 s_\beta v}{v_s} \tag{D.22}$$

$$+ \delta^{(n)} v \left[-\frac{c_\beta^2 m_{H^\pm}^2 s_\beta}{v_s} - \frac{1}{2}|\kappa||\lambda|c_\beta c_{\varphi_y} v_s - \frac{|\lambda|^2 s_\beta \left(3c_\beta^2 v^2 - 2v_s^2\right)}{2v_s} \right]$$

$$+ \delta^{(n)}|\lambda| \left[-\frac{1}{2}|\kappa|c_\beta c_{\varphi_y} v v_s + |\lambda| \left(-\frac{c_\beta^2 s_\beta v^3}{v_s} + 2s_\beta v v_s \right) \right]$$

$$+ \delta^{(n)} t_\beta \left[-\frac{c_\beta^3 m_{H^\pm}^2 \left(c_\beta^2 - 2s_\beta^2\right)v}{v_s} + \frac{1}{2}|\kappa||\lambda|c_\beta^2 c_{\varphi_y} s_\beta v v_s \right.$$

$$\left. - \frac{|\lambda|^2 c_\beta^3 v \left(\left(c_\beta^2 - 2s_\beta^2\right)v^2 - 2v_s^2 \right)}{2v_s} \right] - \frac{1}{2}|\lambda|c_\beta c_{\varphi_y} \delta^{(n)}|\kappa| v v_s$$

$$+ \delta^{(n)} v_s \left[-\frac{1}{2}|\kappa||\lambda|c_\beta c_{\varphi_y} v + \frac{c_\beta^2 m_{H^\pm}^2 s_\beta v}{v_s^2} + \frac{|\lambda|^2 s_\beta v \left(c_\beta^2 v^2 + 2v_s^2\right)}{2v_s^2} \right]$$

$$(\Delta^{(n)} \mathcal{M}_{hh}^2)_{h_u a} = \frac{\delta^{(n)} T_{a_d}}{v} \tag{D.23}$$

$$(\Delta^{(n)} \mathcal{M}_{hh}^2)_{h_u a_s} = \frac{3}{2}|\kappa||\lambda|c_\beta \delta^{(n)}v s_{\varphi_y} v_s + \frac{3}{2}|\kappa||\lambda|c_\beta \delta^{(n)}v_s s_{\varphi_y} v + \frac{3}{2}|\lambda|c_\beta \delta^{(n)}|\kappa| s_{\varphi_y} v v_s \tag{D.24}$$

$$+ \frac{c_\beta \delta^{(n)} T_{a_d}}{s_\beta v_s} + \frac{3}{2}|\kappa|c_\beta \delta^{(n)}|\lambda| s_{\varphi_y} v v_s - \frac{3}{2}|\kappa||\lambda|c_\beta^2 \delta^{(n)} t_\beta s_\beta s_{\varphi_y} v v_s$$

$$(\Delta^{(n)} \mathcal{M}_{hh}^2)_{h_s h_s} = \delta^{(n)} v \left[-\frac{1}{2}|\kappa||\lambda|s_{2\beta}(c_{\varphi_y} + 3s_{\varphi_y}t_{\varphi_\omega})v + \frac{m_{H^\pm}^2 s_{2\beta}^2 v}{2v_s^2} + \frac{|\lambda|^2 s_{2\beta}^2 v^3}{2v_s^2} \right] \tag{D.25}$$

$$- \frac{c_\beta^4 \delta^{(n)} T_{h_u} s_\beta v}{v_s^2} - \frac{c_\beta \delta^{(n)} T_{h_d} s_\beta^4 v}{v_s^2} - \frac{c_\beta \delta^{(n)} T_{a_d} t_{\varphi_\omega} v}{v_s^2} + \frac{\delta^{(n)} m_{H^\pm}^2 s_{2\beta}^2 v^2}{4v_s^2}$$

$$+ \delta^{(n)}|\lambda| \left[-\frac{1}{4}|\kappa|s_{2\beta}(c_{\varphi_y} + 3s_{\varphi_y}t_{\varphi_\omega})v^2 + \frac{|\lambda|s_{2\beta}^2 v^4}{4v_s^2} \right]$$

$$+ \delta^{(n)}t_\beta \left[-\frac{1}{2}|\kappa||\lambda|c_{2\beta}c_\beta^2(c_{\varphi_y} + 3s_{\varphi_y}t_{\varphi_\omega})v^2 + \frac{2c_{2\beta}c_\beta^3 m_{H^\pm}^2 s_\beta v^2}{v_s^2} \right.$$

$$\left. + \frac{|\lambda|^2 c_{2\beta}c_\beta^3 s_\beta v^4}{v_s^2} \right] + \frac{|\kappa|v_s \delta^{(n)}\mathrm{Re}(A_\kappa)}{\sqrt{2}c_{\varphi_\omega}} + \frac{\delta^{(n)}T_{h_s}}{v_s} + \frac{\delta^{(n)}T_{a_s}t_{\varphi_\omega}}{v_s}$$

$$+ \delta^{(n)}v_s \left[\frac{|\kappa|\mathrm{Re}(A_\kappa)}{\sqrt{2}c_{\varphi_\omega}} - \frac{m_{H^\pm}^2 s_{2\beta}^2 v^2}{2v_s^3} - \frac{|\lambda|^2 s_{2\beta}^2 v^4}{4v_s^3} + 4|\kappa|^2 v_s \right]$$

$$+ \delta^{(n)}|\kappa| \left[-\frac{1}{4}|\lambda|s_{2\beta}(c_{\varphi_y} + 3s_{\varphi_y}t_{\varphi_\omega})v^2 + \frac{\mathrm{Re}(A_\kappa)v_s}{\sqrt{2}c_{\varphi_\omega}} + 4|\kappa|v_s^2 \right]$$

$$(\Delta^{(n)}\mathcal{M}_{hh}^2)_{h_s a} = -\frac{1}{2}|\lambda|\delta^{(n)}|\kappa|s_{\varphi_y}vv_s - \frac{1}{2}|\kappa|\delta^{(n)}|\lambda|s_{\varphi_y}vv_s - \frac{1}{2}|\kappa||\lambda|\delta^{(n)}v_s s_{\varphi_y}v \tag{D.26}$$

$$+ \frac{\delta^{(n)}T_{a_d}}{s_\beta v_s} - \frac{1}{2}|\kappa||\lambda|\delta^{(n)}v s_{\varphi_y}v_s$$

$$(\Delta^{(n)}\mathcal{M}_{hh}^2)_{h_s a_s} = -2|\kappa||\lambda|\delta^{(n)}v s_{2\beta}s_{\varphi_y}v - \frac{2c_\beta \delta^{(n)}T_{a_d}v}{v_s^2} + \frac{2\delta^{(n)}T_{a_s}}{v_s} - |\kappa|\delta^{(n)}|\lambda|s_{2\beta}s_{\varphi_y}v^2 \tag{D.27}$$

$$- 2|\kappa||\lambda|c_\beta^2 c_{2\beta}\delta^{(n)}t_\beta s_{\varphi_y}v^2 - |\lambda|\delta^{(n)}|\kappa|s_{2\beta}s_{\varphi_y}v^2$$

$$(\Delta^{(n)}\mathcal{M}_{hh}^2)_{aa} = \delta^{(n)}m_{H^\pm}^2 + |\lambda|^2 v\delta^{(n)}v + |\lambda|\delta^{(n)}|\lambda|v^2 \tag{D.28}$$

$$(\Delta^{(n)}\mathcal{M}_{hh}^2)_{aa_s} = -\frac{c_\beta^3 \delta^{(n)}T_{h_u}}{v_s} - \frac{\delta^{(n)}T_{h_d}s_\beta^3}{v_s} + \frac{\delta^{(n)}m_{H^\pm}^2 s_{2\beta}v}{2v_s} - \frac{3}{2}|\lambda|\ c_{\varphi_y}\delta^{(n)}|\kappa|vv_s \tag{D.29}$$

$$+ \delta^{(n)}v \left[\frac{m_{H^\pm}^2 s_{2\beta}}{2v_s} + \frac{3|\lambda|^2 s_{2\beta}v^2}{4v_s} - \frac{3}{2}|\kappa||\lambda|c_{\varphi_y}v_s \right]$$

$$+ \delta^{(n)}v_s \left[-\frac{3}{2}|\kappa||\lambda|c_{\varphi_y}v - \frac{m_{H^\pm}^2 s_{2\beta}v}{2v_s^2} - \frac{|\lambda|^2 s_{2\beta}v^3}{4v_s^2} \right]$$

$$+ \delta^{(n)}t_\beta \left[\frac{c_\beta^2 c_{2\beta}m_{H^\pm}^2 v}{v_s} + \frac{|\lambda|^2 c_{2\beta}c_\beta^2 v^3}{2v_s} \right]$$

$$+ \delta^{(n)}|\lambda| \left[\frac{|\lambda|s_{2\beta}v^3}{2v_s} - \frac{3}{2}|\kappa|c_{\varphi_y}vv_s \right]$$

$$(\Delta^{(n)}\mathcal{M}_{hh}^2)_{a_s a_s} = \delta^{(n)}v \left[\frac{3}{2}|\kappa||\lambda|s_{2\beta}(c_{\varphi_y} + 3s_{\varphi_y}t_{\varphi_\omega})v + \frac{m_{H^\pm}^2 s_{2\beta}^2 v}{2v_s^2} + \frac{|\lambda|^2 s_{2\beta}^2 v^3}{2v_s^2} \right] \tag{D.30}$$

$$- \frac{c_\beta^4 \delta^{(n)}T_{h_u}s_\beta v}{v_s^2} - \frac{c_\beta \delta^{(n)}T_{h_d}s_\beta^4 v}{v_s^2} + \frac{3c_\beta \delta^{(n)}T_{a_d}t_{\varphi_\omega}v}{v_s^2} - \frac{3\delta^{(n)}T_{a_s}t_{\varphi_\omega}}{v_s}$$

$$+ \delta^{(\mathrm{n})} v_s \left[-\frac{3|\kappa|\mathrm{Re}(A_\kappa)}{\sqrt{2}c_{\varphi_\omega}} - \frac{m_{H^\pm}^2 s_{2\beta}^2 v^2}{2v_s^3} - \frac{|\lambda|^2 s_{2\beta}^2 v^4}{4v_s^3} \right]$$

$$+ \delta^{(\mathrm{n})} |\lambda| \left[\frac{3}{4}|\kappa| s_{2\beta}(c_{\varphi_y} + 3s_{\varphi_y} t_{\varphi_\omega}) v^2 + \frac{|\lambda| s_{2\beta}^2 v^4}{4v_s^2} \right] + \frac{\delta^{(\mathrm{n})} T_{h_s}}{v_s}$$

$$+ \delta^{(\mathrm{n})} t_\beta \left[\frac{3}{2}|\kappa||\lambda| c_{2\beta} c_\beta^2 (c_{\varphi_y} + 3s_{\varphi_y} t_{\varphi_\omega}) v^2 + \frac{2c_{2\beta} c_\beta^3 m_{H^\pm}^2 s_\beta v^2}{v_s^2} \right.$$

$$\left. + \frac{|\lambda|^2 c_{2\beta} c_\beta^3 s_\beta v^4}{v_s^2} \right] - \frac{3|\kappa| v_s \delta^{(\mathrm{n})} \mathrm{Re}(A_\kappa)}{\sqrt{2}c_{\varphi_\omega}} + \frac{\delta^{(\mathrm{n})} m_{H^\pm}^2 s_{2\beta}^2 v^2}{4v_s^2}$$

$$+ \delta^{(\mathrm{n})} |\kappa| \left[\frac{3}{4}|\lambda| s_{2\beta}(c_{\varphi_y} + 3s_{\varphi_y} t_{\varphi_\omega}) v^2 - \frac{3\mathrm{Re}(A_\kappa) v_s}{\sqrt{2}c_{\varphi_\omega}} \right],$$

while the contribution consisting of products of one-loop CTs explicitly reads

$$(\Delta^{(1)(1)} \mathcal{M}_{hh}^2)_{h_d h_d} = |\lambda|^2 (\delta^{(1)} v)^2 s_\beta^2 - \frac{2\delta^{(1)} T_{h_d} \delta^{(1)} v \left(c_\beta^3 + 2c_\beta s_\beta^2 \right)}{v^2} + \frac{2c_\beta^2 \delta^{(1)} T_{h_u} \delta^{(1)} v s_\beta}{v^2} \qquad \text{(D.31)}$$

$$+ 4|\lambda| \delta^{(1)} |\lambda| \delta^{(1)} v s_\beta^2 v + (\delta^{(1)} |\lambda|)^2 s_\beta^2 v^2 + c_\beta^6 (\delta^{(1)} t_\beta)^2 \left(|\lambda|^2 v^2 + 2m_{H^\pm}^2 \right)$$

$$+ 4c_\beta^3 \delta^{(1)} t_\beta s_\beta \left(|\lambda| \delta^{(1)} |\lambda| v^2 + \delta^{(1)} m_{H^\pm}^2 \right) + 4|\lambda|^2 c_\beta^3 \delta^{(1)} t_\beta \delta^{(1)} v s_\beta v$$

$$- \frac{2c_\beta^5 \delta^{(1)} t_\beta \delta^{(1)} T_{h_u}}{v} + \frac{2c_\beta^4 \delta^{(1)} t_\beta \delta^{(1)} T_{h_d} s_\beta}{v}$$

$$(\Delta^{(1)(1)} \mathcal{M}_{hh}^2)_{h_d h_u} = 2|\lambda| \delta^{(1)} |\lambda| \delta^{(1)} v s_{2\beta} v - \frac{2c_\beta^3 \delta^{(1)} T_{h_u} \delta^{(1)} v}{v^2} - \frac{2\delta^{(1)} T_{h_d} \delta^{(1)} v s_\beta^3}{v^2} \qquad \text{(D.32)}$$

$$+ \frac{1}{2}|\lambda|^2 (\delta^{(1)} v)^2 s_{2\beta} + 2|\lambda|^2 c_{2\beta} c_\beta^2 \delta^{(1)} t_\beta \delta^{(1)} v v - \frac{2c_\beta^4 \delta^{(1)} t_\beta \delta^{(1)} T_{h_u} s_\beta}{v} + \frac{2c_\beta^3 \delta^{(1)} t_\beta \delta^{(1)} T_{h_d} s_\beta^2}{v}$$

$$+ c_\beta^5 (\delta^{(1)} t_\beta)^2 s_\beta \left(2m_{H^\pm}^2 - |\lambda|^2 v^2 \right) - 2c_{2\beta} c_\beta^2 \delta^{(1)} t_\beta \left(\delta^{(1)} m_{H^\pm}^2 - |\lambda| \delta^{(1)} |\lambda| v^2 \right)$$

$$+ \frac{1}{2} (\delta^{(1)} |\lambda|)^2 s_{2\beta} v^2$$

$$(\Delta^{(1)(1)} \mathcal{M}_{hh}^2)_{h_d h_s} = -\frac{3|\lambda|^2 c_\beta (\delta^{(1)} v)^2 s_\beta^2 v}{v_s} - \frac{2c_\beta (\delta^{(1)} m_{H^\pm}^2) \delta^{(1)} v s_\beta^2}{v_s} + \frac{4c_\beta^3 \delta^{(1)} t_\beta \delta^{(1)} T_{h_d} s_\beta^3}{v_s} \qquad \text{(D.33)}$$

$$+ \delta^{(1)} |\lambda| \delta^{(1)} v \left[|\lambda| c_\beta \left(4v_s - \frac{6s_\beta^2 v^2}{v_s} \right) - |\kappa| c_{\varphi_y} s_\beta v_s \right] + c_\beta (\delta^{(1)} |\lambda|)^2 \left(2v v_s - \frac{s_\beta^2 v^3}{v_s} \right)$$

$$+ \frac{c_\beta^2 \delta^{(1)} t_\beta v \left(2s_\beta \left(s_\beta^2 - 2c_\beta^2 \right) \left(|\lambda| \delta^{(1)} |\lambda| v^2 + \delta^{(1)} m_{H^\pm}^2 \right) \right)}{v_s}$$

$$- \frac{1}{2}|\kappa| c_\beta^3 c_{\varphi_y} v v_s \delta^{(1)} |\lambda| \delta^{(1)} t_\beta - \frac{c_\beta^5 (\delta^{(1)} t_\beta)^2 v \left(c_\beta^2 - 2s_\beta^2 \right) \left(|\lambda|^2 v^2 + 2m_{H^\pm}^2 \right)}{v_s}$$

$$+ \delta^{(1)} t_\beta \delta^{(1)} v \left[-|\kappa||\lambda| c_\beta^3 c_{\varphi_y} v_s - \frac{|\lambda|^2 c_\beta^2 s_\beta \left(6c_\beta^2 v^2 - 3s_\beta^2 v^2 + 2v_s^2 \right)}{v_s} \right.$$

$$+ \frac{2c_\beta^2 m_{H^\pm}^2 s_\beta \left(s_\beta^2 - 2c_\beta^2\right)}{v_s}\Bigg] + \frac{2c_{2\beta}c_\beta^4 \delta^{(1)}t_\beta \delta^{(1)}T_{h_u}}{v_s}$$

$$(\Delta^{(1)(1)}\mathcal{M}_{hh}^2)_{h_d a} = -\frac{2c_\beta \delta^{(1)}T_{a_d}\delta^{(1)}v}{s_\beta v^2} - \frac{2c_\beta^4 \delta^{(1)}T_{a_d}\delta^{(1)}t_\beta}{s_\beta^2 v} \tag{D.34}$$

$$(\Delta^{(1)(1)}\mathcal{M}_{hh}^2)_{h_d a_s} = -\frac{2c_\beta \delta^{(1)}T_{a_d}\delta^{(1)}v}{s_\beta v^2} - \frac{2c_\beta^4 \delta^{(1)}T_{a_d}\delta^{(1)}t_\beta}{s_\beta^2 v} + 3|\kappa|\delta^{(1)}|\lambda|\delta^{(1)}v s_\beta s_{\varphi_y}v_s \tag{D.35}$$

$$+ 3|\kappa|c_\beta^3 \delta^{(1)}|\lambda|\delta^{(1)}t_\beta s_{\varphi_y}v v_s + 3|\kappa||\lambda|c_\beta^3 \delta^{(1)}t_\beta \delta^{(1)}v s_{\varphi_y}v_s$$

$$(\Delta^{(1)(1)}\mathcal{M}_{hh}^2)_{h_u h_u} = \frac{1}{2}|\lambda|^2 c_\beta^2 (\delta^{(1)}v)^2 + 2v|\lambda|c_\beta^2 \delta^{(1)}|\lambda|\delta^{(1)}v + \frac{1}{2}v^2 c_\beta^2 (\delta^{(1)}|\lambda|)^2 \tag{D.36}$$

$$- 2s_\beta c_\beta^3 \delta^{(1)}m_{H^\pm}^2 \delta^{(1)}t_\beta + 3m_{H^\pm}^2 s_\beta^2 c_\beta^4 (\delta^{(1)}t_\beta)^2 + \frac{c_\beta s_\beta^2 \delta^{(1)}v\delta^{(1)}T_{h_d}}{v^2} + \frac{c_\beta^2 s_\beta^3 \delta^{(1)}t_\beta \delta^{(1)}T_{h_d}}{v}$$

$$- \frac{2c_\beta^4 s_\beta \delta^{(1)}v\delta^{(1)}T_{h_u}}{v^2} - \frac{c_\beta^3 s_\beta^2 \delta^{(1)}t_\beta \delta^{(1)}T_{h_u}}{v} - \frac{3s_\beta^3 c_\beta^2 \delta^{(1)}v\delta^{(1)}T_{h_u}}{v^2} - \frac{s_\beta^5 \delta^{(1)}v\delta^{(1)}T_{h_u}}{v^2}$$

$$+ \frac{1}{2}|\lambda|^2 v^2 c_\beta^4 (1 - 2c_{2\beta})(\delta^{(1)}t_\beta)^2 - 2|\lambda|^2 v c_\beta^3 s_\beta \delta^{(1)}t_\beta \delta^{(1)}v - 2|\lambda|v^2 c_\beta^3 s_\beta \delta^{(1)}|\lambda|\delta^{(1)}t_\beta$$

$$(\Delta^{(1)(1)}\mathcal{M}_{hh}^2)_{h_u h_s} = -\frac{3|\lambda|^2 c_\beta^2 (\delta^{(1)}v)^2 s_\beta v}{v_s} - \frac{2c_\beta^2 (\delta^{(1)}m_{H^\pm})^2 \delta^{(1)}v s_\beta}{v_s} - \frac{4c_\beta^5 \delta^{(1)}t_\beta \delta^{(1)}T_{h_u}s_\beta}{v_s} \tag{D.37}$$

$$+ \delta^{(1)}|\lambda|\delta^{(1)}v \left[|\lambda|\left(4s_\beta v_s - \frac{6c_\beta^2 s_\beta v^2}{v_s}\right) - |\kappa|c_\beta c_{\varphi_y}v_s\right] + \frac{2c_{2\beta}c_\beta^2 \delta^{(1)}t_\beta \delta^{(1)}T_{h_d}s_\beta^2}{v_s}$$

$$+ \frac{c_\beta^2 \delta^{(1)}t_\beta v \left(\delta^{(1)}|\lambda|v_s^2(|\kappa|c_{\varphi_y}s_\beta + 4|\lambda|c_\beta) - 2c_\beta(c_\beta^2 - 2s_\beta^2)\left(|\lambda|\delta^{(1)}|\lambda|v^2 + \delta^{(1)}m_{H^\pm}^2\right)\right)}{v_s}$$

$$+ \frac{c_\beta^4 (\delta^{(1)}t_\beta)^2 s_\beta v \left(2c_\beta^2 - s_\beta^2\right)\left(|\lambda|^2 v^2 + 2m_{H^\pm}^2\right)}{v_s} + (\delta^{(1)}|\lambda|)^2 \left[2s_\beta v v_s - \frac{c_\beta^2 s_\beta v^3}{v_s}\right]$$

$$+ \delta^{(1)}t_\beta \delta^{(1)}v \left[|\kappa||\lambda|c_\beta^2 c_{\varphi_y}s_\beta v_s - \frac{|\lambda|^2 c_\beta^3 \left(3v^2(c_\beta^2 - 2s_\beta^2) - 2v_s^2\right)}{v_s}\right.$$

$$\left. - \frac{2c_\beta^3 m_{H^\pm}^2 \left(c_\beta^2 - 2s_\beta^2\right)}{v_s}\right]$$

$$(\Delta^{(1)(1)}\mathcal{M}_{hh}^2)_{h_u a} = -\frac{2\delta^{(1)}T_{a_d}\delta^{(1)}v}{v^2} - \frac{2c_\beta^3 \delta^{(1)}T_{a_d}\delta^{(1)}t_\beta}{s_\beta v} \tag{D.38}$$

$$(\Delta^{(1)(1)}\mathcal{M}_{hh}^2)_{h_u a_s} = 3|\kappa|c_\beta \delta^{(1)}|\lambda|\delta^{(1)}v s_{\varphi_y}v_s + c_\beta^2 \delta^{(1)}t_\beta \left(-3|\kappa|\delta^{(1)}|\lambda|s_\beta s_{\varphi_y}v v_s - \frac{2\delta^{(1)}T_{a_d}}{s_\beta^2 v_s}\right) \tag{D.39}$$

$$- 3|\kappa||\lambda|c_\beta^2 \delta^{(1)}t_\beta \delta^{(1)}v s_\beta s_{\varphi_y}v_s$$

$$(\Delta^{(1)(1)}\mathcal{M}^2_{hh})_{h_s h_s} = (\delta^{(1)}v)^2\left(-\frac{1}{2}|\kappa||\lambda|s_{2\beta}(c_{\varphi_y}+3s_{\varphi_y}t_{\varphi_\omega})+\frac{3|\lambda|^2 s_{2\beta}^2 v^2}{2v_s^2}+\frac{m_{H^\pm}^2 s_{2\beta}^2}{2v_s^2}\right) \quad \text{(D.40)}$$

$$-\frac{2c_\beta^4 \delta^{(1)}T_{h_u}\delta^{(1)}vs_\beta}{v_s^2}-\frac{2c_\beta\delta^{(1)}T_{a_d}\delta^{(1)}vt_{\varphi_\omega}}{v_s^2}-\frac{2c_\beta\delta^{(1)}T_{h_d}\delta^{(1)}vs_\beta^4}{v_s^2}+\frac{(\delta^{(1)}|\lambda|)^2 s_{2\beta}^2 v^4}{4v_s^2}$$

$$+\frac{\delta^{(1)}m_{H^\pm}^2\delta^{(1)}vs_{2\beta}^2 v}{v_s^2}+\delta^{(1)}|\lambda|\delta^{(1)}v\left(\frac{2|\lambda|s_{2\beta}^2 v^3}{v_s^2}-|\kappa|s_{2\beta}v(c_{\varphi_y}+3s_{\varphi_y}t_{\varphi_\omega})\right)$$

$$+\frac{c_\beta^4(\delta^{(1)}t_\beta)^2 v^2\left(\frac{1}{2}|\kappa||\lambda|s_{2\beta}v_s^2(c_{\varphi_y}+3s_{\varphi_y}t_{\varphi_\omega})+\left(|\lambda|^2 v^2+2m_{H^\pm}^2\right)\left(c_\beta^4-s_{2\beta}^2+s_\beta^4\right)\right)}{v_s^2}$$

$$+\delta^{(1)}t_\beta\delta^{(1)}v\left[-2|\kappa||\lambda|c_{2\beta}c_\beta^2 v(c_{\varphi_y}+3s_{\varphi_y}t_{\varphi_\omega})+\frac{8|\lambda|^2 c_{2\beta}c_\beta^3 s_\beta v^3}{v_s^2}+\frac{8c_{2\beta}c_\beta^3 m_{H^\pm}^2 s_\beta v}{v_s^2}\right]$$

$$+\frac{c_\beta^2\delta^{(1)}t_\beta v}{v_s^2}\left[c_{2\beta}v\left(4c_\beta s_\beta\left(|\lambda|\delta^{(1)}|\lambda|v^2+\delta^{(1)}m_{H^\pm}^2\right)-|\kappa|\delta^{(1)}|\lambda|v_s^2(c_{\varphi_y}+3s_{\varphi_y}t_{\varphi_\omega})\right)\right.$$

$$\left.+2\delta^{(1)}T_{a_d}s_\beta t_{\varphi_\omega}\right]+\frac{2c_\beta^2\delta^{(1)}t_\beta\delta^{(1)}T_{h_d}s_\beta^3 v\left(s_\beta^2-2c_\beta^2\right)}{v_s^2}-\frac{2c_\beta^5\delta^{(1)}t_\beta\delta^{(1)}T_{h_u}v\left(c_\beta^2-2s_\beta^2\right)}{v_s^2}$$

$$(\Delta^{(1)(1)}\mathcal{M}^2_{hh})_{h_s a} = -|\kappa|\delta^{(1)}|\lambda|\delta^{(1)}vs_{\varphi_y}v_s-\frac{2c_\beta^3\delta^{(1)}T_{a_d}\delta^{(1)}t_\beta}{s_\beta^2 v_s} \quad \text{(D.41)}$$

$$(\Delta^{(1)(1)}\mathcal{M}^2_{hh})_{h_s a_s} = 4|\kappa||\lambda|c_\beta^5(\delta^{(1)}t_\beta)^2 s_\beta s_{\varphi_y}v^2-4|\kappa|\delta^{(1)}|\lambda|\delta^{(1)}vs_{2\beta}s_{\varphi_y}v-\frac{4c_\beta\delta^{(1)}T_{a_d}\delta^{(1)}v}{v_s^2} \quad \text{(D.42)}$$

$$+\frac{4c_\beta^2\delta^{(1)}t_\beta v\left(|\kappa|\delta^{(1)}|\lambda|s_{\varphi_y}vv_s^2\left(s_\beta^2-c_\beta^2\right)+\delta^{(1)}T_{a_d}s_\beta\right)}{v_s^2}-2|\kappa||\lambda|(\delta^{(1)}v)^2 s_{2\beta}s_{\varphi_y}$$

$$-8|\kappa||\lambda|c_\beta^2\delta^{(1)}t_\beta\delta^{(1)}vs_{\varphi_y}vc_{2\beta}$$

$$(\Delta^{(1)(1)}\mathcal{M}^2_{hh})_{aa} = -2|\kappa||\lambda|(\delta^{(1)}v)^2 s_{2\beta}s_{\varphi_y}+(\delta^{(1)}|\lambda|)^2 v^2+4|\kappa||\lambda|c_\beta^5(\delta^{(1)}t_\beta)^2 s_\beta s_{\varphi_y}v^2 \quad \text{(D.43)}$$

$$-\frac{4c_\beta\delta^{(1)}T_{a_d}\delta^{(1)}v}{v_s^2}+\frac{4c_\beta^2\delta^{(1)}t_\beta v\left(\delta^{(1)}T_{a_d}s_\beta-|\kappa|\delta^{(1)}|\lambda|s_{\varphi_y}vv_s^2 c_{2\beta}\right)}{v_s^2}$$

$$-8|\kappa||\lambda|c_\beta^2\delta^{(1)}t_\beta\delta^{(1)}vs_{\varphi_y}vc_{2\beta}|\lambda|^2\delta^{(1)}v^2+4|\lambda|\delta^{(1)}|\lambda|\delta^{(1)}vv$$

$$-4|\kappa|\delta^{(1)}|\lambda|\delta^{(1)}vs_{2\beta}s_{\varphi_y}v$$

$$(\Delta^{(1)(1)}\mathcal{M}^2_{hh})_{aa_s} = \frac{3|\lambda|^2(\delta^{(1)}v)^2 s_{2\beta}v}{2v_s}+\frac{\delta^{(1)}m_{H^\pm}^2\delta^{(1)}vs_{2\beta}}{v_s}+\frac{2c_\beta^4\delta^{(1)}t_\beta\delta^{(1)}T_{h_u}s_\beta}{v_s} \quad \text{(D.44)}$$

$$+\delta^{(1)}|\lambda|\delta^{(1)}v\left(\frac{3|\lambda|s_{2\beta}v^2}{v_s}-3|\kappa|c_{\varphi_y}v_s\right)+\frac{(\delta^{(1)}|\lambda|)^2 s_{2\beta}v^3}{2v_s}-\frac{2c_\beta^3\delta^{(1)}t_\beta\delta^{(1)}T_{h_d}s_\beta^2}{v_s}$$

$$+\frac{2c_\beta^2\delta^{(1)}t_\beta vc_{2\beta}\left(|\lambda|\delta^{(1)}|\lambda|v^2+\delta^{(1)}m_{H^\pm}^2\right)}{v_s}-\frac{c_\beta^5(\delta^{(1)}t_\beta)^2 s_\beta v\left(|\lambda|^2 v^2+2m_{H^\pm}^2\right)}{v_s}$$

$$+ \delta^{(1)} t_\beta \delta^{(1)} v \left(\frac{3|\lambda|^2 c_{2\beta} c_\beta^2 v^2}{v_s} + \frac{2c_\beta^2 c_{2\beta} m_{H^\pm}^2}{v_s} \right)$$

$$(\Delta^{(1)(1)} \mathcal{M}_{hh}^2)_{a_s a_s} = (\delta^{(1)} v)^2 \left[\frac{3}{2} |\kappa| |\lambda| s_{2\beta} (c_{\varphi_y} + 3 s_{\varphi_y} t_{\varphi_\omega}) + \frac{3|\lambda|^2 s_{2\beta}^2 v^2}{2 v_s^2} + \frac{m_{H^\pm}^2 s_{2\beta}^2}{2 v_s^2} \right] \qquad \text{(D.45)}$$

$$- \frac{2 c_\beta^4 \delta^{(1)} T_{h_u} \delta^{(1)} v s_\beta}{v_s^2} + \frac{6 c_\beta \delta^{(1)} T_{a_d} \delta^{(1)} v t_{\varphi_\omega}}{v_s^2} - \frac{2 c_\beta \delta^{(1)} T_{h_d} \delta^{(1)} v s_\beta^4}{v_s^2} + \frac{\delta^{(1)} m_{H^\pm}^2 \delta^{(1)} v s_{2\beta}^2 v}{v_s^2}$$

$$+ \delta^{(1)} |\lambda| \delta^{(1)} v \left[3|\kappa| s_{2\beta} v (c_{\varphi_y} + 3 s_{\varphi_y} t_{\varphi_\omega}) + \frac{2|\lambda| s_{2\beta}^2 v^3}{v_s^2} \right] + \frac{(\delta^{(1)} |\lambda|)^2 s_{2\beta}^2 v^4}{4 v_s^2}$$

$$+ \delta^{(1)} t_\beta \delta^{(1)} v \left[6|\kappa| |\lambda| c_{2\beta} c_\beta^2 v (c_{\varphi_y} + 3 s_{\varphi_y} t_{\varphi_\omega}) + \frac{8|\lambda|^2 c_{2\beta} c_\beta^3 s_\beta v^3}{v_s^2} + \frac{8 c_{2\beta} c_\beta^3 m_{H^\pm}^2 s_\beta v}{v_s^2} \right]$$

$$+ \frac{2 c_\beta^2 \delta^{(1)} t_\beta \delta^{(1)} T_{h_d} s_\beta^3 v (s_\beta^2 - 2 c_\beta^2)}{v_s^2} - \frac{2 c_\beta^5 \delta^{(1)} t_\beta \delta^{(1)} T_{h_u} v (c_\beta^2 - 2 s_\beta^2)}{v_s^2}$$

$$+ \frac{c_\beta^4 (\delta^{(1)} t_\beta)^2 v^2}{v_s^2} \left[\left(|\lambda|^2 v^2 + 2 m_{H^\pm}^2 \right) \left(c_\beta^4 - s_{2\beta}^2 + s_\beta^4 \right) - \frac{3}{2} |\kappa| |\lambda| s_{2\beta} v_s^2 (c_{\varphi_y} + 3 s_{\varphi_y} t_{\varphi_\omega}) \right]$$

$$+ \frac{c_\beta^2 \delta^{(1)} t_\beta v}{v_s^2} \left[c_{2\beta} v \left(3|\kappa| \delta^{(1)} |\lambda| v_s^2 (c_{\varphi_y} + 3 s_{\varphi_y} t_{\varphi_\omega}) + 4 c_\beta s_\beta \left(|\lambda| \delta^{(1)} |\lambda| v^2 + \delta^{(1)} m_{H^\pm}^2 \right) \right) \right.$$

$$\left. - 6 \delta^{(1)} T_{a_d} s_\beta t_{\varphi_\omega} \right].$$

Therefore, the full CTs of the elements of the neutral Higgs mass matrix with the fields at one-loop level are given by

$$(\delta^{(1)} \mathcal{M}_{hh}^2)_{\phi_i \phi_j} = (\Delta^{(1)} \mathcal{M}_{hh}^2)_{\phi_i \phi_j} \, , \qquad \text{(D.46)}$$

while the CTs at two-loop level read

$$(\delta^{(2)} \mathcal{M}_{hh}^2)_{\phi_i \phi_j} = (\Delta^{(2)} \mathcal{M}_{hh}^2)_{\phi_i \phi_j} + (\Delta^{(1)(1)} \mathcal{M}_{hh}^2)_{\phi_i \phi_j} \, . \qquad \text{(D.47)}$$

D.3. Charged Higgs Boson Mass Matrix at Tree Level

We present the analytic expression of the 2×2 charged Higgs mass matrix as a function of the set of independent parameters in the complex NMSSM, cf. Eq. (14.71), in the following. At tree level, the tadpole parameters vanish and $\beta_c \to \beta$ holds. Nevertheless, we keep both the tadpole parameters and terms with β_c explicitly in the following expressions, since the tadpole parameters and β require renormalization, while β_c does not. The charged Higgs mass matrix reads

$$\mathcal{M}_{h^+ h^-}^2 = \frac{1}{2} \begin{pmatrix} t_\beta & 1 \\ 1 & \frac{1}{t_\beta} \end{pmatrix} \left[m_W^2 s_{2\beta} + \frac{|\lambda| v_s \left(|\kappa| v_s c_{\varphi_\omega} + \sqrt{2} \text{Re}(A_\lambda) \right)}{c_{(\varphi_\omega - \varphi_y)}} - \frac{1}{2} |\lambda|^2 s_{2\beta} v^2 \right]$$

$$+ \begin{pmatrix} \dfrac{T_{h_d} - T_{a_d} t_{\varphi_\omega - \varphi_y}}{v c_\beta} & -\dfrac{T_{a_d} (t_{\varphi_\omega - \varphi_y} + i)}{s_\beta v} \\ -\dfrac{T_{a_d} (t_{\varphi_\omega - \varphi_y} - i)}{s_\beta v} & \dfrac{s_\beta T_{h_u} - c_\beta T_{a_d} t_{\varphi_\omega - \varphi_y}}{s_\beta^2 v} \end{pmatrix} \, . \qquad \text{(D.48)}$$

D.4. Charged Higgs Boson Mass Counterterm at One- and Two-Loop Level

The one-loop CT of the squared charged Higgs boson mass consists of genuine one-loop CT contributions $\Delta^{(1)}m_{H^\pm}^2$, while the two-loop CT contains not only genuine two-loop CT contributions $\Delta^{(2)}m_{H^\pm}^2$, but moreover contributions $\Delta^{(1)(1)}m_{H^\pm}^2$ from products of two one-loop CTs. The genuine CT contributions to n^{th} loop order ($n = 1, 2$) are given by

$$
\Delta^{(n)}m_{H^\pm}^2 = \left[\frac{v_s\left(|\kappa|v_s c_{\varphi_\omega} + \sqrt{2}\mathrm{Re}(A_\lambda)\right)}{s_{2\beta}c_{\varphi_\omega - \varphi_y}} - |\lambda|v^2 \right]\delta^{(n)}|\lambda| + \frac{s_\beta^2}{c_\beta v}\delta^{(n)}T_{h_d} - |\lambda|^2 v \delta^{(n)}v \tag{D.49}
$$
$$
+ \frac{c_\beta^2}{s_\beta v}\delta^{(n)}T_{h_u} + \frac{t_{\varphi_y - \varphi_\omega}}{c_\beta s_\beta^2 v}\delta^{(n)}T_{a_d} - \frac{|\lambda|c_{2\beta}v_s\left(|\kappa|v_s c_{\varphi_\omega} + \sqrt{2}\mathrm{Re}(A_\lambda)\right)}{2s_\beta^2 c_{\varphi_\omega - \varphi_y}}\delta^{(n)}t_\beta
$$
$$
+ \frac{|\lambda|\left(2|\kappa|v_s c_{\varphi_\omega} + \sqrt{2}\mathrm{Re}(A_\lambda)\right)}{s_{2\beta}c_{\varphi_\omega - \varphi_y}}\delta^{(n)}v_s + \frac{|\lambda|v_s^2 c_{\varphi_\omega}}{s_{2\beta}c_{\varphi_\omega - \varphi_y}}\delta^{(n)}|\kappa| + \frac{\sqrt{2}|\lambda|v_s}{s_{2\beta}c_{\varphi_\omega - \varphi_y}}\delta^{(n)}\mathrm{Re}(A_\lambda) \ ,
$$

while the contribution consisting of products of one-loop CTs explicitly reads

$$
\Delta^{(1)(1)}m_{H^\pm}^2 = \frac{|\lambda|c_\beta v_s c_{2\beta}\left(|\kappa|v_s c_{\varphi_\omega} + \sqrt{2}\mathrm{Re}(A_\lambda)\right)}{2s_\beta^3 c_{\varphi_\omega - \varphi_y}}(\delta^{(1)}t_\beta)^2 - \frac{v^2}{2}(\delta^{(1)}|\lambda|)^2 - \frac{|\lambda|^2(\delta^{(1)}v)^2}{2} \tag{D.50}
$$
$$
+ \left(\frac{\sqrt{2}v_s}{s_{2\beta}c_{\varphi_\omega - \varphi_y}}\delta^{(1)}\mathrm{Re}(A_\lambda) - 2|\lambda|v\delta^{(1)}v - \frac{c_{2\beta}v_s\left(|\kappa|v_s c_{\varphi_\omega} + \sqrt{2}\mathrm{Re}(A_\lambda)\right)}{2s_\beta^2 c_{\varphi_\omega - \varphi_y}}\delta^{(1)}t_\beta \right)\delta^{(1)}|\lambda|
$$
$$
- \frac{1}{v^2}\left(\frac{t_{\varphi_y - \varphi_\omega}}{c_\beta s_\beta^2}\delta^{(1)}T_{a_d} + \frac{c_\beta^2}{s_\beta}\delta^{(1)}T_{h_u} + \frac{s_\beta^2}{c_\beta}\delta^{(1)}T_{h_d} \right)\delta^{(1)}v + \frac{s_\beta^3}{v}\delta^{(1)}t_\beta \delta^{(1)}T_{h_d}
$$
$$
- \left(\frac{(s_\beta^2 - 2c_\beta^2)t_{\varphi_\omega - \varphi_y}}{s_\beta^3 v}\delta^{(1)}T_{a_d} + \frac{c_\beta^5}{s_\beta^2 v}\delta^{(1)}T_{h_u} + \frac{|\lambda|c_{2\beta}v_s}{\sqrt{2}s_\beta^2 c_{\varphi_\omega - \varphi_y}}\delta^{(1)}\mathrm{Re}(A_\lambda) \right)\delta^{(1)}t_\beta
$$
$$
+ \frac{2v_s|\kappa|c_{\varphi_\omega} + \sqrt{2}\mathrm{Re}\,A_\lambda}{s_{2\beta}c_{\phi_\omega - \phi_y}}\delta^{(1)}v_s\delta^{(1)}|\lambda| + \frac{\sqrt{2}|\lambda|}{s_{2\beta}c_{\varphi_\omega - \varphi_y}}\delta^{(1)}v_s\delta^{(1)}\mathrm{Re}\,A_\lambda + \frac{2v_s|\lambda|c_{\varphi_\omega}}{s_{2\beta}c_{\varphi_\omega - \varphi_y}}\delta^{(1)}v_s\delta^{(1)}|\kappa|
$$
$$
+ \frac{|\lambda|c_{2\beta}\left(2v_s|\kappa|c_{\varphi_\omega} + \sqrt{2}\mathrm{Re}\,A_\lambda\right)}{2s_\beta^2 c_{\varphi_\omega - \varphi_y}}\delta^{(1)}v_s\delta^{(1)}|t_\beta| + \frac{v_s^2 c_{\varphi_\omega}}{s_{2\beta}c_{\varphi_\omega - \varphi_y}}\delta^{(1)}|\kappa|\delta^{(1)}|\lambda|
$$
$$
- \frac{2v_s^2|\lambda|c_\beta^2 c_{2\beta}c_{\varphi_\omega}}{s_{2\beta}c_{\varphi_\omega - \varphi_y}}\delta^{(1)}|\kappa|\delta^{(1)}t_\beta + \frac{|\kappa||\lambda|c_{\varphi_\omega}}{s_{2\beta}c_{\varphi_\omega - \varphi_y}}(\delta^{(1)}v_s)^2 \ .
$$

Therefore, the full CT of the squared charged Higgs mass at one-loop level is given by

$$
\delta^{(1)}m_{H^\pm}^2 = \Delta^{(1)}m_{H^\pm}^2 \ , \tag{D.51}
$$

while the CT at two-loop level reads

$$
\delta^{(2)}m_{H^\pm}^2 = \Delta^{(2)}m_{H^\pm}^2 + \Delta^{(1)(1)}m_{H^\pm}^2 \ . \tag{D.52}
$$

D.5. Counterterm of $\mathrm{Re}(A_\lambda)$ at One- and Two-Loop

The one-loop CT of $\mathrm{Re}(A_\lambda)$ consists of genuine one-loop CT contributions $\Delta^{(1)}\mathrm{Re}(A_\lambda)$. At two-loop level, the CT does not only contain contributions $\Delta^{(2)}\mathrm{Re}(A_\lambda)$ stemming from genuine

two-loop CTs, but moreover contributions $\Delta^{(1)(1)}\mathrm{Re}(A_\lambda)$ containing the products of one-loop CTs. The genuine CT contributions to n^{th} loop level $(n = 1, 2)$ are given by

$$\Delta^{(n)}\mathrm{Re}(A_\lambda) = \frac{s_{2\beta}c_{\varphi_\omega - \varphi_y}}{\sqrt{2}|\lambda|v_s}\left[\delta^{(n)}m_{H^\pm}^2 + |\lambda|^2 v\delta^{(n)}v + |\lambda|v^2\delta^{(n)}|\lambda| - \frac{c_\beta^2}{vs_\beta}\delta^{(n)}T_{h_u} - \frac{s_\beta^2}{vc_\beta}\delta^{(n)}T_{h_d} \quad \text{(D.53)}\right.$$

$$\left. - \frac{t_{\varphi_y - \varphi_w}}{s_\beta^2 c_\beta v}\delta^{(n)}T_{a_d}\right] + \left(\mathrm{Re}(A_\lambda) + \frac{|\kappa|v_s c_{\varphi_w}}{\sqrt{2}}\right)\left[2\frac{c_\beta^2}{t_{2\beta}}\delta^{(n)}t_\beta - \frac{\delta^{(n)}|\lambda|}{|\lambda|} - \frac{\delta^{(n)}v_s}{v_s}\right]$$

$$- \frac{c_{\varphi_\omega}}{\sqrt{2}}\left(v_s\delta^{(n)}|\kappa| + |\kappa|\delta^{(n)}v_s\right) ,$$

(D.54)

while the contribution consisting of products of one-loop CTs explicitly reads

$$\Delta^{(1)(1)}\mathrm{Re}(A_\lambda) = \frac{s_{2\beta}c_{\varphi_\omega - \varphi_y}}{\sqrt{2}|\lambda|v_s}\left[2|\lambda|v\delta^{(1)}v\delta^{(1)}|\lambda| + \frac{1}{2}|\lambda|^2(\delta^{(1)}v)^2 - \frac{1}{2}|\lambda|^2 c_\beta^4 v^2(\delta^{(1)}t_\beta)^2 \quad \text{(D.55)}\right.$$

$$+ \frac{1}{2}v^2(\delta^{(1)}|\lambda|)^2 + \frac{c_\beta^3}{v^2 t_\beta}\left(\frac{v}{t_\beta}\delta^{(1)}t_\beta + \frac{1}{c_\beta^2}\delta^{(1)}v\right)\delta^{(1)}T_{h_u} + \frac{s_\beta^3}{v^2}\left(\frac{1}{c_\beta}\delta^{(1)}v - vs_\beta\delta^{(1)}t_\beta\right)\delta^{(1)}T_{h_d}$$

$$+ \frac{t_{\varphi_y - \varphi_w}}{s_\beta^2 c_\beta v^2}\left(\delta^{(1)}v + (2c_\beta^2 - s_\beta^2)\frac{v}{t_\beta}\delta^{(1)}t_\beta\right)\delta^{(1)}T_{a_d}\left] - \frac{c_{\varphi_\omega}}{\sqrt{2}}\delta^{(1)}|\kappa|\delta^{(1)}v_s\right.$$

$$+ \left(\mathrm{Re}(A_\lambda) + \frac{|\kappa|v_s c_{\varphi_w}}{\sqrt{2}}\right)\left[\frac{(\delta^{(1)}|\lambda|)^2}{|\lambda|^2} + \frac{(\delta^{(1)}v_s)^2}{v_s^2} + \frac{\delta^{(1)}v_s\delta^{(1)}|\lambda|}{v_s|\lambda|} - c_\beta^4(\delta^{(1)}t_\beta)^2\right.$$

$$\left.\left. - 2\frac{c_\beta^2}{v_s|\lambda|t_{2\beta}}\left(v_s\delta^{(1)}|\lambda| + |\lambda|\delta^{(1)}v_s\right)\delta^{(1)}t_\beta - 2\frac{s_\beta c_\beta^3}{t_{2\beta}}(\delta^{(1)}t_\beta)^2\right]\right].$$

Therefore, the full one-loop CT of $\mathrm{Re}(A_\lambda)$ is given by

$$\delta^{(1)}\mathrm{Re}(A_\lambda) = \Delta^{(1)}\mathrm{Re}(A_\lambda) , \qquad (D.56)$$

while the CT at two-loop level reads

$$\delta^{(2)}\mathrm{Re}(A_\lambda) = \Delta^{(2)}\mathrm{Re}(A_\lambda) + \Delta^{(1)(1)}\mathrm{Re}(A_\lambda) . \qquad (D.57)$$

NMSSM Two-Loop Self-Energy Diagrams

In this appendix, we present all Feynman-diagrammatic contributions to the two-loop self-energies required for the computation of the $\mathcal{O}(\alpha_t^2)$ corrections. For the diagrams shown in Appendices E.1 and E.2, we do not separately show diagrams which differ from the presented ones by an inversion of the fermion current. All placeholders S_i and F_i ($i = 1, 2$) represent the particle content as specified below each individual Feynman diagram. A cross denotes the insertion of one-loop CT contributions of the propagators (*i.e.* the mass CTs) and the vertices. We implicitly sum over the indices $a, b, c, d = 1, 2$, $e = 3, 4, 5$ and $f = 1, ..., 5$ of all virtual particles in the Feynman diagrams.

E.1. Two-Loop Self-Energies of the Neutral Higgs Bosons

The following figure shows all Feynman-diagrammatic contributions to the neutral Higgs boson self-energies required for the computation of the $\mathcal{O}(\alpha_t^2)$ corrections.
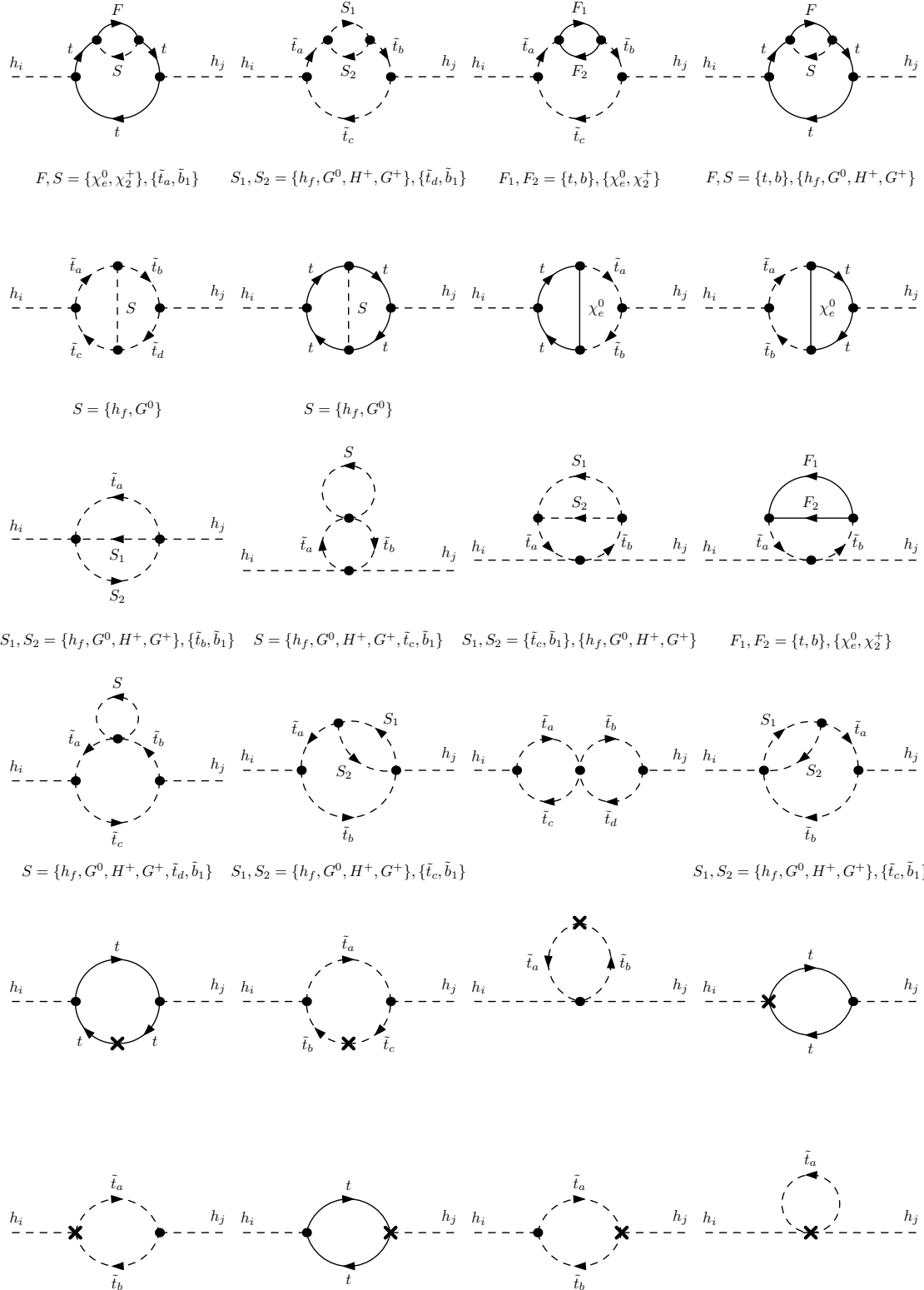
Figure E.1.: Generic neutral Higgs boson two-loop self-energies required for the computation of the $\mathcal{O}(\alpha_t^2)$ corrections of the Higgs masses in the complex NMSSM.

E.2. Two-Loop Self-Energies of the Charged Higgs Bosons

The following figure shows all Feynman-diagrammatic contributions to the neutral Higgs boson self-energies required for the computation of the $\mathcal{O}(\alpha_t^2)$ corrections.
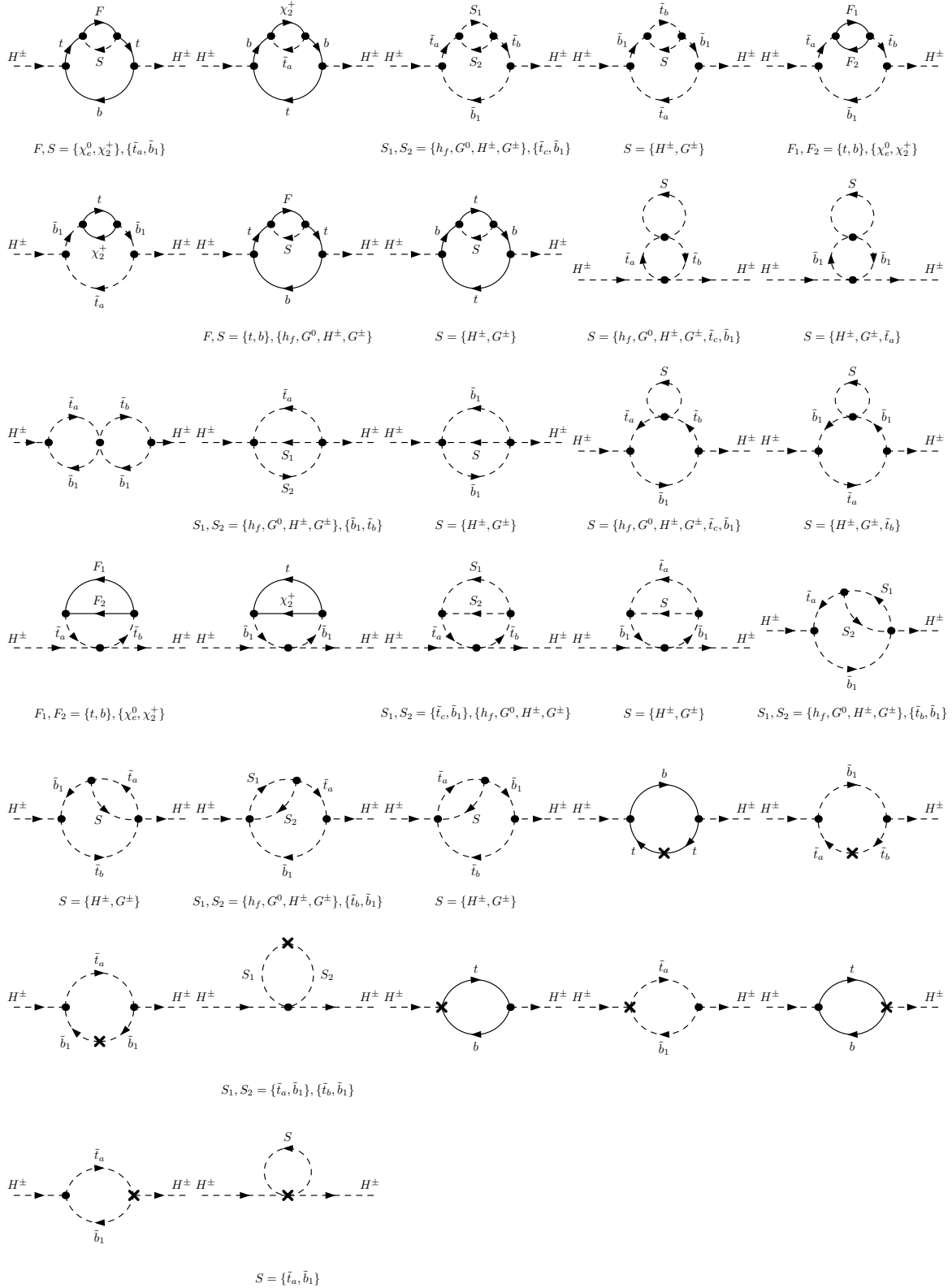
Figure E.2.: Generic charged Higgs boson two-loop self-energies required for the computation of the $\mathcal{O}(\alpha_t^2)$ two-loop CT of the charged Higgs boson mass.

Exemplary Input and Output Files for 2HDECAY

F.1. Exemplary Input File for 2HDECAY

In the following, we show the exemplary shortened input file `2hdecay.in` where we present only the relevant input parameters as described in Sec. 6.2. The first integer in each line corresponds to the line number in the input file and is not part of the actual input.

```
    ...
 6 OMIT ELW2= 0
    ...
 9 2HDM     = 1
    ...
18 ALS(MZ)  = 1.18000e-01
19 MSBAR(2) = 9.50000e-02
20 MCBAR(3) = 0.98600e+00
21 MBBAR(MB)= 4.18000e+00
22 MT       = 1.73200e+02
23 MTAU     = 1.77682e+00
24 MMUON    = 1.056583715e-01
25 1/ALPHA  = 1.37036e+02
26 ALPHAMZ  = 7.754222173973729e-03
27 GF       = 1.1663787e-05
28 GFCALC   = 0.000000000
29 GAMW     = 2.08500e+00
30 GAMZ     = 2.49520e+00
31 MZ       = 9.11876e+01
32 MW       = 8.0385e+01
33 VTB      = 9.9910e-01
34 VTS      = 4.040e-02
35 VTD      = 8.67e-03
36 VCB      = 4.12e-02
37 VCS      = 9.7344e-01
38 VCD      = 2.252e-01
39 VUB      = 3.51e-03
40 VUS      = 2.2534e-01
41 VUD      = 9.7427e-01
    ...
56 PARAM    = 1
57 TYPE     = 1
58 RENSCHEM = 7
59 REFSCHEM = 5
60 *******************
61 TGBET2HDM= 4.23635D0
62 M_12^2   = 28505.5D0
63 INSCALE  = 125.09D0
64 OUTSCALE = MIN
65 ******************* PARAM=1:
```

```
66 ALPHA_H  = -0.189345D0
67 MHL      = 125.09D0
68 MHH      = 381.767D0
69 MHA      = 350.665D0
70 MH+-     = 414.114D0
71 ******************** PARAM=2:
72 LAMBDA1  = 6.368674377530086700D0
73 LAMBDA2  = 0.235570240072350970D0
74 LAMBDA3  = 1.780416490847621700D0
75 LAMBDA4  = -1.526237585404794300D0
76 LAMBDA5  = 0.074592764717552856D0
   ...
```

F.2. Exemplary Output Files for `2HDECAY`

In the following, we show exemplary output files for the BRs and the electroweak partial decay widths. Since we restrict the description of the output file format to exemplary decay channels in Sec. 6.2, we only show shortened output files in the following, while the actual full output files provided by `2HDECAY` contain the BRs and decay widths for all decay channels and for all renormalization schemes that are considered. The first integer in each line corresponds to the line number in the output file and is not part of the actual input.

Exemplary shortened output file `2hdecay_BR.out` **for the BRs:**

```
   ...
51 #           PDG   Width QCD Only
52 DECAY QCD   25    4.22730978E-03 # h decays with QCD corrections only
53                   7              # Renormalization Scheme Number
54      -0.18809815E+00   # Corresponding mixing angle alpha
55       0.43048897E+01   # Corresponding tan(beta)
56       0.28505500E+05   # Corresponding m_12^2
57 #         BR        NDA     ID1     ID2
58      5.93838905E-01    2       5       -5   # BR(h -> b bb )
63      7.76755623E-02    2      21       21   # BR(h -> g g )
   ...
69 #           PDG    Width QCD and EW
70 DECAY QCD&EW    25    4.10575180E-03   # h decays with QCD and EW corrections
71                   7                    # Renormalization Scheme Number
72      -0.18809815E+00   # Corresponding mixing angle alpha
73       0.43048897E+01   # Corresponding tan(beta)
74       0.28505500E+05   # Corresponding m_12^2
75 #         BR        NDA     ID1     ID2
76      5.85412930E-01    2       5       -5   # BR(h -> b bb )
81      7.99752836E-02    2      21       21   # BR(h -> g g )
   ...
```

Exemplary shortened output file `2hdecay_EW.out` **for the electroweak decay widths:**

```
   ...
51 #                  PDG
52 LO DECAY WIDTH    25   # h non-zero LO EW decay widths of on-shell
                             and non-loop induced decays
53                   7   # Renormalization Scheme Number
54      -0.18809815E+00   # Corresponding mixing angle alpha
55       0.43048897E+01   # Corresponding tan(beta)
56       0.28505500E+05   # Corresponding m_12^2
57 #         WIDTH      NDA     ID1     ID2
58      5.96669359E-03    2       5       -5    # GAM(h -> b bb )
59      2.69987831E-04    2     -15       15    # GAM(h -> tau+ tau- )
   ...
64 #                  PDG
65 NLO DECAY WIDTH    25   # h non-zero NLO EW decay widths of on-shell
                             and non-loop induced decays
66                   7 # Renormalization Scheme Number
67      -0.18809815E+00   # Corresponding mixing angle alpha
68       0.43048897E+01   # Corresponding tan(beta)
69       0.28505500E+05   # Corresponding m_12^2
70 #         WIDTH      NDA     ID1     ID2
71      5.71289204E-03    2       5       -5    # GAM(h -> b    bb )
72      2.58765783E-04    2     -15       15    # GAM(h -> tau+ tau- )
   ...
```

References

[1] S. L. Glashow, "Partial-symmetries of weak interactions," *Nuclear Physics* **22** no. 4, (1961) 579 – 588.

[2] P. W. Higgs, "Broken Symmetries and the Masses of Gauge Bosons," *Phys. Rev. Lett.* **13** (Oct, 1964) 508–509.

[3] P. W. Higgs, "Broken symmetries, massless particles and gauge fields," *Physics Letters* **12** no. 2, (1964) 132 – 133.

[4] F. Englert and R. Brout, "Broken Symmetry and the Mass of Gauge Vector Mesons," *Physical Review Letters* **13** (Aug., 1964) 321–323.

[5] G. S. Guralnik, C. R. Hagen, and T. W. Kibble, "Global Conservation Laws and Massless Particles," *Physical Review Letters* **13** (Nov., 1964) 585–587.

[6] T. W. B. Kibble, "Symmetry Breaking in Non-Abelian Gauge Theories," *Phys. Rev.* **155** (Mar, 1967) 1554–1561.

[7] S. Weinberg, "A Model of Leptons," *Phys. Rev. Lett.* **19** (Nov, 1967) 1264–1266.

[8] A. Salam, "Weak and Electromagnetic Interactions," *Conf. Proc.* **C680519** (1968) 367–377.

[9] **Tevatron Electroweak Working Group, CDF, DELPHI, SLD Electroweak and Heavy Flavour Groups, ALEPH, LEP Electroweak Working Group, SLD, OPAL, D0, L3** Collaboration, L. E. W. Group, "Precision Electroweak Measurements and Constraints on the Standard Model," `arXiv:1012.2367 [hep-ex]`.

[10] M. Baak, M. Goebel, J. Haller, A. Hoecker, D. Ludwig, K. Mönig, M. Schott, and J. Stelzer, "Updated Status of the Global Electroweak Fit and Constraints on New Physics," *Eur. Phys. J.* **C72** (2012) 2003, `arXiv:1107.0975 [hep-ph]`.

[11] M. Baak, M. Goebel, J. Haller, A. Hoecker, D. Kennedy, R. Kogler, K. Mönig, M. Schott, and J. Stelzer, "The Electroweak Fit of the Standard Model after the Discovery of a New Boson at the LHC," *Eur. Phys. J.* **C72** (2012) 2205, `arXiv:1209.2716 [hep-ph]`.

[12] **ATLAS** Collaboration, G. Aad *et al.*, "Study of the spin and parity of the Higgs boson in diboson decays with the ATLAS detector," *Eur. Phys. J.* **C75** no. 10, (2015) 476, `arXiv:1506.05669 [hep-ex]`. [Erratum: Eur. Phys. J.C76, no.3, 152(2016), `https://dx.doi.org/10.1140/epjc/s10052-016-3934-y`].

[13] **ATLAS, CMS** Collaboration, G. Aad *et al.*, "Combined Measurement of the Higgs Boson Mass in pp Collisions at $\sqrt{s} = 7$ and 8 TeV with the ATLAS and CMS Experiments," *Phys. Rev. Lett.* **114** (2015) 191803, `arXiv:1503.07589 [hep-ex]`.

[14] **ATLAS, CMS** Collaboration, G. Aad *et al.*, "Measurements of the Higgs boson production and decay rates and constraints on its couplings from a combined ATLAS and CMS analysis of the LHC pp collision data at $\sqrt{s} = 7$ and 8 TeV," *JHEP* **08** (2016) 045, `arXiv:1606.02266 [hep-ex]`.

[15] **ATLAS** Collaboration, G. Aad *et al.*, "Observation of a new particle in the search for the Standard Model Higgs boson with the ATLAS detector at the LHC," *Phys. Lett.* **B716** (2012) 1–29, `arXiv:1207.7214 [hep-ex]`.

[16] **CMS** Collaboration, S. Chatrchyan *et al.*, "Observation of a new boson at a mass of 125 GeV with the CMS experiment at the LHC," *Phys. Lett.* **B716** (2012) 30–61, `arXiv:1207.7235 [hep-ex]`.

[17] T. D. Lee, "A Theory of Spontaneous T Violation," *Phys. Rev. D* **8** (Aug, 1973) 1226–1239.

[18] G. C. Branco, P. M. Ferreira, L. Lavoura, M. N. Rebelo, M. Sher, and J. P. Silva, "Theory and phenomenology of two-Higgs-doublet models," *Phys. Rept.* **516** (2012) 1–102, `arXiv:1106.0034 [hep-ph]`.

[19] C.-Y. Chen, M. Freid, and M. Sher, "Next-to-minimal two Higgs doublet model," *Phys. Rev.* **D89** no. 7, (2014) 075009, `arXiv:1312.3949 [hep-ph]`.

[20] P. Fayet, "Supergauge Invariant Extension of the Higgs Mechanism and a Model for the electron and Its Neutrino," *Nucl. Phys.* **B90** (1975) 104–124.

[21] P. Fayet, "Spontaneously Broken Supersymmetric Theories of Weak, Electromagnetic and Strong Interactions," *Phys. Lett.* **69B** (1977) 489.

[22] P. Fayet, "Supersymmetry and weak, electromagnetic and strong interactions," *Physics Letters B* **64** no. 2, (1976) 159 – 162.

[23] P. Fayet and S. Ferrara, "Supersymmetry," *Phys. Rept.* **32** (1977) 249–334.

[24] S. Dimopoulos and H. Georgi, "Softly broken supersymmetry and SU(5)," *Nuclear Physics B* **193** no. 1, (1981) 150 – 162.

[25] N. Sakai, "Naturalnes in supersymmetric GUTS," *Zeitschrift für Physik C Particles and Fields* **11** no. 2, (Jun, 1981) 153–157.

[26] K. Inoue, A. Kakuto, H. Komatsu, and S. Takeshita, "Low Energy Parameters and Particle Masses in a Supersymmetric Grand Unified Model," *Progress of Theoretical Physics* **67** no. 6, (06, 1982) 1889–1898.

[27] K. Inoue, A. Kakuto, H. Komatsu, and S. Takeshita, "Aspects of Grand Unified Models with Softly Broken Supersymmetry," *Progress of Theoretical Physics* **68** no. 3, (09, 1982) 927–946. [Erratum: Progress of Theoretical Physics, Volume 70, Issue 1, July 1983, Page 330 `https://dx.doi.org/10.1143/PTP.68.927`].

[28] K. Inoue, A. Kakuto, H. Komatsu, and S. Takeshita, "Renormalization of Supersymmetry Breaking Parameters Revisited," *Progress of Theoretical Physics* **71** no. 2, (02, 1984) 413–416.

[29] H. P. Nilles, "Supersymmetry, Supergravity and Particle Physics," *Phys.Rept.* **110** (1984) 1–162.

[30] H. E. Haber and G. L. Kane, "The Search for Supersymmetry: Probing Physics Beyond the Standard Model," *Phys.Rept.* **117** (1985) 75–263.

[31] J. Gunion and H. E. Haber, "Higgs Bosons in Supersymmetric Models. (I).," *Nucl.Phys.* **B272** (1986) 1.

[32] J. Gunion and H. E. Haber, "Higgs Bosons in Supersymmetric Models. (II). Implications for Phenomenology," *Nucl.Phys.* **B278** (1986) 449.

[33] J. F. Gunion, H. E. Haber, G. L. Kane, and S. Dawson, "The Higgs Hunter's Guide," *Front. Phys.* **80** (2000) 1–448.

[34] M. Drees and S. P. Martin, "Implications of SUSY model building," `arXiv:hep-ph/9504324 [hep-ph]`.

[35] J. A. Bagger, "Weak scale supersymmetry: Theory and practice," in *QCD and beyond. Proceedings, Theoretical Advanced Study Institute in Elementary Particle Physics, TASI-95, Boulder, USA, June 4-30, 1995*, pp. 109–162. 1996. `arXiv:hep-ph/9604232 [hep-ph]`.

[36] S. P. Martin, *A Supersymmetry Primer*, pp. 1–98. World Scientific Publishing Co. Pte. Ltd., 1998. `hep-ph/9709356`.

[37] M. Dine, W. Fischler, and M. Srednicki, "A Simple Solution to the Strong CP Problem with a Harmless Axion," *Phys.Lett.* **B104** (1981) 199.

[38] J. R. Ellis, J. Gunion, H. E. Haber, L. Roszkowski, and F. Zwirner, "Higgs Bosons in a Nonminimal Supersymmetric Model," *Phys.Rev.* **D39** (1989) 844.

[39] M. Drees, "Supersymmetric Models with Extended Higgs Sector," *Int.J.Mod.Phys.* **A4** (1989) 3635.

[40] U. Ellwanger, M. Rausch de Traubenberg, and C. A. Savoy, "Particle spectrum in supersymmetric models with a gauge singlet," *Phys.Lett.* **B315** (1993) 331–337, `arXiv:hep-ph/9307322 [hep-ph]`.

[41] U. Ellwanger, M. Rausch de Traubenberg, and C. A. Savoy, "Higgs phenomenology of the supersymmetric model with a gauge singlet," *Z.Phys.* **C67** (1995) 665–670, `arXiv:hep-ph/9502206 [hep-ph]`.

[42] U. Ellwanger, M. Rausch de Traubenberg, and C. A. Savoy, "Phenomenology of supersymmetric models with a singlet," *Nucl.Phys.* **B492** (1997) 21–50, `arXiv:hep-ph/9611251 [hep-ph]`.

[43] T. Elliott, S. King, and P. White, "Unification constraints in the next-to-minimal supersymmetric standard model," *Phys.Lett.* **B351** (1995) 213–219, `arXiv:hep-ph/9406303 [hep-ph]`.

[44] S. King and P. White, "Resolving the constrained minimal and next-to-minimal supersymmetric standard models," *Phys.Rev.* **D52** (1995) 4183–4216, `arXiv:hep-ph/9505326 [hep-ph]`.

[45] M. Maniatis, "The Next-to-Minimal Supersymmetric extension of the Standard Model reviewed," *Int. J. Mod. Phys.* **A25** (2010) 3505–3602, `arXiv:0906.0777 [hep-ph]`.

[46] U. Ellwanger, C. Hugonie, and A. M. Teixeira, "The Next-to-Minimal Supersymmetric Standard Model," *Phys. Rept.* **496** (2010) 1–77, `arXiv:0910.1785 [hep-ph]`.

[47] A. Djouadi, J. Kalinowski, M. Mühlleitner, and M. Spira, "HDECAY: Twenty++ years after," *Comput. Phys. Commun.* **238** (2019) 214–231, `arXiv:1801.09506 [hep-ph]`.

[48] A. Bredenstein, A. Denner, S. Dittmaier, and M. M. Weber, "Precise predictions for the Higgs-boson decay H —> WW/ZZ —> 4 leptons," *Phys. Rev.* **D74** (2006) 013004, `arXiv:hep-ph/0604011 [hep-ph]`.

[49] A. Bredenstein, A. Denner, S. Dittmaier, and M. M. Weber, "Precision calculations for the Higgs decays H —> ZZ/WW —> 4 leptons," *Nucl. Phys. Proc. Suppl.* **160** (2006) 131–135, `arXiv:hep-ph/0607060 [hep-ph]`. [,131(2006)].

[50] A. Bredenstein, A. Denner, S. Dittmaier, and M. M. Weber, "Radiative corrections to the semileptonic and hadronic Higgs-boson decays H —> WW/ZZ —> 4 fermions," *JHEP* **02** (2007) 080, `arXiv:hep-ph/0611234 [hep-ph]`.

[51] L. Altenkamp, S. Dittmaier, and H. Rzehak, "Precision calculations for h → WW/ZZ → 4 fermions in the Two-Higgs-Doublet Model with Prophecy4f," *JHEP* **03** (2018) 110, `arXiv:1710.07598 [hep-ph]`.

[52] D. Eriksson, J. Rathsman, and O. Stål, "2HDMC: Two-Higgs-Doublet Model Calculator Physics and Manual," *Comput. Phys. Commun.* **181** (2010) 189–205, `arXiv:0902.0851 [hep-ph]`.

[53] W. Porod, "SPheno, a program for calculating supersymmetric spectra, SUSY particle decays and SUSY particle production at e+ e- colliders," *Comput. Phys. Commun.* **153** (2003) 275–315, `arXiv:hep-ph/0301101 [hep-ph]`.

[54] W. Porod and F. Staub, "SPheno 3.1: Extensions including flavour, CP-phases and models beyond the MSSM," *Comput. Phys. Commun.* **183** (2012) 2458–2469, `arXiv:1104.1573 [hep-ph]`.

[55] S. Kanemura, M. Kikuchi, K. Sakurai, and K. Yagyu, "H-COUP: a program for one-loop corrected Higgs boson couplings in non-minimal Higgs sectors," *Comput. Phys. Commun.* **233** (2018) 134–144, `arXiv:1710.04603 [hep-ph]`.

[56] M. Krause, M. Mühlleitner, and M. Spira, "2HDECAY - A program for the Calculation of Electroweak One-Loop Corrections to Higgs Decays in the Two-Higgs-Doublet Model Including State-of-the-Art QCD Corrections," `arXiv:1810.00768 [hep-ph]`.

[57] M. Mühlleitner, M. O. P. Sampaio, R. Santos, and J. Wittbrodt, "The N2HDM under Theoretical and Experimental Scrutiny," *JHEP* **03** (2017) 094, `arXiv:1612.01309 [hep-ph]`.

[58] I. Engeln, M. Mühlleitner, and J. Wittbrodt, "N2HDECAY: Higgs Boson Decays in the Different Phases of the N2HDM," *Comput. Phys. Commun.* **234** (2019) 256–262, `arXiv:1805.00966 [hep-ph]`.

[59] U. Ellwanger, "Radiative corrections to the neutral Higgs spectrum in supersymmetry with a gauge singlet," *Phys. Lett.* **B303** (1993) 271–276, `arXiv:hep-ph/9302224 [hep-ph]`.

[60] T. Elliott, S. F. King, and P. L. White, "Supersymmetric Higgs bosons at the limit," *Phys. Lett.* **B305** (1993) 71–77, `arXiv:hep-ph/9302202 [hep-ph]`.

[61] T. Elliott, S. F. King, and P. L. White, "Squark contributions to Higgs boson masses in the next-to-minimal supersymmetric standard model," *Phys. Lett.* **B314** (1993) 56–63, `arXiv:hep-ph/9305282 [hep-ph]`.

[62] T. Elliott, S. F. King, and P. L. White, "Radiative corrections to Higgs boson masses in the next-to-minimal supersymmetric Standard Model," *Phys. Rev.* **D49** (1994) 2435–2456, `arXiv:hep-ph/9308309 [hep-ph]`.

[63] P. N. Pandita, "Radiative corrections to the scalar Higgs masses in a non-minimal supersymmetric Standard Model," *Zeitschrift fur Physik C Particles and Fields* **59** (Dec., 1993) 575–583.

[64] U. Ellwanger and C. Hugonie, "Yukawa induced radiative corrections to the lightest Higgs boson mass in the NMSSM," *Phys. Lett.* **B623** (2005) 93–103, `arXiv:hep-ph/0504269 [hep-ph]`.

[65] G. Degrassi and P. Slavich, "On the radiative corrections to the neutral Higgs boson masses in the NMSSM," *Nucl. Phys.* **B825** (2010) 119–150, `arXiv:0907.4682 [hep-ph]`.

[66] F. Staub, W. Porod, and B. Herrmann, "The Electroweak sector of the NMSSM at the one-loop level," *JHEP* **10** (2010) 040, `arXiv:1007.4049 [hep-ph]`.

[67] K. Ender, T. Graf, M. Mühlleitner, and H. Rzehak, "Analysis of the NMSSM Higgs Boson Masses at One-Loop Level," *Phys. Rev.* **D85** (2012) 075024, `arXiv:1111.4952 [hep-ph]`.

[68] P. Drechsel, L. Galeta, S. Heinemeyer, and G. Weiglein, "Precise Predictions for the Higgs-Boson Masses in the NMSSM," *Eur. Phys. J.* **C77** no. 1, (2017) 42, `arXiv:1601.08100 [hep-ph]`.

[69] G. Belanger, V. Bizouard, F. Boudjema, and G. Chalons, "One-loop renormalization of the NMSSM in SloopS: The neutralino-chargino and sfermion sectors," *Phys. Rev.* **D93** no. 11, (2016) 115031, `arXiv:1602.05495 [hep-ph]`.

[70] G. Bélanger, V. Bizouard, F. Boudjema, and G. Chalons, "One-loop renormalization of the NMSSM in SloopS. II. The Higgs sector," *Phys. Rev.* **D96** no. 1, (2017) 015040, `arXiv:1705.02209 [hep-ph]`.

[71] M. D. Goodsell, K. Nickel, and F. Staub, "Two-loop corrections to the Higgs masses in the NMSSM," *Phys. Rev.* **D91** (2015) 035021, `arXiv:1411.4665 [hep-ph]`.

[72] S. W. Ham, J. Kim, S. K. Oh, and D. Son, "Charged Higgs boson in the next-to-minimal supersymmetric standard model with explicit CP violation," *Phys. Rev.* **D64** (2001) 035007, `arXiv:hep-ph/0104144 [hep-ph]`.

[73] S. W. Ham, S. K. Oh, and D. Son, "Neutral Higgs sector of the next-to-minimal supersymmetric standard model with explicit CP violation," *Phys. Rev.* **D65** (2002) 075004, `arXiv:hep-ph/0110052 [hep-ph]`.

[74] S. W. Ham, Y. S. Jeong, and S. K. Oh, "Radiative CP violation in the Higgs sector of the next-to-minimal supersymmetric model," `arXiv:hep-ph/0308264 [hep-ph]`.

[75] K. Funakubo and S. Tao, "The Higgs sector in the Next-to-MSSM," *Prog. Theor. Phys.* **113** (2005) 821–842, `arXiv:hep-ph/0409294 [hep-ph]`.

[76] S. W. Ham, S. H. Kim, S. K. OH, and D. Son, "Higgs bosons of the NMSSM with explicit CP violation at the ILC," *Phys. Rev.* **D76** (2007) 115013, `arXiv:0708.2755 [hep-ph]`.

[77] F. Domingo, P. Drechsel, and S. Paßehr, "On-Shell neutral Higgs bosons in the NMSSM with complex parameters," *Eur. Phys. J.* **C77** no. 8, (2017) 562, `arXiv:1706.00437 [hep-ph]`.

[78] K. Cheung, T.-J. Hou, J. S. Lee, and E. Senaha, "Higgs Boson Sector of the Next-to-Minimal Supersymmetric Standard Model with CP Violation," *Phys. Rev.* **D82** (2010) 075007, `arXiv:1006.1458 [hep-ph]`.

[79] T. Graf, R. Gröber, M. Mühlleitner, H. Rzehak, and K. Walz, "Higgs Boson Masses in the Complex NMSSM at One-Loop Level," *JHEP* **10** (2012) 122, `arXiv:1206.6806` `[hep-ph]`.

[80] J. Baglio, R. Gröber, M. Mühlleitner, D. T. Nhung, H. Rzehak, M. Spira, J. Streicher, and K. Walz, "NMSSMCALC: A program package for the calculation of loop-corrected Higgs boson masses and decay widths in the (complex) NMSSM," *Comput. Phys. Commun.* **185** no. 12, (2014) 3372–3391, `arXiv:1312.4788` `[hep-ph]`.

[81] M. Mühlleitner, D. T. Nhung, H. Rzehak, and K. Walz, "Two-loop contributions of the order $\mathcal{O}(\alpha_t \alpha_s)$ to the masses of the Higgs bosons in the CP-violating NMSSM," *JHEP* **05** (2015) 128, `arXiv:1412.0918` `[hep-ph]`.

[82] T. N. Dao, R. Gröber, M. Krause, M. Mühlleitner, and H. Rzehak, "Two-Loop $\mathcal{O}(\alpha_t^2)$ Corrections to the Neutral Higgs Boson Masses in the CP-Violating NMSSM," `arXiv:1903.11358` `[hep-ph]`.

[83] M. Krause and M. Mühlleitner, "ewN2HDECAY - A program for the Calculation of Electroweak One-Loop Corrections to Higgs Decays in the Next-to-Minimal Two-Higgs-Doublet Model Including State-of-the-Art QCD Corrections," `arXiv:1904.02103` `[hep-ph]`.

[84] H. G. Liddell, R. Scott, and H. S. Jones, *A Greek-English lexicon*. Clarendon Press, Oxford [u.a.], 1996.

[85] S. M. Cohen, *Aristotle's Metaphysics*. Metaphysics Research Lab, Stanford University, winter 2016 ed., 2016. `http://plato.stanford.edu/entries/aristotle-metaphysics/`.

[86] S. Berryman, *Ancient Atomism*. Metaphysics Research Lab, Stanford University, winter 2016 ed., 2016. `https://plato.stanford.edu/entries/atomism-ancient/`.

[87] N. Robotti, "The discovery of the electron: I," *European Journal of Physics* **18** no. 3, (May, 1997) 133–138.

[88] B. M. Peake, "The discovery of the electron, proton, and neutron," *Journal of Chemical Education* **66** no. 9, (1989) 738.

[89] D. Griffiths, *Introduction to Elementary Particles*. Physics textbook. Wiley, 2008.

[90] H. Kragh, *Quantum Generations: A History of Physics in the Twentieth Century*. History and philosophy of science. Princeton University Press, 2002.

[91] W. Pauli, "The Connection Between Spin and Statistics," *Phys. Rev.* **58** (Oct, 1940) 716–722.

[92] M. Fierz, "Über die relativistische Theorie kräftefreier Teilchen mit beliebigem Spin," *Helvetica Physica Acta* **12** (Jan, 1939) 3–37.

[93] T. D. Lee, *History of Weak Interactions*, pp. 1–27. Springer US, Boston, MA, 1993.

[94] M. E. Peskin and D. V. Schroeder, *An Introduction to quantum field theory*. Advanced book program. Westview Press Reading (Mass.), 1995.

[95] **CDF** Collaboration, F. Abe *et al.*, "Observation of Top Quark Production in $\overline{p}p$ Collisions with the Collider Detector at Fermilab," *Phys. Rev. Lett.* **74** (1995) 2626–2631, `arXiv:hep-ex/9503002` `[hep-ex]`.

[96] **D0** Collaboration, S. Abachi *et al.*, "Search for high mass top quark production in $p\bar{p}$ collisions at $\sqrt{s} = 1.8$ TeV," *Phys. Rev. Lett.* **74** (1995) 2422–2426, `arXiv:hep-ex/9411001 [hep-ex]`.

[97] **DONUT** Collaboration, K. Kodama *et al.*, "Observation of tau neutrino interactions," *Phys. Lett.* **B504** (2001) 218–224, `arXiv:hep-ex/0012035 [hep-ex]`.

[98] **Particle Data Group** Collaboration, M. Tanabashi *et al.*, "Review of Particle Physics," *Phys. Rev.* **D98** no. 3, (2018) 030001.

[99] G. S. Guralnik, C. R. Hagen, and T. W. B. Kibble, "Global Conservation Laws and Massless Particles," *Phys. Rev. Lett.* **13** (Nov, 1964) 585–587.

[100] T. Nakano and K. Nishijima, "Charge Independence for V-particles*," *Progress of Theoretical Physics* **10** no. 5, (11, 1953) 581–582.

[101] M. Gell-Mann, "The interpretation of the new particles as displaced charge multiplets," *Il Nuovo Cimento (1955-1965)* **4** no. 2, (Apr, 1956) 848–866.

[102] **ATLAS** Collaboration, ATLAS, "Combined measurements of Higgs boson production and decay using up to 80 fb^{-1} of proton–proton collision data at $\sqrt{s} = 13$ TeV collected with the ATLAS experiment," Tech. Rep. ATLAS-CONF-2018-031, CERN, Geneva, Jul, 2018. `https://cds.cern.ch/record/2629412`.

[103] **Planck** Collaboration, N. Aghanim *et al.*, "Planck 2018 results. VI. Cosmological parameters," `arXiv:1807.06209 [astro-ph.CO]`.

[104] C. Gross, A. Polosa, A. Strumia, A. Urbano, and W. Xue, "Dark Matter in the Standard Model?," *Phys. Rev.* **D98** no. 6, (2018) 063005, `arXiv:1803.10242 [hep-ph]`.

[105] L. Canetti, M. Drewes, and M. Shaposhnikov, "Matter and Antimatter in the Universe," *New J. Phys.* **14** (2012) 095012, `arXiv:1204.4186 [hep-ph]`.

[106] A. D. Sakharov, "Violation of CP Invariance, C Asymmetry, and Baryon Asymmetry of the Universe," *Pisma Zh. Eksp. Teor. Fiz.* **5** (1967) 32–35. [Usp. Fiz. Nauk161,61(1991)].

[107] N. Cabibbo, "Unitary symmetry and leptonic decays," *Phys. Rev. Lett.* **10** (Jun, 1963) 531–533.

[108] M. Kobayashi and T. Maskawa, "CP Violation in the Renormalizable Theory of Weak Interaction," *Prog. Theor. Phys.* **49** (1973) 652–657.

[109] M. Trodden, "Electroweak baryogenesis," *Rev. Mod. Phys.* **71** (1999) 1463–1500, `arXiv:hep-ph/9803479 [hep-ph]`.

[110] T. Padmanabhan, "Thermodynamical Aspects of Gravity: New insights," *Rept. Prog. Phys.* **73** (2010) 046901, `arXiv:0911.5004 [gr-qc]`.

[111] E. P. Verlinde, "On the Origin of Gravity and the Laws of Newton," *JHEP* **04** (2011) 029, `arXiv:1001.0785 [hep-th]`.

[112] K. Pardo, "Testing Emergent Gravity with Isolated Dwarf Galaxies," `arXiv:1706.00785 [astro-ph.CO]`.

[113] S. Weinberg, "The Cosmological Constant Problem," *Rev. Mod. Phys.* **61** (Jan, 1989) 1–23.

[114] S. M. Carroll, "The Cosmological constant," *Living Rev. Rel.* **4** (2001) 1, `arXiv:astro-ph/0004075 [astro-ph]`.

[115] K. Arun, S. Gudennavar, and C. Sivaram, "Dark matter, dark energy, and alternate models: A review," *Advances in Space Research* **60** no. 1, (2017) 166 – 186.

[116] **Super-Kamiokande** Collaboration, Y. Fukuda *et al.*, "Measurements of the solar neutrino flux from Super-Kamiokande's first 300 days," *Phys. Rev. Lett.* **81** (1998) 1158–1162, `arXiv:hep-ex/9805021 [hep-ex]`. [Erratum: Phys. Rev. Lett.81, 4279(1998), `https://dx.doi.org/10.1103/PhysRevLett.81.4279`].

[117] **KATRIN** Collaboration, S. Mertens, "Status of the KATRIN Experiment and Prospects to Search for keV-mass Sterile Neutrinos in Tritium β-decay," *Physics Procedia* **61** (2015) 267 – 273. 13th International Conference on Topics in Astroparticle and Underground Physics, TAUP 2013.

[118] T. Blum, A. Denig, I. Logashenko, E. de Rafael, B. L. Roberts, T. Teubner, and G. Venanzoni, "The Muon $(g - 2)$ Theory Value: Present and Future," `arXiv:1311.2198 [hep-ph]`.

[119] S. Bifani, S. Descotes-Genon, A. Romero Vidal, and M.-H. Schune, "Review of Lepton Universality tests in B decays," *J. Phys.* **G46** no. 2, (2019) 023001, `arXiv:1809.06229 [hep-ex]`.

[120] M. Dine, "TASI lectures on the strong CP problem," in *Flavor physics for the millennium. Proceedings, Theoretical Advanced Study Institute in elementary particle physics, TASI 2000, Boulder, USA, June 4-30, 2000*, pp. 349–369. 2000. `arXiv:hep-ph/0011376 [hep-ph]`.

[121] G. F. Giudice, *Naturally Speaking: The Naturalness Criterion and Physics at the LHC*, pp. 155–178. World Scientific Publishing Co, 2008.

[122] J. D. Wells, "The Utility of Naturalness, and how its Application to Quantum Electrodynamics envisages the Standard Model and Higgs Boson," *Stud. Hist. Phil. Sci.* **B49** (2015) 102–108, `arXiv:1305.3434 [hep-ph]`.

[123] J. F. Gunion, H. E. Haber, and J. Wudka, "Sum rules for Higgs bosons," *Phys. Rev. D* **43** (Feb, 1991) 904–912.

[124] **CMS** Collaboration, A. M. Sirunyan *et al.*, "Search for the flavor-changing neutral current interactions of the top quark and the Higgs boson which decays into a pair of b quarks at $\sqrt{s} = 13$ TeV," *JHEP* **06** (2018) 102, `arXiv:1712.02399 [hep-ex]`.

[125] **ATLAS** Collaboration, M. Aaboud *et al.*, "Search for flavour-changing neutral current top-quark decays $t \to qZ$ in proton-proton collisions at $\sqrt{s} = 13$ TeV with the ATLAS detector," *JHEP* **07** (2018) 176, `arXiv:1803.09923 [hep-ex]`.

[126] S. L. Glashow, J. Iliopoulos, and L. Maiani, "Weak Interactions with Lepton-Hadron Symmetry," *Phys. Rev. D* **2** (Oct, 1970) 1285–1292.

[127] L. Lopez Honorez, E. Nezri, J. F. Oliver, and M. H. G. Tytgat, "The Inert Doublet Model: An Archetype for Dark Matter," *JCAP* **0702** (2007) 028, `arXiv:hep-ph/0612275 [hep-ph]`.

[128] E. M. Dolle and S. Su, "Inert Dark Matter," *Phys. Rev.* **D80** (2009) 055012, `arXiv:0906.1609 [hep-ph]`.

[129] A. Ilnicka, M. Krawczyk, and T. Robens, "Inert Doublet Model in light of LHC Run I and astrophysical data," *Phys. Rev.* **D93** no. 5, (2016) 055026, `arXiv:1508.01671 [hep-ph]`.

[130] A. Belyaev, G. Cacciapaglia, I. P. Ivanov, F. Rojas-Abatte, and M. Thomas, "Anatomy of the Inert Two Higgs Doublet Model in the light of the LHC and non-LHC Dark Matter Searches," *Phys. Rev.* **D97** no. 3, (2018) 035011, `arXiv:1612.00511 [hep-ph]`.

[131] I. Engeln, "Phenomenological Comparison of the Dark Phases of the Next-to-Two-Higgs-Doublet Model," Master's thesis, Karlsruher Institut für Technologie, Mar, 2018. `https://www.itp.kit.edu/_media/publications/masterthesis_isabellengeln.pdf`.

[132] D. Azevedo, P. M. Ferreira, M. M. Muhlleitner, S. Patel, R. Santos, and J. Wittbrodt, "CP in the dark," *JHEP* **11** (2018) 091, `arXiv:1807.10322 [hep-ph]`.

[133] S. R. Coleman and J. Mandula, "All Possible Symmetries of the S Matrix," *Phys. Rev.* **159** (1967) 1251–1256.

[134] R. Haag, J. T. Łopuszański, and M. Sohnius, "All possible generators of supersymmetries of the s-matrix," *Nuclear Physics B* **88** no. 2, (1975) 257 – 274.

[135] J. H. Schwarz and N. Seiberg, "String theory, supersymmetry, unification, and all that," *Rev. Mod. Phys.* **71** (1999) S112–S120, `arXiv:hep-th/9803179 [hep-th]`.

[136] L. Girardello and M. Grisaru, "Soft breaking of supersymmetry," *Nuclear Physics B* **194** no. 1, (1982) 65 – 76.

[137] S. P. Martin, "Dimensionless supersymmetry breaking couplings, flat directions, and the origin of intermediate mass scales," *Phys. Rev.* **D61** (2000) 035004, `arXiv:hep-ph/9907550 [hep-ph]`.

[138] K. S. Babu, C. F. Kolda, J. March-Russell, and F. Wilczek, "CP violation, Higgs couplings, and supersymmetry," *Phys. Rev.* **D59** (1999) 016004, `arXiv:hep-ph/9804355 [hep-ph]`.

[139] **Super-Kamiokande** Collaboration, K. Abe *et al.*, "Search for proton decay via $p \to e^+\pi^0$ and $p \to \mu^+\pi^0$ in 0.31 megaton·years exposure of the Super-Kamiokande water Cherenkov detector," *Phys. Rev.* **D95** no. 1, (2017) 012004, `arXiv:1610.03597 [hep-ex]`.

[140] F. Franke and H. Fraas, "Neutralinos and Higgs bosons in the next-to-minimal supersymmetric standard model," *Int.J.Mod.Phys.* **A12** (1997) 479–534, `arXiv:hep-ph/9512366 [hep-ph]`.

[141] S. F. King, M. Mühlleitner, R. Nevzorov, and K. Walz, "Exploring the CP-violating NMSSM: EDM constraints and phenomenology," *Nucl. Phys.* **B901** (2015) 526–555, `arXiv:1508.03255 [hep-ph]`.

[142] S. F. King, M. Mühlleitner, R. Nevzorov, and K. Walz, "Discovery Prospects for NMSSM Higgs bosons at the high-energy Large Hadron Collider," *Phys. Rev.* **D90** no. 9, (2014) 095014, `arXiv:1408.1120 [hep-ph]`.

[143] M. Srednicki, *Quantum Field Theory*. Cambridge University Press, 2007.

[144] M. Böhm, A. Denner, and H. Joos, *Gauge Theories of the Strong and Electroweak Interaction*. Vieweg+Teubner Verlag, 2012.

[145] K. G. Wilson, "Renormalization Group and Strong Interactions," *Phys. Rev.* **D3** (1971) 1818.

[146] K. G. Wilson and M. E. Fisher, "Critical exponents in 3.99 dimensions," *Phys. Rev. Lett.* **28** (1972) 240–243.

[147] J. F. Ashmore, "A method of gauge-invariant regularization," *Lettere al Nuovo Cimento (1971-1985)* **4** no. 8, (Jun, 1972) 289–290.

[148] C. G. Bollini and J. J. Giambiagi, "Dimensional Renormalization: The Number of Dimensions as a Regularizing Parameter," *Nuovo Cim.* **B12** (1972) 20–26.

[149] G. 't Hooft and M. J. G. Veltman, "Regularization and Renormalization of Gauge Fields," *Nucl. Phys.* **B44** (1972) 189–213.

[150] W. Siegel, "Supersymmetric dimensional regularization via dimensional reduction," *Physics Letters B* **84** no. 2, (1979) 193 – 196.

[151] D. Stöckinger, "Regularization by dimensional reduction: consistency, quantum action principle, and supersymmetry," *JHEP* **03** (2005) 076, `arXiv:hep-ph/0503129 [hep-ph]`.

[152] S. L. Adler, "Axial-vector vertex in spinor electrodynamics," *Phys. Rev.* **177** (Jan, 1969) 2426–2438.

[153] J. S. Bell and R. Jackiw, "A PCAC puzzle: $\pi^0 \to \gamma\gamma$ in the σ model," *Nuovo Cim.* **A60** (1969) 47–61.

[154] W. A. Bardeen, "Anomalous Ward identities in Spinor Field Theories," *Phys. Rev.* **184** (1969) 1848–1857.

[155] H.-L. Yu and W. B. Yeung, "Dimensional regularization and the γ_5 axial anomaly," *Phys. Rev.* **D35** (1987) 3955.

[156] M. S. Chanowitz, M. Furman, and I. Hinchliffe, "The axial current in dimensional regularization," *Nucl. Phys.* **B159** (1979) 225–243.

[157] F. Jegerlehner, "Facts of life with γ_5," *Eur. Phys. J.* **C18** (2001) 673–679, `arXiv:hep-th/0005255 [hep-th]`.

[158] W. Beenakker, R. Hopker, and P. M. Zerwas, "SUSY-QCD decays of squarks and gluinos," *Phys. Lett.* **B378** (1996) 159–166, `arXiv:hep-ph/9602378 [hep-ph]`.

[159] W. Hollik, E. Kraus, and D. Stöckinger, "Renormalization and symmetry conditions in supersymmetric QED," *Eur. Phys. J.* **C11** (1999) 365–381, `arXiv:hep-ph/9907393 [hep-ph]`.

[160] W. Hollik and D. Stöckinger, "Regularization and supersymmetry-restoring counterterms in supersymmetric QCD," *Eur. Phys. J.* **C20** (2001) 105–119, `arXiv:hep-ph/0103009 [hep-ph]`.

[161] I. Fischer, W. Hollik, M. Roth, and D. Stöckinger, "Restoration of supersymmetric Slavnov-Taylor and Ward identities in presence of soft and spontaneous symmetry breaking," *Phys. Rev.* **D69** (2004) 015004, `arXiv:hep-ph/0310191 [hep-ph]`.

[162] I. Jack and D. R. T. Jones, *Regularization of supersymmetric theories*, pp. 149–167. World Scientific Publishing Co. Pte. Ltd., 1998. `hep-ph/9707278`.

[163] D. M. Capper, D. R. T. Jones, and P. van Nieuwenhuizen, "Regularization by Dimensional Reduction of Supersymmetric and Non-Supersymmetric Gauge Theories," *Nucl. Phys.* **B167** (1980) 479–499.

[164] W. Hollik and D. Stöckinger, "MSSM Higgs-boson mass predictions and two-loop non-supersymmetric counterterms," *Phys. Lett.* **B634** (2006) 63–68, `arXiv:hep-ph/0509298 [hep-ph]`.

[165] R. Harlander, P. Kant, L. Mihaila, and M. Steinhauser, "Dimensional Reduction applied to QCD at three loops," *JHEP* **09** (2006) 053, `arXiv:hep-ph/0607240 [hep-ph]`.

[166] D. Stöckinger and J. Unger, "Three-loop MSSM Higgs-boson mass predictions and regularization by dimensional reduction," *Nucl. Phys.* **B935** (2018) 1–16, `arXiv:1804.05619 [hep-ph]`.

[167] C. Csaki, "The Minimal supersymmetric standard model (MSSM)," *Mod. Phys. Lett.* **A11** (1996) 599, `arXiv:hep-ph/9606414 [hep-ph]`.

[168] R. Santos and A. Barroso, "Renormalization of two-Higgs-doublet models," *Phys. Rev.* **D56** (1997) 5366–5385, `arXiv:hep-ph/9701257 [hep-ph]`.

[169] G. Källén, "On the definition of the Renormalization Constants in Quantum Electrodynamics," *Helv. Phys. Acta* **25** no. 4, (1952) 417.

[170] H. Lehmann, "Über Eigenschaften von Ausbreitungsfunktionen und Renormierungskonstanten quantisierter Felder," *Il Nuovo Cimento (1943-1954)* **11** no. 4, (2008) 342–357.

[171] I. Jack, D. R. T. Jones, S. P. Martin, M. T. Vaughn, and Y. Yamada, "Decoupling of the ε-scalar mass in softly broken supersymmetry," *Phys. Rev.* **D50** (1994) R5481–R5483, `arXiv:hep-ph/9407291 [hep-ph]`.

[172] S. P. Martin, "Two loop effective potential for a general renormalizable theory and softly broken supersymmetry," *Phys. Rev.* **D65** (2002) 116003, `arXiv:hep-ph/0111209 [hep-ph]`.

[173] R. V. Harlander, J. Klappert, A. D. Ochoa Franco, and A. Voigt, "The light CP-even MSSM Higgs mass resummed to fourth logarithmic order," *Eur. Phys. J.* **C78** no. 10, (2018) 874, `arXiv:1807.03509 [hep-ph]`.

[174] R. Harlander, P. Kant, L. Mihaila, and M. Steinhauser, "Dimensional reduction applied to QCD at higher orders," in *Proceedings, 15th International Workshop on Deep-inelastic scattering and related subjects (DIS 2007). Vol. 1 and 2: Munich, Germany, April 16-20, 2007*, pp. 991–994. 2007. `arXiv:0706.2982 [hep-ph]`.

[175] P. Kant, "Dimensional Reduction Applied to Non-SUSY Theories," in *SUSY 2007 Proceedings, 15th International Conference on Supersymmetry and Unification of Fundamental Interactions, July 26 - August 1, 2007, Karlsruhe, Germany*. 2007. `arXiv:0710.2490 [hep-th]`.

[176] H. Lehmann, K. Symanzik, and W. Zimmermann, "Zur Formulierung quantisierter Feldtheorien," *Il Nuovo Cimento (1955-1965)* **1** no. 1, (Jan, 1955) 205–225.

[177] G. 't Hooft, "Renormalization of massless Yang-Mills fields," *Nuclear Physics B* **33** no. 1, (1971) 173 – 199.

[178] J. Taylor, "Ward identities and charge renormalization of the Yang-Mills field," *Nuclear Physics B* **33** no. 2, (1971) 436 – 444.

[179] A. A. Slavnov, "Ward identities in gauge theories," *Theoretical and Mathematical Physics* **10** no. 2, (Feb, 1972) 99–104.

[180] T. Kinoshita, "Mass singularities of Feynman amplitudes," *J. Math. Phys.* **3** (1962) 650–677.

[181] T. D. Lee and M. Nauenberg, "Degenerate Systems and Mass Singularities," *Phys. Rev.* **133** (Mar, 1964) B1549–B1562.

[182] M. D. Goodsell, S. Liebler, and F. Staub, "Generic calculation of two-body partial decay widths at the full one-loop level," *The European Physical Journal C* **77** no. 11, (Nov, 2017) 758, `arXiv:1703.09237 [hep-ph]`.

[183] A. Denner, "Techniques for Calculation of Electroweak Radiative Corrections at the One-Loop Level and Results for *W*-physics at LEP 200," *Fortsch. Phys.* **41** (1993) 307–420, `arXiv:0709.1075 [hep-ph]`.

[184] W. J. Marciano and A. Sirlin, "Dimensional Regularization of Infrared Divergences," *Nucl. Phys.* **B88** (1975) 86–98.

[185] G. Degrassi, S. Di Vita, J. Elias-Miro, J. R. Espinosa, G. F. Giudice, G. Isidori, and A. Strumia, "Higgs mass and vacuum stability in the Standard Model at NNLO," *JHEP* **08** (2012) 098, `arXiv:1205.6497 [hep-ph]`.

[186] A. V. Bednyakov, B. A. Kniehl, A. F. Pikelner, and O. L. Veretin, "Stability of the Electroweak Vacuum: Gauge Independence and Advanced Precision," *Phys. Rev. Lett.* **115** no. 20, (2015) 201802, `arXiv:1507.08833 [hep-ph]`.

[187] C. Runge, "Ueber die numerische Auflösung von Differentialgleichungen," *Mathematische Annalen* **46** no. 2, (Jun, 1895) 167–178.

[188] W. Kutta, "Beitrag zur näherungsweisen Integration totaler Differentialgleichungen," *Zeit. Math. Phys.* **46** (1901) 435–53.

[189] L. Altenkamp, S. Dittmaier, and H. Rzehak, "Renormalization schemes for the Two-Higgs-Doublet Model and applications to h → WW/ZZ → 4 fermions," *JHEP* **09** (2017) 134, `arXiv:1704.02645 [hep-ph]`.

[190] A. V. Konychev, "On the renormalization scheme dependence in quantum field theory," `arXiv:hep-ph/9712477 [hep-ph]`.

[191] L. D. Faddeev and V. N. Popov, "Feynman Diagrams for the Yang-Mills Field," *Phys. Lett.* **B25** (1967) 29–30.

[192] T. Appelquist, J. Carazzone, J. T. Goldman, and H. R. Quinn, "Renormalization and Gauge Independence in Spontaneously Broken Gauge Theories," *Phys. Rev.* **D8** (1973) 1747–1756.

[193] N. K. Nielsen, "On the Gauge Dependence of Spontaneous Symmetry Breaking in Gauge Theories," *Nucl. Phys.* **B101** (1975) 173–188.

[194] G. Costa and M. Tonin, "Renormalization of non-abelian local gauge theories," *La Rivista del Nuovo Cimento (1971-1977)* **5** no. 1, (Jan, 1975) 29–107.

[195] E. Kazes, T. E. Feuchtwang, P. H. Cutler, and H. Grotch, "Gauge Invariance and Gauge Independence of the S Matrix in Nonrelativistic Quantum Mechanics and Relativistic Quantum Field Theories," *Annals Phys.* **142** (1982) 80–94.

[196] P. Gambino and P. A. Grassi, "Nielsen identities of the SM and the definition of mass," *Phys. Rev.* **D62** (2000) 076002, `arXiv:hep-ph/9907254 [hep-ph]`.

[197] W. Kummer, "On the gauge independence of the S matrix," *Eur. Phys. J.* **C21** (2001) 175–179, `arXiv:hep-th/0104123 [hep-th]`.

[198] C. Becchi, A. Rouet, and R. Stora, "Renormalization of Gauge Theories," *Annals Phys.* **98** (1976) 287–321.

[199] M. Z. Iofa and I. V. Tyutin, "Gauge invariance of spontaneously broken non-Abelian theories in the Bogolyubov-Parasyuk-Hepp-Zimmermann method," *Theoretical and Mathematical Physics* **27** no. 1, (Apr, 1976) 316–322.

[200] S. Pokorski and P. Landshoff, *Gauge Field Theories.* Cambridge Monographs on Mathematical Physics. Cambridge University Press, 2000.

[201] J. M. Cornwall and J. Papavassiliou, "Gauge-invariant three-gluon vertex in QCD," *Phys. Rev.* **D40** (1989) 3474.

[202] J. Papavassiliou, "Gauge-invariant proper self-energies and vertices in gauge theories with broken symmetry," *Phys. Rev.* **D41** (1990) 3179.

[203] G. Degrassi and A. Sirlin, "Gauge-invariant self-energies and vertex parts of the standard model in the pinch technique framework," *Phys. Rev. D* **46** (Oct, 1992) 3104–3116.

[204] J. Papavassiliou, "Gauge-independent transverse and longitudinal self-energies and vertices via the pinch technique," *Phys. Rev.* **D50** (1994) 5958–5970, `arXiv:hep-ph/9406258 [hep-ph]`.

[205] N. J. Watson, "Universality of the pinch technique gauge boson selfenergies," *Phys. Lett.* **B349** (1995) 155–164, `arXiv:hep-ph/9412319 [hep-ph]`.

[206] J. Papavassiliou and A. Pilaftsis, "Gauge Invariance and Unstable Particles," *Phys. Rev. Lett.* **75** (1995) 3060–3063, `arXiv:hep-ph/9506417 [hep-ph]`.

[207] D. Binosi, "Electroweak pinch technique to all orders," *J. Phys.* **G30** (2004) 1021–1064, `arXiv:hep-ph/0401182 [hep-ph]`.

[208] D. Binosi and J. Papavassiliou, "Pinch technique: Theory and applications," *Phys. Rept.* **479** (2009) 1–152, `arXiv:0909.2536 [hep-ph]`.

[209] H. Kluberg-Stern and J. B. Zuber, "Renormalization of non-abelian Gauge Theories in a Background Field Gauge. I. Green's Functions," *Phys. Rev.* **D12** (1975) 482–488.

[210] H. Kluberg-Stern and J. B. Zuber, "Renormalization of non-Abelian gauge theories in a background-field gauge. II. Gauge-invariant operators," *Phys. Rev. D* **12** (Nov, 1975) 3159–3180.

[211] D. G. Boulware, "Gauge dependence of the effective action," *Phys. Rev.* **D23** (1981) 389.

[212] L. F. Abbott, "The background field method beyond one loop," *Nucl. Phys.* **B185** (1981) 189–203.

[213] L. F. Abbott, "Introduction to the Background Field Method," *Acta Phys. Polon.* **B13** (1982) 33.

[214] C. F. Hart, "Theory and renormalization of the gauge-invariant effective action," *Phys. Rev. D* **28** (10, 1983) 1993–2006.

[215] A. Denner, G. Weiglein, and S. Dittmaier, "Application of the background field method to the electroweak standard model," *Nucl. Phys.* **B440** (1995) 95–128, `arXiv:hep-ph/9410338 [hep-ph]`.

[216] A. Denner, S. Dittmaier, and J.-N. Lang, "Renormalization of mixing angles," *JHEP* **11** (2018) 104, `arXiv:1808.03466 [hep-ph]`.

[217] A. Djouadi, J. Kalinowski, and M. Spira, "HDECAY: A Program for Higgs boson decays in the standard model and its supersymmetric extension," *Comput. Phys. Commun.* **108** (1998) 56–74, arXiv:hep-ph/9704448 [hep-ph].

[218] K. Fujikawa, B. W. Lee, and A. I. Sanda, "Generalized Renormalizable Gauge Formulation of Spontaneously Broken Gauge Theories," *Phys. Rev.* **D6** (1972) 2923–2943.

[219] Y.-P. Yao, "Quantization and Gauge Freedom in a Theory with Spontaneously Broken Symmetry," *Phys. Rev.* **D7** (1973) 1647–1660.

[220] J. Velhinho, R. Santos, and A. Barroso, "Tree level vacuum stability in two-Higgs-doublet models," *Physics Letters B* **322** no. 3, (1994) 213 – 218.

[221] J. F. Gunion and H. E. Haber, "CP-conserving two-Higgs-doublet model: The approach to the decoupling limit," *Phys. Rev.* **D67** (2003) 075019, arXiv:hep-ph/0207010 [hep-ph].

[222] S. Kanemura, Y. Okada, E. Senaha, and C. P. Yuan, "Higgs coupling constants as a probe of new physics," *Phys. Rev.* **D70** (2004) 115002, arXiv:hep-ph/0408364 [hep-ph].

[223] L. Baulieu, "Perturbative Gauge Theories," *Phys. Rept.* **129** (1985) 1.

[224] S. L. Glashow and S. Weinberg, "Natural Conservation Laws for Neutral Currents," *Phys. Rev. D* **15** (Apr, 1977) 1958–1965.

[225] D. López-Val and J. Solà, "Neutral Higgs-pair production at linear colliders within the general two-Higgs-doublet model: Quantum effects and triple Higgs boson self-interactions," *Phys. Rev.* **D81** (2010) 033003, arXiv:0908.2898 [hep-ph].

[226] M. Krause, "On the Renormalization of the Two-Higgs-Doublet Model," Master's thesis, Karlsruher Institut für Technologie (KIT), Institut für theoretische Physik (ITP), Karlsruhe, May, 2016. https://www.itp.kit.edu/_media/publications/masterthesismarcel.pdf.

[227] M. Krause, R. Lorenz, M. Mühlleitner, R. Santos, and H. Ziesche, "Gauge-independent Renormalization of the 2-Higgs-Doublet Model," *JHEP* **09** (2016) 143, arXiv:1605.04853 [hep-ph].

[228] M. Krause, M. Mühlleitner, R. Santos, and H. Ziesche, "Higgs-to-Higgs boson decays in a 2HDM at next-to-leading order," *Phys. Rev.* **D95** no. 7, (2017) 075019, arXiv:1609.04185 [hep-ph].

[229] A. Denner, L. Jenniches, J.-N. Lang, and C. Sturm, "Gauge-independent $\overline{MS}$ renormalization in the 2HDM," *JHEP* **09** (2016) 115, arXiv:1607.07352 [hep-ph].

[230] S. Kanemura, M. Kikuchi, and K. Yagyu, "Fingerprinting the extended Higgs sector using one-loop corrected Higgs boson couplings and future precision measurements," *Nucl. Phys.* **B896** (2015) 80–137, arXiv:1502.07716 [hep-ph].

[231] J. Fleischer and F. Jegerlehner, "Radiative corrections to Higgs-boson decays in the Weinberg-Salam model," *Phys. Rev. D* **23** (May, 1981) 2001–2026.

[232] P. Gambino, P. A. Grassi, and F. Madricardo, "Fermion mixing renormalization and gauge invariance," *Phys. Lett.* **B454** (1999) 98–104, arXiv:hep-ph/9811470 [hep-ph].

[233] A. Barroso, L. Brucher, and R. Santos, "Renormalization of the Cabibbo-Kobayashi-Maskawa matrix," *Phys. Rev.* **D62** (2000) 096003, `arXiv:hep-ph/0004136 [hep-ph]`.

[234] B. A. Kniehl, F. Madricardo, and M. Steinhauser, "Gauge-independent W-boson partial decay widths," *Phys. Rev.* **D62** (2000) 073010, `arXiv:hep-ph/0005060 [hep-ph]`.

[235] A. Pilaftsis, "Gauge and scheme dependence of mixing matrix renormalization," *Phys. Rev.* **D65** (2002) 115013, `arXiv:hep-ph/0203210 [hep-ph]`.

[236] Y. Yamada, "Gauge dependence of the on-shell renormalized mixing matrices," *Phys. Rev.* **D64** (2001) 036008, `arXiv:hep-ph/0103046 [hep-ph]`.

[237] K. P. O. Diener and B. A. Kniehl, "On-mass-shell renormalization of fermion mixing matrices," *Nucl. Phys.* **B617** (2001) 291–307, `arXiv:hep-ph/0109110 [hep-ph]`.

[238] A. Freitas and D. Stöckinger, "Gauge dependence and renormalization of tan β in the minimal supersymmetric standard model," *Phys. Rev.* **D66** (2002) 095014, `arXiv:hep-ph/0205281 [hep-ph]`.

[239] R. Lorenz, "Full One-Loop Electroweak Corrections to the Decays $H^+ \to W^+\ h/H$ in the Two-Higgs-Doublet Model," Master's thesis, Karlsruher Institut für Technologie (KIT), Institut für theoretische Physik (ITP), Karlsruhe, Jun, 2015. `https://www.itp.kit.edu/prep/diploma/PSFiles/MasterRobinL.pdf`.

[240] J. R. Espinosa and Y. Yamada, "Scale- and gauge-independent mixing angles for scalar particles," *Phys. Rev.* **D67** (2003) 036003, `arXiv:hep-ph/0207351 [hep-ph]`.

[241] J. A. Coarasa Perez, D. Garcia, J. Guasch, R. A. Jimenez, and J. Sola, "Quantum effects on $t \to H^+ b$ in the MSSM: a window to 'virtual' supersymmetry?," *Eur. Phys. J.* **C2** (1998) 373–392, `arXiv:hep-ph/9607485 [hep-ph]`.

[242] R. Santos, A. Barroso, and L. Brucher, "Top quark loop corrections to the decay $H^+ \to h^0 W^+$ in the two-Higgs doublet model," *Phys. Lett.* **B391** (1997) 429–433, `arXiv:hep-ph/9608376 [hep-ph]`.

[243] A. Denner, E. Kraus, and M. Roth, "Physical renormalization condition for the quark-mixing matrix," *Phys. Rev.* **D70** (2004) 033002, `arXiv:hep-ph/0402130 [hep-ph]`.

[244] B. Pontecorvo, "Inverse beta processes and nonconservation of lepton charge," *Sov. Phys. JETP* **7** (1958) 172–173. `http://www.jetp.ac.ru/cgi-bin/e/index/e/7/1/p172?a=list`.

[245] Z. Maki, M. Nakagawa, and S. Sakata, "Remarks on the Unified Model of Elementary Particles," *Progress of Theoretical Physics* **28** no. 5, (11, 1962) 870–880.

[246] M. Böhm, H. Spiesberger, and W. Hollik, "On the 1-Loop Renormalization of the Electroweak Standard Model and its Application to Leptonic Processes," *Fortsch. Phys.* **34** (1986) 687–751.

[247] W. R. Inc., *Mathematica, Version 11.3*. Wolfram Research, Inc., 2018. Champaign, IL.

[248] T. Hahn, "Generating Feynman diagrams and amplitudes with FeynArts 3," *Comput. Phys. Commun.* **140** (2001) 418–431, `arXiv:hep-ph/0012260 [hep-ph]`.

[249] G. 't Hooft and M. J. G. Veltman, "Scalar one-loop integrals," *Nucl. Phys.* **B153** (1979) 365–401.

[250] R. Mertig, M. Böhm, and A. Denner, "Feyn Calc - Computer-algebraic calculation of Feynman amplitudes," *Comput. Phys. Commun.* **64** (1991) 345–359.

[251] V. Shtabovenko, R. Mertig, and F. Orellana, "New Developments in FeynCalc 9.0," *Comput. Phys. Commun.* **207** (2016) 432–444, arXiv:1601.01167 [hep-ph].

[252] T. Hahn and M. Pérez-Victoria, "Automated one-loop calculations in four and D dimensions," *Comput. Phys. Commun.* **118** (1999) 153–165, arXiv:hep-ph/9807565 [hep-ph].

[253] P. Z. Skands *et al.*, "SUSY Les Houches accord: interfacing SUSY spectrum calculators, decay packages, and event generators," *JHEP* **07** (2004) 036, arXiv:hep-ph/0311123 [hep-ph].

[254] B. C. Allanach *et al.*, "SUSY Les Houches Accord 2," *Comput. Phys. Commun.* **180** (2009) 8–25, arXiv:0801.0045 [hep-ph].

[255] M. Krause, D. López-Val, M. Mühlleitner, and R. Santos, "Gauge-independent Renormalization of the N2HDM," *JHEP* **12** (2017) 077, arXiv:1708.01578 [hep-ph].

[256] **HPQCD** Collaboration, I. Allison *et al.*, "High-precision charm-quark mass from current-current correlators in lattice and continuum QCD," *Phys. Rev.* **D78** (2008) 054513, arXiv:0805.2999 [hep-lat].

[257] P. Basler, M. Krause, M. Mühlleitner, J. Wittbrodt, and A. Wlotzka, "Strong first order electroweak phase transition in the CP-conserving 2HDM revisited," *JHEP* **02** (2017) 121, arXiv:1612.04086 [hep-ph].

[258] M. Mühlleitner, M. O. P. Sampaio, R. Santos, and J. Wittbrodt, "Phenomenological comparison of models with extended Higgs sectors," *JHEP* **08** (2017) 132, arXiv:1703.07750 [hep-ph].

[259] M. Misiak and M. Steinhauser, "Weak radiative decays of the B meson and bounds on $M_{H^\pm}$ in the Two-Higgs-Doublet Model," *Eur. Phys. J.* **C77** no. 3, (2017) 201, arXiv:1702.04571 [hep-ph].

[260] R. Coimbra, M. O. P. Sampaio, and R. Santos, "ScannerS: Constraining the phase diagram of a complex scalar singlet at the LHC," *Eur. Phys. J.* **C73** (2013) 2428, arXiv:1301.2599 [hep-ph].

[261] P. M. Ferreira, R. Guedes, M. O. P. Sampaio, and R. Santos, "Wrong sign and symmetric limits and non-decoupling in 2HDMs," *JHEP* **12** (2014) 067, arXiv:1409.6723 [hep-ph].

[262] P. Bechtle, O. Brein, S. Heinemeyer, G. Weiglein, and K. E. Williams, "HiggsBounds: Confronting arbitrary Higgs sectors with exclusion bounds from LEP and the Tevatron," *Comput. Phys. Commun.* **181** (2010) 138–167, arXiv:0811.4169 [hep-ph].

[263] P. Bechtle, O. Brein, S. Heinemeyer, G. Weiglein, and K. E. Williams, "HiggsBounds 2.0.0: Confronting neutral and charged Higgs sector predictions with exclusion bounds from LEP and the Tevatron," *Comput. Phys. Commun.* **182** (2011) 2605–2631, arXiv:1102.1898 [hep-ph].

[264] P. Bechtle, O. Brein, S. Heinemeyer, O. Stål, T. Stefaniak, G. Weiglein, and K. E. Williams, "HiggsBounds − 4: improved tests of extended Higgs sectors against exclusion bounds from LEP, the Tevatron and the LHC," *Eur. Phys. J.* **C74** no. 3, (2014) 2693, arXiv:1311.0055 [hep-ph].

[265] P. Bechtle, S. Heinemeyer, O. Stål, T. Stefaniak, and G. Weiglein, "*HiggsSignals*: Confronting arbitrary Higgs sectors with measurements at the Tevatron and the LHC," *Eur. Phys. J.* **C74** no. 2, (2014) 2711, `arXiv:1305.1933 [hep-ph]`.

[266] M. Sperling, D. Stöckinger, and A. Voigt, "Renormalization of vacuum expectation values in spontaneously broken gauge theories," *JHEP* **07** (2013) 132, `arXiv:1305.1548 [hep-ph]`.

[267] F. Staub, "Automatic calculation of supersymmetric renormalization group equations and loop corrections," *Comput. Phys. Commun.* **182** (2011) 808–833, `arXiv:1002.0840 [hep-ph]`.

[268] F. Staub, "SARAH 3.2: Dirac Gauginos, UFO output, and more," *Comput. Phys. Commun.* **184** (2013) 1792–1809, `arXiv:1207.0906 [hep-ph]`.

[269] F. Staub, "SARAH 4 : A tool for (not only SUSY) model builders," *Comput. Phys. Commun.* **185** (2014) 1773–1790, `arXiv:1309.7223 [hep-ph]`.

[270] M. D. Goodsell, K. Nickel, and F. Staub, "Two-Loop Higgs mass calculations in supersymmetric models beyond the MSSM with SARAH and SPheno," *Eur. Phys. J.* **C75** no. 1, (2015) 32, `arXiv:1411.0675 [hep-ph]`.

[271] J. E. Kim and H. Nilles, "The μ-problem and the strong CP-problem," *Physics Letters B* **138** no. 1, (1984) 150 – 154.

[272] R. D. Peccei and H. R. Quinn, "CP Conservation in the Presence of Pseudoparticles," *Phys. Rev. Lett.* **38** (Jun, 1977) 1440–1443.

[273] R. D. Peccei and H. R. Quinn, "Constraints imposed by CP conservation in the presence of pseudoparticles," *Phys. Rev. D* **16** (Sep, 1977) 1791–1797.

[274] D. Miller, R. Nevzorov, and P. Zerwas, "The Higgs sector of the next-to-minimal supersymmetric standard model," *Nuclear Physics B* **681** no. 1, (2004) 3 – 30.

[275] S. Dimopoulos and S. D. Thomas, "Dynamical relaxation of the supersymmetric CP violating phases," *Nucl. Phys.* **B465** (1996) 23–33, `arXiv:hep-ph/9510220 [hep-ph]`.

[276] S. Heinemeyer, W. Hollik, H. Rzehak, and G. Weiglein, "The Higgs sector of the complex MSSM at two-loop order: QCD contributions," *Phys. Lett.* **B652** (2007) 300–309, `arXiv:0705.0746 [hep-ph]`.

[277] S. Heinemeyer, H. Rzehak, and C. Schappacher, "Proposals for bottom quark/squark renormalization in the complex MSSM," *Phys. Rev.* **D82** (2010) 075010, `arXiv:1007.0689 [hep-ph]`.

[278] G. Degrassi, S. Di Vita, and P. Slavich, "Two-loop QCD corrections to the MSSM Higgs masses beyond the effective-potential approximation," *Eur. Phys. J.* **C75** no. 2, (2015) 61, `arXiv:1410.3432 [hep-ph]`.

[279] S. Borowka, T. Hahn, S. Heinemeyer, G. Heinrich, and W. Hollik, "Renormalization scheme dependence of the two-loop QCD corrections to the neutral Higgs-boson masses in the MSSM," *Eur. Phys. J.* **C75** no. 9, (2015) 424, `arXiv:1505.03133 [hep-ph]`.

[280] M. Frank, *Strahlungskorrekturen im Higgs-Sektor des Minimalen Supersymmetrischen Standardmodells mit CP-Verletzung.* PhD thesis, Universität (TH) Karlsruhe, 2003. Berlin 2003. Fak. f. Physik, Diss. v. 06.12.2002.

[281] M. Sperling, D. Stöckinger, and A. Voigt, "Renormalization of vacuum expectation values in spontaneously broken gauge theories: two-loop results," *JHEP* **01** (2014) 068, `arXiv:1310.7629 [hep-ph]`.

[282] A. Brignole, "Radiative corrections to the supersymmetric neutral Higgs boson masses," *Phys. Lett.* **B281** (1992) 284–294.

[283] P. H. Chankowski, S. Pokorski, and J. Rosiek, "One loop corrections to the supersymmetric Higgs boson couplings and LEP phenomenology," *Phys. Lett.* **B286** (1992) 307–314.

[284] P. H. Chankowski, S. Pokorski, and J. Rosiek, "Complete on-shell renormalization scheme for the minimal supersymmetric Higgs sector," *Nucl. Phys.* **B423** (1994) 437–496, `arXiv:hep-ph/9303309 [hep-ph]`.

[285] A. Dabelstein, "The one-loop renormalization of the MSSM Higgs sector and its application to the neutral scalar Higgs masses," *Z. Phys.* **C67** (1995) 495–512, `arXiv:hep-ph/9409375 [hep-ph]`.

[286] A. Dabelstein, "Fermionic decays of neutral MSSM Higgs bosons at the one-loop level," *Nucl. Phys.* **B456** (1995) 25–56, `arXiv:hep-ph/9503443 [hep-ph]`.

[287] A. K. Cyrol, M. Mitter, and N. Strodthoff, "FormTracer - A Mathematica tracing package using FORM," *Comput. Phys. Commun.* **219** (2017) 346–352, `arXiv:1610.09331 [hep-ph]`.

[288] S. A. Larin, "The renormalization of the axial anomaly in dimensional regularization," *Phys. Lett.* **B303** (1993) 113–118, `arXiv:hep-ph/9302240 [hep-ph]`.

[289] R. Mertig and R. Scharf, "TARCER: A Mathematica program for the reduction of two-loop propagator integrals," *Comput. Phys. Commun.* **111** (1998) 265–273, `arXiv:hep-ph/9801383 [hep-ph]`.

[290] U. Nierste, D. Müller, and M. Böhm, "Two-loop relevant parts of D-dimensional massive scalar one-loop integrals," *Zeitschrift für Physik C - Particles and Fields* **57** no. 4, (Dec, 1993) 605–613.

[291] S. P. Martin and D. G. Robertson, "TSIL: a program for the calculation of two-loop self-energy integrals," *Comput. Phys. Commun.* **174** (2006) 133–151, `arXiv:hep-ph/0501132 [hep-ph]`.

[292] S. Heinemeyer, W. Hollik, and G. Weiglein, "The masses of the neutral CP-even Higgs bosons in the MSSM: Accurate analysis at the two-loop level," *The European Physical Journal C - Particles and Fields* **9** no. 2, (Jun, 1999) 343–366, `arXiv:hep-ph/9812472 [hep-ph]`.

[293] S. Heinemeyer, W. Hollik, and G. Weiglein, "FeynHiggs: a program for the calculation of the masses of the neutral CP-even Higgs bosons in the MSSM," *Computer Physics Communications* **124** no. 1, (2000) 76 – 89, `arXiv:hep-ph/9812320 [hep-ph]`.

[294] G. Degrassi, S. Heinemeyer, W. Hollik, P. Slavich, and G. Weiglein, "Towards high precision predictions for the MSSM Higgs sector," *Eur. Phys. J.* **C28** (2003) 133–143, `arXiv:hep-ph/0212020 [hep-ph]`.

[295] M. Frank, T. Hahn, S. Heinemeyer, W. Hollik, H. Rzehak, and G. Weiglein, "The Higgs Boson Masses and Mixings of the Complex MSSM in the Feynman-Diagrammatic Approach," *JHEP* **02** (2007) 047, `arXiv:hep-ph/0611326 [hep-ph]`.

[296] T. Hahn, S. Heinemeyer, W. Hollik, H. Rzehak, and G. Weiglein, "High-Precision Predictions for the Light *CP*-Even Higgs Boson Mass of the Minimal Supersymmetric Standard Model," *Phys. Rev. Lett.* **112** (Apr, 2014) 141801, `arXiv:1312.4937 [hep-ph]`.

[297] W. Hollik and S. Paßehr, "Higgs boson masses and mixings in the complex MSSM with two-loop top-Yukawa-coupling corrections," *JHEP* **10** (2014) 171, `arXiv:1409.1687 [hep-ph]`.

[298] W. Hollik and S. Paßehr, "Two-loop top-Yukawa-coupling corrections to the charged Higgs-boson mass in the MSSM," *The European Physical Journal C* **75** no. 7, (Jul, 2015) 336, `arXiv:1502.02394 [hep-ph]`.

[299] H. Bahl and W. Hollik, "Precise prediction for the light MSSM Higgs-boson mass combining effective field theory and fixed-order calculations," *The European Physical Journal C* **76** no. 9, (Sep, 2016) 499, `arXiv:1608.01880 [hep-ph]`.

[300] H. Bahl, S. Heinemeyer, W. Hollik, and G. Weiglein, "Reconciling EFT and hybrid calculations of the light MSSM Higgs-boson mass," *The European Physical Journal C* **78** no. 1, (Jan, 2018) 57, `arXiv:1706.00346 [hep-ph]`.

[301] P. Drechsel, R. Gröber, S. Heinemeyer, M. Mühlleitner, H. Rzehak, and G. Weiglein, "Higgs-boson masses and mixing matrices in the NMSSM: analysis of on-shell calculations," *The European Physical Journal C* **77** no. 6, (Jun, 2017) 366, `arXiv:1612.07681 [hep-ph]`.

[302] A. Brignole, G. Degrassi, P. Slavich, and F. Zwirner, "On the $\mathcal{O}(\alpha_t^2)$ two-loop corrections to the neutral Higgs boson masses in the MSSM," *Nuclear Physics B* **631** no. 1, (2002) 195 – 218, `arXiv:hep-ph/0112177 [hep-ph]`.

[303] A. Denner, S. Dittmaier, M. Grazzini, R. V. Harlander, R. S. Thorne, M. Spira, and M. Steinhauser, "Standard Model input parameters for Higgs physics,". `https://cds.cern.ch/record/2047636`.

[304] R. Costa, M. Mühlleitner, M. O. P. Sampaio, and R. Santos, "Singlet extensions of the Standard Model at LHC Run 2: benchmarks and comparison with the NMSSM," *JHEP* **06** (2016) 034, `arXiv:1512.05355 [hep-ph]`.

[305] D. Azevedo, P. Ferreira, M. M. Mühlleitner, R. Santos, and J. Wittbrodt, "Models with extended Higgs sectors at future e^+e^- colliders," *Phys. Rev.* **D99** no. 5, (2019) 055013, `arXiv:1808.00755 [hep-ph]`.

[306] F. Staub, P. Athron, U. Ellwanger, R. Gröber, M. Mühlleitner, P. Slavich, and A. Voigt, "Higgs mass predictions of public NMSSM spectrum generators," *Comput. Phys. Commun.* **202** (2016) 113–130, `arXiv:1507.05093 [hep-ph]`.

[307] **ATLAS** Collaboration, G. Aad *et al.*, "Summary of the searches for squarks and gluinos using $\sqrt{s} = 8$ TeV *pp* collisions with the ATLAS experiment at the LHC," *JHEP* **10** (2015) 054, `arXiv:1507.05525 [hep-ex]`.

[308] **ATLAS** Collaboration, M. Aaboud *et al.*, "Search for top squarks in final states with one isolated lepton, jets, and missing transverse momentum in $\sqrt{s} = 13$ TeV *pp* collisions with the ATLAS detector," *Phys. Rev.* **D94** no. 5, (2016) 052009, `arXiv:1606.03903 [hep-ex]`.

[309] S. Inoue, M. J. Ramsey-Musolf, and Y. Zhang, "CP-violating phenomenology of flavor conserving two Higgs doublet models," *Phys. Rev.* **D89** no. 11, (2014) 115023, `arXiv:1403.4257 [hep-ph]`.

[310] V. Andreev, D. Ang, D. DeMille, J. Doyle, G. Gabrielse, J. Haefner, N. R. Hutzler, Z. Lasner, C. Meisenhelder, B. R. O'Leary, C. D. Panda, A. West, E. P. West, and X. Wu, "Improved limit on the electric dipole moment of the electron," *Nature* **562** (10, 2018) 355–360.

[311] L. Lewin, *Polylogarithms and associated functions.* North Holland, 1981.

[312] R. Scharf and J. B. Tausk, "Scalar two-loop integrals for gauge boson self-energy diagrams with a massless fermion loop," *Nucl. Phys.* **B412** (1994) 523–552.

[313] S. P. Martin, "Complete two-loop effective potential approximation to the lightest Higgs scalar boson mass in supersymmetry," *Phys. Rev.* **D67** (2003) 095012, `arXiv:hep-ph/0211366 [hep-ph]`.

[314] S. P. Martin, "Taming the Goldstone contributions to the effective potential," *Phys. Rev.* **D90** no. 1, (2014) 016013, `arXiv:1406.2355 [hep-ph]`.

[315] J. Braathen and M. D. Goodsell, "Avoiding the Goldstone Boson Catastrophe in general renormalisable field theories at two loops," *JHEP* **12** (2016) 056, `arXiv:1609.06977 [hep-ph]`.

[316] J. Braathen, M. D. Goodsell, and F. Staub, "Supersymmetric and non-supersymmetric models without catastrophic Goldstone bosons," *Eur. Phys. J.* **C77** no. 11, (2017) 757, `arXiv:1706.05372 [hep-ph]`.

[317] O. V. Tarasov, "Connection between Feynman integrals having different values of the space-time dimension," *Phys. Rev.* **D54** (1996) 6479–6490, `arXiv:hep-th/9606018 [hep-th]`.

[318] O. V. Tarasov, "Generalized recurrence relations for two-loop propagator integrals with arbitrary masses," *Nucl. Phys.* **B502** (1997) 455–482, `arXiv:hep-ph/9703319 [hep-ph]`.

[319] S. P. Martin, "Evaluation of two-loop self-energy basis integrals using differential equations," *Phys. Rev.* **D68** (2003) 075002, `arXiv:hep-ph/0307101 [hep-ph]`.

[320] F. Berends and J. Tausk, "On the numerical evaluation of scalar two-loop self-energy diagrams," *Nuclear Physics B* **421** (06, 1994) 456–470.

[321] H. A. Rzehak, *Zwei-Schleifen-Beiträge im supersymmetrischen Higgs-Sektor.* PhD thesis, Technische Universität München, 2005. `https://mediatum.ub.tum.de/603098`. München 2005. Max-Planck-Institut fur Physik (Werner-Heisenberg-Institut), Diss. v. 27.06.2005.